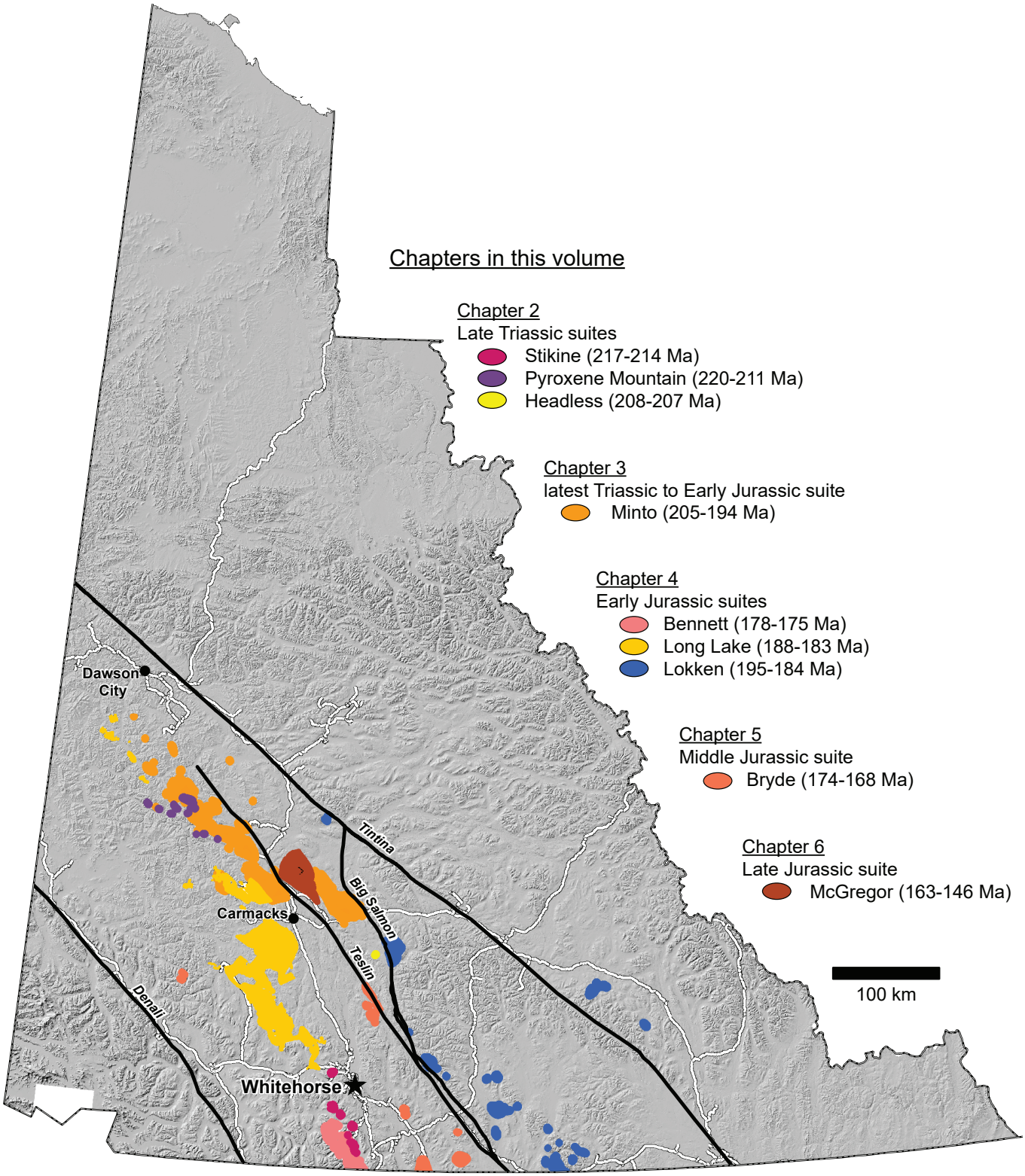


Yukon Geological Survey Open File 2020-1

Atlas of Late Triassic to Jurassic plutons in the Intermontane terranes of Yukon

Patrick J. Sack and Maurice Colpron
James L. Crowley
James J. Ryan
Murray M. Allan
Luke P. Beranek
Nancy L. Joyce

with contributions from:
James K. Mortensen
Steve Israel
John B. Chapman


Chapters in this volume
Chapter 2
Late Triassic suites
Stikine (217-214 Ma)
Pyroxene Mountain (220-211 Ma)
Headless (208-207 Ma)
Chapter 3
latest Triassic to Early Jurassic suite
Minto (205-194 Ma)
Chapter 4
Early Jurassic suites
Bennett (178-175 Ma)
Long Lake (188-183 Ma)
Lokken (195-184 Ma)
Chapter 5
Middle Jurassic suite
Bryde (174-168 Ma)
Chapter 6
Late Jurassic suite
McGregor (163-146 Ma)
Dawson City
Carmacks
Whitehorse
Tintina
Big Salmon
Teslin
Denali
100 km

Yukon

Atlas of Late Triassic to Jurassic plutons in the Intermontane terranes of Yukon

Patrick J. Sack and Maurice Colpron (Yukon Geological Survey)

James L. Crowley (Boise State University)

James J. Ryan (Geological Survey of Canada)

Murray M. Allan (Mineral Deposit Research Unit, University of British Columbia; now at Teck Resources Limited)

Luke P. Beranek (Memorial University of Newfoundland)

Nancy L. Joyce (Geological Survey of Canada)

with contributions from:

James K. Mortensen (University of British Columbia, emeritus)

Steve Israel (Yukon Geological Survey; now at Archer Cathro and Associates, 1981 Limited)

John B. Chapman (Geological Survey of Canada; now at Rio Tinto)

Published under the authority of the Department of Energy, Mines and Resources, Government of Yukon
Printed in Whitehorse, Yukon, 2020

Publié avec l'autorisation du Ministères de l'Énergie, des Mines et des Ressources du gouvernement du Yukon
Imprimé à Whitehorse (Yukon) en 2020.

© Department of Energy, Mines and Resources, Government of Yukon

This, and other Yukon Geological Survey publications, may be obtained from:

Yukon Geological Survey
102-300 Main Street
Box 2703 (K-102)
Whitehorse, Yukon, Canada Y1A 2C6
email geology@gov.yk.ca

Visit the Yukon Geological Survey web site at https://yukon.ca/en/science-and-natural-resources/geology

In referring to this publication, please use the following citation:
Sack, P.J., Colpron, M., Crowley, J.L., Ryan, J.J., Allan, M.M., Beranek, L.P. and Joyce, N.L., 2020. Atlas of Late Triassic to Jurassic plutons in the Intermontane terranes of Yukon. Yukon Geological Survey, Open File 2020-1, 365 p.

Front cover: YGS geologist Maurice Colpron taking notes in front of tors of weathered granite, station 15PS096 in the Big Creek batholith.

Inside front cover: Late Triassic to Jurassic plutons that intrude the Intermontane terranes in Yukon.

Back cover: MDRU geologist Murray Allan heading towards tors to collect a sample for Al-in-Hbl geobarometry, station 14PS125 in the northern part of the Aishihik batholith.

Preface

The Atlas of Late Triassic to Jurassic plutons in the Intermontane terranes of Yukon presents a significant body of work, both in terms of the volume of new data generated and the measure of existing information compiled. The idea for the project was conceived in 2014 at a geoscience research planning workshop in Whitehorse. Workshop participants noted that Late Triassic to Jurassic plutons in the Intermontane belt of British Columbia are host to a number of important porphyry-style copper ± gold ± molybdenum deposits, and that coeval (and presumably co-magmatic) plutons occur in Yukon but have seen limited exploration.

The authors focused on plutons in south-central Yukon, assembling detailed field and petrographic descriptions and documenting geophysical signatures and physical rock property data. New and existing isotopic data have enabled the plutons to be subdivided into nine suites, and geochemical and thermobarometric data yield information about the magma source and emplacement depth of each suite. The volume also includes detailed descriptions of the mineral occurrences associated with each pluton and provides MINFILE references to enable users to find further information on these showings and their associated exploration histories.

The Atlas is intentionally description and data-heavy, and will serve as a comprehensive resource for information on Late Triassic to Jurassic magmatism and metallogeny in Yukon.

Funding for this project was provided by the Yukon Geological Survey; additional support from NRCan's Geomapping for Energy and Minerals (GEM) program contributed to geochronological, geochemical and isotopic analyses.

Carolyn Relf
Director, Yukon Geological Survey

Table of Contents

Preface i

Chapter 1 Introduction

Overview 1

Structure of the Atlas 5

Data sets 6

Contributions 16

Acknowledgements 17

Abbreviations commonly used in this Atlas 18

- Mineral abbreviations 18
- Dating techniques 18
- Other analytical terms 18
- Geoscience institutions 18

Definitions 18

- Pluton nomenclature 18
- Geochronology terminology 19
- Closure temperatures 19
- Crustal levels 19
- Migmatites 20
- Mineral occurrences 20

Chapter 2 Late Triassic (Stikine, Pyroxene Mountain & Headless suites)

Summary 21

Introduction 22

Stikine suite 25

- Tally-Ho plutons 27
- Red Ridge pluton 31
- Friday Creek pluton 38
- Ibex pluton 42
- King Lake pluton 45

Pyroxene Mountain suite 51

- Pyroxene Mountain–Fort Selkirk area 51
- Mount Nansen area 56

Headless suite 57

Geochemistry 60
Major elements 60
Trace elements 60
Zircon chemistry 62
Isotopes 63
Discussion 65

Chapter 3 Latest Triassic–Early Jurassic (Minto suite)

Summary 69
Introduction 70
Granite Mountain batholith 74
Minto pluton 95
Yukon River, Pelly and Walhalla plutons 111
Tatchun batholith 124
Mount Nansen and Big Creek areas 139
Geochemistry 141
Major elements 141
Trace elements 143
Zircon chemistry 145
Isotopes 146
Discussion 146

Chapter 4 Early Jurassic (Long Lake, Bennett & Lokken suites)

Summary 149
Introduction 150
Long Lake suite 155
Aishihik batholith 156
Big Creek batholith 190
Granite Mountain batholith 199
Bennett suite 209
Bennett batholith 213
Alligator Lake plutons 219
Lokken suite 222
Lokken batholith 223
Macmillan Range plutons 230
Thirtymile Lake plutons 235
Sawtooth plutons 241
Englishman plutons 246

Logjam plutons 250
Swift River sill 257
Finlayson plutons 261
Geochemistry 267
Major elements 267
Trace elements 270
Zircon chemistry 275
Isotopes 277
Discussion 280

Chapter 5 Middle Jurassic (Bryde suite)

Summary 283
Introduction 284
Teslin Crossing stock 287
Michie stock 298
Mount Bryde stock 304
Fourth of July batholith 309
Geochemistry 315
Major elements 315
Trace elements 315
Zircon chemistry 319
Isotopes 319
Discussion 321

Chapter 6 Late Jurassic (McGregor suite)

Summary 323
Introduction 324
McGregor batholith 327
Geochemistry 343
Major elements 343
Trace elements 343
Zircon chemistry 347
Isotopes 348
Discussion 349

References 353

Appendices Appendices are available as digital files only.

Appendix 1 Geochronology compilation

Appendix 2 Sample master

Appendix 3 Boise State University LA-ICPMS summary and data

Appendix 4 Boise State University CA-TIMS summary and data

Appendix 5 Al-in-Hbl geobarometry

Appendix 6 $^{40}Ar/^{39}Ar$ summary and data

Appendix 7 ID-TIMS summary and data

Appendix 8 Whole rock geochemistry

Appendix 9 Sr, Nd and Pb isotope summary and data

Appendix 10 Zircon Hf isotope summary and data

Appendix 11 University of British Columbia LA-ICPMS summary and data

Appendix 12 SIMS summary and data

Appendix 13 Polished and stained images

Chapter 1
Introduction

Overview

Late Triassic to Jurassic granitoid plutons intrude the Intermontane terranes in British Columbia, Yukon and easternmost Alaska (Fig. 1-1). In British Columbia, these plutons are associated with significant porphyry Cu ± Mo ± Au mineralization, but comparatively few copper occurrences are known along the northern extension of this belt in Yukon (Mortensen *et al.*, 1995; Logan and Mihalynuk, 2014) and there is no known mineralization associated with Late Triassic to Jurassic plutons in eastern Alaska (Dusel-Bacon *et al.*, 2015). Significant copper mineralization is identified at the Minto and Carmacks Copper deposits in central Yukon (Fig. 1-2), but the style of mineralization at these enigmatic deposits is not typical of porphyry deposits. Both Minto and Carmacks Copper are hosted in Early Jurassic granitoid plutons and have thus been inferred to relate to porphyry deposits of this age in British Columbia (*e.g.*, Logan and Mihalynuk, 2014). Poor understanding of the Yukon deposits and their host intrusions are factors that have hindered exploration. To fill this gap in knowledge, the Yukon Geological Survey initiated a comprehensive study of Late Triassic to Jurassic plutons in 2014 (Relf, 2015) aimed at better defining their geology and mineral potential. For this study, most plutons in southern Yukon of known or inferred Late Triassic to Jurassic age were visited, mainly between 2014 and 2015. Archival collections and data acquired during regional mapping projects of the Yukon Geological Survey and Geological Survey of Canada since 1998 were also compiled as part of this study. This Atlas presents the extensive geochronological, geochemical, isotopic and geobarometric data sets that have been acquired and compiled for these Late Triassic to Jurassic plutons in southern Yukon.

This study focuses on the Late Triassic to Jurassic plutons exposed between the Yukon-British Columbia border at 60°N and the latitude of Stewart Crossing (~63°20'N) in central Yukon (Fig. 1-2; Table 1-1). Plutons of this age also extend to the northwest into western Yukon and east-central Alaska (Fig. 1-1) but were not examined for the present study. The Late Triassic to Jurassic plutons intrude rocks of the Intermontane terranes including Yukon-Tanana, Stikinia, Quesnellia and Cache Creek. The younger, Middle Jurassic plutons also intrude Jurassic sedimentary strata of Whitehorse trough (Fig. 1-2). The Yukon-Tanana terrane consists of metasedimentary, metavolcanic and metaplutonic rocks that record development of a series of magmatic arcs of mid to late Paleozoic age that were constructed on a metasedimentary sequence of western Laurentian affinity (Mortensen, 1992; Colpron *et al.*, 2006a, 2007a; Nelson *et al.*, 2006; Piercey and Colpron, 2009). In Yukon, Stikinia and Quesnellia comprise mainly Upper Triassic arc volcanic and sedimentary rocks and local exposures of older, upper Paleozoic metavolcanic and metasedimentary sequences of arc and back-arc affinities (Hart, 1997a; Colpron *et al.*, 2006a). The dominantly Upper Triassic volcanic and volcaniclastic rocks of Quesnellia and Stikinia have similar composition and stratigraphic relationships which make them difficult to differentiate in central Yukon. The boundary between these two terranes is typically defined by the Teslin fault, the northern expression of the Thibert fault that marks the boundary between Quesnellia and the Cache Creek terrane in northern British Columbia. The position of the Teslin fault, and therefore the Quesnellia–Stikinia boundary, is, however, poorly constrained in central Yukon. Both Quesnellia and Stikinia in Yukon are inferred to have been developed atop a 'basement' comprising mid-Paleozoic and older elements of the Yukon-Tanana terrane (*e.g.*, Nelson *et al.*, 2013).

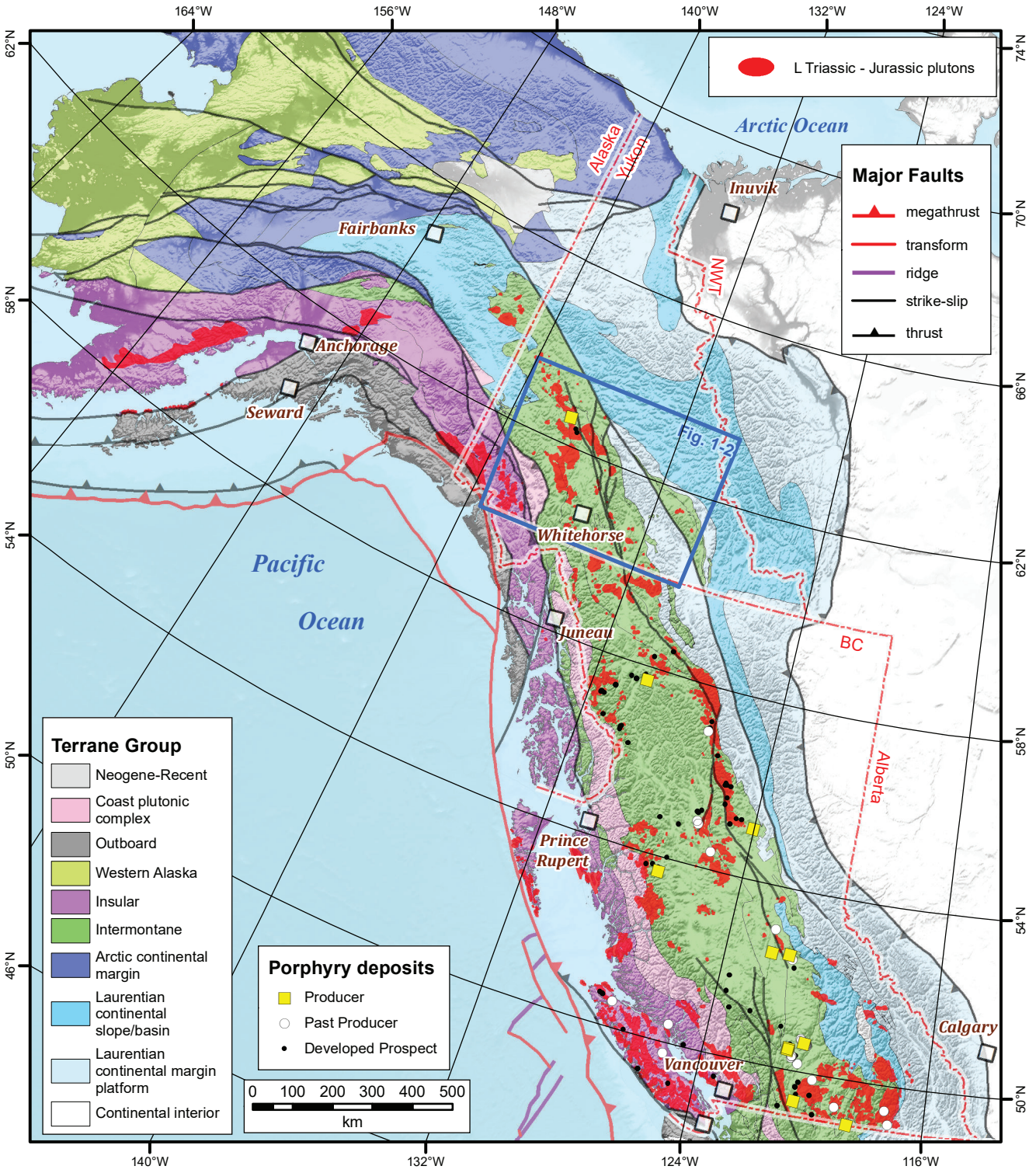


Figure 1-1. *Distribution of Late Triassic to Jurassic plutons and significant Cu ± Mo ± Au porphyry deposits in the northern Cordillera. Simplified terrane map modified after Colpron and Nelson (2011). Plutons are from Cui et al. (2017) for British Columbia, YGS (2020a) for Yukon, and Wilson et al. (2015) for Alaska. Porphyry deposits are from BC MINFILE (BCGS, 2019) and Yukon MINFILE (YGS, 2020b) databases.*

The Cache Creek terrane in southern Yukon comprises mainly Pennsylvanian to Permian limestone massifs, uppermost Permian to Middle Triassic volcanic and volcaniclastic rocks, variably serpentinized ultramafic rocks, and an overlying succession of Upper Triassic to Lower Jurassic chert and immature clastic rocks that are inferred to be in part equivalent with strata of the Laberge Group in the Whitehorse trough to the north (Colpron *et al.*, 2015; Bickerton *et al.*, 2020). The Whitehorse trough is an Early to Middle Jurassic synorogenic marine sedimentary basin that developed during convergence of the Intermontane terranes and is in part coeval with Early Jurassic magmatism that generated the plutons described in this Atlas (Colpron *et al.*, 2015; Bordet *et al.*, 2019). The Whitehorse trough overlaps Stikinia, Quesnellia and Cache Creek terranes (Fig. 1-2).

In Yukon, the Late Triassic to Jurassic plutons are subdivided into nine plutonic suites based mainly on composition and age, but also to some extent on their relationship with their host terrane, and geographic distribution (Table 1-1). From oldest to youngest, these suites are:

1. the Late Triassic Pyroxene Mountain (220–211 Ma), Stikine (217–214 Ma) and Headless (208–207 Ma) suites (Chapter 2);
2. the latest Triassic to Early Jurassic Minto suite (205–194 Ma; Chapter 3);
3. the Early Jurassic Lokken (195–184 Ma), Long Lake (188–183 Ma) and Bennett (178–175 Ma) suites (Chapter 4);
4. the Middle Jurassic Bryde suite (174–168 Ma; Chapter 5); and
5. the Late Jurassic McGregor suite (163–146 Ma; Chapter 6).

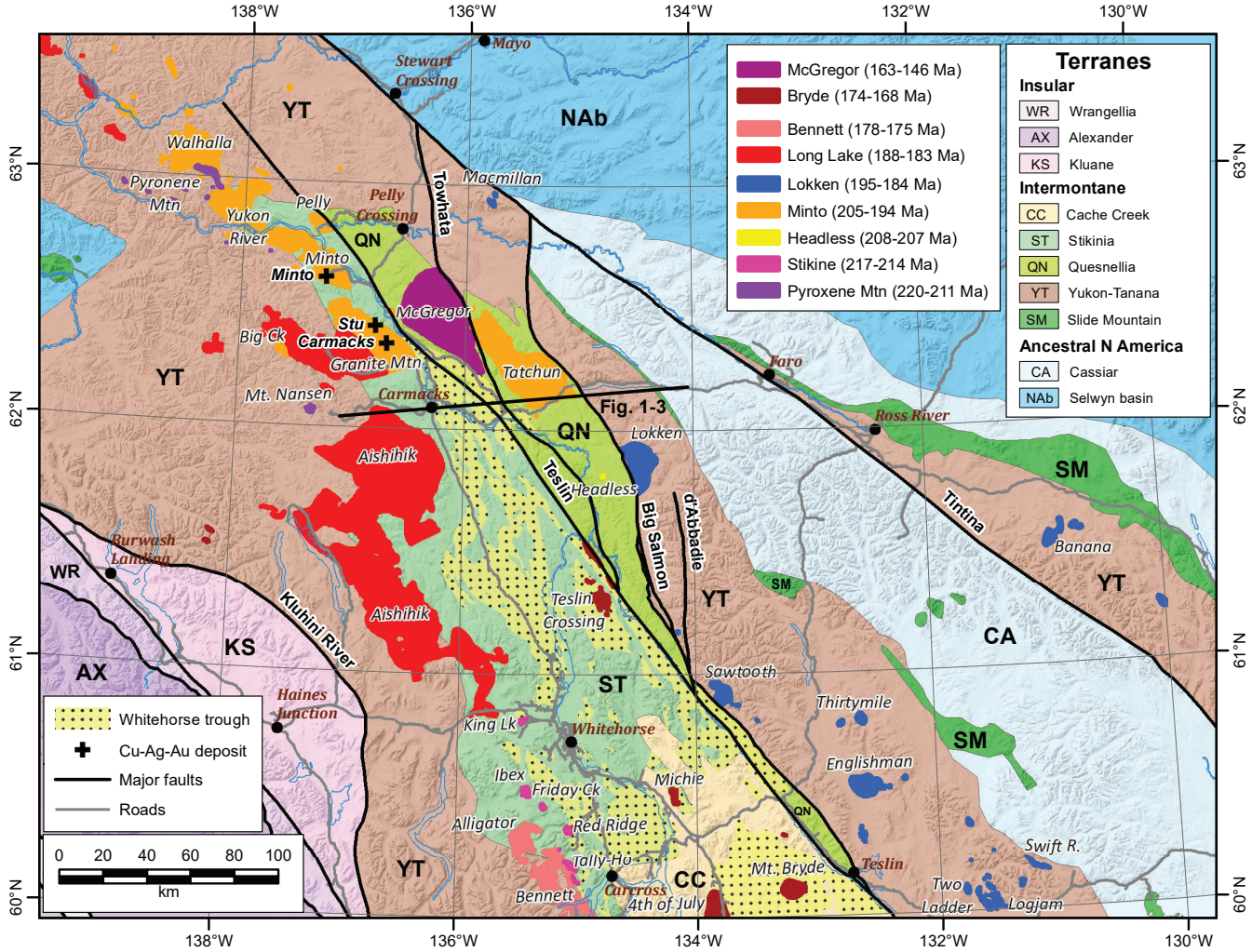


Figure 1-2. *Distribution of Late Triassic to Jurassic plutons in southern Yukon. The names of plutons described in this Atlas are indicated. Note that the Tadru plug (described in Chapter 2) is too small to be shown here. Terrane map is modified after Colpron and Nelson (2011). Plutons and distribution of Whitehorse trough strata are from YGS (2020a).*

In general, the Late Triassic to Jurassic plutons lack an association with coeval volcanic rocks in Yukon. Possible exceptions are plutons of the Stikine and Pyroxene Mountain suites which are broadly coeval with volcanic and volcaniclastic rocks of the Upper Triassic Lewes River Group in Stikinia (Carnian to Norian?; Wheeler, 1961; Tempelman-Kluit, 1984; Hart, 1997a; Bordet *et al.*, 2019), and small plugs of the Headless suite which intrude coeval rocks of the Upper Triassic Semenof formation in Quesnellia east of the Teslin fault (Tempelman-Kluit, 1984, 2009; Simard, 2003). Pyroclastic rocks of the Pliensbachian (*ca.* 188–184 Ma, Lower Jurassic; Colpron and Friedman, 2008) Nordenskiöld facies in the Whitehorse trough are coeval with magmatism of the Long Lake suite to the west and Lokken suite to the east, but no record of Early Jurassic volcanism is known outside of the Whitehorse trough in Yukon. Early Jurassic volcanism occurs in the Hazelton Group of northern British Columbia (Nelson *et al.*, 2013). In Yukon, metamorphic studies and mica cooling ages indicate exhumation of the Yukon-Tanana terrane, and the Early Jurassic plutons it hosts, during deposition of the Whitehorse trough sediments in Early to Middle Jurassic (Colpron *et al.*, 2015).

The Intermontane terranes of southern Yukon are dissected by a series of Late Cretaceous strike-slip faults, including the Teslin, d'Abbadie, Big Salmon and Towhata faults (Fig. 1-2). Near the Yukon-British Columbia border, the Teslin fault and its southern extension, the Thibert fault, is inferred to have as much as 130 km of dextral offset (Gabrielse *et al.*, 2006). South of 61°N latitude, the Teslin-Thibert fault separates Quesnellia, to the east, from Cache Creek terrane, to the west. North of 61°N, the Teslin fault loses apparent stratigraphic offset as it juxtaposes lithologically similar Upper Triassic rocks of the Lewes River Group and Semenof formation, and locally Lower to Middle Jurassic strata of the Laberge Group (Whitehorse trough). The displacement recorded along the Teslin fault near 60°N is inferred to be partitioned into splays of the d'Abbadie, Big Salmon and Towhata faults (Fig. 1-2), which collectively account for ~125 km of dextral displacement (Nelson and Colpron, 2007; Nelson *et al.*, 2013).

Table 1-1. *Summary of Late Triassic to Jurassic plutonic suites in the Intermontane terranes of Yukon.*

Chapter	Suite	Plutons	Age range (Ma)	Host terrane(s)
2 – Late Triassic	Stikine	Tally-Ho, Red Ridge, Friday Ck, Ibex Mtn, King Lk	217–214	ST
	Proxene Mountain	Pyroxene Mtn, Mt Nansen	220–211	YT
	Headless	Headless, Tadru	208–207	QN
3 – latest Triassic to Early Jurassic	Minto	Tatchun, NE Granite Mtn, Minto, Yukon Rv, Pelly, Walhalla	205–194	ST/YT, ± QN
4 – Early Jurassic	Long Lake	Aishihik, Big Ck, SW Granite Mtn	188–183	ST/YT
	Bennett	Bennett, Alligator Lk	178–175	ST/YT
	Lokken	Logjam, Two Ladder, Swift Rv, Englishman, Thirtymile, Sawtooth, Banana, Lokken, Macmillan	195–184	YT
5 – Middle Jurassic	Bryde	Fourth of July, Mt. Bryde, Michie, Teslin Crossing	174–168	WT, ST, CC
6 – Late Jurassic	McGregor	McGregor	163–146	QN

Notes:
Ck – creek; Mtn – mountain; Lk – lake; Rv – river.
CC – Cache Creek; QN – Quesnellia; ST – Stikinia; WT – Whitehorse trough; YT – Yukon-Tanana.

In seismic and magnetotelluric (MT) profiles across southern Yukon (SNORCLE line 3), the Teslin fault appears to be underlain by east-dipping anomalies that project to mid-crustal levels (Cook *et al.*, 2004; Dehkordi *et al.*, 2019). Farther north, in central Yukon, a recent interpretation of seismic and gravity data across the Intermontane terranes shows the Big Salmon fault as a deeper and more laterally continuous crustal structure than the Teslin fault at this latitude (Fig. 1-3; Calvert *et al.*, 2017). The northern extent of these Cretaceous faults and the Intermontane terranes are truncated by the Cenozoic Tintina fault, which has displaced the Yukon-Tanana terrane of the Finlayson Lake area as much as 430 km to the southeast (Fig. 1-2; Gabrielse *et al.*, 2006).

Structure of the Atlas

This Atlas provides systematic descriptions for each pluton visited during the course of this study and/or regional mapping activities in central Yukon (*e.g.*, Colpron *et al.*, 2002; Gordey and Ryan, 2005; Ryan *et al.*, 2010, 2013, 2016). These descriptions are primarily organized by geologic epoch and plutonic suite (Table 1-1). Accordingly, the main chapters cover the Late Triassic (Chapter 2), Early Jurassic (Chapter 4), Middle Jurassic (Chapter 5) and Late Jurassic (Chapter 6) epochs. The exception to this basic organization is the Minto suite, which straddles the Late Triassic to Early Jurassic epochs and is described separately in Chapter 3. This is in part due to its metallogenetic significance (host to Minto and Carmacks Copper deposits) and to the more extensive studies conducted on plutons of this suite (*e.g.*, Tafti, 2005; Hood, 2012; Kovacs, 2018).

Each chapter follows the same basic structure. Each section within a chapter opens with a summary of the plutonic suite and its regional setting followed by systematic descriptions for each pluton or group of plutons (Table 1-1).

The descriptions of individual plutons, or group of related plutons, begin with the local geology, physiography, and detailed petrography based on outcrop, hand sample and thin section observations. These are extensively illustrated with maps and photographs. Detailed maps for each pluton, or group of plutons, are derived from the Yukon digital bedrock geology compilation (YGS, 2020b) and use standard symbolization for faults and contacts throughout this Atlas (Fig. 1-4); MINFILE labels are restricted to major occurrences.

This is followed by characterization of the oxidation state for each phase in the pluton, as inferred from magnetic susceptibility data (*e.g.*, Hart *et al.*, 2004a,b) and aeromagnetic maps, and description of mineral occurrences spatially associated with the pluton. A geochronology section reviews previous attempts at dating the pluton and, for most plutons described in this Atlas, we present new high precision dating of zircons using combined LA-ICPMS and CA-TIMS analyses (Table 1-2).

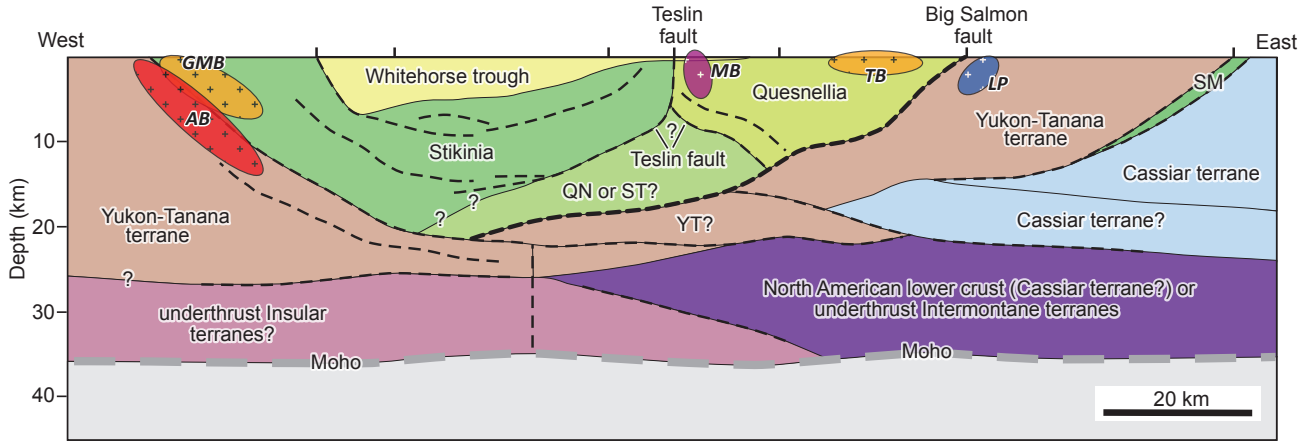


Figure 1-3. *Crustal architecture of the Intermontane terranes in central Yukon (modified after Calvert et al., 2017). Approximate line of section is indicated on Figure 1-2. Approximate positions of selected Jurassic plutons are projected into the line of section: AB – Aishihik batholith; GMB – Granite Mountain batholith; LP – Lokken pluton; MB – McGregor batholith; TB – Tatchun batholith. Other abbreviations: QN – Quesnellia; SM – Slide Mountain; YT – Yukon-Tanana.*

Individual pluton sections typically close with characterization of the crystallization pressure and temperature estimates for compositions amenable to the Al-in-Hbl geobarometric method (Table 1-3); crystallization temperatures are also collected from zircon trace element data acquired by LA-ICPMS analyses.

Each chapter follows with a presentation of the geochemical and isotopic data (Table 1-4) acquired for each suite. Data for each pluton are described together to facilitate discussion of geochemical and isotopic trends within each suite. The chapters conclude with a brief discussion of the key characteristics of each suite and a summary of their mineral potential.

The goal of this Atlas is to present an objective summary of observations and data acquired from Late Triassic to Jurassic plutons intruding the Intermontane terranes in southern Yukon. Accordingly, interpretation of these data is generally limited to first order interpretations of complex geochronological data, exhumation history or mineralizing systems. The data sets compiled for this Atlas are presented in a series of digital Appendices that are described below. At the end of this chapter is a list of abbreviations and definitions.

Data sets

The data compiled for this Atlas are primarily derived from field observations and samples collected between 2014 and 2018, with the majority of sampling occurring in 2014 and 2015 for plutons south of the Minto mine (Fig. 1-2). Data for the Minto, Pelly, Yukon River and Walhalla plutons (Minto suite) were mainly collected as part of regional mapping programs of the Yukon Geological Survey and Geological Survey of Canada, and a number of previously unpublished geochemical and geochronological data acquired for these projects are included in this Atlas. Archival data also augment the new data collected for this study from the Tatchun, Granite Mountain, Big Creek and Aishihik plutons. Table 1-5 summarizes the new and archival data compiled for this Atlas. The data sets are presented in a series of digital Appendices, generally as Microsoft Excel spreadsheets. Detailed methods for each analytical technique are also included in each Appendix.

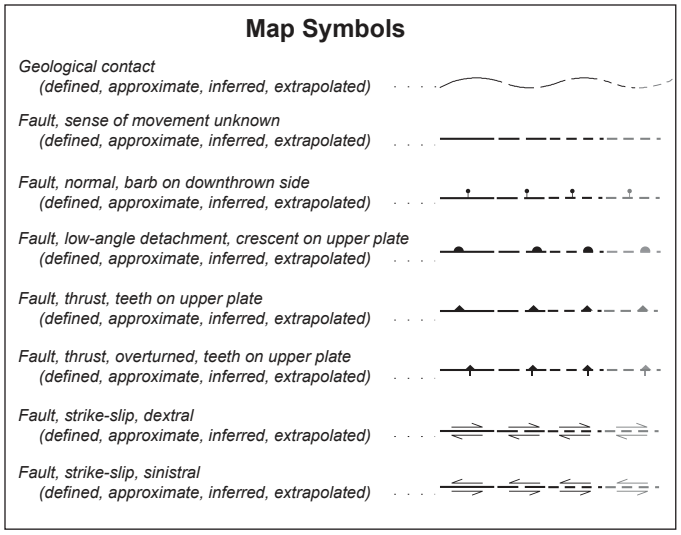


Figure 1-4. *Symbol legend for geological contacts and faults used on all detailed maps in this Atlas. Symbology is adapted from Colpron et al. (2016a).*

Appendix 1 is a compilation of all known U-Pb, $^{40}Ar/^{39}Ar$ and K/Ar dates for Late Triassic to Jurassic plutons in southern Yukon, including the new data presented in this Atlas. These data were extracted from the Yukon-wide geochronological data set available from http://data.geology.gov.yk.ca/Compilation/22 (YGS, 2020c).

Appendix 2 is a summary of field stations and samples collected for this study and compiled from archival data. Appendix 2 gives for each sample: 1) the type of analyses performed; 2) basic petrologic attributes, including estimated modal abundance of Qz, Kfs, Pl and mafic minerals from image analysis of cobaltinitrite-stained slabs; and 3) a measure of the magnetic susceptibility for the sample. The detailed methods describe the use of ImageJ© software (Rasband, 1997–2016) for estimation of modal abundance. For samples without a cobaltinitrite-stained slab, modal mineralogy was estimated visually on hand samples and thin sections. For most samples, lithology is determined using these modal mineralogy data and a QAP diagram simplified from Le Bas and Streckeisen (1991). For a few samples with only geochemical data (mostly archival samples with the prefix 11RAYJC), lithology was determined using the major element TAS classification of Middlemost (1994). Table A2-1 describes in more detail the column headers used in the main table for Appendix 2.

Table 1-2. *Summary of new U-Pb CA-TIMS results for Late Triassic to Jurassic plutons in southern Yukon.*

Sample	Latitude	Longitude	Pluton	Lithology	Weighted mean $^{206}Pb/^{238}U$ date (Ma)	± (Ma)	total n	n in weighted mean	MSWD	pof	Inheritance from LA-ICPMS	Comments
Stikine suite												
15PS050-1	60.36106	-135.07205	Red Ridge	granodiorite	**216.48**	**0.06**	6	6	1.09	0.37	none apparent	
15PS054-1	60.46463	-135.28794	Friday Creek	granodiorite	**215.17**	**0.06**	6	6	1.01	0.41	none apparent	
15PS133-1	60.52913	-135.43400	Ibex	granodiorite	**214.42**	**0.07**	6	5	0.72	0.58	none apparent	1 older at 214.68 ± 0.15 Ma
08MC089-1	60.808327	-135.482953	King Lake	granodiorite	**216.35**	**0.23**	5	4	0.66			
Minto suite												
14PS145	62.1153	-135.42444	Tatchun	granodiorite	**203.32**	**0.06**	8	5	1.29	0.27	2 components at 342 ± 8 and 320 ± 10 Ma	1 older at 204.81 ± 0.14 Ma and 2 strongly discordant
S09-16-01A	62.62015	-137.2447	Minto	mineralized gneiss, no igneous textures	**198.22**	**0.06**	6	6	1.83	0.10	1 at 325 ± 14 Ma	GSC SHRIMP is 197.0 ± 1.9 Ma (external error)
S09-16-01D	62.62015	-137.2447	Minto	granodiorite	**196.39**	**0.11**	12	4	1.05	0.37	3 at 326 ± 32 Ma 11 at 214 ± 4 Ma	4 youngest from double polished zircon. 8 older from double and single polished. GSC SHRIMP is 197.7 ± 1.8 Ma (external error)
15PS101-1	62.3209	-135.71469	Tatchun	monzodiorite	**196.13**	**0.09**	6	2	0.32	0.57	3 at 341 ± 10 Ma	4 older from 196.4 Ma to much older.
14PS073	62.3349	-136.51932	Granite Mtn	monzodiorite	**194.71**	**0.07**	6	5	0.85	0.50	none apparent	1 younger at 194.33 ± 0.14 Ma
STU80-7-286.5	62.41588	-136.8497	Granite Mtn	mafic enclave	***scatter***		5	0			none apparent	Range from 194.99 ± 0.13 to 206.27 ± 0.14 Ma
Lokken suite												
14MC-142	60.8179	-132.6472	Thirtymile	monzodiorite	**194.71**	**0.07**	6	5	0.83	0.53	none apparent	
14PS184a	61.9053	-134.36940	Lokken	monzodiorite	**192.20**	**0.06**	7	5	0.41	0.75	none apparent	2 older at 192.44 ± 0.13 and 192.53 ± 0.13 Ma
15MC003	62.9430	-135.79855	Macmillan	monzonite	**192.12**	**0.07**	5	5	1.10	0.36	none apparent	
14PS226	60.0413	-131.66808	Two Ladder	monzodiorite	**188.18**	**0.05**	6	6	0.72	0.61	none apparent	

Note: All samples analyzed at BSU, except 08MC089-1 which was analyzed at UBC.

Table 1-2 continued.

Sample	Latitude	Longitude	Pluton	Lithology	Weighted mean $^{206}Pb/^{238}U$ date (Ma)	± (Ma)	total n	n in weighted mean	MSWD	pof	Inheritance from LA-ICPMS	Comments
Lokken suite continued												
14PS225	60.0331	-131.55230	Logjam	monzonite	**184.21**	**0.05**	6	6	1.36	0.24	3 components at 2285 ± 40 Ma 348 ± 8, and 198 ± 5 Ma	
14PS222	60.5363	-132.50719	Englishman	monzonite	**188.05**	**0.05**	6	6	0.33	0.90	none apparent	
14PS218	60.9218	-133.74924	Sawtooth	monzodiorite	**184.28**	**0.07**	6	4	1.27	0.27	4 components at 1698 ± 82, 605 ± 42, 232 ± 9 Ma	1 older at 184.64 ± 0.12 Ma and 1 older discordant analysis
16PS027	61.53528	-130.96681	Finlayson Lake (Banana)	monzonite	**185.95**	**0.05**	6	6	0.90	0.48	2 grains at ~200 Ma	
Long Lake suite												
14PS182	62.3930	-137.09773	Granite Mtn	granodiorite	**187.46**	**0.07**	6	4	1.93	0.10	2 components at 350 ± 16 and 204 ± 5 Ma	2 older at 187.76 ± 0.13 and 190.66 ± 0.13 Ma
14PS114-1	62.3061	-136.9690	Granite Mtn	granodiorite	**186.38**	**0.07**	6	3	2.38	0.09	none apparent	3 older at 186.70 ± 0.13, 186.90 ± 0.13, and 186.97 ± 0.13 Ma
15PS071-1	61.69203	-136.28988	Aishihik 1	monzodiorite	**186.22**	**0.10**	6	6	2.28	0.04	none apparent	
14PS154-1	61.6013	-137.3813	Aishihik 1	tonalite	**184.69**	**0.06**	6	5	1.44	0.22	4 components at 571 ± 21, 374 ± 18, 275 ± 12 and 200 Ma	1 older at 186.94 ± 0.13 Ma
14PS120-1	62.0380	-136.7286	Aishihik 2	granodiorite	**184.06**	**0.06**	6	5	1.21	0.30	6 components at 2606 ± 46, 1741 ± 62, 346 ± 10, 263 ± 10, 250 ± 7, and 199 ± 5 Ma	1 older at 184.25 ± 0.12 Ma
14PS162-1	61.0865	-136.32462	Aishihik 1	tonalite	**184.06**	**0.05**	6	6	1.21	0.30	4 components at 377 ± 12, 326 ± 14, 273 ± 16, and 208 ± 7 Ma	
15SI078	61.3679	-136.9590	Aishihik 1	granodiorite	**183.28**	**0.07**	6	3	2.66	0.07	2 components at 345 ± 10 Ma and 199 ± 4 Ma	1 older at 183.48 ± 0.13 Ma and 2 fragments from 1 grain at 184.5 Ma

Note: All samples analyzed at BSU, except 08MC089-1 which was analyzed at UBC.

Table 1-2 continued.

Sample	Latitude	Longitude	Pluton	Lithology	Weighted mean $^{206}Pb/^{238}U$ date (Ma)	± (Ma)	total n	n in weighted mean	MSWD	pof	Inheritance from LA-ICPMS	Comments
Long Lake suite continued												
14PS165-1	61.3339	-136.6787	Aishihik 2	granite	***scatter***		6	0	0.88	0.47	7 components at 374 ± 13, 353 ± 14, 325 ± 15, 306 ± 13, 229 ± 9, 209 ± 7, and 196 ± 4 Ma	Range from 184.69 ± 0.14 to 181.49 ± 0.13; most are closer to older end; LA-ICPMS date of 183.8 ± 0.6 Ma best estimate of crystallization
15PS099-1	62.37125	-137.67214	Big Ck	monzodiorite	**185.04**	**0.06**	6	5	1.11	0.35		
15PS094-1	62.28278	-137.11144	Big Ck	syenite	**182.83**	**0.05**	6	6	0.81	0.54	1 component at 324 ± 11 Ma	
Bennett suite												
15PS032-1	60.13068	-135.17345	Bennett	granodiorite	**178.18**	**0.06**	7	5	2.07	0.08	none apparent	2 older at 178.44 ± 0.12 and 178.48 ± 0.12 Ma
Bryde suite												
15PS003-1	60.0300	-133.8562	Fourth of July	diorite	**173.44**	**0.05**	6	6	0.86	0.51	1 at 215 ± 12 Ma	
15PS123-1	60.12305	-133.18851	Mt. Bryde	monzodiorite	**172.51**	**0.05**	6	6	0.23	0.95	none apparent	
15PS082-1	61.28733	-134.80464	Teslin Crossing	monzodiorite	**171.62**	**0.05**	6	6	1.01	0.41	none apparent	
15PS010-1	60.47758	-134.18810	Michie	monzonite	**168.09**	**0.05**	6	6	1.25	0.28	none apparent	
McGregor suite												
14PS181	62.5782	-136.11845	McGregor	granodiorite	**163.42**	**0.05**	6	6	1.45	0.23	none apparent	
14PS171-2	62.5782	-136.11845	McGregor	leucocratic dike	**161.18**	**0.05**	6	6	1.73	0.12	2 components at 318 ± 7 and 198 ± 4 Ma	
14PS171-1	62.5782	-136.11845	McGregor	granodiorite	**161.16**	**0.05**	6	5	1.87	0.10	none apparent	1 older at 162.64 ± 0.11 Ma

Note: All samples analyzed at BSU, except 08MC089-1 which was analyzed at UBC.

Table 1-3. *Summary of geobarometry results for Late Triassic to Jurassic plutons in southern Yukon.*

Sample	Latitude	Longitude	Pluton	Plagioclase X_{an} [a]	1σ [b]	Amphibole $Al^{(TOT)}$	1σ [c]	T (°C)	1σ [d]	P (kbar)	1σ_{reg} [e]	1σ_{Al} [f]	1σ_{T} [g]	1$\sigma_{Al,T}$ [h]	1σ_{TOT} [i]	Depth (km)	1σ [j]	Notes
Stikine suite																		
15PS054	60.4646	-135.2879	Friday Creek	0.289	0.025	1.472	0.047	743	10	3.09	0.6	0.23	0.17	0.27	0.87	11.7	3.3	XAn in range
15PS056	60.4518	-135.2798	Friday Creek	0.293	0.025	1.510	0.063	729	9	3.49	0.6	0.31	0.15	0.32	0.92	13.2	3.5	XAn in range
Minto suite																		
01GGA166B2	63.1355	-138.6759	Walhalla Creek	0.203	0.018	2.061	0.047	732	8	5.86	0.6	0.22	0.16	0.26	0.86	22.1	3.3	XAn < 0.25
11RAYJC037A2	62.6466	-137.3092	Minto	0.259	0.032	2.128	0.055	762	12	5.49	0.6	0.24	0.30	0.38	0.98	20.7	3.7	XAn in range
CDB-10-078a	62.6210	-137.2523	Minto	0.262	0.031	2.108	0.065	748	11	5.72	0.6	0.29	0.25	0.38	0.98	21.6	3.7	XAn in range
14PS048	62.3087	-136.7076	Granite Mtn	0.252	0.033	2.028	0.045	724	12	5.86	0.6	0.20	0.23	0.31	0.91	22.1	3.4	XAn in range
14PS183	62.4686	-137.0456	Granite Mtn	0.279	0.025	1.869	0.069	731	9	5.03	0.6	0.31	0.17	0.35	0.95	19.0	3.6	XAn in range
STU80-7_286.5'	62.4159	-136.8497	Granite Mtn	0.284	0.019	1.864	0.047	744	7	4.77	0.6	0.21	0.14	0.25	0.85	18.0	3.2	XAn in range
14PS142	62.4072	-135.8628	Tatchun	0.108	0.025	2.020	0.023	663	17	6.75	0.6	0.11	0.19	0.23	0.83	25.5	3.1	XAn < 0.25
MA14-TB10	62.3031	-135.5224	Tatchun	0.206	0.022	2.122	0.057	721	9	6.36	0.6	0.26	0.18	0.31	0.91	24.0	3.4	XAn < 0.25
MA14-TB2	62.4518	-135.8270	Tatchun	0.141	0.040	2.314	0.047	721	23	7.21	0.6	0.22	0.45	0.51	1.11	27.2	4.2	XAn < 0.25
MA14-TB4	62.3766	-135.6654	Tatchun	0.188	0.034	2.433	0.060	766	16	6.68	0.6	0.29	0.41	0.49	1.09	25.2	4.1	XAn < 0.25
Lokken suite																		
15MC003	62.9430	-135.7986	Macmillan Range	0.479	0.039	1.776	0.038	817	13	2.62	0.6	0.17	0.38	0.41	1.01	9.9	3.8	XAn > 0.35
15PS107	61.7724	-134.4638	Lokken	0.273	0.026	1.534	0.028	759	11	3.06	0.6	0.14	0.21	0.25	0.85	11.5	3.2	XAn in range

Notes:

[a] XAn refers to mole fraction of anorthite component in plagioclase
[b] error in plagioclase composition is estimated from the standard deviation of plagioclase compositions (both within-grain and between-grain)
[c] error in Al^{TOT} is calculated from the 1σ error in Al_2O_3
[d] error in T is propagated from the error in the plagioclase composition (at fixed hornblende composition)
[e] $\sigma_{(REG)}$ refers to the approximate 1σ regression error of the Anderson and Smith (1995) geobarometer
[f] σ_{Al} refers to the 1σ error in pressure due to uncertainty in the Al^{TOT}
[g] σ_{T} refers to the 1σ error in pressure due to uncertainty in crystallization temperature
[h] $\sigma_{Al,T}$ is the propagated 1σ error in pressure due to errors in Al^{TOT} and T
[i] σ_{TOT} is the estimated total error in pressure calculated by adding the regression error and propagated (Al_{TOT} and T) errors
[j] error in depth taking into account the combined uncertainty in pressure (σ_{TOT})

Table 1-3 continued.

Sample	Latitude	Longitude	Pluton	Plagioclase X_{an} [a]	1σ [b]	Amphibole $Al^{(TOT)}$	1σ [c]	T (°C)	1σ [d]	P (kbar)	$1\sigma_{reg}$ [e]	$1\sigma_{Al}$ [f]	$1\sigma_{T}$ [g]	$1\sigma_{Al,T}$ [h]	$1\sigma_{TOT}$ [i]	Depth (km)	1σ [j]	Notes
Long Lake suite																		
14PS159	61.5549	-136.7508	Aishihik	0.267	0.016	1.750	0.035	731	6	4.52	0.6	0.16	0.11	0.19	0.79	17.1	3.0	XAn in range
14PS162	61.0865	-136.3246	Aishihik	0.328	0.046	2.125	0.055	739	15	6.00	0.6	0.23	0.32	0.40	1.00	22.7	3.8	XAn in range
14PS167	61.3688	-136.8342	Aishihik	0.330	0.016	1.951	0.078	737	5	5.29	0.6	0.34	0.10	0.36	0.96	20.0	3.6	XAn in range
15PS071	61.6920	-136.2899	Aishihik	0.254	0.060	1.169	0.129	705	25	2.28	0.6	0.56	0.27	0.65	1.25	8.6	4.7	XAn in range
MA14-AB1	62.0382	-136.7274	Aishihik	0.318	0.027	1.711	0.083	741	10	4.16	0.6	0.39	0.18	0.40	1.00	15.7	3.8	XAn in range
MA14-AB10	61.7923	-136.2892	Aishihik	0.377	0.032	1.790	0.088	764	11	4.02	0.6	0.40	0.24	0.44	1.04	15.2	3.9	XAn > 0.35
MA14-AB8	61.8817	-136.9347	Aishihik	0.213	0.018	1.392	0.049	697	8	3.40	0.6	0.25	0.09	0.25	0.85	12.8	3.2	XAn < 0.25
Bennett suite																		
15PS043	60.2152	-135.0980	Bennett	0.212	0.020	1.462	0.105	718	9	3.45	0.6	0.42	0.13	0.49	1.09	13.0	4.1	XAn < 0.25
15PS130	60.2745	-135.4733	Alligator Lake	0.240	0.080	0.927	0.176	649	34	1.51	0.6	0.88	0.07	0.87	1.47	5.7	5.6	apparent P < 2kbar
Bryde suite																		
15PS002	60.0224	-133.8460	Fourth of July	0.410	0.052	0.699	0.069	672	18	0.33	0.6	0.37	0.07	0.34	0.94	1.2	3.5	XAn > 0.35; apparent P < 2kbar
McGregor suite																		
14PS171	62.5782	-136.1185	McGregor	0.116	0.024	1.540	0.176	659	16	4.46	0.6	0.90	0.12	0.87	1.47	16.8	5.5	XAn < 0.25
14PS173	62.5697	-136.4479	McGregor	0.170	0.017	1.712	0.098	664	8	5.25	0.6	0.48	0.08	0.48	1.08	19.8	4.1	XAn < 0.25

Notes:

[a] XAn refers to mole fraction of anorthite component in plagioclase
[b] error in plagioclase composition is estimated from the standard deviation of plagioclase compositions (both within-grain and between-grain)
[c] error in Al^{TOT} is calculated from the 1σ error in Al_2O_3
[d] error in T is propagated from the error in the plagioclase composition (at fixed hornblende composition)
[e] $\sigma_{(REG)}$ refers to the approximate 1σ regression error of the Anderson and Smith (1995) geobarometer
[f] σ_{Al} refers to the 1σ error in pressure due to uncertainty in the Al^{TOT}
[g] σ_{T} refers to the 1σ error in pressure due to uncertainty in crystallization temperature
[h] $\sigma_{Al,T}$ is the propagated 1σ error in pressure due to errors in Al^{TOT} and T
[i] σ_{TOT} is the estimated total error in pressure calculated by adding the regression error and propagated (Al_{TOT} and T) errors
[j] error in depth taking into account the combined uncertainty in pressure (σ_{TOT})

***Table 1-4**. Radiogenic isotope data for Late Triassic to Jurassic plutons in southern Yukon.*

Sample	Latitude	Longitude	Pluton	Age (Ma)	Age control	Rb [(a)] (ppm)	Sr [(a)] (ppm)	$^{87}Rb/^{86}Sr$	$^{87}Sr/^{86}Sr$	2σ [(b)]	$^{87}Sr/^{86}Sr_i$
Stikine suite											
15PS054-1	60.4646	-135.2879	Friday Creek	215.17	dated	53	688	0.0770	0.704748	0.000016	0.704067
15PS133-1	60.5291	-135.4340	Ibex	214.42	dated	45	808	0.0557	0.704513	0.000015	0.704022
Minto suite											
14PS145-1	62.1153	-135.4244	Tatchun	203.32	dated	80	1142	0.0701	0.705294	0.000019	0.704700
03RAY303-A1	63.0088	-138.2703	Walhalla Creek	198	estimated	70	729	0.0957	0.705826	0.000022	0.705046
10RAYJR032-A1	62.7948	-137.9319	Yukon River	198	estimated	37	963	0.0384	0.705077	0.000017	0.704766
15PS101-1	62.3209	-135.7147	Tatchun	196.13	dated	50	1118	0.0447	0.705205	0.000020	0.704828
CDB10-063-A1	62.6437	-137.1259	Minto	196	estimated	68	740	0.0919	0.706129	0.000016	0.705388
14PS048-1	62.3087	-136.7076	Granite Mtn	195	estimated	18	1010	0.0178	0.705580	0.000017	0.705437
14PS183-1	62.4686	-137.0456	Granite Mtn	195	estimated	47	842	0.0558	0.706687	0.000019	0.706239
14PS073-1	62.3349	-136.5193	Granite Mtn	194.71	dated	61	1257	0.0485	0.705075	0.000018	0.704700
Lokken suite											
14MC142-1	60.8179	-132.6472	Thirtymile	194.67	dated	99	857	0.1155	0.706853	0.000015	0.705900
14PS184a-1	61.9053	-134.3694	Lokken	192.2	dated	120	813	0.1476	0.706905	0.000016	0.705700
14PS226-1	60.0413	-131.6681	Two Ladder	188.18	dated	151	324	0.4660	0.708799	0.000016	0.705200
14PS222-1	60.5363	-132.5072	Englishman	188.05	dated	87	996	0.0873	0.705106	0.000013	0.704400
14PS218-1	60.9218	-133.7492	Sawtooth	184.28	dated	63	398	0.1583	0.706210	0.000015	0.705000
Long Lake suite											
14PS182-1	62.3930	-137.0977	Granite Mtn	187.46	dated	22	1091	0.0202	0.705769	0.000015	0.705600
14PS154-1	61.6013	-137.3813	Aishihik	186.71	dated	25	899	0.0278	0.706305	0.000019	0.706100
14PS148-1	61.6977	-136.2874	Aishihik	186.23	dated	46	1058	0.0435	0.706640	0.000020	0.706300
15PS099-1	62.3713	-137.6721	Big Ck	185.04	dated	85	1191	0.0714	0.705614	0.000016	0.705077
14PS120-1	62.0380	-136.7286	Aishihik	184.11	dated	51	815	0.0626	0.706997	0.000014	0.706500
14PS162-1	61.0865	-136.3246	Aishihik	184.08	dated	41	704	0.0582	0.706254	0.000016	0.705800
14PS165-1	61.3339	-136.6787	Aishihik	183	estimated	102	909	0.1122	0.706303	0.000015	0.705500
Bennett suite											
15PS032-1	60.1307	-135.1735	Bennett	178.18	dated	92	976	0.0943	0.705879	0.000019	0.705189
15PS132-1	60.3614	-135.4659	Alligator Lake	175	estimated	28	749	0.0374	0.705606	0.000020	0.705337
Bryde suite											
15PS003-1	60.0300	-133.8562	Fourth of July	173.44	dated	45	380	0.1184	0.705302	0.000019	0.704457
15PS123-1	60.1231	-133.1885	Mt Bryde	172.51	dated	49	587	0.0835	0.704865	0.000019	0.704273
15PS082-1	61.2873	-134.8046	Teslin Crossing	171.62	dated	71	1004	0.0707	0.704497	0.000170	0.703998
15PS010-1	60.4776	-134.1881	Michie	168.09	dated	377	1131	0.3333	0.707260	0.000024	0.704956
McGregor suite											
14PS181-1	62.3859	-136.0950	McGregor	163.42	dated	50	1346	0.0371	0.705772	0.000150	0.705500
14PS171-2	62.5782	-136.1185	McGregor	161.18	dated	73	3019	0.0242	0.705565	0.000019	0.705400

Notes:

[a] Sr and Rb values determined by metaborate/tetraborate fusion followed by analysis using Inductively Coupled Plasma-Mass Spectrometry at Activation Laboratories

[b] Uncertainties are presented as ±2 standard errors (2σ)

[c] Sm and Nd values were determined by acid digestion followed by thermal ionization mass spectrometry at Carleton University

[d)] Pb isotope ratios are corrected for fractionation against the NBS 981 (Todt et al., 1996)

Table 1-4 continued.

Sample	Nd [c] (ppm)	Sm [c] (ppm)	$^{147}Sm/^{144}Nd$	$^{143}Nd/^{144}Nd$	2σ[b]	$^{143}Nd/^{144}Nd_i$	2σ[b]	εNd (CHUR)$_T$	2σ[b]
Stikine suite									
15PS054-1	11.00	2.13	0.116180	0.512795	0.000010	0.512631	0.000010	5.3	0.2
15PS133-1	15.40	3.52	0.121745	0.512800	0.000010	0.512630	0.000010	5.2	0.2
Minto suite									
14PS145-1	10.30	2.15	0.117740	0.512577	0.000010	0.512432	0.000010	0.9	0.2
03RAY303-A1	15.46	3.13	0.121851	0.512555	0.000010	0.512397	0.000011	0.3	0.2
10RAYJR032-A1	19.40	4.48	0.132205	0.512614	0.000010	0.512444	0.000011	1.2	0.2
15PS101-1	9.78	1.88	0.118858	0.512513	0.000010	0.512360	0.000010	-0.4	0.2
CDB10-063-A1	13.80	2.57	0.112359	0.512462	0.000010	0.512317	0.000011	-1.3	0.2
14PS048-1	12.80	2.61	0.122010	0.512465	0.000010	0.512310	0.000011	-1.5	0.2
14PS183-1	19.20	3.89	0.116430	0.512352	0.000010	0.512203	0.000011	-3.6	0.2
14PS073-1	24.10	4.12	0.111181	0.512597	0.000010	0.512460	0.000010	1.3	0.2
Lokken suite									
14MC142-1	17.30	3.40	0.123075	0.512416	0.000010	0.512259	0.000010	-2.5	0.2
14PS184a-1	13.80	2.83	0.125986	0.512331	0.000010	0.512176	0.000010	-4.3	0.2
14PS226-1	13.60	2.59	0.129948	0.512483	0.000010	0.512264	0.000010	-1.4	0.2
14PS222-1	13.50	2.92	0.120745	0.512409	0.000010	0.512261	0.000010	-2.6	0.2
14PS218-1	11.50	2.67	0.134502	0.512535	0.000010	0.512369	0.000010	-0.6	0.2
Long Lake suite									
14PS182-1	16.70	3.11	0.118201	0.512456	0.000010	0.512310	0.000010	-1.7	0.2
14PS154-1	22.50	4.46	0.125187	0.512376	0.000010	0.512222	0.000010	-3.4	0.2
14PS148-1	10.60	2.04	0.107084	0.512284	0.000010	0.512152	0.000010	-4.8	0.2
15PS099-1	28.20	5.35	0.120690	0.512405	0.000010	0.512259	0.000010	-2.8	0.2
14PS120-1	22.40	4.26	0.117539	0.512241	0.000010	0.512097	0.000010	-5.9	0.2
14PS162-1	14.50	3.43	0.139441	0.512493	0.000010	0.512321	0.000010	-1.5	0.2
14PS165-1	3.93	0.75	0.124732	0.512339	0.000010	0.512185	0.000011	-4.2	0.2
Bennett suite									
15PS032-1	14.10	2.57	0.109628	0.512409	0.000010	0.512282	0.000010	-2.5	0.2
15PS132-1	17.40	4.15	0.131523	0.512437	0.000010	0.512286	0.000011	-2.5	0.2
Bryde suite									
15PS003-1	18.80	4.36	0.126408	0.512677	0.000010	0.512323	0.000010	2.3	0.2
15PS123-1	17.10	3.52	0.132005	0.512668	0.000010	0.512519	0.000010	2.0	0.2
15PS082-1	23.70	4.29	0.109850	0.512720	0.000010	0.512596	0.000010	3.5	0.2
15PS010-1	26.60	4.45	0.105648	0.512566	0.000010	0.512450	0.000010	0.5	0.2
McGregor suite									
14PS181-1	45.40	7.54	0.098915	0.512529	0.000010	0.512407	0.000010	-0.1	0.2
14PS171-2	98.00	15.90	0.097548	0.512569	0.000010	0.512448	0.000010	0.7	0.2

Notes:

[a] Sr and Rb values determined by metaborate/tetraborate fusion followed by analysis using Inductively Coupled Plasma-Mass Spectrometry at Activation Laboratories

[b] Uncertainties are presented as ±2 standard errors (2σ)

[c] Sm and Nd values were determined by acid digestion followed by thermal ionization mass spectrometry at Carleton University

[d] Pb isotope ratios are corrected for fractionation against the NBS 981 (Todt et al., 1996)

Table 1-4 continued.

Sample	$^{208}Pb/^{204}Pbcor^{(d)}$	$2\sigma^{(b)}$	$^{207}Pb/^{204}Pbcor^{(d)}$	$2\sigma^{(b)}$	$^{206}Pb/^{204}Pbcor^{(d)}$	$2\sigma^{(b)}$
Stikine suite						
15PS054-1	38.2871	0.006	15.5855	0.002	18.7088	0.002
15PS133-1	38.3253	0.003	15.5835	0.001	18.7850	0.002
Minto suite						
14PS145-1	38.4328	0.002	15.6107	0.001	18.7487	0.001
03RAY303-A1	38.4970	0.002	15.6287	0.001	18.6527	0.001
03RAY303-A1	38.4779	0.007	15.6227	0.003	18.6297	0.003
15PS101-1	38.3815	0.002	15.5946	0.001	18.7319	0.001
CDB10-063-A1	38.5161	0.003	15.6237	0.001	18.7459	0.001
14PS048-1	38.6155	0.004	15.6367	0.001	18.8552	0.001
14PS183-1	38.7622	0.003	15.6598	0.001	18.9493	0.001
14PS073-1						
Lokken suite						
14MC142-1	38.8429	0.004	15.6799	0.001	19.0244	0.001
14PS184a-1						
14PS226-1	38.8328	0.005	15.6889	0.001	18.9562	0.001
14PS222-1	38.7183	0.002	15.6719	0.001	19.0936	0.001
14PS218-1	38.6288	0.003	15.6488	0.001	18.9061	0.001
Long Lake suite						
14PS182-1	38.8298	0.002	15.6779	0.001	18.9593	0.001
14PS154-1	38.8710	0.002	15.6819	0.001	19.0274	0.001
14PS148-1	38.9725	0.002	15.6849	0.001	19.0745	0.001
15PS099-1	38.7140	0.002	15.6297	0.001	19.0305	0.001
14PS120-1	39.0117	0.007	15.6940	0.002	19.0936	0.002
14PS162-1	38.8147	0.002	15.6869	0.001	19.0084	0.001
14PS165-1	38.9484	0.006	15.7020	0.002	19.1567	0.002
Bennett suite						
15PS032-1	38.7381	0.005	15.6357	0.002	19.1257	0.002
15PS132-1	38.7712	0.004	15.6427	0.002	19.1277	0.002
Bryde suite						
15PS003-1	38.6738	0.003	15.6467	0.001	18.9223	0.001
15PS123-1	38.6637	0.005	15.6437	0.002	18.9634	0.002
15PS082-1	38.7853	0.007	15.6397	0.003	19.1929	0.004
15PS010-1	38.6346	0.004	15.6257	0.002	18.9754	0.002
McGregor suite						
14PS181-1	38.9665	0.006	15.7130	0.002	19.0625	0.001
14PS171-2						

Notes:

[a] Sr and Rb values determined by metaborate/tetraborate fusion followed by analysis using Inductively Coupled Plasma-Mass Spectrometry at Activation Laboratories

[b] Uncertainties are presented as ±2 standard errors (2σ)

[c] Sm and Nd values were determined by acid digestion followed by thermal ionization mass spectrometry at Carleton University

[d] Pb isotope ratios are corrected for fractionation against the NBS 981 (Todt et al., 1996)

Appendix 3 includes cathodoluminescence (CL) images of zircon and the laser ablation-inductively coupled plasma mass spectrometry (LA-ICPMS) methods and data for analyses conducted on 36 samples at the Isotope Geology Laboratory at Boise State University (BSU). Cathodoluminescence imaging was done on most zircon grains analyzed at BSU. The response (brightness) of CL images corresponds to trace element abundance and is used to characterize populations. LA-ICPMS dating was done on nearly all samples analyzed by chemical abrasion–thermal ionization mass spectrometry (CA-TIMS) for this study. Approximately 30 LA-ICPMS spots in each sample were analyzed to characterize the zircon population(s) present. Analyses were conducted with a quadrupole ICPMS using a 25 µm spot size and a 30 second ablation time. The primary use of LA-ICPMS data in this Atlas is to broadly characterize the age and trace element composition of zircon before CA-TIMS dating. Zircon grains dated by CA-TIMS were selected from the youngest statistically coherent LA-ICPMS population with similar chemical composition and CL response. For inherited grains, these data aid in characterizing the nature of the crust with which the magma has interacted. For autocrysts, the trace element data reflect magmatic processes such as temperature of crystallization and degree of crustal contamination. The Ti-in-zircon crystallization temperature is calculated from trace element data acquired by LA-ICPMS analysis using the equations of Watson *et al.* (2006).

Appendix 4 includes a summary of the new CA-TIMS dates and data tables for 36 samples analyzed for this study. Most samples (n = 35) were analyzed at the Isotope Geology Laboratory BSU, and methods for these analyses are given. A single sample from the Stikine suite (08MC089-1) was previously analyzed at the Pacific Centre for Isotopic and Geochemical Research

Table 1-5. *Summary of data presented in this Atlas.*

Data type	Data set	Lab	New data	Archival data	Total	Appendix
Geochronology (U-Pb zircon)	CA-TIMS	BSU, UBC	36		36	4
	SIMS	GSC		1	1	12
	ID-TIMS	UBC, GSC		5	5	7
	LA-ICPMS	BSU, UBC	36	5	41	3, 11
Geochronology (Ar)	Ms	GSC	1		1	6
	Hbl		17	4	21	
	Bt		21	1	22	
Lithogeochemistry		various	125	62	187	8
Isotopes	Sr	Carleton U	30		30	9
	Nd		30		30	
	Pb (Kfs)		27		27	
	Hf (Zrn)	MUN	22		22	10
Geobarometry	Al-in-Hbl	UBC	26		26	5

of the University of British Columbia following the methods described in Logan *et al.* (2007). A sample from the Minto pluton (S09-16-01D) with complex zircon was first prepared using a laser-cutting technique to isolate the igneous component from these zircons before CA-TIMS dating. Details of this approach are provided in methods for Appendix 4 and Kovacs *et al.* (2020). In this Atlas, only the internal error based on analytical uncertainties is given at 2σ for weighted mean dates presented in the text and summary tables. In most cases, we use the weighted mean date of CA-TIMS analyses with this internal error as the crystallization age of the sample. Further error propagation for comparison with dates from other geochronological methods using the U-Pb decay scheme (*e.g.*, LA-ICPMS) or other decay schemes (*e.g.*, $^{40}Ar/^{39}Ar$, $^{187}Re/^{187}Os$) are detailed in the methods document and given in the data tables.

Appendix 5 contains electron microprobe analysis (EMPA) data for plagioclase and hornblende used to calculate emplacement pressure using the Al-in-Hbl geobarometer for 26 samples of Late Triassic to Jurassic plutons. A methods document, summary file, and file with the raw EMPA data for each sample are included in Appendix 5. The total error includes the regression error, aluminium and temperature errors, and is between ± 0.8–1.0 kbar for all samples (13–24% error, equivalent to ± 3.0–3.5 km). All errors are at the 1σ level of uncertainty. The Al-in-Hbl geobarometer is used in this Atlas to estimate the emplacement depth of the plutons (*e.g.*, Hammarstrom and Zen, 1986). The solidus curve for hornblende-bearing melts of calc-alkaline composition is relatively insensitive to temperature above ~2 kbar, but is relatively temperature-dependent below ~2 kbar which means the Al-in-Hbl geobarometer shouldn't be used in rocks emplaced at pressures ≤2 kbar (~7 km depth; Hollister *et al.*, 1987). In this study, most samples have calculated emplacement pressures >2 kbar; for the few that do not, we infer a maximum emplacement pressure of ≤2 kbar.

Appendix 6 includes new and previously unpublished $^{40}Ar/^{39}Ar$ data for hornblende, muscovite and biotite separates from 25 samples of Late Triassic to Jurassic plutons. Appendix 6 contains a methods document and data file with a summary of results as well as individual analyses. Errors on weighted mean plateau dates are at 2σ uncertainty and are based on internal error only. These data constrain the cooling and exhumation history for the plutons; for the two-mica phase of the McGregor batholith, a muscovite analysis also provides a minimum constraint for the emplacement age of this phase.

Appendix 7 includes isotopic dilution-thermal ionization mass spectrometry (ID-TIMS) methods and data tables for three previously unpublished U-Pb zircon dates from samples collected during regional mapping programs of the Yukon Geological Survey and analyzed at UBC and GSC Ottawa. Errors on weighted mean dates are given at 2σ uncertainty and based on internal analytical uncertainties only. We use the weighted mean date of ID-TIMS analyses to determine the crystallization ages of these samples.

Appendix 8 contains new and previously unpublished whole-rock lithogeochemical data for 187 samples of Late Triassic and Jurassic plutons in southern Yukon. This appendix includes the lithogeochemical data as well as methods, precision and accuracy for new data collected for this study. Analytical data for 30 samples with the 11RAYJC prefix have data included here but the analytical technique and quality control are unknown; these data are not included in accuracy and precision calculations. YGS samples were analyzed using fusion preparation and ICPMS analysis. Fusion preparation completely dissolves refractory minerals such as zircon, titanite and monazite, and when combined with ICPMS analysis, ensures high-quality data for low-level trace elements such as the REE used in many geochemical plots. Precision for major elements and REE is typically <5% and for trace elements is <10%. Accuracy of major element and REE analyses is <10% and for trace elements is <20%. Detection limits, precision and accuracy for each element are in Table A08-1, a tab in Appendix 8–WRx geochem data.

Appendix 9 contains whole-rock and K-feldspar radiogenic isotope data for 30 samples from Late Triassic to Jurassic plutons in southern Yukon. This appendix includes a methods document and a data table. Strontium, neodymium and lead isotopes were analyzed using TIMS. Whole-rock strontium and neodymium data are from analysis of whole-rock geochemical pulps. Lead isotopes analyses were conducted on powders from K-feldspar separates. Strontium and Nd isotopes are proxies for magma source (juvenile *vs.* evolved) and Pb isotopes indicate crustal contamination. These proxies are useful for determining magma source and contamination which influences the metals available in magmatic-hydrothermal systems (*e.g.*, Thompson *et al.*, 1999).

Appendix 10 contains Hf isotopic data for zircons from 22 of the samples analyzed by LA-ICPMS and CA-TIMS at BSU (data in Appendices 3 and 4). The Hf data were acquired at MUN on the same zircon mounts used at BSU with spot locations from each lab adjacent so the data are as related as possible. Hafnium isotopes in zircon are proxies for magma source (juvenile *vs.* evolved). In inherited grains this helps constrain basement geologic history. In autocrysts, these data contribute to understanding magma source.

Appendix 11 includes a method document and previously unpublished LA-ICPMS U-Pb zircon data collected at UBC.

Appendix 12 includes a method document and previously unpublished SIMS U-Pb zircon data collected at GSC–Ottawa. The instrument used to collect these data was a Sensitive High-Resolution Ion MicroProbe (SHRIMP) and commonly, the dates derived from these data are referred to as SHRIMP dates. We use the generic technique, secondary ion mass spectrometry (SIMS) to refer to the data collected.

Appendix 13 contains photographs of fresh and cobaltinitrite-stained rock slabs used for QAP classification summarized in Appendix 2.

Contributions

This Atlas presents an extensive data set for Late Triassic to Jurassic plutons intruding the Intermontane terranes in Yukon. Compilation of such a large and varied data set is only possible through collaboration between many geologists, whose contributions are outlined below:

Patrick Sack and Maurice Colpron (Yukon Geological Survey)

Patrick and Maurice co-led this study for the Yukon Geological Survey. They jointly designed the scope and objectives of the study, and compiled the data presented in this Atlas. Patrick led the field studies in 2014 and 2015, with contributions from Maurice mostly in 2014. Maurice contributed regional knowledge of the Intermontane terranes and Jurassic plutons in Yukon based on previous regional mapping activities.

Patrick wrote the majority of material presented in this Atlas, with contributions and edits from Maurice. Maurice analyzed and described the geochemical data and wrote the discussions and summary for complex geochronological data. Maurice prepared the maps for this Atlas.

Jim Crowley (Boise State University)

Jim produced all geochronological data generated at the Isotope Geology Laboratory of Boise State University (Appendices 3 and 4). Jim participated in the fieldwork in 2015 and assisted with interpretation of the geochronological data through ongoing discussions throughout the study. Jim contributed to writing and editing parts of this Atlas, and provided guidance in graphical presentation of the LA-ICPMS and CA-TIMS data.

Jim Ryan (Geological Survey of Canada, Vancouver)

Jim contributed to this Atlas by providing access to archival samples and unpublished geochemical and geochronological data collected as part of regional mapping activities by the Geological Survey of Canada between 2001 and 2014. Jim contributed to writing parts of Chapter 2 (Pyroxene Mountain suite) and Chapter 3 (Yukon River and Walhalla plutons), and provided photographs and descriptions for these plutons.

Murray Allan (Mineral Deposit Research Unit, University of British Columbia)

Murray participated in fieldwork in the northern Aishihik batholith and the Tatchun batholith in 2014. Murray analyzed samples with suitable mineralogy for Al-in-Hbl geobarometry at UBC, and did calculations and error propagation for pressure and temperature estimates presented in Appendix 5.

Luke Beranek (Memorial University of Newfoundland)

Luke used LA-ICPMS techniques to determine the Hf isotope compositions of previously dated zircons at Memorial University of Newfoundland.

Nancy Joyce (Geological Survey of Canada, Ottawa)

Nancy produced the new $^{40}Ar/^{39}Ar$ data presented in this Atlas. She also retrieved unpublished U-Pb zircon ID-TIMS and SIMS data from the GSC archives.

Jim Mortensen (University of British Columbia)

Jim provided the unpublished U-Pb data for ID-TIMS analyses of samples collected during regional mapping programs (Tatchun batholith and Headless plug), and unpublished LA-ICPMS analyses from the Big Creek, McGregor and Teslin Crossing plutons.

Steve Israel (Yukon Geological Survey)

Steve contributed geochronological and geochemical data from samples collected during regional mapping of the Aishihik Lake region.

John Chapman (Geological Survey of Canada, Vancouver)

John provided geochemical data for the Aishihik, Big Creek, Granite Mountain, McGregor, Minto and Walhalla plutons. John also provided photos of mineralized core from the Minto deposit.

Acknowledgements

In addition to a thorough review by co-authors, we would like to acknowledge the following people for review and constructive criticism of an earlier draft of this document: Carolyn Relf, Leyla Weston, David Moynihan, Tyler Ambrose and Rosie Cobbett. Don Lougheed and Josh Pillsbury ably assisted Patrick in the field during 2014 and 2015, respectively. Josh completed an honours thesis on the Bennett pluton (Pillsbury, 2016). Prospectors and geologists Jean Pautler, Scott Casselman, Nikolett Kovacs, Bill Harris, Emily and Jesse Halle, Ivan Elash, Doug McIlveen, Roisin Kerr and Heather Burrell welcomed us on their properties, showed us their rocks and engaged in geology discussions which helped us understand the enigmatic mineralized rocks associated with these intrusions. Thank you to Karen MacFarlane for editorial handling and layout.

Abbreviations commonly used in this Atlas

Mineral abbreviations

Mineral abbreviations are from Whitney and Evans (2010) with the following exceptions:

Epidote – identified according to two mechanisms of formation:

- Ep1 = magmatic epidote defined by euhedral grain boundaries in contact with mafic phases, typically biotite and/or hornblende (Zen and Hammarstrom, 1984). Magmatic epidote is interpreted to have formed during magma crystallization;
- Ep2 = secondary epidote is sub to anhedral and typically associated with feldspars or interstitial to mafic phenocrysts. Interpretation of secondary epidote genesis is not made, except to infer it is post-magmatic crystallization.

Dating techniques

CA-TIMS – chemical abrasion–thermal ionization mass spectrometry

ID-TIMS – isotopic dilution–thermal ionization mass spectrometry

LA-ICPMS – laser ablation–inductively coupled mass spectrometry

SIMS – secondary ion mass spectrometry

TIMS – thermal ionization mass spectrometry

Age *vs.* date – we use the age-versus-date distinction noted by Schoene (2014); age is an interpretation whereas date is the analytical result.

Other analytical terms

Al-in-Hbl – aluminum-in-hornblende

ASI – Alumina saturation index

BSE – bulk-silicate Earth

CHUR – chondritic uniform reservoir

CL – cathodoluminescence

EMPA– electron microprobe analysis

LILE – large-ion lithophile elements

MALI – modified alkali-lime index

TAS – total alkali-silica

MSWD – mean squared weighted deviation

PM – primitive mantle

pof – probability of fit

PPL – plane polarized light

QAP – quartz-alkali-feldspar-plagioclase diagram of Le Bas and Streckeisen (1991)

REE – rare-earth elements; with LREE for light REE and HREE for heavy REE

UCC – upper continental crust

VAG – volcanic arc granitoid

XPL – cross-polarized light

Geoscience institutions

BSU – Boise State University

GSC – Geological Survey of Canada

YGS – Yukon Geological Survey

UBC – University of British Columbia

MDRU – Mineral Deposits Research Unit (at UBC)

MUN – Memorial University of Newfoundland

Definitions

Strike and dip measurements are presented using the right-hand-rule with the format strike/dip. Strike measurements are three digits and dip are two, both are in degrees (*e.g.*, N305/48).

Pluton nomenclature

Batholith – intrusive body with >100 km² expression at surface that is discordant with surrounding rocks.

Lopolith – intrusive body that is roughly concordant with a roughly horizontal top and a shallow convex base. It also may have a feeder pipe below.

Pluton – dimensionless term for intrusive body without any implied emplacement geometry.

Plug – intrusive body with <1 km² expression at surface that is discordant with surrounding rocks.

Stock – intrusive body with >1 to <100 km² expression at surface that is discordant with surrounding rocks.

Geochronology terminology

Zircon interpretation (from Miller et al., 2007)

Antecryst: Refers to zircon crystals that crystallized from an earlier pulse of magma and which are incorporated in a later pulse(s). Antecrysts are slightly older than autocrysts (within several m.y. in the present study) and here are within the age range of the suite to which an igneous body belongs. For example, the range of the Minto suite is 205–194 Ma, and for rocks with an autocryst population used to calculate the crystallization age of the rock, slightly older grains up to 205 Ma are termed antecrysts. Crystals grown in the discrete pulses of magma intrusion may well share similar chemical or petrographic characteristics.

Autocryst: A term for zircon crystals or crystal growth that in a spatial and temporal sense is associated exclusively with a distinct pulse or increment of magma. Depending on the age range of a plutonic suite and the age of a sample, it may be difficult to distinguish autocrysts from antecrysts in large and growing magma bodies as growth cannot necessarily be associated spatially to a single pulse of melt. Ideally, crystallization ages are calculated from the autocryst population in a sample.

Inherited grain: Zircon crystals (or parts of crystals) are distinguished by being appreciably older (≥10s of m.y. in the present study) than the majority of zircons in a sample of igneous rock. They may also be characterized by geochemical characteristics that differ from the vast majority of zircons in the rock (*e.g.*, U, Th concentrations, U/Th ratio).

Xenocryst: Zircon crystals incorporated from surrounding host rock during transit and emplacement, which are broadly coeval with crystallization age (≤10 m.y. in the present study). For example, in the Stikine suite, *ca.* 215 to 225 Ma zircon crystals are likely sourced from Late Triassic volcanic rocks and are referred to as xenocrysts. The line between antecryst and xenocryst can be blurry. As with inherited crystals, xenocrysts would also presumably have to be older than the majority of zircon crystals in any igneous rock sample and may also be characterized by geochemical signatures that are distinct from the majority of zircon crystals in the rock.

$^{40}Ar/^{39}Ar$ interpretation (after McDougall and Harrison, 1999)

Integrated age – $^{40}Ar/^{39}Ar$ age calculated by summing results from all steps in a single step-heating experiment. Equivalent to a total fusion age or K/Ar age.

Plateau age – $^{40}Ar/^{39}Ar$ age calculated from at least three contiguous steps with concordant ages (within 1σ) that represent a significant proportion of ^{39}Ar released (>30%).

Pseudo-plateau (or plateau-like) age – $^{40}Ar/^{39}Ar$ age calculated from a series of contiguous steps that define a relatively flat portion of the age spectrum but that are not all concordant with 1σ.

The initial atmospheric $^{40}Ar/^{36}Ar$ value of 298.56 from Lee *et al.* (2006) is used in this Atlas.

Closure temperatures

Table 1-6 summarizes the closure temperatures used to interpret geochronological results presented in this Atlas. Closure temperatures are from Hodges (2014).

Table 1-6. *Closure temperature estimates for minerals analyzed in this study.*

Mineral	Isotopic system	T (Celsius)
Zircon	U-Pb	960
Titanite	U-Pb	670
Hornblende	$^{40}Ar/^{39}Ar$	570
Muscovite	$^{40}Ar/^{39}Ar$	490
Biotite	$^{40}Ar/^{39}Ar$	350

Crustal levels

We use the following definitions for crustal levels; pressures calculated assuming a lithostatic gradient of 3.7 km/kbar. Upper crust from 0 to 7 km depth (0 to 1.9 kbar); middle crust from 7 to 20 km depth (1.9 to 5.4 kbar); and lower crust below 20 km depth (>5.4 kbar). The definition for upper crust used here corresponds broadly with depths of emplacement typically inferred for 'normal' porphyry systems (Seedorff *et al.*, 2005, 2008) and the lower limit (~2 kbar) of resolution for the Al-in-hornblende geobarometer (Hollister *et al.*, 1987).

Migmatites

The nomenclature of Sawyer (2008) is applied to describe partially melted rocks, leucocratic melt (leucosome), melanocratic residuum (melanosome), and unmelted rocks.

Mineral occurrences

Yukon MINFILE occurrence numbers (unique ID for each mineral occurrence) are in square brackets *e.g.*, [105D 100]. Further information on each occurrence can be found at http://data.geology.gov.yk.ca/.

Chapter 2
Late Triassic

Stikine suite (217–214 Ma)
Pyroxene Mountain suite (220–211 Ma)
Headless suite (208–207 Ma)

Summary

Late Triassic plutons intrude Upper Triassic volcanic arc rocks of Stikinia and Quesnellia, and Paleozoic metamorphic rocks of Yukon-Tanana terrane in southern Yukon. The Stikine suite, exposed south and west of Whitehorse, was examined in five areas for this study, from south to north: Tally-Ho Mountain, Red Ridge, Friday Creek, Ibex Mountain and King Lake. Individual plutons are single or multiphase and either intrude Lewes River Group volcanic and volcaniclastic rocks (Upper Triassic, Stikinia), or are unconformably overlain by Jurassic and younger sedimentary rocks. The plutons are mostly medium-grained and equigranular hornblende (augite) granodiorite with subordinate monzonite to monzodiorite. Uranium-lead zircon CA-TIMS dating of four of these plutons indicate a tightly constrained 217–214 Ma range for the Stikine plutonic suite. Aluminum-in-hornblende geobarometry for the Friday Creek pluton suggests emplacement depths ranging from 8.5 to 16.7 km. The Pyroxene Mountain suite comprises small plutons, or rafts in younger plutons, of medium to coarse-grained hornblende gabbro, pyroxenite, hornblendite, monzodiorite and granodiorite that intrude the Yukon-Tanana terrane west and northwest of Carmacks. Previous dating of these bodies suggested a range of 220–211 Ma; new $^{40}Ar/^{39}Ar$ hornblende dates range from 218–214 Ma and support correlation with the more precisely dated Stikine suite (217–214 Ma). Diorite of the Headless suite intrudes Upper Triassic volcanic rocks of Quesnellia east of Carmacks. They are distinctly younger at 208–207 Ma than plutons of the Stikine and Pyroxene Mountain suites to the west. Geochemical and isotopic data (Sr_i of ~0.704, εNd_t = 5.2 to 5.3, and $^{207}Pb/^{204}Pb$ of ~15.58) from Late Triassic plutons in southern Yukon are consistent with emplacement in a juvenile arc setting and show no indication of interaction with evolved crustal material. The tectonic setting and magmatic conditions of Late Triassic plutons are compatible with development of Cu (± Mo, Au) mineralization and emplacement depths suggest they may be more prospective for deeper (≥10 km) mineral deposit models. Two areas of northern Stikinia and Quesnellia that are underlain by Upper Triassic volcanic rocks are characterized by anomalous stream sediment geochemistry that may suggest potential for buried porphyry systems in these areas.

Introduction

Late Triassic plutons are associated with arc volcanic rocks of Stikinia and occur in two clusters in southern Yukon. South and west of Whitehorse, the Stikine suite (217–214 Ma) comprises small plutons that intrude Upper Triassic volcanic and volcaniclastic rocks of the Lewes River Group near the western edge of Stikinia (Fig. 2-1; Hart, 1995). A second cluster of small Late Triassic plutons occurs near the northern apex of Stikinia and Quesnellia, in the Carmacks area (Fig. 2-1). West of Pelly Crossing, small plutons assigned to the Pyroxene Mountain suite (220–211 Ma; Ryan *et al.*, 2013) intrude metamorphic rocks of the Yukon-Tanana terrane. West of Carmacks, a series of small monzodiorite plutons also intrude metamorphic rocks of the Yukon-Tanana terrane near Mount Nansen (Ryan *et al.*, 2016) and are described below with the Pyroxene Mountain suite; one of these plutons is dated at *ca.* 211 Ma (Klöcking *et al.*, 2016). Northeast of the Teslin fault, two small *ca.* 207 Ma felsic plugs (including the Headless plug) intrude Upper Triassic volcanic rocks of Quesnellia (Semenof formation; Tempelman-Kluit, 1984, 2009). Our field study focused on plutons of the Stikine suite exposed between Whitehorse and Carcross (Table 2-1). Plutons of the Pyroxene Mountain and Headless suites were not visited for the present study but are summarized later in the chapter based on previous work.

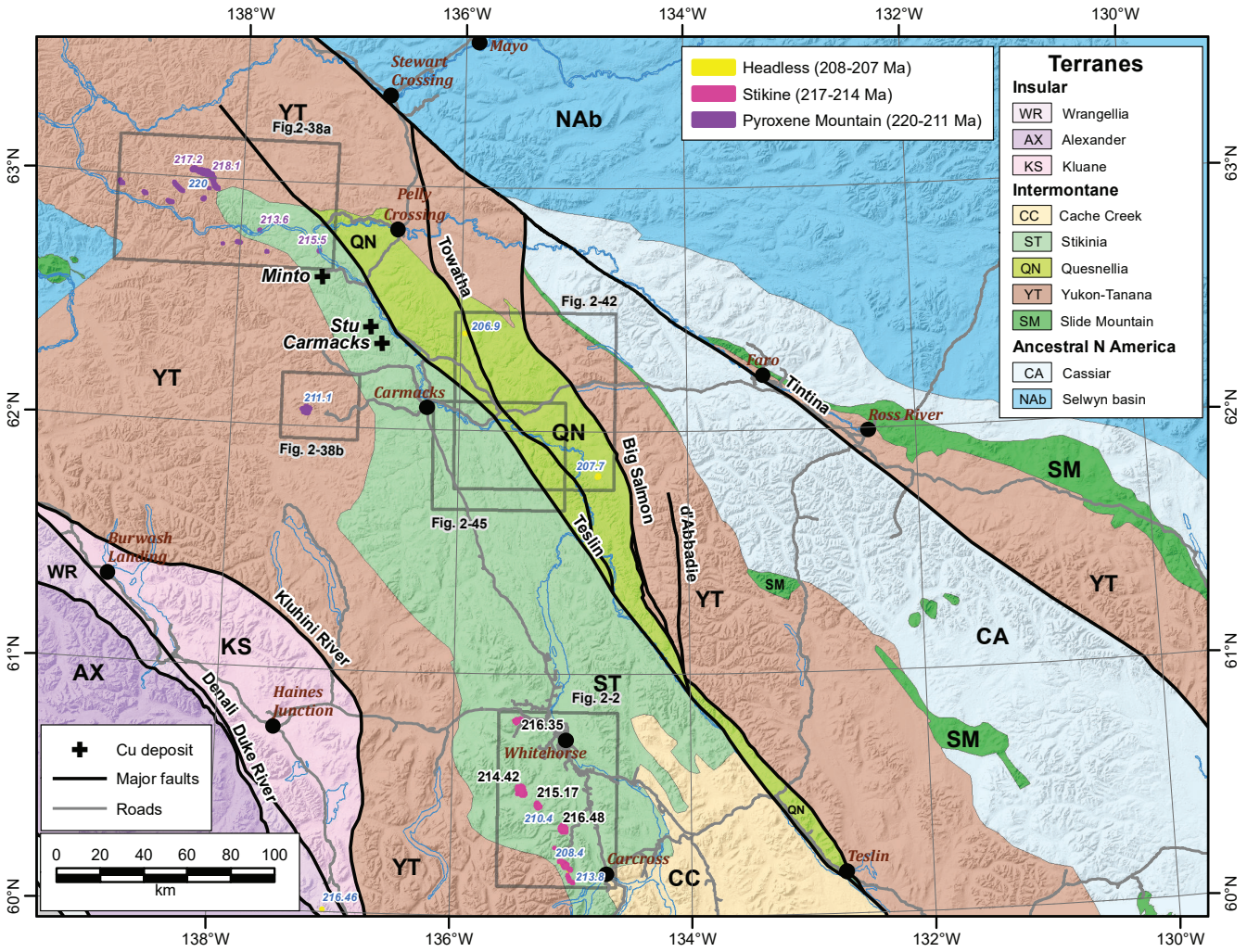


***Figure 2-1**. Distribution of Late Triassic plutons inferred to be related to mafic volcanic rocks of Stikinia and Quesnellia in southern Yukon. U-Pb dates are indicated next to plutons—black numbers are zircon CA-TIMS ages (this study); blue, italicized numbers indicate samples dated by other U-Pb techniques from previous work, and purple numbers are Ar/Ar date for Pyroxene Mountain plutons (see Appendix 1 for geochronology compilation). Terrane map is modified after Colpron and Nelson (2011).*

Table 2-1. *Summary of characteristics for Late Triassic plutons of the Stikine, Pyroxene Mountain and Headless suites in Yukon.*

Pluton	NTS	Area (km^2)	Terrane[1]	Rock[2]	Composition[3]	Oxidation state[4]	Age (Ma)[5]	Al-in-Hbl barometry (kbar)[6]	Ti-in-Zrn temp. (°C)[7]	Isotopes[8]	Inheritance[9]	Comment	Reference
Stikine suite													
Tally-Ho	105D/2-3	<2.2	ST	Aug (Hbl) monzonite to monzodiorite; pyroxenite	alkalic-calcic, to mildly alkalic	strongly oxidized	213.8 ± 0.6	–	–	–	–	UBC, TIMS, single concordant multi-grains fraction	Hart (1995); this study
Red Ridge	105D/6	6.5	ST	Hbl granodiorite	alkalic-calcic, to mildly alkalic	weakly to moderately oxidized	216.48 ± 0.06	–	633–724	–	–	BSU, CA-TIMS (n = 6)	this study
Friday Creek	105D/6	2.7	ST	Hbl-Bt granodiorite	calc-alkalic	weakly oxidized	215.17 ± 0.06	3–3.5	714–780	εNd: 5.3 Sr_i: 0.70407 $^{207/204}$Pb: 15.58 εHf_{zm}: 9.7-11	–	BSU, CA-TIMS (n = 6)	this study
Ibex	105D/11	12.3	ST	Hbl (Bt) granodiorite-tonalite	calc-alkalic to alkalic-calcic	oxidized	214.42 ± 0.07	–	652–788	εNd: 5.2 Sr_i: 0.70402 $^{207/204}$Pb: 15.58 εHf_{zm}: 9.9-11.6	–	BSU, CA-TIMS (n=5)	this study
King Lake	105D/14	3.5	ST	Hbl (Aug) monzonite, monzodiorite, granodiorite	alkalic-calcic	moderately oxidized	216.35 ± 0.23	–	–	–	–	UBC, CA-TIMS (n = 4)	this study
Pyroxene Mountain suite													
Pyroxene	115J14-15; 115O/1	<30	YT	Hbl gabbro, diorite, granodiorite; pyroxenite	cumulate	–	218.1 ± 1.6	–	–	–	–	GSC, Ar/Ar Hbl 99.2% ^{39}Ar	Joyce *et al.* (2015)
Mt. Nansen	115I/3	<6	YT	Hbl-Bt monzodiorite, Qz monzonite	calc-alkalic	–	211.1 ± 0.9	–	–	–	–	UBC, LA-ICPMS Zrn (n = 20)	Klöcking *et al.* (2016)
Headless suite													
Headless	105E/15	1	QN	Hbl Qz diorite	calc-alkalic	–	207.7 ± 0.4	–	–	–	–	UBC, TIMS, single concordant multi-grain fraction	Mortensen (unpub., 2002)
Tadru	105L/5	0.1	QN	felsite	alkalic-calcic?	–	206.9 ± 0.7	–	–	–	–	UBC, TIMS, single concordant multi-grain fraction	this study

Notes:

[1] host terrane to intrusion. QN – Quesnellia; ST – Stikinia; YT – Yukon-Tanana
[2] lithology from Figs. 2-3 and 2-46. Aug – augite; Bt – biotite; Hbl – hornblende; Qz – quartz
[3] composition from Fig. 2-48b
[4] oxidation state from Fig. 2-4
[5] best age from pluton, as discussed in text
[6] crystallization pressure estimates from Al-in-hornblende barometry, Appendix 5
[7] crystallization temperature from Ti-in-zircon thermometry, Appendix 3
[8] whole rock Nd and Sr data; K-feldspar Pb data (Appendix 9); Hf in zircon data (Appendix 10)
[9] inheritance determined from U-Pb LA-ICPMS analyses of zircon (Appendix 3)

Upper Triassic (Norian) rocks of Stikinia and Quesnellia in Yukon are coeval with significant porphyry mineralization in British Columbia (*e.g.*, the 222 Ma Schaft Creek deposit, the 210–205 Ma Galore Creek deposit, and the 210–206 Ma Highland Valley deposit; Logan and Mihalynuk, 2014). The continuity and similarity of Stikinia and Quesnellia throughout the Canadian Cordillera and the temporal overlap between Upper Triassic rocks of Yukon and British Columbia, suggest a similar metallogeny between the two regions. Below, we consider porphyry systems (*i.e.*, porphyry Cu ± Mo-Au, epithermal Au and Cu-Au skarn deposits) as the most likely Late Triassic mineralization styles.

Stikine suite

The Stikine suite comprises a number of small (<12.5 km²), subcircular to locally northwest-elongate plutons that intrude Stikinia near its western margin with the Yukon-Tanana terrane (Hart, 1995). Plutons of the Stikine suite are exposed in five main areas between Carcross and Whitehorse, from south to north: Tally-Ho, Red Ridge, Friday Creek, Ibex Mountain and King Lake (Fig. 2-2; Table 2-1). At a number of localities, contact relationships clearly show that these plutons were intruded into mafic volcanic and volcaniclastic rocks of the Upper Triassic Povoas formation (Carnian–Norian?). Elsewhere, these plutons are unconformably overlain by Lower Jurassic sedimentary rocks of the Laberge Group or intruded by Cretaceous or Paleogene plutons (Fig. 2-2; Hart, 1997b; Hart and Radloff, 1990).

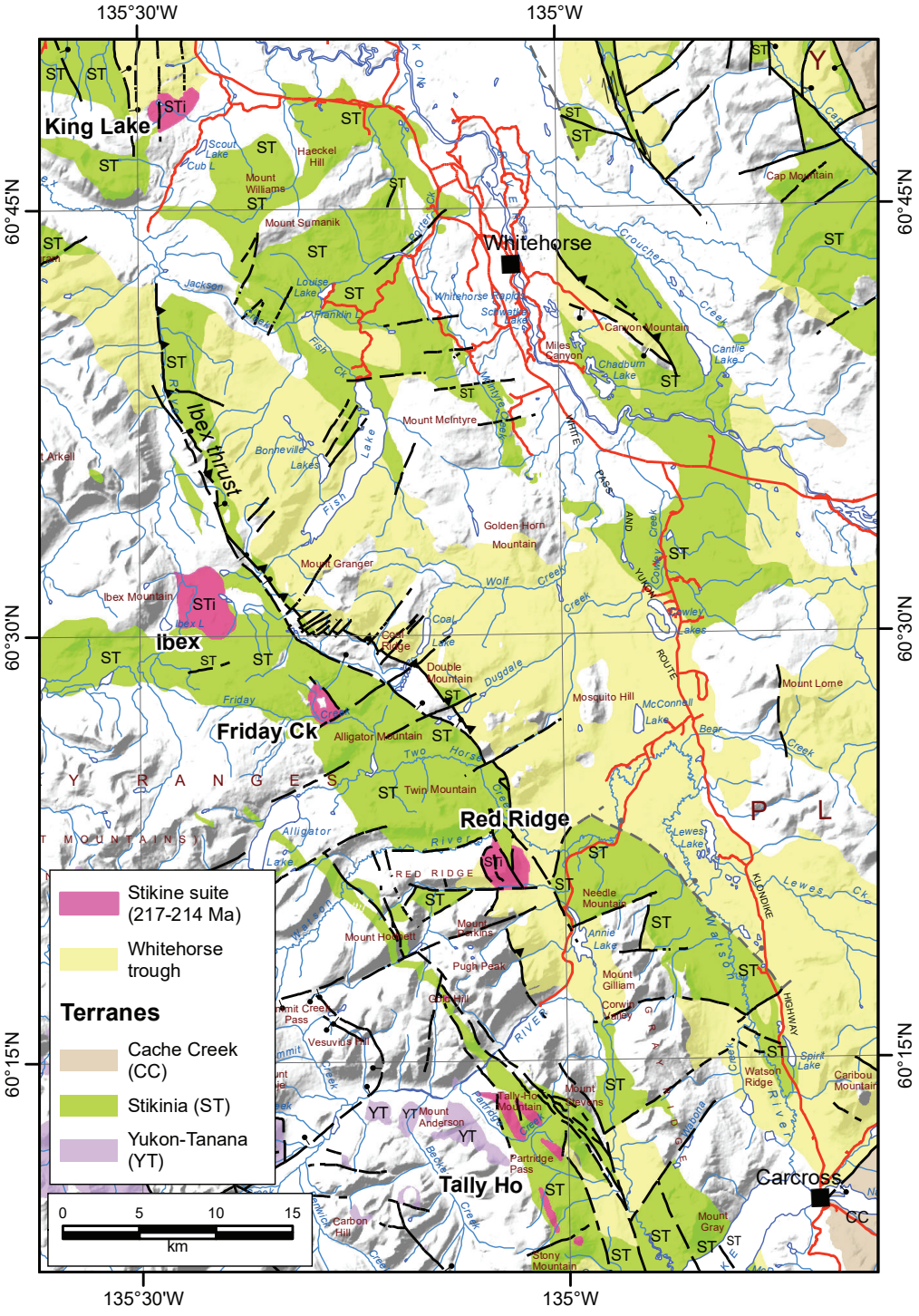


Figure 2-2. *Distribution of Stikine suite plutons in southern Yukon. These plutons intrude the western edge of Stikinia and are locally unconformably overlain by clastic rocks of the Whitehorse trough. The five main areas of exposures described in the text are indicated. Note that plutons of the Stikine suite occur mainly in the footwall of the southwest-verging Ibex thrust. Fault symbology as in Figure 1-4.*

Uranium-lead zircon geochronology from Stikine suite plutons yield a tight cluster of dates in the 217–214 Ma range (*see* below; Appendix 1). These plutons are mostly equigranular and medium-grained granodiorite with local monzodiorite and monzonite phases (Fig. 2-3; Appendix 2). Hornblende is the dominant mafic mineral in these plutons, with biotite usually present in subordinate amounts; Tally-Ho and King Lake plutons have varying amounts of altered pyroxene cores with hornblende rims. Alteration of these plutons varies from weak (*e.g.*, Friday Creek pluton) to intense (*e.g.*, Red Ridge pluton) and secondary epidote is common. The Stikine suite plutons are magnetic and weakly oxidized to oxidized (Fig. 2-4; Appendix 2), and susceptibilities range from 0.12 to 23.8 × 10^{-3} SI units (mean 7.2 × 10^{-3} SI units; n = 18). Copper-molybdenum prospects are locally associated with the Red Ridge and King Lake plutons (Fig. 2-2).

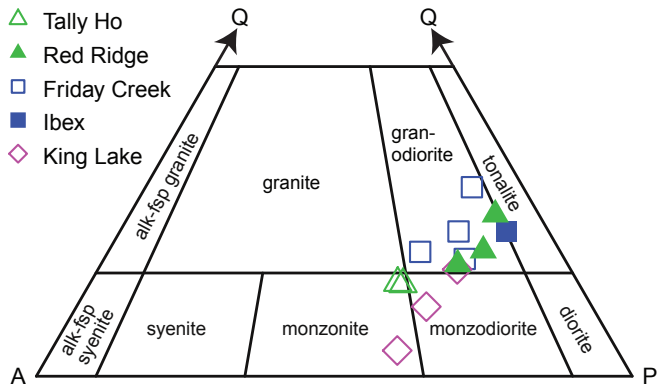


Figure 2-3. *Simplified quartz-alkali-feldspar-plagioclase (QAP) plot (Le Bas and Streckeisen, 1991) with Stikine suite pluton data (Appendix 2).*

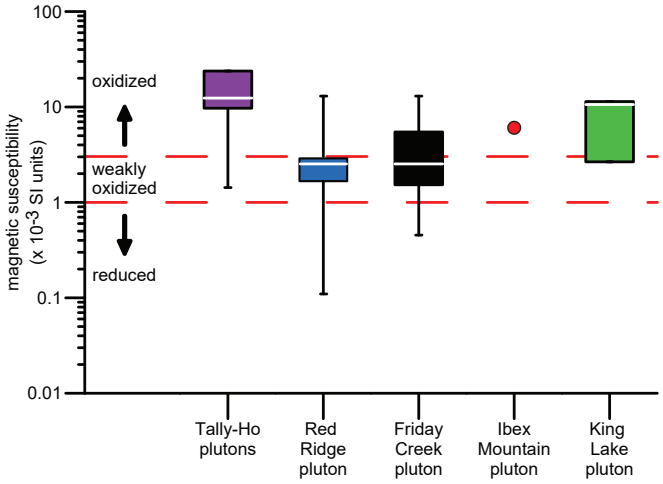
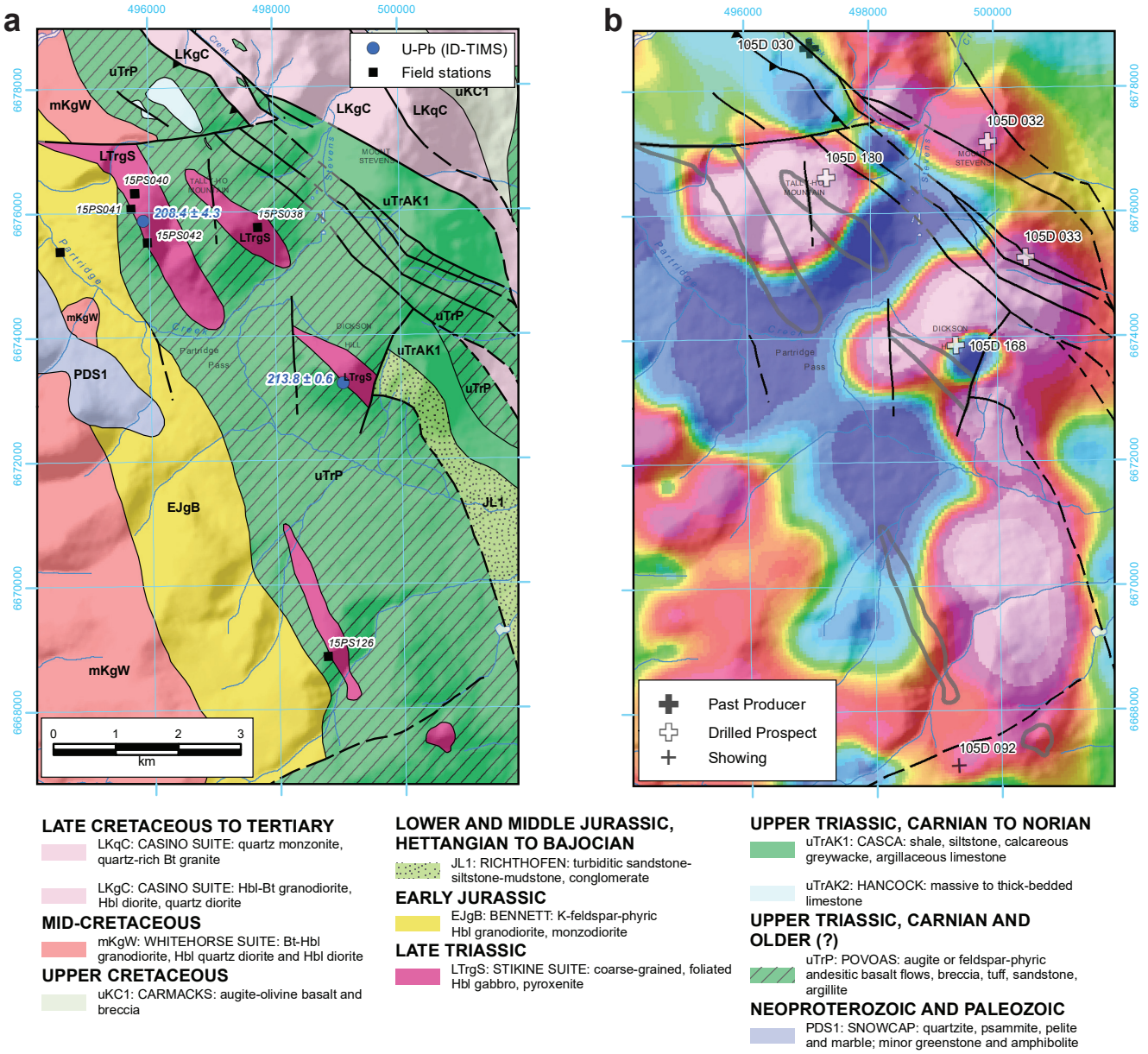


Figure 2-4. *Box and whisker plot of magnetic susceptibility measurements for each Stikine suite pluton (Appendix 2). Divisions between reduced to weakly oxidized (1 × 10^{-3} SI units), and weakly oxidized to oxidized (3 × 10^{-3} SI units) are from Hart et al. (2004a,b). Ends of boxes are 75th and 25th percentile of data, white line within boxes indicate median (50th percentile) of data, whiskers 95th and 5th percentile.*

Tally-Ho plutons

The Tally-Ho plutons are located on Tally-Ho Mountain and Dickson Hill in the Partridge Pass area, approximately 20 km west of Carcross (Figs. 2-2 and 2-5a). The Tally-Ho plutons are small (0.2 to 2.1 km²), elongate northwest and concordant with the regional structures in the area (Fig. 2-6; Hart, 1995). A small body of serpentinized pyroxenite on Tally-Ho Mountain is likely associated with these plutons (Hart and Radloff, 1990; Tizzard *et al.*, 2009).

The plutons are foliated (Fig. 2-7) and experienced the same deformation history as greenstone of the Povoas formation (Hart and Radloff, 1990). Hart (1995) suggested that the Tally-Ho plutons are comagmatic with mafic volcanic rocks of the Povoas formation based on their similar mineralogy, spatial relationship and Late Triassic ages. The following descriptions are based on field observations from two Tally-Ho plutons exposed on Tally-Ho Mountain (Figs. 2-2 and 2-5a).



LATE CRETACEOUS TO TERTIARY

LKqC: CASINO SUITE: quartz monzonite, quartz-rich Bt granite

LKgC: CASINO SUITE: Hbl-Bt granodiorite, Hbl diorite, quartz diorite

MID-CRETACEOUS

mKgW: WHITEHORSE SUITE: Bt-Hbl granodiorite, Hbl quartz diorite and Hbl diorite

UPPER CRETACEOUS

uKC1: CARMACKS: augite-olivine basalt and breccia

LOWER AND MIDDLE JURASSIC, HETTANGIAN TO BAJOCIAN

JL1: RICHTHOFEN: turbiditic sandstone-siltstone-mudstone, conglomerate

EARLY JURASSIC

EJgB: BENNETT: K-feldspar-phyric Hbl granodiorite, monzodiorite

LATE TRIASSIC

LTrgS: STIKINE SUITE: coarse-grained, foliated Hbl gabbro, pyroxenite

UPPER TRIASSIC, CARNIAN TO NORIAN

uTrAK1: CASCA: shale, siltstone, calcareous greywacke, argillaceous limestone

uTrAK2: HANCOCK: massive to thick-bedded limestone

UPPER TRIASSIC, CARNIAN AND OLDER (?)

uTrP: POVOAS: augite or feldspar-phyric andesitic basalt flows, breccia, tuff, sandstone, argillite

NEOPROTEROZOIC AND PALEOZOIC

PDS1: SNOWCAP: quartzite, psammite, pelite and marble; minor greenstone and amphibolite

Figure 2-5. (a) *Geological map of the Tally-Ho area. Geology from YGS (2020a); fault symbology as in Figure 1-4.* ***(b)*** *Reduced to pole, first vertical derivative aeromagnetic map of the Tally-Ho plutons (Aurora Geosciences Ltd. and Bruce, 2017a) showing distribution of Cu-Ag-Au MINFILE occurrences. Grid is UTM NAD83, zone 8.*

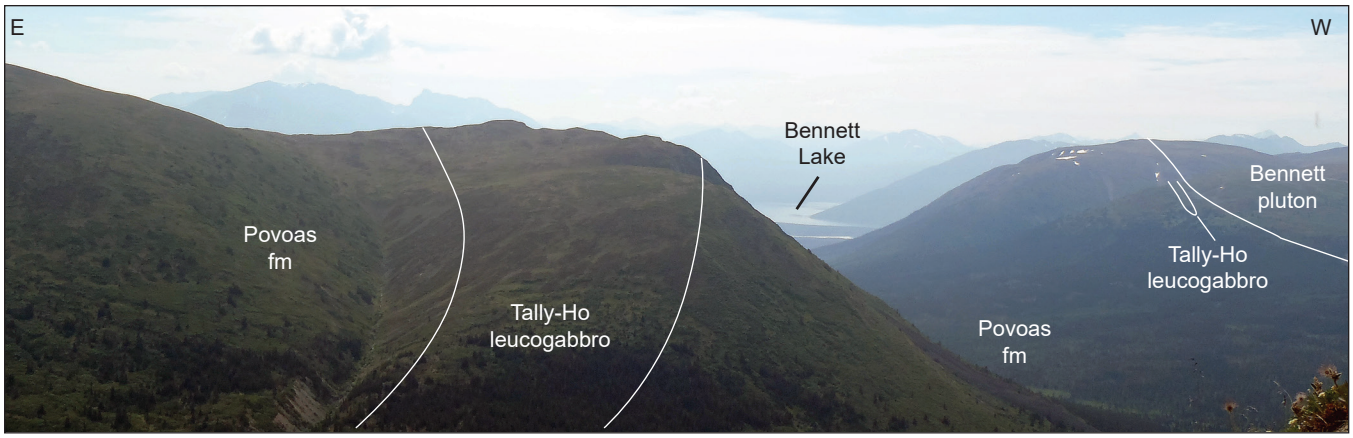


Figure 2-6. *Looking south along-strike from station 15PS038 on Tally-Ho Mountain towards Bennett Lake. Deformed rocks of the Povoas formation and Tally-Ho leucogabbro comprise the Tally-Ho 'shear zone', the western edge of which is marked by undeformed Bennett pluton rocks. fm = formation.*

Petrography

The Tally-Ho plutons are coarse-grained, porphyritic and foliated 'leucogabbro' that contain equal proportions of felsic and mafic minerals. In outcrop and hand sample, these rocks have a distinct spotted and leucocratic appearance due to the large (0.5 to 2 cm) plagioclase phenocrysts in a groundmass of coarse-grained mafic minerals and fine-grained white K-feldspar (Figs. 2-7 and 2-8). Two representative samples plot in the monzonite field of the simplified QAP diagram (Fig. 2-3). Mafic minerals are typically augite with hornblende rims (Fig. 2-9). Plagioclase and K-feldspar are intensely saussuritized and sericitized, respectively; hornblende and biotite are moderately chloritized and commonly exhibit an anastomosing alignment outlining the foliation in the rock. These rocks are typically described as 'leucogabbro' in the field (*e.g.*, Hart and Radloff, 1990; Hart, 1995; Tizzard *et al.*, 2009), although the presence of fine-grained white K-feldspar in the groundmass indicate a more alkalic monzonite composition (Figs. 2-3 and 2-8).



Figure 2-7. *Foliated leucogabbro from Tally-Ho Mountain 500 m south of station 15PS042.* ***(a)*** *Outcrop of foliated leucogabbro with a pervasive anastomosing foliation at N305/48 (solid line) superposed by broadly spaced kink bands at N195/90 (dashed line). Hammer is 45 cm long.* ***(b)*** *Fresh surface of outcrop in (a), only the pervasive anastomosing foliation is seen at this scale.*

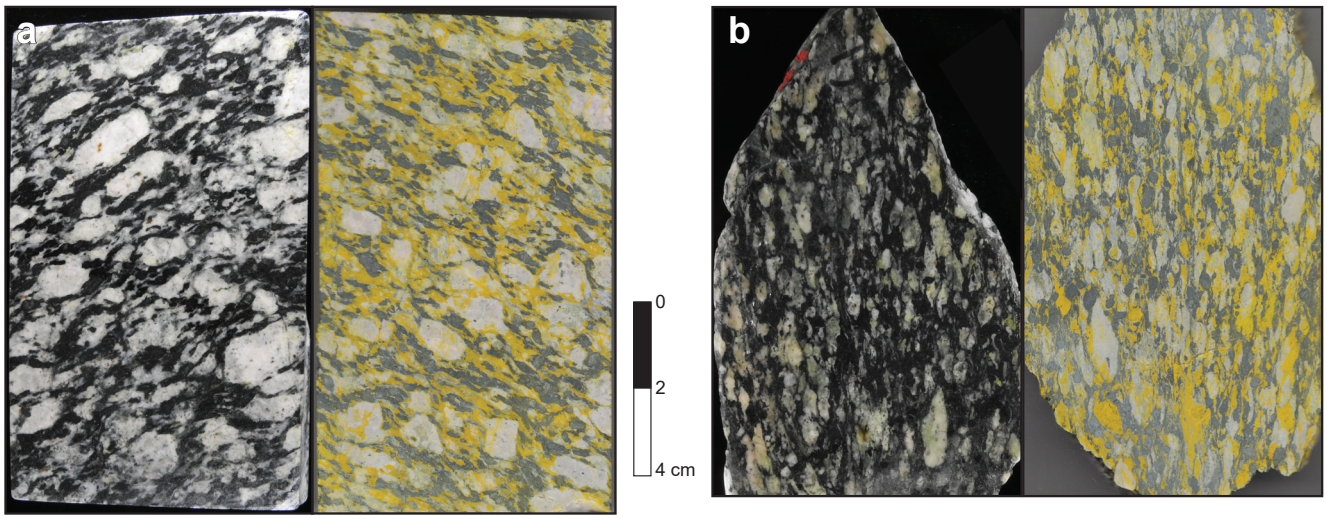


Figure 2-8. *Representative samples of Tally-Ho leucogabbro. Fresh polished surface (left) and a cobaltinitrite-stained cut surface (right).* ***(a)*** *15PS040-2,* ***(b)*** *15PS042-1. Scale is the same for both samples, yellow-stained mineral is K-feldspar.*

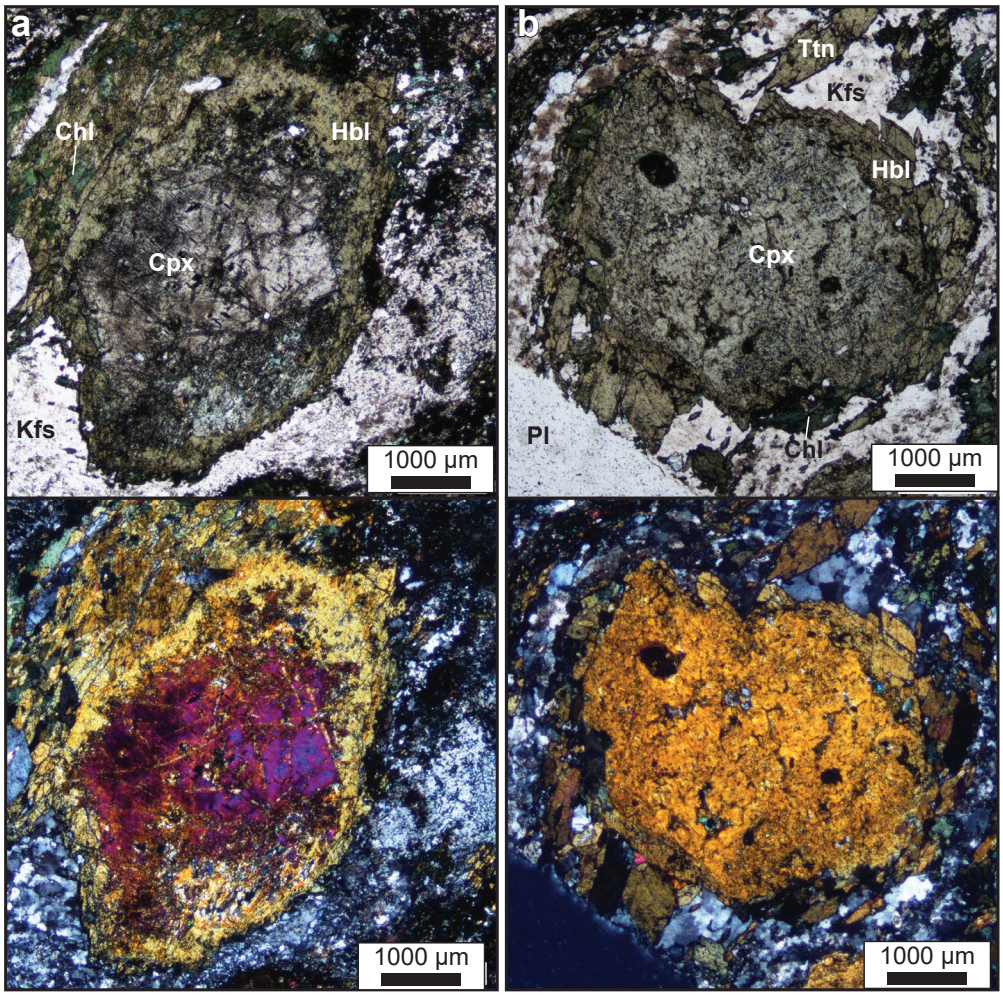


Figure 2-9. *Transmitted light photomicrograph pairs for samples of the Tally-Ho plutons; plane polarized light (upper) and cross-polarized light (lower). Coarse-grained augite phenocrysts with hornblende rims locally altered to chlorite within a groundmass of mostly fine-grained K-feldspar.* ***(a)*** *15PS040-2,* ***(b)*** *15PS042-1.*

Oxidation state and mineral occurrences

The Tally-Ho plutons are magnetic with susceptibilities ranging from 1.43 to 23.80 × 10^{-3} SI units (mean 13.86 × 10^{-3} SI units; n = 4), indicating that they are strongly oxidized (Fig. 2-4). The Silver Queen [105D 180] and Dickson Hill [105D 168] occurrences are located on Tally-Ho Mountain and Dickson Hill, respectively (Fig. 2-5b). The Silver Queen occurrence is a set of discordant epithermal quartz veins interpreted to relate to Eocene magmatism (Hart and Radloff, 1990). The Dickson Hill occurrence includes the Odd vein which is up to 2 m wide, concordant with the regional foliation, and shows little to no wallrock alteration (Hart and Radloff, 1990). Limited primary fluid inclusion evidence suggests that the veins were formed at temperatures above 500°C. These characteristics are interpreted as indicating a metamorphic origin for these veins, possibly related to the regional deformation (Hart and Radloff, 1990). There are no known mineral occurrences directly associated with the Late Triassic plutons in this area (YGS, 2020b).

Geochronology

Two Tally-Ho plutons (Tally-Ho Mountain and Dickson Hill) were previously dated (Fig. 2-5a). Both samples were analyzed by U-Pb ID-TIMS technique, using multi-grain, air-abraded zircon fractions. Hart (1995) reports a single concordant date of 213.8 ± 0.6 Ma from a fraction of strongly abraded coarse zircons recovered from leucogabbro on Dickson Hill (Fig. 2-10a; analyzed at UBC). A second fraction of finer grained zircons is strongly discordant. To the west, on Tally-Ho Mountain, Tizzard *et al.* (2009) dated another leucogabbro sample (Fig. 2-5). They analyzed three fractions of unabraded zircons which yielded slightly discordant (5–8%) results with $^{206}Pb/^{238}U$ dates ranging from 214.9 ± 0.3 Ma to 219.2 ± 0.3 Ma. A linear regression through the three discordant fractions yield a lower intercept on concordia at 208.4 ± 4.3 Ma which Tizzard *et al.* (2009) interpreted as the age of the rock (Fig. 2-10b; analyzed at University of Alberta). Our attempt at improving the geochronology of the Tally-Ho plutons was unsuccessful, as our sample 15PS040-1 did not yield zircon. Although we have not been able to date the Tally-Ho plutons more precisely, we consider Hart's (1995) *ca.* 214 Ma date more reliable than the discordant analyses of Tizzard *et al.* (2009) because it is more consistent with our dating of other plutons in this suite (*see* below).

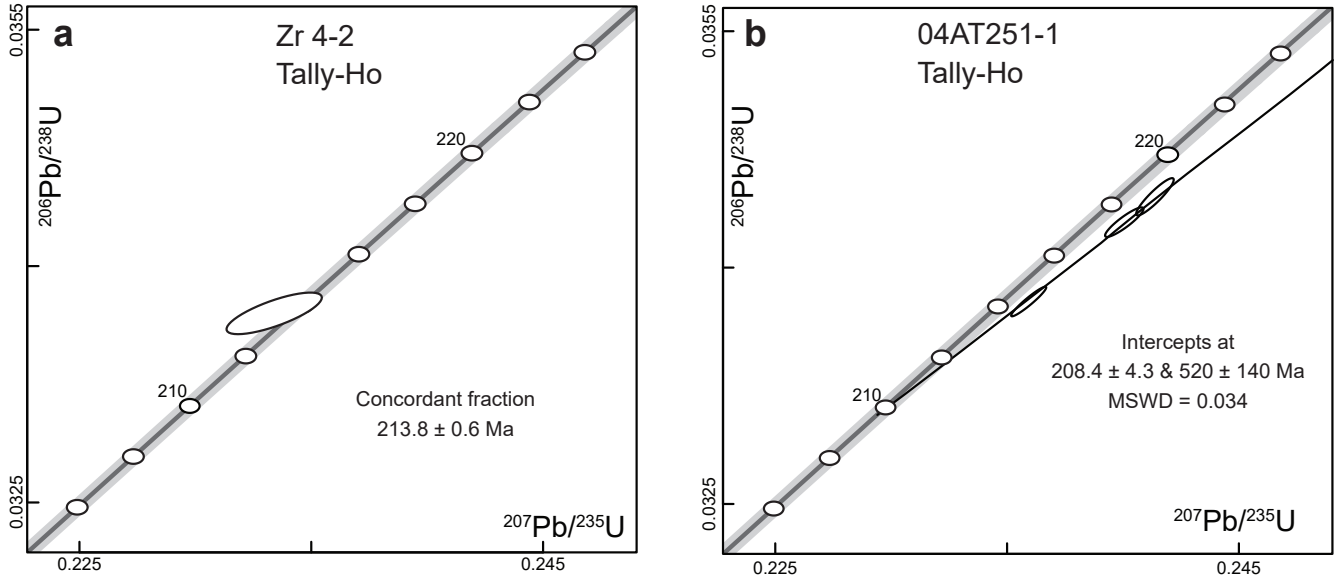
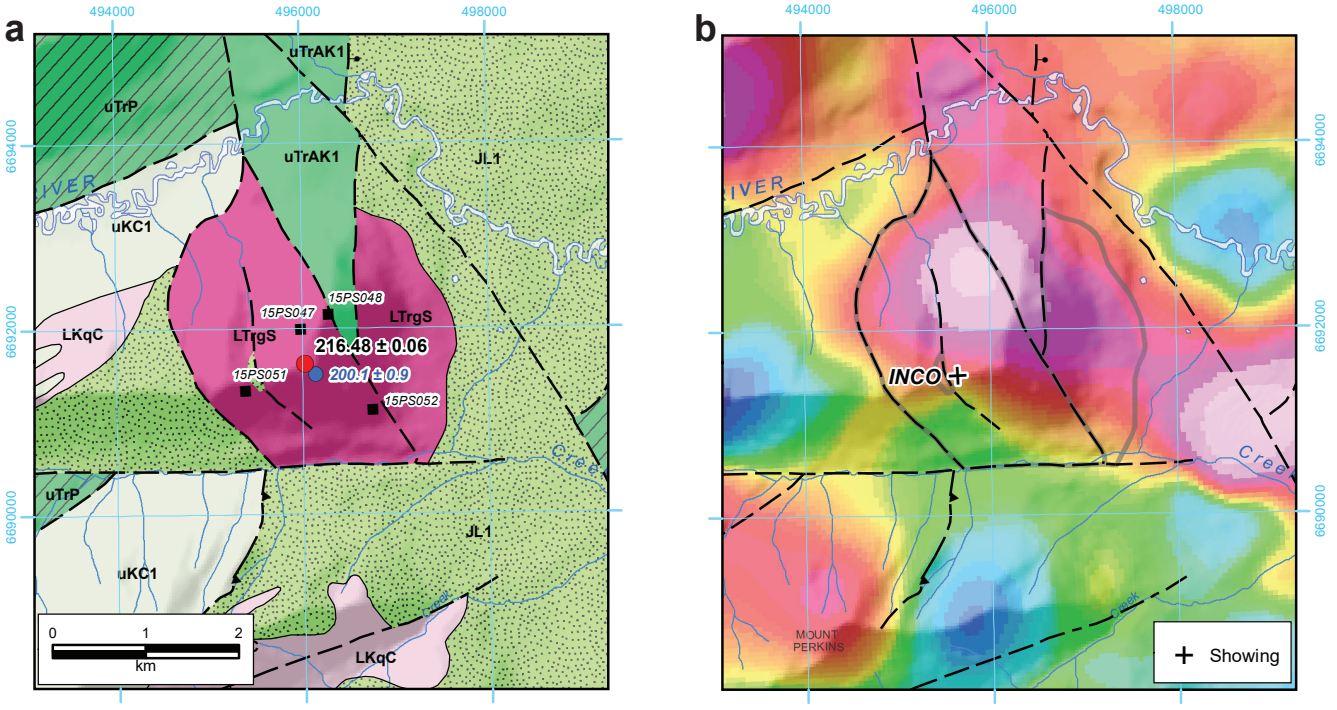


Figure 2-10. *Concordia diagrams showing previous results of U-Pb zircon geochronology for Tally-Ho leucogabbro.* ***(a)*** *sample from Dickson Hill dated by Hart (1995);* ***(b)*** *sample from Tally-Ho Mountain dated by Tizzard et al. (2009). Both samples were dated using multi-grain zircon fractions with the ID-TIMS technique. Sample from Hart (1995) was air-abraded, whereas the Tizzard et al. (2009) sample was unabraded.*

Red Ridge pluton

The Red Ridge pluton is a 6.5 km² body located on the eastern end of Red Ridge between Thompson Creek and the Watson River, approximately 30 km northwest of Carcross (Fig. 2-2). It is exposed in a circular erosional window through clastic sedimentary rocks of the Laberge Group, the defining unit of the Whitehorse trough (Fig. 2-11a; Hart and Radloff, 1990). Two phases of medium-grained, hornblende-rich granodiorite, a mesocratic and a leucocratic phase, make up the composite Red Ridge pluton. The irregular, fluidal contact between the two phases suggests they are comagmatic, although the leucocratic phase locally has a very thin chilled margin (Fig. 2-12). The northern part of the Red Ridge pluton is cut by north and west-northwest striking faults which juxtapose rocks of the Upper Triassic Casca member (Aksala formation) of the Lewes River Group, with the middle part of the pluton (Fig. 2-11; Hart and Radloff, 1990). Near the western contact (15PS048), locally abundant intrusive breccia with subround mafic volcanic fragments in a granodiorite matrix (Fig. 2-13) suggests the fault reactivated a primary intrusive contact.



LATE CRETACEOUS TO TERTIARY
LKqC: CASINO SUITE: quartz monzonite, quartz-rich Bt granite

UPPER CRETACEOUS
uKC1: CARMACKS: augite-olivine basalt and breccia

LOWER AND MIDDLE JURASSIC, HETTANGIAN TO BAJOCIAN
JL1: RICHTHOFEN: turbiditic sandstone-siltstone-mudstone, conglomerate

LATE TRIASSIC
LTrgS: STIKINE SUITE: coarse-grained, foliated, gabbroic Hbl orthogneiss

UPPER TRIASSIC, CARNIAN TO NORIAN
uTrAK1: CASCA: shale, siltstone, calcareous greywacke, argillaceous limestone

UPPER TRIASSIC, CARNIAN AND OLDER (?)
uTrP: POVOAS: augite or feldspar-phyric andesitic basalt flows, breccia, tuff, sandstone argillite

U-Pb (CA-TIMS)
U-Pb (ID-TIMS)
Field stations

***Figure 2-11**. **(a)** Geology of the Red Ridge area. Geology from YGS (2020a); fault symbology as in Figure 1-4. **(b)** Reduced to pole, first vertical derivative aeromagnetic map of the Red Ridge pluton (Aurora Geosciences Ltd. and Bruce, 2017a) showing location of the INCO MINFILE occurrence. Grid is UTM NAD83, zone 8.*



Figure 2-12. *Road-cut through the central part of the Red Ridge pluton, station 15PS047, showing the composite nature of the pluton with textures indicative of coeval emplacement.* ***(a)*** *Outcrop scale, hammer is 45 cm long.* ***(b)*** *Irregular fluidal contact between coarser grained mesocratic and finer grained leucocratic granodiorite, hammer head 13 cm.* ***(c)*** *Irregular contact and a 2 mm chilled margin in the leucocratic phase, pencil lead 2 mm.*

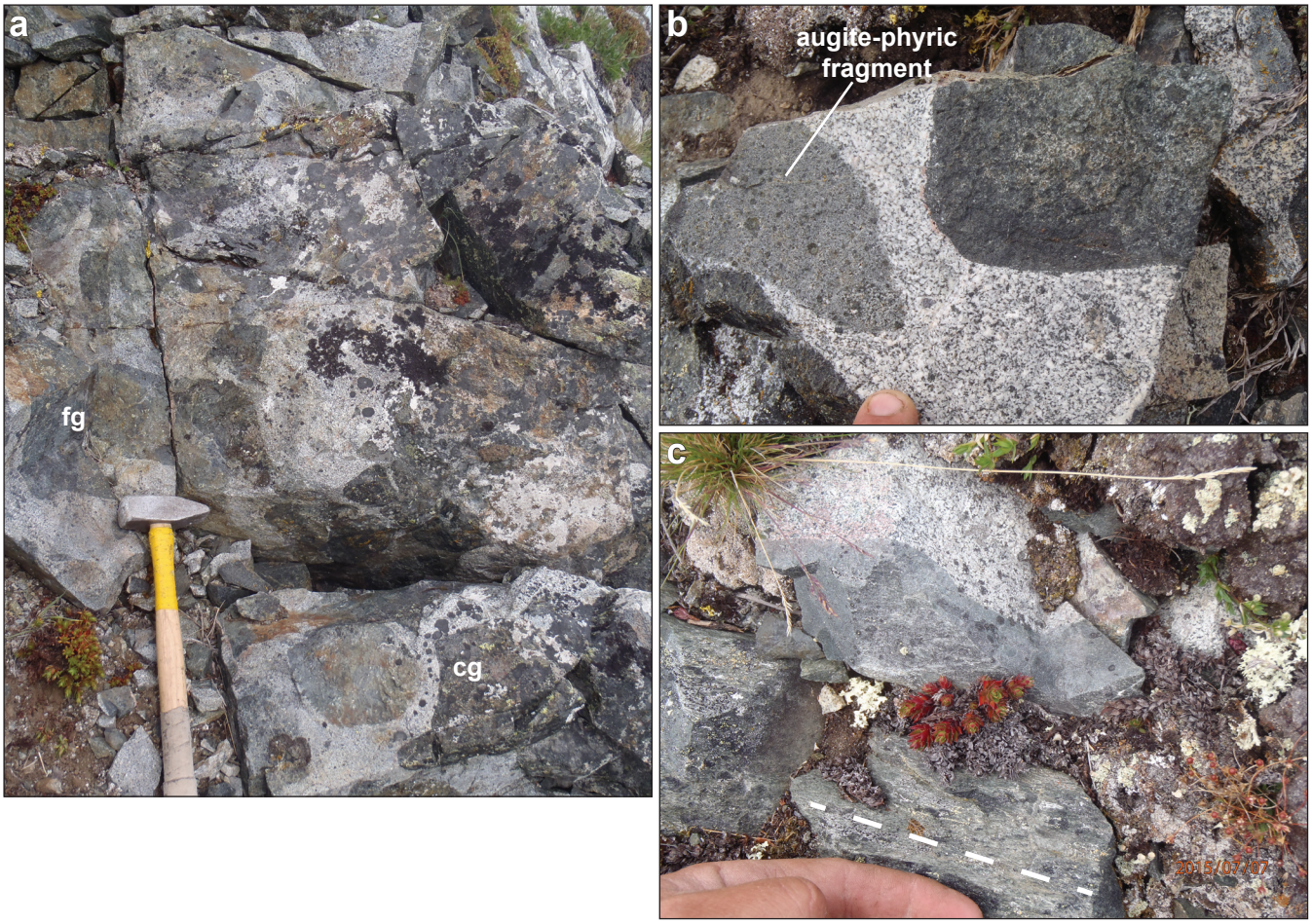


Figure 2-13. *Intrusive breccia at station 15PS048, near the centre of the Red Ridge pluton, suggests a primary intrusive relationship with country rocks.* ***(a)*** *Angular to round fragments of fine-grained (fg) and coarse-grained (cg) mafic volcanic rocks within granodiorite, hammer 45 cm long.* ***(b)*** *Augite-phyric basalt fragment within granodiorite.* ***(c)*** *Foliated mafic volcanic rock fragment within granodiorite, dashed line parallel with foliation.*

Petrography

Both phases of the Red Ridge pluton are equigranular, medium-grained hornblende granodiorite (Fig. 2-14). The mesocratic phase is slightly more mafic with less K-feldspar and more plagioclase than the leucocratic phase. Both phases plot in the granodiorite field of the simplified QAP diagram (Fig. 2-3). Most grains are euhedral and equigranular; mafic minerals compose between 10% (leucocratic phase) and 50% (mesocractic phase) of the rock. Hornblende is the main mafic mineral but minor biotite is also present (Fig. 2-15), as are trace amounts of magnetite and titanite. Plagioclase and K-feldspar are moderately to intensely saussuritized and sericitized, respectively; hornblende and biotite are moderately altered to chlorite. Epidote occurs as an alteration mineral, commonly with propylitic alteration of mafic minerals to chlorite + carbonate + epidote and feldspar phenocrysts to albite (Fig. 2-15).

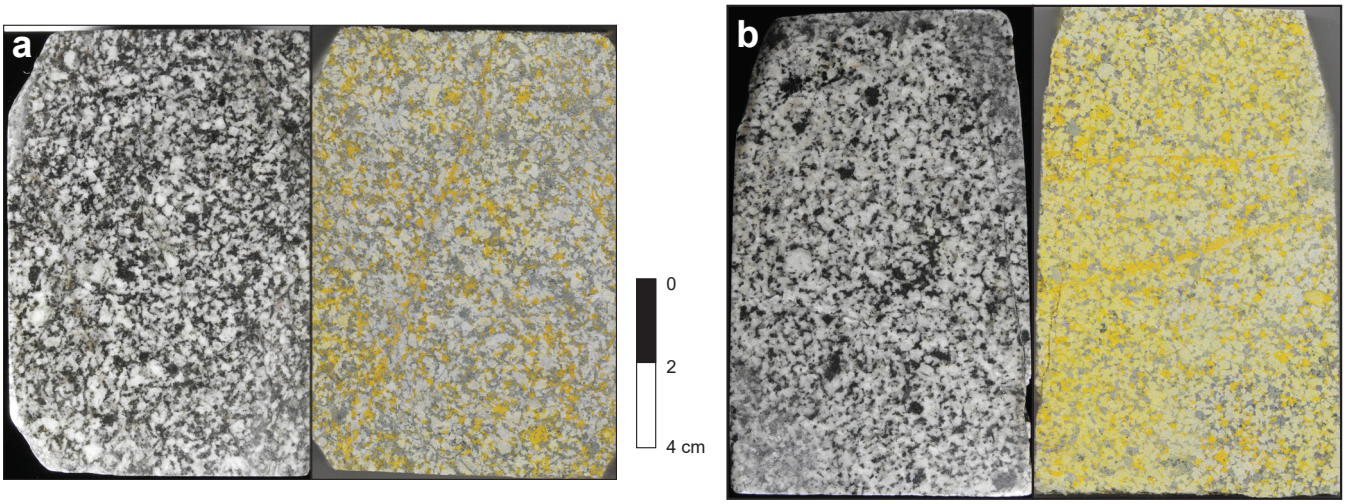


Figure 2-14. *Representative samples of the Red Ridge pluton. Each sample shown with a fresh polished surface (left) and a cobaltinitrite-stained cut surface (right).* ***(a)*** *Mesocratic phase, 15PS052-1;* ***(b)*** *leucocratic phase, 15PS050-1. Note K-feldspar is stained yellow.*

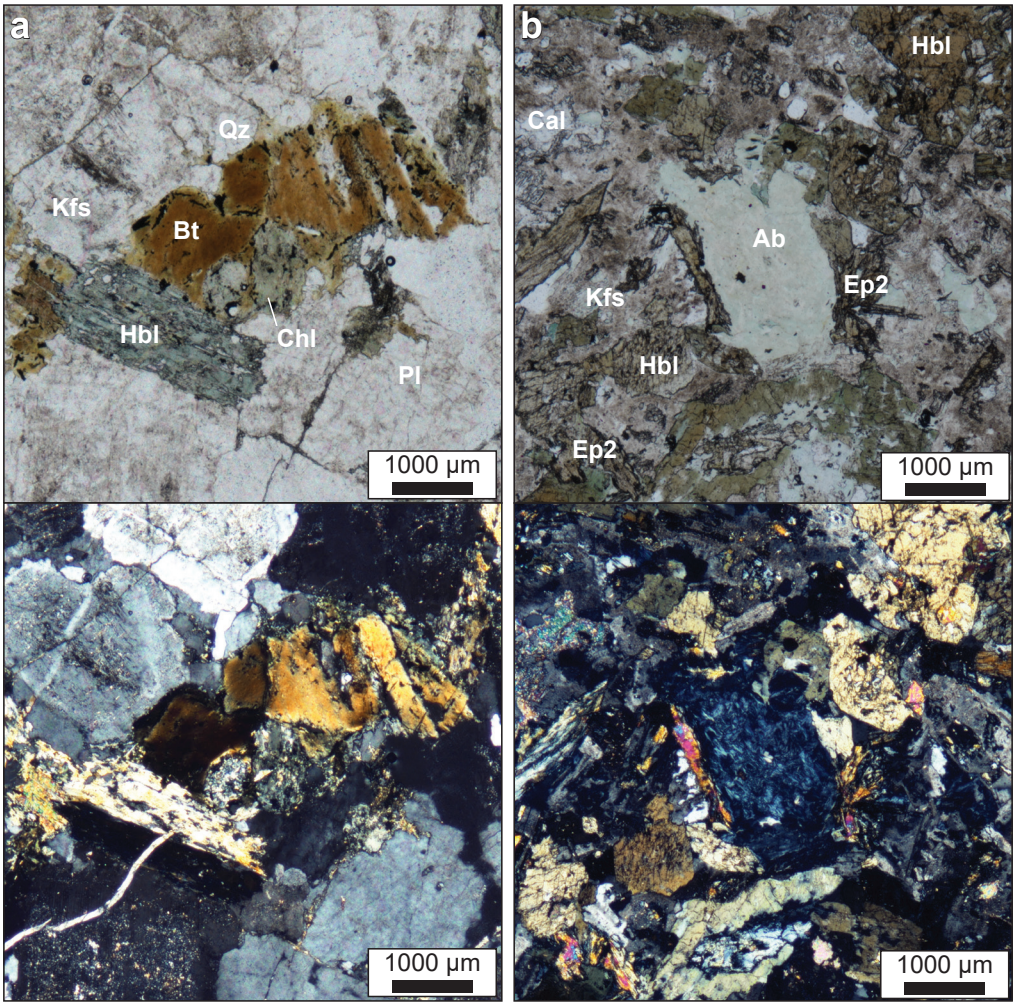


Figure 2-15. *Transmitted light photomicrograph pairs for samples of the Red Ridge pluton; plane polarized light (upper) and cross-polarized light (lower).* ***(a)*** *Typical poikilitic hornblende phenocryst with biotite weakly altered to chlorite, 15PS050-1.* ***(b)*** *Propylitic alteration assemblage of albite, calcite and secondary epidote, 15PS047-1.*

Oxidation state and mineral occurrences

The Red Ridge pluton is magnetic and weakly to moderately oxidized with susceptibilities ranging from 0.12 to 12.50 × 10^{-3} SI units (mean 4.03 × 10^{-3} SI units, n = 5; Fig. 2-4). It is host to the Inco occurrence [105D 100] (Fig. 2-11b), which has two different styles of mineralization: 1) polymetallic Au-Ag quartz veins associated with brittle fault zones and crosscutting Eocene rhyolite dikes (Hart, 1995); and 2) porphyry-style Cu-Mo veining within the pluton. Most of the exploration focus has been on mineralization associated with north-striking, steeply-dipping Eocene rhyolite dikes associated regionally with gold mineralization in the Wheaton district 20 km to the southwest (Henneberry, 1988). In the southwestern part of the pluton a silica and pyrite altered zone of brittlely deformed granodiorite (Fig. 2-16a,b) trends north and may be associated with Eocene rhyolite dikes. In the central portion of the pluton, chalcopyrite, chalcocite(?) and malachite occur on fracture surfaces and within thin (≤1 cm) vuggy quartz veins and micro-breccias oriented N145/70. These quartz veins and barren K-feldspar veins have diffuse margins with the granodiorite and appear to be comagmatic (Fig. 2-16c–f).

Geochronology

Hornblende granodiorite from the Red Ridge pluton was dated by Hart (1995) at 200.1 ± 0.9 Ma (Fig. 2-17), based on two overlapping concordant zircon fractions (Y88-33-3, U-Pb, ID-TIMS on multi-grain fractions, UBC). A third fraction yielded a younger date of *ca.* 189 Ma which was presumed to reflect Pb loss.

We resampled the Red Ridge granodiorite approximately 165 m northwest of Hart's site (Fig. 2-11a). Our sample 15PS050-1 yielded stubby, prismatic zircons with concentric zoning suggesting magmatic growth and absence of inherited cores (Fig. 2-18a). Thirty-two LA-ICPMS spot analyses yielded $^{206}Pb/^{238}U$ dates between 229 and 205 Ma, and a weighted mean of 215.5 ± 1.9 Ma (Fig. 2-18b; Appendix 3). Six zircon grains were analyzed by CA-TIMS and yielded concordant $^{206}Pb/^{238}U$ dates ranging from 216.58 ± 0.15 to 216.37 ± 0.15 Ma, and a weighted mean crystallization date of 216.48 ± 0.06 Ma (MSWD = 1.09; Fig. 2-18c; Appendix 4). Our results from the Red Ridge pluton confirm it is part of the Late Triassic Stikine suite but are distinctly older than the previous date reported by Hart (1995). Although varying phases are observed in this pluton, evidence indicates they are comagmatic and related mainly to varying abundance of hornblende and are thus unlikely to be significantly different in age. Considering that Hart's sample already exhibited evidence of Pb loss, it is likely that all analyses in the sample were affected by Pb loss. Our more precise CA-TIMS date of 216.48 ± 0.06 Ma is therefore considered the crystallization age of the Red Ridge pluton (Fig. 2-18c).

Thermometry

Ti-in-zircon temperature estimates, from sample 15PS050-1 in the Red Ridge pluton range from 633–724°C (Appendix 3).



Figure 2-16. *Two styles of mineralization are observed within the Red Ridge pluton: breccia zones with quartz-pyrite alteration (a and b) and vuggy veins with copper mineralization (c–f).* ***(a)*** *Monomict breccia with granodiorite fragments within a quartz-pyrite cement.* ***(b)*** *Fine-grained pyritic and siliceous rock, likely same material as the cement in a.* ***(c)*** *Fe and Cu-oxides on fractures.* ***(d)*** *Surface of vuggy quartz vein with malachite.* ***(e)*** *Vuggy quartz vein (1 cm wide) with chalcocite(?) and malachite, pencil lead is 2 mm thick.* ***(f)*** *At least two orientations of K-feldspar veins crosscutting granodiorite. a and b from station 15PS051; c to f from station 15PS050.*

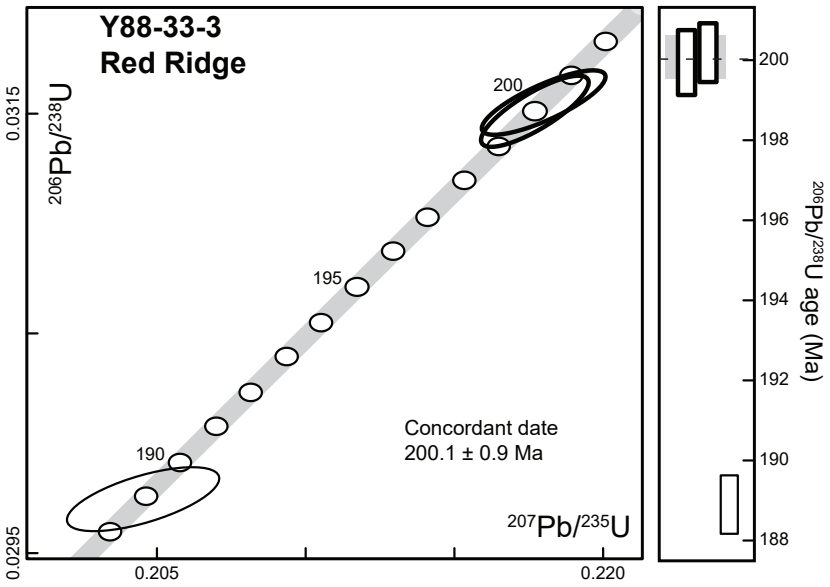
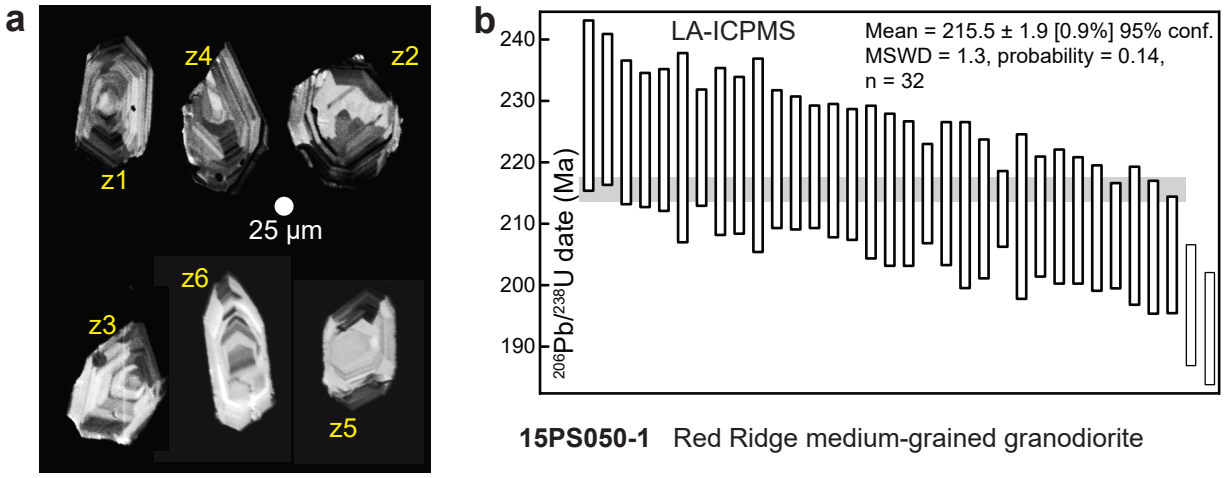


Figure 2-17. *U-Pb concordia diagram for Y88-33-3, Red Ridge pluton (Hart, 1995). Zircon analyses included in the weighted mean $^{206}Pb/^{238}U$ crystallization age are represented by solid bold ellipses. The light grey band surrounding concordia account for decay constant uncertainties. Ranked $^{206}Pb/^{238}U$ dates are shown to the right of the concordia diagram. Box heights are 2σ uncertainties. Horizontal dashed line corresponds to the concordia age where the height of the grey band indicates uncertainty. Line-type designations on bar charts mimic those described for the concordia diagram.*



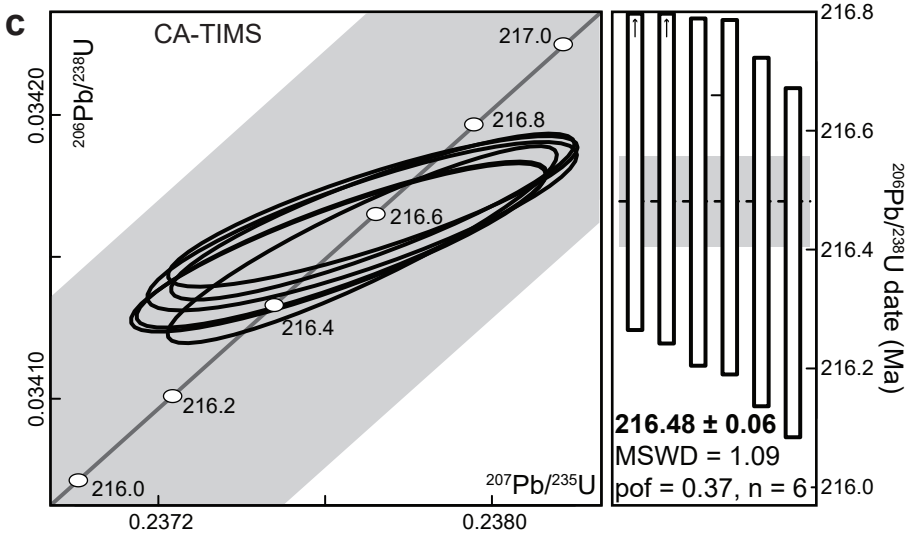


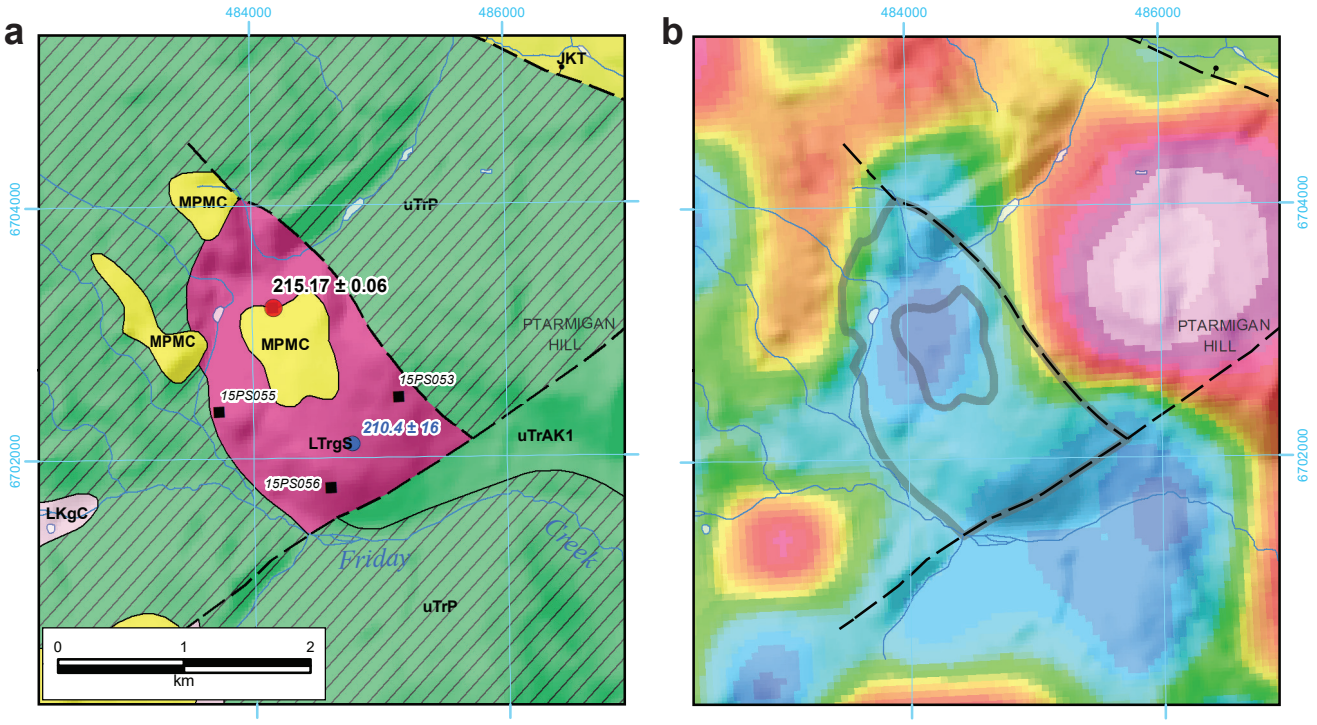
Figure 2-18. *U-Pb zircon geochronology results from 15PS050-1.*
(a) *Cathodoluminescence images of zircon analyzed by CA-TIMS, with analysis label.*
(b) *Ranked plot of $^{206}Pb/^{238}U$ dates determined by LA-ICPMS.*
(c) *Concordia plot of CA-TIMS dates. Analyses included in CA-TIMS weighted mean date calculation are shown by bold ellipses; ellipses with thin lines are not used in calculation. The light grey band around concordia (dark grey line) illustrates the decay constant uncertainties. Ranked $^{206}Pb/^{238}U$ date plot is to the right of the concordia plot, with the weighted mean date shown by the grey band. Line-type designations are the same as the concordia plot. Small arrows indicate error bars extend slightly beyond limit of plot. Errors in all plots are at 2σ. MSWD = mean squared weighted deviation, pof = probability of fit, n = number of analyses included in age calculation.*

Friday Creek pluton

The Friday Creek pluton is located on the western knob of Ptarmigan Hill on the north side of Friday Creek (Figs. 2-2 and 2-19a). It is a 2.7 km² body with a slight northwest-trending elongation. The pluton is faulted against rocks of the Lewes River Group on its southeastern and northeastern sides (Fig. 2-19a); its western margin is not exposed but is inferred to represent either an intrusive contact into the Povoas formation or an unconformity (Hart, 1995). Thin flows of the Neogene Miles Canyon basalt locally unconformably overlie the pluton (Fig. 2-19a).

Petrography

The Friday Creek pluton is a simple, single-phase body of unfoliated, medium-grained granodiorite that is commonly leucocratic on weathered surfaces with a slight pinkish tinge on fresh surfaces (Fig. 2-20); large titanite phenocrysts up to 5 mm are common (Figs. 2-21 and 2-22). All samples from the Friday Creek pluton plot in the granodiorite field of the QAP diagram (Fig. 2-3). Most grains are equigranular, subhedral to seriate (Fig. 2-22). Plagioclase and K-feldspar are weakly to moderately saussuritized and sericitized, respectively; mafic minerals are weakly altered to chlorite. Hornblende and biotite make up 5–10% of the rock, typically with hornblende more abundant than biotite. Accessory minerals include small possibly magmatic epidote (Fig. 2-22a) and titanite (Figs. 2-21 and 2-22c).



MIOCENE TO PLIOCENE

MPMC: MILES CANYON: columnar jointed olivine basalt flows

LATE CRETACEOUS TO TERTIARY

LKgC: CASINO SUITE: Hbl-Bt granodiorite, Hbl diorite, quartz diorite

UPPER JURASSIC AND LOWER CRETACEOUS

JKT: TANTALUS: chert pebble conglomerate and gritty quartz-chert-feldspar sandstone

LATE TRIASSIC

LTrgS: STIKINE SUITE: coarse-grained, foliated, gabbroic Hbl orthogneiss

UPPER TRIASSIC, CARNIAN TO NORIAN

uTrAK1: CASCA: shale, siltstone, calcareous greywacke, argillaceous limestone

UPPER TRIASSIC, CARNIAN AND OLDER (?)

uTrP: POVOAS: augite or feldspar-phyric andesitic basalt flows, breccia, tuff, sandstone, argillite

U-Pb (CA-TIMS)

U-Pb (ID-TIMS)

Field stations

Figure 2-19. (a) *Geology of the Friday Creek area. Geology from YGS (2020a); fault symbology as in Figure 1-4.* ***(b)*** *Reduced to pole, first vertical derivative aeromagnetic map of the Friday Creek area (Aurora Geosciences Ltd. and Bruce, 2017a). Grid is UTM NAD83, zone 8.*



Figure 2-20. *Fresh surface of granodiorite sample 15PS053-1, Friday Creek pluton.*

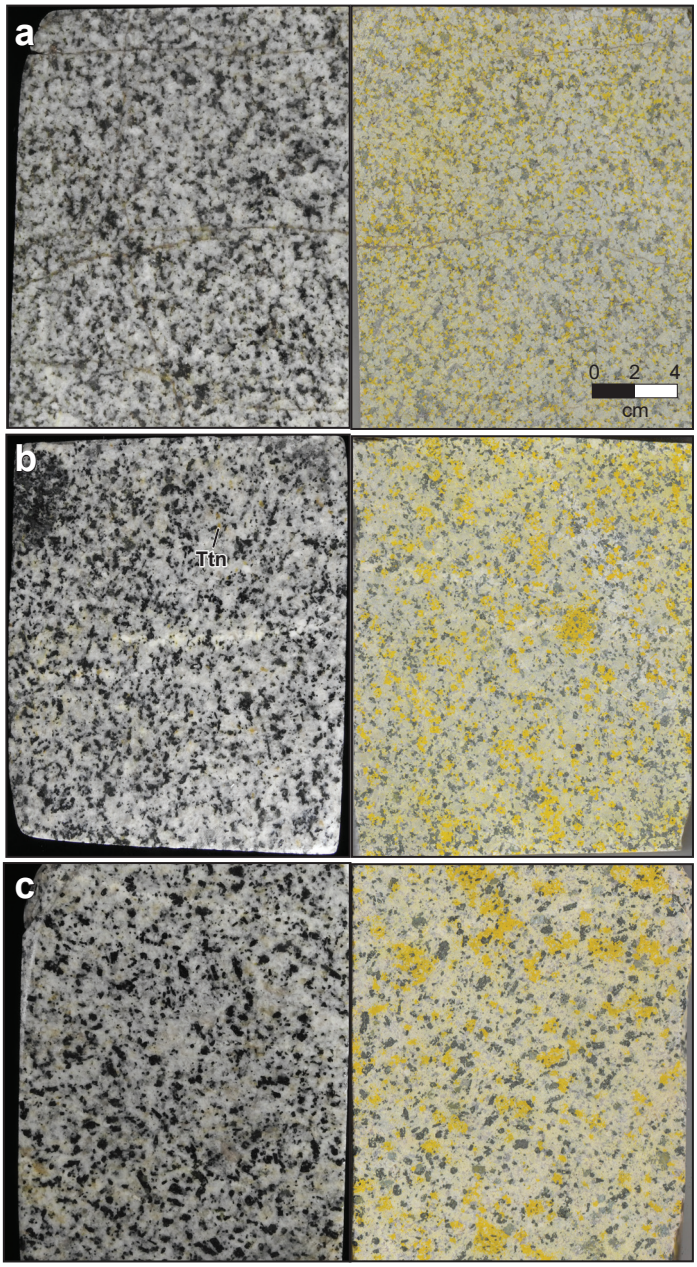


Figure 2-21. *Representative samples of the Friday Creek pluton. Fresh polished surface (left) and a cobaltinitrite-stained surface (right).* ***(a)*** *15PS055-1,* ***(b)*** *15PS054-1,* ***(c)*** *15PS056-1. Note K-feldspar is yellow. In b, small light brown mineral is titanite (Ttn).*

Oxidation state and mineral occurrences

The Friday Creek pluton is weakly oxidized, with susceptibilities ranging from 0.45 to 13.0 × 10^{-3} SI units (Fig. 2-4; mean 4.6 × 10^{-3} SI units; n = 5), and underlain by an aeromagnetic low (Fig. 2-19b). No known mineral occurrences are associated with this pluton (YGS, 2020b).

Geochronology

Hart (1995) previously reported a U-Pb zircon date of 210 +16/-1 Ma from the Friday Creek pluton, based on two nearly concordant, multi-grain fractions analyzed by ID-TIMS at UBC. We collected a sample of granodiorite from the Friday Creek pluton approximately 1.2 km northwest of the locality sampled by Hart (1995), below the unconformity with a Neogene basalt flow (Fig. 2-19a). Sample 15PS054-1 yielded stubby prismatic zircons with faint concentric zoning and an absence of inherited cores (Fig. 2-23a). LA-ICPMS analyses of 28 zircons have $^{206}Pb/^{238}U$ dates between 223 and 205 Ma, and a weighted mean of 212.2 ± 1.9 Ma (Fig. 2-23b; Appendix 3). Six zircon grains analyzed by CA-TIMS yielded concordant $^{206}Pb/^{238}U$ dates that range from 215.29 ± 0.15 to 215.08 ± 0.15 Ma (Appendix 4), with a weighted mean date of 215.17 ± 0.06 Ma (MSWD = 1.01, n = 6; Fig. 2-23c). This more precise date is considered the crystallization age of the Friday Creek pluton.

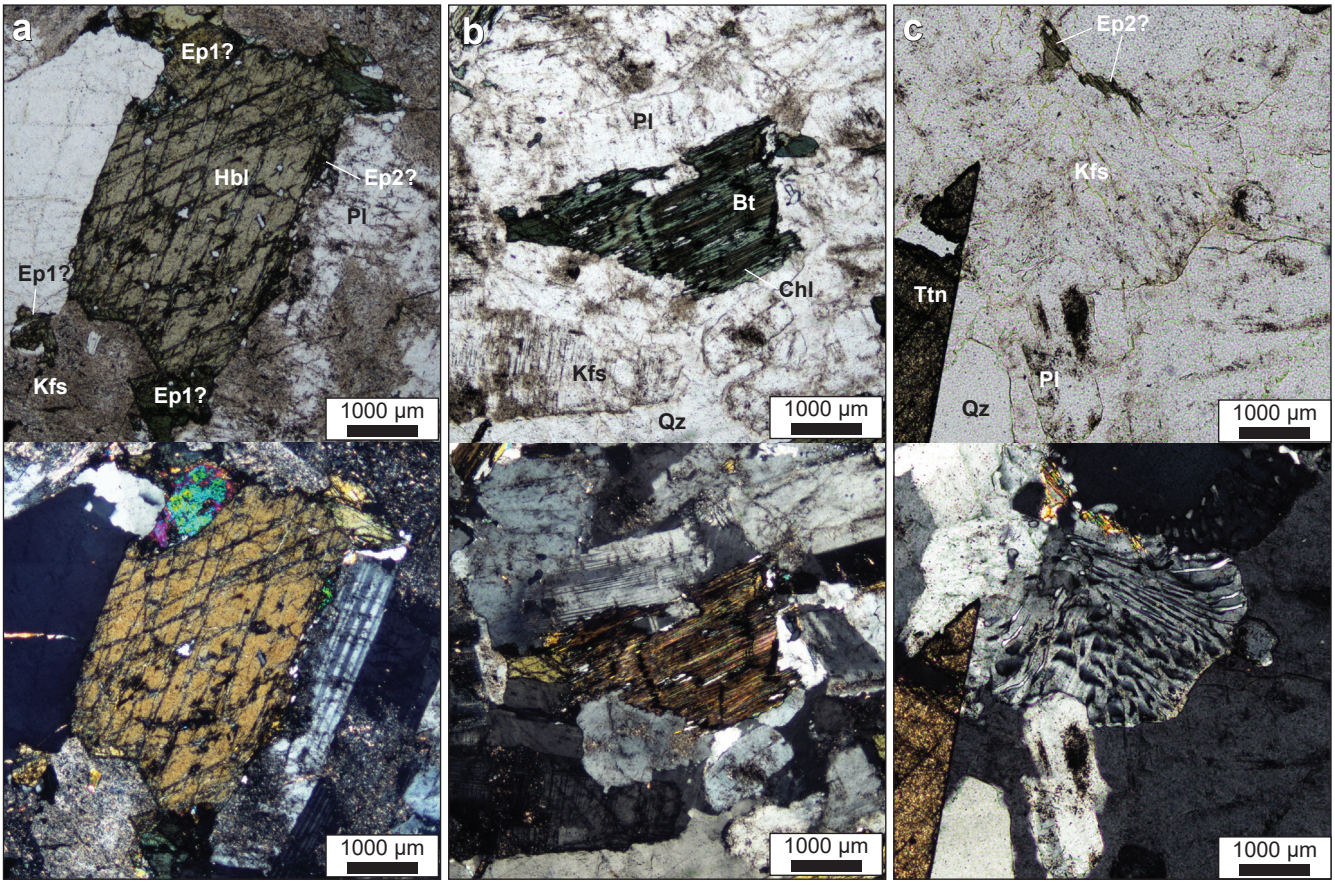


Figure 2-22. *Transmitted light photomicrograph pairs for samples of the Friday Creek pluton; plane polarized light (upper) and cross-polarized light (lower).* ***(a)*** and ***(b)*** *15PS053-1,* ***(c)*** *15PS056-1.*

Thermobarometry

Granodiorite from the Friday Creek pluton contains the suitable mineral assemblage for Al-in-Hbl geobarometry. Two samples were analyzed (15PS054-1 and 15PS056-1; Appendix 5). Al^{TOT} in hornblende from these samples are 1.47–1.51 and plagioclase has X_{An} of 0.29, indicating crystallization pressure estimates of 3.09 ± 0.87 to 3.49 ± 0.92 kbar (Appendix 5; emplacement depths of 11.7 to 13.2 km) and solidus temperatures of 729–743°C. This is broadly consistent with Ti-in-zircon temperature estimates of *ca.* 714–780°C for sample 15PS054-1 (Appendix 3).

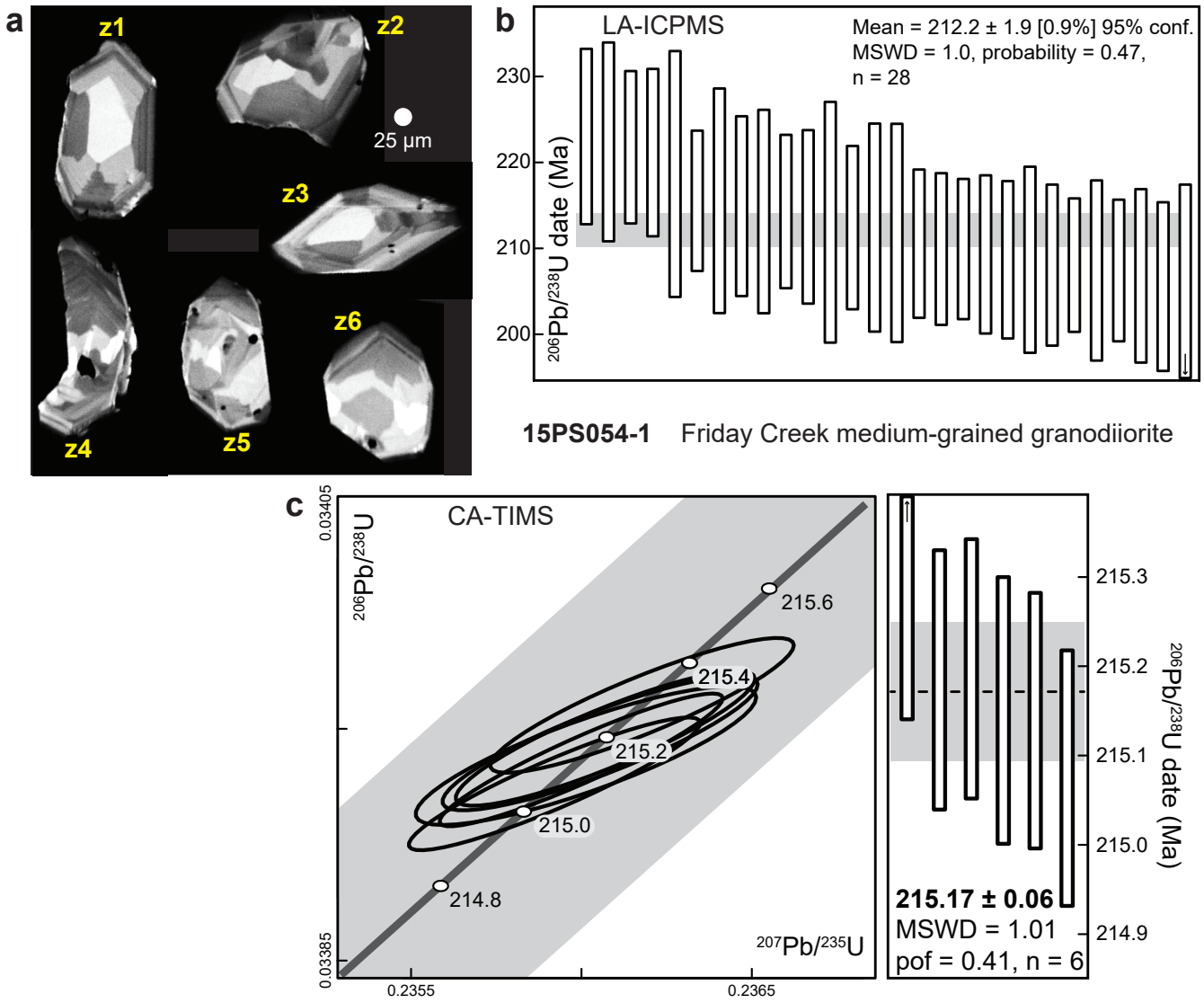


Figure 2-23. *U-Pb zircon geochronology results from 15PS054-1.* ***(a)*** *Cathodoluminescence images of zircon analyzed by CA-TIMS, with analysis label.* ***(b)*** *Ranked plot of $^{206}Pb/^{238}U$ dates determined by LA-ICPMS.* ***(c)*** *Concordia plot of CA-TIMS dates. Analyses included in CA-TIMS weighted mean date calculation are shown by bold ellipses; ellipses with thin lines are not used in calculation. The light grey band around concordia (dark grey line) illustrates the decay constant uncertainties. Ranked $^{206}Pb/^{238}U$ date plot is to the right of the concordia plot, with the weighted mean date shown by the grey band. Line-type designations are the same as the concordia plot. Small arrows indicate error bars extend slightly beyond limit of plot. Errors in all plots are at 2σ. MSWD = mean squared weighted deviation, pof = probability of fit, n = number of analyses included in age calculation.*

Ibex pluton

The Ibex pluton is a 12.3 km² body in the upper Ibex valley between Fish Lake and Ibex Mountain (Figs. 2-2 and 2-24a). This is the largest pluton in the Stikine suite, but it is generally poorly exposed and there are only a few outcrops on hilltops and in stream cuts; it coincides in part with a magnetic high (Fig. 2-24b). The southern and eastern contacts of the pluton are mapped as intruding the Povoas formation whereas to the north the pluton is intruded by the mid-Cretaceous Whitehorse suite and to the west by the Paleocene Ruby Range suite (Fig. 2-24a). We visited a single locality in the north-central part of the pluton within an incised stream cut that flows into the Ibex River from the east (Fig. 2-24a). The exposure at station 15PS133 is generally rubbly and weathered (Fig. 2-25).

Petrography

On weathered and fresh surfaces the rock is slightly pink, medium grained and unfoliated (Fig. 2-26). It is a granodiorite-tonalite (Fig. 2-3) with an overall equigranular texture. K-feldspar occurs as anhedral poikilitic clots with inclusions of plagioclase and quartz (Fig. 2-27). Most grains are subhedral and seriate. Hornblende is the most common mafic mineral with minor biotite, together they make up 10–15% of the rock. Hornblende is fresh, whereas biotite is intensely altered to chlorite. Plagioclase and K-feldspar are moderately to intensely saussuritized and sericitized, respectively (Fig. 2-28).

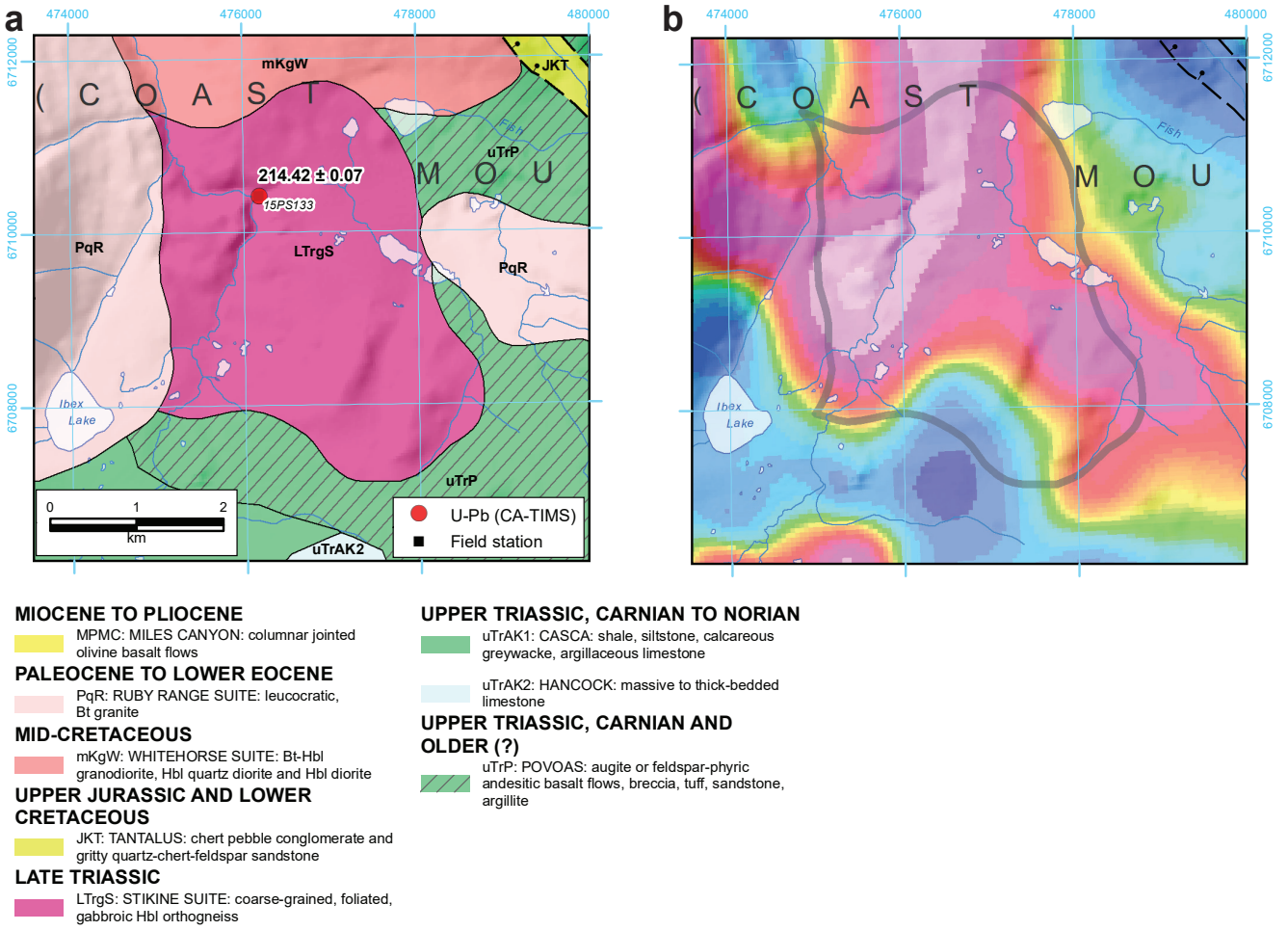


Figure 2-24. (a) *Geology of the Ibex pluton area. Geology from YGS (2020a); fault symbology as in Figure 1-4.* ***(b)*** *Reduced to pole, first vertical derivative aeromagnetic map of the Ibex pluton (Aurora Geosciences Ltd. and Bruce, 2017a). Grid is UTM NAD83, zone 8.*



Figure 2-25. *Poorly exposed rubbly outcrop in the bank of a side stream to the upper Ibex River, station 15PS133.*

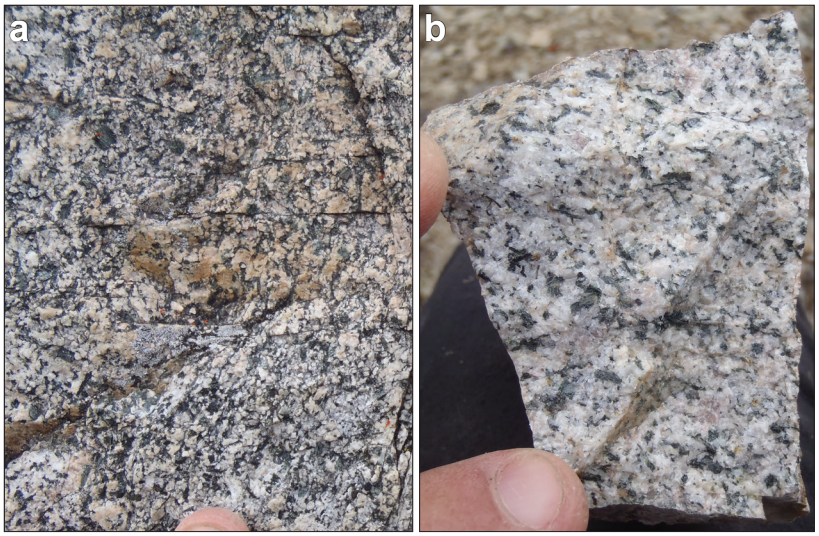


Figure 2-26. *Weathered* ***(a)*** *and fresh* ***(b)*** *exposures of the Ibex pluton at station 15PS133.*

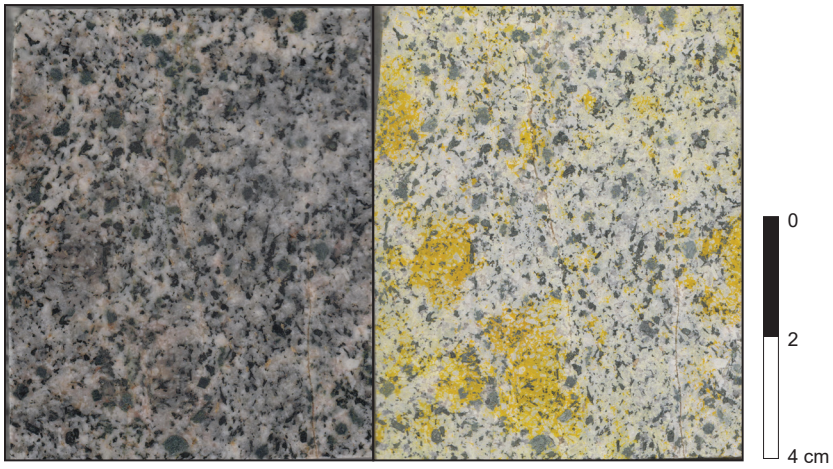


Figure 2-27. *Sample 15PS133-1 from the Ibex pluton, polished surface (left) and a cobaltinitrite-stained cut surface (right).*

Oxidation state and mineral occurrences

The Ibex pluton is magnetic with a susceptibility of 6.05×10^{-3} SI units (Figs. 2-4 and 2-24b). No known mineral occurrences are associated with this pluton (YGS, 2020b).

Geochronology

We report here the first date for the Ibex pluton (Table 2-1). Sample 15PS133-1 yielded prismatic zircons with a >2:1 elongation ratio and concentric, magmatic zoning (Fig. 2-29a). There is no evidence of inherited cores in the CL images or in LA-ICPMS analyses of 28 zircons with $^{206}Pb/^{238}U$ dates ranging from 230 to 203 Ma (weighted mean of 214.5 ± 1.9 Ma; Fig. 2-29b; Appendix 3). CA-TIMS analyses of six zircon grains from sample 15PS133-1 yielded concordant $^{206}Pb/^{238}U$ dates that range from 214.49 ± 0.15 to 214.34 ± 0.15 Ma (Fig. 2-29c; Appendix 4). One of these grains is slightly older and is interpreted as either an antecryst or a xenocryst; the weighted mean crystallization date of the five younger grains is 214.42 ± 0.07 Ma (MSWD = 0.72, n = 5; Fig. 2-29c).

Thermometry

Ti-in-zircon thermometry for the Ibex pluton indicate crystallization temperature ranging from 652–788°C (Appendix 3).

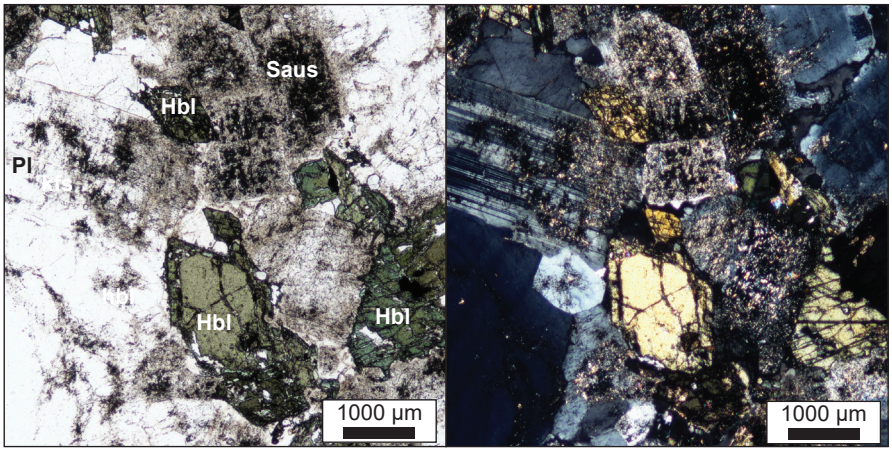


Figure 2-28. *Transmitted light photomicrograph pair for 15PS133-1 from the Ibex pluton; (left) plane polarized light and (right) cross-polarized light.*

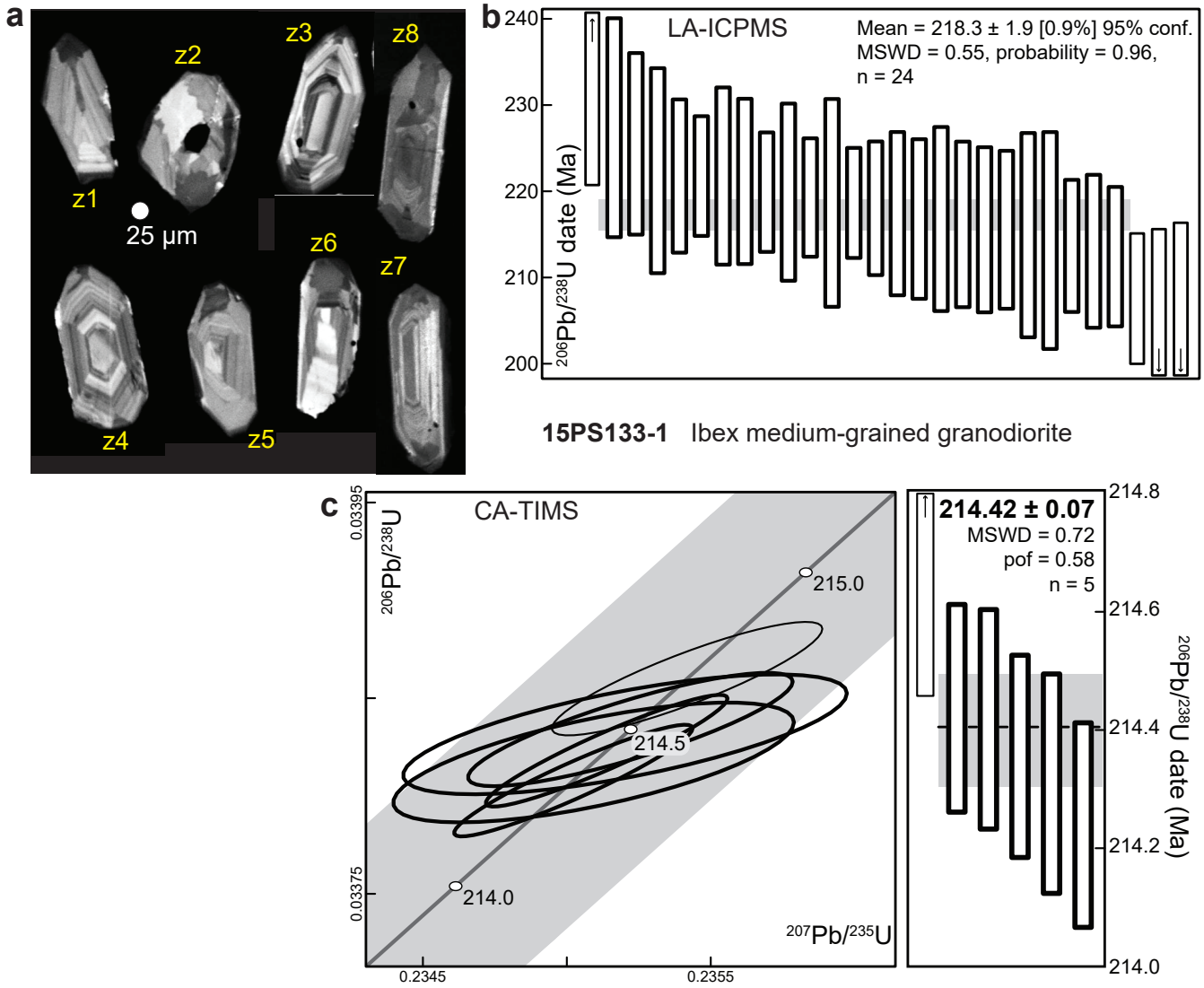


Figure 2-29. *U-Pb zircon geochronology results from 15PS133-1. (a) Cathodoluminescence images of zircon analyzed by CA-TIMS, with analysis label. (b) Ranked plot of $^{206}Pb/^{238}U$ dates determined by LA-ICPMS. (c) Concordia plot of CA-TIMS dates. Analyses included in CA-TIMS weighted mean date calculation are shown by bold ellipses; ellipses with thin lines are not used in calculation. The light grey band around concordia (dark grey line) illustrates the decay constant uncertainties. Ranked $^{206}Pb/^{238}U$ date plot is to the right of the concordia plot, with the weighted mean date shown by the grey band. Line-type designations are the same as the concordia plot. Small arrows indicate error bars extend slightly beyond limit of plot. Errors in all plots are at 2σ. MSWD = mean squared weighted deviation, pof = probability of fit, n = number of analyses included in age calculation.*

King Lake pluton

The King Lake pluton is located 6 km south of the Alaska Highway, approximately 24 km northwest of Whitehorse in the Scout Lake area, near a small water body known as King Lake (Figs. 2-2 and 2-30a). It is a semicircular pluton with a mapped area of 3.5 km², although its southeastern side is covered by Quaternary deposits obscuring its true size and shape (Fig. 2-30a). The pluton is bound in part on its western edge by a north-striking fault juxtaposing monzodiorite with Upper Triassic mafic volcanic rocks of the Povoas formation and Lower Jurassic sedimentary rocks of the Richthofen formation (Laberge Group). A small semicircular part of the pluton extends west of the fault and comprises granodiorite unconformably overlain by Laberge Group strata (Fig. 2-30a). The northern contact is also mapped as an unconformity beneath Lower Jurassic clastic and tuffaceous rocks of the Nordenskiöld facies and Richthofen formation (Laberge Group; Hart, 1997a). Along the northeastern edge of the pluton, beneath the sub-Jurassic unconformity, thin granodiorite dikes intrude monomictic basalt breccia of the Povoas formation (Fig. 2-31).

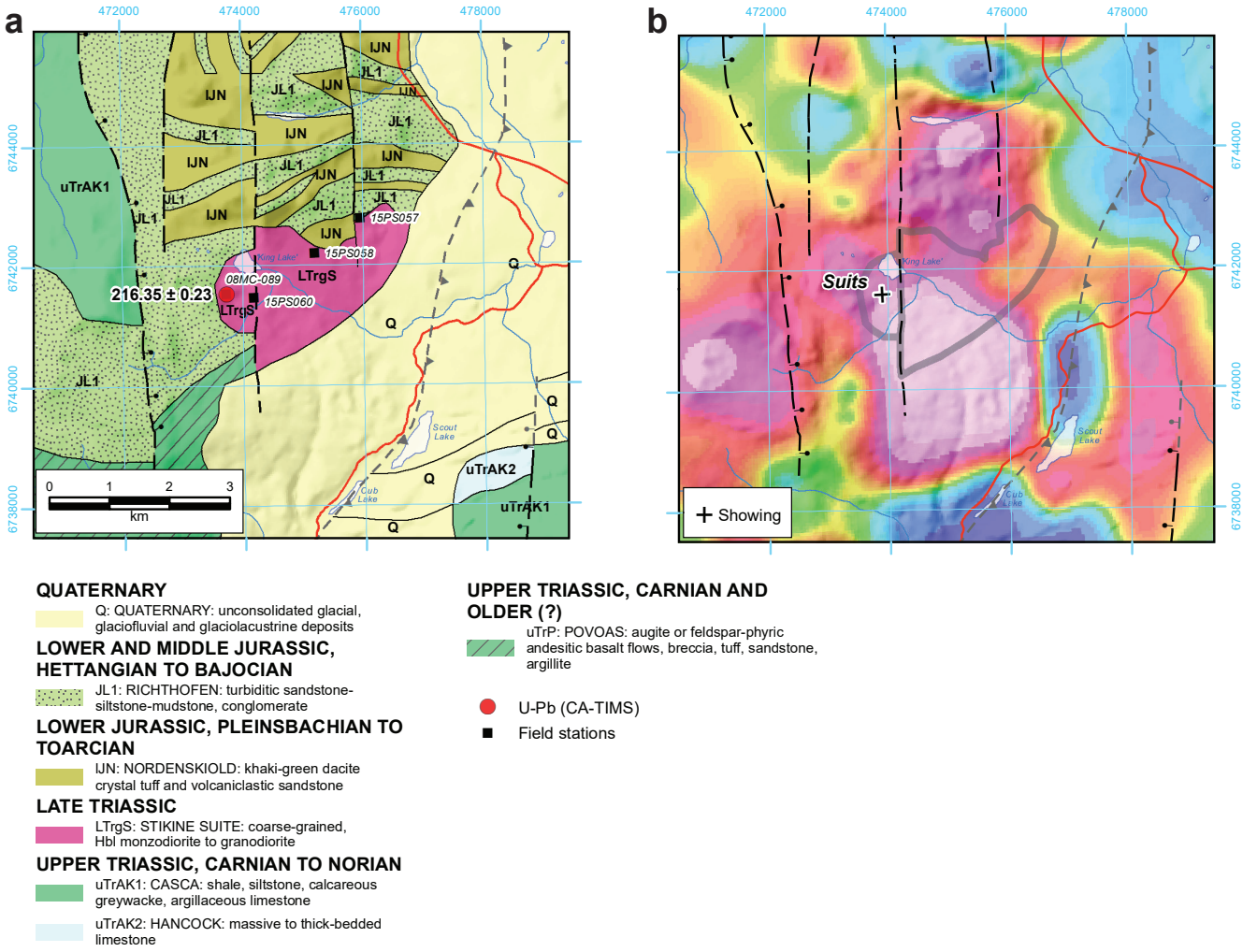


Figure 2-30. (a) *Geology of the King Lake pluton area. Geology from YGS (2020a); fault symbology as in Figure 1-4.* ***(b)*** *Reduced to pole, first vertical derivative aeromagnetic map of the King Lake area (Aurora Geosciences Ltd. and Bruce, 2017a). The location of the Suits MINFILE occurrence [105D 104] is shown. Grid is UTM NAD83, zone 8.*

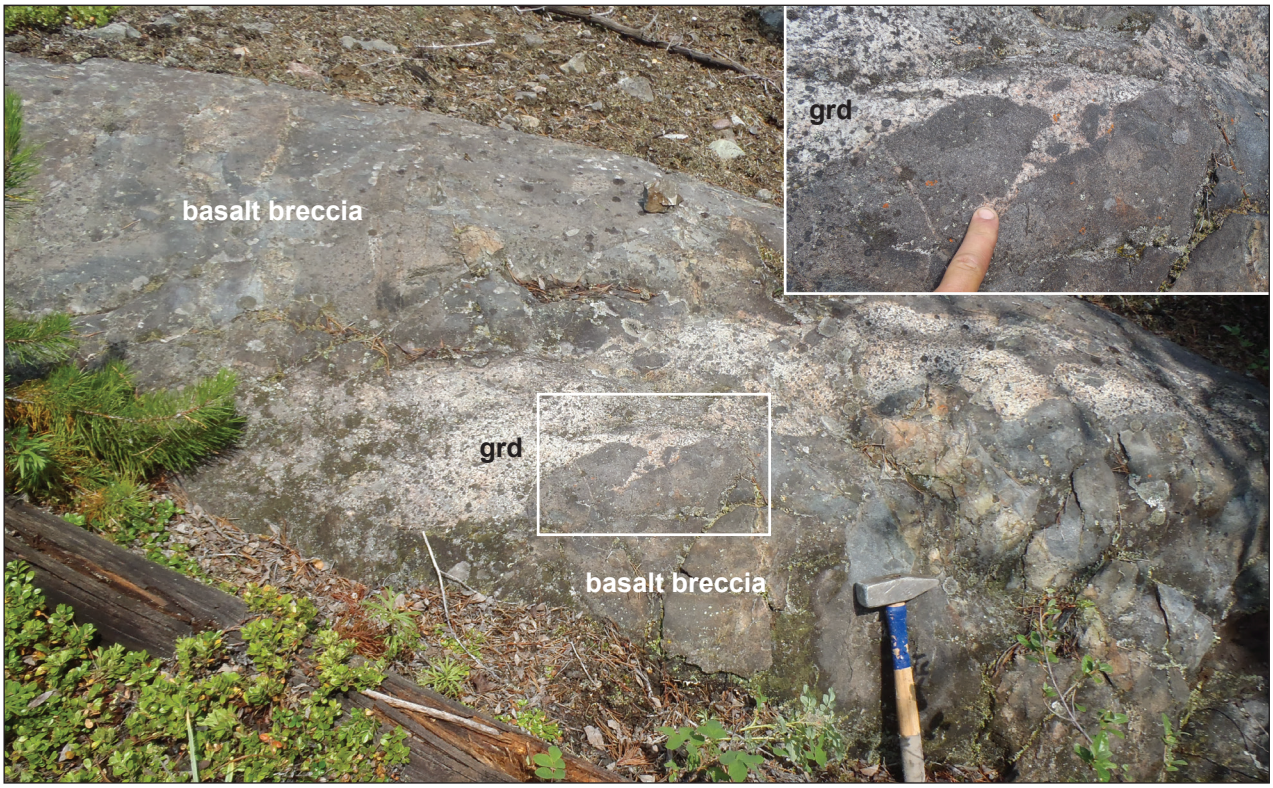


Figure 2-31. *Outcrop of granodiorite dike intruding monomictic basalt breccia, hammer 45 cm long; 15PS057. This relationship of granodiorite dike intruding basaltic rocks is similar to that seen at station 08MC089, where the granodiorite was dated at 216 Ma (Fig. 2-30; Appendix 4). grd = granodiorite.*

Petrography

The King Lake pluton is multiphase with a granodiorite phase and a monzodiorite to monzonite phase (Figs. 2-3 and 2-32). Both phases are unfoliated and medium grained, though the granodiorite is slightly coarser grained than the monzodiorite (Figs. 2-32 and 2-33). In both phases, all minerals are relatively fresh and hornblende and biotite are present in equal amounts. Hornblende in the monzodiorite locally contains cores of augite (Fig. 2-34). In the granodiorite, total mafic mineral content is approximately 10% whereas it ranges from 30–50% in the monzodiorite (Fig. 2-32). The granodiorite comprises mostly euhedral grains and the monzodiorite mostly subhedral grains (Fig. 2-33).

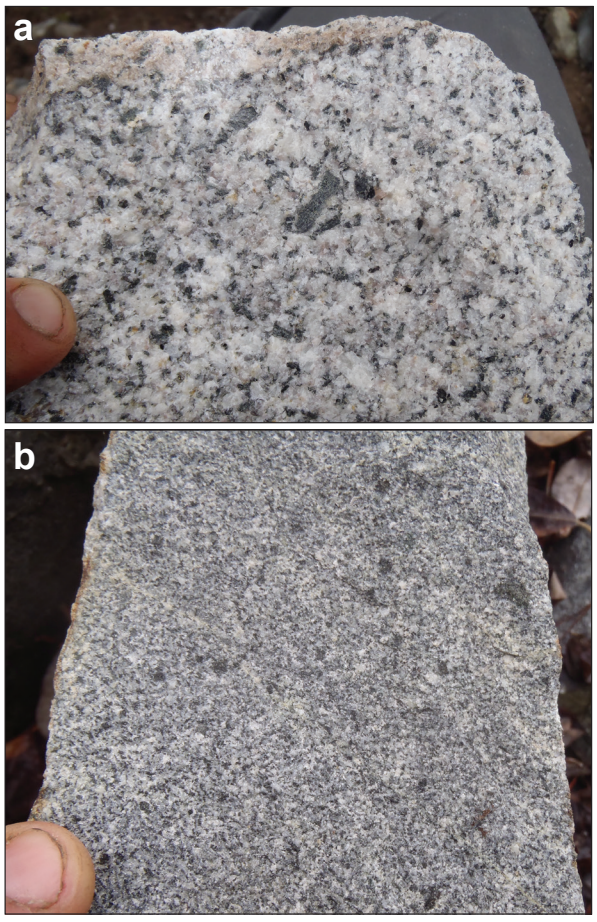


Figure 2-32. *Fresh broken surfaces of two King Lake pluton phases.* ***(a)*** *Equigranular medium-grained granodiorite dike, 15PS057-1;* ***(b)*** *fine to medium-grained monzodiorite, 15PS060-1.*

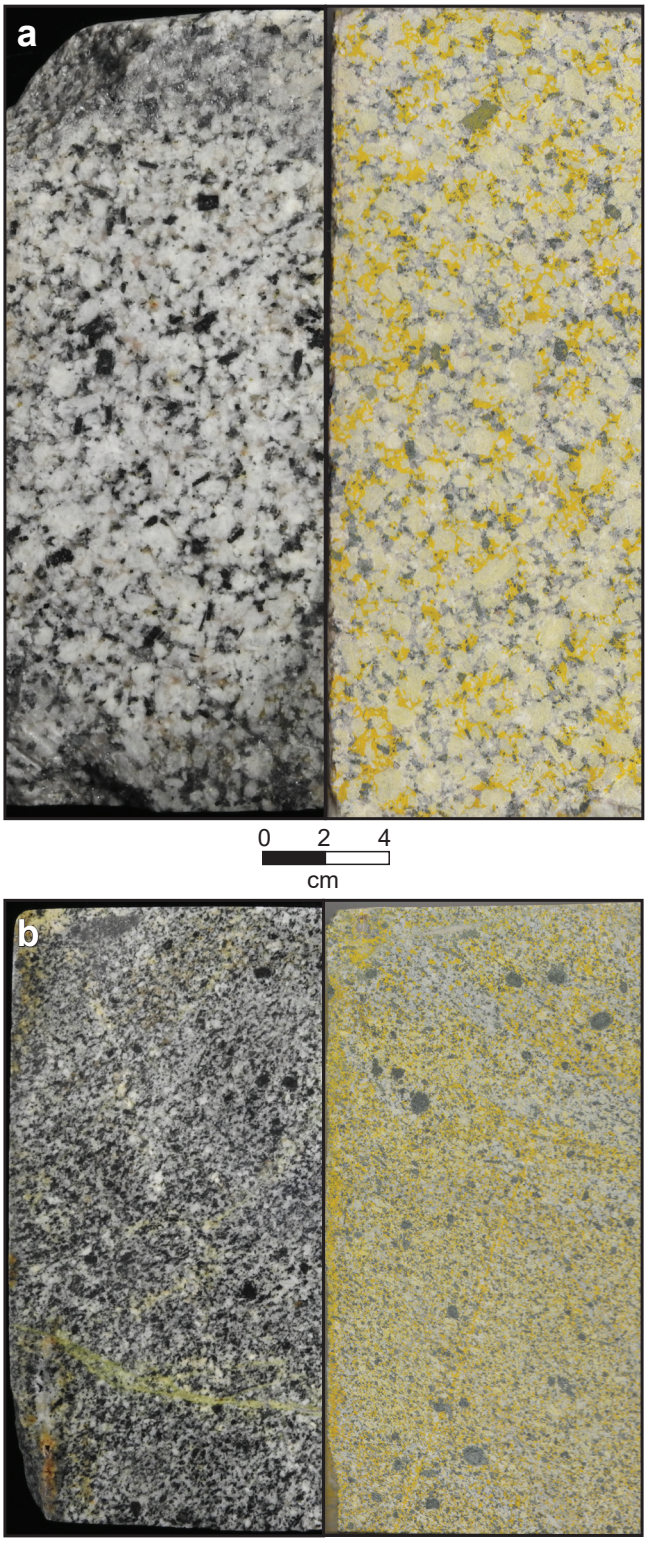


Figure 2-33. *Representative samples showing the multiphase nature of the King Lake pluton. Each sample shown with a fresh polished surface (left) and a cobaltinitrite-stained cut surface (right).* ***(a)*** *15PS057-1,* ***(b)*** *15PS060-1.*

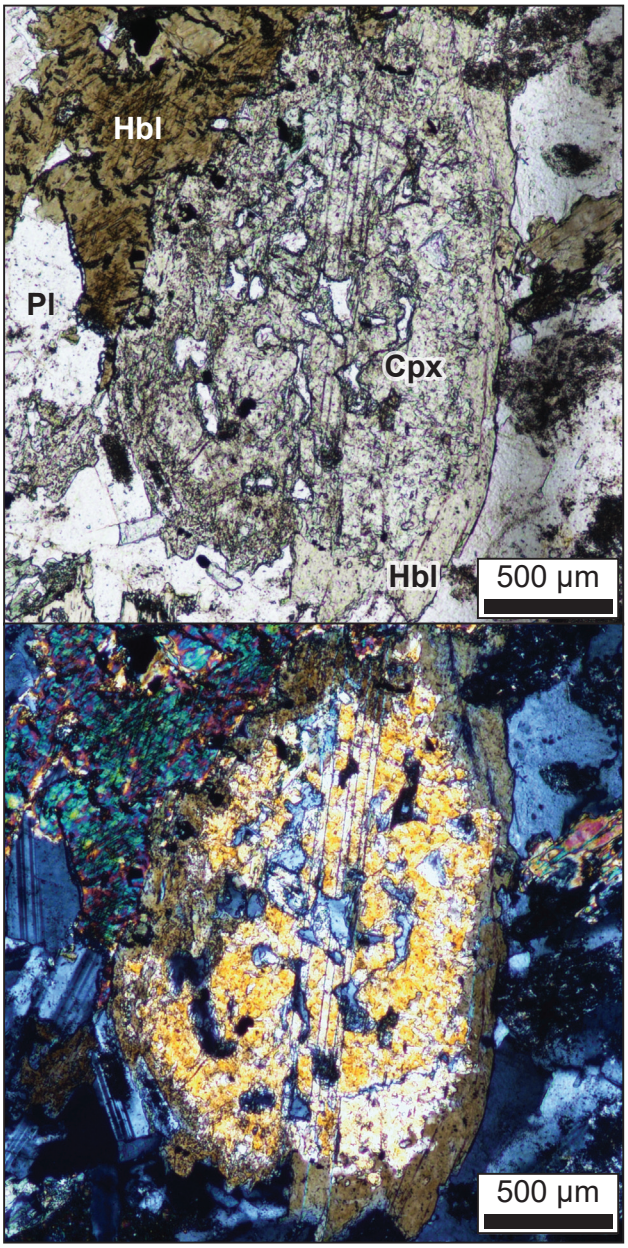


Figure 2-34. *Clinopyroxene (augite) core overgrown by hornblende in monzodiorite of the King Lake pluton, 15PS058. Transmitted light photomicrograph pair; (upper) plane polarized light and (lower) cross-polarized light.*

Oxidation state and mineral occurrences

The King Lake pluton is magnetic and moderately oxidized with susceptibilities ranging from 2.66 to 11.4 × 10^{-3} SI units (mean 8.22 × 10^{-3} SI units, n = 3; Figs. 2-4 and 2-30b). A single Cu showing, Suits [105D 104], occurs in the western part of the King Lake pluton, just south of King Lake (Fig. 2-30b). The Cu (± Mo, Au) mineralization occurs as veins with chalcopyrite and malachite on fracture surfaces (Fig. 2-35a,b). Barren epidote veins are also spatially associated with Cu mineralization (Fig. 2-35c). Two styles of chalcopyrite-bearing veins are evident, the earliest are fine-grained (<50 µm), 1 to 2 mm-wide epidote-calcite veins with relatively straight and sharp selvages (Fig. 2-36). These thin veins are crosscut by wider (3–5 mm), coarse-grained (>500 µm) quartz-calcite veins with diffuse, irregular selvages (Fig. 2-36). Traynor (1999) reported grab samples assaying up to 0.6% Cu and 0.2% Mo from this occurrence.

Geochronology

A sample of granodiorite associated with Cu mineralization was collected for U-Pb geochronology (08MC089-1; Appendix 4). Five zircon grains were analyzed by CA-TIMS at UBC and yielded concordant $^{206}Pb/^{238}U$ dates that range from 217.99 ± 0.45 to 216.21 ± 0.47 Ma (Fig. 2-37). One analysis is slightly older and is interpreted as either an antecryst or a xenocryst; the weighted mean crystallization age of four zircons is 216.35 ± 0.23 Ma (MSWD = 0.66, n = 4; Fig. 2-37).

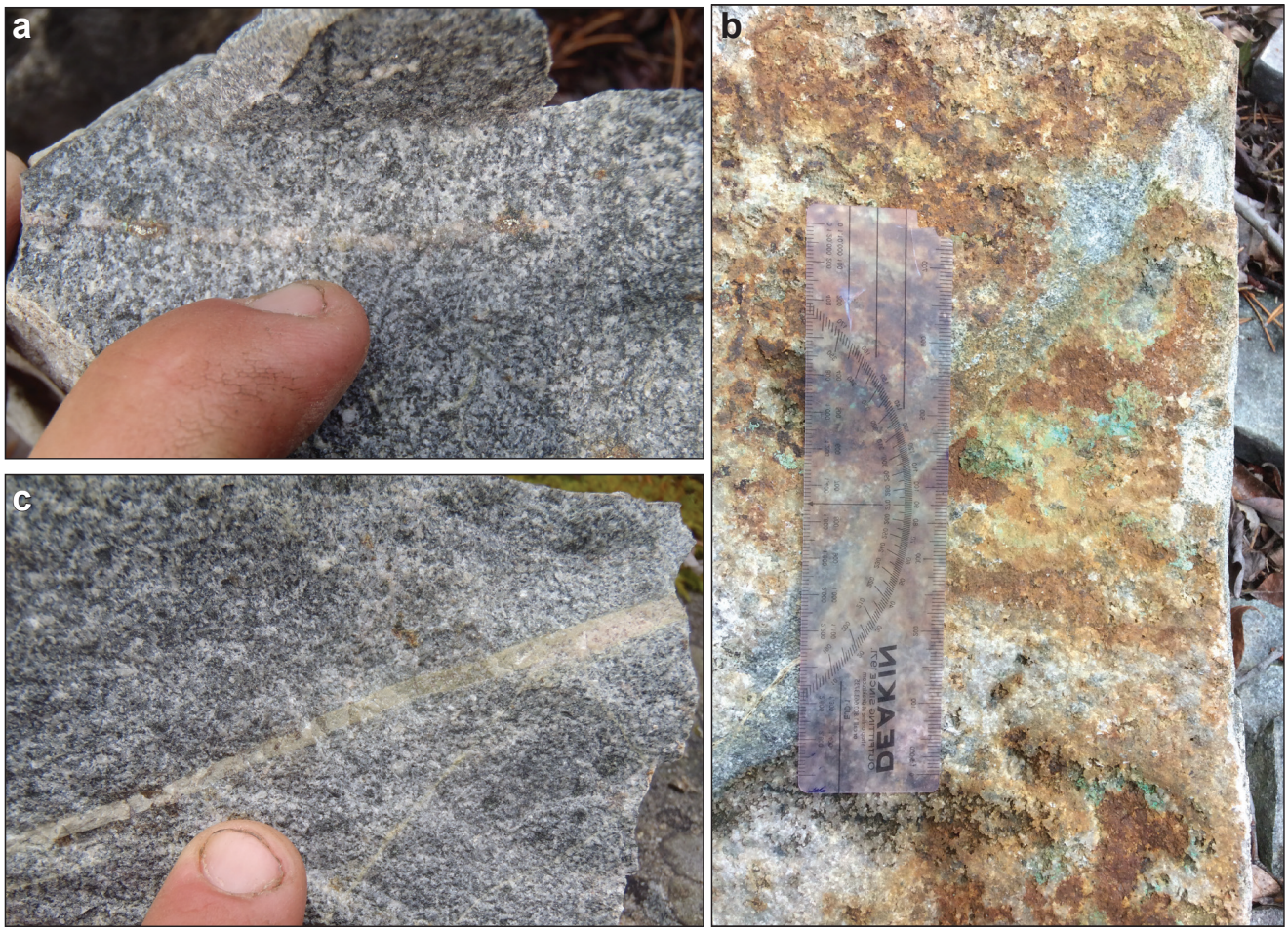


Figure 2-35. *Copper mineralization at the Suits mineral occurrence [105D 104] south of King Lake, station 15PS060 (Fig. 2-30).* ***(a)*** *Thin quartz vein with chalcopyrite in the monzodiorite phase of the King Lake pluton.* ***(b)*** *Fe and Cu-oxides on a fracture surface.* ***(c)*** *Barren epidote vein.*

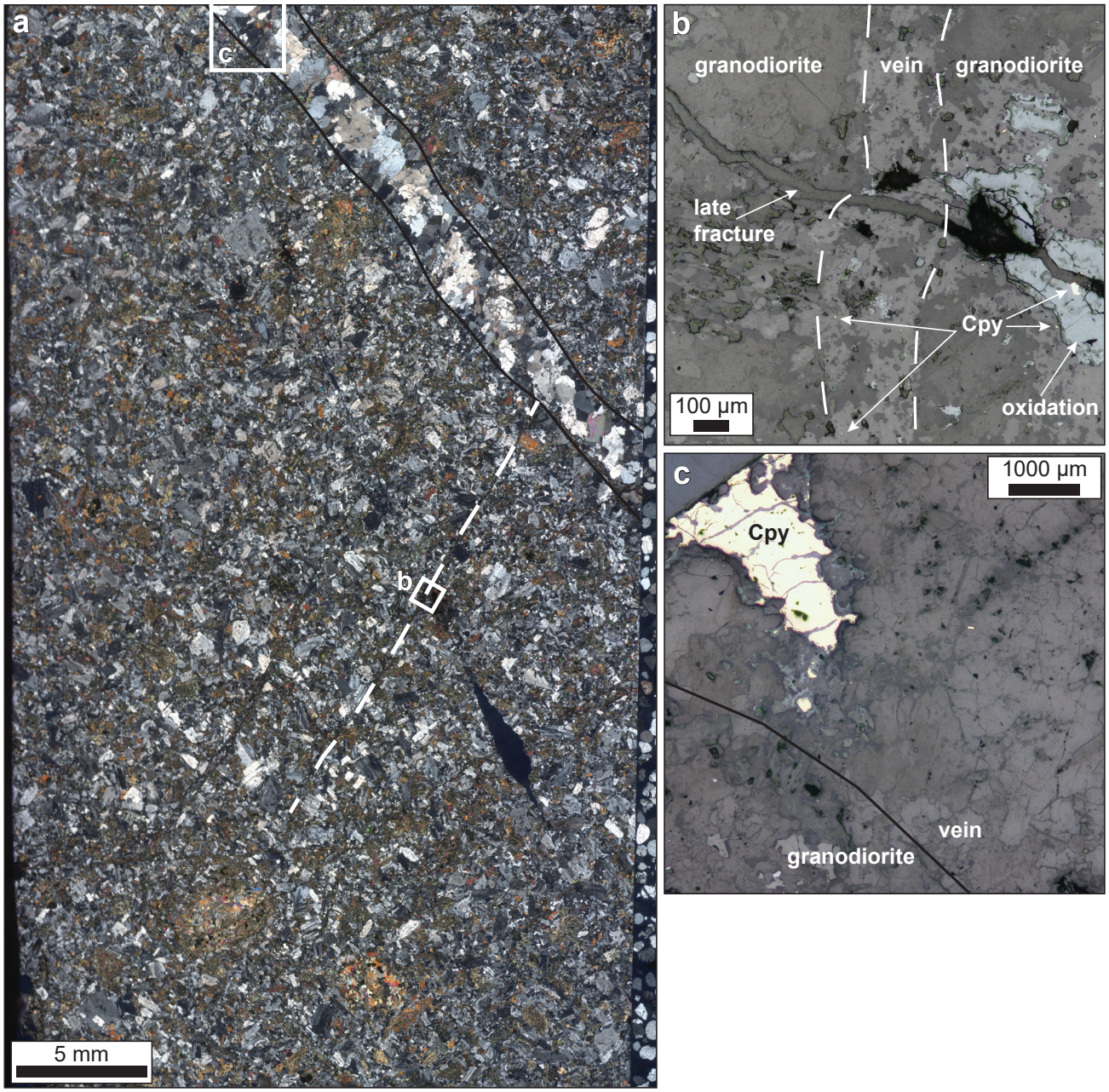


Figure 2-36. *Copper-bearing veins at the Suits occurrence [105D 104] within the King Lake pluton, 15PS060-2.* ***(a)*** *Scan of thin section, cross-polarized transmitted light, showing two vein sets and location of reflected light images shown in b and c. Note early thin veins are crosscut by thicker, coarse-grained vein.* ***(b)*** *Early, thin epidote-calcite veins with disseminated very fine chalcopyrite grains (Cpy). Late fracture enables oxidation and possibly remobilized copper.* ***(c)*** *Later, thick and coarser grained quartz-calcite veins with large chalcopyrite grain.*

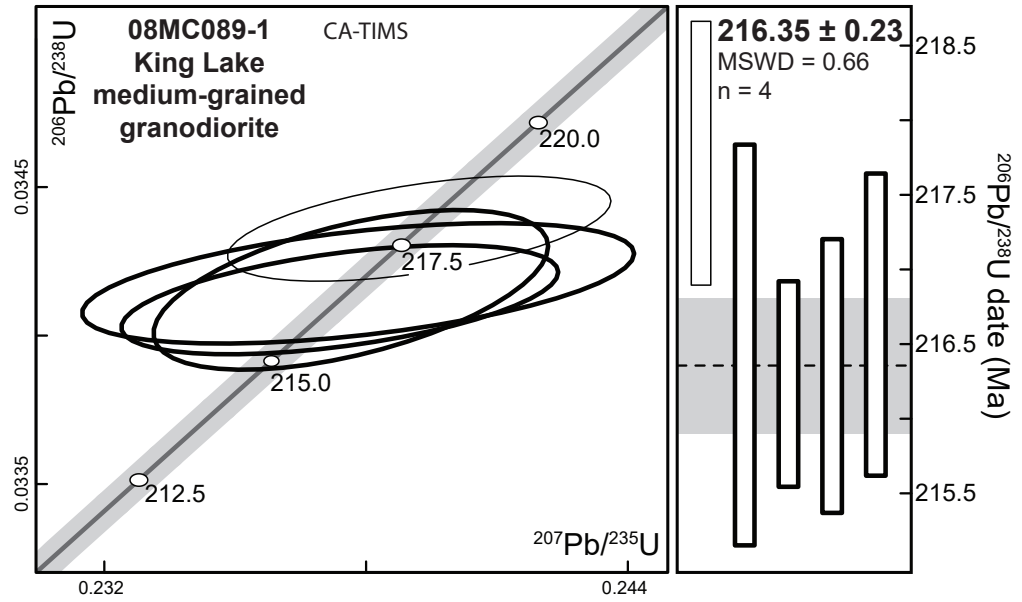


Figure 2-37. *U-Pb zircon geochronology results from 08MC089-1. Concordia diagram (left) and ranked $^{206}Pb/^{238}U$ dates (right) for 5 zircons analyzed by CA-TIMS from 08MC089-1 (Appendix 4). Zircon analyses included in the weighted mean $^{206}Pb/^{238}U$ date (n = 4) are represented by solid bold ellipses on concordia and boxes in ranked plot. Thin ellipse and box are excluded from age calculation. The light grey band around Concordia (dark grey) shows the decay constant uncertainties. Bar heights in ranked plot are 2σ uncertainties. The horizontal dashed line represents the weighted mean date of 4 CA-TIMS analyses with the 2σ uncertainty shown by the grey band. MSWD = mean squared weighted deviation.*

Pyroxene Mountain suite

Plutons assigned to the Pyroxene Mountain suite are primarily tabular bodies that are interpreted to intrude metamorphic rocks of the Yukon-Tanana terrane near the northern apex of Stikinia in central Yukon (Fig. 2-1). These plutons were not examined in detail for the present study; the descriptions below are summarized from field observations from previous work (Gordey and Ryan, 2005; Ryan *et al.*, 2013).

Pyroxene Mountain–Fort Selkirk area

The Pyroxene Mountain suite takes its name from prominent exposures of dark green to black clinopyroxenite and hornblendite on Pyroxene Mountain, the largest body of the suite, ~90 km west-northwest of Pelly Crossing (Figs. 2-1 and 2-38a; Ryan *et al.*, 2013). The rocks are typically medium to coarse-grained clinopyroxenite with 5–30 mm pyroxene crystals (Fig. 2-39a),

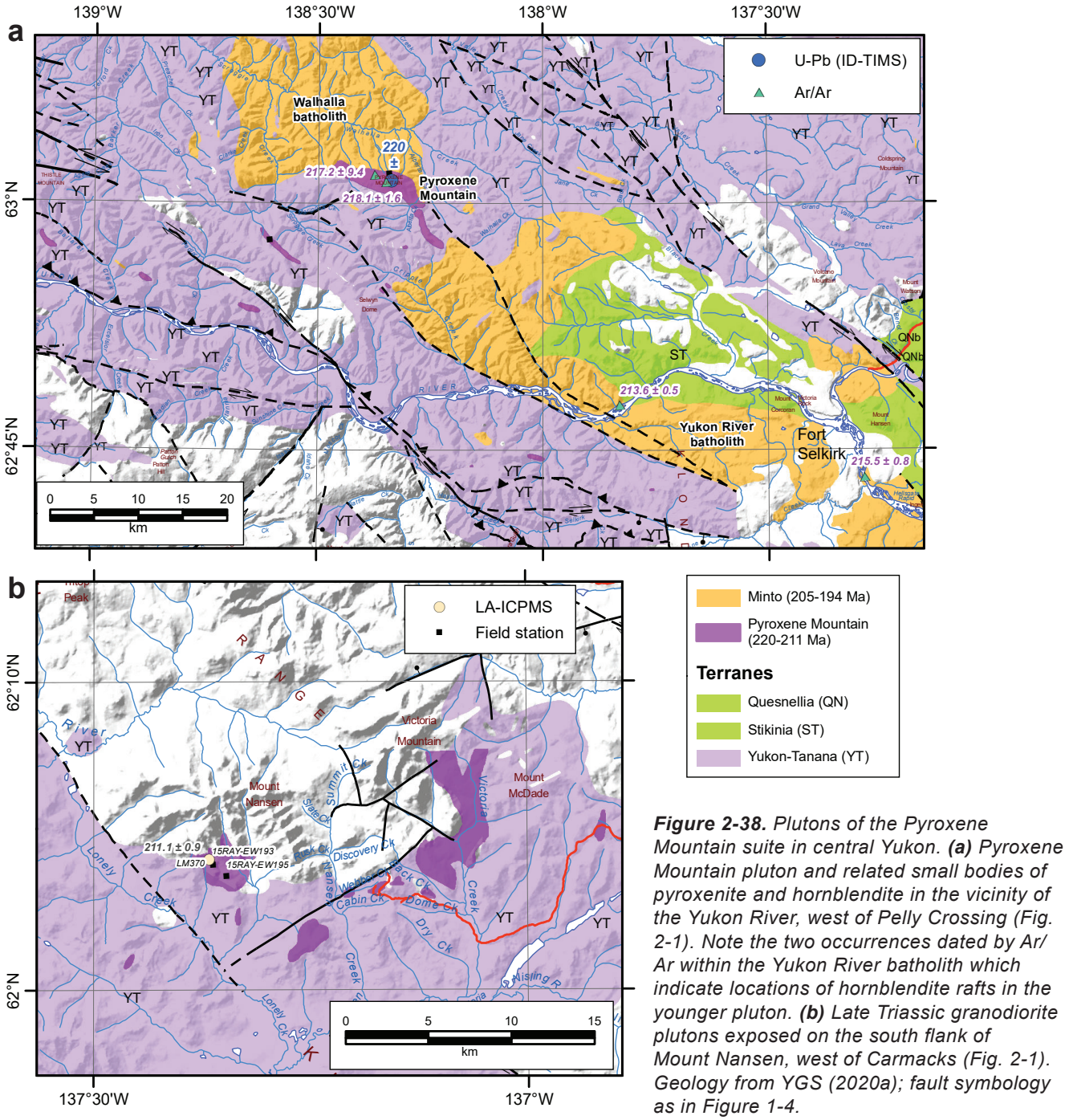


Figure 2-38. *Plutons of the Pyroxene Mountain suite in central Yukon.* ***(a)*** *Pyroxene Mountain pluton and related small bodies of pyroxenite and hornblendite in the vicinity of the Yukon River, west of Pelly Crossing (Fig. 2-1). Note the two occurrences dated by Ar/Ar within the Yukon River batholith which indicate locations of hornblendite rafts in the younger pluton.* ***(b)*** *Late Triassic granodiorite plutons exposed on the south flank of Mount Nansen, west of Carmacks (Fig. 2-1). Geology from YGS (2020a); fault symbology as in Figure 1-4.*

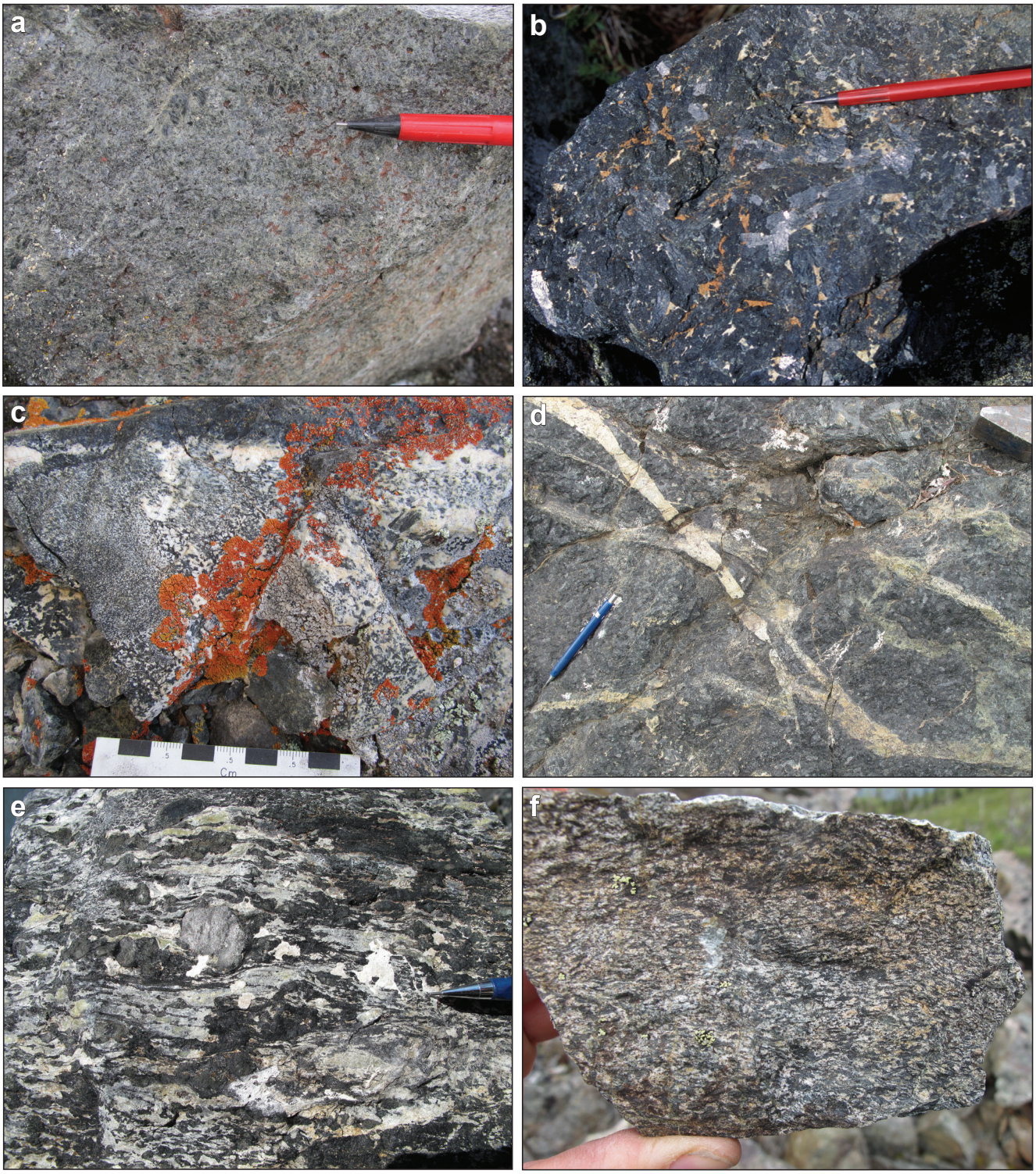


Figure 2-39. *Representative lithology of the Pyroxene Mountain suite in central Yukon.* ***(a)*** *Clinopyroxenite of the Pyroxene Mountain pluton, 14RAY099.* ***(b)*** *Very coarse grained hornblendite from the margin of the Pyroxene Mountain pluton, 01RAY-09-20.* ***(c)*** *Pegmatitic gabbro, Pyroxene Mountain pluton, 11RAYAZ036.* ***(d)*** *Very coarse grained hornblendite cut by felsic dikes occurs as a raft within the Yukon River batholith, 10RAYJR031.* ***(e)*** *Foliated, very coarse grained gabbro from a raft within the Minto pluton, near Fort Selkirk, 10RAYJR104.* ***(f)*** *Weakly foliated coarse-grained monzodiorite from the Mount Nansen area, 15RAY-EW193.*

coarse-grained hornblendite with 5–50 mm hornblende crystals (Fig. 2-39b), and subordinate hornblende gabbro, diorite, trondhjemite and granodiorite. The gabbro is locally pegmatitic (Fig. 2-39c). At Pyroxene Mountain, weakly foliated amphibolite (hornblendite) is developed along the altered margins of a clinopyroxenite core that is generally unfoliated. Veins of hornblendite are locally observed cutting clinopyroxenite. The southern margin of the Pyroxene Mountain body is interpreted to intrude tonalite and granodiorite orthogneiss of the Mississippian Simpson Range suite (Yukon-Tanana terrane; Ryan *et al.*, 2013). Along its northern flank, the Pyroxene Mountain pluton is intruded by Early Jurassic granodiorite of the Walhalla pluton (*ca.* 198 Ma; Minto suite; Fig. 2-38a; *see* Chapter 3). Smaller hornblendite and pyroxenite bodies also occur sporadically southwest of Pyroxene Mountain, on the north side of the Yukon River, and as rafts within the Early Jurassic Yukon River batholith (Figs. 2-38a and 2-39d,e).

Pyroxene Mountain plutons are inferred to be subvolcanic cumulates related to Late Triassic volcanism in Stikinia (Povoas formation; Tempelman-Kluit, 1984, 2009; Ryan *et al.*, 2013). However, a direct relationship between these plutons and the Povoas formation is not observed in the field. The Povoas formation occurs southeast of the northern Yukon River batholith and is isolated from the main pyroxenite massif at Pyroxene Mountain, 15 km to the northwest (Fig. 2-38a). Occurrences of hornblendite lenses within augite-phyric metavolcanic rocks of the Povoas formation in the Fort Selkirk area bear strong similarities to rocks of the Pyroxene Mountain suite, and to amphibolite rafts in the Yukon River batholith (Fig. 39d), supporting comagmatic origins. Rafts of hornblendite and coarse-grained hornblende gabbro within the Early Jurassic pluton are locally strongly foliated (Fig. 2-39e).

Some samples of pyroxenite from Pyroxene Mountain display pristine, unaltered mineralogy, whereas most samples show some degree of alteration, particularly pseudomorphing of pyroxene by hornblende. In gabbroic samples, the plagioclase show various stages of saussuritization.

Geochronology

Previous dating of a hornblendite vein within pyroxenite of the Pyroxene Mountain pluton yielded a $^{40}Ar/^{39}Ar$ hornblende plateau date of 218.1 ± 1.6 Ma (01RAY299B1; Fig. 2-40a; Joyce *et al.*, 2015). Titanite from a trondhjemite dike within the pyroxenite yielded a poor-quality U-Pb date of ~220 Ma (M. Villeneuve, unpublished data, 2003) broadly consistent with the hornblende date.

We present here three new $^{40}Ar/^{39}Ar$ hornblende dates for the Pyroxene Mountain suite (Appendix 6). Sample 11RAYAZ036A is from a hornblende gabbro about 1 km west of sample 01RAY299B1 on Pyroxene Mountain (Fig. 2-38a). It yielded a disturbed age spectrum with dates ranging between 208 ± 9 and 235 ± 3 Ma for 97.3% of ^{39}Ar released (Appendix 6). A poorly resolved inverse isochron yields a date of 217.2 ± 9.4 Ma (MSWD = 80.22) and initial $^{40}Ar/^{36}Ar$ of 358.4 ± 15.9 suggesting that this sample contains excess Ar (Fig. 2-40b; atmospheric $^{40}Ar/^{36}Ar_i$ = 298.56; Lee *et al.*, 2006).

Sample 10RAYJR031A2 is from a raft of hornblendite exposed on the north shore of the Yukon River at the eastern margin of the Yukon River batholith (Fig. 2-38a). Hornblende from this sample yielded a well-defined $^{40}Ar/^{39}Ar$ plateau at 213.6 ± 0.5 Ma (MSWD = 0.81; Fig. 2-40c; Appendix 6). Another sample (10RAYJR013A1) was collected from a raft of hornblende gabbro at the northeastern margin of the Minto pluton, near Fort Selkirk (Fig. 2-38a). Hornblende from this sample yielded a $^{40}Ar/^{39}Ar$ plateau for 72.1% of ^{39}Ar released with a date of 215.5 ± 0.8 Ma (MSWD = 0.24; Fig. 2-40d; Appendix 6). Three lower temperature steps in this sample (25.3% of ^{39}Ar released) yielded younger dates between 206.6 ± 2.7 and 211.2 ± 1.4 Ma that may reflect partial resetting by the Early Jurassic Minto pluton.

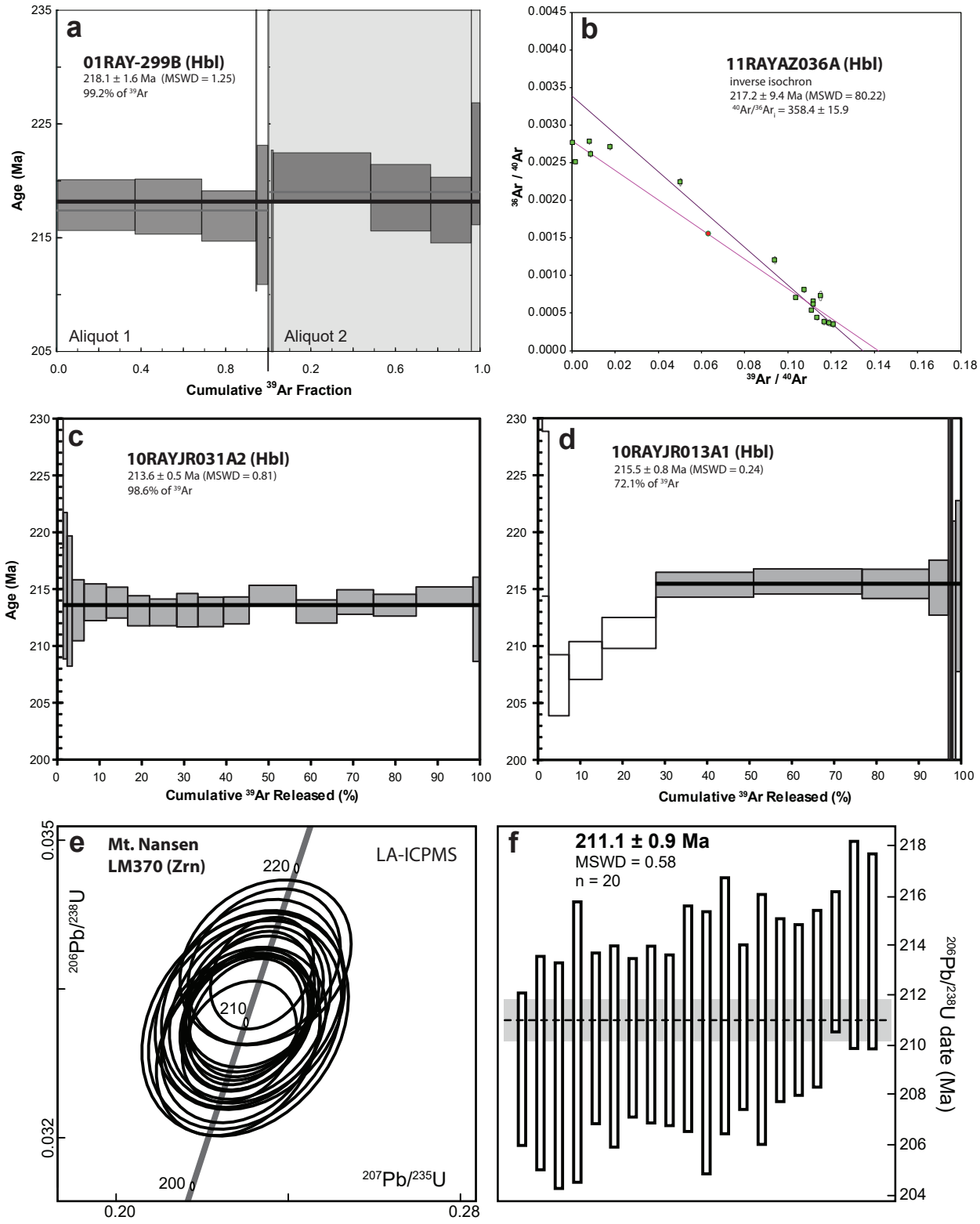


Figure 2-40. *Geochronological data for the Pyroxene Mountain suite.* ***(a)*** *$^{40}Ar/^{39}Ar$ age spectra for 2 aliquots of hornblende from the Pyroxene Mountain pluton (01RAY-299B; from Joyce et al., 2015; Fig. 2-38a).* ***(b)*** *Inverse isochron plot for hornblende from the Pyroxene Mountain pluton (11RAYZA036A, Appendix 6).* ***(c)*** *$^{40}Ar/^{39}Ar$ age spectra for hornblende from an amphibolite raft in the Yukon River pluton (10RAYJR031A2; Appendix 6).* ***(d)*** *$^{40}Ar/^{39}Ar$ age spectra for hornblende from a very coarse grained gabbro raft in the Minto pluton, near Fort Selkirk (10RAYJR013A1; Appendix 6).* ***(e)*** *Concordia diagram and* ***(f)*** *weighted mean plot for LA-ICPMS U-Pb zircon dates from monzodiorite at Mount Nansen (after Klöcking et al., 2016; LM370, Fig. 2-38b).*

Mineral occurrences

The Pyroxene Mountain area has 6 MINFILE occurrences of porphyry Cu (Mo, Au) and related mineralization styles (Fig. 2-41; YGS, 2020b). Of these, 3 are hosted in Paleozoic metamorphic rocks of the Yukon-Tanana terrane in proximity to Cretaceous faults or the mid-Cretaceous Onasick pluton [115I 076, 115J 072, 115O 014]. Two occurrences are hosted in Early Jurassic granodiorite of the Walhalla and Yukon River plutons (Minto suite; discussed in Chapter 3; [115I 102, 115O 085]). The Kerr occurrence [115I 081] is the only drilled porphyry Cu prospect in the area (Fig. 2-41). It is hosted by rocks of the Upper Triassic Povoas formation and the Early Jurassic Yukon River batholith, and consists of disseminated and fracture-controlled pyrite, chalcopyrite and molybdenite hosted by chlorite schist and biotite granodiorite (Sinclair *et al.*, 1976). The northern tip of Stikinia also underlies four single stream sediment anomalies modelled for porphyry Cu (Mo, Au) deposits (Fig. 2-41; Table 2-2; geology levelled, Mackie *et al.*, 2016a,b). These factors combined suggest potential for a porphyry system hosted in Upper Triassic volcanic rocks in this region. The Pyroxene Mountain pluton itself contains a single occurrence, Pyroxene [115O 116], that corresponds with two separate 1 km long coincident electromagnetic conductors and Pt-Pd-Au geochemical soil anomalies (Richards, 1991). Plutons of the Pyroxene Mountain suite are generally magnetic and coincident with magnetic highs on the regional aeromagnetic map (Fig. 2-41b; Hayward and Oneschuk, 2011). In addition, mineralization at the Carmacks Copper and Minto deposits is Late Triassic (*ca.* 217–213 Ma; Kovacs *et al.*, 2020) and thus coeval, and possibly genetically related to rocks of the Pyroxene Mountain suite. This suggests that Pyroxene Mountain suite plutons, and coeval rafts within younger plutons, may be good exploration targets.

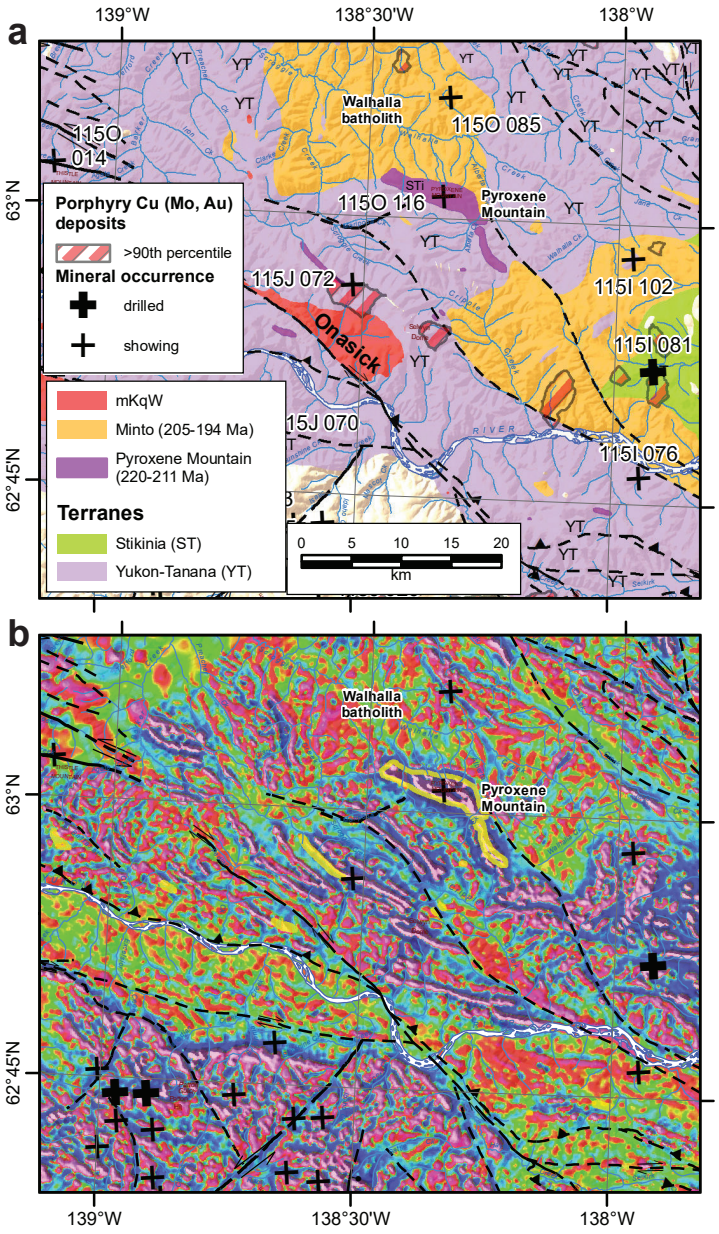


Figure 2-41. (a) *Simplified geology overlain with weighted sums models of regional geochemical stream sediment data in the Pyroxene Mountain area. Red hatched catchment basins represent >90th percentile data when ranked by importance for porphyry Cu (Mo, Au) deposits in the respective NTS sheet (Mackie et al., 2016a,b). Weighted sums modelling and importance rankings for various deposit types are described in more detail in Mackie et al. (2015).* ***(b)*** *First vertical derivative aeromagnetic map of the Pyroxene Mountain area (Hayward and Oneschuk, 2011). Yellow lines outline plutons of the Pyroxene Mountain suite.*

Table 2-2. *Summary of select catchment basins with regional geochemical stream sediment data >90th percentile for geology levelled weighted sum models of Mackie et al. (2016a–f). 90th percentile thresholds from Héon (2003) using data from the Intermontane terranes.*

		Ag (ppb)	Au (ppb)	Cu (ppm)	Mo (ppm)	Tl (ppm)
N Stikina (n = 4)	minimum	66	0.6	13.88	0.46	0.05
	maximum	131	4.8	46.4	3.35	0.09
Clair Lake (n = 15)	minimum	34	0.5	13.1	0.4	0.05
	maximum	143	7	94.8	2.62	0.22
Mt Stutzen (n = 9)	minimum	19	BD	7.05	0.17	BD
	maximum	133	3.2	38.38	2.68	0.28
90th percentile threshold		200	10	43	4	NA

Mount Nansen area

A series of small Late Triassic plutons also intrude the Yukon-Tanana terrane in the Mount Nansen area, approximately 55 km west of Carmacks (Figs. 2-1 and 2-38b). There the rock consists of a coarse-grained, foliated hornblende-biotite monzodiorite to quartz monzonite (Fig. 2-39f) that intrudes amphibolite, orthogneiss, quartzite, and schist of the Yukon-Tanana terrane (Klöcking *et al.*, 2016; Ryan *et al.*, 2016). The northernmost exposures of these plutons are either intruded by the mid-Cretaceous Dawson Range batholith or unconformably overlain by andesitic volcanic rocks of the mid-Cretaceous Mount Nansen Group. Klöcking *et al.* (2016) reported LA-ICPMS U-Pb analyses of zircon from a monzodiorite pluton along the south flank of Mount Nansen, above Lonely Creek (Fig. 2-38b). Their sample LM370 yielded $^{206}Pb/^{238}U$ dates ranging from 214.3 ± 2.0 to 208.8 ± 1.6 Ma, with a weighted mean of 211.1 ± 0.9 Ma (Fig. 2-40e,f). These results may indicate association with Late Triassic intrusive rocks of the Pyroxene Mountain and Stikine suites.

Mineral occurrences

The Mount Nansen area has more than 20 porphyry and epithermal vein occurrences including the Klaza, Mount Nansen and Brown-McDade deposits (Casselman, 2018). These mineral occurrences are all hosted by, and likely all related to, Cretaceous igneous rocks (*e.g.*, Mortensen *et al.*, 2016). The Late Triassic plutons in this area are not associated with known mineral occurrences (YGS, 2020b), although the Cretaceous mineralizing systems could possibly mask older Late Triassic mineralization.

Headless suite

Two small plugs of felsic to intermediate plutonic rocks intrude mafic volcanic rocks of the Upper Triassic Semenof formation, a major component of Quesnellia in southern Yukon (Fig. 2-1; Tempelman-Kluit, 1984, 2009; Simard, 2003; Simard and Devine, 2003; Colpron *et al.*, 2016a). These two plugs, east of the Teslin fault were described and sampled during regional mapping (Tempelman-Kluit, 1984, 2009; Colpron *et al.*, 2002, 2003). The Headless plug, ~42 km south of Little Salmon Lake (Fig. 2-42), is a small body (~1 km^2) of hornblende diorite that intrudes mafic volcaniclastic rocks of the Semenof formation (Upper Triassic; Tempelman-Kluit, 1984, 2009). The diorite is medium grained and equigranular, and locally contains mafic xenoliths and schlieren up to a few centimetres in size. Hornblende is fresh and euhedral, and makes up to 20% of the rock, with intergrown euhedral plagioclase (>70%), interstitial quartz (≤10%) and minor titanite (Fig. 2-43). The plagioclase is mildly saussuritized.

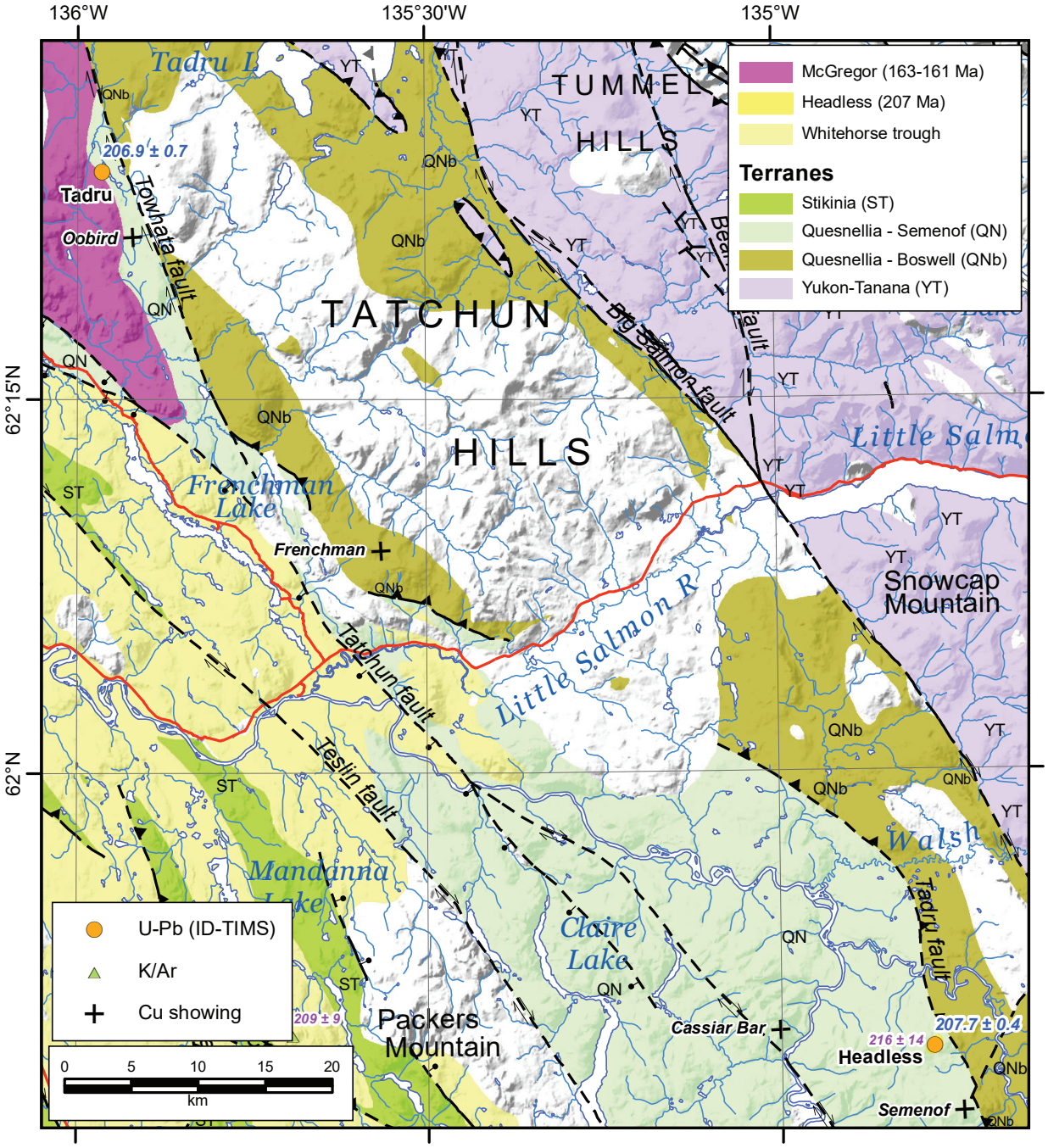


Figure 2-42. *Occurrences of small plugs and dikes of the Headless suite in Quesnellia, central Yukon.*

North of Frenchman Lake and ~15 km southwest of Tadru Lake (Fig. 2-42, Tadru), a 2 m wide dike of quartz-feldspar porphyry intrudes augite-phyric basalt of the Semenof formation (inferred to be Povoas formation by Colpron *et al.*, 2002, 2003). The dike is fine-grained, weakly foliated and concordant with foliation in the basalt near the Towhata fault. These rocks are intruded by granodiorite of the Middle Jurassic McGregor pluton to the west (Fig. 2-42).

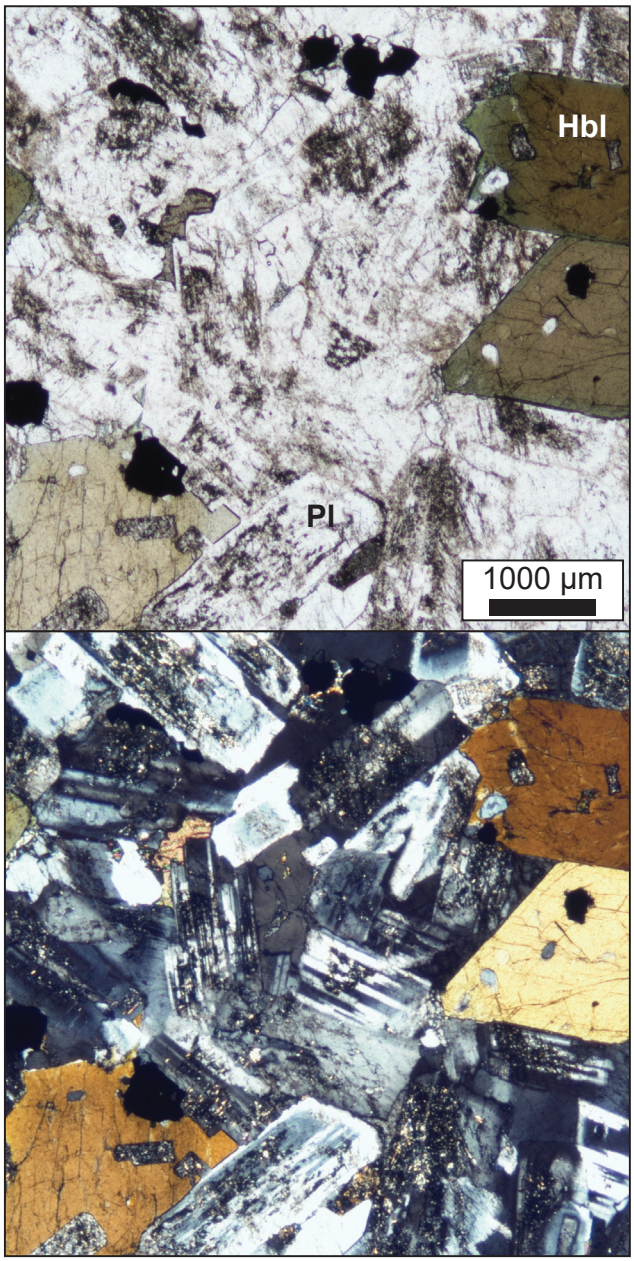


Figure 2-43. *Transmitted light photomicrograph pair for 01MC296 from the Headless plug; plane polarized light (upper) and cross-polarized light (lower).*

Geochronology

Stevens *et al.* (1982a) reported a K-Ar date of 216 ± 14 Ma for hornblende from the Headless plug (Fig. 2-42). We collected a sample for U-Pb geochronology during reconnaissance fieldwork in 2001. Sample 01MC296 yielded a large amount of zircon, most of which comprises elongate, euhedral, pale yellow prisms with no optically visible zoning or cores. Four fractions of strongly air-abraded zircon were analyzed by ID-TIMS at the University of British Columbia (J.K. Mortensen, unpublished data, 2002). Fraction B yielded a concordant analysis with a $^{206}Pb/^{238}U$ date of 207.7 ± 0.4 Ma, which is interpreted to be the crystallization age of the rock (Fig. 2-44a). The other three fractions yield slightly older U/Pb and Pb/Pb dates and are interpreted to have contained a minor component of older, inherited zircon.

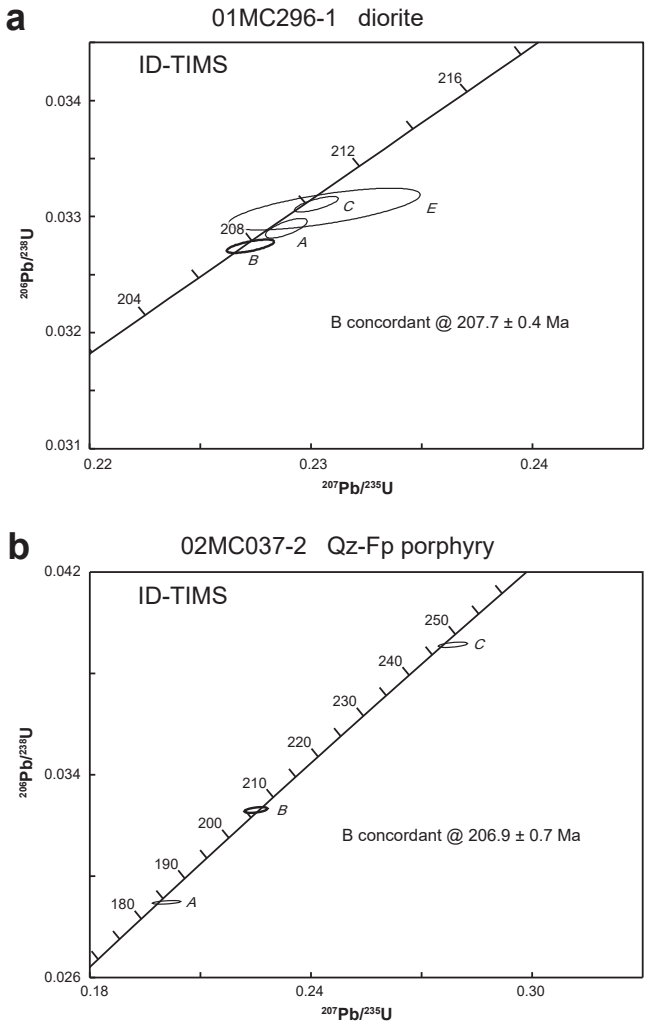


Figure 2-44. *Concordia diagrams for multi-grain, air abraded zircon fractions analyzed by ID-TIMS at UBC (J.K. Mortensen, unpublished data, 2002).*
(a) *01MC296;* ***(b)*** *02MC037-2.*

A sample of quartz-feldspar porphyry at the Tadru locality (02MC037-2) yielded 3 zircon fractions that were analyzed by ID-TIMS at UBC. Fraction B is concordant with a $^{206}Pb/^{238}U$ date of 206.9 ± 0.7 Ma (Fig. 2-44b; Appendix 7). Two other zircon fractions are slightly discordant; fraction C is interpreted to contain older inherited components, whereas the younger fraction A is inferred to have suffered Pb loss.

Mineral occurrences

The mineral potential associated with the Headless plug and Tadru dike has not been studied in detail, but it is notable that occurrences of disseminated chalcopyrite, bornite, azurite and malachite in mafic volcanic rocks of the Upper Triassic Semenof formation occur within 5–10 km of these intrusions (Fig. 2-42; Semenof [105E 014] and Cassiar Bar [105E 016] occurrences near Headless plug; Oobird [105L 061] south of the Tadru dike; YGS, 2020b). In addition, two areas partly underlain by Upper Triassic volcanic rocks west of the Headless plug contain sizeable regional stream sediment anomalies in weighted sum modelling for porphyry Cu and epithermal deposits (Table 2-2; Fig. 2-45; Mackie *et al.*, 2016c–f). The largest of these anomalies is located 20 km west of the Headless plug and is centred on Claire Lake (Fig. 2-45). The anomaly consists of 15 samples over a contiguous drainage area of 350 km² with ≥90th percentile stream sediment data when levelled for geology and modelled for porphyry copper and epithermal deposits (Table 2-2; Mackie *et al.*, 2016f). The Claire Lake anomaly straddles the Teslin fault and is underlain by felsic volcanic rocks of the Cretaceous Mt. Nansen Group to the west, and Upper Triassic mafic volcanic rocks of the Semenof formation to the east (Fig. 2-45). Both units and the fault may contribute to this anomaly.

The Mount Stutzen anomaly corresponds to a large (120 km²) multi-sample stream sediment anomaly partly underlain by a thrust imbricate of Upper Triassic volcanic rocks in the northern Whitehorse trough (Table 2-2; Fig. 2-45; Mackie *et al.*, 2016c–f). The presence of these two large regional stream sediment geochemistry anomalies associated with Upper Triassic volcanic rocks of Stikinia and Quesnellia could indicate prospectivity for Late Triassic porphyry and epithermal deposits in the area southeast of Carmacks.

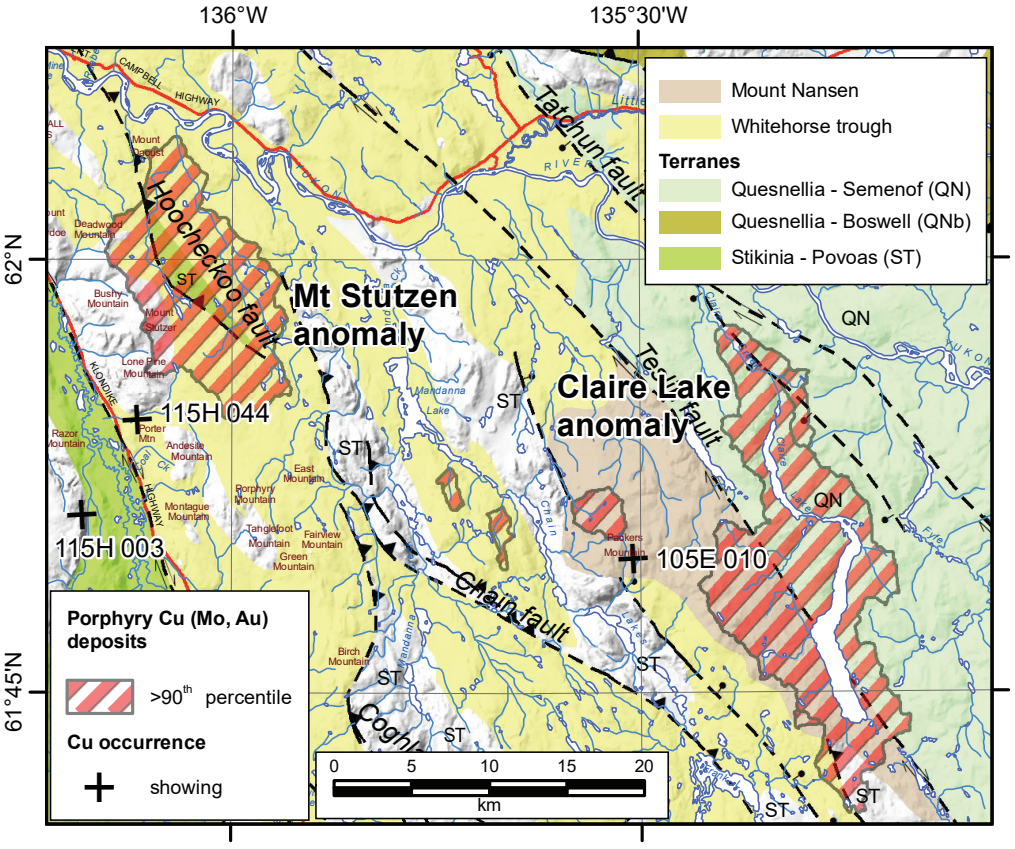


Figure 2-45. *Simplified geology overlain with weighted sums models of regional geochemical stream sediment data. Red hatched catchment basins represent >90th percentile data when ranked by importance for porphyry Cu (Mo, Au) deposits in the respective NTS sheet (Mackie et al., 2016c–f). Weighted sums modelling and importance rankings for various deposit types are described in more detail in Mackie et al. (2015).*

Geochemistry

Fourteen samples from Stikine suite plutons were analyzed for whole-rock geochemistry as part of this study (Appendix 8). One sample from the Tally-Ho leucogabbro is from a fractionated felsic pod and not representative of its dominant lithology, and one sample from the Red Ridge pluton shows evidence of propylitic alteration and has a loss-on-ignition value of 3.2% (Appendix 8). The remaining samples (n = 12) include at least one from each of the five plutons described above and are considered representative of the Stikine suite.

Only a few (7) samples from the Pyroxene Mountain suite were analyzed for major and trace element geochemistry (Klöcking *et al.*, 2016; Ryan *et al.*, 2018; Appendix 8). Of these, four samples from the Pyroxene Mountain area (Fig. 2-38a) are mostly from coarse-grained (to pegmatitic), mafic-ultramafic pyroxenite and gabbro that may be cumulate phases and not representative of the bulk composition of the magma. More typical medium to coarse-grained diorite and gabbro were sampled from the Mount Nansen area (Appendix 8).

Only one sample from each of the two Headless plugs were analyzed for major and trace elements geochemistry (Appendix 8). Sample 02MC037-2 from the Tadru dike (Fig. 2-41) is highly fractionated with high $Si0_2$ values and is also not considered representative of the bulk magma composition (Fig. 2-46).

Major elements

Samples from the Late Triassic plutons in southern Yukon show a wide range of SiO_2 values, with two main clusters at 48–55% and 61–67% (Figs. 2-46 and 2-47). Most samples have magnesian, calc-alkalic to alkali-calcic, metaluminous compositions, with samples from the Tally Ho, King Lake and Red Ridge plutons (Stikine suite) exhibiting slight alkalic tendencies (Figs. 2-3, and 2-46 to 2-48). In general, the Late Triassic plutons plot along linear fractionation trends showing Na_2O enrichment, and depletion in FeO*, MgO, TiO_2 and CaO with increasing SiO_2 values. The Pyroxene Mountain samples form a distinct cluster with low SiO_2, Na_2O and K_2O, and high MgO, FeO* and CaO values consistent with a probable cumulate origin.

Trace elements

Trace element patterns for samples of the Stikine suite show trends typical of subduction-related arc magmas with negative Nb and Ti anomalies (Sun and McDonough, 1989), Th/Nb_N of ~7.3, and La/Yb_N of ~8.3 on primitive mantle normalized plots (Fig. 2-49a), and slight depletion in LILE compared to average upper continental crust (Fig. 2-49b). Small negative Sm, Y and Ti (relative to Zr) anomalies (Fig. 2-49a) indicate minor fractionation (Pearce, 1996) in the Stikine suite.

Samples from the Mount Nansen area have generally flatter patterns (La/Yb_N of ~5) with a less pronounced

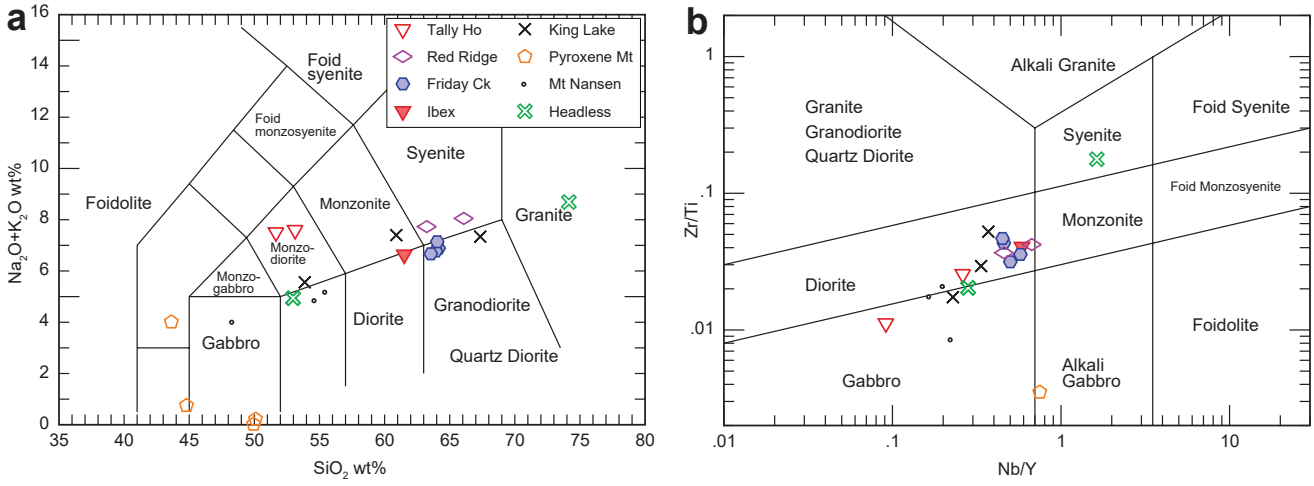


Figure 2-46. (a) *Total alkali-silica diagram for Late Triassic plutons in southern Yukon (adapted from Le Bas et al., 1986, for plutonic rocks).* ***(b)*** *Zr/Ti vs. Nb/Y classification diagram of Winchester and Floyd (1977) as modified by Pearce (1996).*

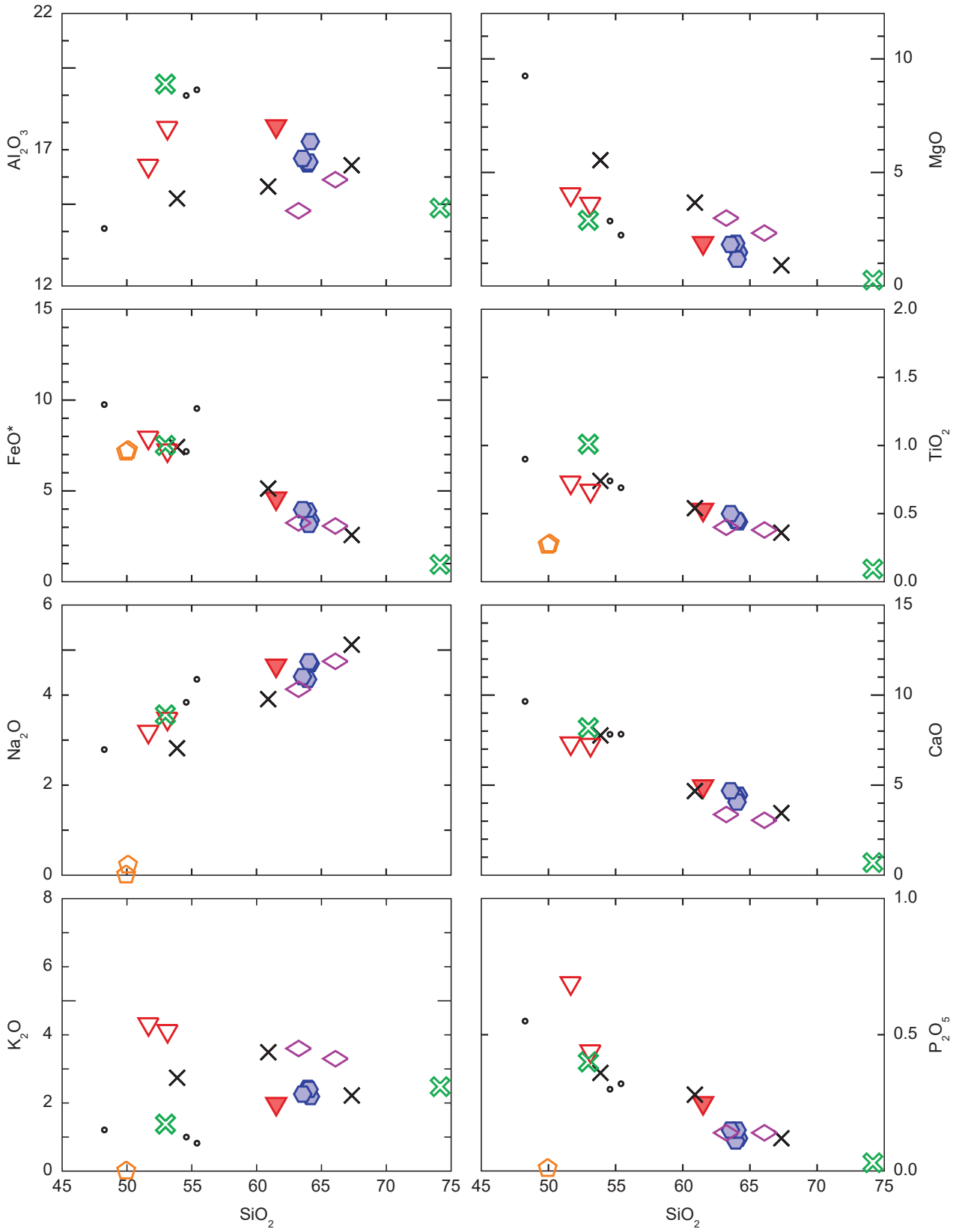


Figure 2-47. *Major elements vs. SiO_2 Harker plots for Late Triassic samples. Symbols as in Fig. 2-46.*

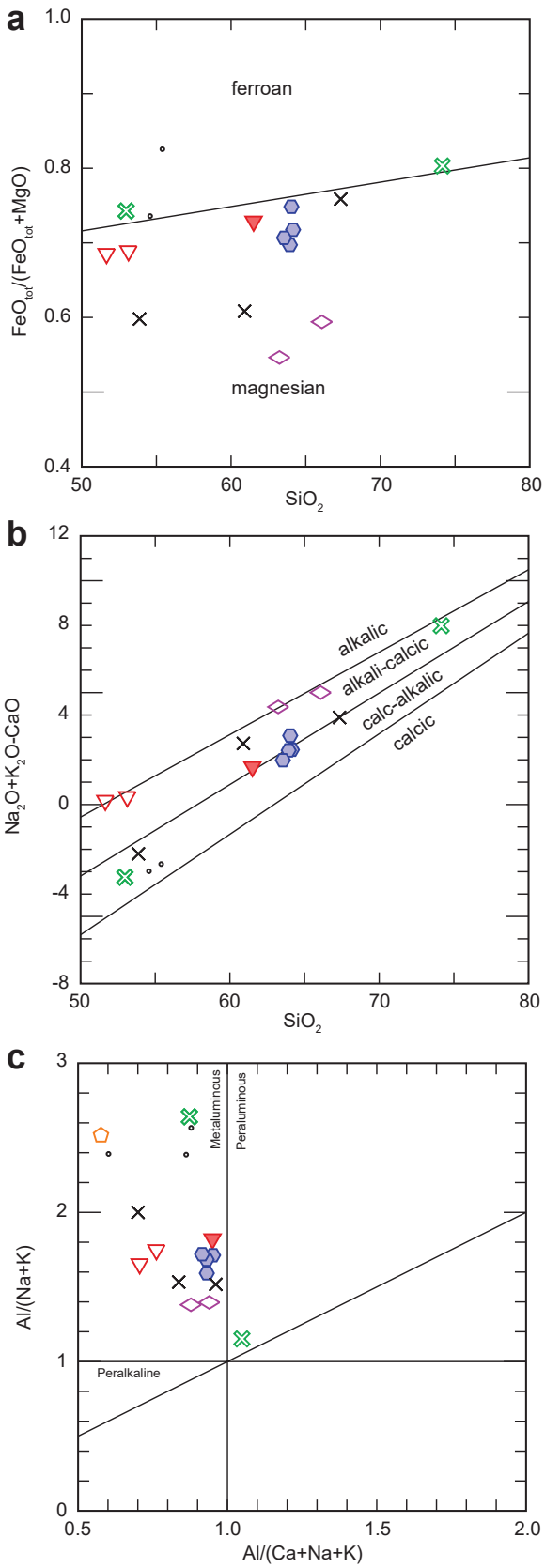


Figure 2-48. *Geochemical classification using criteria of Frost et al. (2001).* ***(a)*** *Fe-number,* ***(b)*** *modified alkali-lime index (MALI), and* ***(c)*** *alumina saturation index (ASI; from Shand, 1943). Symbols as in Figure 2-46.*

negative Nb anomaly (Th/Nb$_N$ of ~2.5) on primitive mantle-normalized plots (Fig. 2-49c), and strong depletion in Th, Zr and Hf relative to average upper continental crust (Fig. 2-49d). These patterns are typical for granitic rocks with a ferroan island arc (tholeiitic) composition (Frost *et al.*, 2001). Two of the Pyroxene Mountain samples are strongly depleted in LILE and exhibit strong negative Zr anomalies consistent with their coarse-grained, cumulate origins (Fig. 2-49c,d). A coarse-grained hornblende gabbro collected west of Scroggie Creek (Fig. 2-38a) has trace element patterns (La/Yb$_N$ = 8.4, and slight negative Zr anomaly) that more closely match samples from the Mount Nansen area, except for its Th depletion relative to Nb (Th/Nb$_N$ = 0.3; Fig. 2-49c).

The sample from the Headless plug, intruding volcanic rocks of the Semenof formation (Quesnellia) east of Teslin fault (Fig. 2-42), also has trace element patterns comparable to those from the Mount Nansen area with relatively flat primitive mantle-normalized pattern (La/Yb$_N$ = 3.4) and slight negative Nb and Ti anomalies (Th/Nb$_N$ = 1.7; Fig. 2-49e). The highly fractionated dike sampled at the Tadru occurrence exhibits strongly depleted trace element patterns with strong enrichments in Zr and Hf (Fig. 2-49e,f). All Late Triassic samples plot in the volcanic arc field on the Yb/Ta tectonic discrimination diagram (Fig. 2-50; Pearce *et al.*, 1984) and fall within the 'I-type' classification of Chappell and White (2001; Fig. 2-51).

Zircon chemistry

Zircons from three samples of the Stikine suite dated in this study were also analyzed for trace elements using the LA-ICPMS at Boise State University (Appendix 3). Zircons from all three samples have a similar range in Hf of 7700–10400 ppm, with a few analyses from the Red Ridge pluton yielding slightly higher Hf content up to 11 500 ppm (Fig. 2-52a–c). The Stikine suite plutons yielded Ti-in-zircon temperatures ranging from ~650–800°C, with zircons from the Friday Creek pluton yielding consistently high temperatures (mean = 752°C) and those from the Red Ridge pluton plotting near the lower end of the range (mean = 685°C; Fig. 2-52a). There is no apparent change in Ti-in-zircon temperature with increasing Hf content in Stikine suite samples.

Zircons from Stikine suite samples have U and Y contents consistent with granodiorite to tonalite compositions (Fig. 2-52b) and plot within the continental arc field of the U/Yb *vs.* Gd/Yb discriminant diagram of Grimes *et al.* (2015).

Isotopes

One sample from the Friday Creek pluton, 15PS054-1, and one from the Ibex Mountain pluton, 15PS133-1, were analyzed for whole-rock Sr and Nd isotopes, and Pb isotopes in K-feldspar (Appendix 9). Initial $^{87}Sr/^{86}Sr$ (Sr_i) values for both samples are near 0.704, initial $^{143}Nd/^{144}Nd$ values are 0.5126 (εNd_t = 5.2–5.3), and $^{207}Pb/^{204}Pb$ values are near 15.58 (Appendix 9). These results are consistent with juvenile magma sources that are relatively uncontaminated by crustal material (*e.g.*, Armstrong, 1988).

A subset of the zircon from these same samples was analyzed for Lu-Hf by LA-ICPMS at Memorial University of Newfoundland (Appendix 10). The location of loss spots were chosen to match U-Pb LA-ICPMS analyses from Boise State University (Appendix 3). Zircons from both the Friday Creek and Ibex plutons yielded εHf_i values of +9.7 to +11.5 which are also indicative of juvenile magma sources (Fig. 2-53). The Stikine suite plutons are the most juvenile magmatic rocks of all Late Triassic to Jurassic plutons in the Intermontane terranes of Yukon.

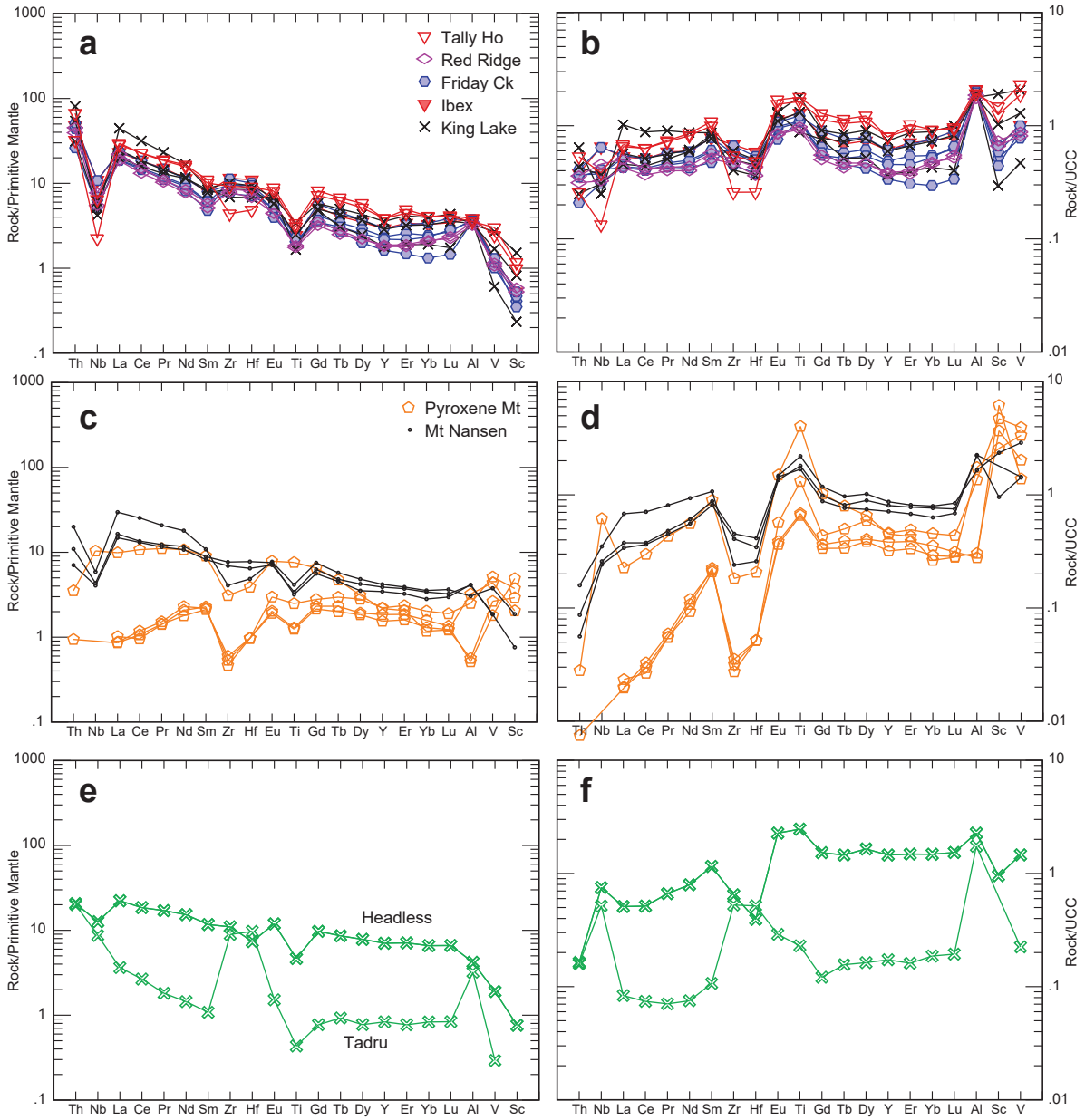


Figure 2-49. *Left - Primitive mantle normalized spider plots using values from McDonough and Sun (1995). Right - Upper continental crust (UCC) normalized spider plots using values from McLennan (2001).* ***(a*** *and* ***b)*** *Stikine suite;* ***(c*** *and* ***d)*** *Pyroxene Mountain suite;* ***(e*** *and* ***f)*** *Headless suite.*

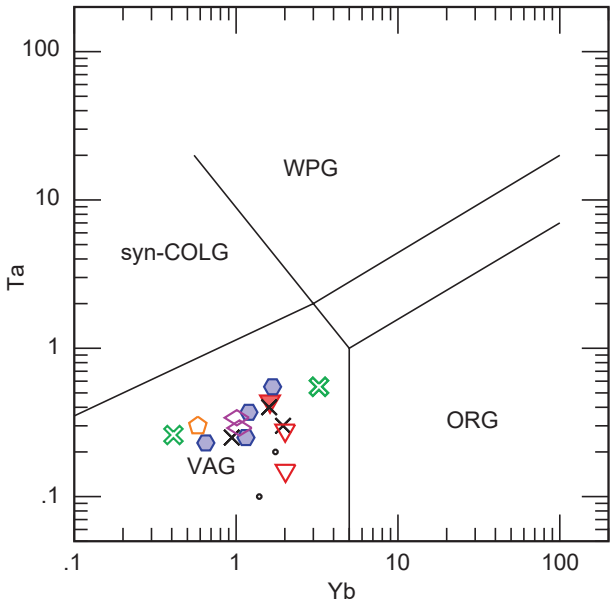


Figure 2-50. *Tectonic discrimination diagram for granitoid rocks from Pearce et al. (1984). VAG = volcanic arc granite, ORG = ocean ridge granite, WPG = within plate granite and COLG = collisional granite. Symbols as in Fig. 2-46.*

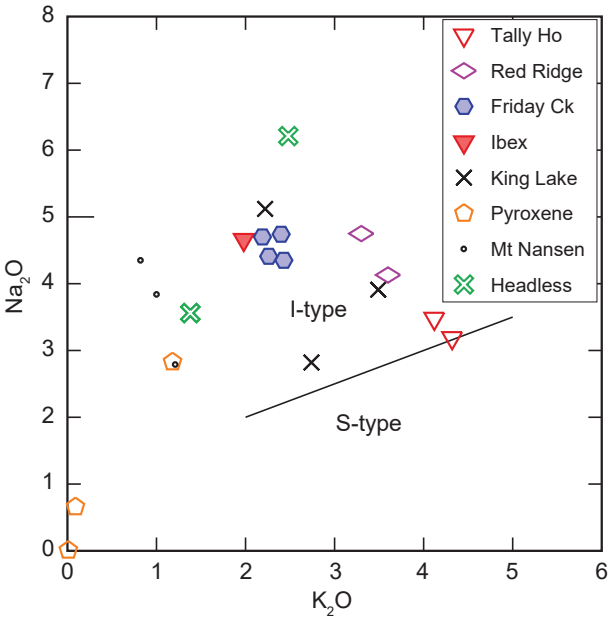


Figure 2-51. *Na_2O vs K_2O for Late Triassic plutons in Yukon. The boundary between 'I-type' and 'S-type' granitoid rocks is from Chappell and White (1974).*

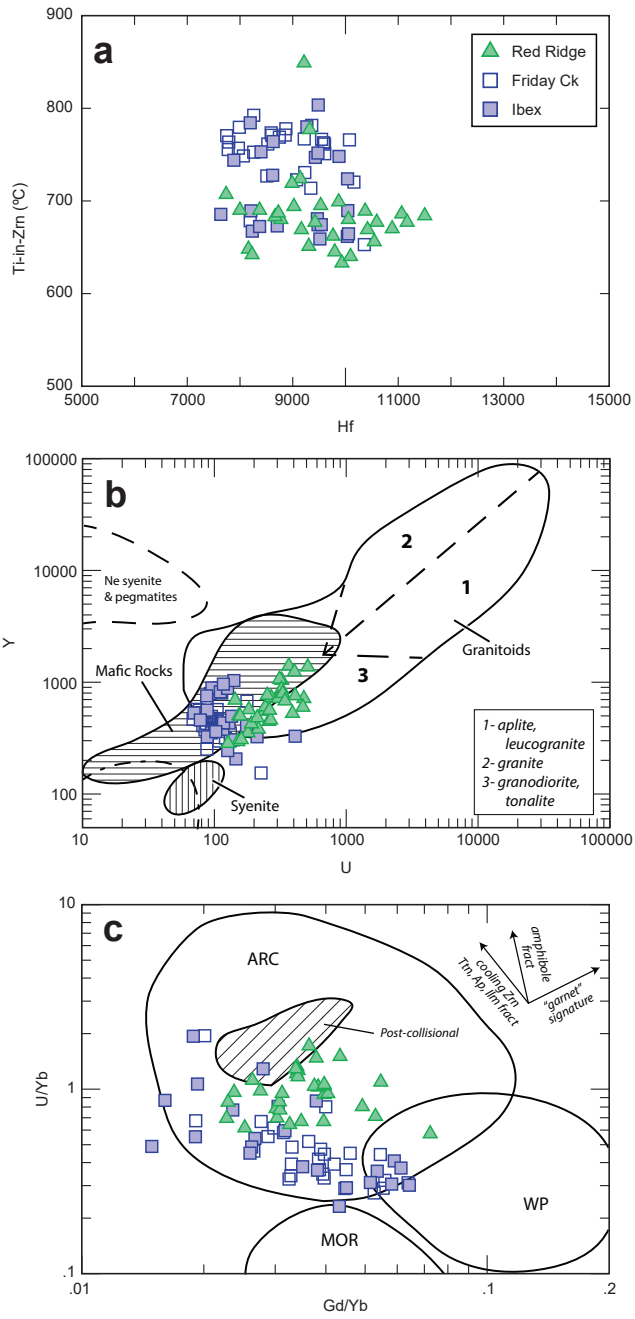


Figure 2-52. *Trace element zircon chemistry from LA-ICPMS analyses of samples from the Stikine suite (Appendix 3).* ***(a)*** *Plot of crystallization temperature estimates (Ti-in-zircon) vs. Hf concentrations in zircons.* ***(b)*** *Y vs. U classification diagram of Belousova et al. (2002).* ***(c)*** *Discriminant diagram of Grimes et al. (2015). Fract = fractionation.*

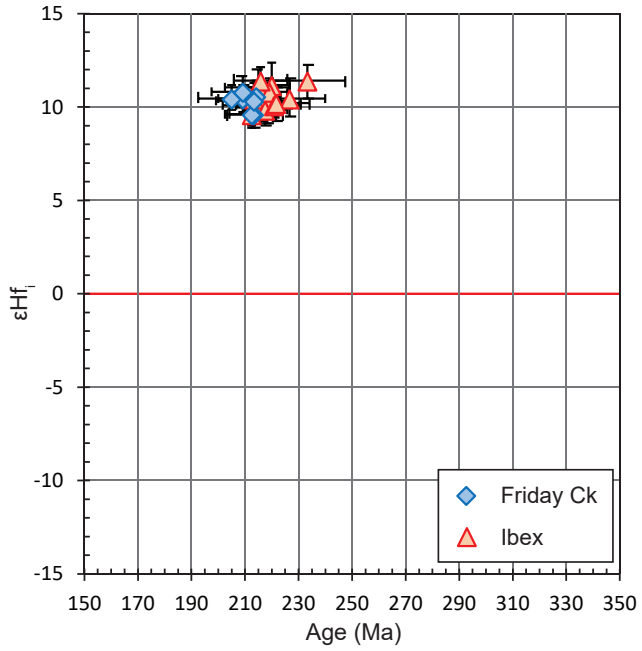


Figure 2-53. *Hf isotopic data for selected zircons from the Friday Creek and Ibex plutons, Stikine suite (Appendix 9). Error bars are 2σ.*

Discussion

Late Triassic plutons inferred to be related to arc volcanism in northern Stikinia intrude the Upper Triassic Lewes River Group southwest of Whitehorse and metamorphic rocks of the Yukon-Tanana terrane northwest of Carmacks (Fig. 2-1). Our dating of the Stikine suite southwest of Whitehorse (Fig. 2-2) using the CA-TIMS method on zircon tightly constrains it to *ca.* 217–214 Ma (Fig. 2-54), and refines the previous, less precise range of *ca.* 220–208 Ma (Hart, 1995). The Stikine suite plutons have the geochemical characteristics of calc-alkalic to alkali-calcic arc magma emplaced above a subduction zone (Figs. 2-48 to 2-50) with juvenile isotopic compositions (Appendix 9) consistent with derivation from the mantle wedge. The lack of inheritance in zircons from Stikine suite plutons (Appendix 3) and their juvenile isotopic compositions (Appendix 10; Fig. 2-53) show no evidence for interaction with evolved continental crust, supporting this interpretation. Geobarometric estimates from one Stikine suite pluton (Friday Creek; Appendix 5) suggest emplacement in the middle crust (~3.0–3.5 kbar, or 12–13 km); this is consistent with a maximum lower greenschist (chlorite grade or generally lower) metamorphism of country rocks intruded by Stikine plutons (Read *et al.*, 1991).

Plutons of the Pyroxene Mountain suite, west and north of Carmacks (Fig. 2-1), have not yielded as precise dates as those from the Stikine suite (Fig. 2-54). The *ca.* 218 Ma hornblende date from the Pyroxene Mountain pluton (Joyce *et al.*, 2015), and $^{40}Ar/^{39}Ar$ hornblende dates of 216–214 Ma from amphibolite rafts in the Yukon River batholith and Minto pluton (Fig. 2-40; Appendix 6) support correlation with the Stikine suite. Similar dates in the 217–214 Ma range are also evident in inherited zircons from the Minto pluton and Granite Mountain batholith (Minto suite; *see* Chapter 3). The range of U-Pb zircon LA-ICPMS dates for a pluton near Mount Nansen (Fig. 2-40c) is comparable to LA-ICPMS dates in our dated Stikine suite samples (Figs. 2-18b, 2-23b and 2-29b) and could reflect a similar age in the 217–214 Ma range if dated more precisely. The geochemistry of more representative samples from the Mount Nansen area resemble that of Stikine suite plutons to the south, although they appear to be slightly more tholeiitic (Fig. 2-49). If future more precise dating of the Pyroxene Mountain plutons confirms their correlation with the Stikine suite, then these intrusions provide a strong argument that Yukon-Tanana forms the “basement” upon which Triassic volcanism in Stikinia was deposited.

Small diorite plugs of the Headless suite yielded dates of *ca.* 207 Ma (Fig. 2-44; Appendix 7). Although these samples are not as precisely dated as our Stikine suite samples, the results from the Headless suite are consistently younger and unlikely to be as old as 217–214 Ma (Fig. 2-54). Therefore, the Headless suite is unlikely to be directly correlated with the Stikine and Pyroxene Mountain suites which intrude Stikinia. The Headless suite intrudes coeval volcanic strata of the Semenof formation (Colpron *et al.*, 2003) and therefore can be inferred to have been emplaced at high crustal levels.

The Stikine plutonic suite is part of the Stikine magmatic arc (Nelson *et al.*, 2013) and the plutons have geochemistry consistent with subduction-derived magmas indicating a tectonic setting amenable to development of porphyry-style mineralization. In general, the plutons are weakly to strongly oxidized, with juvenile isotopic signatures indicating that metals such as Cu and Mo may have been available, and mobile, for mineralization processes (Fig. 2-55; Thompson *et al.*, 1999).

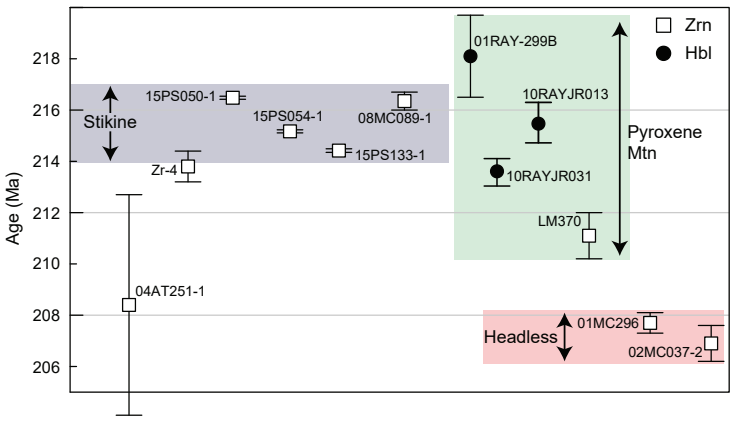


Figure 2-54. *Summary plot of $^{206}Pb/^{238}U$ zircon dates and one $^{40}Ar/^{39}Ar$ hornblende date from Late Triassic plutons in Yukon. Error bars are 2σ. Shaded grey area represents the refined age range of the Stikine plutonic suite from the present study. The green area indicates range of the Pyroxene Mountain suite from existing data, and the pink area is range of unpublished dates from the Headless plugs in Quesnellia. Geochronological data is from compilation in Appendix 1.*

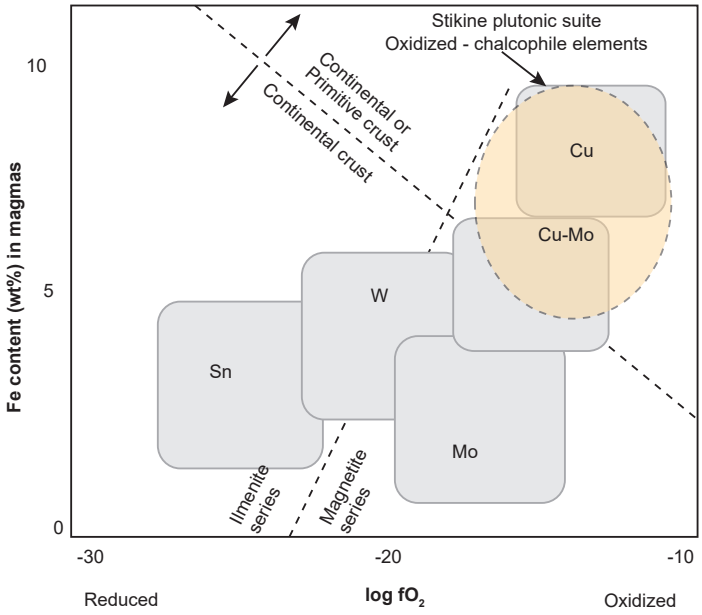


Figure 2-55. *Schematic plot of degree of fractionation, shown by the Fe content, versus oxidation state (fO_2) for calc-alkalic to alkalic magmas associated with magmatic-hydrothermal mineralization (modified from Thompson et al., 1999). The generalized position of the Stikine plutonic suite, with a potential Cu-Au (chalcophile) association is shown by the orange ellipse. Boundary between the magnetite and ilmenite magma series is from Ishihara (1977).*

Pluton emplacement depth for the Friday Creek pluton, the only Stikine suite pluton amenable to the Al-in-Hbl geobarometry, is between 8.5 and 16.7 km (when considering errors). These are near the deeper end of emplacement depths inferred for 'deep porphyry' systems (Seedorff *et al.*, 2008), and may suggest that Late Triassic plutons in Yukon are more prospective for deposit styles such as skarns. One notable exception may be the Red Ridge pluton which hosts Cu (± Mo) sulphides within veins that have open space textures suggestive of emplacement at a shallow (<10 km?) crustal level. Alteration in this pluton precludes estimation of emplacement depths using the Al-in-Hbl geobarometer, but Ti-in-zircon thermometry for the Red Ridge pluton (~685°C; Appendix 3) are ~70°C lower than that of the Friday Creek pluton (~752°C; Fig. 2-52), and may suggest a shallower emplacement depth for the Red Ridge pluton. The King Lake pluton is also associated with Cu (± Mo, Au) mineralization, but this pluton does not have suitable mineralogy for Al-in-Hbl geobarometry and its emplacement depth remains unknown. However, the lack of open space textures within mineralized veins suggest a deeper (>10 km?) emplacement depth and thus the King Lake pluton may be more prospective for skarn mineralization.

Most porphyry deposits form in the upper 5 km of the crust (Seedorff *et al.*, 2005) with broadly coeval volcanic rocks commonly making up a significant proportion of the surface geology (Sillitoe and Perello, 2005). In some cases, the volcanic rocks can also host significant porphyry mineralization (*e.g.*, Copper Mountain; Preto, 1972). Within Stikinia and Quesnellia in Yukon, the Povoas (Lewes River Group) and Semenof formations are regionally extensive Upper Triassic volcanic units that are broadly correlative with the Nicola, Stuhini and Takla groups of British Columbia (*e.g.*, Souther, 1991).

They are generally only mildly metamorphosed in central Yukon and locally intruded by high-level subvolcanic plugs, such as the Headless plugs in northern Quesnellia (Figs. 2-1 and 2-42). The region east of Carmacks is generally poorly exposed and Late Triassic intrusions are apparently sparse. Yet the presence of large, multi-sample stream sediment anomalies near the northern apex of Triassic Stikinia and Quesnellia (Fig. 2-45) suggests potential for buried porphyry systems in this region. We also note that mineralized meta-igneous rafts at the Carmacks Copper and Minto deposits are Late Triassic (*ca.* 217 Ma) and that the porphyry copper mineralization is >213 Ma (Kovacs *et al.*, 2020). These rafts were deformed and metamorphosed prior to being engulfed by latest Triassic to earliest Jurassic Minto suite plutons (*ca.* 205 to 194 Ma; *see* Chapter 3). Occurrences of *ca.* 218 to 214 Ma meta-igneous rafts and bodies within the Pyroxene Mountain, Yukon River, Minto and Granite Mountain batholiths are potential targets for Minto-style, Late Triassic mineralization.

Chapter 3
Latest Triassic–Early Jurassic

Minto suite (205–194 Ma)

Summary

Plutons of the Minto suite (205–194 Ma) form large batholiths that intrude Quesnellia, Stikinia and the Yukon-Tanana terranes in central Yukon. They comprise mainly granodiorite of metaluminous, calc-alkalic to weakly alkalic compositions and have isotopic compositions consistent with a small degree of assimilation of older crust ($^{87}Sr/^{86}Sr_i$ = 0.7047 to 0.7062; εNd_t = -3.6 to +1.3). This is reflected in Mississippian and Late Triassic inherited zircon components in samples from the Granite Mountain, Minto and Tatchun plutons. The Minto suite plutons were emplaced at middle to lower crustal levels, based on Al-in-hornblende geobarometry of 5–6 kbar (or ~20 km depth) west of Teslin fault, and 6–7 kbar (or ~25 km depth) in Tatchun batholith to the east. These emplacement levels are consistent with the greenschist to amphibolite metamorphic grade of surrounding country rocks. $^{40}Ar/^{39}Ar$ cooling ages suggest rapid cooling and exhumation of the Tatchun batholith, east of Teslin fault (~15 km in ≤2 m.y., or 2.1–7.5 mm/yr), and slower exhumation and cooling of the Minto and Granite Mountain plutons to the west (~10 km in ~8–14 m.y., or 0.7–1.3 mm/yr).

Copper-gold mineralization at the Minto and Carmacks Copper deposits is hosted in foliated and variably migmatized rafts and xenoliths of intermediate to mafic meta-igneous rocks, some of which are dated at *ca.* 217–214 Ma. Textural variations in the hypogene ore and Re-Os dating of molybdenite indicate that original ore formation occurred in the Late Triassic (*ca.* 217–213 Ma) and was locally remobilized during intrusion of the Minto suite and migmatization of the host rafts at *ca.* 198–196 Ma.

Introduction

The latest Triassic to Early Jurassic Minto suite (205–194 Ma) forms large plutons and batholiths that intrude the northern apex of exposures of Triassic volcanic rocks of Stikinia and Quesnellia, and mid-Paleozoic metamorphic 'basement' rocks of the Yukon-Tanana terrane along a northwest-trending belt that extends to north of Carmacks (Fig. 3-1). The two main intrusive complexes comprising the Minto suite occur on either side of the Teslin fault. To the west of Teslin fault, the Granite Mountain, Minto, and Yukon River plutons probably form a single large batholith, ~120 km long by 15–25 km wide, whose mapped extents are separated by relatively thin cover of Late Cretaceous and younger basalt—the Upper Cretaceous Carmacks Group (uKC) and the Pliocene–Pleistocene Selkirk Lavas (TQS; Fig. 3-2). This large plutonic complex intrudes the boundary between Stikinia and Yukon-Tanana terranes, and its southern portion hosts Cu-Ag-Au mineralization at Minto [115I 021, 022], Carmacks Copper (*aka.* Williams Creek) [115I 008] and Stu [115I 011]. Several Minto suite plugs and stocks are also present in the Mount Nansen area. To the northwest, the Walhalla pluton intrudes the Yukon-Tanana terrane but may connect at depth with the batholithic complex to the south (Fig. 3-2; extending the composite batholith to ~150 km in strike length). To the east, the Pelly pluton is separated from the main part of the Yukon River batholith by Triassic metavolcanic rocks of Stikinia and Selkirk volcanic flows.

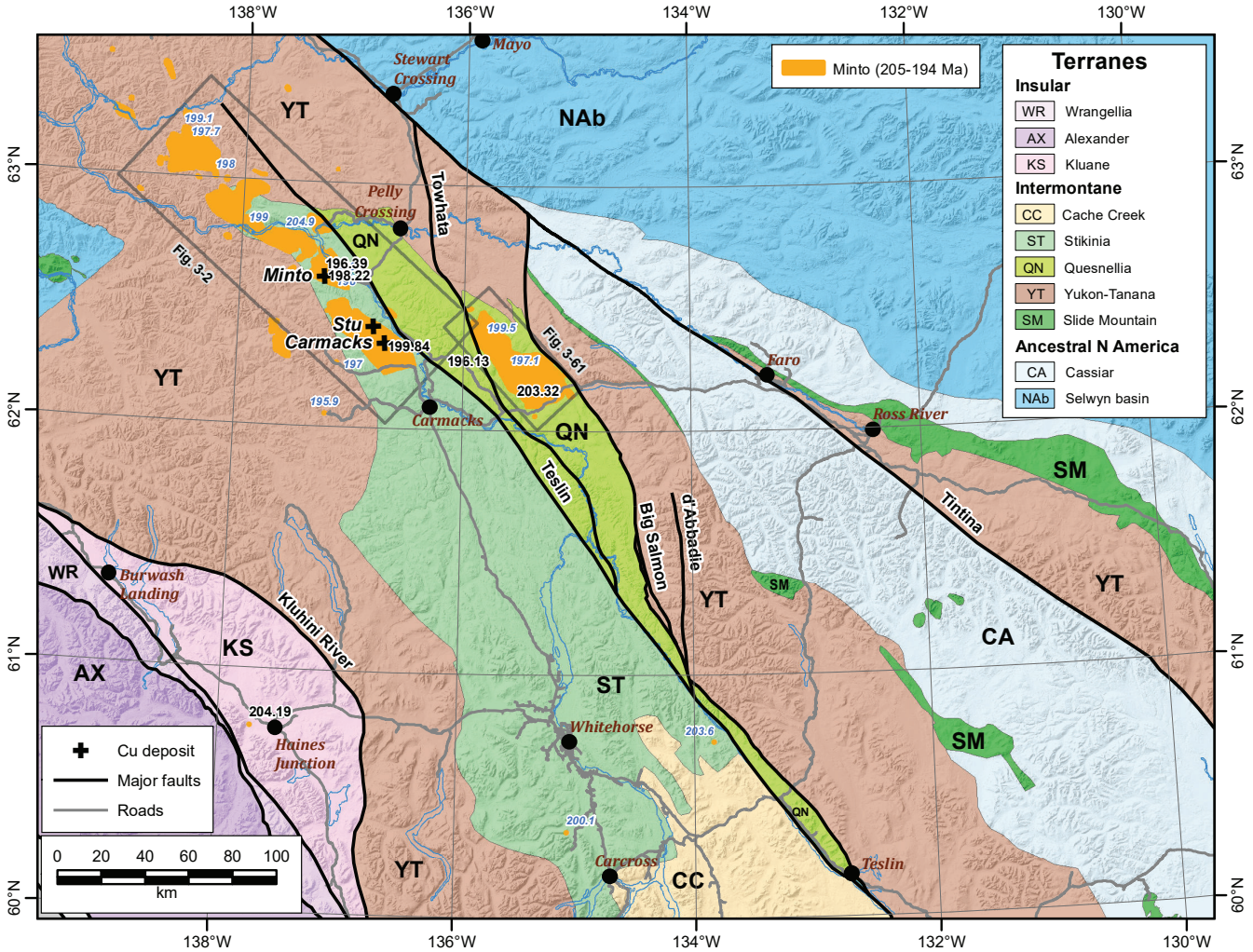
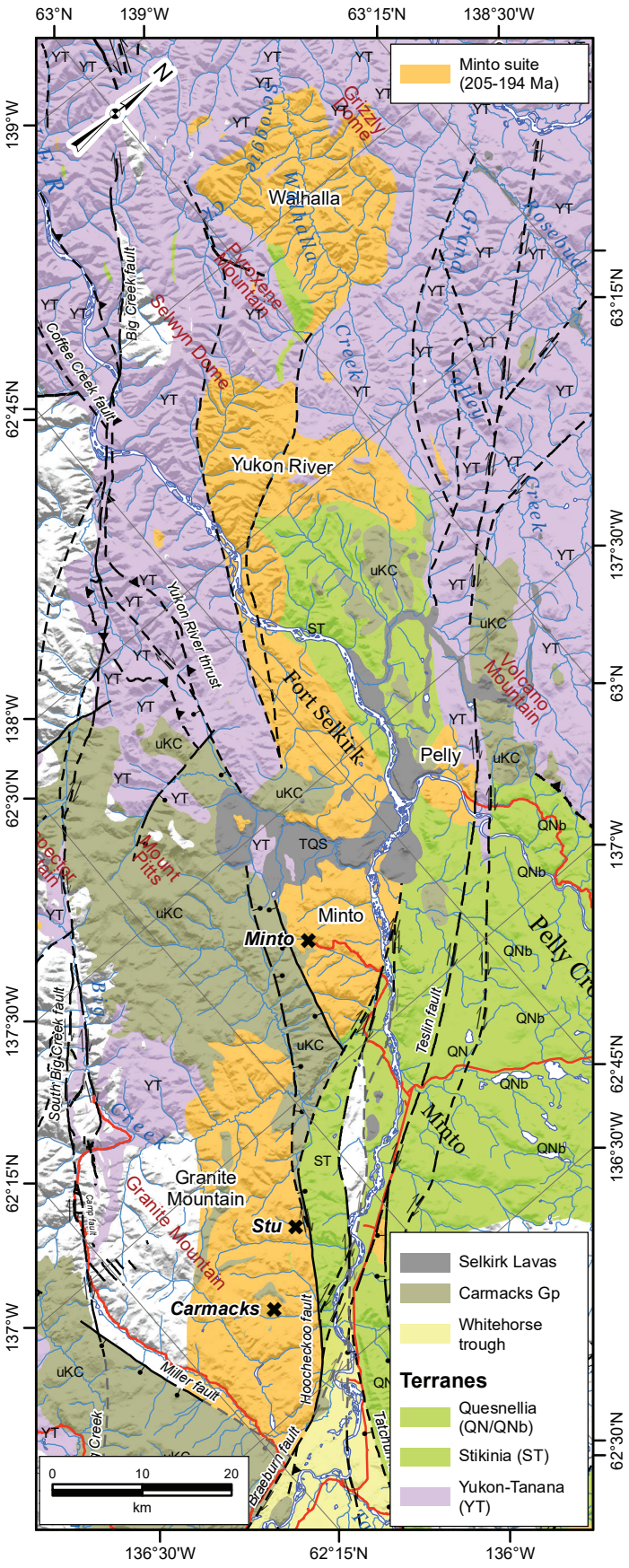


Figure 3-1. *Distribution of latest Triassic to Early Jurassic plutons of the Minto suite in southern Yukon. U-Pb dates are indicated next to plutons, black numbers are zircon CA-TIMS ages (this study); blue, italicized numbers indicate samples dated by other U-Pb techniques from previous work (see Appendix 1 for geochronology compilation). Terrane map is modified after Colpron and Nelson (2011).*



East of the Teslin fault, the Tatchun batholith is similar in composition and age to Minto suite plutons to the west, and is considered to be part of this suite (Fig. 3-1). The Tatchun batholith is ~50 km long by 10–20 km wide and intrudes upper Paleozoic metavolcanic rocks of Quesnellia in the hanging wall of the Tadru fault, which juxtaposes the upper Paleozoic Boswell assemblage (Moose and Boswell formations of Simard, 2003; YGS, 2020a) with Upper Triassic rocks of the Semenof formation (Tempelman-Kluit, 1984, 2009; Colpron *et al.*, 2002).

The Minto suite plutons comprise mostly Hbl ± Bt granodiorite with subordinate granite, monzonite and monzodiorite (Table 3-1; Fig. 3-3). These plutons were constructed from multiple pulses of magma ranging from *ca.* 205–194 Ma and displaying a wide range of textures from medium-grained equigranular to coarse-grained K-feldspar porphyritic phases. The bulk of these plutons lack deformation features but locally they are strongly foliated to gneissic. The Minto plutons are dominantly magnetic, and weakly oxidized to oxidized (Fig. 3-4).

These plutons were originally assigned to the Late Triassic Klotassin plutonic suite (Tempelman-Kluit and Wanless, 1975), but were later reassigned to the Aishihik plutonic suite after realization that Klotassin plutons included both Cretaceous and Jurassic bodies (*e.g.*, Johnston and Erdmer, 1995a; Johnston *et al.*, 1996). Johnston *et al.* (1996) assigned an age range of *ca.* 192–185 Ma for granodiorite of the Aishihik plutonic suite, based on available dating from the Aishihik batholith in southern Yukon. Granodiorite of the Aishihik batholith is intruded by 'younger', more felsic

Figure 3-2. *Distribution of the latest Triassic to Early Jurassic Minto suite (205–194 Ma) plutons between the Teslin and Big Creek faults, northwest of Carmacks. Exposures of the Granite Mountain, Minto and Yukon River plutons are separated by overlapping younger volcanic rocks of the Upper Cretaceous Carmacks Group and the Pliocene-Pleistocene Selkirk Lavas, suggesting that these plutons may form part of a single large batholith, ~120 km long × 15–25 km wide. Geology after YGS (2020a); fault symbology as in Figure 1-4. Note that the geographic reference frame has been rotated with North pointing to the upper right of the page.*

Table 3-1. *Summary of characteristics for latest Triassic to Early Jurassic plutons of the Minto suite in Yukon.*

Pluton	NTS	Area (km^2)	Terrane[1]	Rock[2]	Composition[3]	Oxidation state[4]	Age (Ma)[5]	Al-in-Hbl barometry (kbar)[6]	Ti-in-Zrn temp. (°C)[7]	Isotopes[8]	Inheritance[9]	Comment	Reference
Granite Mountain (northeast)	115I/6–8	500	ST/YT	Hbl-Bt Qz monzonite, diorite, granodiorite	calc-alkalic to alkali-calcic; peraluminous	weakly to moderately oxidized	199.84 ± 0.14 194.71 ± 0.07	4.8–5.9	730–792	εNd: -3.6–1.3 Sr_i: 0.70407 $^{207/204}$Pb: 15.58 $εHf_{zrn}$: 6.0–7.5	–	BSU, CA-TIMS	Kovacs *et al.* (2020); this study
Minto	115I/11	170	ST/YT	Bt ± Hbl granodiorite	calc-alkalic to alkali-calcic; peraluminous	oxidized	198.22 ± 0.06 196.39 ± 0.11	5.5–5.7	544–720	εNd: -1.3 Sr_i: 0.7054 $^{207/204}$Pb: 15.62 $εHf_{zrn}$: 0.8–10.9	325, 214 Ma	BSU, CA-TIMS	this study
Yukon River	115I/11–14, 115J/16	506	ST/YT	Hbl-Bt granodiorite; Two-mica monzonite, granodiorite	alkali-calcic to mildly alkalic; peraluminous	reduced to weakly oxidized	199.0 ± 2.0	–	–	εNd: 1.2 Sr_i: 0.7048 $^{207/204}$Pb: 15.62	–	GSC, SIMS	this study
Pelly	115I/14	43.4	ST/YT	Bt (Hbl) granodiorite-monzonite	alkali-calcic to mildly alkalic; peraluminous	weakly oxidized	204.9 ± 3.3	–	–	–	–	GSC, SIMS	Knight *et al.* (2013)
Walhalla	115O/1–2	345	YT	Hbl-Bt granodiorite; tonalite	calcic to alkali-calcic; peraluminous	reduced to weakly oxidized	199.1 ± 6.8	–	–	εNd: 0.3 Sr_i: 0.7048 $^{207/204}$Pb: 15.63	–	UBC, ID-TIMS, multi-grains fraction	J.K. Mortensen, unpubl.
Tatchun	105L/3–6	712	QN	Kfs porphyritic Hbl-Bt granodiorite; Bt monzodiorite; tonalite	alkali-calcic to alkalic; peraluminous	weakly to moderately oxidized; tonalite is reduced	203.32 ± 0.06 196.13 ± 0.09	6.4–7.2	597–630	εNd: -0.4–0.9 Sr_i: 0.70475 $^{207/204}$Pb: 15.60 $εHf_{zrn}$: 0.5–5.0	342, 320 Ma	BSU, CA-TIMS	this study

Notes:

[1] host terrane to intrusion; QN – Quesnellia; ST – Stikinia; YT – Yukon-Tanana

[2] lithology from Figs. 3-3 and 3-80. Aug – augite; Bt –biotite; Hbl – hornblende; Qz – quartz

[3] composition from Fig. 3-82b

[4] oxidation state from Fig. 3-4

[5] best age from pluton, as discussed in text

[6] crystallization pressure estimates from Al-in-hornblende barometry, Appendix 5

[7] crystallization temperature from Ti-in-zircon thermometry, Appendix 3

[8] whole rock Nd and Sr data; K-feldspar Pb data (Appendix 9); Hf in zircon data (Appendix 10)

[9] inheritance determined from U-Pb LA-ICPMS analyses of zircon (Appendix 3)

quartz monzonite and granite of the Long Lake suite (pink quartz monzonite of Tempelman-Kluit, 1974a,b; Woodsworth *et al.*, 1991; Johnston and Erdmer, 1995a) that also yielded a *ca.* 186 Ma date (Johnston *et al.*, 1996; *see* Chapter 4 for further description of the Long Lake suite).

Because the granodiorite composition of the Granite Mountain, Minto, Yukon River and Tatchun batholiths are similar to early phases of the Aishihik batholith, they were shown as part of the Aishihik suite on the compilation map of Gordey and Makepeace (2001). Due to their importance as hosts to Cu-Ag-Au mineralization, the Minto and Granite Mountain plutons came to be considered "type" Aishihik suite, even though they yielded dates ranging from *ca.* 204–196 Ma (Breitsprecher and Mortensen, 2004; Tafti, 2005; Colpron, 2011; Hood, 2012) which is older than granodiorite in the Aishihik batholith (Johnston *et al.*, 1996).

In a recent study of the Aishihik batholith, Joyce *et al.* (2016) found that no part of the batholith matches the expanded definition of the Aishihik suite, and suggested abandoning this name to avoid confusion and proposed the name Minto suite for the *ca.* 204–196 Ma granodiorite in plutons north of Carmacks (Colpron *et al.*, 2016b). The Aishihik batholith was found to be dominated by the Long Lake suite (Joyce *et al.*, 2016; *see* Chapter 4).

Our study of the Minto suite focuses primarily on the Granite Mountain, Tatchun and Minto plutons. Also integrated here are unpublished observations and data acquired during regional mapping projects by the Yukon Geological Survey and Geological Survey of Canada (for the Tatchun, Minto, Pelly, Yukon River and Walhalla plutons; *e.g.*, Colpron *et al.*, 2002, 2003; Colpron and Ryan, 2010; Ryan *et al.*, 2010, 2013; Knight *et al.*, 2013), as well as from three Master's theses focused on the Minto and Carmacks Copper deposits (Tafti, 2005; Hood, 2012; Kovacs, 2018). Two historic samples (J.K. Mortensen), one from Mount Nansen area and one from the Big Creek batholith, were analyzed by LA-ICPMS for U-Pb dating of zircon at UBC and are also reported here.

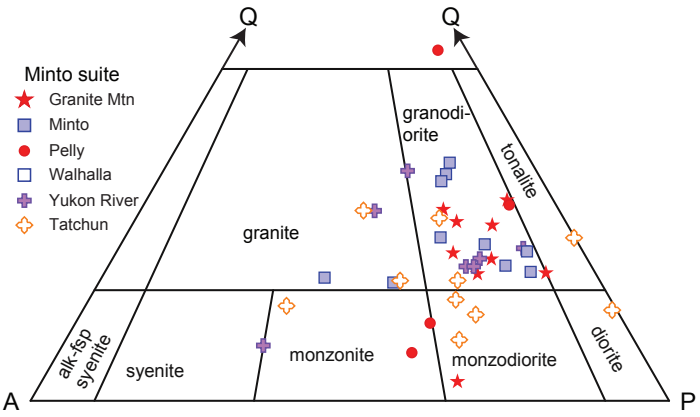


Figure 3-3. *Simplified quartz-alkali-feldspar-plagioclase (QAP) plot for samples of the Minto suite (after Le Bas and Streckeisen, 1991).*

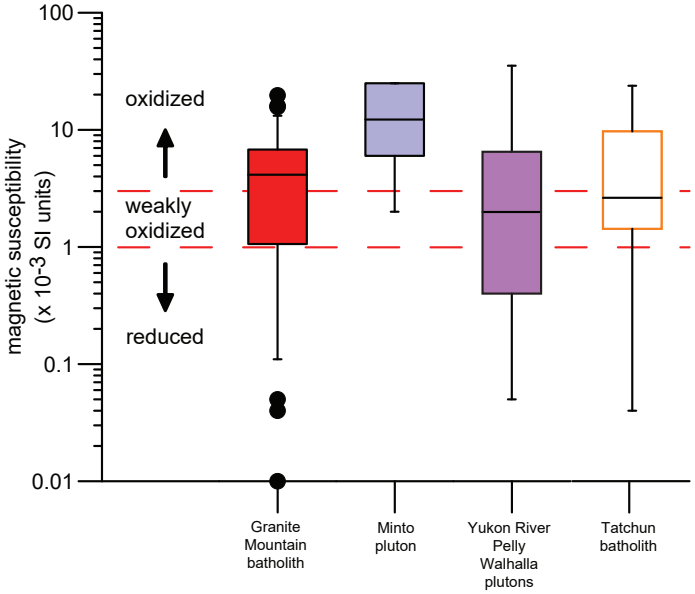


Figure 3-4. Box and whisker plot of magnetic susceptibility measurements for plutons of the Minto suite (Appendix 2). Divisions between reduced to weakly oxidized (1×10^{-3} SI units), and weakly oxidized to oxidized (3×10^{-3} SI units) are from Hart et al. (2004a,b). Ends of boxes are 75th and 25th percentile of data, black line within boxes indicates median (50th percentile) of data, whiskers 95th and 5th percentile. Colours are as in Fig. 3-3.

Granite Mountain batholith

The composite Granite Mountain batholith is located ~30 km northwest of Carmacks (Fig. 3-1; Table 3-1). It comprises an older northeastern portion assigned to the Minto plutonic suite (205–194 Ma), and a younger southwestern portion assigned to the Long Lake plutonic suite (188–182 Ma; Fig. 3-5). This section focuses on the older, northeastern portion of the batholith; rocks of the younger southwestern portion are described in Chapter 4. The batholith is elongate, northwest trending and has a total mapped exposure of 720 km^2; approximately 500 km^2 is assigned to the Minto suite and 220 km^2 to the Long Lake suite (Fig. 3-5). The batholith intrudes Mississippian granodiorite-tonalite gneiss of the Yukon-Tanana terrane along its western margin (Simpson Range plutonic suite; Allan and Friend, 2018; Carlson, 1987).

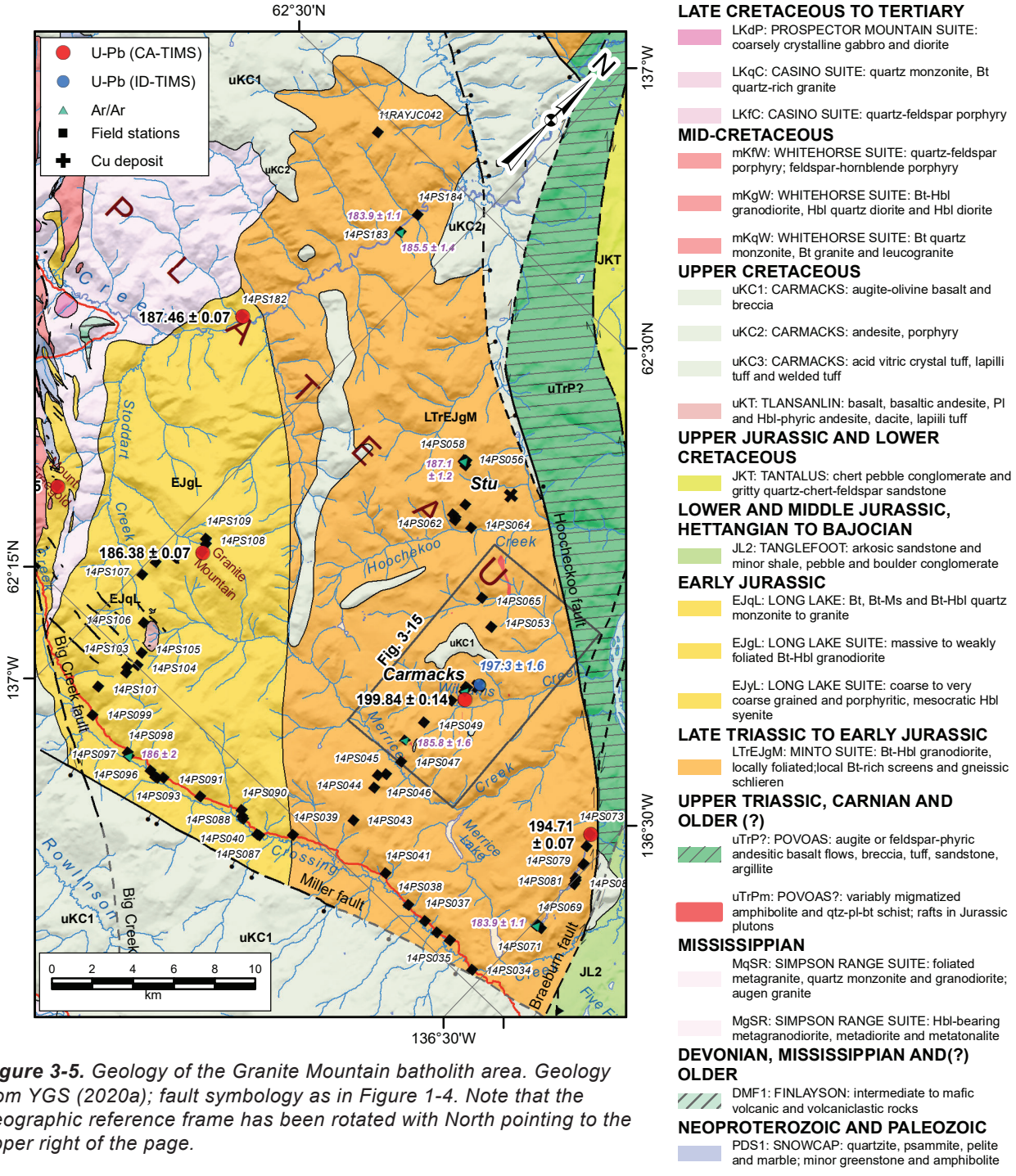


Figure 3-5. *Geology of the Granite Mountain batholith area. Geology from YGS (2020a); fault symbology as in Figure 1-4. Note that the geographic reference frame has been rotated with North pointing to the upper right of the page.*

Its northeastern contact is mapped as a Late Cretaceous fault against Upper Triassic rocks of the Povoas formation (Stikinia; Fig. 3-5). Xenoliths of mafic volcanic rock within granodiorite near the northeast margin of the Granite Mountain batholith suggest a primary intrusive relationship with the Triassic volcanic rocks of Stikinia (Fig. 3-6). Cretaceous faulting was focused along this contact and may have resulted in local epidote alteration of the granodiorite. The northern part of the Granite Mountain batholith is unconformably overlain by mafic volcanic rocks of the Upper Cretaceous Carmacks Group (*ca.* 73–68 Ma; Grond *et al.*, 1984), with local development of a thin basal conglomerate (Carlson, 1987). Carmacks Group basalt also occurs along a few narrow ridges overlying the central part of the Granite Mountain batholith (Fig. 3-5). The southern margin of the batholith is defined by the Miller fault which down-drops the Upper Cretaceous Carmacks Group against Early Jurassic granodiorite (Tempelman-Kluit, 1984). Locally, dacite dikes related to the Early Cretaceous Mt. Nansen Group intrude the batholith (Tempelman-Kluit, 1984).

The northeastern portion of the Granite Mountain batholith is composed predominantly of a medium to coarse-grained granodiorite that locally has a weak to moderate magmatic foliation and/or is K-feldspar porphyritic. The foliation is best developed in the outer 2–3 km of the batholith where it is generally subparallel to the batholith margin (Fig. 3-7). The northeastern part of the Granite Mountain batholith locally contains large xenoliths and rafts of schist and amphibolite characterized by an older, penetrative foliation striking NW to NNW and dipping steeply to the NE to ENE (Kovacs *et al.*, 2017; Sack *et al.*, 2016). The rafts locally host Cu-Ag-Au mineralization at the Carmacks Copper deposit and Stu occurrence (Fig. 3-5). In both instances these rafts of mineralized rock occur at, or near, the contact between an eastern more mafic monzodiorite phase and a western felsic to intermediate granodiorite phase (Kovacs *et al.*, 2017; Sack *et al.*, 2016). Hornblende-rich diorite, or 'hornblendite' is noted locally and may be an early restite phase of the batholith. In one location near the eastern margin of the batholith, 'hornblendite' contains disseminated and fine-grained interstitial chalcopyrite (Fig. 3-8) suggesting a relationship to early Cu mineralization such as that seen at Carmacks Copper (Kovacs *et al.*, 2017).

The following descriptions are primarily from the southeastern portion of the Granite Mountain batholith, in the vicinity of the Carmacks Copper deposit and Stu occurrence, where detailed work has been done (Tafti, 2005; Sack *et al.*, 2016; Kovacs *et al.*, 2017; Kovacs, 2018).

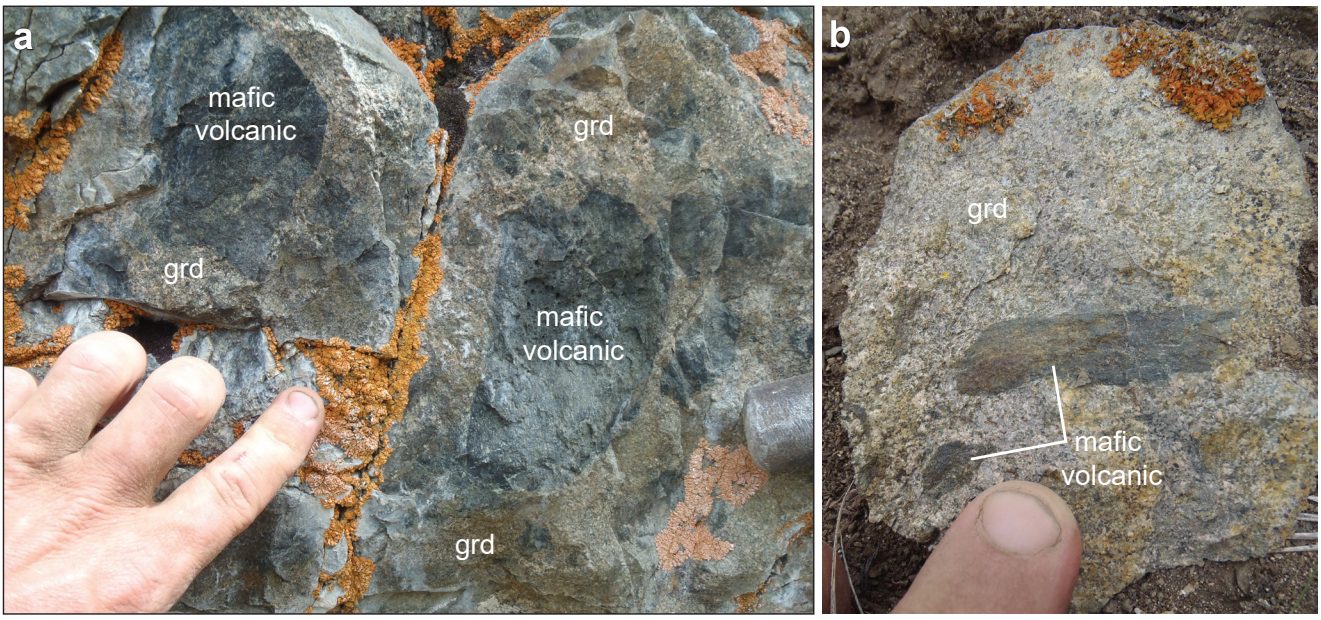


Figure 3-6. *Intrusive relationship between mafic volcanic country rock and Granite Mountain batholith.* ***(a)*** *Outcrop of mafic volcanic fragments within altered granodiorite.* ***(b)*** *Float with small, weakly foliated, mafic volcanic fragments within altered granodiorite. Both photographs from station 14PS080; grd = granodiorite.*

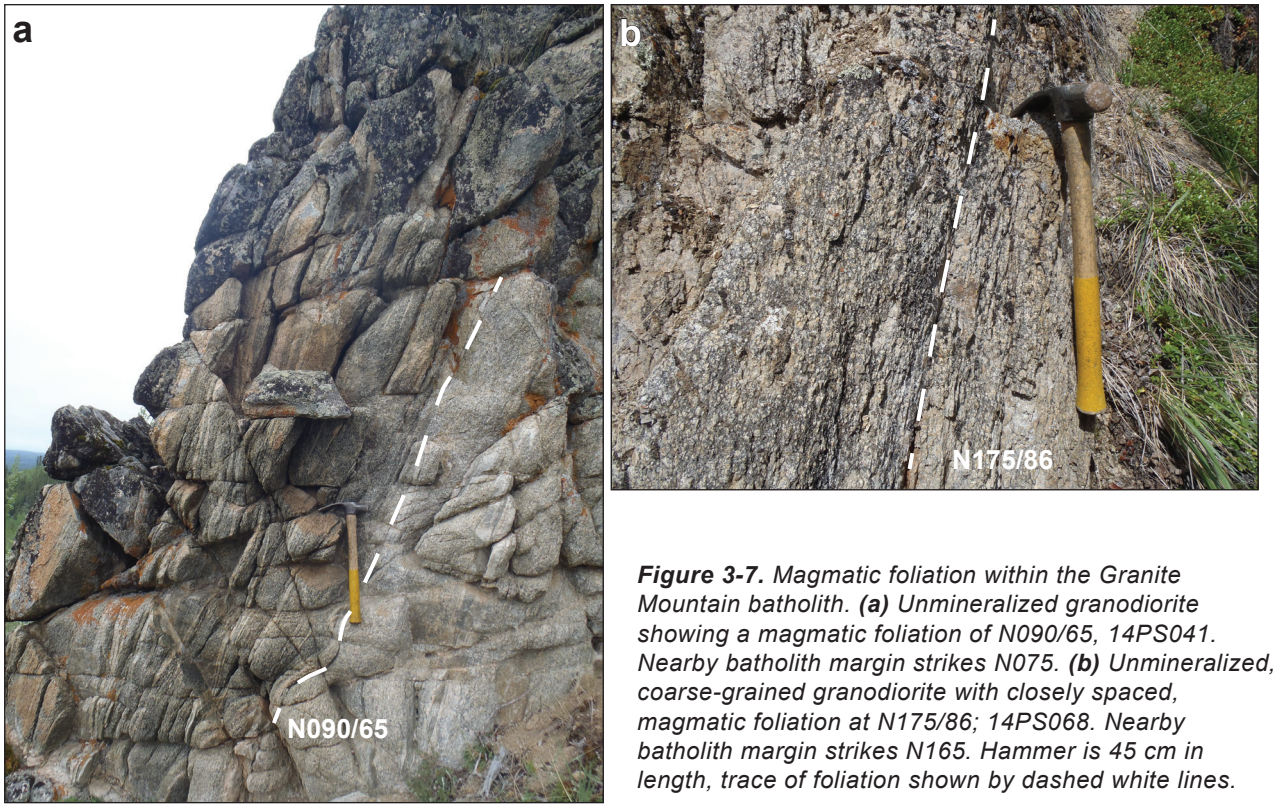


Figure 3-7. *Magmatic foliation within the Granite Mountain batholith.* ***(a)*** *Unmineralized granodiorite showing a magmatic foliation of N090/65, 14PS041. Nearby batholith margin strikes N075.* ***(b)*** *Unmineralized, coarse-grained granodiorite with closely spaced, magmatic foliation at N175/86; 14PS068. Nearby batholith margin strikes N165. Hammer is 45 cm in length, trace of foliation shown by dashed white lines.*

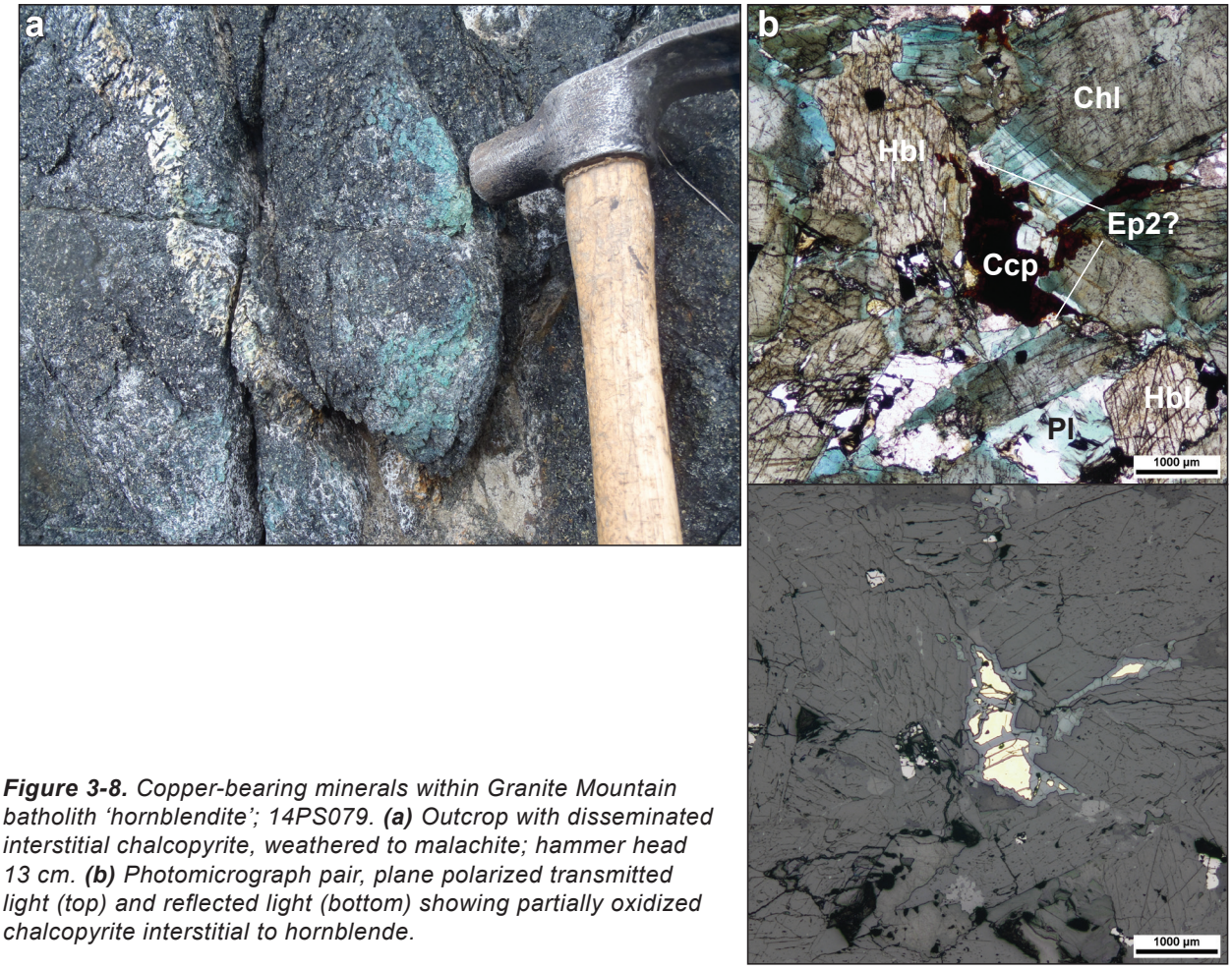


Figure 3-8. *Copper-bearing minerals within Granite Mountain batholith 'hornblendite'; 14PS079.* ***(a)*** *Outcrop with disseminated interstitial chalcopyrite, weathered to malachite; hammer head 13 cm.* ***(b)*** *Photomicrograph pair, plane polarized transmitted light (top) and reflected light (bottom) showing partially oxidized chalcopyrite interstitial to hornblende.*

Petrography

At least three phases of unfoliated granitoid rocks are recognized within the older, northeastern part of the Granite Mountain batholith (Kovacs *et al.*, 2017; Sack *et al.*, 2016). From oldest to youngest the three phases are: 1) an early mafic phase that ranges from monzonite to diorite and is medium-grained, equigranular to plagioclase porphyritic (Kovacs *et al.*, 2017; Fig. 3-9); 2) an intermediate granodiorite phase that is medium to coarse-grained, equigranular to K-feldspar porphyritic (Fig. 3-10a,b); and 3) late dikes that range from medium-grained, equigranular monzonite to monzodiorite, through to pegmatite or aplite (Fig. 3-10c; Kovacs *et al.*, 2017). In all three phases, the rocks are seriate to porphyritic, with fresh to weakly sericitized K-feldspar, and weakly to intensely saussuritized plagioclase (Fig. 3-11). Mafic minerals are unaltered, make up to 40% of the rock and typically include both biotite and hornblende in equal proportions. Epidote is present in all three phases both as magmatic and alteration minerals (Ep1 and Ep2, respectively in Fig. 3-11a,b); titanite is a ubiquitous trace mineral. Locally, near phase boundaries and/or contacts with large rafts of country rock, the granitoid rocks contain a magmatic foliation and show myrmekitic textures in thin section (vermicular intergrowths of quartz in plagioclase near K-feldspar grains; Fig. 3-11c; Kovacs *et al.*, 2017; Kovacs, 2018; this study). This texture indicates late stage, subsolidus metasomatism of K-feldspar near internal batholith boundaries (Barker, 1970).

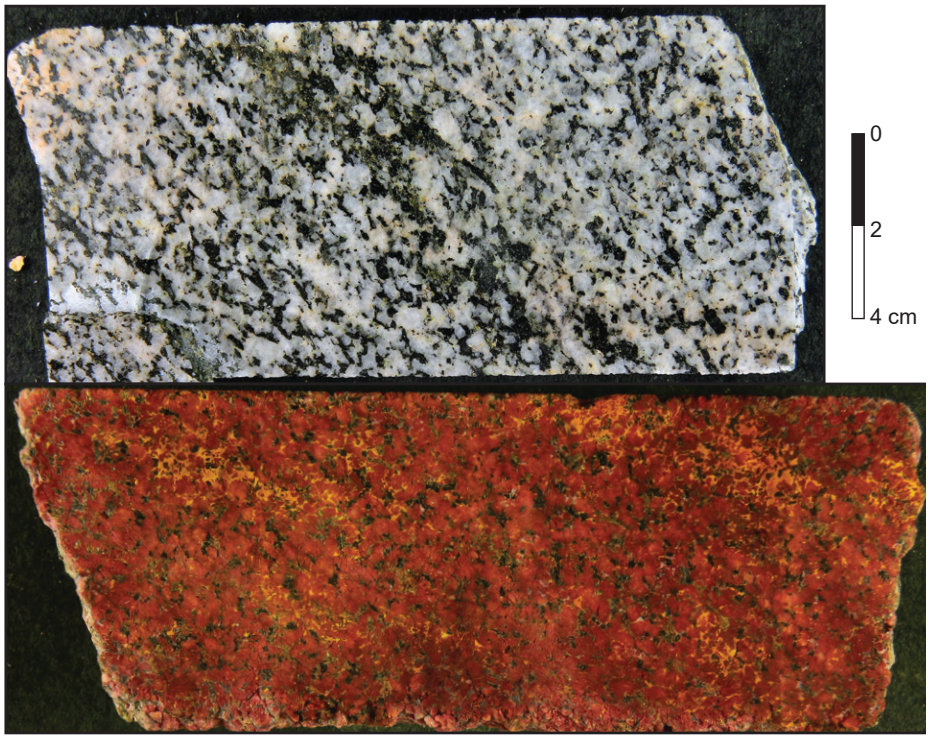


Figure 3-9. *Earliest phase of the Minto suite portion of the Granite Mountain batholith, monzodiorite from the eastern portion of the Carmacks Copper property (from Kovacs et al., 2017). Fresh polished surface (upper) and cobaltinitrite-stained surface (lower). Red-stained mineral is plagioclase, yellow-stained is K-feldspar and unstained, milky-white mineral is quartz.*

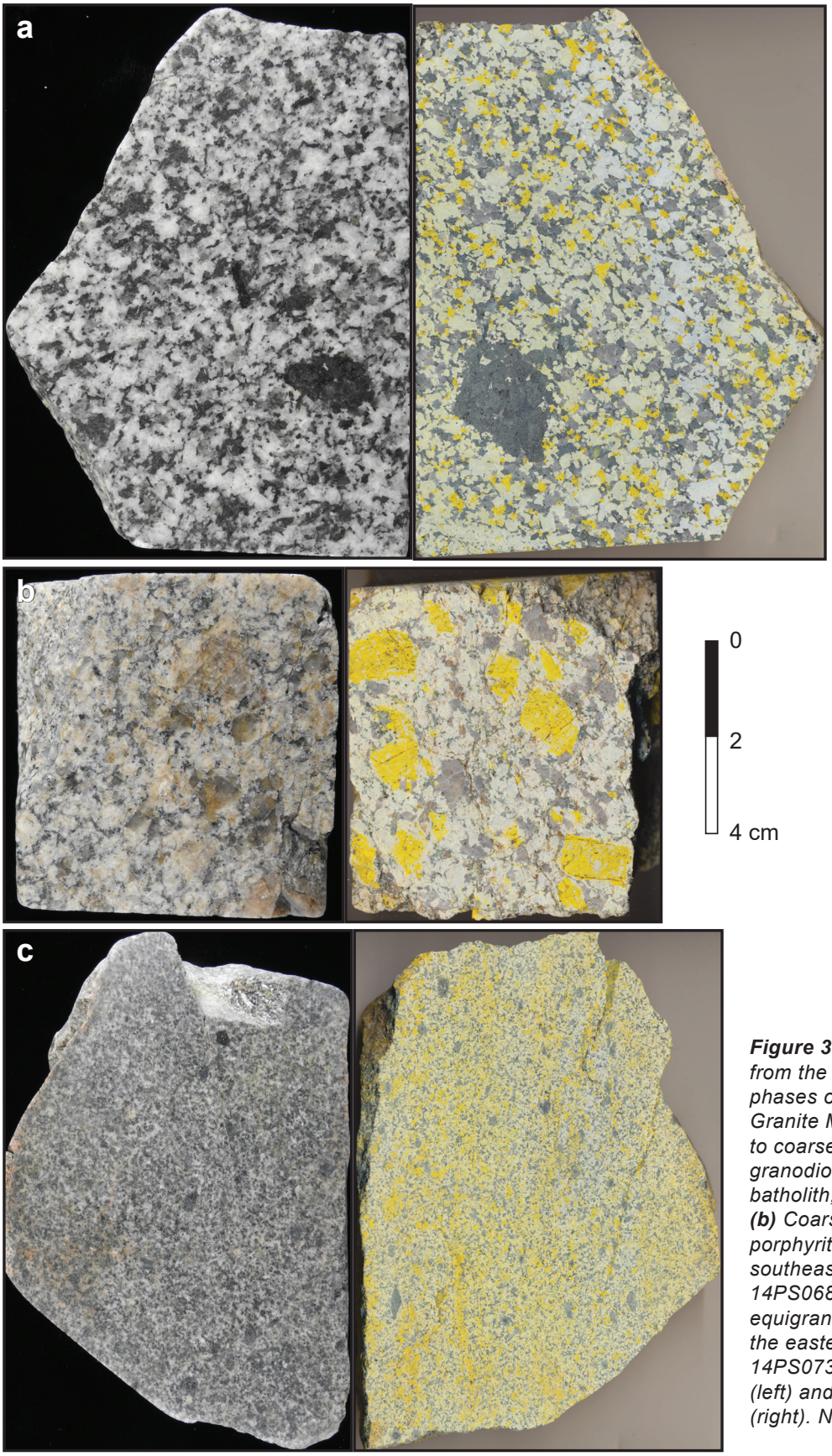


Figure 3-10. *Representative samples from the intermediate and felsic phases of the Minto portion of the Granite Mountain batholith.* ***(a)*** *Medium to coarse-grained, equigranular granodiorite from the northern end of the batholith, 14PS183-1.* ***(b)*** *Coarse-grained, K-feldspar porphyritic granodiorite from the southeastern portion of the batholith, 14PS068-1.* ***(c)*** *Medium-grained equigranular monzodiorite from near the eastern margin of the batholith, 14PS073-1. Fresh polished surface (left) and a cobaltinitrite-stained surface (right). Note K-feldspar is yellow.*

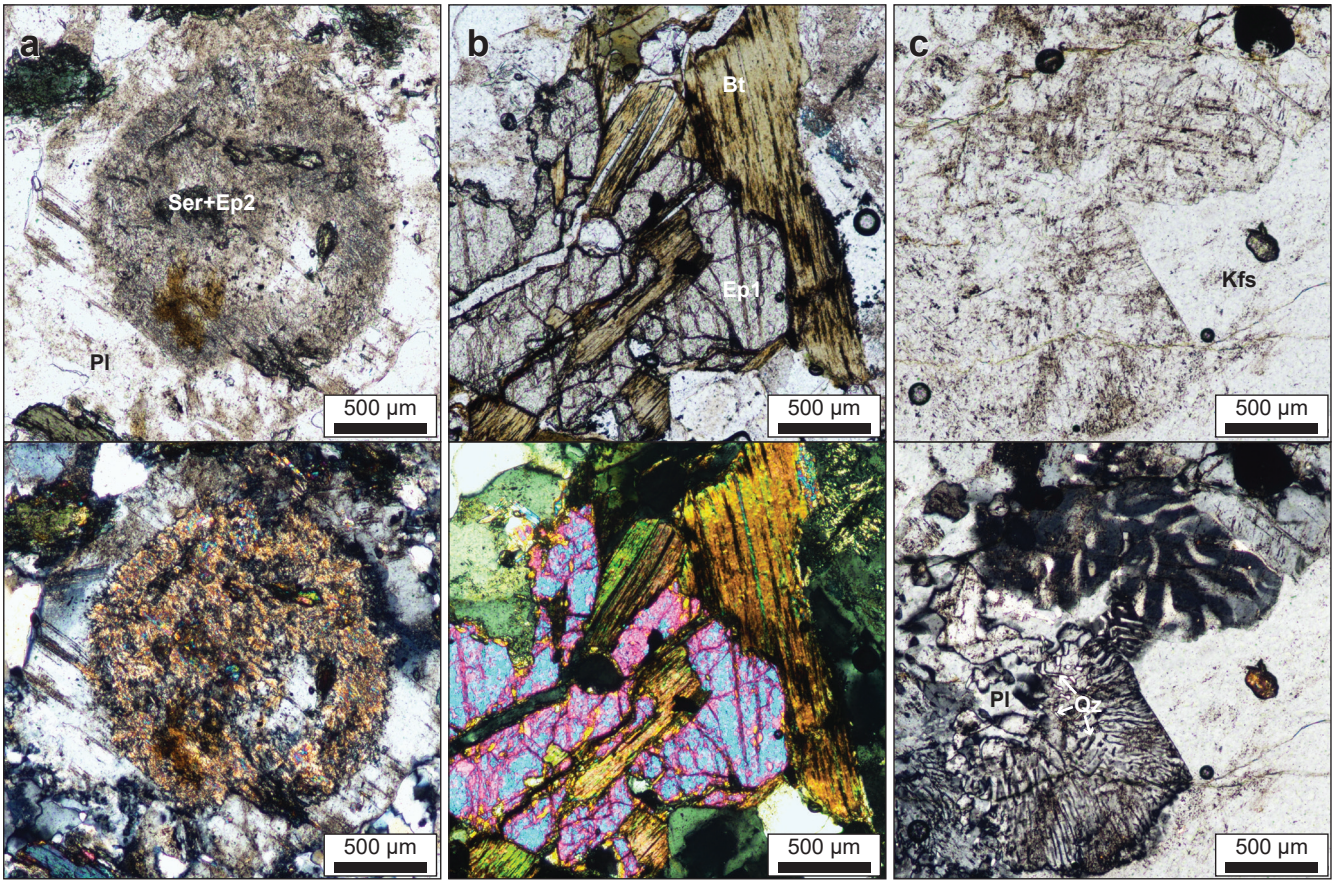


Figure 3-11. *Transmitted light photomicrograph pairs, plane polarized light (upper) and cross-polarized light (lower), from the Granite Mountain batholith.* ***(a)*** *Plagioclase with an intensely saussuritized (sericite and epidote) core; 14PS073-1.* ***(b)*** *Euhedral epidote intergrown with biotite; 11RAY042A1.* ***(c)*** *Vermicular intergrowths of quartz and plagioclase (myrmekite) on the margin of a coarse K-feldspar, 14PS068-1.*

Oxidation state and mineral occurrences

The monzonite to diorite phase has magnetic susceptibilities ranging from 0.17 to 9.6 × 10^{-3} SI units (mean 5.19 × 10^{-3} SI units; n = 27), while the intermediate rocks (*e.g.*, granodiorite) have similar values but a slightly larger range of 0.17 to 16.00 × 10^{-3} SI units (mean 3.23 × 10^{-3} SI units; n = 10; Appendix 2). Late monzonite and aplite dikes have much lower magnetic susceptibilities ranging from 0.05 to 0.25 × 10^{-3} SI units (mean 0.15 × 10^{-3} SI units; n = 4). Mafic rafts associated with copper mineralization at the Carmacks Copper deposit generally have relatively low magnetic susceptibilities with a median of 0.49 × 10^{-3} SI units (n = 697) but locally, are highly magnetic with susceptibilities up to 65 × 10^{-3} SI units (Fig. 3-12a). The relatively low magnetic character of the Carmacks Copper orebodies does not appear to be influenced by weathering (*i.e.*, magnetite destruction associated with oxidation) as there is no correlation between magnetic susceptibility and downhole depth (Fig. 3-12b). Similar observations at the Stu occurrence indicate the supergene mineralization at that location also results in a relative magnetic low feature (median of 0.48 × 10^{-3} SI units; n = 15) but is locally magnetic with susceptibilities up to 24 × 10^{-3} SI units. At Stu, several of the highest magnetic susceptibility measurements are from oxidized rocks in trenches. Mafic volcanic rocks of the Carmacks Group are typically highly magnetic with susceptibilities >10 × 10^{-3} SI units and their exposures over the Granite Mountain batholith correspond with the strongest magnetic gradients in the area (Fig. 3-13).

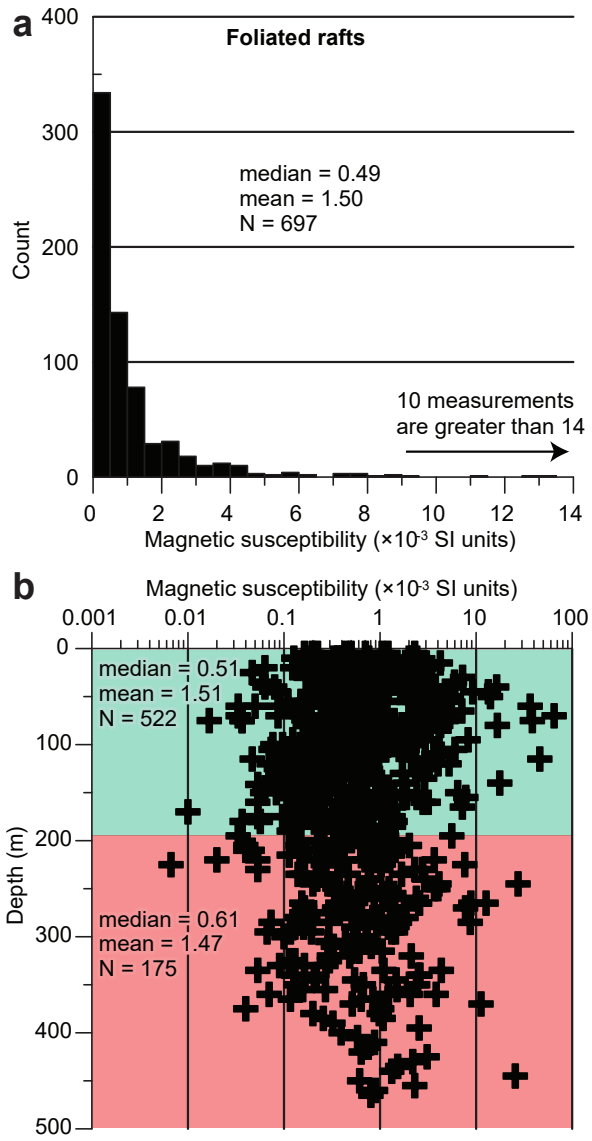


Fig. 3-12. (a) *Magnetic susceptibility data from mafic rafts at the Carmacks Copper deposits. Data from Milton (written communication, 2018). Histogram plot showing a skewed distribution to low (<1) values.* ***(b)*** *Same data plotted against depth showing the lack of correlation between magnetic susceptibility and downhole depth, suggesting that oxidation of magnetite is not a control on magnetic susceptibility. Statistics subdivided into above (green) and below (red) 200 m, the approximate depth of oxidation in the main zone of the Carmacks Copper deposit.*

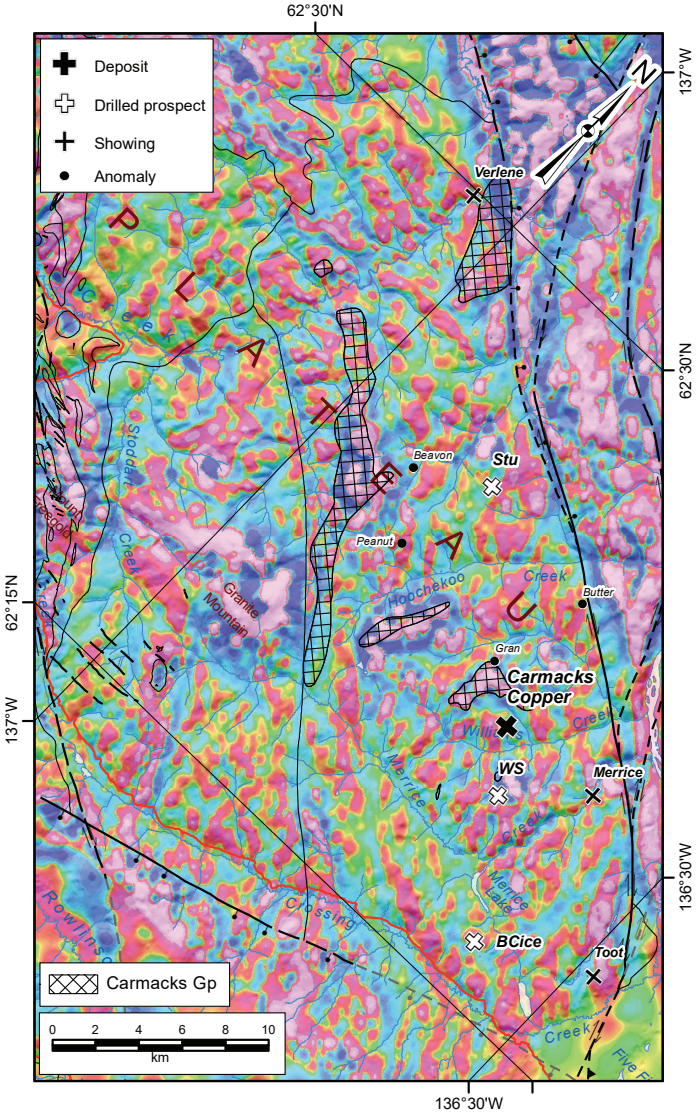


Figure 3-13. *Reduced to pole, first vertical derivative aeromagnetic map of the Granite Mountain batholith (Aurora Geosciences Ltd. and Bruce, 2017b) showing distribution of Cu-Ag-Au MINFILE occurrences in the eastern part of the batholith, and mapped exposures of Carmacks Group overlying the granodiorite (cross-hatch). Note that the geographic reference frame has been rotated with North pointing to the upper right of the page. Fault symbology as in Figure 1-4.*

The Minto suite portion of the Granite Mountain batholith hosts eleven Cu (± Ag, Au) mineral occurrences (Fig. 3-13; Table 3-2; YGS, 2020b). The Stu, Carmacks Copper and Toot occurrences were visited as part of this study (Table 3-2). Most of the copper occurrences were discovered and heavily explored in the mid-1970s to early 1980s, following the discovery and initial definition of the Minto and Carmacks Copper deposits (Sack *et al.*, 2017). The level of knowledge for these occurrences varies from the relatively well-studied Carmacks Copper deposit (*e.g.*, Abbott, 1971; Tafti, 2005; Kovacs *et al.*, 2017; Kovacs, 2018), to those with reconnaissance drilling such as Stu (Paulter, 2009; Sack *et al.*, 2016),

Table 3-2. *Summary of MINFILE occurrences hosted by the Granite Mountain batholith (modified from YGS, 2020b).*

MINFILE number	Name	Latitude	Longitude	Deposit type	Deposit status	Commodities
115I 008	Carmacks Copper	62.34888	-136.69361	Minto-style	deposit	Cu, Au, Ag
115I 006	BCice	62.27555	-136.58194	Minto-style	drilled prospect	Cu, Au
115I 007	WS	62.32611	-136.65666	Minto-style	drilled prospect	Cu, Ag, Au
115I 011	Stu	62.41640	-136.85128	Minto-style	drilled prospect	Cu, Ag, Au
115I 108	Toot	62.29916	-136.48388	Minto-style	showing	Cu
115I 009	Merrice	62.35333	-136.59527	Qz vein	showing	Cu, Ag, Au
115I 014	Verlene	62.49805	-137.04416	Minto-style	showing	Cu, Ag, Au
115I 126	Butter	62.40722	-136.72000	Minto-style	anomaly	Au, Cu
115I 127	Peanut	62.37361	-136.87416	Minto-style	anomaly	Au, Cu
115I 128	Gran	62.36500	-136.74138	Minto-style	anomaly	Cu
115I 089	Beavon	62.39944	-136.91333	Minto-style	anomaly	Cu

through to soil and prospecting anomalies such as the Verlene occurrence ([115I 014]; Table 3-2; Fig. 3-13). Ten of the occurrences in the Granite Mountain batholith are similar in that they are Cu (± Ag, Au) occurrences (Table 3-2) associated with foliated rocks. The eleventh occurrence is the Merrice ([115I 009]; Table 3-2) which is a poorly understood set of quartz veins, with disseminated chalcopyrite and bornite, that were discovered in the early 1900s (YGS, 2020b).

Carmacks Copper deposit

At Carmacks Copper, the orebodies are mostly hosted by northwest-striking rafts of foliated mafic schist and amphibolite engulfed, and partially migmatized by unfoliated granodiorite of the Minto suite in the northeastern part of the Granite Mountain batholith (Fig. 3-14). Supergene processes have affected the upper portion of the orebodies and locally remobilized copper into surrounding Granite Mountain batholith rocks. The current resource for the deposit includes six zones in two areas, the main area comprises Zones 1, 7 and 4, the southern area comprises Zones 2000S, 12 and 13 (Fig. 3-15; JDS Energy and Mining Ltd., 2016). Eight other mineralized zones have been discovered on the property but are not included in current resource estimates (Fig. 3-15). Zones 1, 7 and 4 host 12.07 Mt of oxide (1.06% copper, 0.46 g/t gold, 4.6 g/t silver) and 8.37 Mt of sulphide mineralization (0.73% copper, 0.20 g/t gold, 2.1 g/t silver; Table 3-3). Zones 2000S, 12 and 13 host 4.69 Mt of oxide (0.46% copper, 0.12 g/t gold, 1.9 g/t silver) and 8.70 Mt of sulphide mineralization (0.58% copper, 0.13 g/t gold, 2.1 g/t silver; Table 3-3).



Figure 3-14. *Trench exposure at the Carmacks Copper deposit (Zone 7, station 14PS067) showing the common features of the mineralization—foliated host rocks with Cu-oxides (brown) engulfed and intruded by unfoliated granodiorite (light grey). Strike and dip of foliation within schist is N310/80. Intrusive contact between granodiorite and schist shown by solid black line; trace of foliation shown by dashed white line. Hammer is 45 cm in length.*

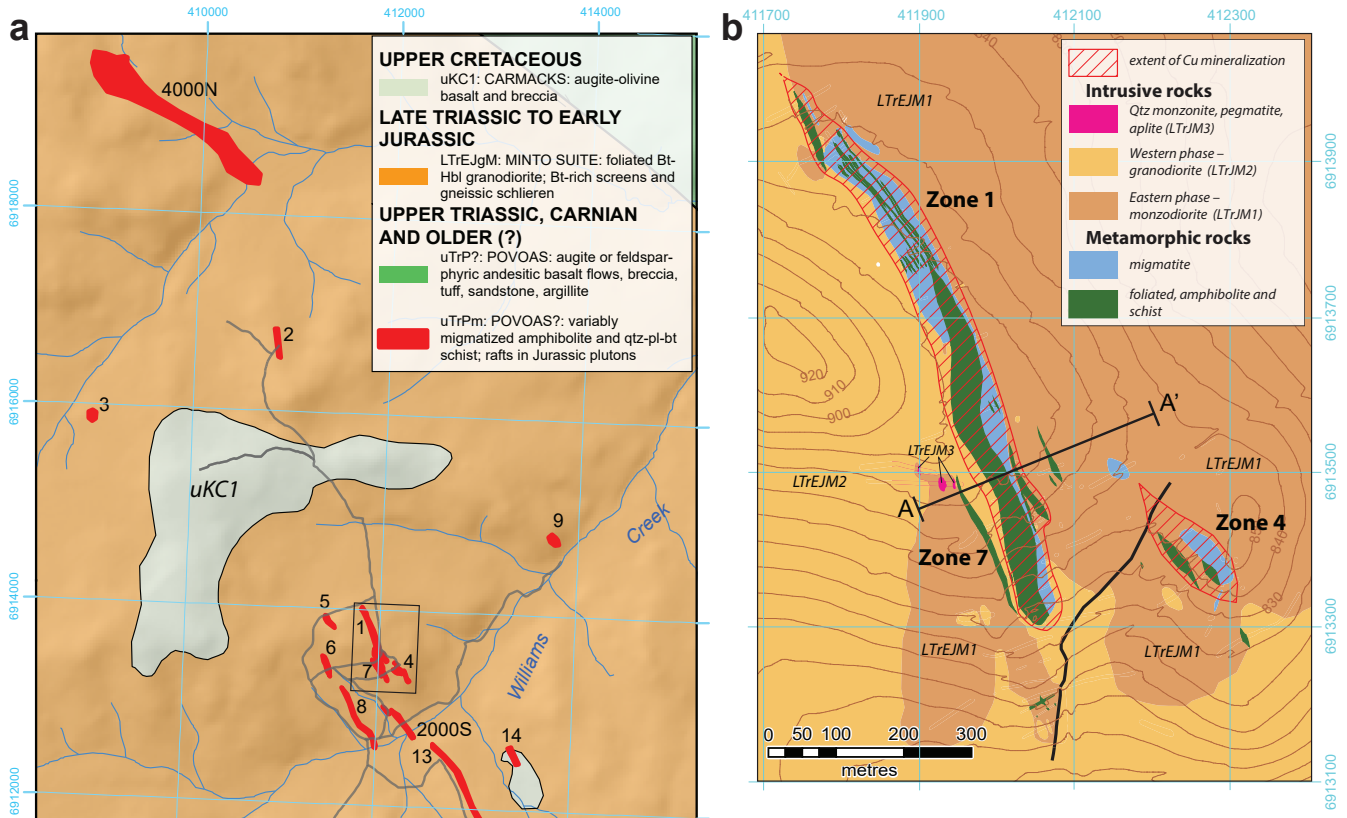


Figure 3-15. (a) *Detailed geological map showing distribution of mineralized rafts of amphibolite and intermediate schist within granodiorite at the Carmacks Copper deposit (after Kovacs et al., 2020). Numbers indicate the mineralized zones.* ***(b)*** *Detailed map of the main zones at the Carmacks Copper deposit (after Kovacs, 2018; Kovacs et al., 2020). This map shows the various phases of the Granite Mountain batholith in this area, and the relationship between migmatized and relatively intact metamorphic rafts in the main deposit area.*

Combined, Zones 1, 7 and 4 make up the largest deposit on the property with a 700 m strike length and up to 100 m in width (Fig. 3-15b; JDS Energy and Mining Ltd., 2016). Mineralization in Zone 4 is interpreted as an apparent 250 m sinistral offset of Zones 1 and 7 across a post-mineralization brittle fault (Fig. 3-15b; Kovacs, 2018). The main area zones are oxidized to approximately 200 m below surface with hypogene mineralization extending to at least 450 m down dip; mineralization is open at depth (Fig. 3-16; JDS Energy and Mining Ltd., 2016). Zones 12 and 13 have a combined strike length of 1.2 km with the widest part of Zone 13 up to 100 m in width (Fig. 3-15a). The continuity of Zones 12 and 13 has not been demonstrated and in Zone 12, the rafts bifurcate and split into several parallel splays offset by post-mineralization faulting (JDS Energy and Mining Ltd., 2016). Zone 2000S is between the main area and Zone 13 and has a 300 m strike length and 30 m width. The oxidation in Zones 2000S, 12 and 13 extends 40 to 80 m below surface (JDS Energy and Mining Ltd., 2016). In Zones 1, 7 and 2000S the orebodies are defined by roughly elongate, ellipsoidal shells that strike northwest and dip steeply to the east (Fig. 3-16; Kovacs, 2018). In contrast, the orebody in Zone 4 is flat lying (Kovacs, 2018) and those at Zones 12 and 13 also strike northwest but dip moderately (~45°) to the east.

Table 3-3. Carmacks Copper mineral resource summary.

Deposit	Class	Cut-off	Tonnes (000)	Total Cu (%)	Soluble Cu (%)	Sulphide Cu (%)	Au (ppm)	Ag (ppm)	Cu (lbs)	Cu (Tonnes)	Au (oz)	Au (Tonnes)	Ag (oz)	Ag (Tonnes)	Type	Year calculated
Main (1,4,7)	Measured	0.25% CuT	4,031	1.10	0.90	0.20	0.59	5.65	79,942,167	36,261	84,044	2.4	803,432	22.8	Oxide + Transition	2016
	Indicated	0.25% CuT	7,949	1.04	0.83	0.20	0.40	4.05	146,144,039	66,290	110,863	3.1	1,134,623	32.2		
	Inferred	0.25% CuT	90	0.73	0.53	0.20	0.13	1.82	1,043,888	474	404	0.0	5,774	0.2		
	M+I+Inf	**0.25% CuT**	**12,070**	**1.06**	**0.85**	**0.20**	**0.46**	**4.57**	**227,130,094**	**103,025**	**195,311**	**5.5**	**1,943,830**	**55.1**		
	Measured	0.25% CuT	695	0.80	0.02	0.77	0.26	2.50	11,798,024	5,352	6,374	0.2	61,289	1.7	Sulphide	
	Indicated	0.25% CuT	3,645	0.74	0.03	0.71	0.21	2.30	57,054,463	25,880	27,000	0.8	295,720	8.4		
	Inferred	0.25% CuT	4,031	0.71	0.01	0.70	0.18	1.90	62,207,763	28,217	25,594	0.7	270,160	7.7		
	M+I+Inf	**0.25% CuT**	**8,371**	**0.73**	**0.02**	**0.71**	**0.20**	**2.12**	**131,060,250**	**59,448**	**58,969**	**1.7**	**627,168**	**17.8**		
South (2000S, 12,13)	Measured	0.15% CuOx	3,409	0.46	0.34	0.12	0.12	1.80	34,571,528	15,681	14,430	0.4	216,448	6.1	Oxide + Transition	2018
	Indicated	0.15% CuOx	895	0.50	0.36	0.14	0.12	2.20	9,865,675	4,475	3,788	0.1	69,455	2.0		
	Inferred	0.15% CuOx	389	0.34	0.27	0.07	0.12	1.65	2,915,830	1,323	1,647	0.0	22,641	0.6		
	M+I+Inf	**0.15% CuOx**	**4,693**	**0.46**	**0.34**	**0.12**	**0.12**	**1.86**	**47,353,033**	**21,479**	**19,865**	**0.6**	**308,543**	**8.7**		
	Measured	0.25% CuT	1,136	0.59	0.11	0.49	0.13	2.30	12,271,797	5,566	5,209	0.1	92,164	2.6	Sulphide	
	Indicated	0.25% CuT	3,280	0.63	0.07	0.56	0.13	2.30	40,494,460	18,368	15,041	0.4	266,107	7.5		
	Inferred	0.25% CuT	4,281	0.54	0.05	0.49	0.12	1.90	46,246,093	20,977	18,121	0.5	286,915	8.1		
	M+I+Inf	**0.25% CuT**	**8,697**	**0.58**	**0.07**	**0.52**	**0.13**	**2.10**	**99,012,350**	**44,911**	**38,371**	**1.1**	**645,186**	**18.3**		
Global resource (M+I+Inf all zones)			**33,831**						**504,555,727**	**228,863**	**312,515**	**8.9**	**3,524,728**	**99.9**		

Notes:

2016 resources recalculated from 2016 PEA (JDS Energy and Mining Ltd., 2016); 2018 from April 9, 2018 Copper North Mining Corp. news release. Contained Cu calculated using Total Cu for all zones because metallurgical tests show >100% recovery of soluble copper, indicating the leach method is more aggressive than the soluble copper assay method (J. Milton written communication, December 2018).

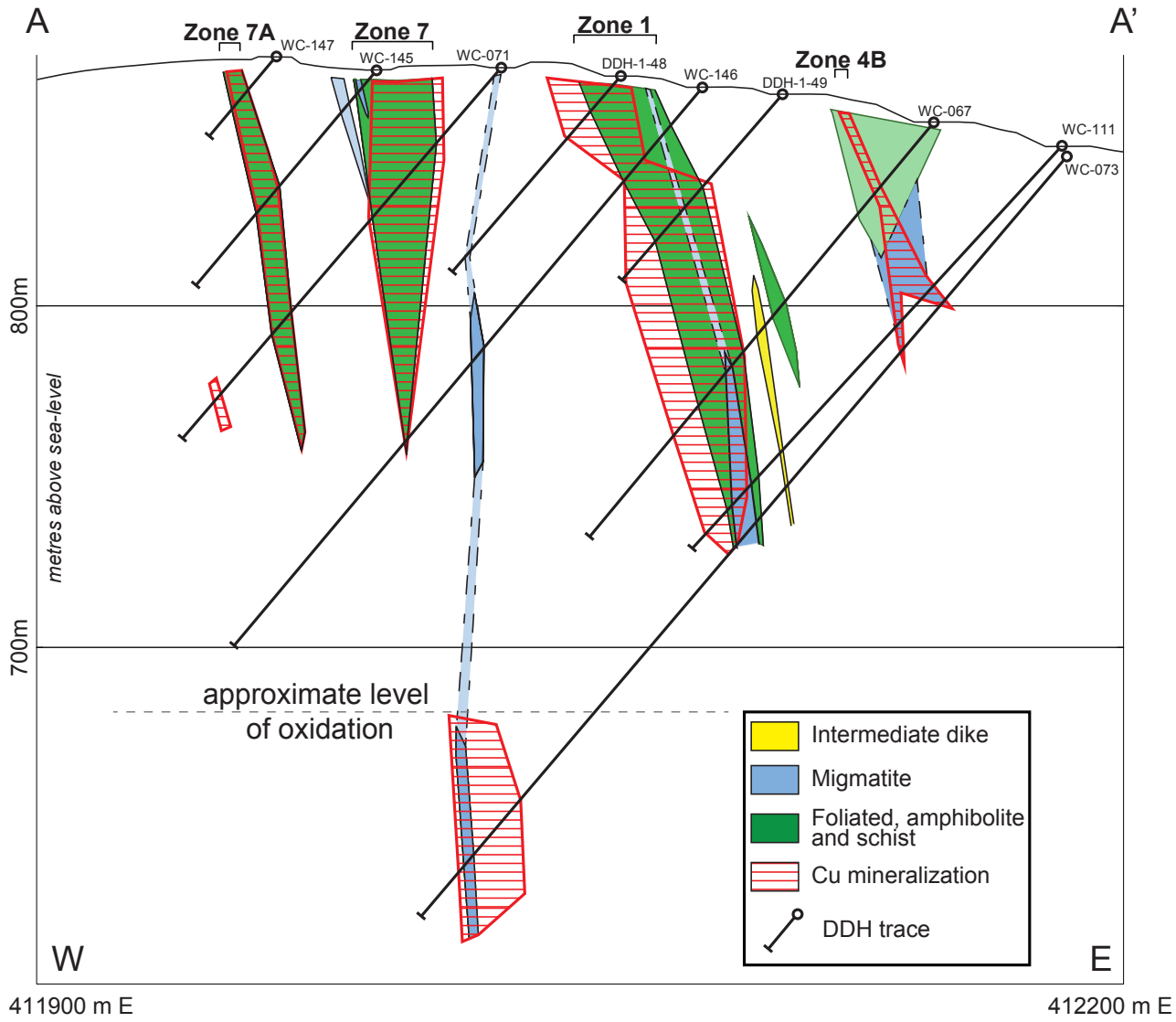


Figure 3-16. *Cross section 200N (50 m thick, oriented N066) through southern part of the main area; UTM NAD 83, Zone 8, looking north. Location of cross section shown on Figure 3-15. White area is unfoliated granodiorite to monzodiorite. Faded colours indicate our interpretation which utilizes surface mapping and terminology of Kovacs (2018). Extent of Cu mineralization based on total copper and oxide copper assays. Intermediate dike is likely related to the Upper Cretaceous Carmacks Group volcanic rocks. Modified from Casselman (2008). DDH = diamond drill hole.*

The majority of the resource at Carmacks Copper is within the upper oxidized portion of the orebodies (Table 3-3) where weathering has created 1 to 3% pore space and supergene minerals commonly line and in-fill cavities as irregular and coliform masses, fill fractures and rim sulphides (JDS Energy and Mining Ltd., 2016). The majority of the copper in the supergene portions is in malachite, cuprite, azurite and tenorite, with trace amounts of covellite, digenite, djurleite and native copper (Fig. 3-17; JDS Energy and Mining Ltd., 2016). Non-copper-bearing supergene minerals include limonite, goethite, specular hematite and gypsum (JDS Energy and Mining Ltd., 2016).

Hypogene copper-bearing minerals in the Carmacks Copper deposit are bornite and chalcopyrite (Tafti, 2005; Kovacs, 2018). Non-copper-bearing hypogene minerals include magnetite, pyrite, pyrrhotite and carbonate, with trace amounts of native gold and bismuth, molybdenite, bismuthinite and arsenopyrite (JDS Energy and Mining Ltd., 2016). In Zones 1 and 7,



Figure 3-17. *Supergene copper mineralization at Zone 1, Carmacks Copper deposits.* ***(a)*** *'Discovery trench', showing abundant supergene copper, most obvious is blue-green malachite but azurite and tenorite are also common. Approximate location of (b) shown in centre left.* ***(b)*** *Close-up of quartz-plagioclase-biotite schist, migmatite and a late dike. Supergene copper mineralization coating all three rock types; hammer head 13 cm.* ***(c)*** *Reflected light image of a hypogene copper mineral (bornite) weathering to a supergene copper mineral (covellite) with specular hematite (from trench 91-11; Tafti, 2005).*

hypogene copper mineralization is zoned from bornite in the north to chalcopyrite, and finally to minor pyrite-pyrrhotite in the south (JDS Energy and Mining Ltd., 2016). Gold is associated with bornite and as a result, gold values are higher in the northern half of the main area (average 0.75 g/t Au) and lower in the southern half (average 0.27 g/t Au; JDS Energy and Mining Ltd., 2016). In the lower hypogene portions of the orebodies, sulphide minerals have three distinct textural and rock associations (Fig. 3-18). The least metamorphosed sections of amphibolite and schist contain either disseminated chalcopyrite and pyrite or foliaform chalcopyrite and bornite, whereas migmatized portions of the rafts are characterized by net-textured bornite and chalcopyrite (Kovacs, 2018). Disseminated and foliaform sulphides are interpreted as the earliest mineralization (*i.e.*, pre-Granite Mountain batholith) whereas net-textured sulphides have been partially melted and locally remobilized, likely as a result of the Granite Mountain batholith engulfing the rafts (Kovacs, 2018).

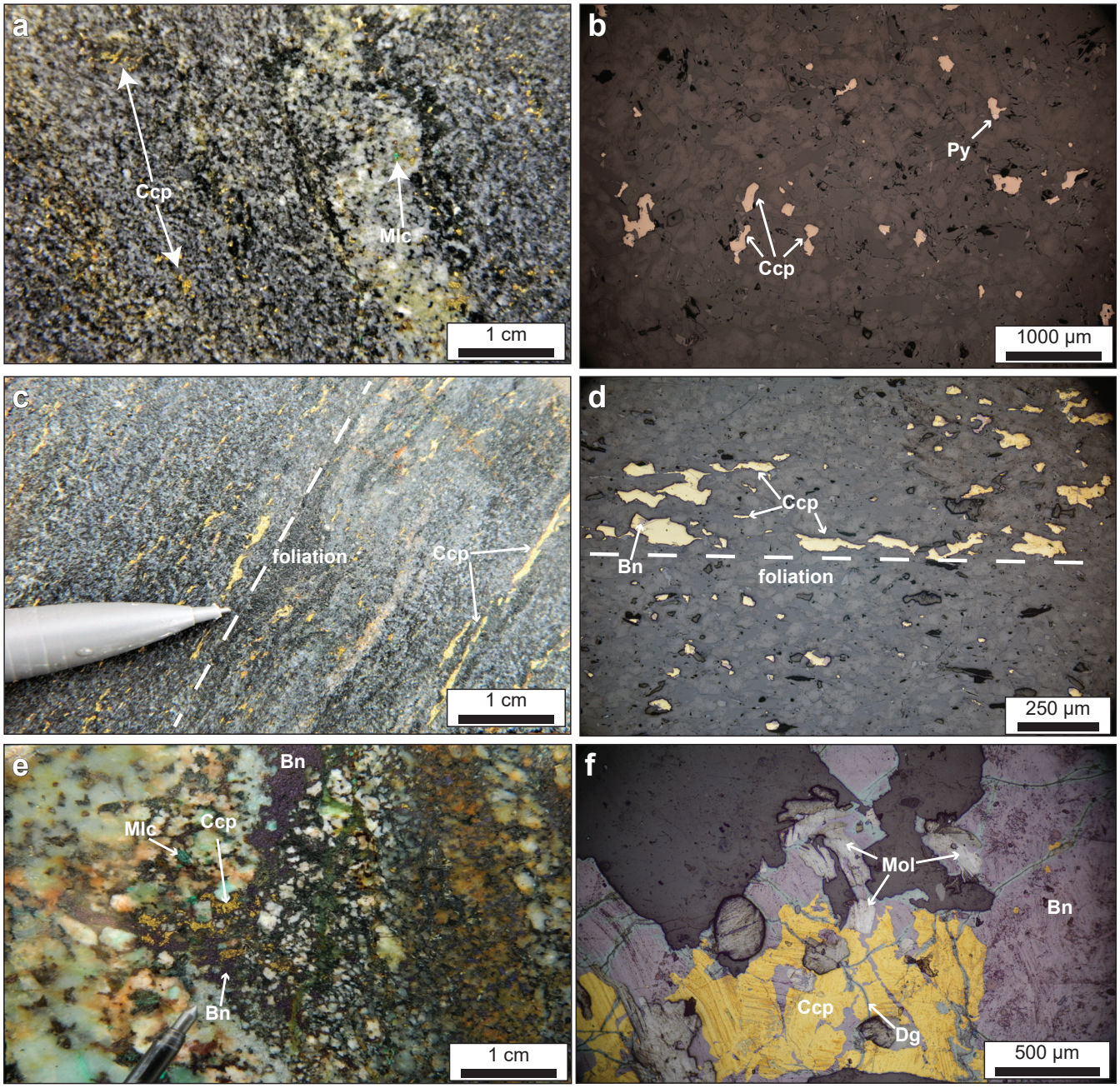


Figure 3-18. *Disseminated, foliaform and net-textured hypogene copper mineralization at the Carmacks Copper deposits. All images from Kovacs (2018).* ***(a)*** *Disseminated chalcopyrite mineralization in the quartz-plagioclase-biotite schist, CN15024-44.5 m.* ***(b)*** *Reflected light photomicrograph of disseminated chalcopyrite ± pyrite, CN15024-54.88 m.* ***(c)*** *Foliaform chalcopyrite mineralization in the amphibolite, WC005-254.4 m.* ***(d)*** *Reflected light photomicrograph of foliaform chalcopyrite-bornite mineralization in amphibolite, WC005-254.4 m.* ***(e)*** *Net-textured bornite-chalcopyrite mineralization in diatexite migmatite, WC002-148 m.* ***(f)*** *Reflected light photomicrograph of net-textured bornite-chalcopyrite mineralization in migmatite, WC008-174.31 m.*

Geochronology

U-Pb

The bulk of geochronological studies of the Granite Mountain batholith were conducted at the Carmacks Copper deposit as part of two Master's theses (Tafti, 2005; Kovacs, 2018). The earlier study of Tafti (2005) used standard ID-TIMS methods on air abraded, multi-grain zircon fractions (analyzed at UBC) and yielded a wide range of $^{206}Pb/^{238}U$ dates between 216 and 185 Ma suggesting a mixture of complex zircons, including inherited and Pb-loss components (Fig. 3-19). The majority of zircon $^{206}Pb/^{238}U$ dates in Tafti's samples range between ~200 and 195 Ma indicating an average date of *ca.* 198 Ma for granodiorite host at Carmacks Copper. Older zircon components (>200 Ma) are most common in samples from mineralized rafts of mafic schist and amphibolite, but also occur as inferred xenocrysts in *ca.* 197 Ma K-feldspar porphyritic granodiorite (Fig. 3-19; Tafti, 2005).

The more recent study of Kovacs (2018) employed more modern dating techniques, including CL imaging of zircon and a combination of LA-ICPMS and CA-TIMS methods on single grains (analyzed at UBC). Zoned igneous zircons from three samples of granodiorite to monzodiorite intrusive hosts at Carmacks Copper yielded CA-TIMS dates of 195.14 ± 0.25 Ma, 195.11 ± 0.19 Ma and 194.34 ± 0.16 Ma (Fig. 3-19; Kovacs, 2018). One sample of K-feldspar porphyritic granodiorite contained an older, inherited zircon with a $^{206}Pb/^{238}U$ date of *ca.* 200 Ma. A sample of diatexite migmatite collected at the margin of a mineralized amphibolite raft yielded a slightly older CA-TIMS crystallization date of 197.41 ± 0.17 Ma, and also contained an older, inherited component at *ca.* 199 Ma (Fig. 3-19; Kovacs, 2018).

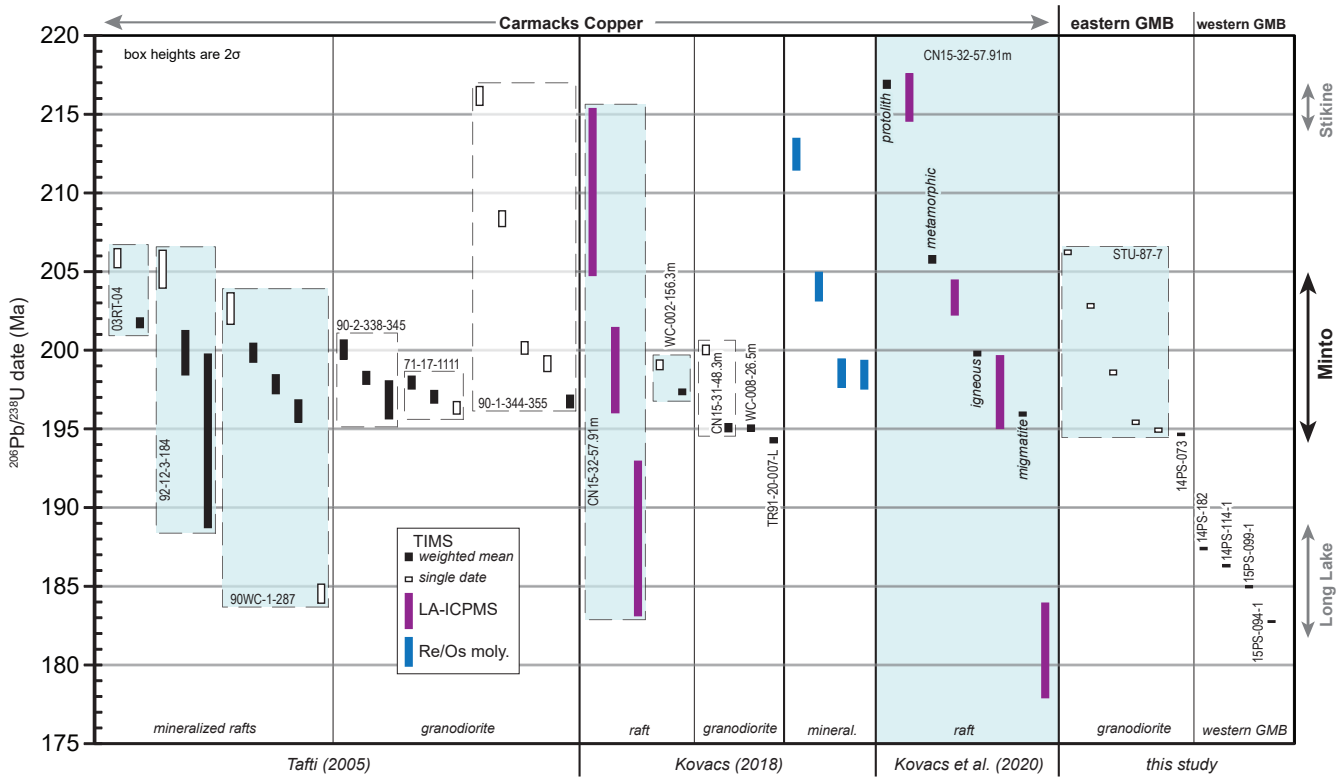


Figure 3-19. *Summary of $^{206}Pb/^{238}U$ zircon dates from the Granite Mountain batholith. The majority of samples dated were collected at the Carmacks Copper deposit (Tafti, 2005; Kovacs, 2018). New CA-TIMS dates from the eastern margin of Granite Mountain batholith collected for this study are shown at right (eastern GMB). Also shown are younger dates from the western portion of the batholith for comparison at far right (western GMB; see Chapter 4). Re-Os dates from molybdenite in ore at the Carmacks Copper deposits are also shown for comparison (Kovacs, 2018). Samples shown with blue shading were collected from mineralized foliated rafts at the Carmacks Copper and Stu occurrences. Double arrows along the right edge of the diagram indicate age ranges of the Stikine (217–214 Ma), Minto (205–194 Ma) and Long Lake (188–184 Ma) suites.*

Zircons from a sample of quartz-plagioclase-biotite schist collected from a foliated, partially melted raft within the Granite Mountain batholith (CN15-32-57.91m, Zone 13; Kovacs, 2018) exhibit complexities in CL images with older cores, CL-bright concentrically zoned domains, and irregular, CL-dark domains likely reflecting metamorphism and/or partial melting (Fig. 3-20). In an attempt to resolve this complexity, Kovacs (2018) used the LA-ICPMS method to *in situ* date the various zircon components (Fig. 3-19). The oldest component identified consists of a single core dated at 347.6 ± 6.4 Ma (Kovacs, 2018; not shown on Fig. 3-19). Concentrically zoned, CL-bright zircon with moderate U concentrations yielded a weighted mean date of 210.1 ± 5.3 Ma (n = 5; Fig. 3-19) that Kovacs (2018) interprets as the crystallization age of the mafic protolith. These igneous zircons are overprinted by patchy, CL-grey, homogeneous and convoluted zircon sectors that likely formed as a result of metamorphic recrystallization or migmatization. These yielded a weighted mean date of 198.8 ± 2.7 Ma (n = 16; Fig. 3-19). Outer, CL-dark zircon rims probably result from Pb loss at *ca.* 188.1 ± 4.9 Ma (Fig. 3-19).

In order to refine these results, zircon grains from sample CH15-32-57.91m were further analyzed at Boise State University. Zircons were polished and imaged on two sides of 30–40 μm wafers, and U-Pb and trace element data were collected by LA-ICPMS. From these results, major zircon components were isolated by laser-cutting and analyzed by CA-TIMS. At least 5 zircon components are recognized in LA-ICPMS and CA-TIMS analyses from this sample (Kovacs *et al.*, 2020):

1. Older cores (n = 2) defining an inherited component with a LA-ICPMS weighted mean date of 356 ± 9 Ma (not shown on Fig. 3-19).
2. A population (n = 11) of zircons having CL-dark rims and heterogeneous chemical composition with a weighted mean LA-ICPMS date of 216.1 ± 1.5 Ma. Cores isolated by laser-cutting from this population yielded a CA-TIMS date of 217.53 ± 0.16 Ma (n = 2, Fig. 3-19; labelled "*protolith*").
3. The majority of LA-ICPMS analyses (n = 67) have homogeneous chemical compositions typical of arc magma and are inferred to represent an igneous population with a weighted mean date of 203.4 ± 1.1 Ma. Nine cores isolated by laser-cutting yielded a weighted mean CA-TIMS date of 199.84 ± 0.14 Ma (Fig. 3-19; labelled "*igneous*").

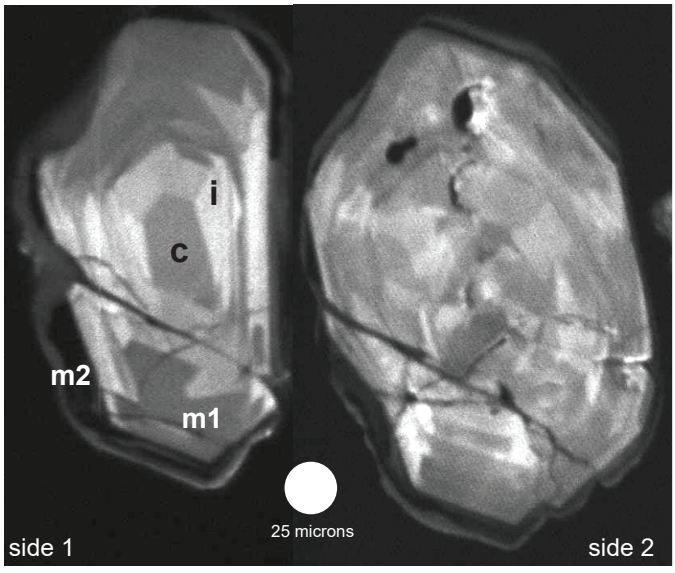


Figure 3-20. *Cathodoluminescence (CL) images of two sides of a doubly polished zircon from sample CN15-32-57.91m (Zone 13; Carmacks Copper deposit). Zircons from this sample exhibit complex internal morphology evidenced by the mottled texture in CL images (cf. side 2). Imaging of side 1 shows a distinct CL-grey core (c) surrounded by a brighter, concentrically zoned domain representing igneous growth (i), outer irregular CL-grey zones (m1), and a CL-dark rim (m2), the latter interpreted as resulting from metamorphism and/or partial melting.*

4. Eighteen zircon domains with CL-dark rims and cores have chemical compositions typical of secondary zircon formed during metamorphism and partial melting. They show a spread in age from *ca.* 207 to 189 Ma and yield a weighted mean LA-ICPMS date of 197.4 ± 2.3 Ma. Laser-cut fragments from these metamorphic zircons yield two clusters of equivalent CA-TIMS dates at 205.82 ± 0.23 Ma (n = 3; labelled "*metamorphic*") and 196.01 ± 0.12 Ma (n = 4; Fig. 3-19; labelled "*migmatite*").
5. An even younger metamorphic zircon component is represented by two equivalent LA-ICPMS analyses of 181.4 ± 3.0 Ma (Fig. 3-19).

For this study, two samples of granodiorite from the northeastern part of the Granite Mountain batholith were collected outside of the well-studied Carmacks Copper project and analyzed by LA-ICPMS and CA-TIMS methods at Boise State University. Sample STU80-7-286.5 is from a diorite enclave within granodiorite at the Stu occurrence, ~11 km northwest of Carmacks Copper (Figs. 3-5 and 3-13). The sample yielded numerous stubby, prismatic zircons with magmatic zoning (Fig. 3-21a). Thirty LA-ICPMS spot analyses yielded $^{206}Pb/^{238}U$ dates between 218 and 183 Ma, and a weighted mean of 194.0 ± 1.7 Ma (n = 28; Fig. 3-21b). Five zircons free of inclusions were selected for CA-TIMS and yielded non-equivalent $^{206}Pb/^{238}U$ dates scattered from 206.27 ± 0.14 to 194.99 ± 0.13 Ma (Fig. 3-21c), a pattern similar to complex zircons found in the Carmacks Copper deposit (Fig. 3-19).

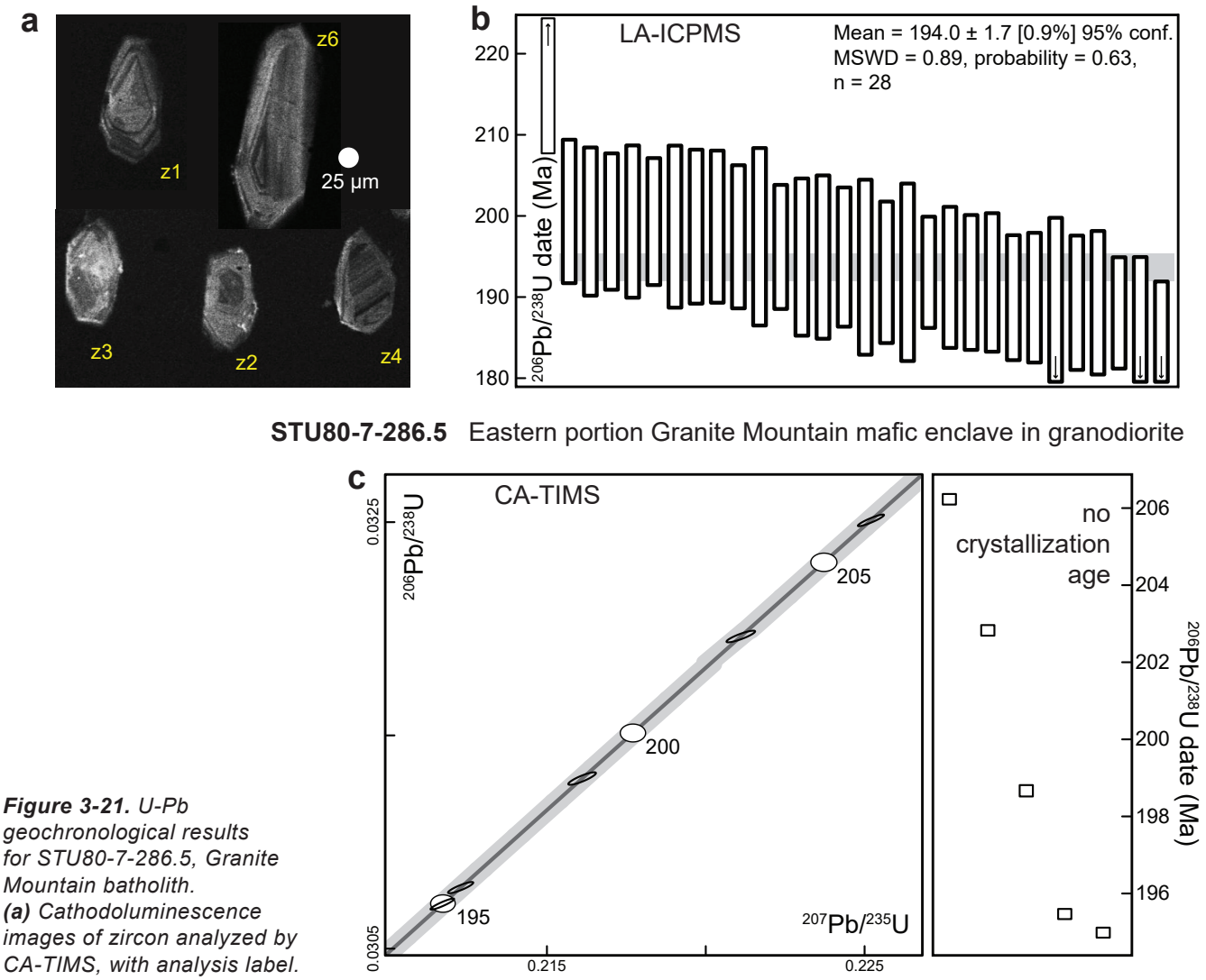


Figure 3-21. *U-Pb geochronological results for STU80-7-286.5, Granite Mountain batholith.* ***(a)*** *Cathodoluminescence images of zircon analyzed by CA-TIMS, with analysis label.* ***(b)*** *Ranked plot of $^{206}Pb/^{238}U$ dates determined by LA-ICPMS.* ***(c)*** *Concordia plot of CA-TIMS dates. The light grey band around concordia (dark grey line) illustrates the decay constant uncertainties. Ranked $^{206}Pb/^{238}U$ date plot is to the right of the concordia plot. Errors in all plots are at 2σ. MSWD = mean squared weighted deviation, n = number of analyses included in age calculation.*

Sample 14PS073-1 is a monzodiorite from the youngest phase recognized from relative crosscutting relationships along the eastern margin of the Granite Mountain batholith, ~9 km east of Carmacks Copper (Fig. 3-5). This sample yielded small, prismatic zircon needles (Fig. 3-22a). Thirty-two LA-ICPMS spot analyses yielded $^{206}Pb/^{238}U$ dates between 216 and 187 Ma, and a weighted mean of 197.6 ± 2.2 Ma (n = 31; Fig. 3-22b). Six zircons from 14PS073-1 were analyzed by CA-TIMS; five yielded equivalent $^{206}Pb/^{238}U$ dates of 194.71 ± 0.07 Ma (MSWD = 0.85, n = 5) and one grain is slightly younger at 194.31 ± 0.14 Ma (Fig. 3-22c).

Re-Os

Kovacs (2018) also provided constraints on mineralization at Carmacks Copper by dating molybdenite aliquots from 4 samples using the $^{187}Re/^{187}Os$ method. Molybdenite occurs with copper sulphide minerals and exhibits two textural types: Type 1 molybdenite comprises anhedral to subhedral, kinked and locally sieve-textured grains; and Type 2 molybdenite consists of euhedral to subhedral flakes intergrown with net-textured sulphides. The four samples yielded $^{187}Re/^{187}Os$ dates ranging from 212.5 ± 1.2 to 198.5 ± 0.9 Ma, representing various degrees of mixing of the two types of molybdenite in these samples; older dates are inferred to represent the approximate age of Type 1, and younger dates that of Type 2 molybdenite (Kovacs, 2018; Kovacs *et al.*, 2020).

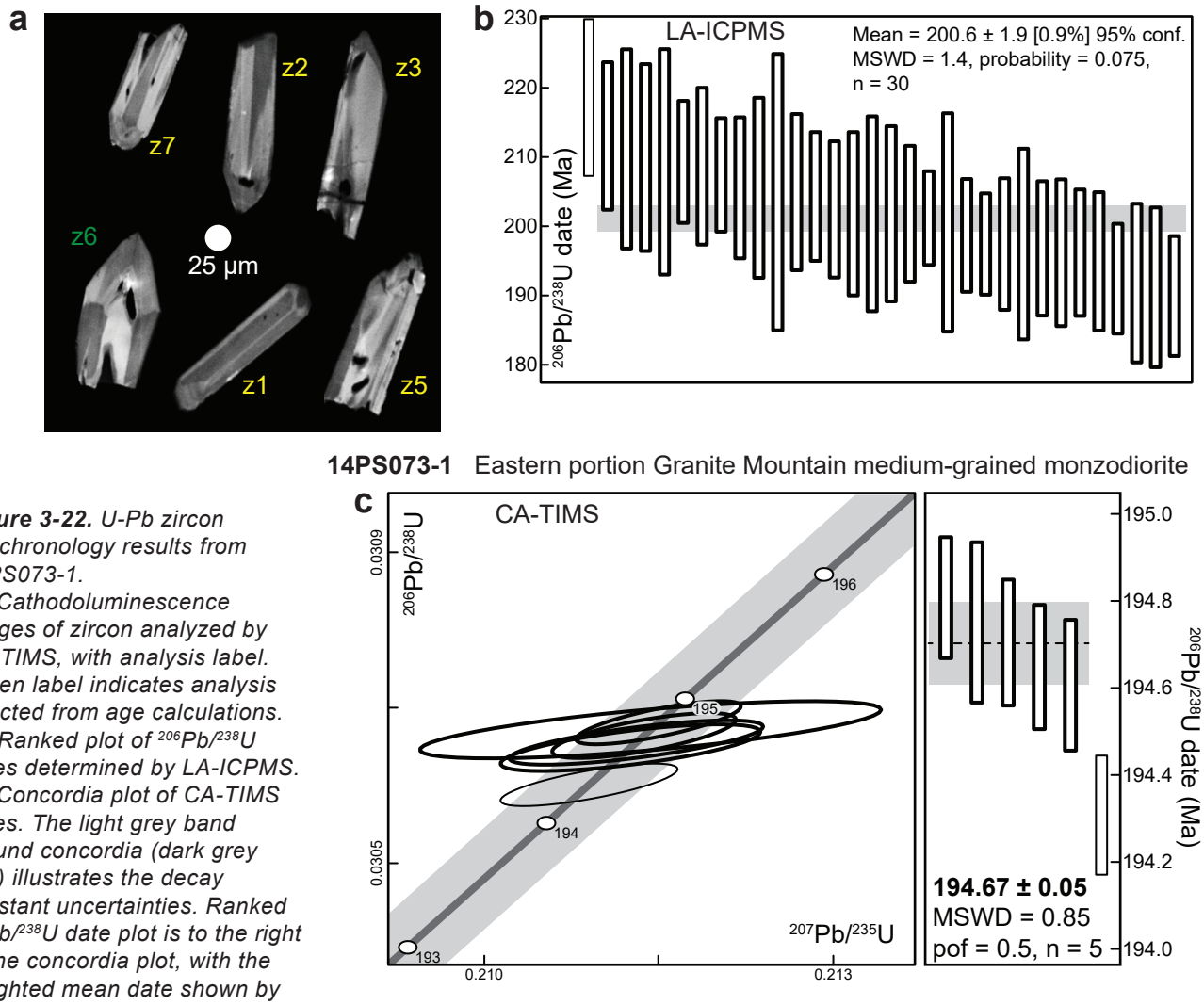


Figure 3-22. *U-Pb zircon geochronology results from 14PS073-1.*
(a) *Cathodoluminescence images of zircon analyzed by CA-TIMS, with analysis label. Green label indicates analysis rejected from age calculations.*
(b) *Ranked plot of $^{206}Pb/^{238}U$ dates determined by LA-ICPMS.*
(c) *Concordia plot of CA-TIMS dates. The light grey band around concordia (dark grey line) illustrates the decay constant uncertainties. Ranked $^{206}Pb/^{238}U$ date plot is to the right of the concordia plot, with the weighted mean date shown by the grey band. Analyses included in weighted mean date calculation are bold; analyses with thin lines are not used in calculation. Line-type designations are the same in all plots. Errors in all plots are at 2σ. MSWD = mean squared weighted deviation, pof = probability of fit, n = number of analyses included in age calculation.*

Ar-Ar

Hornblende and biotite from 4 samples of granodiorite from the northeastern part of the Granite Mountain batholith were analyzed by the $^{40}Ar/^{39}Ar$ method at the GSC laboratory in Ottawa (laser, step-heating; Appendix 6). Hornblende from three of these samples (14PS048, 14PS063 and 14PS183) yielded well-defined plateau ages between 187.0 ± 1.3 and 183.4 ± 1.4 Ma (Figs. 3-23 and 3-24). Biotite from all samples shows evidence of argon loss in early steps and plateau-like regions in mid to high temperature steps yielding cooling ages ranging from 187.1 ± 1.2 to 183.9 ± 1.1 Ma (Figs. 3-23 and 3-24). The concordance of hornblende and biotite ages from these samples suggest that the northeastern part of the Granite Mountain batholith cooled rapidly between the ~570°C closure of argon in hornblende and the ~350°C closure temperature for biotite (Fig. 3-25; Table 1-6). Our new $^{40}Ar/^{39}Ar$ dates are

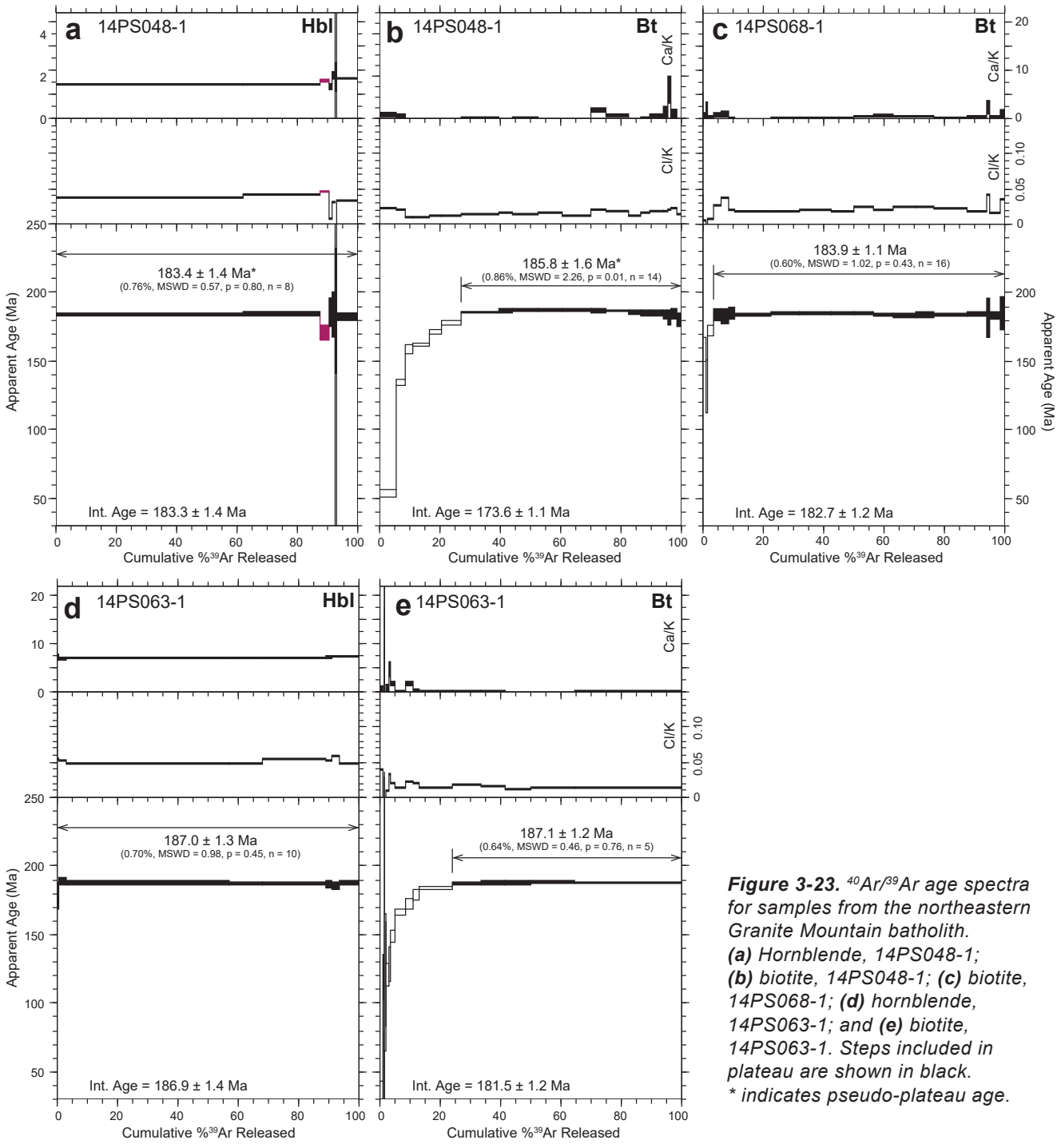


Figure 3-23. *$^{40}Ar/^{39}Ar$ age spectra for samples from the northeastern Granite Mountain batholith.* ***(a)*** *Hornblende, 14PS048-1;* ***(b)*** *biotite, 14PS048-1;* ***(c)*** *biotite, 14PS068-1;* ***(d)*** *hornblende, 14PS063-1; and* ***(e)*** *biotite, 14PS063-1. Steps included in plateau are shown in black. * indicates pseudo-plateau age.*

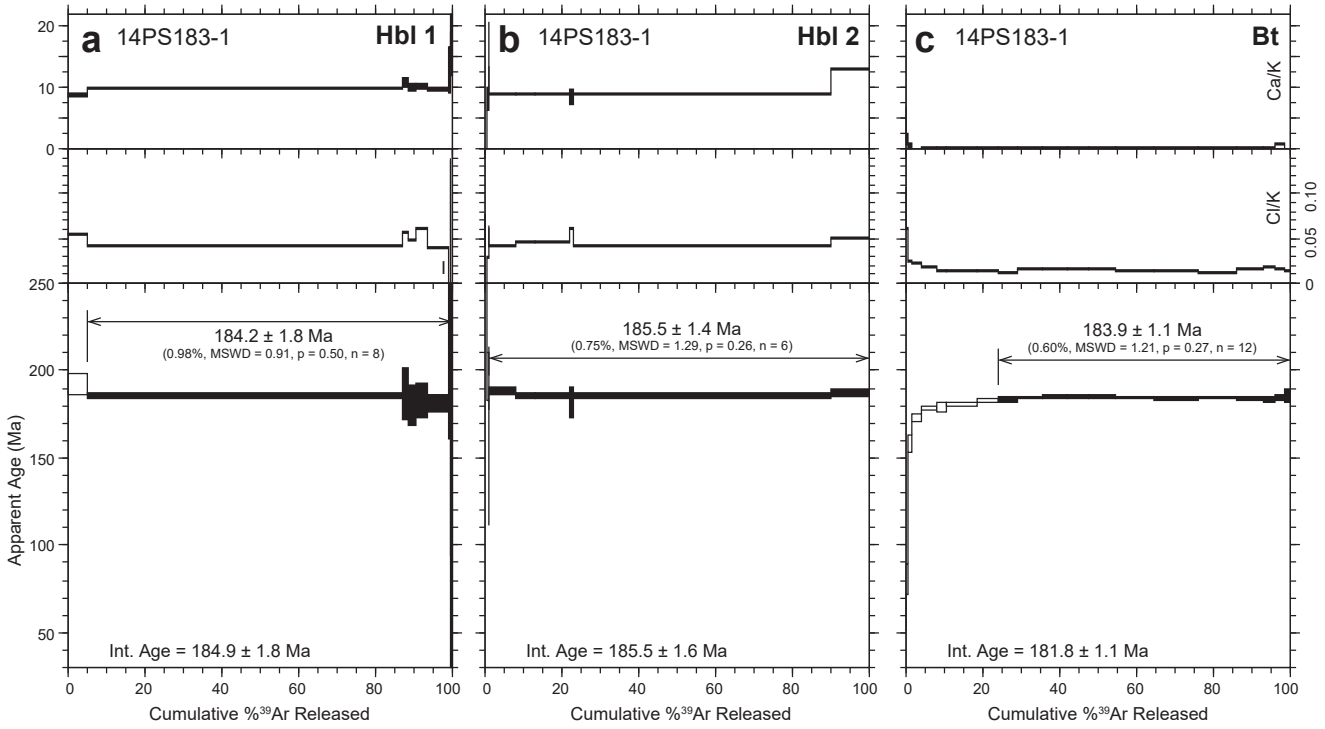


Figure 3-24. *$^{40}Ar/^{39}Ar$ age spectra for sample 14PS183-1 from the northern Granite Mountain batholith.* ***(a)*** *Hornblende, aliquot 1;* ***(b)*** *hornblende, aliquot 2; and* ***(c)*** *biotite. Steps included in plateau are shown in black.*

systematically younger than previous hornblende (191.3 ± 0.8 Ma, 90-1-344-355; Tafti, 2005) and biotite dates (197.1 ± 1.2 Ma, VNCH-98-14a; Joyce *et al.*, 2015) from the Carmacks Copper deposit (Figs. 3-25 and 3-26). The new $^{40}Ar/^{39}Ar$ dates are also 8–12 m.y. younger than U-Pb zircon crystallization ages (*ca.* 200–195 Ma) for the northeastern part of the Granite Mountain batholith (Figs. 3-19 and 3-25). These more closely resemble the U-Pb zircon crystallization ages (*ca.* 187–183 Ma) and a $^{40}Ar/^{39}Ar$ hornblende date from the southwestern part of the batholith (Figs. 3-25 and 3-26; *see* Chapter 4 for further discussion).

Summary of geochronological results

The complexity of zircons in the Granite Mountain batholith resulted in an apparent scatter of dates when analyzed by standard ID-TIMS methods on multi-grain fractions (*e.g.*, Tafti, 2005; Fig. 3-19). By using more modern techniques, including CL imaging and analyses of single zircon crystals by CA-TIMS, Kovacs (2018) was able to refine dating of the granodiorite in the northeastern Granite Mountain batholith to 197–194 Ma, but still recognized older components of *ca.* 200 Ma in some samples (Fig. 3-19). Our analysis of sample 14PS073 yielded comparable results with a date of 194.71 ± 0.14 Ma (Fig. 3-22). The detailed analysis of zircons from a mineralized raft at the Carmacks Copper deposit, using a combination of LA-ICPMS and CA-TIMS

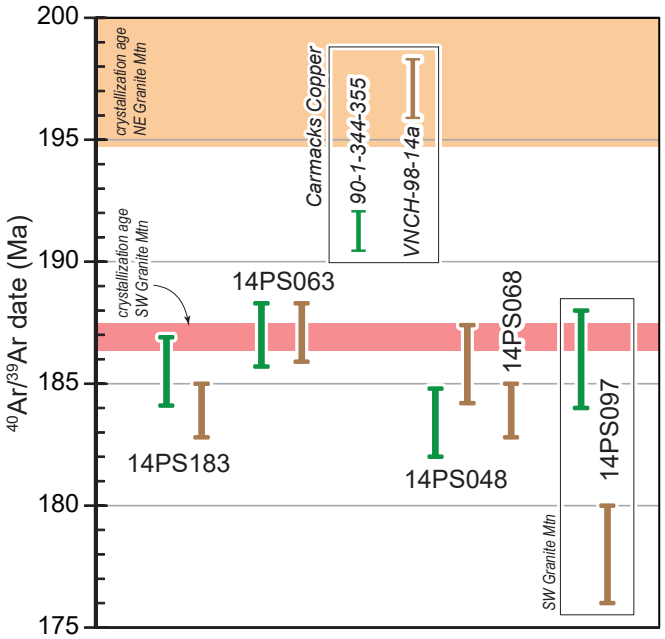


Figure 3-25. *Summary of $^{40}Ar/^{39}Ar$ dates from the Granite Mountain batholith. Most results are from this study (Appendix 5); samples from the Carmacks Copper deposit are from Tafti (2005; 90-1-344-355) and Joyce et al. (2015; VNCH-98-14a). Orange band at top indicates range of U-Pb crystallization dates from the northeastern part of the Granite Mountain batholith (ca. 200–195 Ma); red band near centre of diagram indicates range of U-Pb zircon crystallization dates for the younger, southwestern part of the Granite Mountain batholith (ca. 187.5 to 186.4 Ma; Long Lake suite, see Chapter 4).*

on laser-cut fragments, help further resolve the complex history of the Granite Mountain batholith (sample CN15-32-57.91m, Fig. 3-19; Kovacs *et al.*, 2020). Using this approach, Kovacs *et al.* (2020) established the age of protolith for rafts in the Granite Mountain batholith at 217.53 ± 0.16 Ma, thereby indicating correlation with rocks of the Stikine and Pyroxene Mountain plutonic suites or Upper Triassic basalts of the Povoas formation (*see* Chapter 2). A first episode of metamorphic zircon growth occurred at 205.82 ± 0.23 Ma and likely reflects timing of burial and metamorphism of the protolith. The main phase of zircon growth recorded in this sample is at 199.84 ± 0.14 Ma and is interpreted as an early phase of the Granite Mountain batholith. A second episode of metamorphic zircon growth at 196.01 ± 0.12 Ma likely reflects migmatization of the rafts during intrusion of the main phases of the batholith at 197–194 Ma (Kovacs, 2018; this study). Finally, a younger population of metamorphic zircons at *ca.* 188–181 Ma likely reflects Pb loss associated with intrusion of the younger, southwestern part of the batholith (*ca.* 187–183 Ma; *see* Chapter 4). The detailed analysis of zircons in sample CN15-32-57.91m by Kovacs *et al.* (2020) provides a solid framework to explain the apparent scatter of dates in older samples analyzed by ID-TIMS on multi-grain fractions (Fig. 3-19).

Rhenium-osmium dating of molybdenite from the Carmacks Copper ore suggests that the mineralization is Late Triassic, with the oldest date of 212.5 ± 1.2 Ma providing a minimum estimate of the age of mineralization (Kovacs, 2018). The younger $^{187}Re/^{187}Os$ dates of *ca.* 198 Ma likely reflect timing of recrystallization of the ore during intrusion of the various phases of the Granite Mountain batholith beginning at *ca.* 200 Ma and ending at *ca.* 195 Ma (Fig. 3-19).

Finally, $^{40}Ar/^{39}Ar$ results from this study suggest that the northeastern part of the Granite Mountain batholith likely did not cool below ~570°C until *ca.* 187 Ma, or that intrusion of the younger, southwestern part of the batholith reheated the older granodiorite well above the ~570°C closure temperature for argon in hornblende.

Thermobarometry

Three samples from the Minto suite portion of the Granite Mountain batholith, 14PS048-1, 14PS183-1 and STU80-7-286.5, contain the suitable mineral assemblage for Al-in-Hbl geobarometry (Appendix 3). Al^{TOT} in hornblende for these samples is between 2.03 and 1.86% with cotectic plagioclase that has X_{An} of 0.28 to 0.25. Crystallization pressure estimates derived from these data are between

5.86 ± 0.91 and 4.77 ± 0.85 kbar (Fig. 3-26; Appendix 5; emplacement depths between 22.1 and 18.0 km). Solidus temperatures between 724 and 744°C derived using the amphibole-plagioclase thermometer of Holland and Blundy (1994) are slightly lower than the Ti-in-zircon temperature estimate of 772°C from sample 14PS073-1 (Watson *et al.*, 2006; Appendix 3). Our new data are consistent with previous studies by McCausland *et al.* (2002; n = 12) and Tafti (2005; n = 2) who report Al^{TOT} in hornblende between 2.20 and 1.86, with cotectic plagioclase X_{An} from 0.32 to 0.20, and amphibole-plagioclase temperatures from 711 to 771°C. Crystallization pressure estimates derived using these prior data are between 5.97 and 4.52 kbar (Fig. 3-26; emplacement depths between 22.6 and 16.1 km). Our Ti-in-zircon temperature of 772°C is also consistent with that of Kovacs (2018) who reports Ti-in-zircon temperatures of 632–838°C for Granite Mountain batholith rocks, and 762–868°C for zircon formed during migmatization of rafts at the Carmacks Copper deposit.

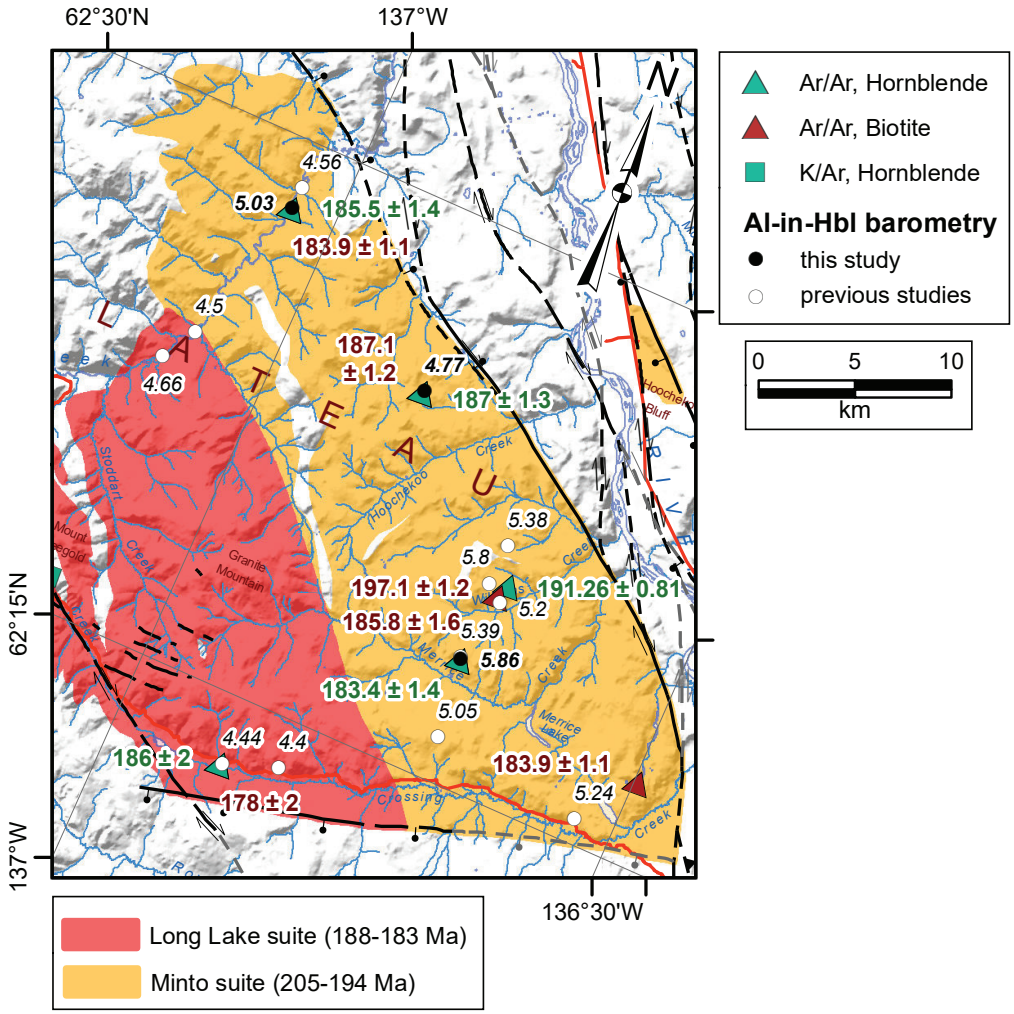


Figure 3-26. *Distribution of $^{40}Ar/^{39}Ar$ dates and pressure estimates from Al-in-hornblende geobarometry in the Granite Mountain batholith. Hornblende dates are labelled green; biotite have brown labels. Al-in-hornblende results from Tafti (2005) and McCausland et al. (2002), and from this study (Appendix 5). Fault symbology as in Figure 1-4.*

Minto pluton

The Minto pluton, ~40 km southwest of Pelly Crossing, is host to Cu-Ag-Au mineralization at the Minto mine (Fig. 3-1; Table 3-1). It has an exposed surface area of 170 km² and, similar to the Granite Mountain batholith, it straddles the boundary between Stikinia and Yukon-Tanana terranes (Fig. 3-2). The pluton intrudes Upper Triassic augite-phyric basalt of the Lewes River Group (Stikinia) to the east and is inferred to intrude Early Mississippian metaplutonic rocks of the Simpson Range plutonic suite (Yukon-Tanana terrane) to the west (Fig. 3-27; Tempelman-Kluit, 1984). This relationship is covered by Pliocene-Pleistocene basalt flows of the Selkirk Volcanic Group (Tempelman-Kluit, 1984; Jackson *et al.*, 1996; Nelson *et al.*, 2009), which separates the Minto pluton from the larger Yukon River batholith to the northwest (Fig. 3-2). Along its eastern margin, the Minto pluton is locally faulted against rocks of the Lewes River Group along the Ingersoll fault (Tempelman-Kluit, 1984; Fig. 3-27). To the south, the Minto pluton is locally overlain by red-weathering conglomerate and sandstone, and basalt of the Upper Cretaceous Carmacks Group which is down-dropped along a normal fault (Tempelman-Kluit, 1984). The conglomerate is polymictic, clast-supported, with cobble to boulder-sized clasts and includes mineralized clasts from the Minto orebodies (Hood, 2012). Detrital zircon from two samples of sandstone matrix from conglomerate indicate a

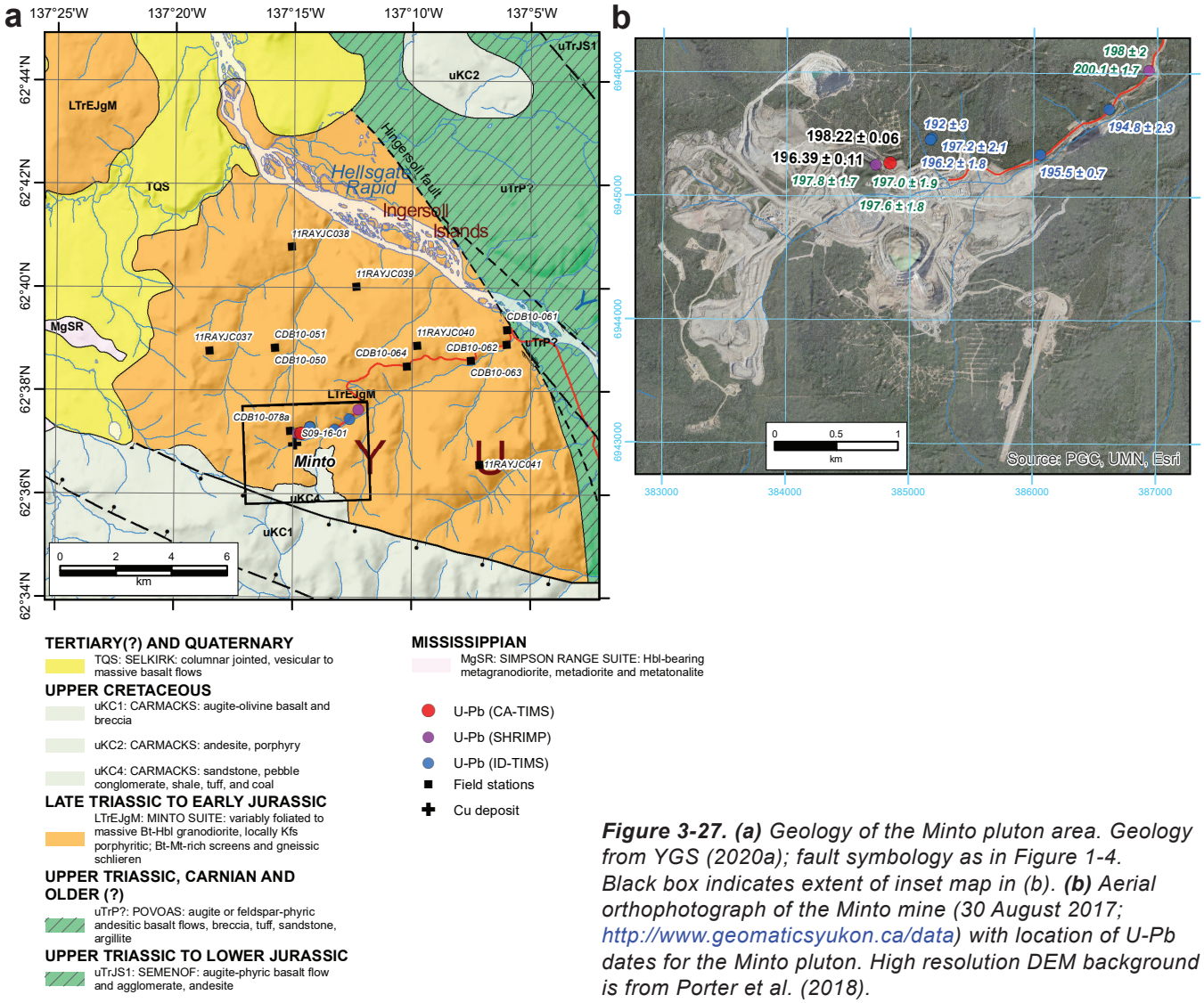


Figure 3-27. (a) *Geology of the Minto pluton area. Geology from YGS (2020a); fault symbology as in Figure 1-4. Black box indicates extent of inset map in (b).* ***(b)*** *Aerial orthophotograph of the Minto mine (30 August 2017; http://www.geomaticsyukon.ca/data) with location of U-Pb dates for the Minto pluton. High resolution DEM background is from Porter et al. (2018).*

Campanian (*ca.* 78 Ma) maximum depositional age (M. Colpron, unpublished data, 2008), and support the interpretation that this is a basal Carmacks clastic unit. At the Minto mine, Jurassic granodiorite and Cretaceous conglomerate are locally imbricated by a series of reverse faults with offsets in the order of tens of metres (Fig. 3-28).

The Minto pluton comprises mainly granodiorite and monzogranite (Fig. 3-3) that are variably medium-grained and equigranular to coarse-grained K-feldspar porphyritic, and generally undeformed (Fig. 3-29). These rocks intrude a series of stacked, tabular bodies of foliated granitoid, gneiss and migmatite that dip gently to the north and host the copper mineralization at the Minto mine (Fig. 3-30; Mercer and Sagman, 2012).



Figure 3-28. (a) *Reverse fault placed granodiorite of the Minto pluton over Upper Cretaceous conglomerate. Photo taken from eastern wall of main Minto pit, spring 2010. Bench height is approximately 5 m.* ***(b)*** *Close-up view of Upper Cretaceous conglomerate from exposure along the Minto mine airstrip. Hammer handle is approximately 3 cm wide.*

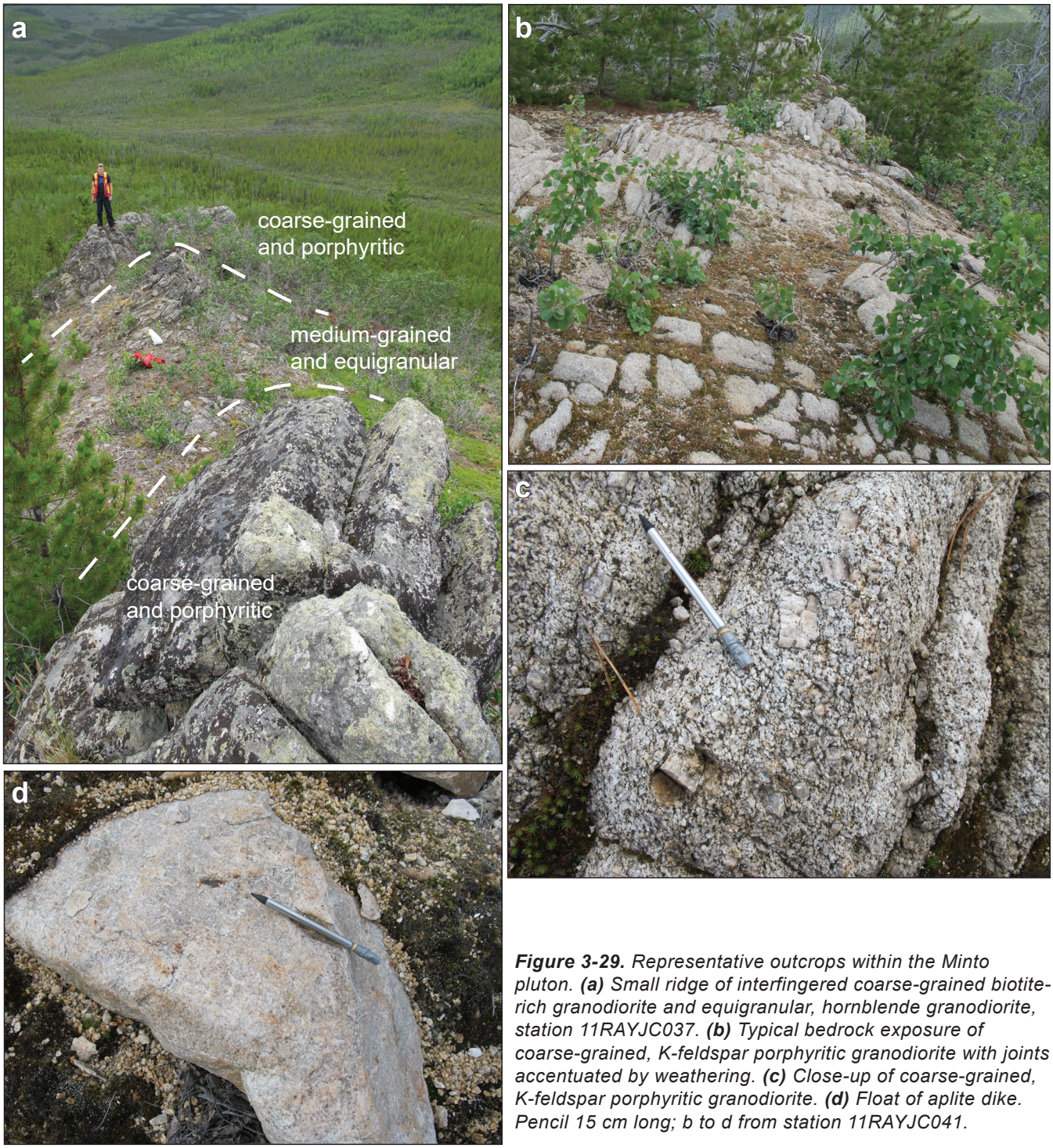


Figure 3-29. *Representative outcrops within the Minto pluton.* ***(a)*** *Small ridge of interfingered coarse-grained biotite-rich granodiorite and equigranular, hornblende granodiorite, station 11RAYJC037.* ***(b)*** *Typical bedrock exposure of coarse-grained, K-feldspar porphyritic granodiorite with joints accentuated by weathering.* ***(c)*** *Close-up of coarse-grained, K-feldspar porphyritic granodiorite.* ***(d)*** *Float of aplite dike. Pencil 15 cm long; b to d from station 11RAYJC041.*

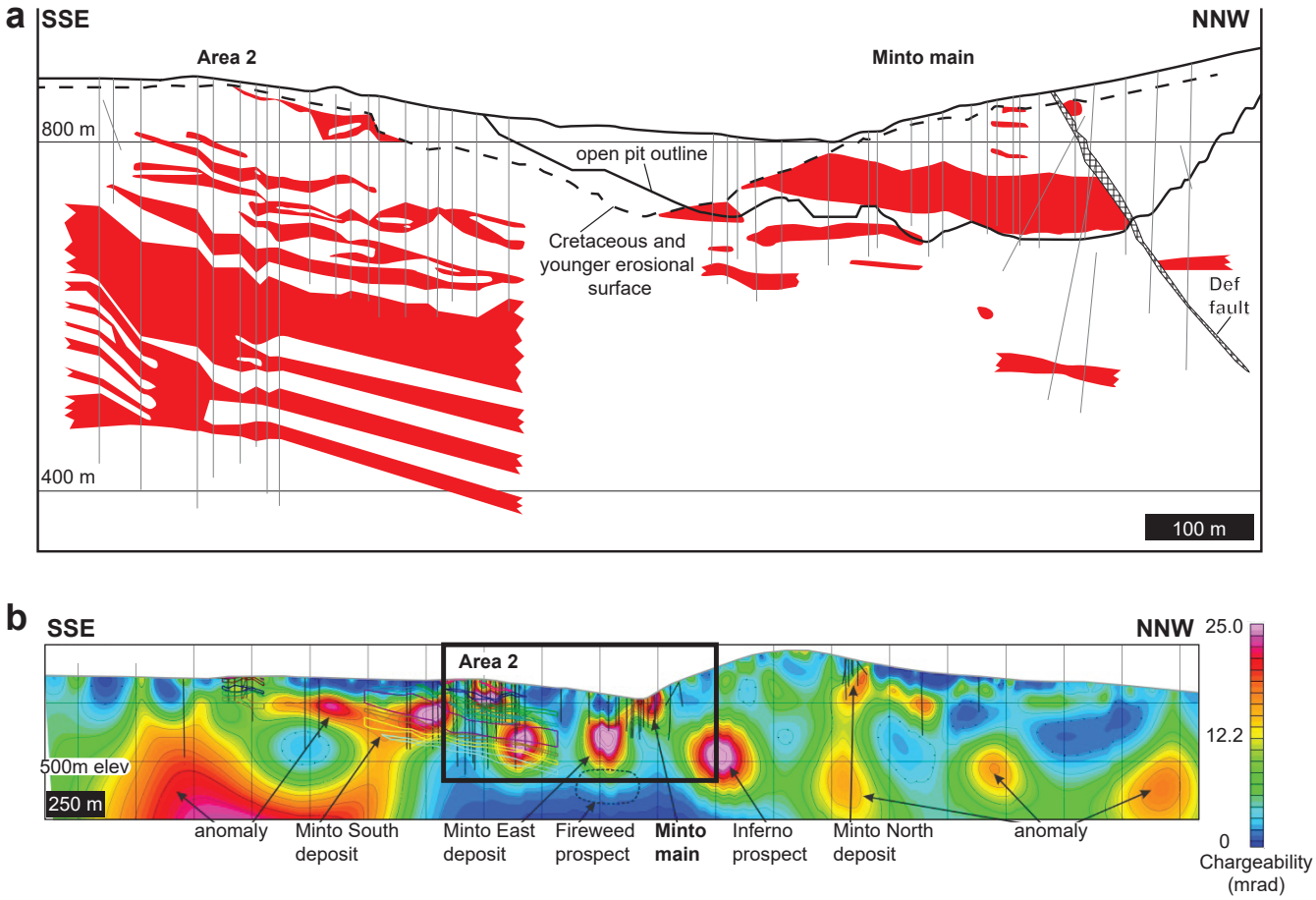


Figure 3-30. (a) *Vertical section through the Minto deposit prior to mining development, ca. 2007 (after Hood et al., 2009). Copper occurs within shallow-dipping bands of foliated and gneissic rocks (red).* ***(b)*** *Smooth IP chargeability from DC resistivity along Line 3 of a Titan-24 survey of the Minto property (after Verweerd et al., 2010; Mercer and Sagman, 2012). Note correspondence of high chargeability anomalies with known deposits.*

Petrography

Granodiorite is the dominant rock type in the Minto pluton (Fig. 3-3) although compositions tending to tonalite or diorite and a late aplite phase are also present (Fig. 3-29d). The rocks vary from crowded, coarse-grained, K-feldspar porphyritic to medium-grained and equigranular (Fig. 3-31); porphyritic rocks are slightly more resistant to weathering than equigranular rocks (Fig. 3-29a). In general, the granodiorite contains 30 to 50% plagioclase, 10 to 40% K-feldspar, 20 to 40% quartz, and 5 to 20% total biotite ± hornblende (Hood, 2012; this study). Accessory minerals include magnetite, epidote, titanite, apatite and zircon, all of which have sharp euhedral crystal faces in thin section (Hood, 2012). K-feldspar occurs most commonly as phenocrysts 1 to 3 cm long, with inclusions of biotite, plagioclase, hornblende, epidote and zircon common along growth zones. Tonalite and diorite are generally slightly coarser grained and typically contain plagioclase as both euhedral crystals up to 1 cm in length and anhedral equigranular crystals that are evenly distributed (Hood, 2012). Quartz forms anhedral masses interstitial to feldspar, but locally forms glomeroporphyritic masses up to 1 cm in diameter (Fig. 3-32a,b). Vermicular intergrowths of quartz in plagioclase form myrmekitic textures in nearly all samples from the pluton (Fig. 3-32c). Biotite and hornblende are the most common mafic minerals; they are typically <1 cm, and comprise up to 20% of the granodiorite (Fig. 3-33). Magmatic epidote is a ubiquitous accessory mineral in Minto pluton samples (Fig. 3-33).

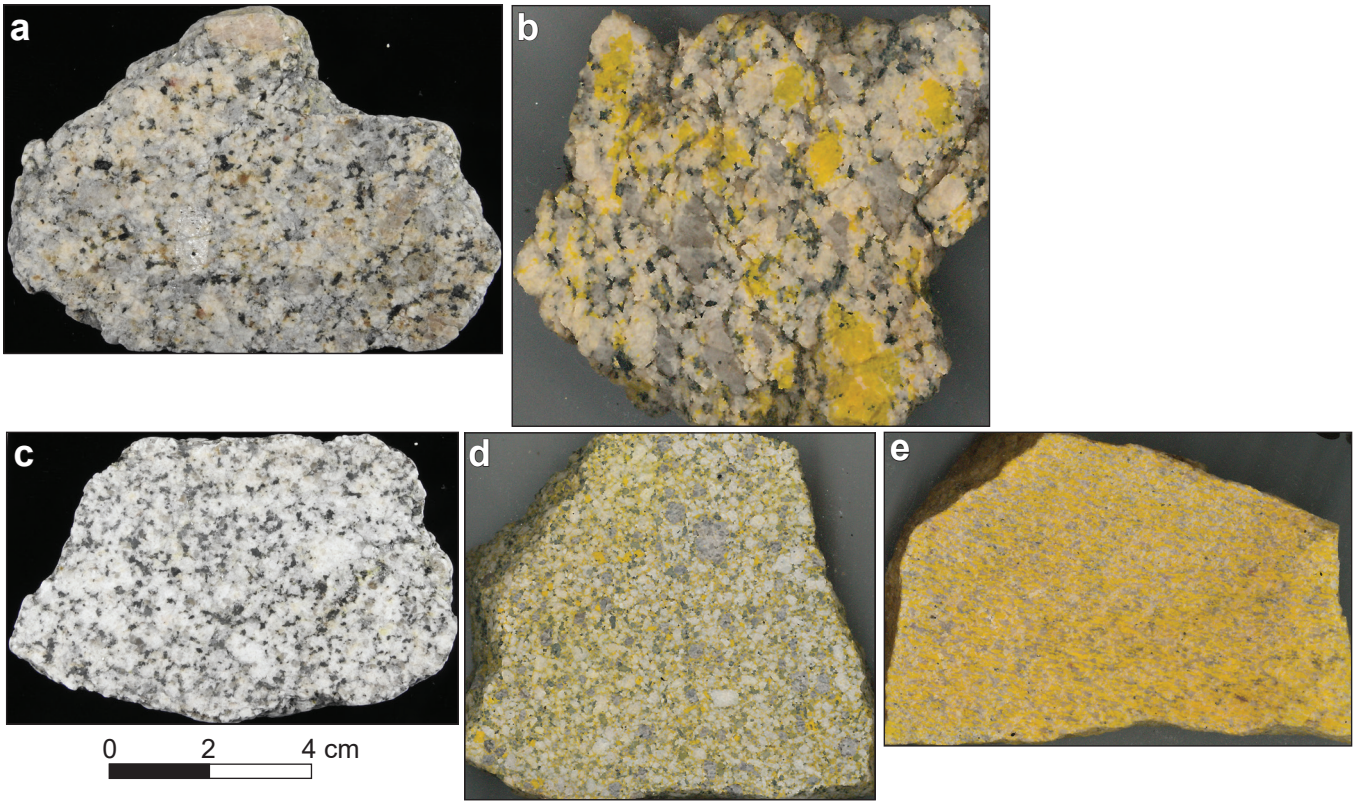


Figure 3-31. *Representative samples from the Minto pluton.* ***(a** and **b)** Coarse-grained, porphyritic granodiorite; a-11RAYJC040A, b-11RAYJC039A.* ***(c** and **d)** Medium-grained equigranular monzodiorite; c-11RAYJC042A, d-11RAYJC038A.* ***(e)** Monzonitic aplite; 11RAYJC041B. (a and c) Fresh polished surface and (b, d and e) cobaltinitrite-stained surface. Note K-feldspar is yellow.*

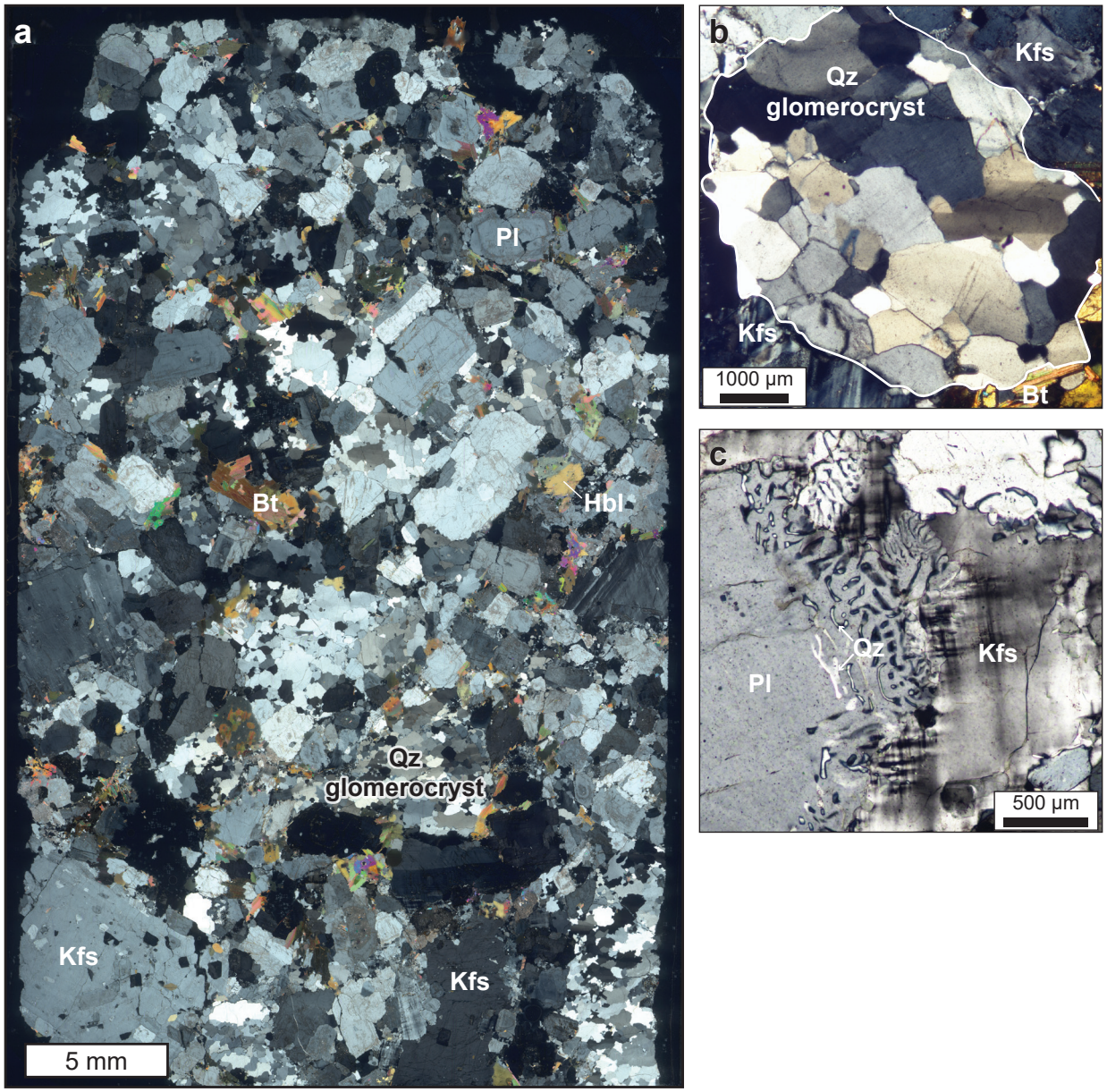


Figure 3-32. *Transmitted, cross-polarized light images from the Minto pluton.* ***(a)*** *Full thin section scan of representative K-feldspar porphyritic granodiorite; 11RAYJC040A.* ***(b)*** *Glomeroporphyritic quartz (outlined in solid white) within granodiorite; 11RAYJC036A.* ***(c)*** *Vermicular intergrowths of quartz and plagioclase (myrmekite) at the boundary with K-feldspar, 11RAYJC039A.*

Oxidation state and mineral occurrences

Unfoliated rocks of the Minto pluton have magnetic susceptibilities ranging from 2.00 to 25.00 × 10^{-3} SI units (mean 12.88 × 10^{-3} SI units; n = 4; Fig. 3-4). Increased magnetite content is frequently logged in mineralized intervals of diamond drill core at the Minto deposits and the magnetic susceptibility of these rocks is typically 10s to 100s × 10^{-3} SI units (Hood, 2012), higher than that of the surrounding unmineralized rocks (Mercer and Sagman, 2012). Hematite or hematite/magnetite domains correspond to brittle structures with low magnetic susceptibility suggesting supergene oxidation processes have locally partially or completely destroyed magnetite (Mercer and Sagman, 2012).

Nine MINFILE occurrences are located within the Minto pluton (Table 3-4; Fig. 3-34; YGS, 2020b). At the Minto mine, (represented by two MINFILE occurrences—Minto Main zone [115I 021] and Minto North [115I 022]) mineralization is identified in

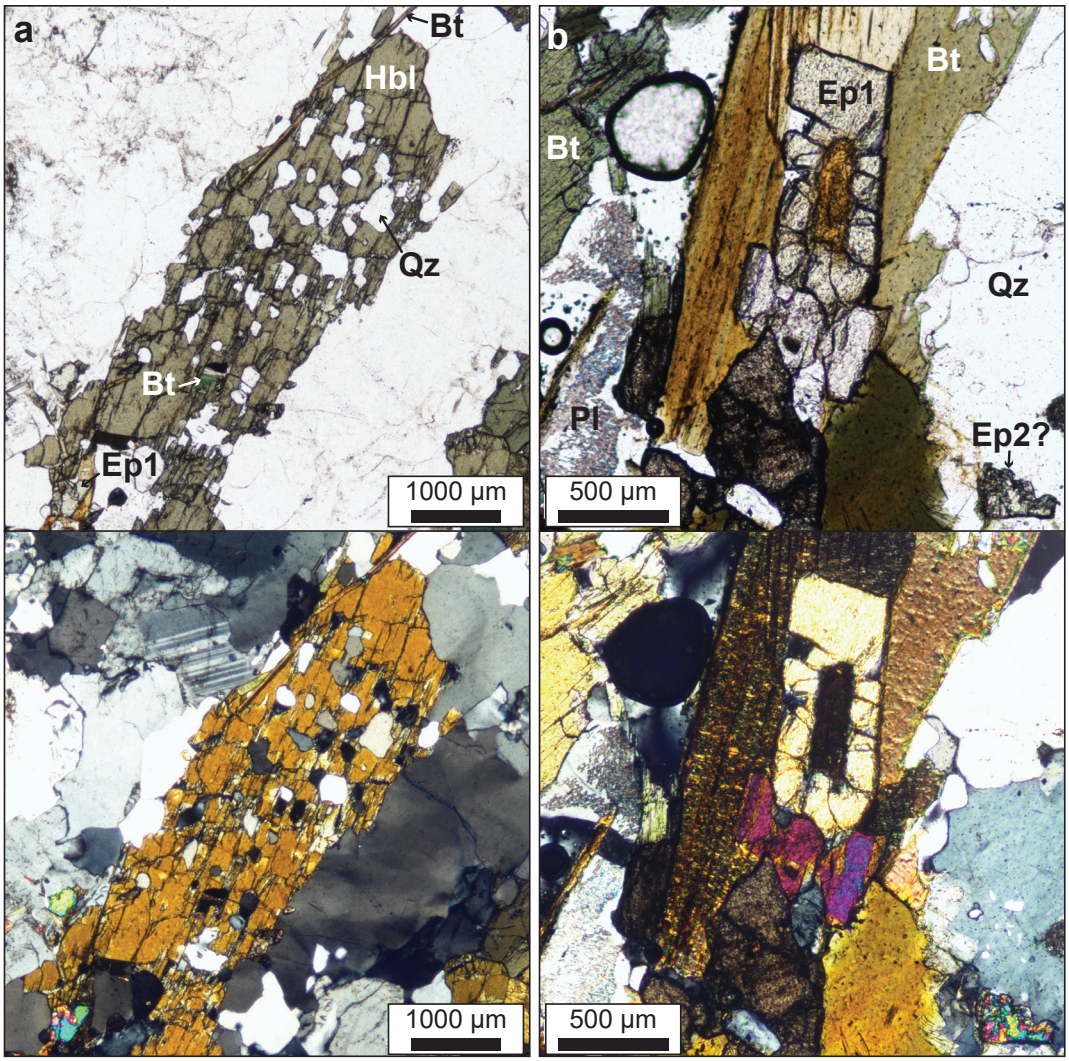


Figure 3-33. *Transmitted light photomicrograph pairs, plane polarized light (upper) and cross-polarized light (lower), of typical mafic minerals in the Minto pluton.* ***(a)*** *Poikilitic hornblende with plagioclase and quartz inclusions. Small euhedral epidote in the bottom left of image.* ***(b)*** *Large, zoned euhedral magmatic epidote surrounded by biotite. Both from 11RAYJC037A.*

8 zones (Fig. 3-34 inset) for a global resource of 63 Mt of sulphide ore grading 1.15% Cu, 0.42 g/t Au and 4.2 g/t Ag (Table 3-5; Sack *et al.*, 2017). Minto mine produced 12.9 Mt of ore between 2007 and 2017, containing 747.4 Mlb of Cu, 247 koz of Au and 2.2 Moz of Ag (S. Casselman, 2018). Two other occurrences, Pal [115I 023] and Comanche [115I 074] have each had between 800 and 1000 m of diamond drilling that intersected mineralized rocks similar to those mined in the Minto deposits. The Coin occurrence [115I 020] comprises disseminated and stringer chalcopyrite, bornite and native copper in altered mafic volcanic rocks of the Upper Triassic Povoas formation (Figs. 3-27 and 3-34; Sinclair, 1977). Although there is foliated granodiorite near mineralization, and 300 m of diamond drilling was done at the Coin occurrence, it is unclear if mineralization is similar to that at the Minto mine (Sinclair, 1977). Four other occurrences, Ori [115I 079], Northair [115I 075], Boylen [115I 097] and Giant [115I 094] are untested geochemical or geophysical anomalies that are likely related to the Minto occurrences.

Table 3-4. *Summary of MINFILE occurrences hosted by the Minto pluton (modified from YGS, 2020b).*

MINFILE number	Name	Latitude	Longitude	Deposit type	Deposit status	Commodities
115I 021	Minto	62.6092	-137.2383	Minto-type	Producer	Cu, Ag, Au
115I 022	Minto North	62.6258	-137.2439	Minto-type	Producer	Cu, Ag, Au
115I 020	Coin	62.6222	-137.0633	Minto-type?	Drilled Prospect	Cu, Ag, Au
115I 023	Pal	62.6100	-137.2039	Minto-type	Drilled Prospect	Cu, Ag, Au
115I 074	Comanche	62.6130	-137.3125	Minto-type	Drilled Prospect	Cu
115I 079	Ori	62.6694	-137.2958	Minto-type?	Anomaly	Cu, Au
115I 075	Northair	62.6444	-137.1344	Minto-type?	Anomaly	Cu
115I 097	Boylen	62.6353	-137.1925	Minto-type?	Anomaly	Cu
115I 094	Giant	62.6686	-137.3692	Minto-type?	Anomaly	Cu

Table 3-5. *Global Minto resource recalculated from Mercer and Sagman (2012) for Minto South, Ridgetop, Minto North and Minto East deposits (their Tables 1-2 through 1-5 respectively).*

	Tonnes (000)	Cu (%)	Au (ppm)	Ag (ppm)	Cu (lbs)	Cu (tonnes)	Au (oz)	Au (tonnes)	Ag (oz)	Ag (tonnes)
Total M&I	54,513	1.21	0.45	4.4	1,449,715,364	657,579.29	771,233	21.9	7,696,197	218.2
Total Inferred	8,491	0.81	0.24	2.9	151,741,000	68,828.50	64,300	1.8	787,000	22.3
Global Resource (M&I plus Inf)	63,004	1.15	0.42	4.2	1,601,456,364	726,407.80	835,533	23.7	8,483,197	240.5

Notes:

Minto Main deposit estimate is from SRK (2008; their Table 1-5, Dec 2007 Model). The Dec 2007 model, was done after approximately 6 months of mining and doesn't include mined out material; it is considered a slight underestimate. A cut-off grade of 0.5% Total Cu was used for each estimate.

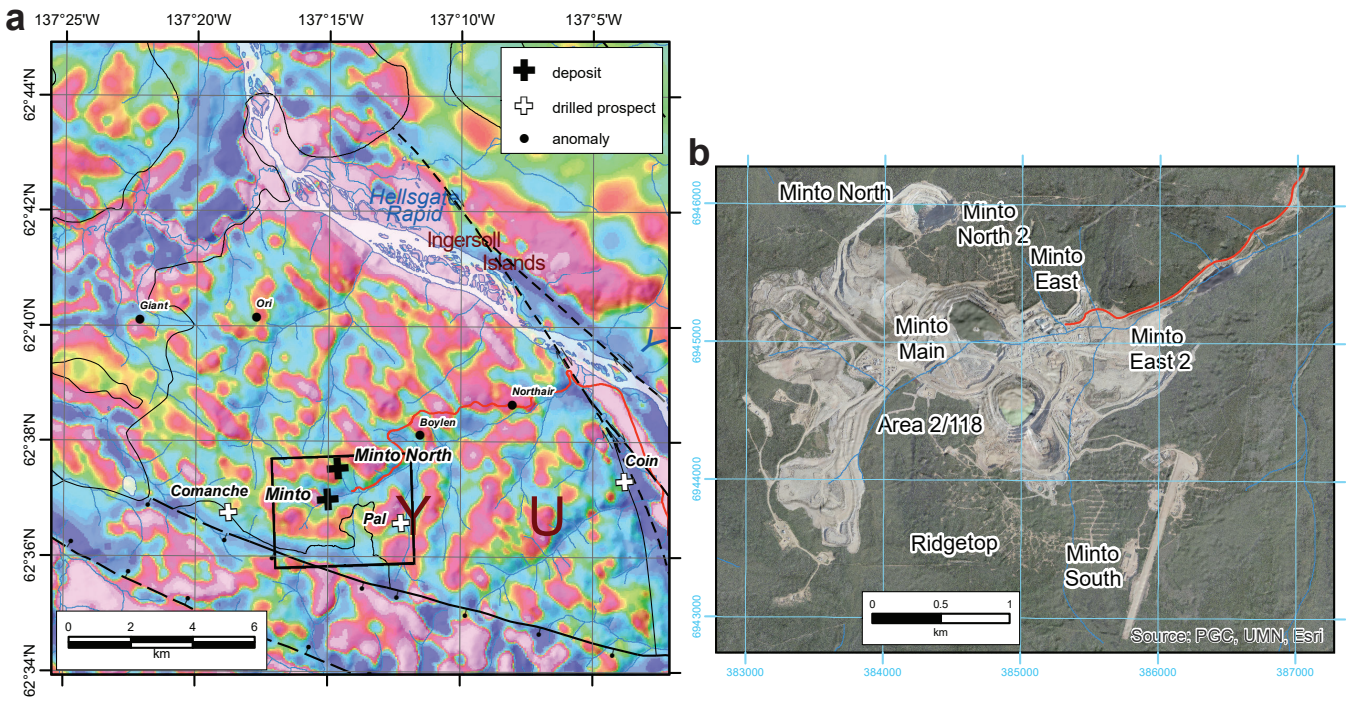


Figure 3-34. (a) *Reduced to pole, first vertical derivative aeromagnetic map of the Minto pluton (Aurora Geosciences Ltd. and Bruce, 2017b) showing distribution of Cu-Ag-Au MINFILE occurrences and anomalies. Fault symbology as in Figure 1-4.* ***(b)*** *Aerial orthophotograph showing location of the various orebodies at the Minto mine (30 August 2017; http://www.geomaticsyukon.ca/data). High resolution DEM background is from Porter et al. (2018).*

Minto mine

The Minto deposits have been studied and described by Pearson and Clark (1979), Tafti (2005) and Hood (2012). The mineralized rocks comprise alternating mafic and felsic layers that are moderately to strongly foliated and recrystallized, these rocks have been partially melted and migmatized (Fig. 3-35). Individual orebodies of foliated rock are up to tens of metres thick and form gently dipping horizons which can be traced laterally for more than one kilometre in diamond drill core; these horizons are stacked in parallel to subparallel sequences (Fig. 3-30a; Mercer and Sagman, 2012). Individual mafic layers are millimetres to centimetres thick and consist of moderately aligned biotite, hornblende, epidote, magnetite and titanite separated by thicker felsic layers that are centimetres to tens of centimetres thick and composed of medium to coarse-grained quartz and plagioclase with lesser amounts of biotite, hornblende, epidote, magnetite and titanite (Fig. 3-36; Hood, 2012). Higher grade ore typically occurs within thicker layered, coarser grained and more siliceous rocks, while lower grade ore is often associated with thin, discontinuously layered and more mafic rocks (Mercer and Sagman, 2012). Contacts between foliated and unfoliated rocks are typically sharp, marked by rapid change in grain size, with foliation and gneissic banding commonly at high angle to contacts with unfoliated rocks; locally, K-feldspar phenocrysts from unfoliated granodiorite impinge on foliation (Fig. 3-37). These observations suggest an intrusive relationship between unmineralized and

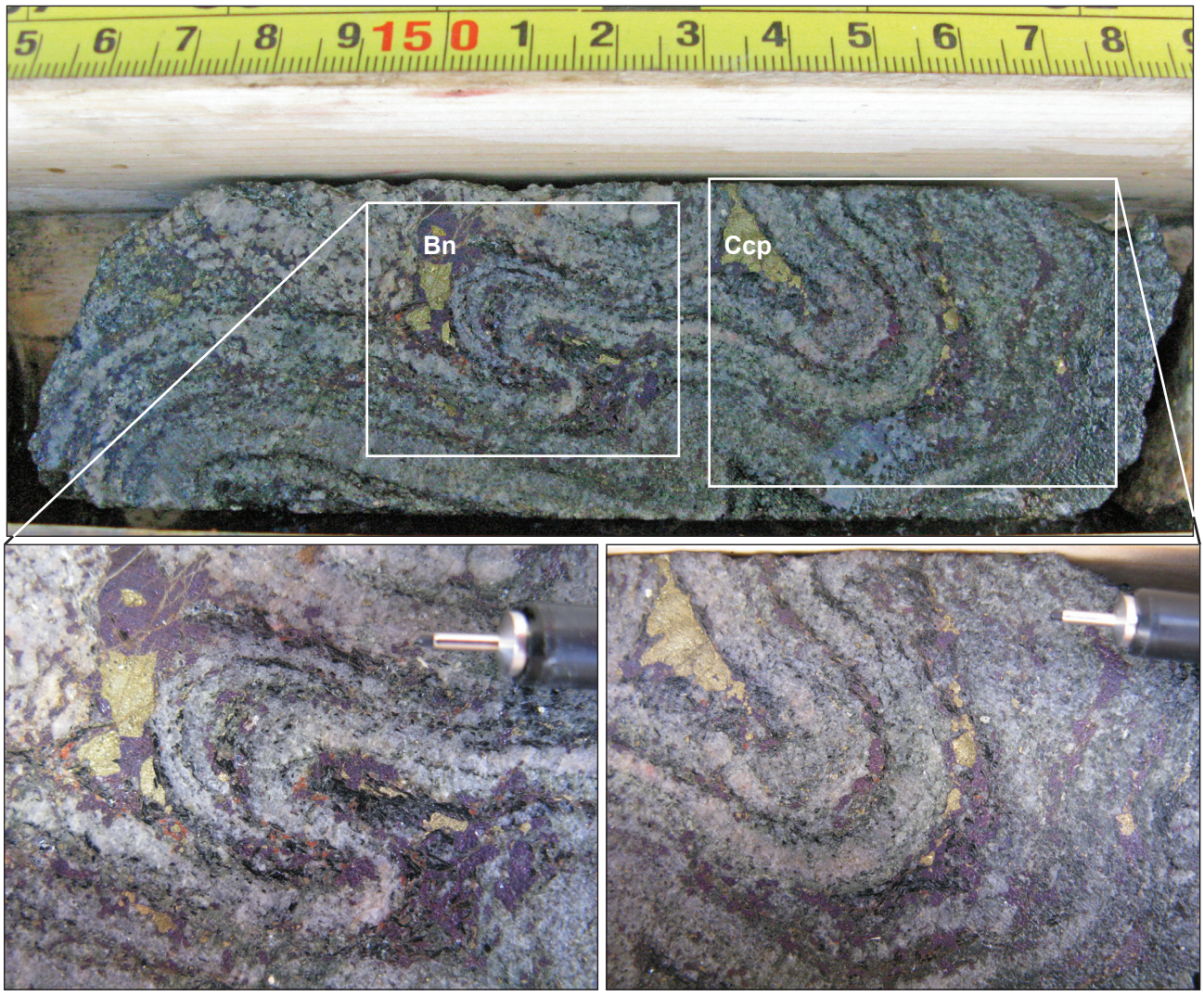


Figure 3-35. *Ptygmatic folding within migmatitic mineralized rocks in diamond drill hole 09SWC390 at approximately 81 m depth, Minto North deposit. Copper sulphides (chalcopyrite and bornite) are locally remobilized and concentrated in fold hinges.*

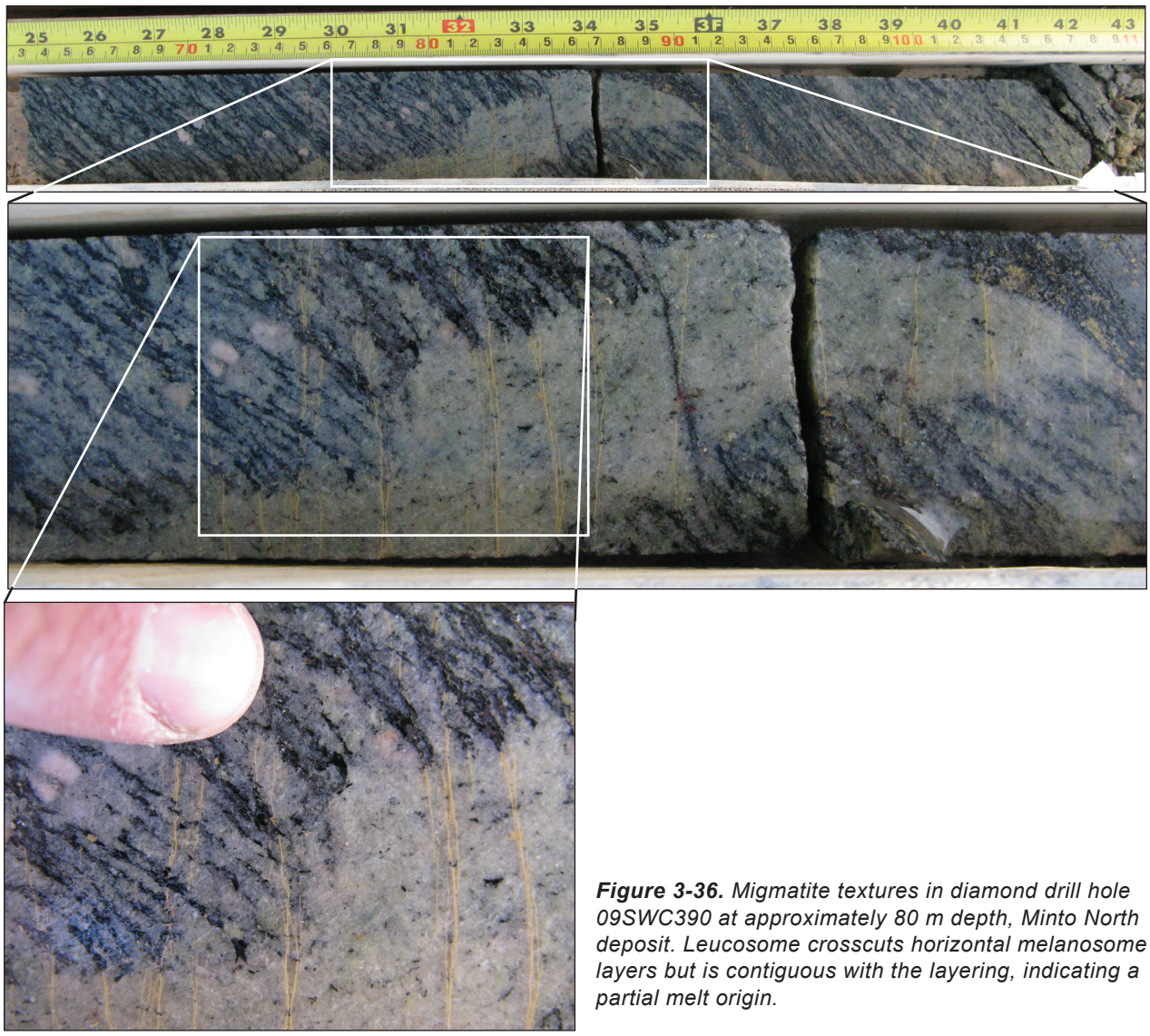


Figure 3-36. *Migmatite textures in diamond drill hole 09SWC390 at approximately 80 m depth, Minto North deposit. Leucosome crosscuts horizontal melanosome layers but is contiguous with the layering, indicating a partial melt origin.*

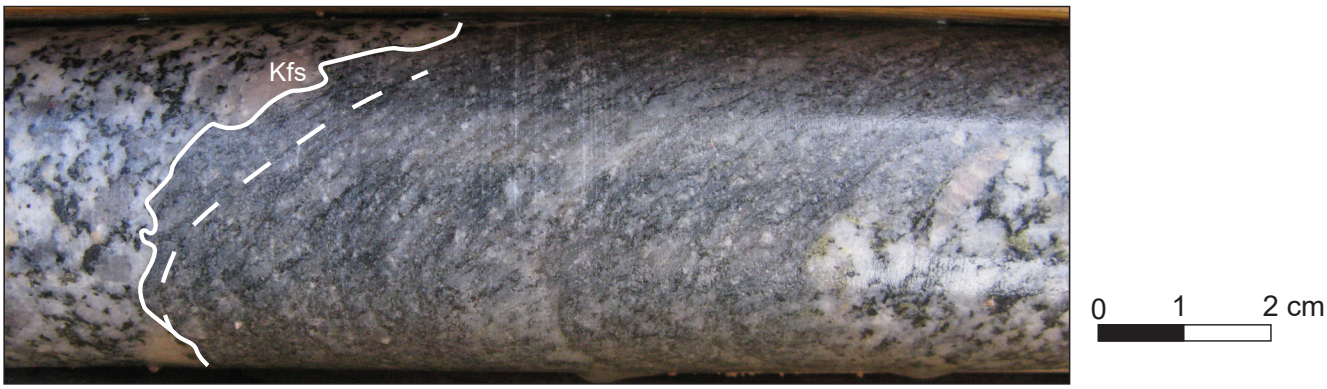


Figure 3-37. *Contact relationship between foliated and unfoliated rocks in the Minto North deposit; diamond drill hole 09SWC457 at approximately 23 m depth. Truncation of foliation (dashed white line) by the irregular contact (solid white line) between foliated and unfoliated rocks. Also, note the K-feldspar phenocryst which impinges foliated rock.*

mineralized rocks (Hood, 2012). As described in the Carmacks Copper deposit (Kovacs, 2018), the mineralized horizons at Minto appear to represent differentially migmatized rafts intruded by the main phase granodiorite of the Minto pluton (Fig. 3-38). However, this process is generally more advanced at Minto and gneissic horizons were commonly inferred to be derived from plutonic protoliths in previous studies (*e.g.*, Tafti, 2005; Hood, 2012).

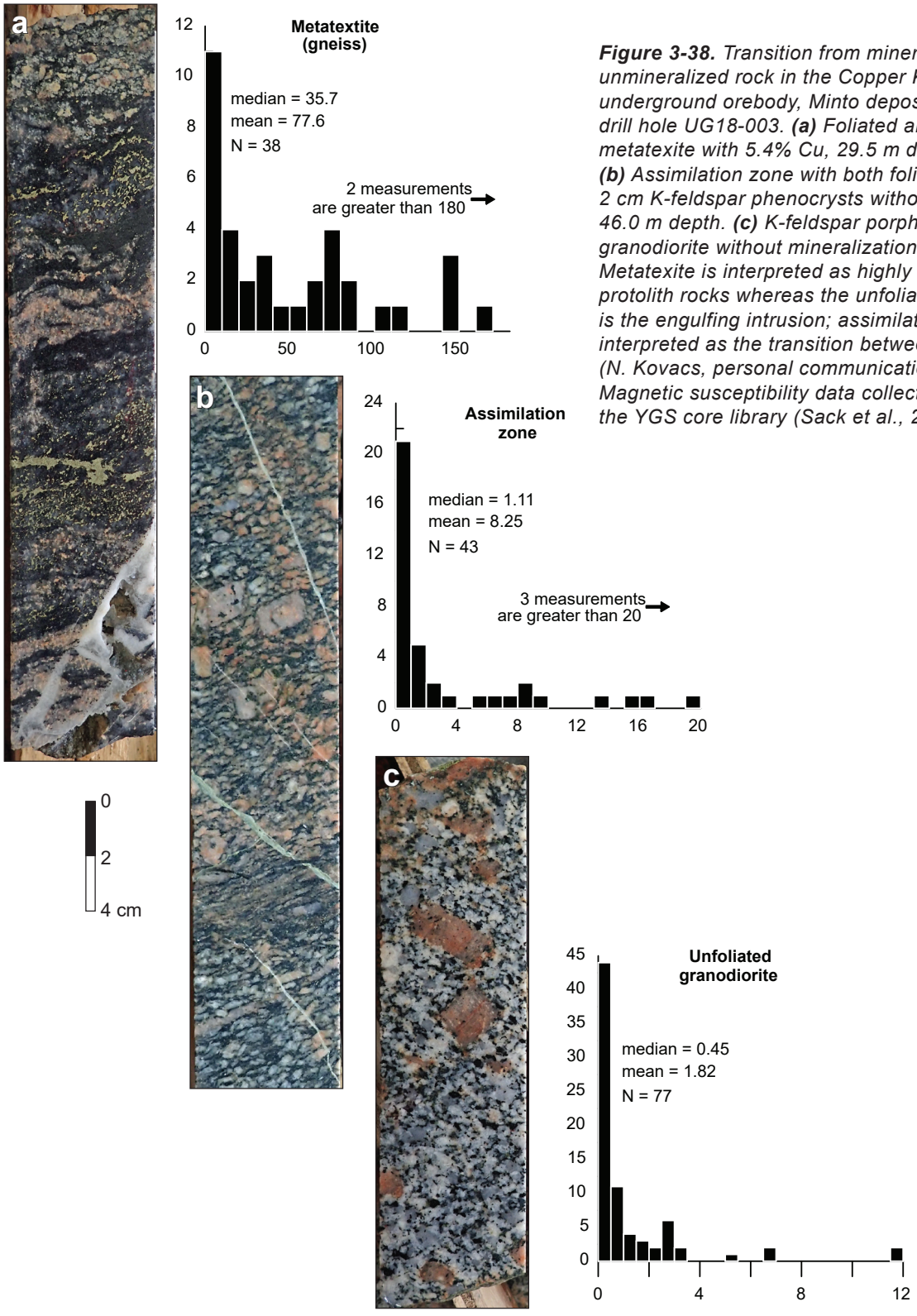


Figure 3-38. *Transition from mineralized to unmineralized rock in the Copper Keel West underground orebody, Minto deposits, diamond drill hole UG18-003.* ***(a)*** *Foliated and mineralized metatexite with 5.4% Cu, 29.5 m depth.* ***(b)*** *Assimilation zone with both foliated rock and 2 cm K-feldspar phenocrysts without mineralization, 46.0 m depth.* ***(c)*** *K-feldspar porphyritic unfoliated granodiorite without mineralization, 49.5 m depth. Metatexite is interpreted as highly metamorphosed protolith rocks whereas the unfoliated granodiorite is the engulfing intrusion; assimilation zone is interpreted as the transition between the two (N. Kovacs, personal communication, 2018). Magnetic susceptibility data collected on core from the YGS core library (Sack et al., 2017).*

Hypogene ore minerals in the Minto deposits are mainly chalcopyrite and bornite, with rare chalcocite and minor pyrite (Mercer and Sagman, 2012). The sulphides occur as disseminated and foliaform stringers along foliation planes and commonly display a net-texture suggesting recrystallization of original ore minerals (Figs. 3-35 and 3-38; N. Kovacs, pers. comm., 2018). Magnetite and biotite are commonly abundant in association with ore sulphides (Fig. 3-38a). Magnetite content decreases from migmatized rafts (median = 35.7×10^{-3} SI units; metatexite), to foliated granodiorite (median = 8.25×10^{-3} SI units; assimilation zone), and finally to unfoliated granodiorite (median = 0.37×10^{-3} SI units; Fig. 3-38). The magnetite and biotite enrichment and K-feldspar replacement of plagioclase observed in the ore zones are interpreted as part of a strong potassic alteration associated with the Minto mineralization (Mercer and Sagman, 2012; Hood, 2012). Supergene mineralization consisting of chalcocite, malachite and minor azurite and native copper, is localized near surface extensions of the orebodies (commonly beneath exposure of the Upper Cretaceous conglomerate), and along late faults such as the DEF fault (Fig. 3-30).

Geochronology

All previous geochronological studies of the Minto pluton were conducted on samples collected in the vicinity of the Minto mine (Fig. 3-27 inset). Early attempts on multi-grain, unabraded zircon fractions yielded a single concordant date at 192 ± 3 Ma (Fig. 3-39; Appendix 1; Tempelman-Kluit and Wanless, 1980). Tafti (2005) subsequently dated 7 samples from the Minto mine using ID-TIMS on air-abraded, multi-grain zircon fractions and unabraded titanite fractions (only zircon compiled in Fig. 3-39; Appendix 1; analyzed at UBC). Most samples yielded discordant results for zircon with $^{206}Pb/^{238}U$ dates scattered between *ca.* 223 and 194 Ma, and interpreted concordia ages ranging from 197.8 ± 2.5 to 195.5 ± 0.7 Ma (Tafti, 2005). These results from multi-grain fractions likely represent mixing of various inherited components with igneous zircons, and possibly some Pb loss.

In an attempt to improve the dating of the Minto deposit, Hood (2012) analyzed single zircons from six samples using the RG-SIMS method (analyzed at GSC Ottawa). Samples were selected to represent the range of igneous protoliths encountered in the Minto mine area, and four of these samples were collected from a sequence of crosscutting intrusive phases stacked over 4 m in the Main open pit, with the oldest being a strongly foliated mineralized gneiss and the youngest phase a massive, unfoliated K-feldspar porphyritic granodiorite (Fig. 3-40). Spot analyses of zircon from the samples yielded a range of $^{206}Pb/^{238}U$ dates scattered between *ca.* 350 and 188 Ma, with most analyses between 205 and 190 Ma (Fig. 3-39). The interpreted concordia ages range from 200.1 ± 1.1 to 197.0 ± 1.4 Ma for these samples, with the four well-constrained samples from the Minto Main pit (Fig. 3-40) yielding overlapping concordia ages between 197.8 ± 1.3 and 197.0 ± 1.4 Ma (Hood, 2012, p. 110). Taken at face value, the interpreted concordia ages suggest that the relatively youngest, massive granodiorite phase (S09-16-01D; Fig. 3-40) is older at *ca.* 198 Ma than the foliated, mineralized gneiss it cuts (S09-16-01A; *ca.* 197 Ma). However, when considering only $^{206}Pb/^{238}U$ dates from the dominant age components from each of these samples, the mineralized banded gneiss sample (S09-16-01A) appears slightly older at 198.4 ± 1.0 Ma (n = 26, MSWD = 2.1) than the massive granodiorite (S09-16-01D) with a date of 195.8 ± 1.0 Ma (n = 9, MSWD = 1.6; Fig. 3-39).

We reanalyzed these two samples from the Minto Main open pit using the combination of LA-ICPMS and CA-TIMS methods at Boise State University (Appendices 3 and 4). The first sample, S09-16-01A, from a mineralized quartzofeldspathic gneiss (Fig. 3-40), yielded stubby, sub-equant zircons with concentric, magmatic zoning, and some inherited cores (Fig. 3-41a). Fifteen LA-ICPMS spots were analyzed from 14 zircons and yielded $^{206}Pb/^{238}U$ dates between 325 and 192 Ma, with a weighted mean of 196.1 ± 2.6 Ma for the youngest 11 analyses (Fig. 3-41b; Appendix 3). The Mississippian (*ca.* 325 Ma) and Late Triassic (211-207 Ma) dates are interpreted as inherited zircon components. Six zircons with young LA-ICPMS dates were analyzed by CA-TIMS and yielded concordant $^{206}Pb/^{238}U$ dates that range from 198.36 ± 0.15 to 198.09 ± 0.15 Ma, with a weighted mean of 198.22 ± 0.06 Ma (MSWD = 1.83, n = 6; Fig. 3-41c) interpreted as the crystallization age of this sample.

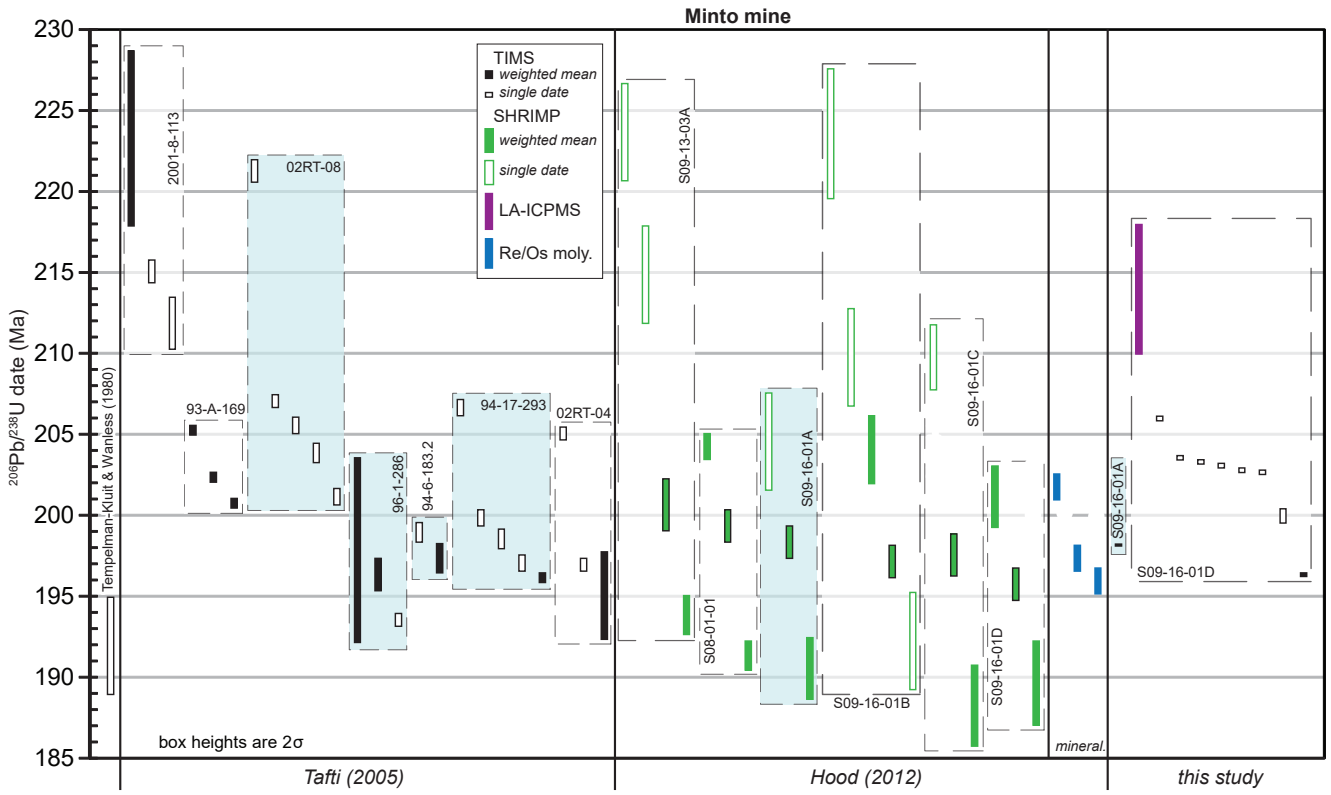


Figure 3-39. *Summary of $^{206}Pb/^{238}U$ zircon dates from the Minto pluton (Appendix 1). All samples were collected at the Minto mine. Dates by Tafti (2005) and Tempelman-Kluit and Wanless (1980) were analyzed by ID-TIMS on multi-grain zircon fractions. Hood (2012) dated single grains by SIMS at the GSC; the weighted mean $^{206}Pb/^{238}U$ date for the dominant population in SIMS analyses is outline in black. Hood (2012) also dated molybdenite in mineralized samples by Re/Os (blue bars). New CA-TIMS dates collected for this study are shown at right (reanalysis of 2 samples analyzed by Hood, 2012; Appendix 4).*

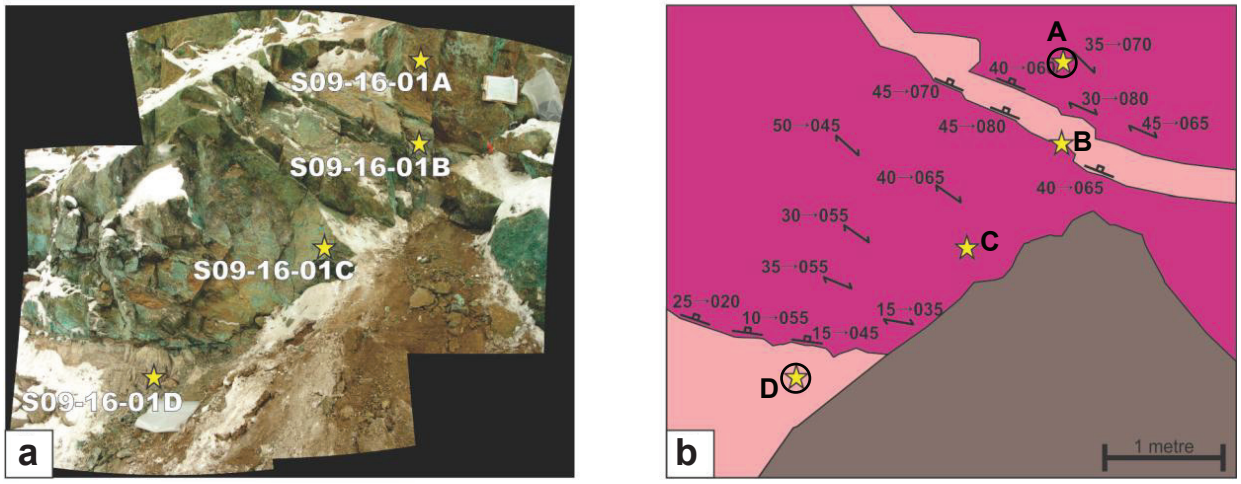


Figure 3-40. *Photo-mosaic **(a)** and outcrop sketch **(b)** showing relationship between mineralized gneiss (magenta) and massive granodiorite (pink) in the Minto Main open pit (from Hood, 2012, p. 85). Sample locations indicated by yellow stars. Samples reanalyzed in this study are indicated by black circles in b.*

S09-16-01A Minto foliated mineralized gneiss

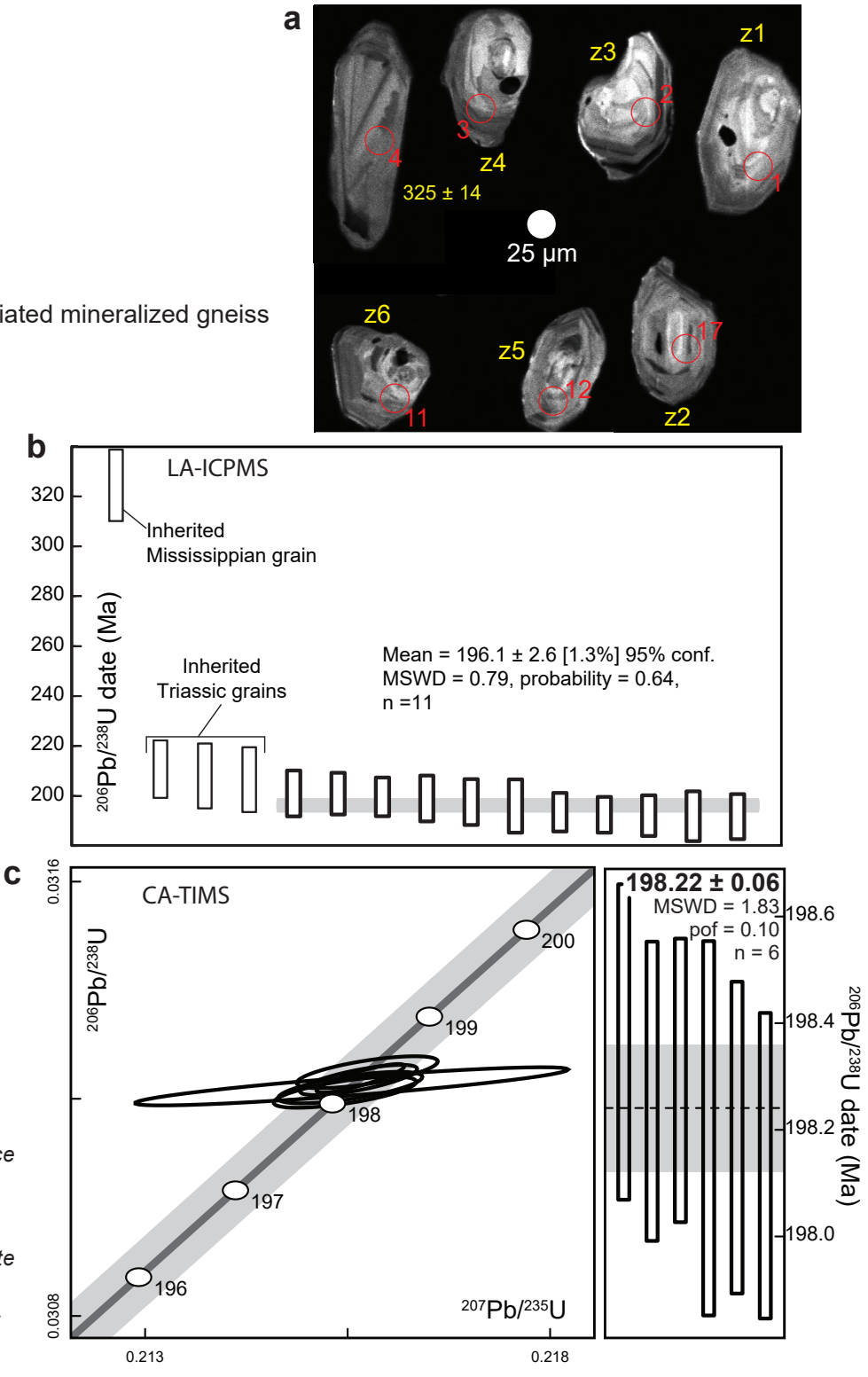


Figure 3-41. *U-Pb geochronological results for sample S09-16-01A, Minto pluton.* ***(a)*** *Cathodoluminescence images of magmatic zircons dated by CA-TIMS (z1-6) and of one inherited zircon dated at 325 ± 14 Ma. Red circles indicate LA-ICPMS analysis spots with corresponding analysis number.* ***(b)*** *Ranked plot of LA-ICPMS $^{206}Pb/^{238}U$ dates (Appendix 3).* ***(c)*** *Concordia diagram (right) and ranked 206Pb/238U dates (left) for 6 zircons analyzed by CA-TIMS (Appendix 4). The light grey band around Concordia (dark grey line) shows the decay constant uncertainties. Analyses included in weighted mean date calculations are bold. Line-type designations are the same in all plots. Errors in all plots are at 2σ. MSWD = mean squared weighted deviation, pof = probability of fit, n = number of analyses included in age calculation.*

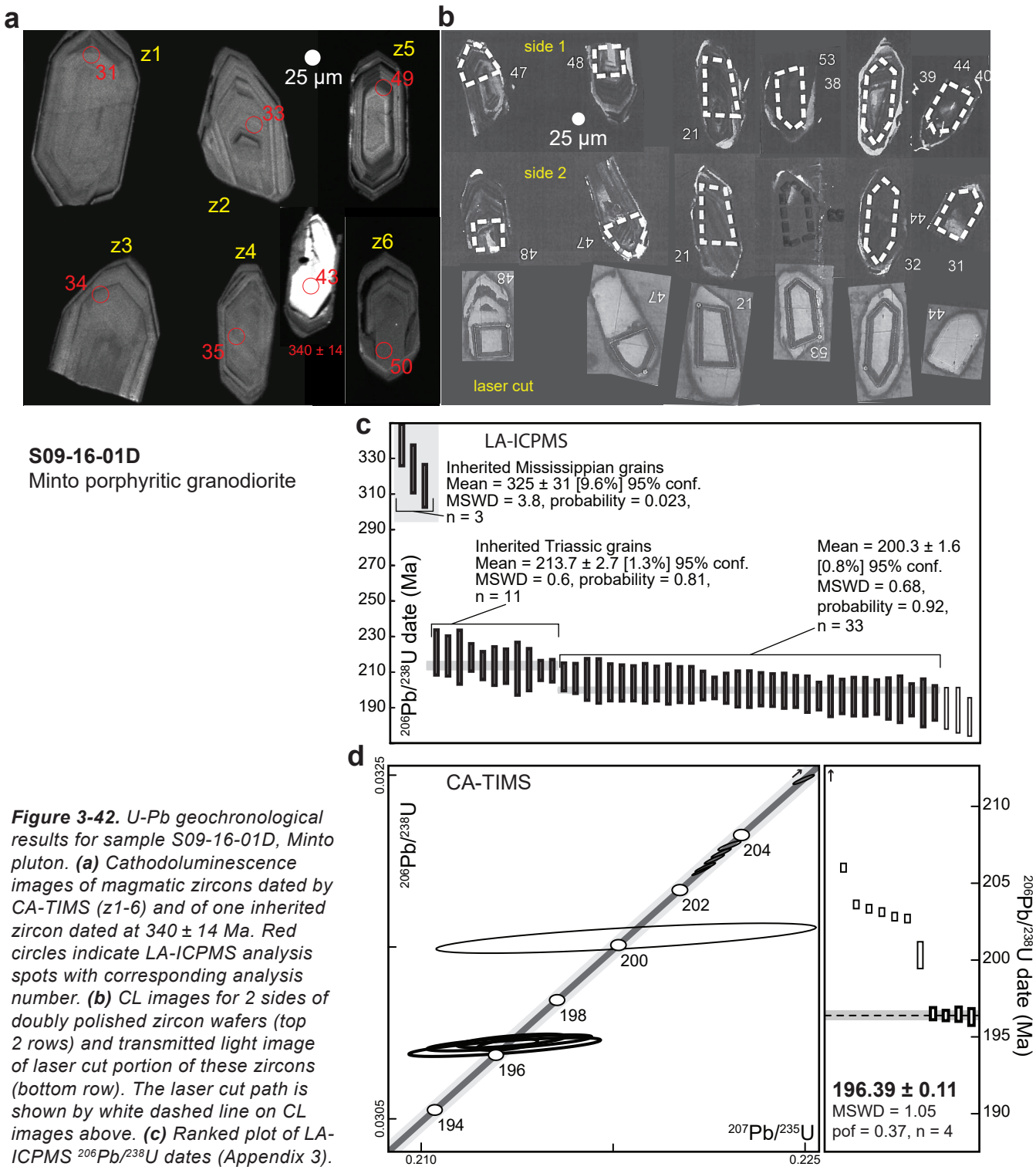
The second sample from the Minto Main open pit, S09-16-01D, is a massive, coarse-grained K-feldspar porphyritic granodiorite that crosscuts the mineralized quartzofeldspathic gneiss (Fig. 3-40). This sample yielded abundant prismatic zircons with ~3:1 aspect ratio, and common CL-bright cores overgrown by concentric, igneous-zoned sectors (Fig. 3-42a; Appendix 3). Some cores are CL-dark and rimmed by thin CL-bright zones, then overgrown by magmatic zircon. Most igneous zircons in this sample also have very thin, low U, CL-bright rims that are only clearly identified in images of unannealed zircon (Fig. 3-42b). Fifty zircons were analyzed by LA-ICPMS and yielded $^{206}Pb/^{238}U$ dates ranging from *ca.* 340 to 185 Ma (Appendix 3). These dates are distributed in three age components: 1) the oldest 3 analyses (340–315 Ma; Fig. 3-42b) are from CL-bright cores that have high total REE concentrations (860–1750 ppm) and are interpreted as inherited zircons; 2) eleven analyses from zoned zircon sectors have $^{206}Pb/^{238}U$ dates between 221 and 211 Ma, with a weighted mean of 213.7 ± 2.7 Ma; and 3) other analyses (n = 36) from zoned, igneous zircon domains range from 207 to 185 Ma, with 33 of these analyses yielding a weighted mean date of 200.3 ± 1.6 Ma (Fig. 3-42c; Appendix 3). The youngest three analyses (190–185 Ma) probably suffered Pb loss.

From these LA-ICPMS results and CL imaging, we selected six zircons that appeared free of inherited components for CA-TIMS analyses (Fig. 3-42a). These yielded $^{206}Pb/^{238}U$ dates scattered between 206.03 ± 0.14 and 202.70 ± 0.14 Ma (Fig. 3-42d; Appendix 4). These results are older than the *ca.* 198 Ma date previously estimated from SIMS data for this sample (Hood, 2012), and apparently older than the mineralized gneiss, dated here by CA-TIMS at 198.22 ± 0.08 Ma (Fig. 3-41), that is intruded by this granodiorite (Fig. 3-40). This apparent contradiction can only be reasonably interpreted as reflecting mixing of older, cryptic inherited components with juvenile growths in these zircons.

To resolve this discrepancy, we polished a number of zircons on two sides to form wafers ~30–40 µm thick, which were then imaged by CL, and analyzed by LA-ICPMS to identify domains with consistent composition and age. From these analyses, homogeneous domains were cut from six of the wafers using a 6 µm-wide laser beam and analyzed by CA-TIMS (Fig. 3-42b; *see* Analytical Methods in Appendix 4 for complete description of the laser cutting technique). Four of these zircon fragments have concordant $^{206}Pb/^{238}U$ dates that range from 196.54 ± 0.20 to 196.28 ± 0.28 Ma, and yield a weighted mean of 196.39 ± 0.11 Ma (Fig. 3-42d; MSWD = 1.05, n = 4). This is interpreted as the crystallization age of this massive granodiorite sample. Two other fragments yielded older $^{206}Pb/^{238}U$ dates of 240.18 ± 0.49 Ma and 200.02 ± 0.44 Ma that are inferred to reflect mixing with older cryptic cores.

Thermobarometry

Two samples from the Minto pluton, CDB10078A and 11RAYJC037A, contain the suitable mineral assemblage for Al-in-Hbl geobarometry (Hammarstrom and Zen, 1986; Appendix 5). Al^{TOT} in hornblende for these samples is 2.11 and 2.13 with cotectic plagioclase that has X_{an} of 0.26 and solidus temperatures between 748 and 762°C, respectively. Crystallization pressure estimates derived from these data are 5.72 ± 0.98 kbar for CDB10078A and 5.49 ± 0.98 kbar for 11RAYJC037A (Appendix 5; emplacement depth of approximately 21 km, respectively). Solidus temperatures derived using the amphibole-plagioclase mineral thermometer of Holland and Blundy (1994) for samples CDB10078A and 11RAYJC037A are higher than average Ti-in-zircon temperature estimates (Watson *et al.*, 2006) of 621 and 684°C for igneous components in samples S09-16-01A and S09-16-01D, respectively (Appendix 3). Older inherited components in S09-16-01D have higher Ti-in-zircon temperatures of 689–734°C. Our new Al-in-Hbl crystallization pressure and amphibole-plagioclase solidus temperature estimates are both slightly lower, but within error of previous estimates by Tafti (2005; n = 5) who reports Al^{TOT} in hornblende of 2.11–2.20, with cotectic plagioclase X_{An} of 0.23–0.27, and amphibole-plagioclase temperatures of 723–738°C. Crystallization pressure estimates derived using the Tafti (2005) data are between 6.13 and 6.63 kbar (emplacement depths of 23.2–25.0 km).



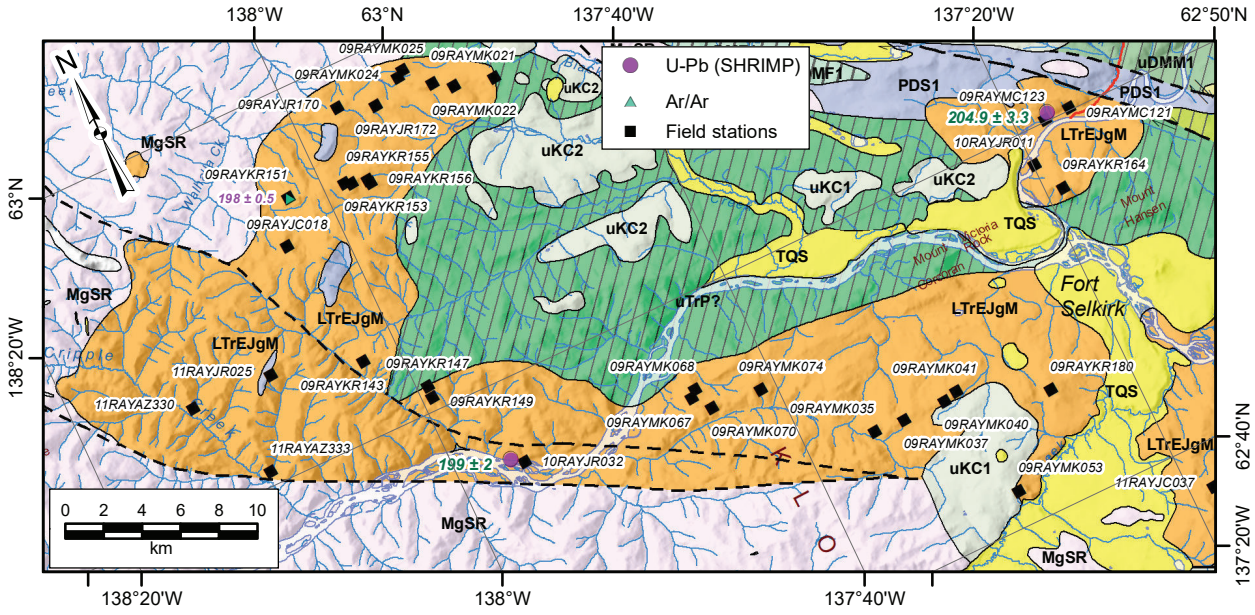
S09-16-01D
Minto porphyritic granodiorite

Figure 3-42. *U-Pb geochronological results for sample S09-16-01D, Minto pluton.* ***(a)*** *Cathodoluminescence images of magmatic zircons dated by CA-TIMS (z1-6) and of one inherited zircon dated at 340 ± 14 Ma. Red circles indicate LA-ICPMS analysis spots with corresponding analysis number.* ***(b)*** *CL images for 2 sides of doubly polished zircon wafers (top 2 rows) and transmitted light image of laser cut portion of these zircons (bottom row). The laser cut path is shown by white dashed line on CL images above.* ***(c)*** *Ranked plot of LA-ICPMS $^{206}Pb/^{238}U$ dates (Appendix 3).* ***(d)*** *Concordia diagram (right) and ranked $^{206}Pb/^{238}U$ dates (left) for 12 zircons analyzed by CA-TIMS (Appendix 4). The light grey band around concordia (dark grey line) shows the decay constant uncertainties. Analyses included in weighted mean date calculations are bold; analyses with thin lines are not used in calculations. Line-type designations are the same in all plots. Errors in all plots are at 2σ. Arrow indicates data extends off of plot. MSWD = mean squared weighted deviation, pof = probability of fit, n = number of analyses included in age calculation.*

Yukon River, Pelly and Walhalla plutons

The Yukon River, Pelly and Walhalla plutons are the northwestern-most of the large Late Triassic to Early Jurassic Minto suite plutons in southern Yukon (Figs. 3-1 and 3-2). These plutons were not visited for this study; they were described and sampled as part of regional mapping programs between 2001 and 2015 (Gordey and Ryan, 2005; Ryan *et al.*, 2010, 2013). Several small (<10 km^2) Late Triassic to Early Jurassic plutons are also mapped northwest of the Walhalla pluton in the Klondike Plateau of western Yukon and eastern Alaska (Gordey and Ryan, 2005; Wilson *et al.*, 2015; Colpron *et al.*, 2016b; YGS, 2020a), but these were not included in this study as only limited data are available from these bodies.

The Yukon River batholith has a mapped extent of 506 km^2. It straddles the Yukon River west of the confluence with the Pelly River at Fort Selkirk, approximately 60 km west of Pelly Crossing (Figs. 3-1 and 3-43; Table 3-1). The Yukon River batholith is generally poorly exposed in rubble and subcrop near hilltops (Fig. 3-44), in creek cuts, and along the banks of the Yukon River. It intrudes along the boundary between Stikinia and Yukon-Tanana terranes, at the northwest termination of exposures of Upper Triassic rocks of Stikinia in central Yukon. Along its northeastern margin, the batholith intrudes Upper Triassic augite-phyric intermediate to mafic volcanic rocks of the Povoas formation (Tempelman-Kluit, 1984; Ryan *et al.*, 2013). The volcanic rocks locally have a well-developed cleavage and are



TERTIARY(?) AND QUATERNARY

TQS: SELKIRK: columnar jointed, vesicular to massive basalt flows

PALEOCENE TO LOWER EOCENE

PRC1: RHYOLITE CREEK: light grey, green, maroon, purple and black rhyolite and dacite

UPPER CRETACEOUS

uKC1: CARMACKS: augite-olivine basalt and breccia

uKC2: CARMACKS: andesite, porphyry

uKC4: CARMACKS: sandstone, pebble conglomerate, shale, tuff, and coal

LATE TRIASSIC TO EARLY JURASSIC

LTrEJgM: MINTO SUITE: variably foliated to massive Bt-Hbl granodiorite, locally Kfs porphyritic; Bt-Mt-rich screens and gneissic schlieren

UPPER TRIASSIC, CARNIAN AND OLDER (?)

uTrP?: POVOAS: augite or feldspar-phyric andesitic basalt flows, breccia, tuff, sandstone, argillite

UPPER TRIASSIC TO LOWER JURASSIC

uTrJS1: SEMENOF: augite-phyric basalt flow and agglomerate, andesite

UPPER CARBONIFEROUS, LOWER AND MIDDLE PENNSYLVANIAN

uCB1: BOSWELL: siliceous argillite, siltstone, sandstone, chert conglomerate, volcanic breccia

MISSISSIPPIAN

MqSR: SIMPSON RANGE SUITE: foliated metagranite, quartz monzonite and granodiorite; augen granite

MgSR: SIMPSON RANGE SUITE: Hbl-bearing metagranodiorite, metadiorite and metatonalite

DEVONIAN, MISSISSIPPIAN AND(?) OLDER

uDMM1: MOOSE: massive and pillow basalt, amphibolite and greenstone

uDMM3: MOOSE: intermediate metavolcanic and metavolcaniclastic rocks

DMF1: FINLAYSON: intermediate to mafic volcanic and volcaniclastic rocks

NEOPROTEROZOIC AND PALEOZOIC

PDS1: SNOWCAP: quartzite, psammite, pelite and marble; minor greenstone and amphibolite

Figure 3-43. *Geology of the area around the Yukon River batholith and Pelly pluton. Geology from YGS (2020a); fault symbology as in Figure 1-4. Note that the geographic reference frame has been rotated with North pointing to the upper left of the page.*



Figure 3-44. *Subcrop near the headwaters of Black Creek showing the poorly exposed nature of the northern portion of the Yukon River batholith, 09RAYMK024.*

metamorphosed to greenschist or sub-greenschist facies (Colpron and Ryan, 2010). The western and southwestern margins intrude Early Mississippian (*ca.* 355–345 Ma) orthogneiss of the Simpson Range plutonic suite, part of the Yukon-Tanana terrane; the southwestern margin is inferred to be reactivated by a fault (Ryan *et al.*, 2013). A fault inferred from an aeromagnetic survey divides the batholith into three sectors: north, southwest and southeast sectors (Fig. 3-45). Small (<3 km^2) pendants of Snowcap assemblage, quartzite and psammitic schist of the Yukon-Tanana basement occur in the southwest and north sectors of the batholith. At its southeastern end, Late Triassic to Early Jurassic granitoid rocks of the Yukon River batholith are unconformably overlain by basalts of the Upper Cretaceous Carmacks Group and the Pliocene-Pleistocene Selkirk Lavas (Ryan *et al.*, 2013), which separates the main batholith from the Minto pluton to the southeast (Figs. 3-2 and 3-43).

The Pelly stock has a mapped extent of 43.4 km^2; it straddles the Pelly River north of its confluence with the Yukon River (Figs. 3-2 and 3-43; Table 3-1). The pluton intrudes Upper Triassic augite-phyric intermediate to mafic metavolcanic rocks of the Povoas formation (Stikinia) to the south and west, and metasedimentary rocks of the Snowcap assemblage (Yukon-Tanana terrane) to the north (Ryan *et al.*, 2010). The northeastern part of the Pelly pluton is cut by the main strand of the Teslin fault (Figs. 3-2 and 3-43). To the southwest, the pluton is unconformably overlain by porphyritic dacite of the Carmacks Group and basalt of the Selkirk volcanics (Ryan *et al.*, 2010).

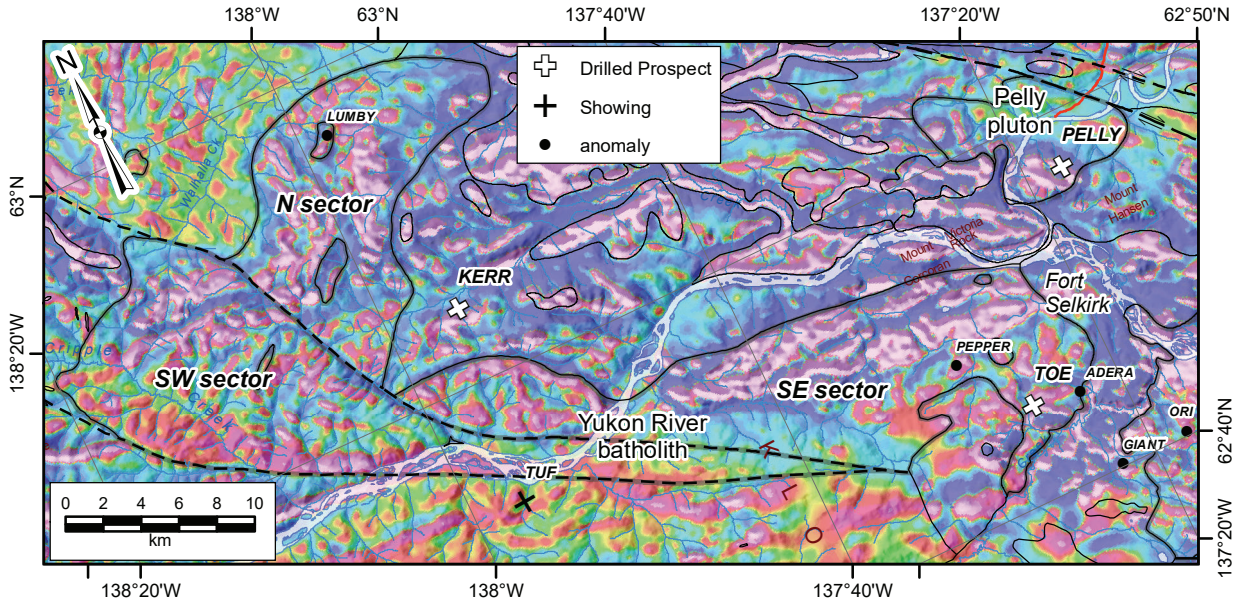


Figure 3-45. *First vertical derivative aeromagnetic map of the Yukon River batholith and Pelly pluton region (Hayward and Oneschuk, 2011) showing distribution of Cu-Ag-Au MINFILE occurrences and anomalies. Note that the geographic reference frame has been rotated with North pointing to the upper left of the page.*

The composite Walhalla batholith has a total mapped extent of 345 km^2 and intrudes rocks of the Yukon-Tanana terrane ~95 km southwest of Stewart Crossing (Figs. 3-1, 3-2 and 3-46). The batholith straddles Walhalla and Scroggie creeks, and cuts older, Late Triassic pyroxenite and gabbro at Pyroxene Mountain (*see* Chapter 2 for description of the Pyroxene Mountain suite; Ryan *et al.*, 2013). The Walhalla batholith intrudes mainly metasedimentary rocks of the Snowcap assemblage; its southern and northwestern margins intrude orthogneiss of the Simpson Range plutonic suite and locally amphibolite of the Finlayson assemblage (Fig. 3-46; Gordey and Ryan, 2005; Ryan *et al.*, 2013). Xenoliths of these host rocks are relatively abundant in the Walhalla pluton. Small (<1–5 km^2) satellite stocks assigned to the Minto plutonic suite are scattered around the Walhalla batholith (Figs. 3-2 and 3-46).

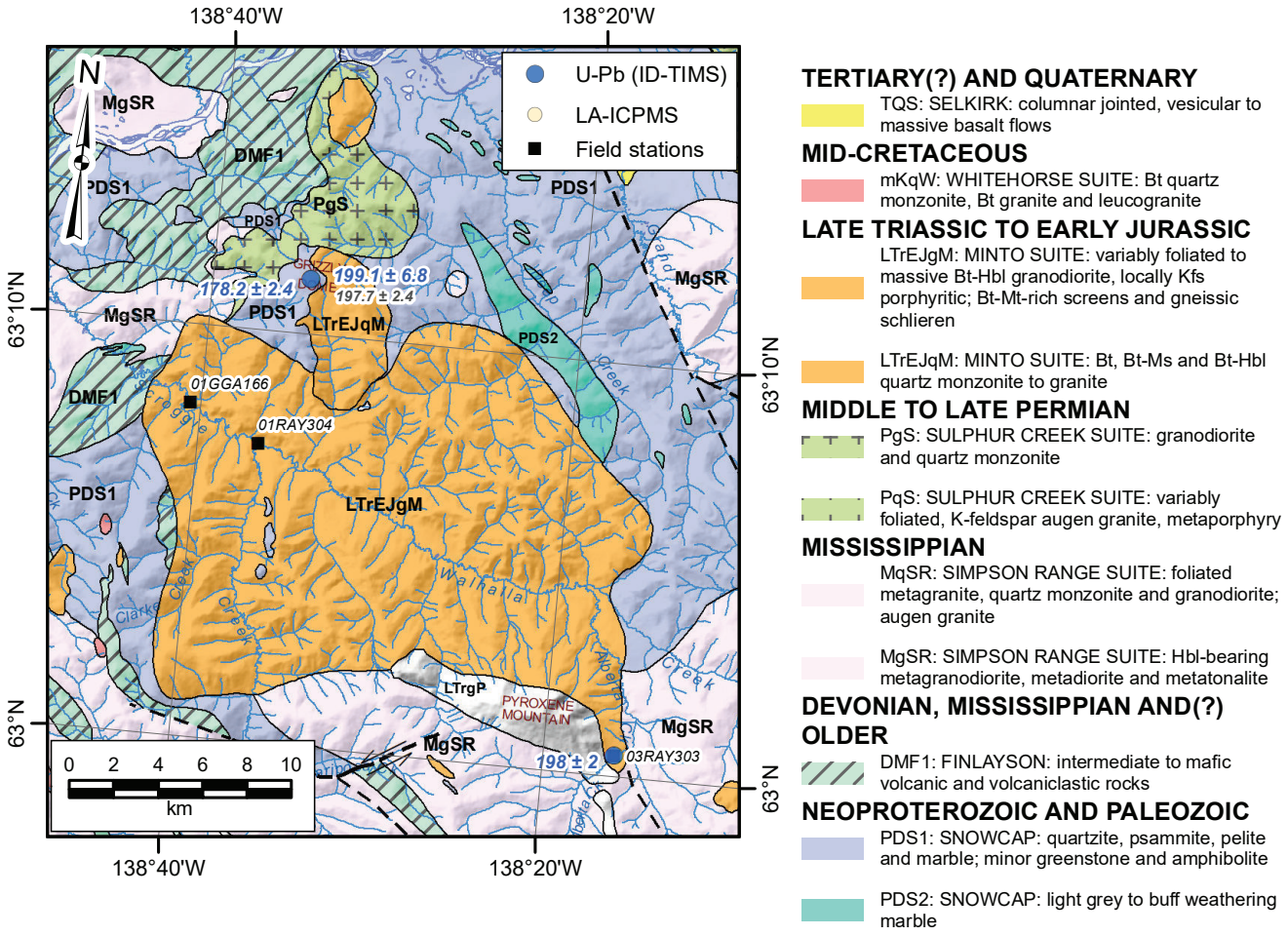


Figure 3-46. *Geology of the Walhalla batholith area. Geology from YGS (2020a); fault symbology as in Figure 1-4.*

Petrography

The Yukon River batholith comprises two main phases (Fig. 3-45). The batholith mainly consists of equigranular to K-feldspar porphyritic, hornblende-biotite granodiorite typical of dominant phases in the Minto plutonic suite (Figs. 3-3 and 3-47; Ryan *et al.*, 2013). In these rocks, biotite and hornblende are typically fresh, and epidote occurs in two distinct forms: as euhedral crystals intergrown with biotite and hornblende (interpreted as magmatic) and as an interstitial mineral without clear grain boundaries (Fig. 3-48). The northern sector of the Yukon River batholith also comprises a two-mica, equigranular to K-feldspar porphyritic monzonite to granodiorite

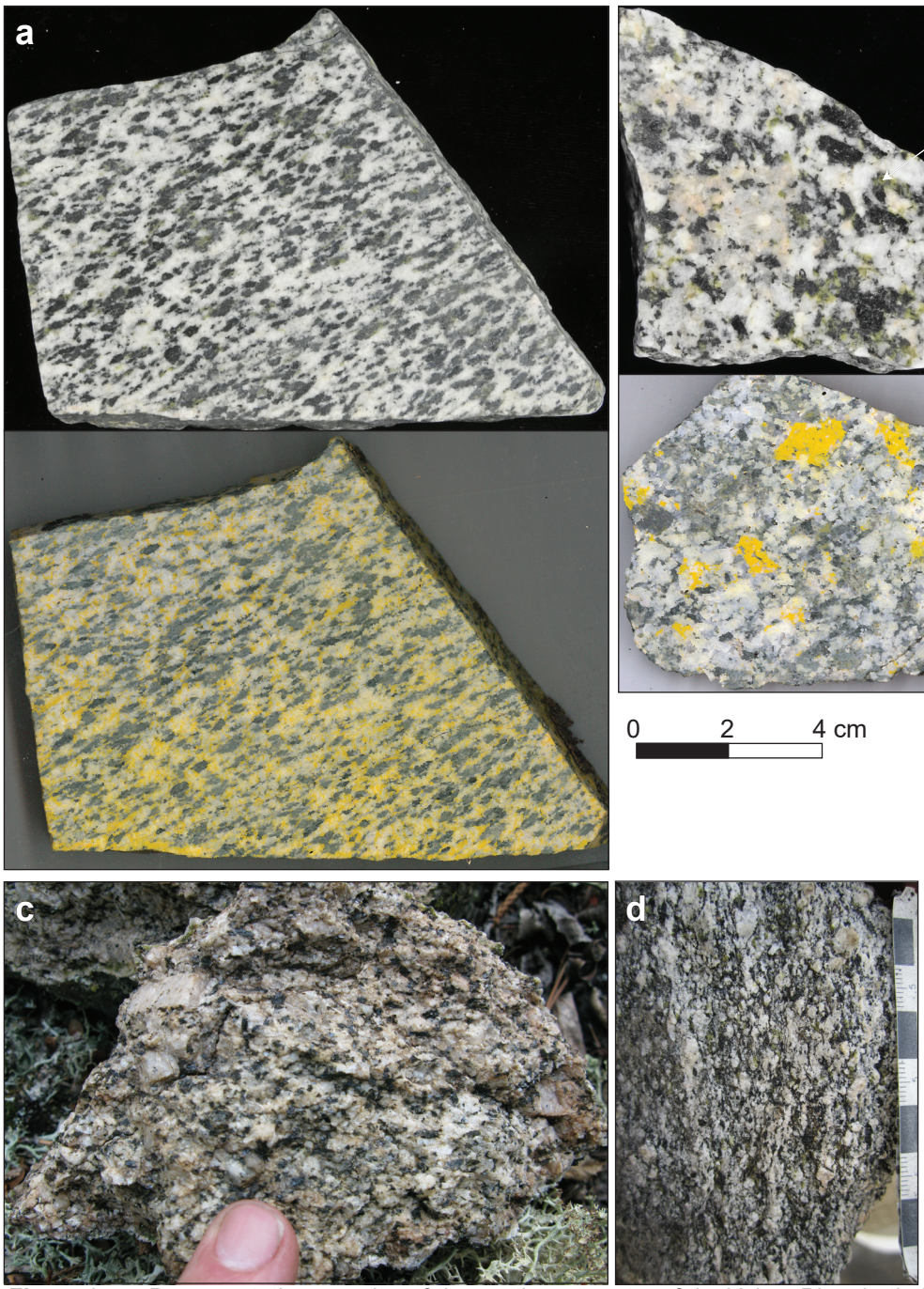


Figure 3-47. *Representative samples of the southwest sector of the Yukon River batholith (a,b). Fresh polished surface (upper) and a cobaltinitrite-stained surface (lower).* ***(a)*** *11RAYAZ333A1,* ***(b)*** *10RAYJR032A1. Note K-feldspar is yellow. In (b), light green mineral is epidote, most of which is magmatic (Ep1; see Fig. 3-48b). Fresh surfaces for rocks from the southeast sector of the batholith (c and d).* ***(c)*** *Porphyritic granodiorite (09RAYMK038);* ***(d)*** *foliated granodiorite (11RAYAZ418).*

phase (Figs. 3-3 and 3-49). Muscovite in this rock is coarse grained (>500 µm) and euhedral (Fig. 3-50a). Biotite is fresh to completely altered to chlorite, and where present, hornblende is fresh to weakly chloritized. Plagioclase and K-feldspar are weakly to strongly saussuritized and sericitized, respectively (Fig. 3-50). Opaque minerals make up to 3% of the rock and are mostly magnetite.

The Pelly stock is an equigranular to K-feldspar porphyritic granodiorite to monzonite (Figs. 3-3 and 3-51). Grains are mostly anhedral to subhedral but locally, K-feldspar occurs as subhedral to euhedral zoned laths (Fig. 3-52); plagioclase is locally light green in colour (Fig. 3-51a). Plagioclase and K-feldspar are weakly to strongly saussuritized and sericitized, respectively (Fig. 3-52). Mafic minerals make up 5 to 10% of the rock, and biotite is more common than hornblende; there are trace amounts of clinopyroxene (Fig. 3-53). Biotite is unaltered and hornblende locally has epidote alteration rims; clinopyroxene phenocrysts are fresh. Opaque minerals make up to 1% of the rock and are mostly magnetite.

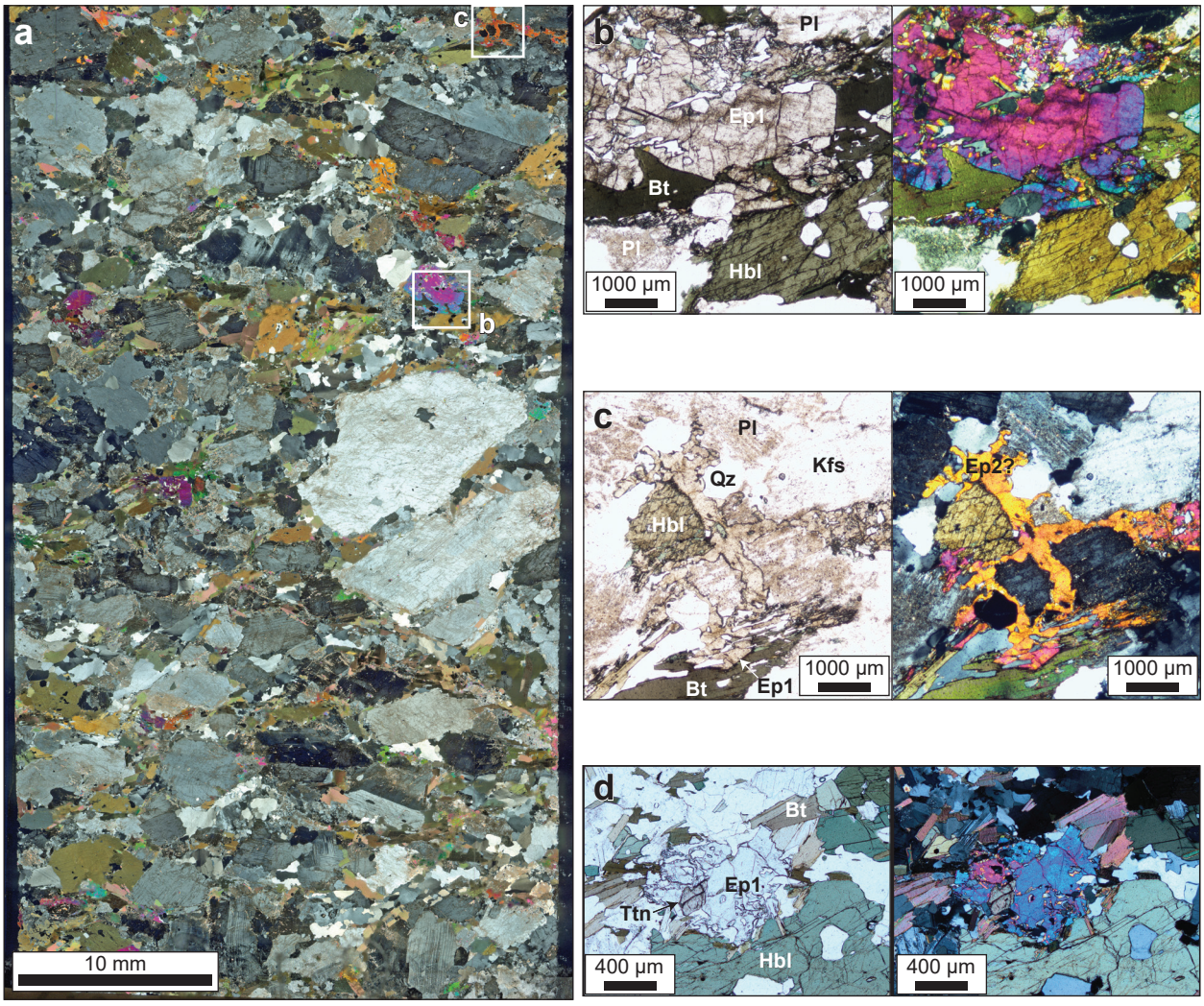


Figure 3-48. *Two generations of epidote within granodiorite of the southwest sector of the Yukon River batholith, 10RAYJR032A1 (a–c).* ***(a)*** *Thin section scan, cross-polarized light with location of b and c shown. (b and c) Transmitted light photomicrograph pairs; plane polarized light (left) and cross-polarized light (right).* ***(b)*** *Early, magmatic epidote with euhedral grain boundaries intergrown with biotite and hornblende.* ***(c)*** *Late, interstitial epidote infilling between plagioclase and quartz grains.* ***(d)*** *Magmatic epidote in granodiorite from the southeast sector of the batholith, 03RAY303. Transmitted light photomicrograph pairs; plane polarized light (left) and cross-polarized light (right).*

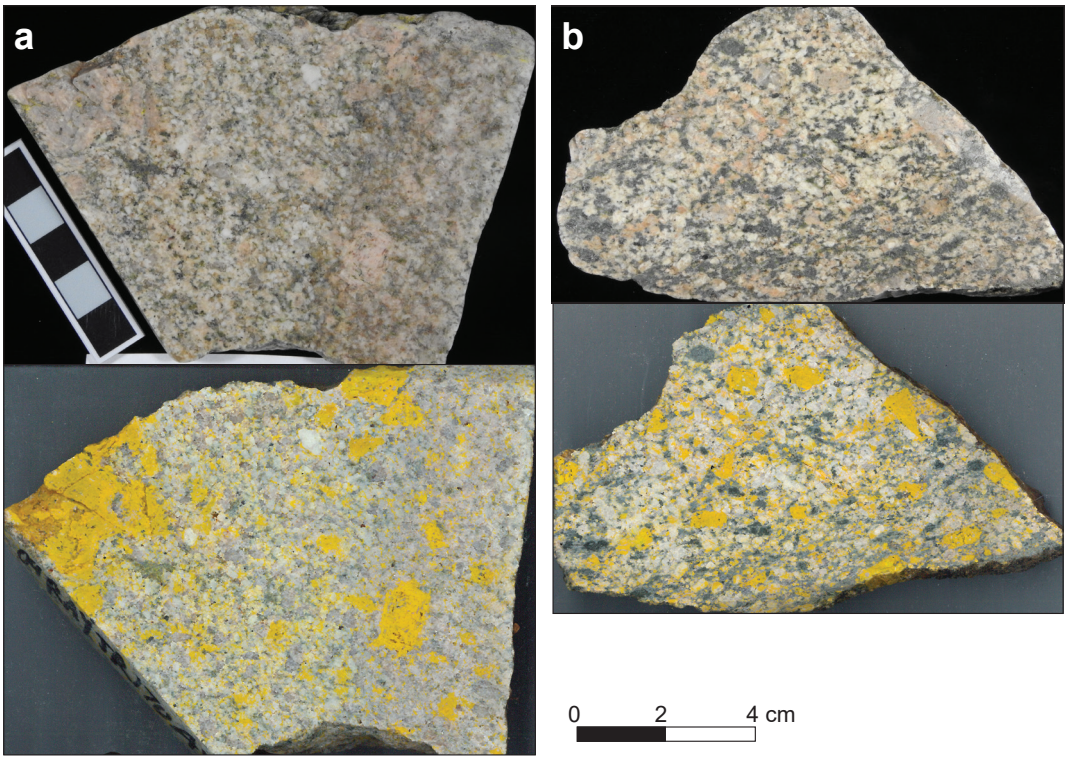


Figure 3-49. *Representative samples of the northern sector of the Yukon River batholith. Slightly weathered polished surface (upper) and a cobaltinitrite-stained surface (lower). Subtle light green tinge on polished surfaces is likely due to strong sericitization of K-feldspar and resembles samples from the central phase of the McGregor batholith (see Chapter 6).* ***(a)*** *Medium-grained, K-feldspar porphyritic granodiorite, 09RAYJR170A1.* ***(b)*** *Medium-grained, equigranular to K-feldspar porphyritic granodiorite, 09RAYKR154A1. Note: K-feldspar is yellow.*

The Walhalla batholith comprises white to beige tonalite and hornblende-biotite granodiorite to monzonite phases that are generally massive to weakly foliated (Fig. 3-54). The northwest margin of the pluton is heterogeneous over a width of 1–3 km. It is polyphase, commonly pegmatitic and leucocratic, with abundant schlieren of resorbed and variably migmatized country rock (Fig. 3-55). The rock is locally strongly foliated, but it is uncertain whether the foliation results from solid-state deformation or is a ghost foliation acquired from migmatized xenoliths. The southeast portion of the pluton, in the vicinity of Alberta Creek (Fig. 3-46), is more homogeneous and similar in character to typical hornblende-bearing granodiorite of the Minto suite.

The granodiorite to monzonite phase is commonly K-feldspar porphyritic (Ryan *et al.*, 2013). The tonalite is coarse grained, equigranular and leucocratic, with 5 to 15% hornblende, biotite and rare euhedral epidote; plagioclase is unaltered. One tonalite sample, 01RAY304, contains coarser grained magmatic muscovite (Fig. 3-56). The primary mafic minerals in the porphyritic granodiorite to monzonite phase are also hornblende and biotite, and these are commonly intergrown with euhedral, magmatic epidote (Fig. 3-57). Plagioclase and K-feldspar in these rocks is weakly to moderately saussuritized and sericitized, respectively. Opaque minerals make up to 1% of the rock and are mostly magnetite.

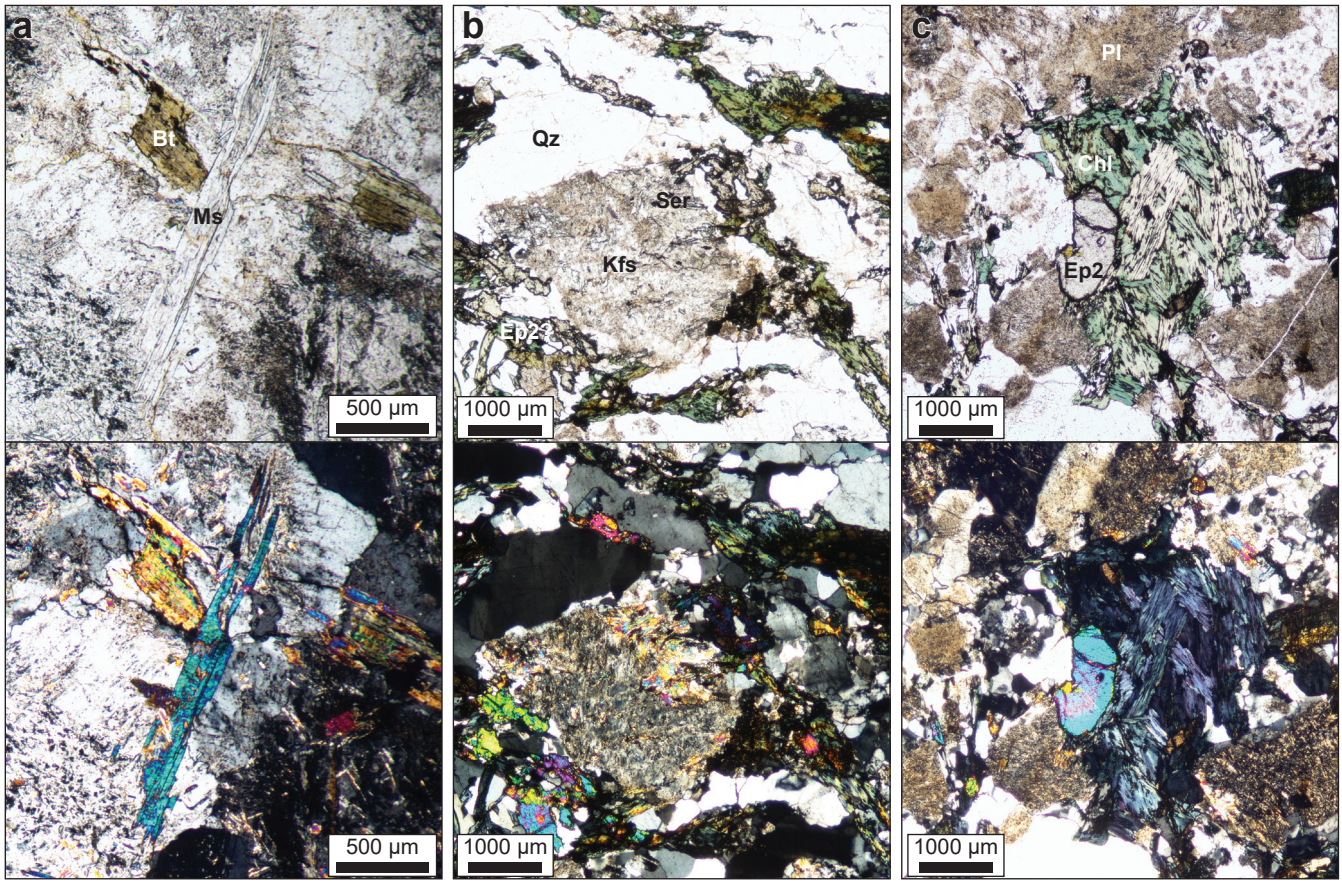


Figure 3-50. *Magmatic muscovite and alteration within the northern sector of the Yukon River batholith. Transmitted light photomicrograph pairs; plane polarized light (upper) and cross-polarized light (lower).* ***(a)*** *Coarse-grained euhedral muscovite interpreted as magmatic in origin, 09RAYJR170A1.* ***(b)*** *Strong sericitization of coarse-grained K-feldspar, likely the cause of the slight green tinge on polished surface of samples from this part of the batholith.* ***(c)*** *Anhedral epidote grain intergrown with chlorite and altered plagioclase. Chlorite is interpreted to have completely replaced biotite. Plagioclase is strongly saussuritized. (b and c) from 09RAYKR154A1.*

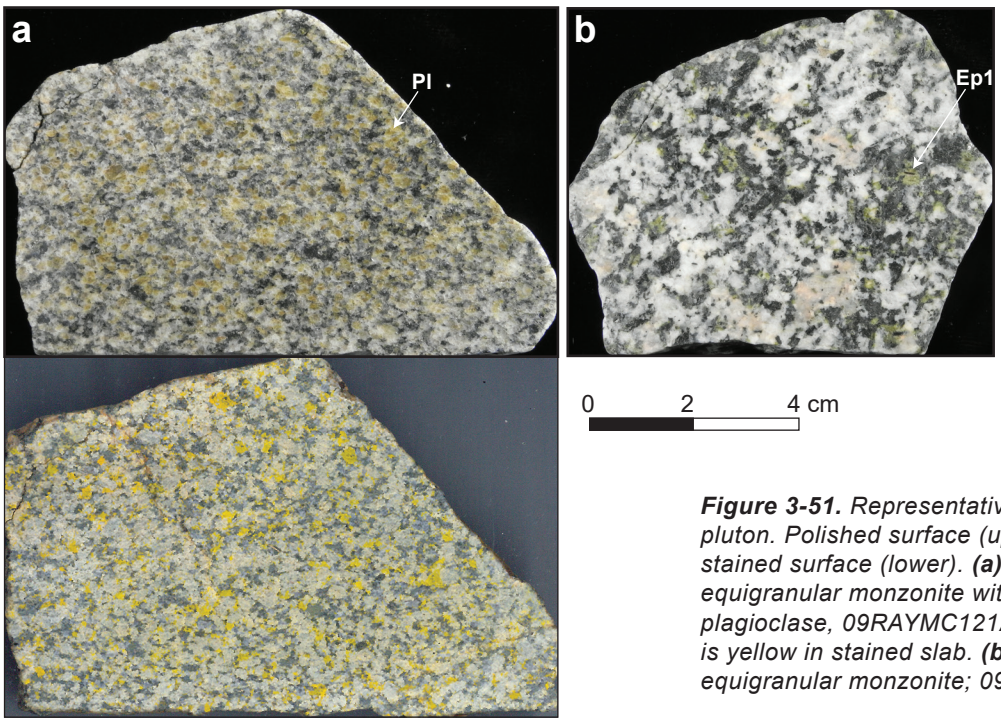


Figure 3-51. *Representative samples of the Pelly pluton. Polished surface (upper) and a cobaltinitrite-stained surface (lower).* ***(a)*** *Medium-grained, equigranular monzonite with brownish-green plagioclase, 09RAYMC121A1. Note K-feldspar is yellow in stained slab.* ***(b)*** *Medium-grained, equigranular monzonite; 09RAYKR164A1.*

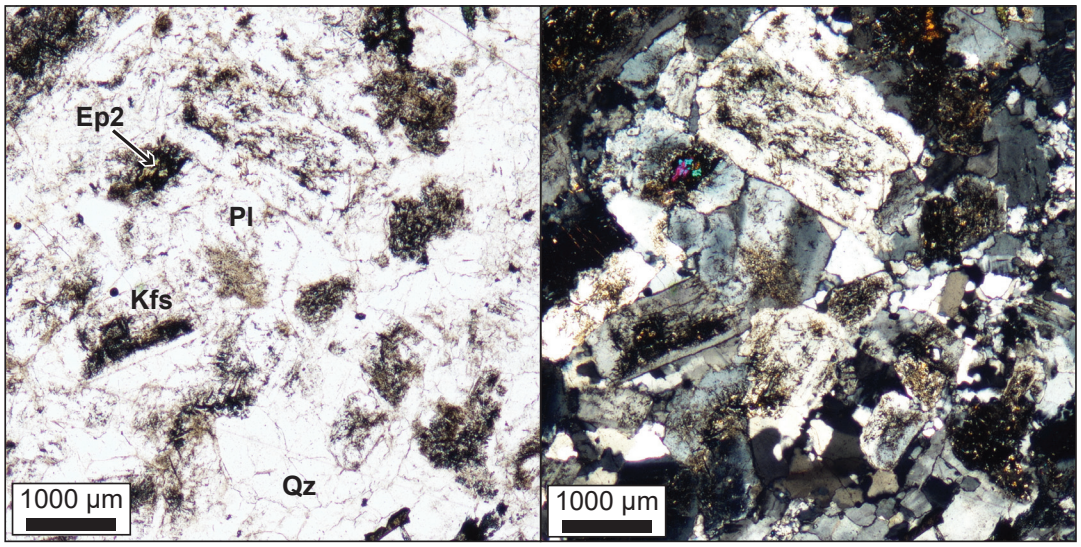


Figure 3-52. *Subhedral to euhedral feldspar laths with weak saussuritization of plagioclase and sericitization of K-feldspar, 09RAYKR164A1. Transmitted light photomicrograph pair; plane polarized light (left) and cross-polarized light (right).*

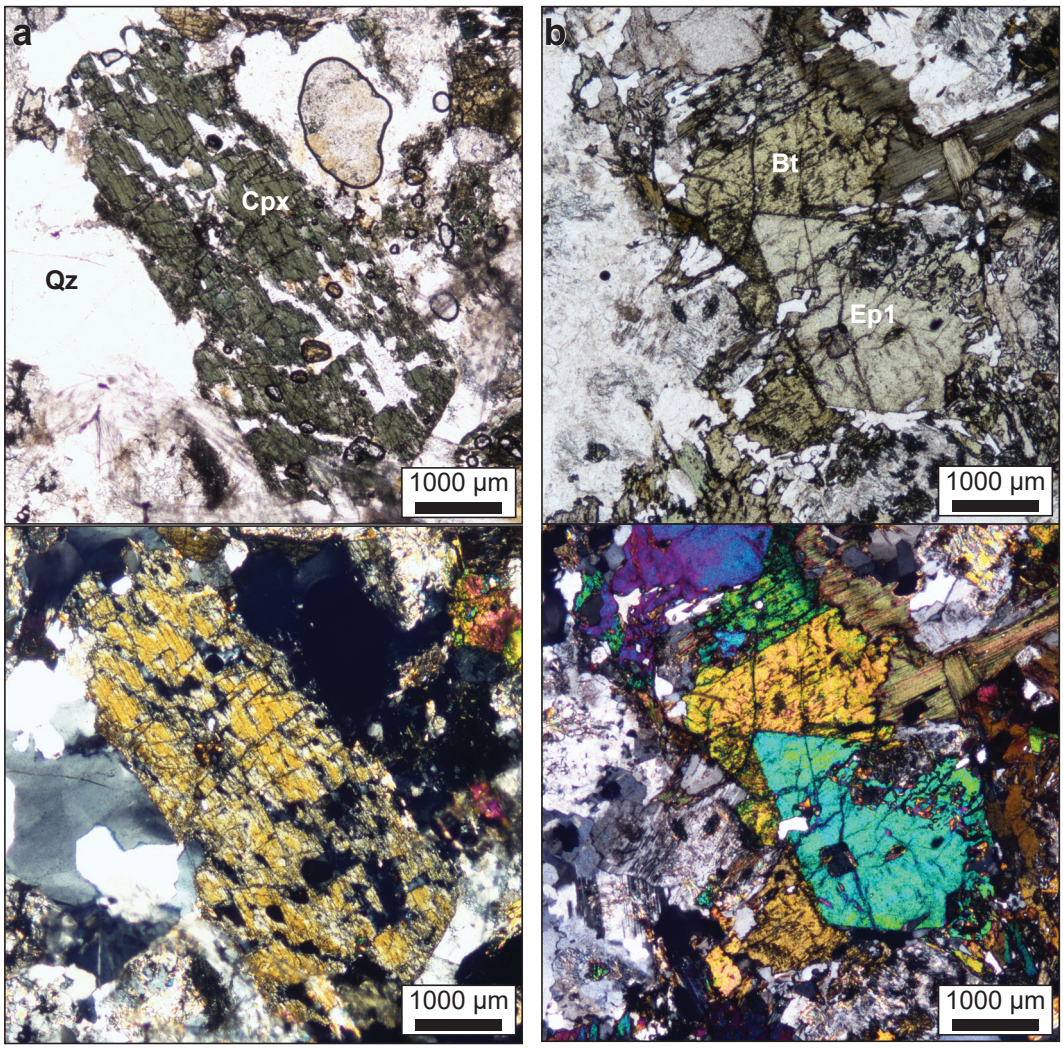


Figure 3-53. *Representative photomicrographs of mafic minerals in 09RAYMC123A1 from the Pelly pluton. Transmitted light photomicrograph pairs; plane polarized light (upper) and cross-polarized light (lower).* ***(a)*** *Rare coarse-grained clinopyroxene phenocryst.* ***(b)*** *Intergrown coarse-grained, euhedral magmatic epidote and biotite.*

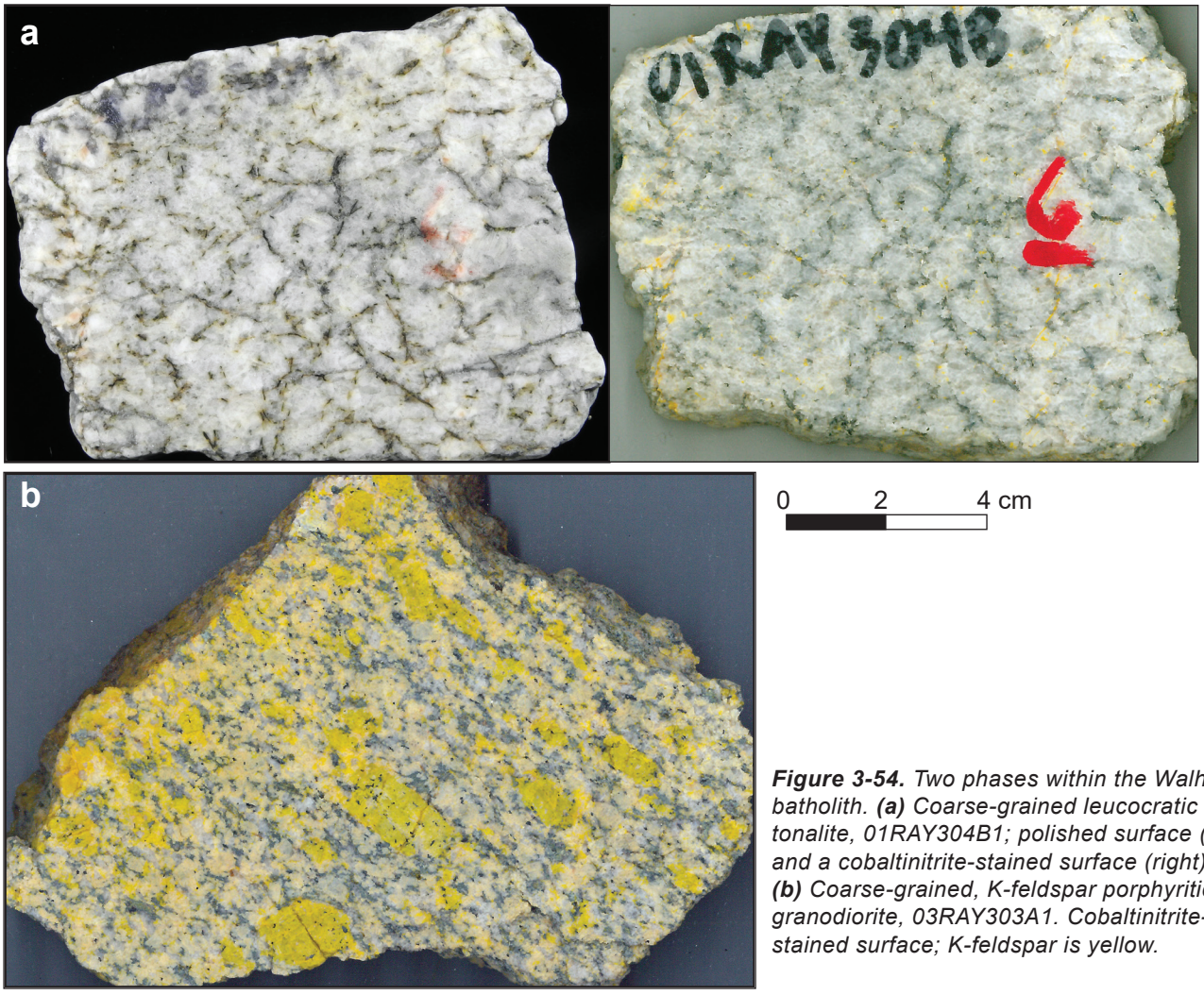


Figure 3-54. *Two phases within the Walhalla batholith.* ***(a)*** *Coarse-grained leucocratic tonalite, 01RAY304B1; polished surface (left) and a cobaltinitrite-stained surface (right).* ***(b)*** *Coarse-grained, K-feldspar porphyritic granodiorite, 03RAY303A1. Cobaltinitrite-stained surface; K-feldspar is yellow.*



Figure 3-55. *Schlieren from the northwest margin of the Walhalla batholith, 01RAY304.*

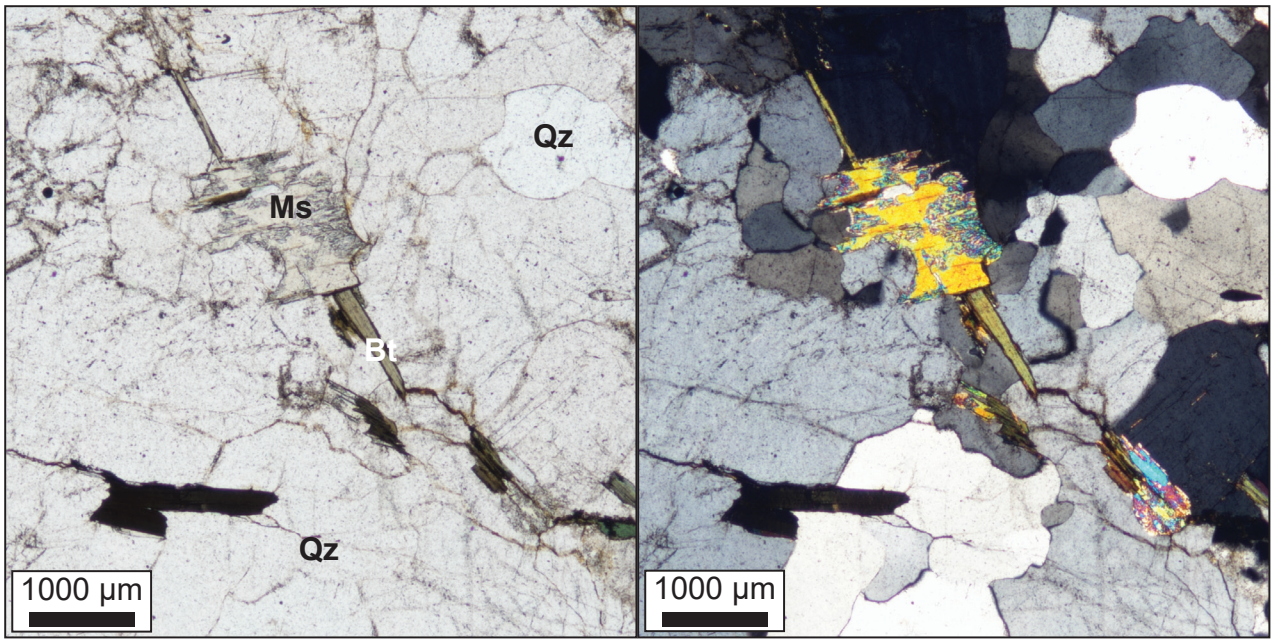


Figure 3-56. *Coarse-grained, euhedral muscovite from the Walhalla batholith, 01RAY304B1. Transmitted light photomicrograph pair; plane polarized light (left) and cross-polarized light (right).*

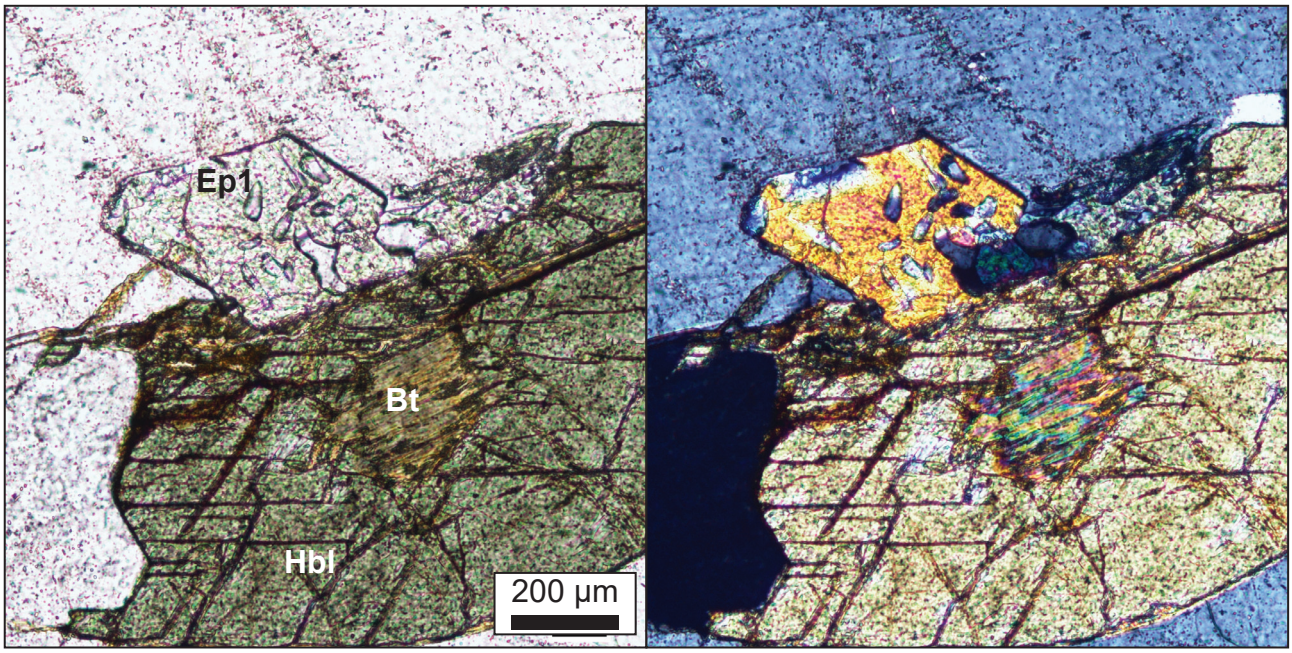


Figure 3-57. *Euhedral magmatic epidote intergrown with unaltered hornblende in 03RAYJR303A1 from the Walhalla batholith. Transmitted light photomicrograph pair; plane polarized light (left) and cross-polarized light (right).*

Oxidation state and mineral occurrences

The Yukon River, Walhalla and Pelly plutons have magnetic susceptibilities that range from 0.21 to 35.3 × 10^{-3} SI units (mean 5.17 × 10^{-3} SI units; n = 37; Fig. 3-4). The mean for the southwest and southeast sectors of the Yukon River batholith are 2.89 × 10^{-3} SI units (n = 14) and 5.23 × 10^{-3} SI units (n = 6), respectively. These are similar to the north sector which has a mean magnetic susceptibility of 5.45 × 10^{-3} SI units (n = 14). The Pelly pluton is slightly more magnetic with a mean susceptibility of 11.80 × 10^{-3} SI units (n = 5). Tempelman-Kluit and Currie (1978) have one magnetic susceptibility measurement of 0.37 × 10^{-3} SI units from the tonalite phase of the Walhalla pluton. Though there are variations within each pluton, and within portions of plutons, these magnetic susceptibility data are consistent with petrographic observations which show magnetite in varying abundances and regional aeromagnetic surveys which show varying magnetic response within each body (*e.g.*, Figs. 3-45 and 3-58).

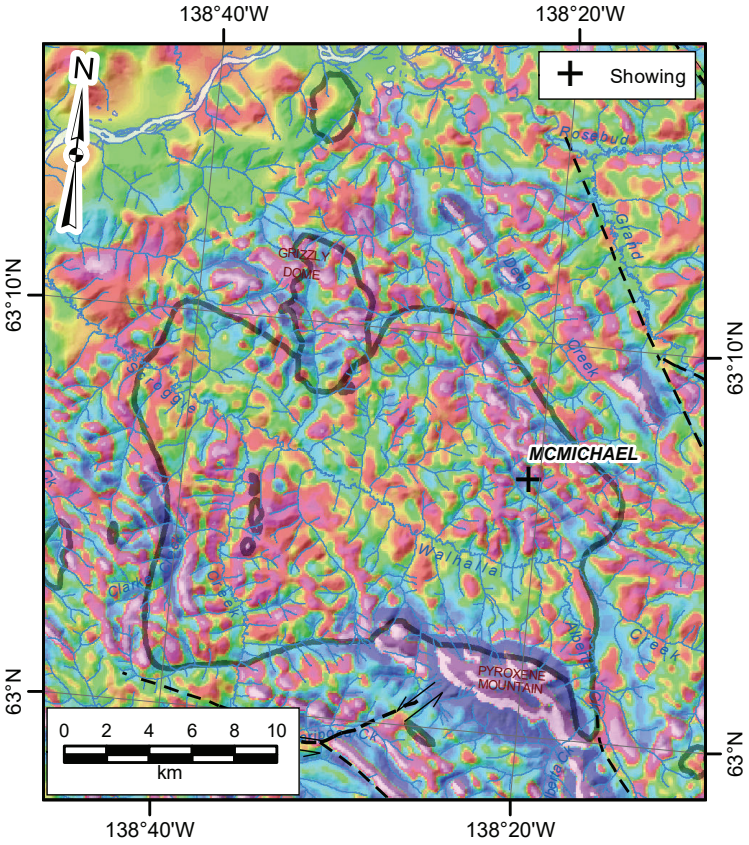


Figure 3-58. *First vertical derivative aeromagnetic map of the Walhalla batholith (Hayward and Oneschuk, 2011) showing a single Cu-Ag-Au MINFILE occurrence within the pluton.*

Several mineral occurrences are hosted by, or are located near, the Yukon River, Walhalla and Pelly plutons (Figs. 3-45 and 3-58). Occurrences surrounding the Yukon River and Walhalla batholiths (*e.g.*, Kerr [115I 081] and Pyroxene [115O 116]) may be related to Late Triassic plutons of the Pyroxene Mountain suite, and are discussed in Chapter 2. A single occurrence within the Walhalla pluton (McMichael [115O 085]) corresponds to weak copper mineralization in granodiorite near a stream sediment anomaly. In the southeast sector of the Yukon River batholith, more than 1000 m were drilled in three holes at the Toe occurrence [115I 124] near Fort Selkirk (Fig. 3-45). The drilling targeted coincident magnetic, induced polarization and MMI Cu-Au geochemical anomalies but failed to intersect mineralization (Sidhu, 2011).

In the southern part of the Pelly pluton, the Pelly occurrence [115I 026] was staked in the early 1970s to cover Cu-Mo soil anomalies near the contact with Upper Triassic mafic volcanic rocks of Stikinia (Figs. 3-43 and 3-45). Minor chalcopyrite and malachite are reported from this area (Ouellette and Pollries, 2010). Six diamond drill holes totaling 833.5 m have been drilled in 1972 and 2010 (Ouellette and Pollries, 2010). Only weak Cu-Au-Mo mineralization was intersected in core, the best interval is 1.9 m of 0.1 ppm Au, 588 ppm As (Ouellette and Pollries, 2010).

Geochronology

The age of the Yukon River batholith is constrained by one U-Pb zircon date of 199 ± 2 Ma (MSWD = 1.0; n = 21; SIMS, Appendix 12) from the southwest sector (Fig. 3-43). The data are relatively consistent at *ca.* 200 Ma, with four inherited Carboniferous grains between 339 and 313 Ma (Fig. 3-59a,b). Hornblende and biotite from granodiorite in the north sector of the batholith were analyzed by the $^{40}Ar/^{39}Ar$ method at the University of Wisconsin–Madison (09RAYKR151A; Appendix 6). The hornblende age spectrum shows evidence of Ar loss in low temperature steps but climbs to a plateau of 198.0 ± 0.5 Ma at mid to high temperatures (Fig. 3-59c). Biotite from the same sample yield a disturbed, hump-shaped age spectrum and an integrated age of *ca.* 194 Ma for 98% of ^{39}Ar released (Fig. 3-59d).

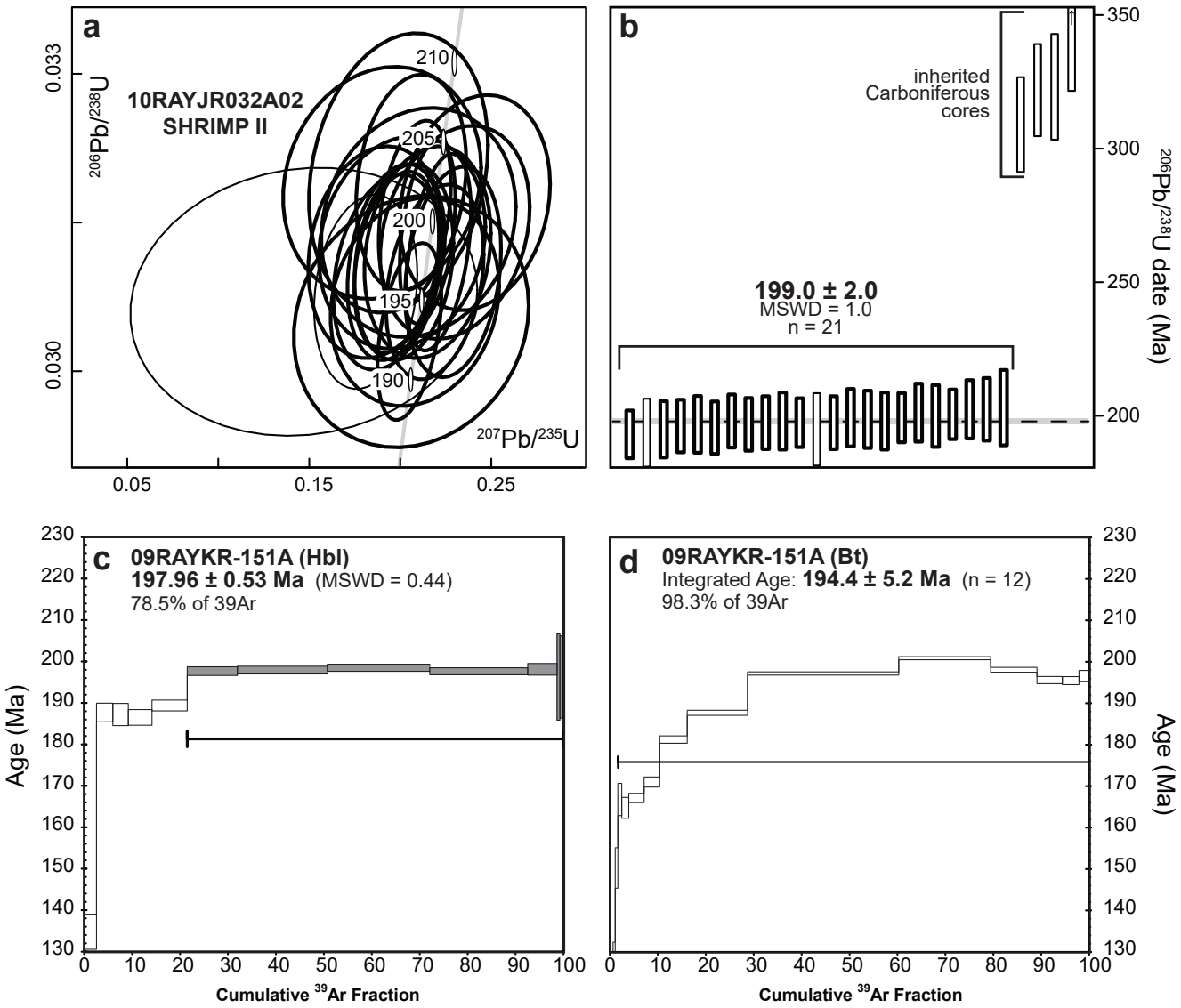


Figure 3-59. *U-Pb geochronological results for the Yukon River batholith.* ***(a)*** *Concordia diagram and* ***(b)*** *ranked $^{206}Pb/^{238}U$ dates for zircons analyzed by SIMS at GSC in Ottawa; 10RAYJR032A02 from the southwest sector of the batholith. Only zircon analyses included in the weighted mean $^{206}Pb/^{238}U$ date are shown by solid bold ellipses on concordia. All analyses are shown in rank plot, with bar heights indicating 2σ uncertainties. The horizontal dashed line represents the weighted mean date of 21 analyses with the 2σ uncertainty shown by the light grey band. MSWD = mean squared weighted deviation. Carboniferous dates reflect an inherited component.* ***(c)*** *$^{40}Ar/^{39}Ar$ age spectra for hornblende from granodiorite in the north sector of the Yukon River batholith (09RAYKR151A; Appendix 6).* ***(d)*** *$^{40}Ar/^{39}Ar$ age spectra for biotite from the same sample.*

The age of the Pelly pluton is constrained by a single U-Pb zircon date of 204.9 ± 3.3 Ma (MSWD = 3.9; n = 13; SIMS; Knight *et al.*, 2013). The data for the Pelly pluton show considerable scatter with a number of discordant analyses affected by common Pb contamination, and others reflecting an inherited Mississippian component (Fig. 3-60). The Walhalla composite pluton has two different ages. Granodiorite from the southeast corner of the pluton is dated at 198 +2/-60 Ma based on U-Pb TIMS analyses of multi-grain zircon fractions from a K-feldspar porphyritic granodiorite (J. Ryan, unpublished data, 2003). A sample from the northern tip of the Walhalla pluton (Grizzly Dome pluton) yielded U-Pb zircon dates of 199.1 ± 6.8 Ma (ID-TIMS, multi-grain fractions) and 197.7 ± 2.4 Ma (LA-ICPMS; J.K. Mortensen, unpublished data, 1999). A pink granite dike from the same outcrop is younger with a titanite U-Pb date of 178.2 ± 2.4 Ma (J. Ryan, unpublished ID-TIMS data, 2002).

Thermobarometry

One sample of tonalite orthogneiss from the northwestern Walhalla batholith contains the suitable mineral assemblage for Al-in-Hbl geobarometry (01GGA166B1; Hammarstrom and Zen, 1986; Appendix 5). Al^{TOT} in hornblende from this sample is 2.06 with cotectic plagioclase X_{An} of 0.20, indicating a crystallization pressure estimate of 5.86 ± 0.6 kbar (Appendix 5; emplacement depths of 18.8 to 25.4 km) and a solidus temperature of 732°C.

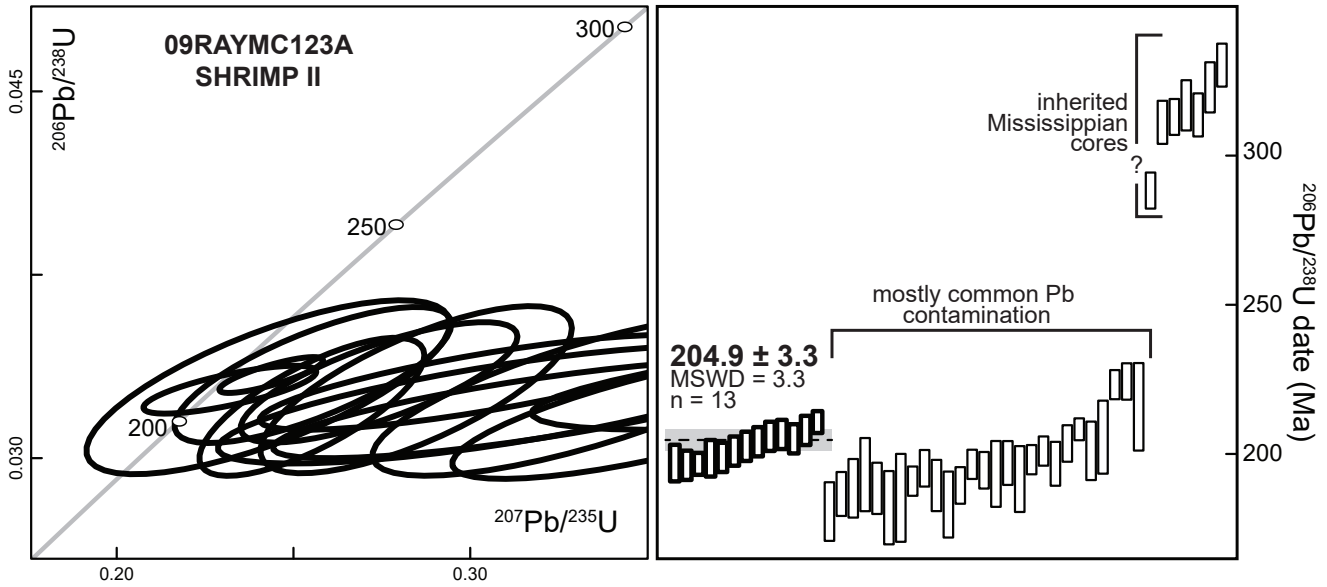


Figure 3-60. *U-Pb geochronological results for sample 09RAYMC123A, Pelly pluton (replotted from Knight et al., 2013). Concordia diagram (left) and ranked $^{206}Pb/^{238}U$ dates (right) for zircons analyzed by SIMS at GSC in Ottawa. Only zircon analyses included in the weighted mean $^{206}Pb/^{238}U$ date are shown by solid bold ellipses on concordia. All analyses reported by Knight et al. (2013) are shown in rank plot, with bar heights indicating 2σ uncertainties. The horizontal dashed line represents the weighted mean date of 13 analyses with the 2σ uncertainty shown by the light grey band. MSWD = mean squared weighted deviation. A large number of analyses in this sample suffered common Pb contamination. Mississippian dates likely reflect an inherited component.*

Tatchun batholith

The Tatchun batholith is an elongate northwest-trending body located ~40 km east of Carmacks (Fig. 3-1), between the Little Salmon River and Tadru Lake, that has a mapped extent of 712 km² (Fig. 3-61). Two small satellite bodies are inferred to be extensions of the Tatchun batholith: 1) a 4.4 km² pluton exposed to the southeast of the Little Salmon River, and separated from the main batholith by Upper Cretaceous basalt of the Carmacks Group; and 2) a 1.4 km² plug intruding amphibolite of the Moose formation (Quesnellia) to the northwest (Fig. 3-61). The Tatchun batholith intrudes mid to late Paleozoic rocks of Quesnellia, including mafic metavolcanic rocks and marble of the Moose formation to the north and east, and sedimentary and volcanic rocks of the Boswell formation to the west (Colpron *et al.*, 2002; Fig. 3-61). The central northeastern margin of the batholith intrudes Carboniferous tonalitic orthogneiss of the Kelly suite. The southern margin of the batholith is unconformably overlain by basalt of the Upper Cretaceous Carmacks Group (Colpron *et al.*, 2002). The western margin of the batholith is locally truncated by the Towhata fault, a Cretaceous dextral strike-slip fault that juxtaposes Jurassic granodiorite with Triassic mafic metavolcanic rocks of the Semenof formation (Quesnellia; Tempelman-Kluit, 1984, 2009; Colpron *et al.*, 2002). The northwestern portion of the pluton is moderately foliated with a mafic mineral alignment fabric striking northwest and dipping moderately to steeply to the northeast (Colpron *et al.*, 2002). This portion of the batholith also locally contains rafts of strongly foliated amphibolite aligned parallel to fabric in the granodiorite (Fig. 3-62). Three main phases are identified in the Tatchun batholith: 1) coarse-grained, K-feldspar porphyritic granodiorite; 2) medium-grained equigranular biotite monzodiorite; and 3) leucocratic tonalite, aplite and pegmatite. These three phases occur throughout the batholith but can locally be observed in the same outcrop (*e.g.*, Fig. 3-63). At the scale of the batholith there appears to be a systematic distribution, with the coarse-grained porphyritic granodiorite forming a border phase, the medium-grained equigranular monzodiorite occupying the central part of the batholith, and the tonalite representing the dominant phase in the northern and eastern portions of the batholith (Fig. 3-61). The regions predominantly underlain by exposures of tonalite are characterized by magnetic lows (Fig. 3-64). The coarse-grained porphyritic border phase weathers to rounded bedrock exposures with a 'knobbly' texture resulting from differential weathering of groundmass (recessive) and K-feldspar phenocrysts up to 5–7 cm long (resistant; Figs. 3-65 and 3-66). The groundmass of this phase has a consistent ratio of 1:2 quartz to plagioclase with the variation in alkali content, and thus the QAP classification relates primarily to abundance of K-feldspar phenocrysts (Fig. 3-67). The medium-grained equigranular central phase weathers in similar rounded shapes as the border phase but with a smoother surface due to the even distribution of mafic and felsic minerals (Fig. 3-68).

Petrography

The three phases of the Tatchun batholith range in composition from quartz monzonite to granodiorite for the coarse-grained porphyritic phase, monzodiorite for the medium-grained equigranular phase and tonalite to diorite for the leucocratic phase (Fig. 3-69). In all three phases, plagioclase and K-feldspar are unaltered to weakly saussuritized and sericitized, respectively; mafic minerals are unaltered (Fig. 3-70). In all three phases, epidote is present mostly as a primary magmatic mineral (Fig. 3-71). Both the coarse-grained porphyritic and medium-grained equigranular phases have a mafic mineral assemblage of hornblende and biotite. However, the coarse-grained phase is hornblende dominant with 2 to 5 times more hornblende than biotite, and the medium-grained phase is biotite dominant with twice as much biotite as hornblende. The leucocratic phase varies from fine to coarse grained and is distinct from the other phases of the pluton as it has ≤5% hornblende, biotite and K-feldspar combined (Figs. 3-69 and 3-72).

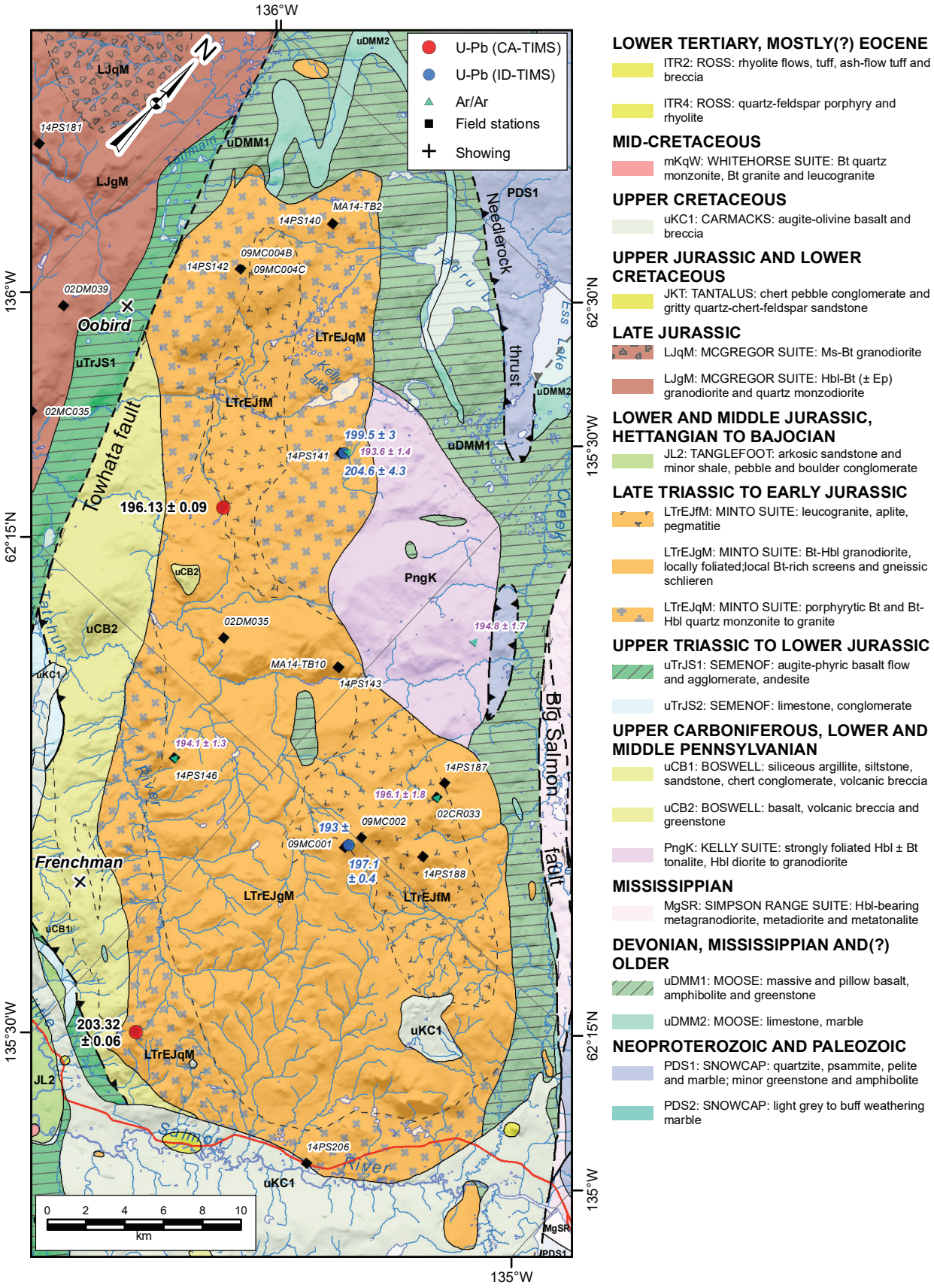


Figure 3-61. *Geology of the Tatchun batholith area. Geology from YGS (2020a); fault symbology as in Figure 1-4. Note that the geographic reference frame has been rotated with North pointing to the upper right of the page.*



Figure 3-62. *Foliated rocks within the Tatchun batholith, station 15PS101.* ***(a)*** *Outcrop of garnet amphibolite in contact with granodiorite. Note subparallel foliation in both rock types. Field of view approximately 2 m across.* ***(b)*** *Close-up of garnet amphibolite, likely a raft of Moose formation within the Tatchun batholith.* ***(c)*** *Broken surface of moderately foliated granodiorite of the Tatchun batholith. Dashed lines indicate foliation trace.*

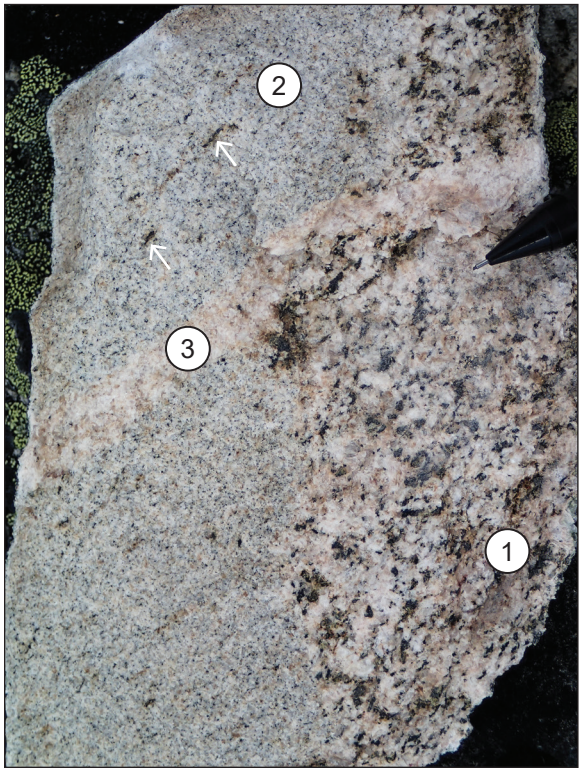


Figure 3-63. *Hand sample containing all three phases of the Tatchun batholith. Numbers show relative intrusive sequence: 1) weakly foliated coarse-grained granodiorite; 2) medium-grained granodiorite with small biotite-rich inclusions of 1 (arrows); and 3) leucogranite dike crosscutting 1 and 2. Station 14PS142, sample approximately 15 cm across.*

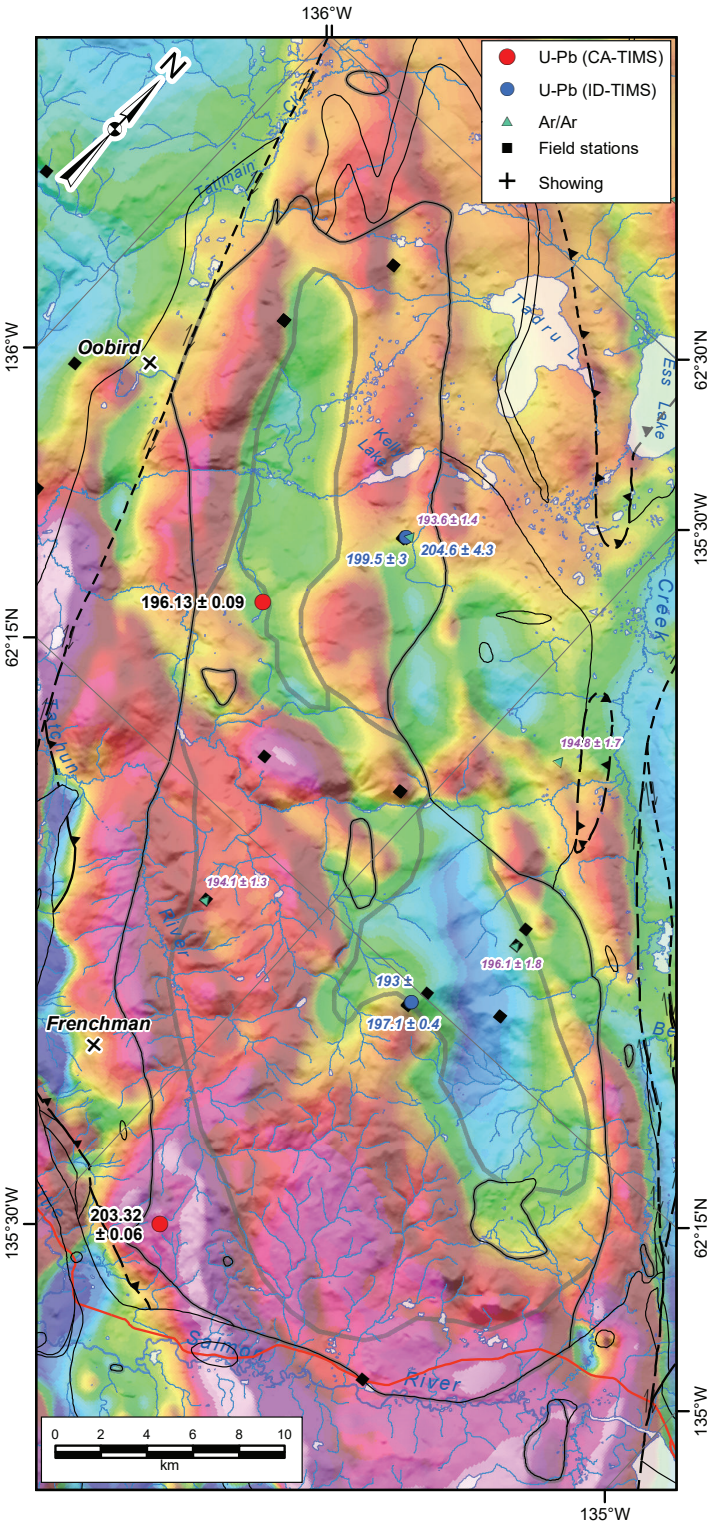


Figure 3-64. *Residual total field aeromagnetic map for the Tatchun batholith area (Hayward and Oneschuk, 2011). Heavy grey lines show interpreted contacts between the three phases of the batholith. Fault symbology as in Figure 1-4. Note that the geographic reference frame has been rotated with North pointing to the upper right of the page.*

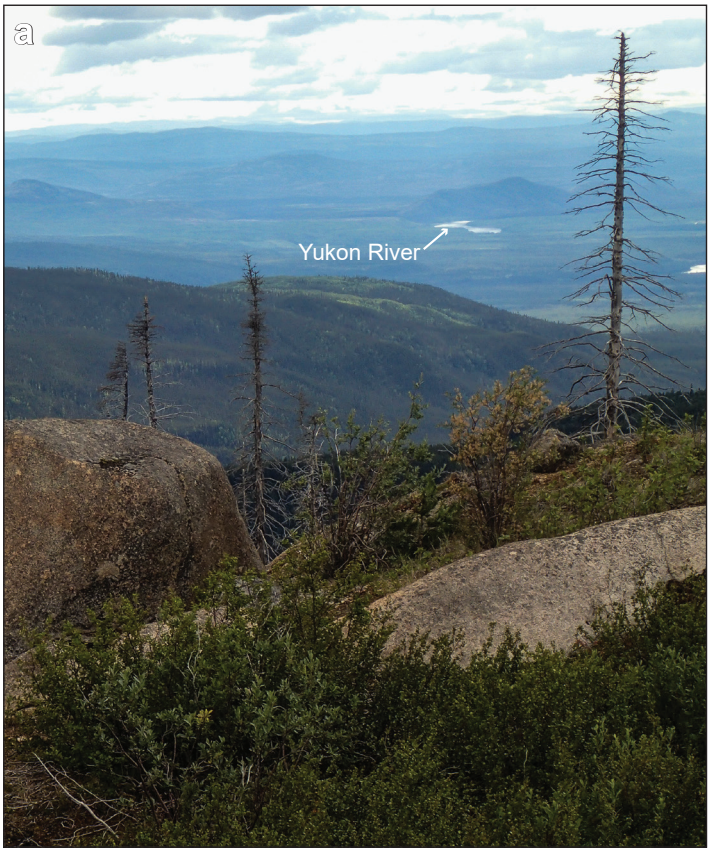




Figure 3-65. *Exposure along the southern part of the Tatchun batholith.* ***(a)*** *View southwest towards the Yukon River showing the forest cover and rounded outcrop typical of the southern portion of the batholith, station 14PS145.* ***(b)*** *Outcrop of weathered, K-feldspar porphyritic granite with a thin, crosscutting, aplite dike; station 14PS206. Hammer 45 cm long.*







Figure 3-66. *Weathered outcrop of coarse-grained, K-feldspar porphyritic granodiorite, station 14PS145.* ***(a)*** *K-feldspar megacrysts are locally ≥5 cm long. Hammer is 45 cm long;* ***(b)*** *close-up of area outlined in (a); lens cap is 4 cm in diameter.* ***(c)*** *Coarse-grained, dark grey quartz and white plagioclase with large K-feldspar phenocrysts.*

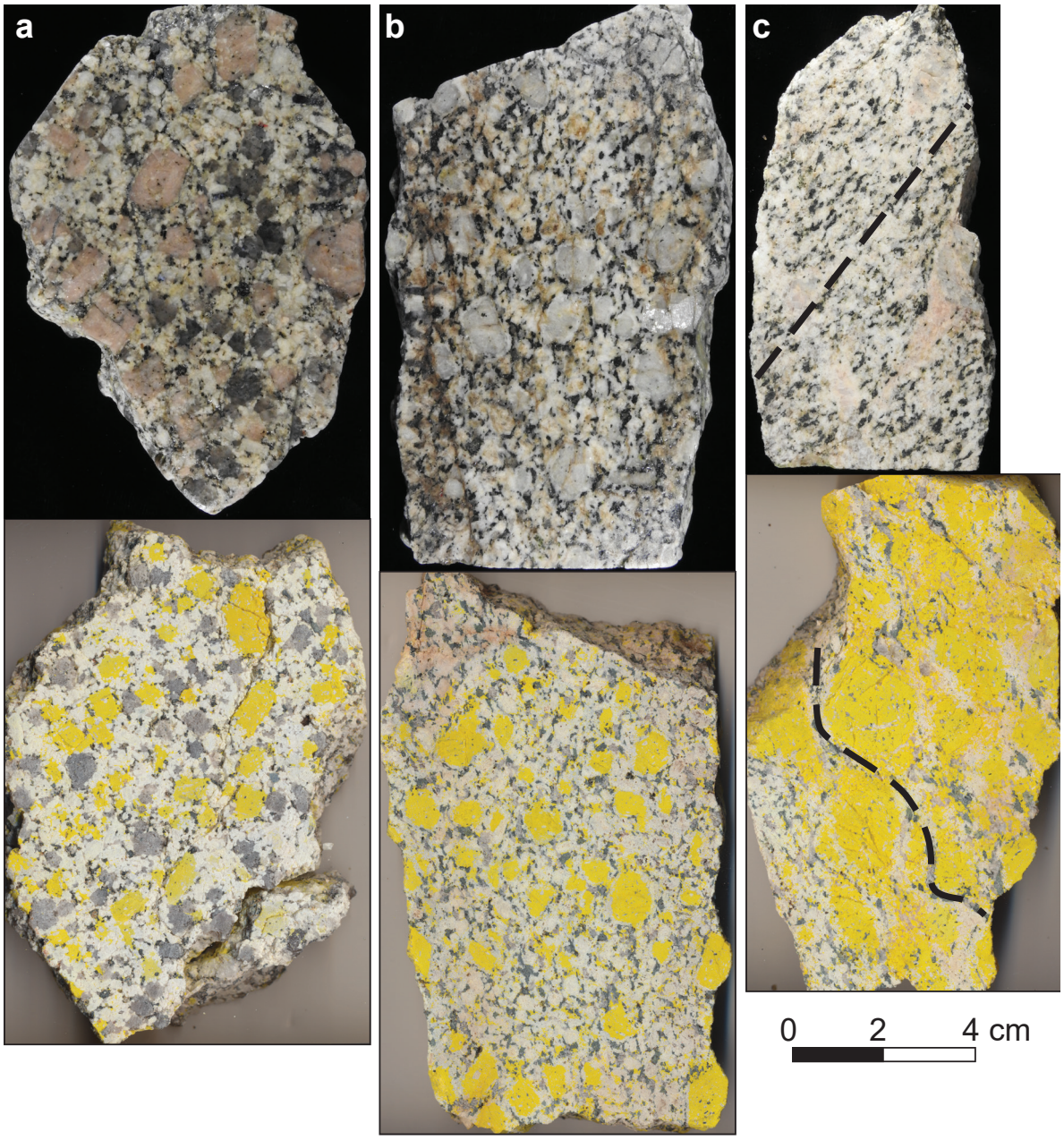


Figure 3-67. *Representative coarse-grained porphyritic samples from the Tatchun batholith. Fresh polished surface (upper) and a cobaltinitrite-stained surface (lower).* ***(a)*** *Coarse-grained K-feldspar porphyritic granodiorite with large, dark grey quartz phenocrysts, 14PS145-1.* ***(b)*** *Coarse-grained K-feldspar porphyritic granodiorite with equigranular groundmass, 14PS187-1.* ***(c)*** *Weakly foliated, K-feldspar porphyritic, coarse-grained granodiorite with slightly elongate K-feldspar phenocrysts, 14PS142-1. Dashed line indicates foliation trace; K-feldspar is stained yellow.*

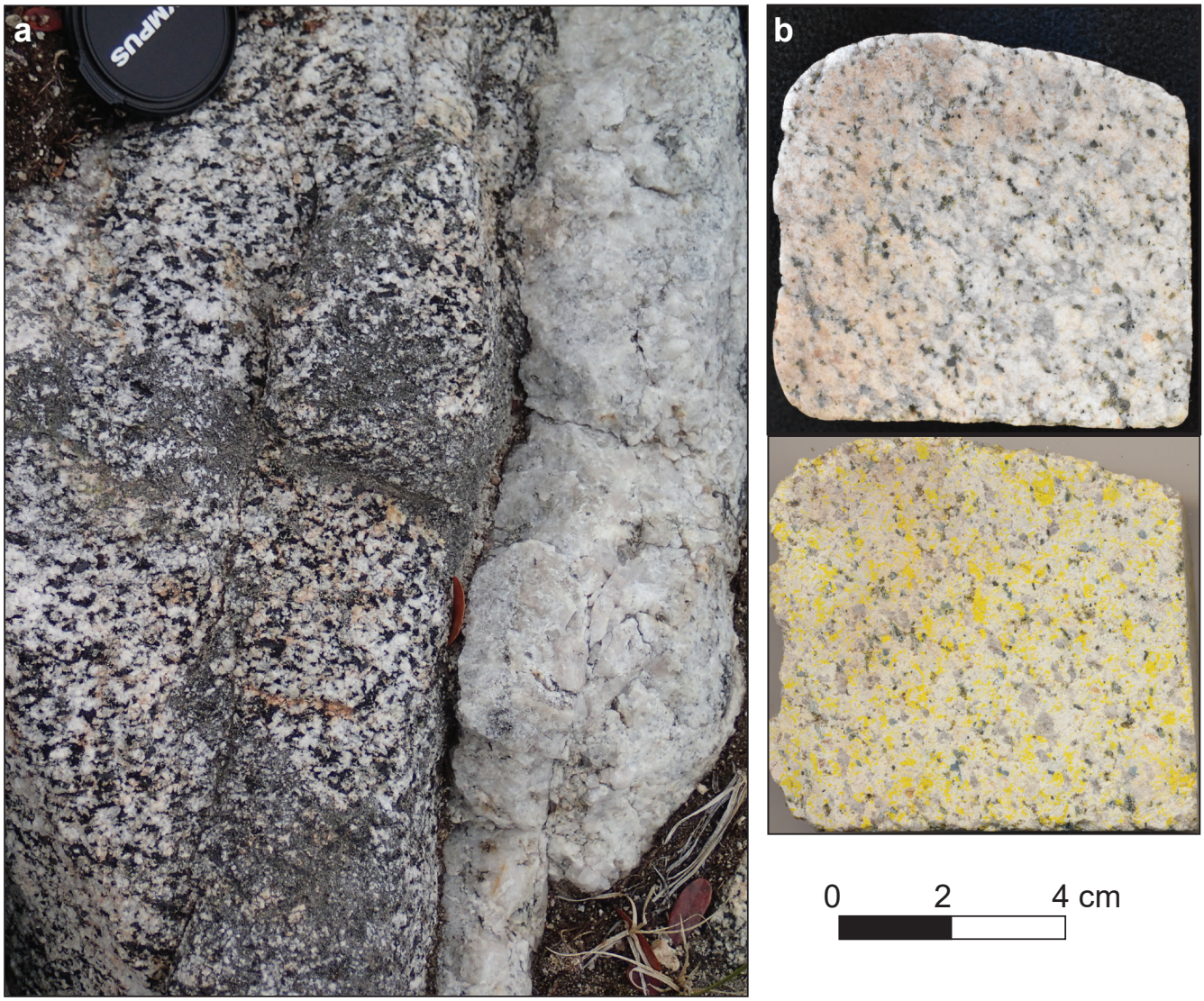


Figure 3-68. *Medium-grained equigranular granodiorite from the central phase of the Tatchun batholith.* ***(a)*** *Outcrop with medium-grained granodiorite cut by leucocratic aplite; 14PS143.* ***(b)*** *Fresh polished surface (upper) and a cobaltinitrite-stained surface (lower); 14PS146-1. K-feldspar is stained yellow.*

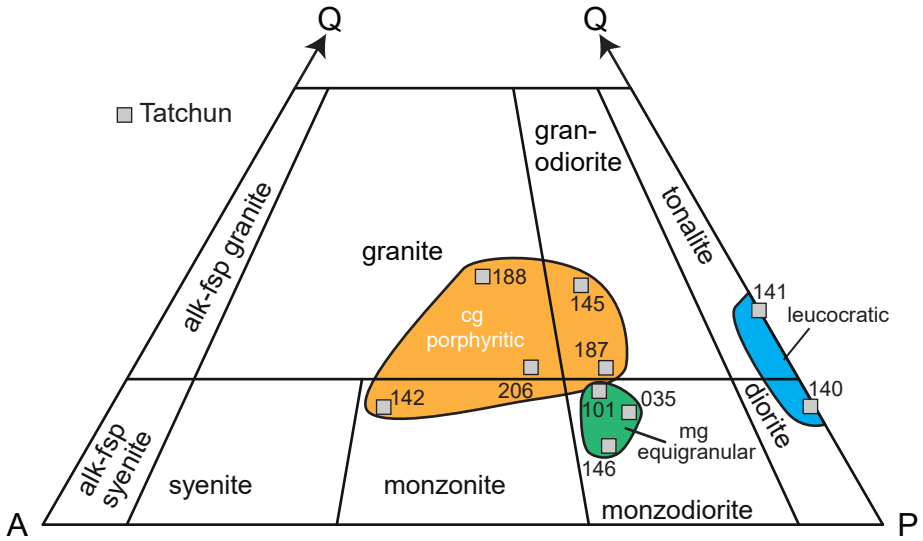


Figure 3-69. *Simplified QAP diagram for Tatchun batholith samples (after Le Bas and Streckeisen, 1991). Numbers beside each sample shortened to station number only for clarity. cg = coarse grained, mg = medium grained.*

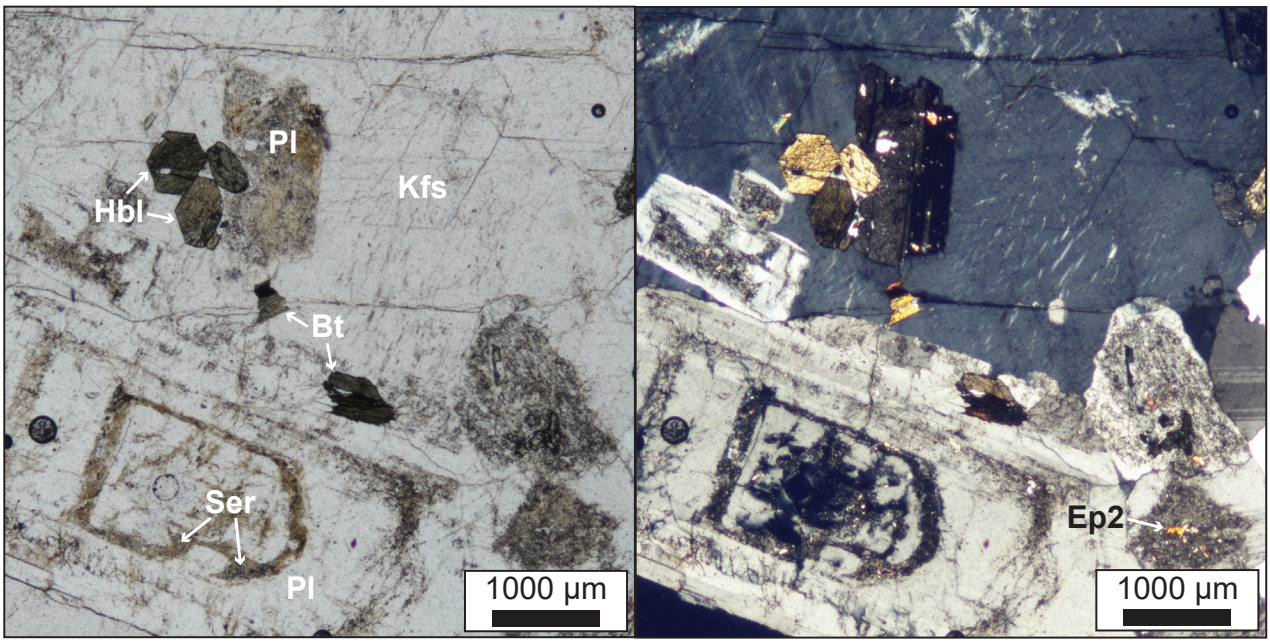


Figure 3-70. *Transmitted light photomicrograph pairs, plane polarized light (left) and cross-polarized light (right), of feldspars from the Tatchun batholith, 14PS145-1. Unaltered coarse-grained K-feldspar and weakly altered plagioclase cores with fine-grained hornblende and biotite. Plagioclase cores saussuritized to sericite and epidote.*

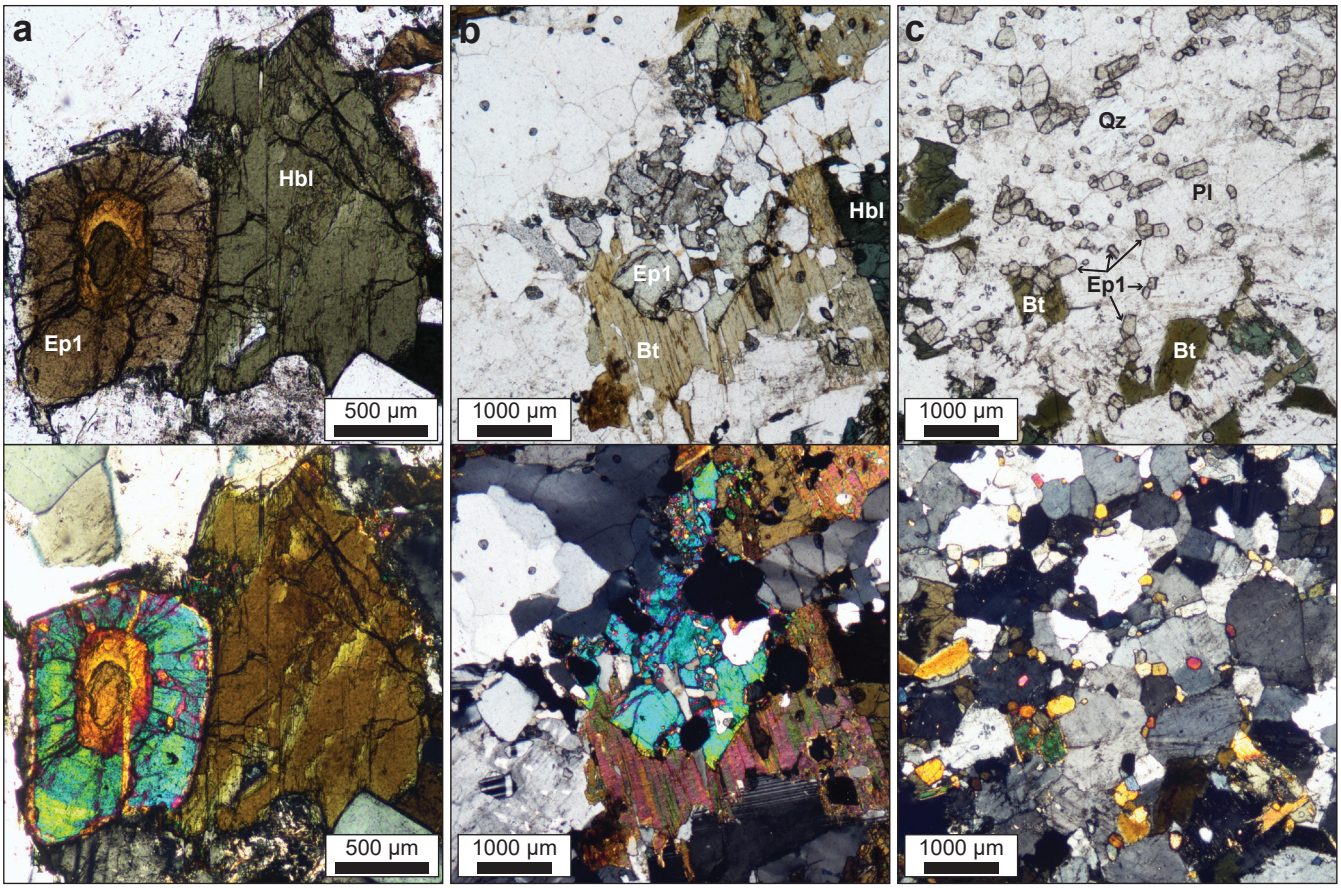


Figure 3-71. *Transmitted light photomicrograph pairs, plane polarized light (upper) and cross-polarized light (lower), showing the variation in magmatic epidote from the Tatchun batholith.* ***(a)*** *Zoned euhedral epidote with a clean linear boundary against hornblende, 02MC030-1.* ***(b)*** *Poikilitic epidote sharing a euhedral boundary with biotite, 14PS141-2.* ***(c)*** *Small euhedral epidote intergrown with both felsic groundmass and biotite, 14PS142-1.*

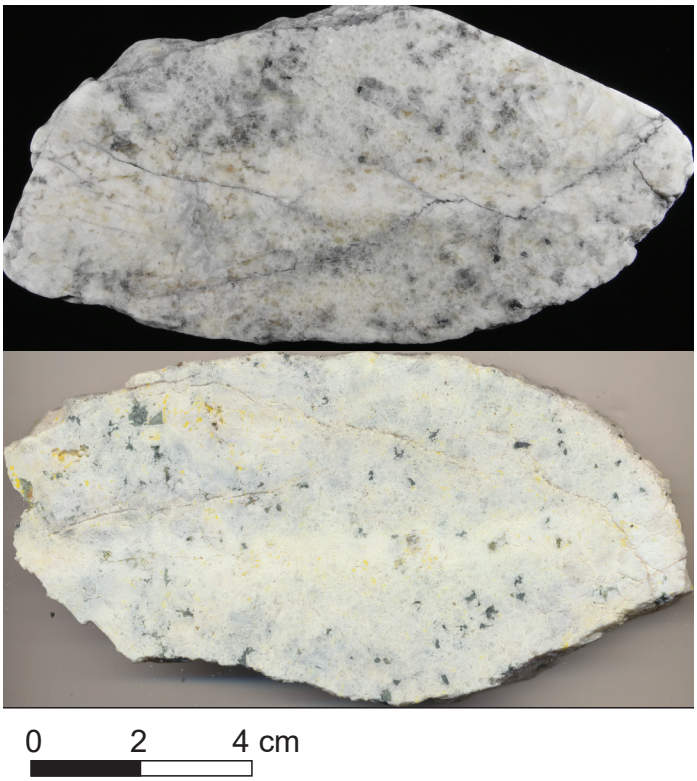


Figure 3-72. *Representative sample of diorite from the leucocratic phase of the Tatchun batholith, 14PS140-1. Fresh polished surface (upper) and a cobaltinitrite-stained surface (lower).*

Oxidation state and mineral occurrences

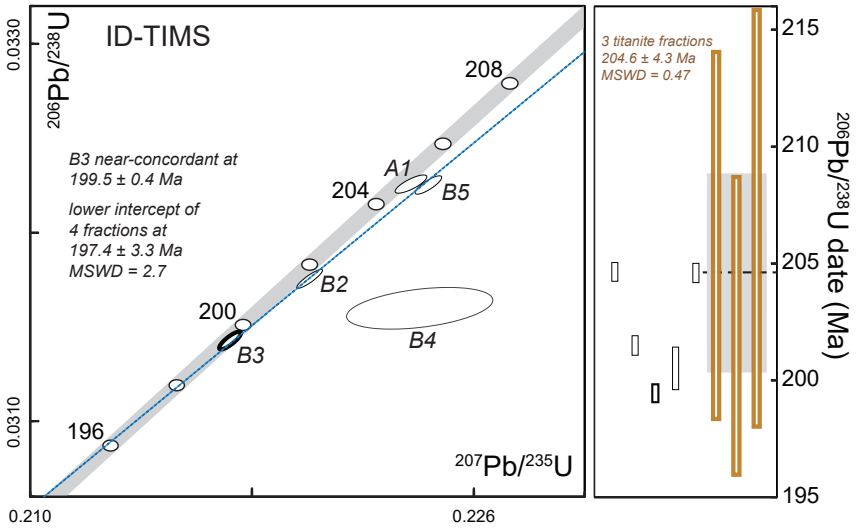
The magnetic susceptibility of the porphyritic border phase ranges from 0.102 to 6.33 × 10^{-3} SI units (mean 1.8 × 10^{-3} SI units; n = 5). The central monzodiorite phase has a magnetic susceptibility between 2.24 and 10.32 × 10^{-3} SI units (mean 4.29 × 10^{-3} SI units; n = 5). The tonalite phase has low magnetic susceptibility, with measurements of 0.02 and 0.23 × 10^{-3} SI units (mean 0.14 × 10^{-3} SI units; n = 2) and its distribution is partially reflected by aeromagnetic lows that characterize the northern and eastern parts of the pluton (Fig. 3-63).

The Oobird [105L 061] and Frenchman [105L 066] occurrences are located within 2 km of the southwestern margin of the Tatchun batholith (Fig. 3-61). The Oobird occurrence mineralization consists of traces of chalcopyrite and bornite with 5 to 20% pyrrhotite and pyrite near a quartz-feldspar porphyry dike. This dike intrudes mafic volcanic rocks of the Upper Triassic Semenof formation and is dated at *ca.* 207 Ma (Headless suite; *see* Chapter 2, Tadru locality in Fig. 2-42). The Frenchman occurrence mineralization consists of malachite and azurite-stained quartz vein float found along the ridge east of Frenchman Lake. It coincides with anomalous copper values up to 130 ppm in a till sample (Bond and Plouffe, 2003).

Geochronology

U-Pb

The age of the coarse-grained K-feldspar porphyritic granite phase of the Tatchun batholith is constrained by U-Pb dating of two samples. Sample 02MC030-1 from the northern margin of the batholith was analyzed by ID-TIMS on multi-grain zircon and titanite fractions at the GSC laboratory in Ottawa by M.E. Villeneuve in 2003. Five zircon fractions yielded discordant results with $^{206}Pb/^{238}U$ dates ranging from 204.67 ± 0.4 to 199.5 ± 0.4 Ma (Appendix 6). A regression through the 4 least discordant fractions has a lower intercept of 197.4 ± 3.3 Ma (Fig. 3-73). We consider the $^{206}Pb/^{238}U$ date of 199.5 ± 0.4 Ma for the least discordant fraction the best estimate for crystallization age of this sample. Three titanite fractions have a weighted average $^{206}Pb/^{238}U$ date of 204.7 ± 4.3 Ma (Fig. 3-73). Together, these early discordant results broadly suggest that the border phase of the Tatchun batholith is dated at *ca.* 205–200 Ma.



02MC030-1 Tatchun border phase porphyritic granodiorite

Figure 3-73. *U-Pb geochronological results for sample 02MC030-1, Tatchun batholith. Concordia diagram (left) and ranked $^{206}Pb/^{238}U$ dates (right) for 5 zircon and 3 titanite fractions analyzed by ID-TIMS at GSC in Ottawa (Appendix 7). Only zircon fractions are plotted on concordia diagram, with most concordant fraction (B3) shown with solid bold ellipse. The light grey band around concordia (dark grey line) shows the decay constant uncertainties. The blue line is regression through the 4 least discordant analyses. Bar heights in ranked plot are 2σ uncertainties. Bars with brown outline are titanite analyses. The horizontal dashed line represents the weighted mean date of the 3 titanite analyses with the 2σ uncertainty shown by the light grey band. MSWD = mean squared weighted deviation.*

Another sample of coarse-grained porphyritic granite from the southern margin of the Tatchun batholith (14PS145-1; Fig. 3-66) was analyzed by LA-ICPMS and CA-TIMS at Boise State University (Appendices 3 and 4). This sample yielded prismatic zircons with an aspect ratio of 2:1, concentric igneous zoning, and inherited cores in some grains (Fig. 3-74a). Fifty-eight LA-ICPMS spots were analyzed and yielded $^{206}Pb/^{238}U$ dates between 361 ± 33 and 184 ± 13 Ma, with a weighted mean of 203.4 ± 1.9 Ma for 37 of 39 young analyses (Fig. 3-74b; Appendix 3). Analyses from inherited cores defined two clusters of Mississippian dates at *ca.* 320 and 342 Ma. Eight of the youngest zircons were selected for CA-TIMS analysis (Appendix 4) with six grains yielding concordant analyses ranging from 204.80 ± 0.14 to 203.18 ± 0.14 Ma; the youngest five grains have a weighted mean date of 203.32 ± 0.06 Ma (MSWD =1.29, n = 5; Fig. 3-74c) which is interpreted as the crystallization age of this rock. Older grains with $^{206}Pb/^{238}U$ dates of 212.58 ± 0.26 and 278.16 ± 0.22 Ma are interpreted to reflect mixing of inherited components.

A sample of medium-grained equigranular monzodiorite from the central phase of the Tatchun batholith (15PS101-1) was also analyzed using a combination of LA-ICPMS and CA-TIMS at Boise State University (Appendices 3 and 4). In this sample, zircons are mostly stubby and prismatic with concentric igneous zoning; some grains contain CL-bright inherited cores (Fig. 3-75a). Fifty-one spots were analyzed by LA-ICPMS and yielded $^{206}Pb/^{238}U$ dates between 348 ± 11 and 185 ± 8 Ma, and a weighted mean date of 197.8 ± 1.4 Ma for 45 of 48 of the youngest zircons (Fig. 3-75b; Appendix 3). An older cluster of three dates at *ca.* 341 Ma are from inherited cores. Six of the youngest zircons were selected for CA-TIMS analysis. Five grains yielded concordant analyses with $^{206}Pb/^{238}U$ dates ranging from 197.07 ± 0.15 to 196.10 ± 0.13 Ma; one older grain is dated at 228.03 ± 0.16 Ma (Fig. 3-75c). The youngest two analyses have a weighted mean $^{206}Pb/^{238}U$ date of 196.13 ± 0.09 Ma (MSWD = 0.32, n = 2) that is considered the crystallization age of this sample.

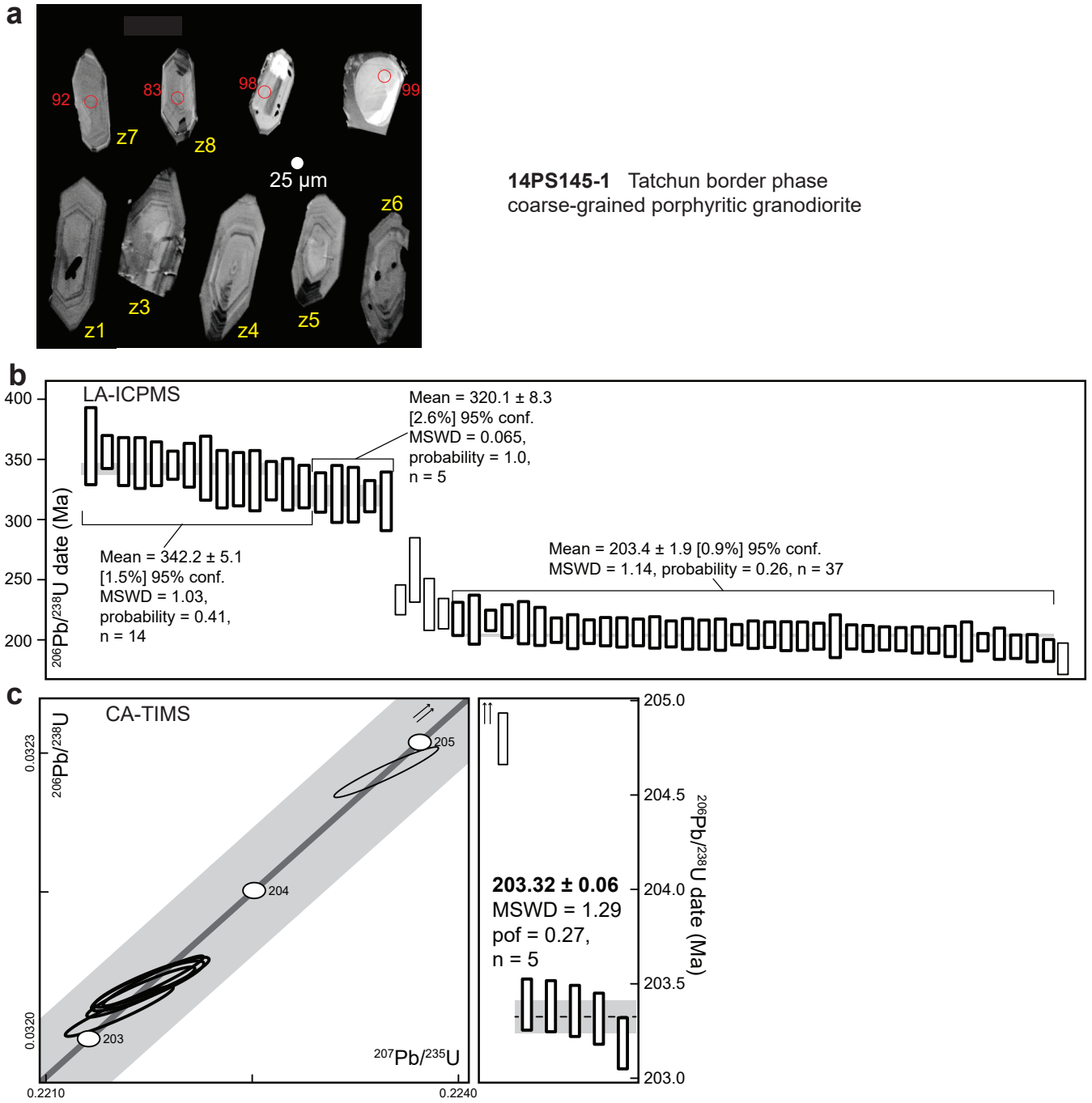


Figure 3-74. *U-Pb zircon geochronology results from 14PS145-1, Tatchun batholith.* ***(a)*** *Cathodoluminescence images of zircon analyzed by LA-ICPMS (red analysis number) and CA-TIMS (yellow analysis number).* ***(b)*** *Ranked plot of $^{206}Pb/^{238}U$ dates determined by LA-ICPMS. Statistics for three populations calculated.* ***(c)*** *Concordia plot of CA-TIMS data (left) with ranked plot of $^{206}Pb/^{238}U$ dates (right). The light grey band around concordia (dark grey line) shows the decay constant uncertainties. Analyses included in weighted mean age (light grey horizontal bar) calculations are bold; analyses with thin lines are not used in calculations. Line-type designations are the same in all plots. Errors in all plots are at 2σ. MSWD = mean squared weighted deviation, pof = probability of fit, n = number of analyses included in age calculation.*

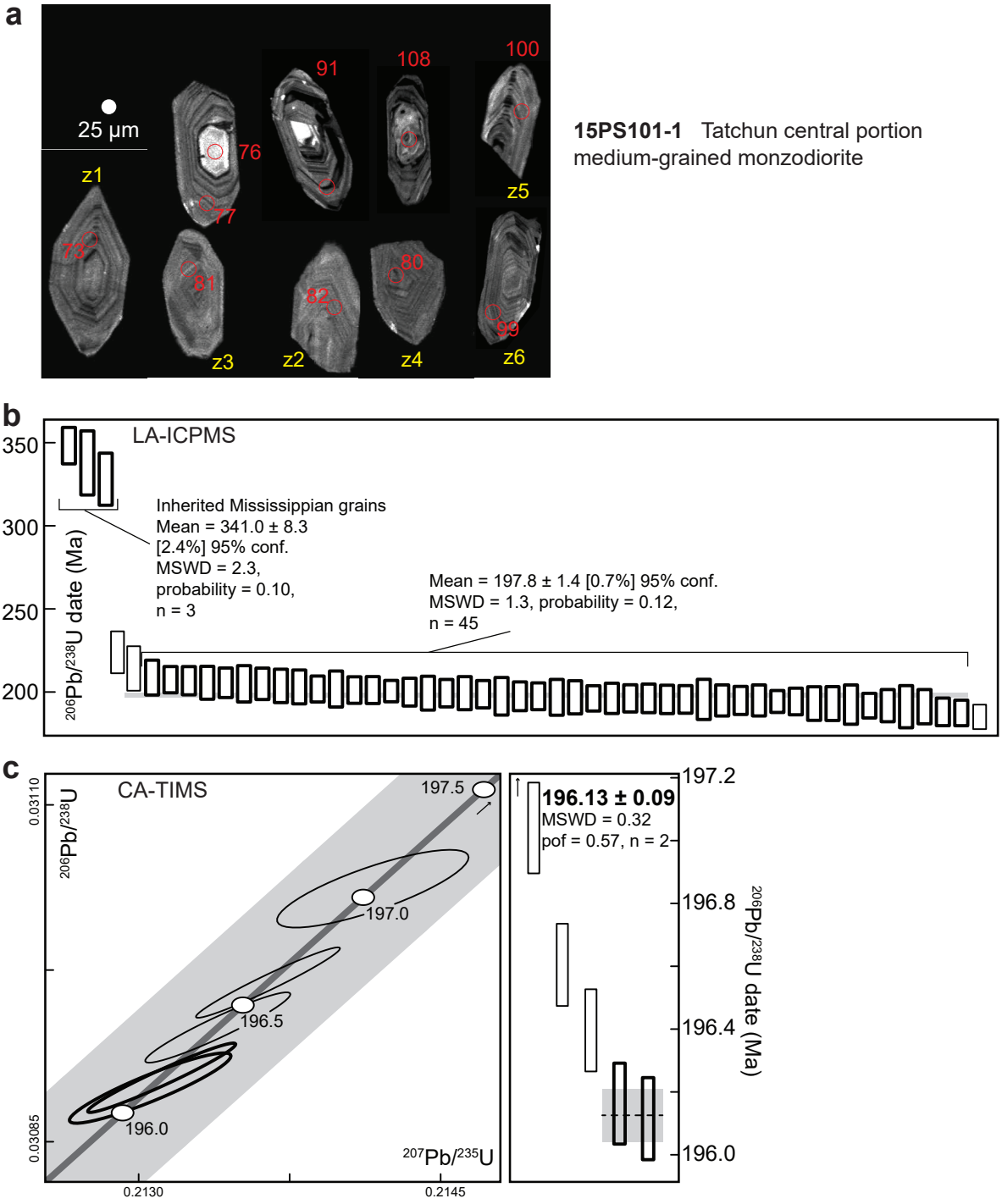


Figure 3-75. *U-Pb geochronological results for sample 15PS101-1, Tatchun batholith.* ***(a)*** *Cathodoluminescence images of representative zircons from this sample, including zircons with inherited cores. LA-ICPMS spots in red numbers, of CA-TIMS analyses in yellow.* ***(b)*** *Ranked plot of LA-ICPMS $^{206}Pb/^{238}U$ dates (Appendix 3).* ***(c)*** *Concordia diagram (left) and ranked $^{206}Pb/^{238}U$ dates (right) for 5 zircons analyzed by CA-TIMS (Appendix 4). The light grey band around concordia (dark grey line) shows the decay constant uncertainties. Analyses included in weighted mean age (light grey horizontal bar) calculations are bold; analyses with thin lines are not used in calculations. Line-type designations are the same in all plots. Errors in all plots are at 2σ. Arrows indicate data extends off of plot. MSWD = mean squared weighted deviation, pof = probability of fit, n = number of analyses included in age calculation.*

The apparent youngest leucocratic tonalite phase of the Tatchun batholith (99MC227-2) was dated at UBC by ID-TIMS on multi-grain zircon and titanite fractions by J.K. Mortensen in 2000 (Appendix 7). A single concordant fraction has a $^{206}Pb/^{238}U$ date of 197.1 ± 0.4 Ma that best constrains the age of this rock; four other fractions are discordant with $^{206}Pb/^{238}U$ dates ranging from 200.4 ± 0.4 to 221.1 ± 0.4 Ma and likely indicate mixing with inherited components (Fig. 3-76). A discordia line anchored at 197.1 Ma has an upper intercept of *ca.* 364 Ma suggesting a mid-Paleozoic inherited component. Two titanite fractions have $^{206}Pb/^{238}U$ dates of 195.2 ± 1.7 and 199.4 ± 1.2 Ma (Appendix 7). Crosscutting relationships viewed in the field consistently show that the leucocratic tonalite phase is the youngest of the three phases in the Tatchun batholith (*cf.* Fig. 3-63). Available geochronological data indicate that the porphyritic border phase is clearly older with dates of *ca.* 203 Ma. However, the medium-grained monzodiorite and leucocratic tonalite phases are apparently close in age with dates of 197–196 Ma.

Ar-Ar

Hornblende and biotite from 3 samples of the Tatchun batholith were analyzed by the $^{40}Ar/^{39}Ar$ method at the GSC laboratory in Ottawa (laser, step-heating). Results from two of these samples (02MC030-1 and 02CR033-1) were reported by Joyce *et al.* (2015); both samples were collected from the northeastern edge of the batholith during regional mapping (Colpron *et al.*, 2002; Fig. 3-77). We present data here for an additional sample collected near the southwestern edge of the batholith (14PS146-1; Appendix 6). In all samples, hornblende shows evidence of excess ^{40}Ar. Two aliquots of hornblende were analyzed from 14PS146-1 (Appendix 6). The first aliquot yielded a stair-stepped age spectrum with apparent ages between 197 and 214 Ma, and an integrated age of 203 ± 3 Ma (Fig. 3-78a). The second aliquot yielded a plateau age of 212.3 ± 3 Ma (Fig. 3-78b), results that are much older than the oldest U-Pb zircon crystallization ages of *ca.* 203 Ma from the Tatchun batholith (Figs. 3-61 and 3-74). Hornblende from sample

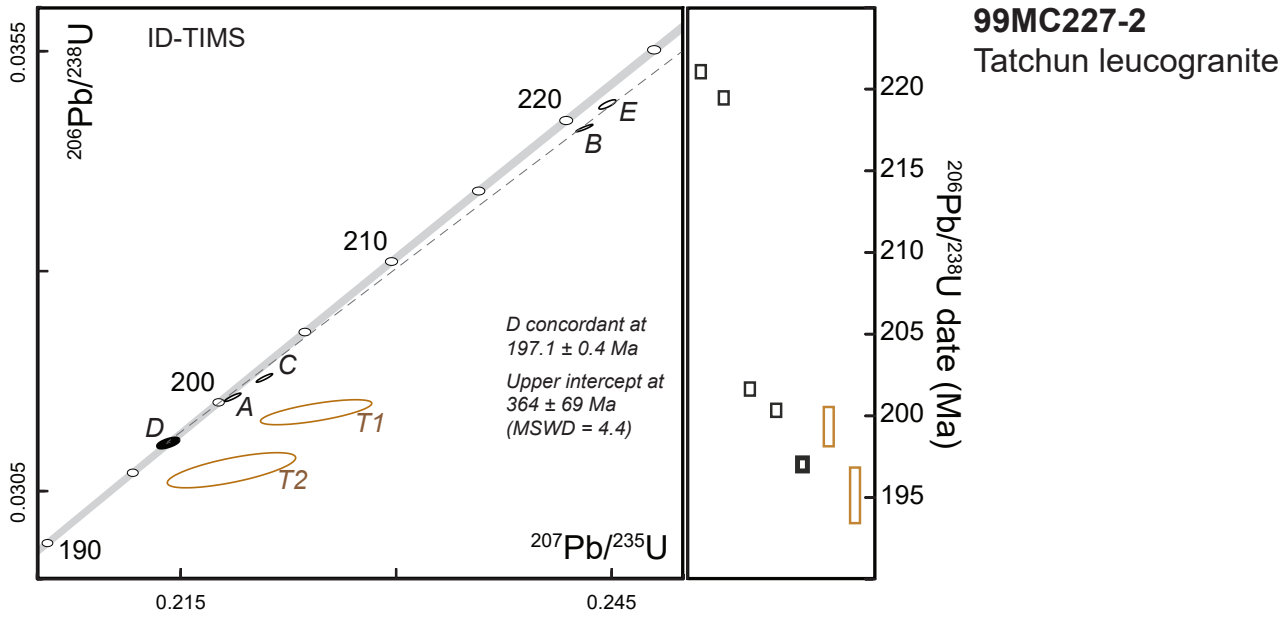


Figure 3-76. *U-Pb geochronological results for sample 99MC227-2, Tatchun batholith. Concordia diagram (left) and ranked $^{206}Pb/^{238}U$ dates (right) for 5 zircon and 2 titanite fractions analyzed by ID-TIMS at UBC (Appendix 7). Fraction D is concordant at 197.1 ± 0.4 Ma and shown by solid bold ellipse. The light grey band on concordia diagram shows the decay constant uncertainties. Dashed discordia line shows regression anchored on concordant fraction D with Devonian upper intercept. Bar heights in ranked plot are 2σ uncertainties. Bars with brown outline are titanite analyses. MSWD = mean squared weighted deviation.*

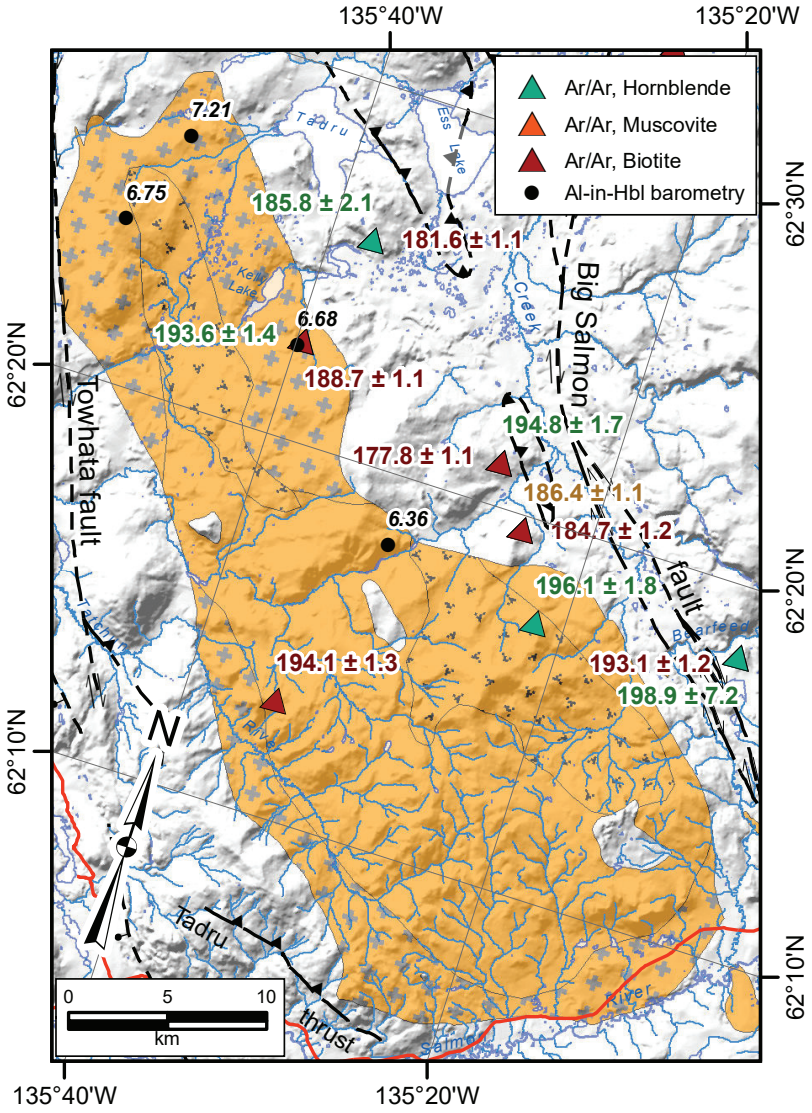


Figure 3-77. *Distribution of $^{40}Ar/^{39}Ar$ dates in the Tatchun batholith and surrounding country rocks. Hornblende dates are labelled dark green; muscovite light brown, and biotite have dark brown labels. Al-in-hornblende pressures are indicated in the batholith for samples from this study (Appendix 5). Fault symbology as in Figure 1-4.*

02MC030 yielded disturbed $^{40}Ar/^{39}Ar$ age spectra with an integrated age of 196 ± 5 Ma, and an inverse isochron date of 193.6 ± 1.4 Ma ($^{40}Ar/^{36}Ar_i$ = 562 ± 16; Joyce *et al.*, 2015). Two aliquots from sample 02CR033-1 have age spectra showing evidence of excess ^{40}Ar in low temperature steps, but reproducible plateaus in higher temperatures at 197.4 ± 1.3 Ma; an inverse isochron indicates an age of 196.1 ± 1.8 Ma ($^{40}Ar/^{36}Ar_i$ = 991 ± 113; Joyce *et al.*, 2015). Hornblende dates from these two samples are more consistent with U-Pb zircon crystallization ages between 203–196 Ma (Figs. 3-73 to 3-76, and 3-79).

Biotite from sample 14PS146-1 has an $^{40}Ar/^{39}Ar$ age spectrum with indicated argon loss in lower temperature steps and a well-defined plateau at 194.1 ± 1.3 Ma in mid to high temperature steps (76.8% of ^{39}Ar released; Fig. 3-78c). This suggests that the southwestern part of the batholith cooled below the ~350°C closure of argon in biotite within ~2 m.y. of crystallization of the main granodiorite phase (Fig. 3-79). Biotite from sample 02MC030-1 yielded a younger plateau age of 188.7 ± 1.1 Ma (94% of ^{39}Ar released; Joyce *et al.*, 2015), suggesting slower cooling for this part of the Tatchun batholith.

Joyce *et al.* (2015) also provide results from hornblende, muscovite and biotite from metamorphic country rocks northeast of the batholith that suggest progressively younger cooling ages to the northeast (mica dates between 186.4 ± 1.1 and 177.8 ± 1.1 Ma; Figs. 3-77 and 3-79). Hornblende and biotite return to older cooling ages east of the Big Salmon fault (Figs. 3-77 and 3-79; Joyce *et al.*, 2015).

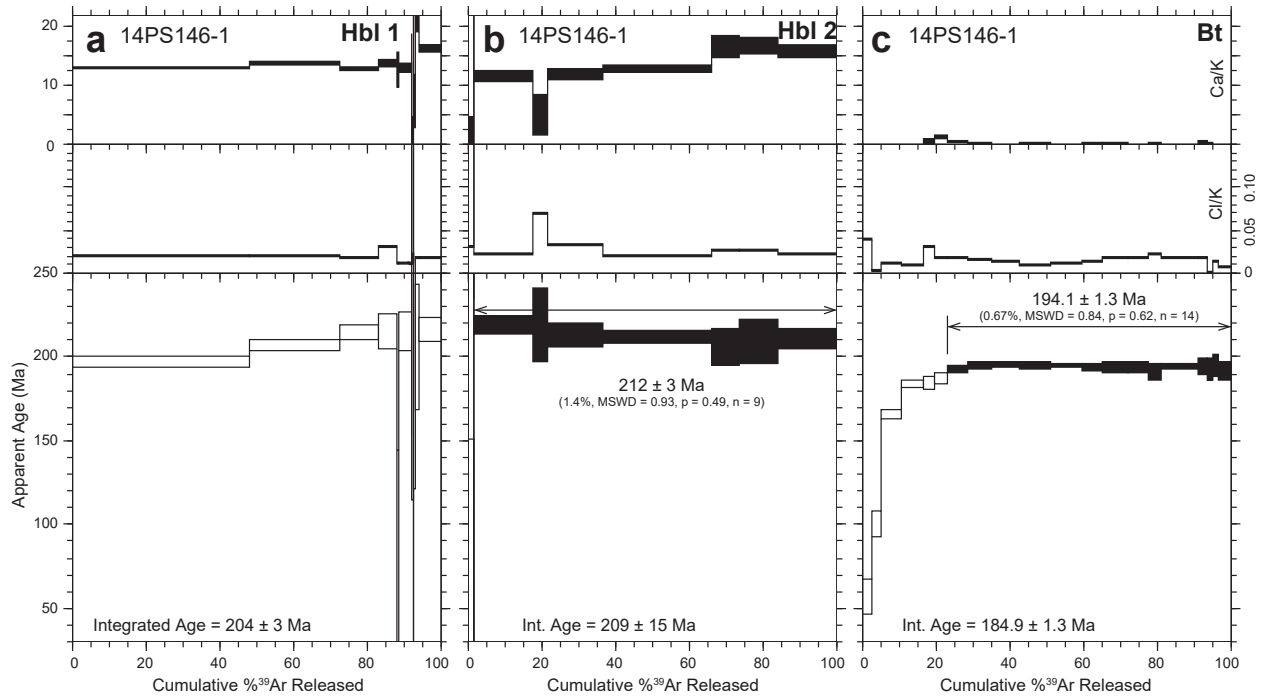


Figure 3-78. *$^{40}Ar/^{39}Ar$ age spectra for hornblende and biotite from sample 14PS146-1, Tatchun batholith (Appendix 6).* ***(a)*** *Hornblende, aliquot 1;* ***(b)*** *hornblende, aliquot 2; and* ***(c)*** *biotite. Steps included in plateau are shown in black.*

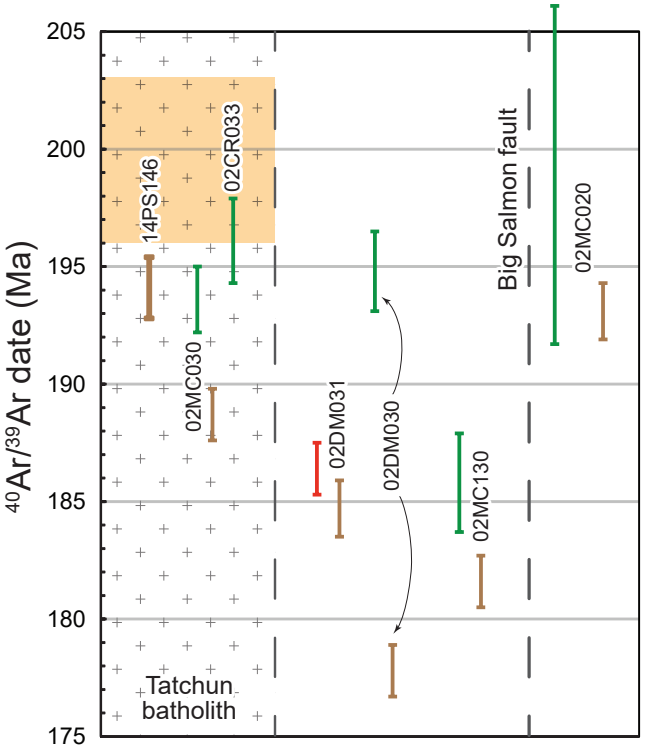


Figure 3-79. *Summary of $^{40}Ar/^{39}Ar$ dates from the Tatchun batholith and surrounding country rocks. Samples are plotted in a relative SW to NE order, with stipple pattern indicating interior of the batholith. Orange bar in upper left indicates range of crystallization ages from U-Pb zircon dates. Green bars indicate hornblende, brown biotite. Most data are from Joyce et al. (2015) with one sample (14PS146-1) from this study (Appendix 6).*

Thermobarometry

Four samples from the Tatchun batholith, three from the porphyritic granodiorite border phase, and one from the monzodiorite central phase contain the suitable mineral assemblage for Al-in-Hbl geobarometry (Hammarstrom and Zen, 1986; Appendix 5). Three of these samples (MA14-TB2, -TB4, and -TB10) are recalculated from Topham *et al.* (2016); the other sample (14PS142-1) is from the present study. Al^{TOT} in hornblende from these samples are between 2.020 and 2.433, with cotectic plagioclase that have X_{An} between 0.11 and 0.21. Amphibole-plagioclase crystallization temperatures are estimated at 663–766°C and crystallization pressure estimates are 6.36 ± 0.6 kbar to 7.21 ± 0.6 kbar (Fig. 3-77; Appendix 5; emplacement depths of 24.0 to 27.2 km). Zircon crystallization temperature estimates, using the Ti-in-zircon thermometer (Watson et al., 2006), are somewhat lower at 597 to 630°C for samples 14PS145-1 and 15PS101-1, respectively (Appendix 3).

Mount Nansen and Big Creek areas

Approximately 50 km west of Carmacks, Late Triassic to Early Jurassic plugs and stocks are scattered in the Mount Nansen area and within the younger Big Creek batholith (Fig. 3-80). These plutons are light coloured, hornblende-biotite granodiorite, diorite, and monzodiorite. They can be weakly to moderately foliated with varying amounts of biotite-rich screens and gneissic schlieren and commonly are K-feldspar porphyritic (Ryan *et al.*, 2016; Allan and Friend, 2018). The age of these plutons is not well constrained and at least two suites are present, the Late Triassic Pyroxene Mountain suite (*ca.* 211 Ma; further information in Chapter 2) and the latest Triassic to earliest Jurassic Minto suite.

We present new LA-ICPMS data collected at UBC (Appendix 11) for two historic samples that yielded ages of *ca.* 195 Ma and are thus interpreted as part of the Minto suite. The first sample is from a plug 1 km west of the Mount Nansen deposit, and collected in 1997 (97VIK-48). This sample yielded a range of $^{206}Pb/^{238}U$ dates between 202 and 190 Ma, with the youngest 19 grains giving a weighted mean date of 195.9 ± 1.0 Ma (Fig. 3-81a,b) that provides the best estimate for the crystallization age of this sample. The second sample is from the southern part of the Big Creek batholith (Fig. 3-80); it was collected by G. Carlson during regional mapping in 1986 (86D-300). This sample yielded a range of $^{206}Pb/^{238}U$ dates between 351 and 186 Ma, with two clusters of dates at *ca.* 330 and 195 Ma (Fig. 3-81c,d). The youngest 16 grains have a weighted mean date of 195.1 ± 1.0 Ma that provides the best estimate for the crystallization age of this sample.

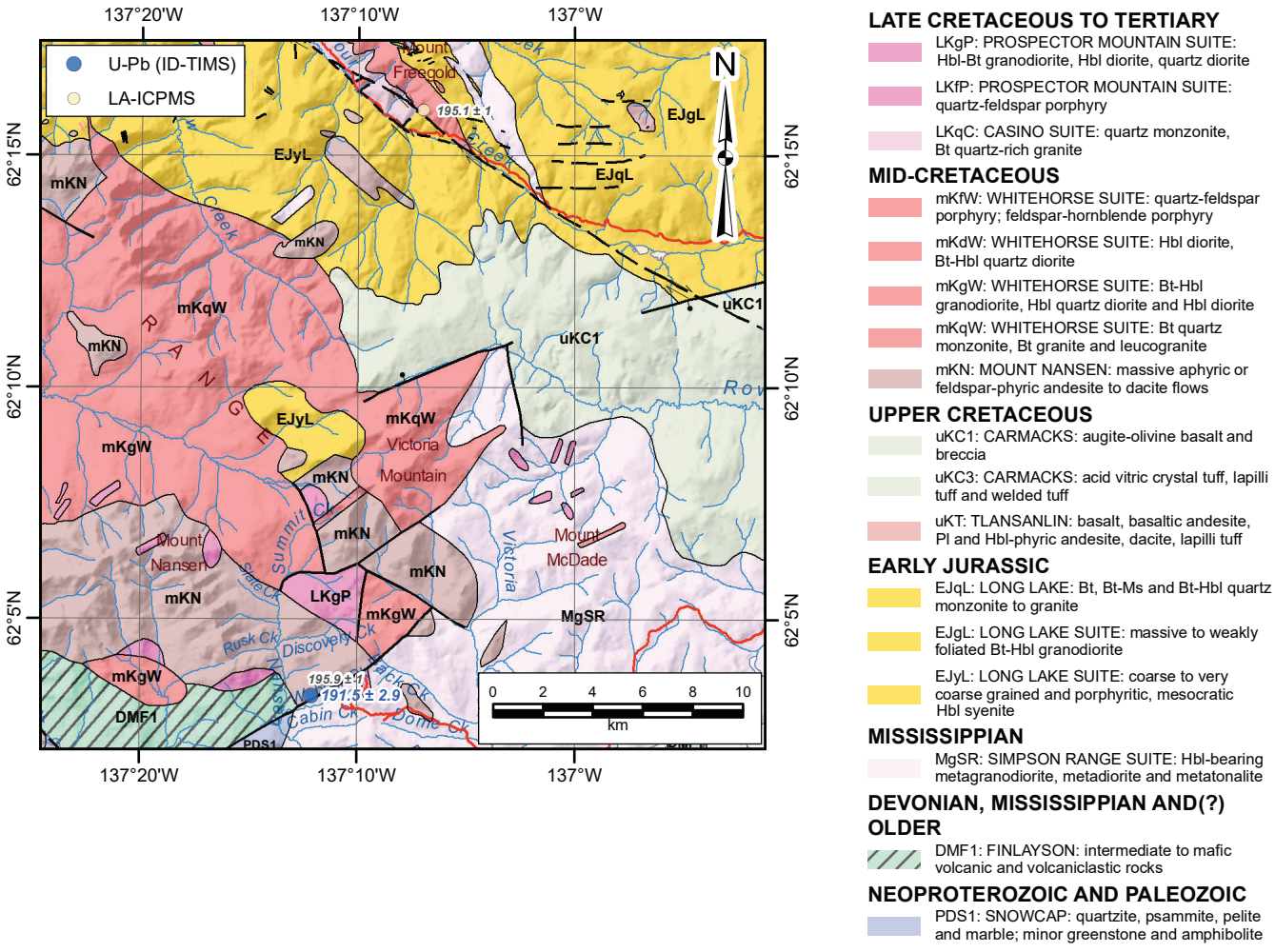


Figure 3-80. *Geology of the Mount Nansen and Big Creek area. Geology from YGS (2020a); fault symbology as in Figure 1-4.*

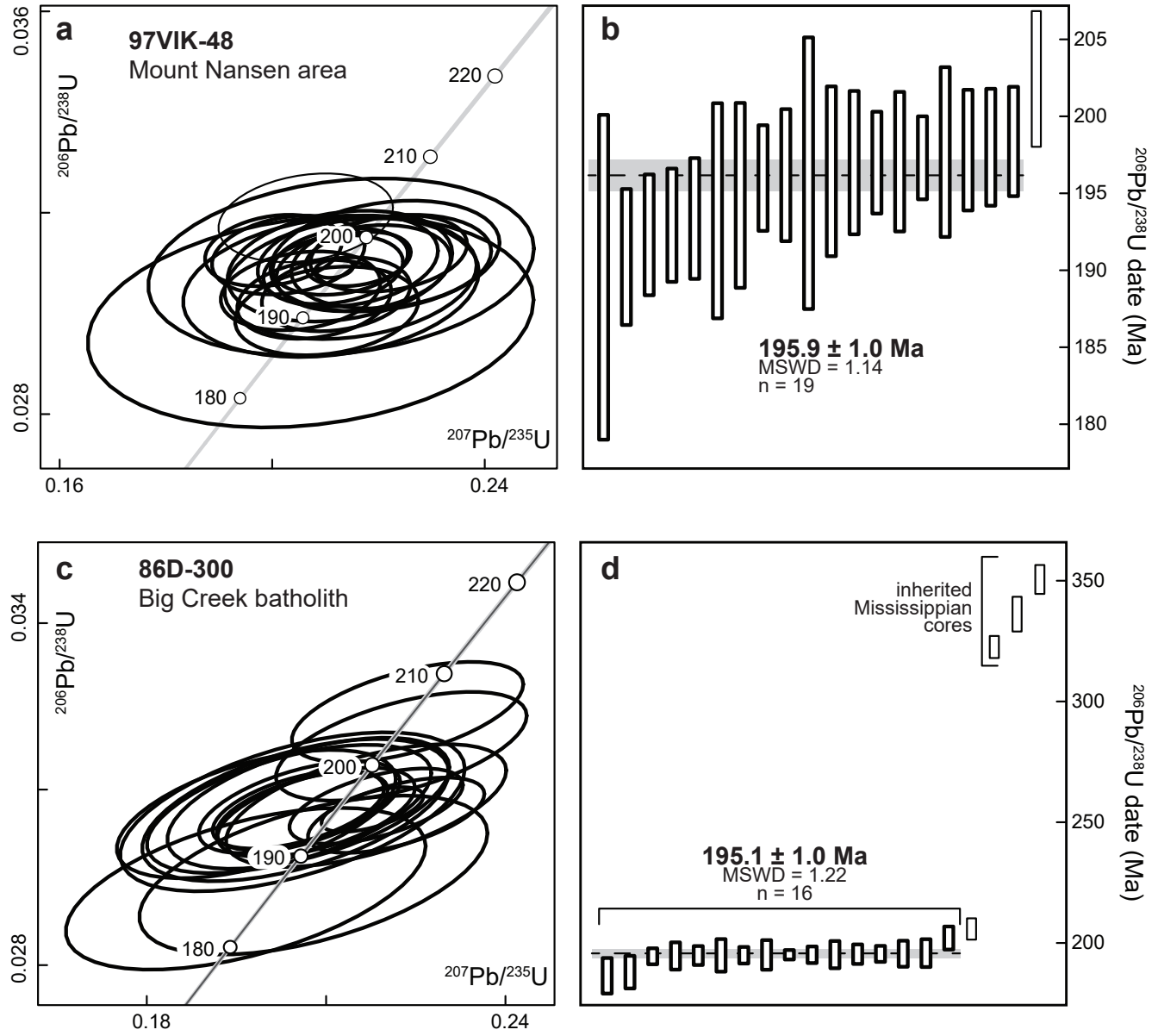


Figure 3-81. *Zircon LA-ICPMS $^{206}Pb/^{238}U$ dates for two historic samples from the Mount Nansen area and Big Creek batholith.* ***(a)*** *Concordia diagram and* ***(b)*** *ranked $^{206}Pb/^{238}U$ dates for zircons analyzed at UBC; 97VIK-48.* ***(c)*** *Concordia diagram and* ***(d)*** *ranked $^{206}Pb/^{238}U$ dates for zircons analyzed at UBC; 86D-300. Only zircon analyses included in the weighted mean $^{206}Pb/^{238}U$ date are shown by solid bold ellipses on concordia. All analyses are shown in ranked plot, with bar heights indicating 2σ uncertainties. The horizontal dashed line represents the weighted mean date of analyses with the 2σ uncertainty shown by the light grey band. MSWD = mean squared weighted deviation. In (d), Mississippian dates likely reflect an inherited component.*

Geochemistry

Sixty samples from Minto suite plutons were analyzed for whole-rock geochemistry (Appendix 8): 17 from the eastern part of the Granite Mountain batholith, 11 from the Minto pluton, 8 from the Yukon River batholith, 4 from the Pelly pluton, 5 from the Walhalla batholith, and 15 from the Tatchun batholith. Samples from the Walhalla, Pelly, Yukon River and Minto plutons were collected during regional mapping activities by the GSC between 2009 and 2011 (Ryan *et al.*, 2018), as were a few of the Granite Mountain samples. It should be noted that the Walhalla batholith samples are from a range of coarse-grained units that may not all reflect bulk compositions of the various phases in this pluton; two of these samples are from foliated rocks that may include components of metamorphic xenoliths common in this pluton. Some of the samples from the Tatchun batholith were analyzed as part of regional mapping by the YGS (Colpron *et al.*, 2002); all other samples were collected for the present study.

Major elements

The majority of samples from the Minto suite have SiO_2 values ranging from ~57 to 74% (diorite to granite) and exhibit linear fractionation trends on major element diagrams (Figs. 3-82a and 3-83). One sample from the Tatchun batholith is more mafic with SiO_2 values of ~53% and a monzodiorite composition (Figs. 3-82 and 3-83). Most of the Minto suite plutons are subalkalic (Fig. 3-82b), with generally magnesian and calc-alkalic to alkali-calcic compositions (Fig. 3-84). A few samples from the Tatchun, Pelly and Walhalla plutons are ferroan and show alkalic tendencies (Figs. 3-82 and 3-84). The Minto suite is metaluminous (Fig. 3-84c). All samples plot in the 'I-type' field of the Chappell and White (2001) classification diagram (Fig. 3-85).

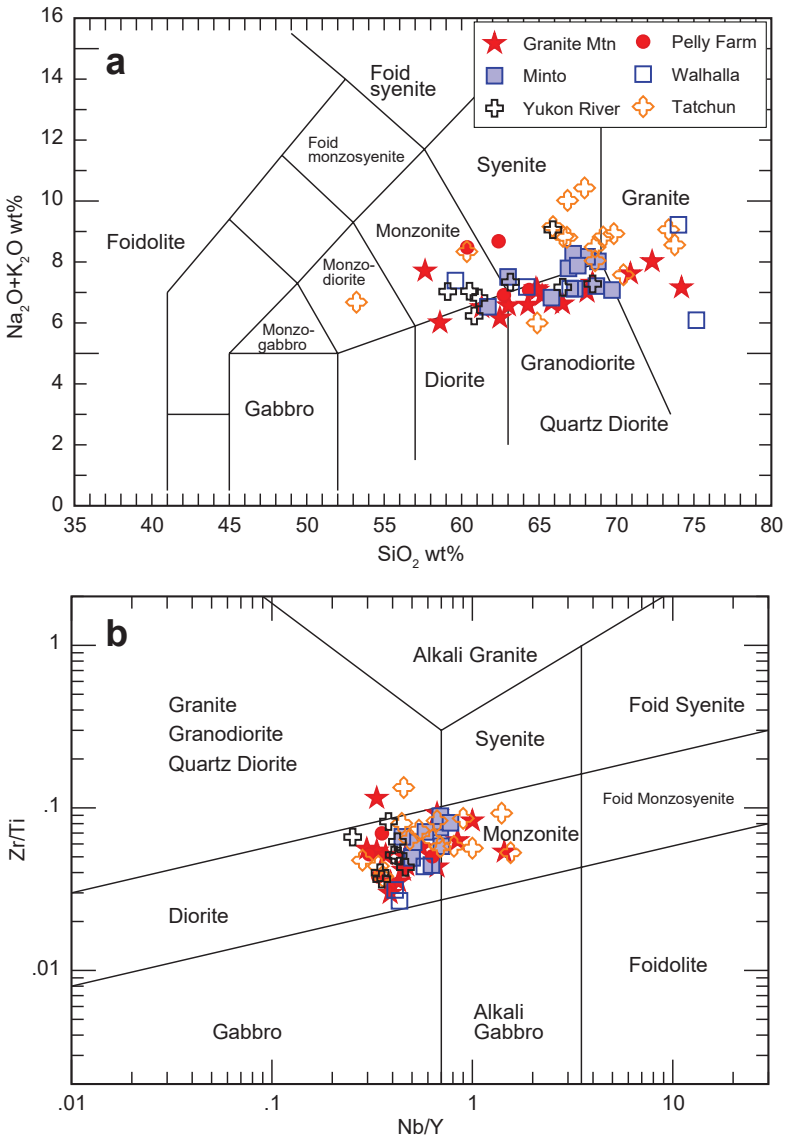


Figure 3-82. (a) *Total alkali-silica diagram for samples of the Minto suite (adapted from Le Bas et al., 1986, for plutonic rocks).* ***(b)*** *Zr/Ti vs. Nb/Y classification diagram of Winchester and Floyd (1977) as modified by Pearce (1996).*

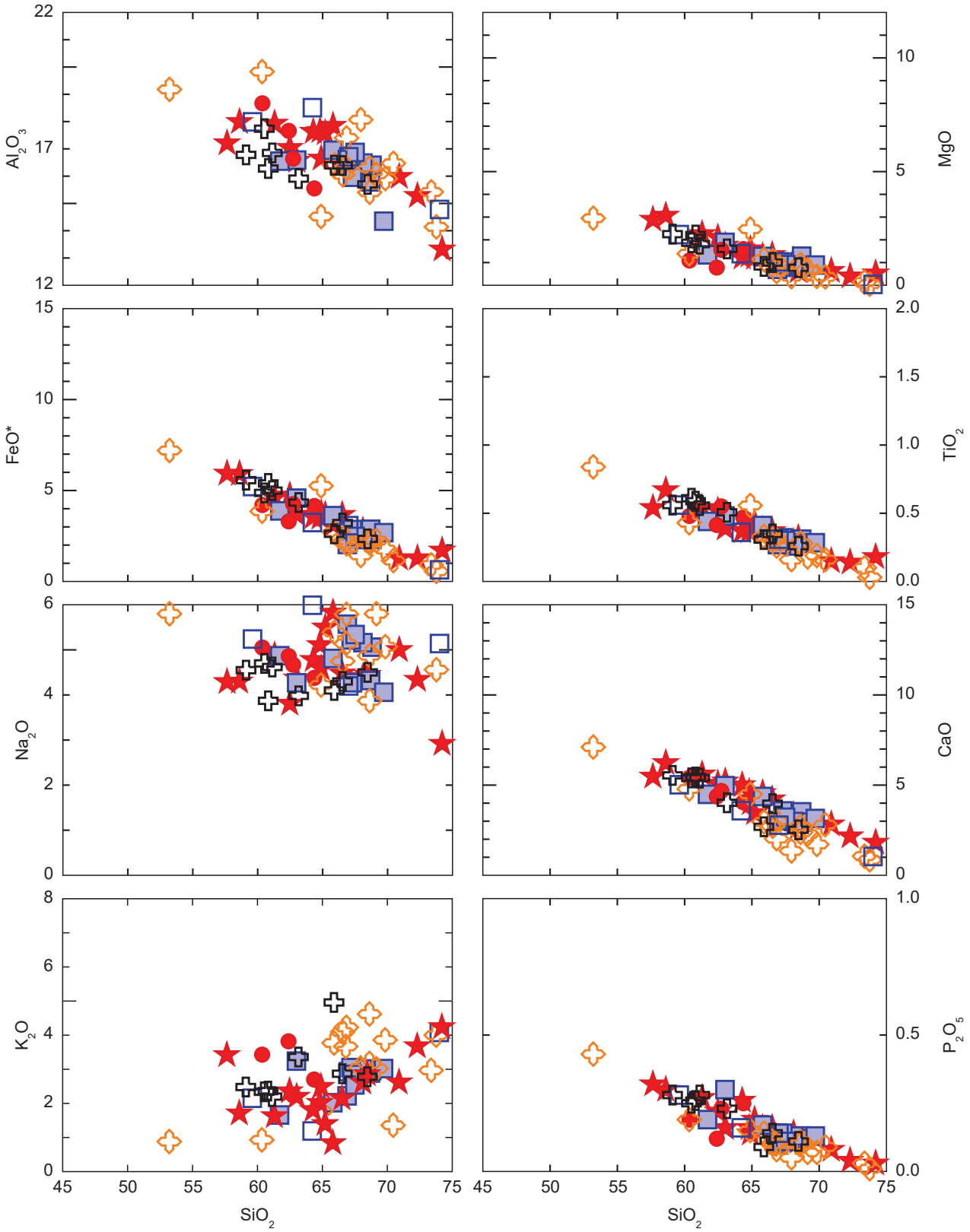


Figure 3-83. *Major elements vs. SiO_2 Harker plots for samples of the Minto suite. Symbols as in Fig. 3-80.*

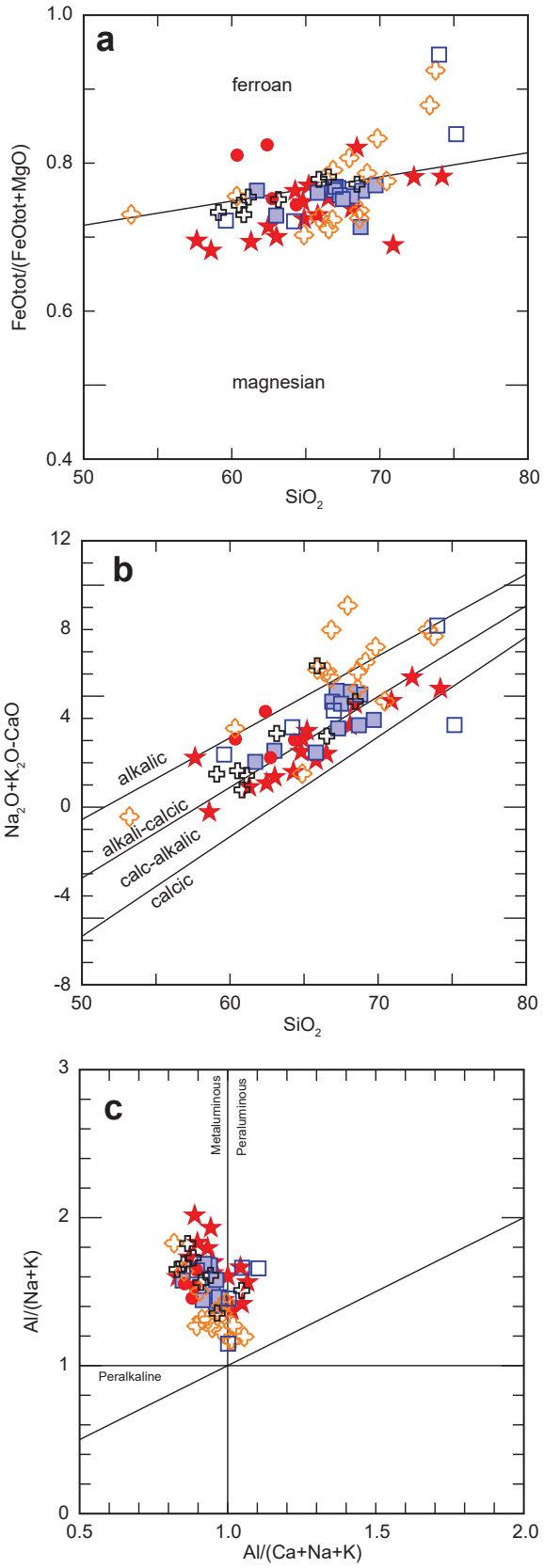


Figure 3-84. *Geochemical classification using criteria of Frost et al. (2001).* ***(a)*** *Fe-number,* ***(b)*** *modified alkali-lime index (MALI), and* ***(c)*** *alumina saturation index (ASI). Symbols as in Fig. 3-80.*

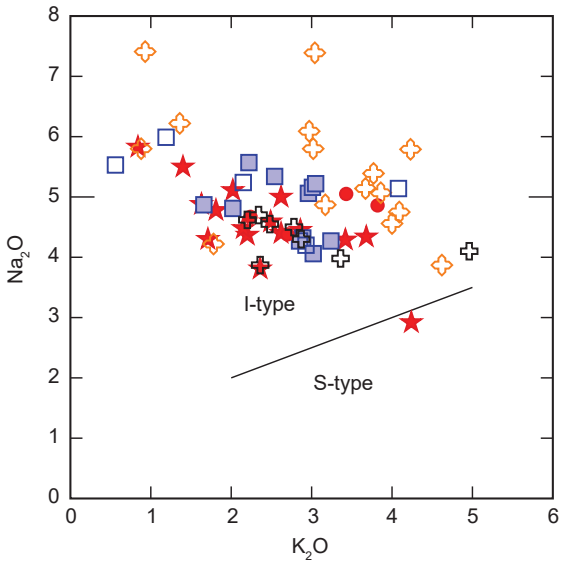


Figure 3-85. *Na_2O vs K_2O for samples of the Minto suite. The boundary between 'I-type' and 'S-type' granitoid rocks is from Chappell and White (1974). Symbols as in Fig. 3-80.*

Trace elements

For the most part, samples from the Minto suite have trace element patterns typical of subduction-related arc magmas, with negative Nb and Ti anomalies on primitive mantle normalized plots (Sun and McDonough, 1989), Th/Nb_N ~7.7 and La/Yb_N of ~7.6 (Fig. 3-86a,c,e,g; Appendix 8). These samples show relatively flat patterns that are only slightly depleted relative to upper continental crust (Fig. 3-86b,d,f,h). The Tatchun batholith exhibits a broader range of trace element concentrations, with the more depleted patterns representing the leucocratic tonalite samples (Fig. 3-86g,h). Samples from the Walhalla batholith display a scatter of trace element patterns consistent with the heterogeneity of this pluton and likely reflects various degrees of contamination by country rocks, or strong fractionation in these generally coarse-grained plutonic rocks (Fig. 3-86e,f). Minto suite samples plot in the arc (VAG) field of the Ta/Yb discrimination diagram of Pearce *et al.* (1984; Fig. 3-87).

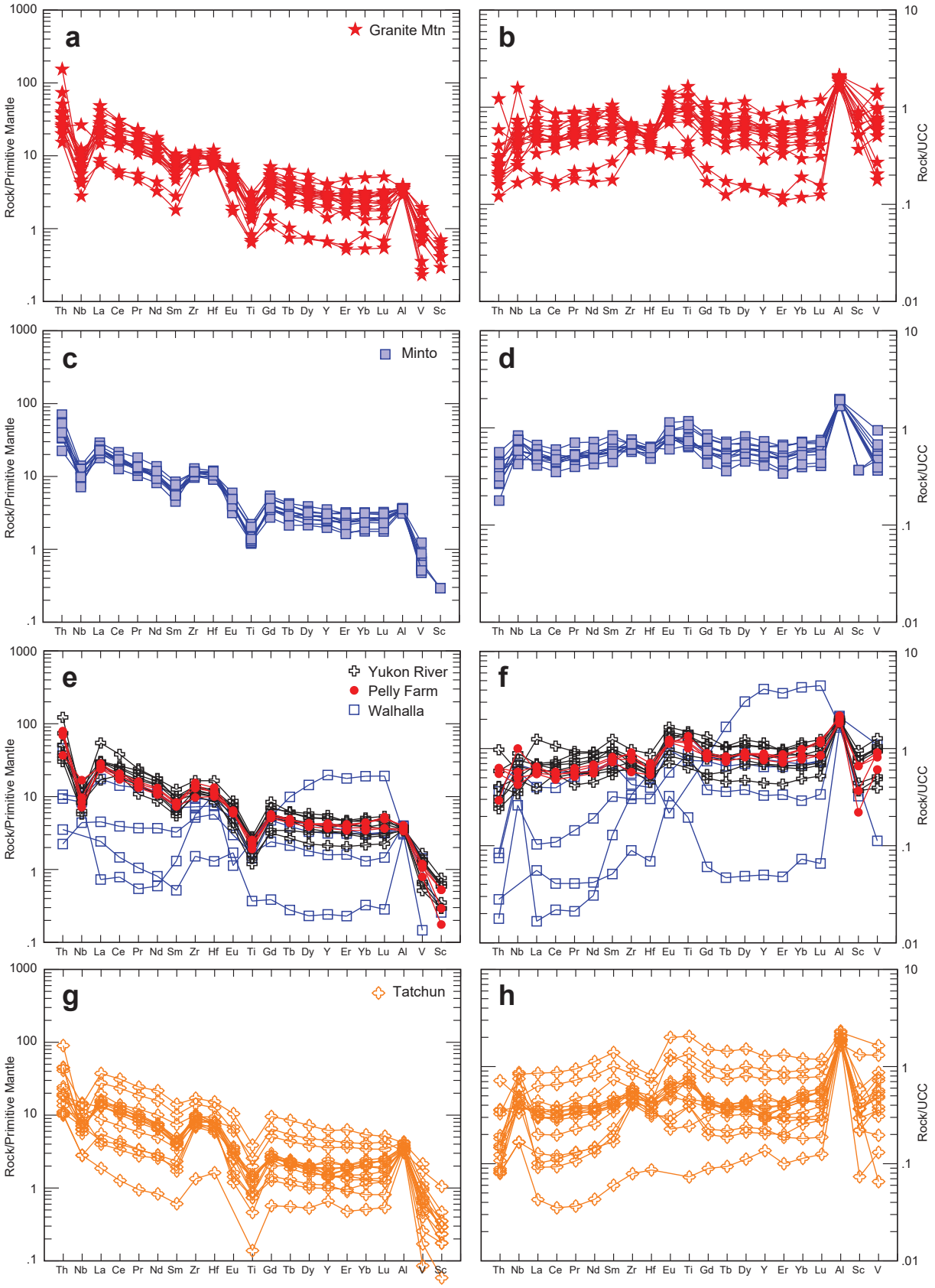


Figure 3-86. *Left – Primitive mantle normalized spider plots using values from McDonough and Sun (1995). Right – Upper continental crust (UCC) normalized spider plots using values from McLennan (2001).* ***(a** and **b)** Granite Mountain batholith; **(c** and **d)** Minto pluton; **(e** and **f)** Yukon River, Pelly and Walhalla plutons; and **(g** and **h)** Tatchun batholith.*

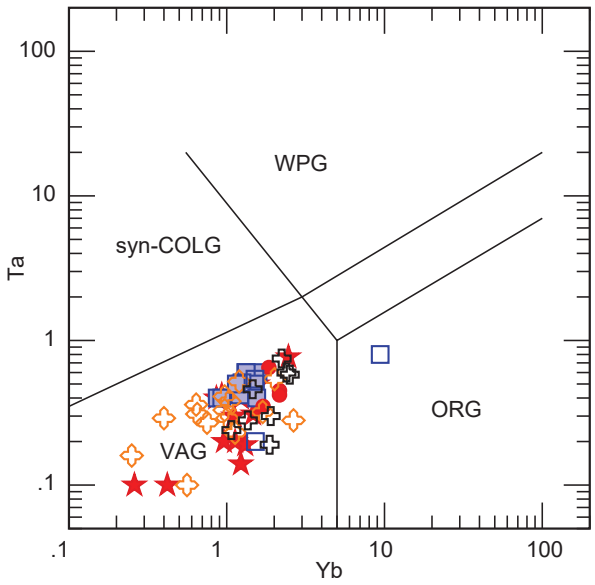


Figure 3-87. *Tectonic discrimination diagram for granites from Pearce et al. (1984). VAG = volcanic arc granite, ORG = ocean ridge granite, WPG = within plate granite and COLG = collisional granite. Symbols as in Fig. 3-80.*

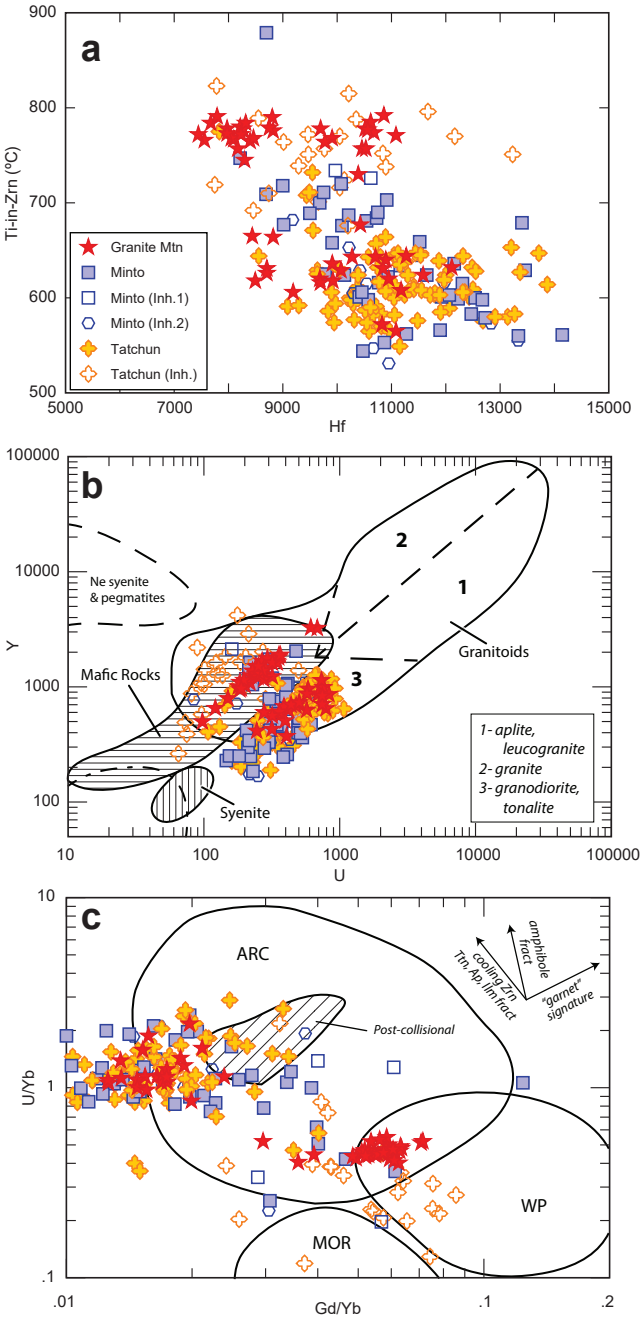


Figure 3-88. *Trace element zircon chemistry from LA-ICPMS analyses of samples from the Minto suite (Appendix 3).* ***(a)*** *Plot of crystallization temperature estimates (Ti-in-zircon) vs. Hf concentrations in zircons.* ***(b)*** *Y vs. U classification diagram of Belousova et al. (2002).* ***(c)*** *Discriminant diagram of Grimes et al. (2015). Open symbols for the Minto and Tatchun samples are analyses of inherited (Inh.) cores; note that two population of inherited zircons are documented in the Minto pluton (see Fig. 3-39).*

Zircon chemistry

Trace element concentrations were measured in zircons from samples of the Granite Mountain, Minto and Tatchun plutons that were analyzed by LA-ICPMS at Boise State University (Appendix 3). Two samples from the Granite Mountain batholith have zircon chemistry that forms two distinct clusters, with zircons from monzodiorite along the eastern edge of the pluton (14PS073) being characterized by higher Ti-in-zircon temperatures (757–791°C) and more mafic arc compositions (lower U/Yb and higher Gd/Yb) than those from diorite of the STU occurrence (STU80-7-286.5; Fig. 3-88). Zircons from the STU sample have more typical arc to post-collisional granodiorite signatures, with Ti-in-zircon temperatures of 606–664°C and U/Yb ~1 (Fig. 3-88). Igneous zircons from the Minto pluton and Tatchun batholith have typical arc compositions broadly similar to those from the STU occurrence. Ti-in-zircon temperatures range from ~550–720°C and U/Yb ~1 are consistent with arc to post-collisional granitoid rocks (Fig. 3-88). Inherited zircon cores from both the Minto and Tatchun plutons are dominantly Mississippian (Figs. 3-41 and 3-42) and

have generally higher Ti-in-zircon temperatures (690–800°C) and more mafic compositions, with lower U/Yb and higher Gd/Yb than the Early Jurassic igneous zircons (Fig. 3-88). Mississippian cores from zircons of the Tatchun batholith have the most juvenile signatures, consistent with the dominantly mafic composition of Carboniferous hosts rocks of Quesnellia (Moose formation; Fig. 3-61). The Late Triassic inherited zircon cores in sample S09-16-01D (*ca.* 214 Ma; Fig. 3-42) from the Minto pluton have similar compositions to the main population of *ca.* 200–196 Ma igneous zircons from this pluton.

Isotopes

Eight samples from the Minto suite were analyzed for whole-rock Sr and Nd isotopes; K-feldspar from 7 Minto samples were also analyzed for Pb isotopes (Appendix 9). The Minto suite samples have initial $^{87}Sr/^{86}Sr$ values ranging from 0.7047 to 0.7062 and initial $^{143}Nd/^{144}Nd$ values of 0.51220 to 0.51246 (εNd_t = -3.6 to 1.3; Fig. 3-89), and $^{207}Pb/^{204}Pb$ values of 15.59 to 15.66, suggesting mixing with evolved crustal components.

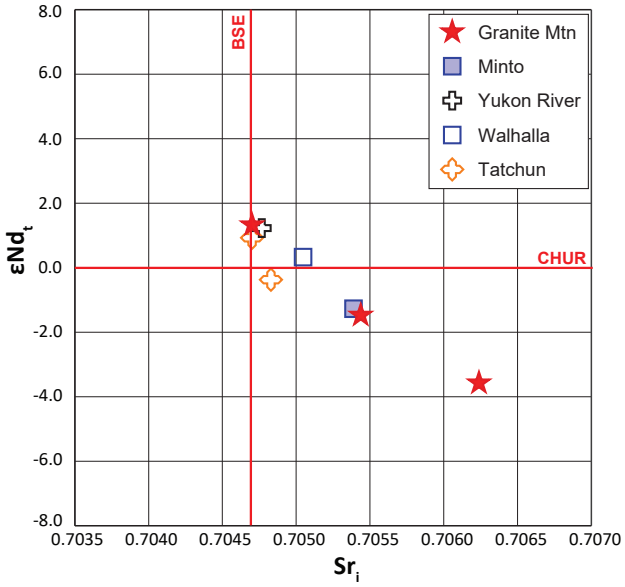


Figure 3-89. *Whole rock Nd and Sr isotopic data for the Minto suite (Appendix 8). Plot of εNd_t vs. initial $^{87}Sr/^{86}Sr$. BSE = bulk silicate Earth; CHUR = chondritic uniform reservoir.*

Zircons from 5 Minto suite samples were also analyzed for Lu-Hf by LA-ICPMS at Memorial University of Newfoundland (Appendix 10). Sampled spots were chosen to match U-Pb LA-ICPMS analyses from Boise State University (Appendix 3). Igneous zircons from the Minto and Tatchun plutons all have similar εHf_i values between 0 and 5 (Fig. 3-90). Zircons in one sample from the Granite Mountain batholith (14PS073) have slightly more juvenile εHf_i values of +6.0 to +7.5 that are consistent with the more mafic composition of these zircons (Fig. 3-90; Appendix 3) and more juvenile overall isotopic composition of this sample ($^{87}Sr/^{86}Sr_i$ = 0.7047; εNd_t = 1.3; Fig. 3-89; Appendix 9). Mississippian zircon cores from the Minto and Tatchun plutons yield generally higher εHf_i values of +3.7 to +10.9 (Fig. 3-90; Appendix 10) suggesting juvenile sources for these xenocrysts, consistent with their trace element chemistry (Fig. 3-88; Appendix 3).

Discussion

Plutons of the Minto suite intrude the boundary between Stikinia and Yukon-Tanana terrane northwest of Carmacks where they probably form part of a single large batholith ~120 km long by ~15–25 km wide (Figs. 3-1 and 3-2; Table 3-1). Northeast of the Teslin fault, the Tatchun batholith intrudes Paleozoic metamorphic rocks of Quesnellia (Figs. 3-1 and 3-61). These plutons comprise mainly monzodiorite and granodiorite, with lesser quartz monzonite, granite and tonalite (Fig. 3-3). They have metaluminous and calc-alkalic to mildly alkalic compositions (Fig. 3-84). Their trace element and isotopic compositions suggest that they are derived from subduction-related magma but with mixing of more evolved crustal material (Figs. 3-86 and 3-91). The zircon crystallization ages from these plutons range mainly from *ca.* 200–194 Ma, with only two samples yielding older crystallization ages of *ca.* 205–203 Ma in the Tatchun and Pelly plutons (Figs. 3-1 and 3-91). These older components are also identified in zircon antecrysts from the Granite Mountain and Minto plutons (Figs. 3-19, 3-39 and 3-42; Appendix 3), and therefore likely record the onset of Minto suite magmatism in central Yukon.

A number of samples from the Granite Mountain, Minto and Tatchun plutons contain Mississippian inherited zircon components (*ca.* 350–320 Ma;

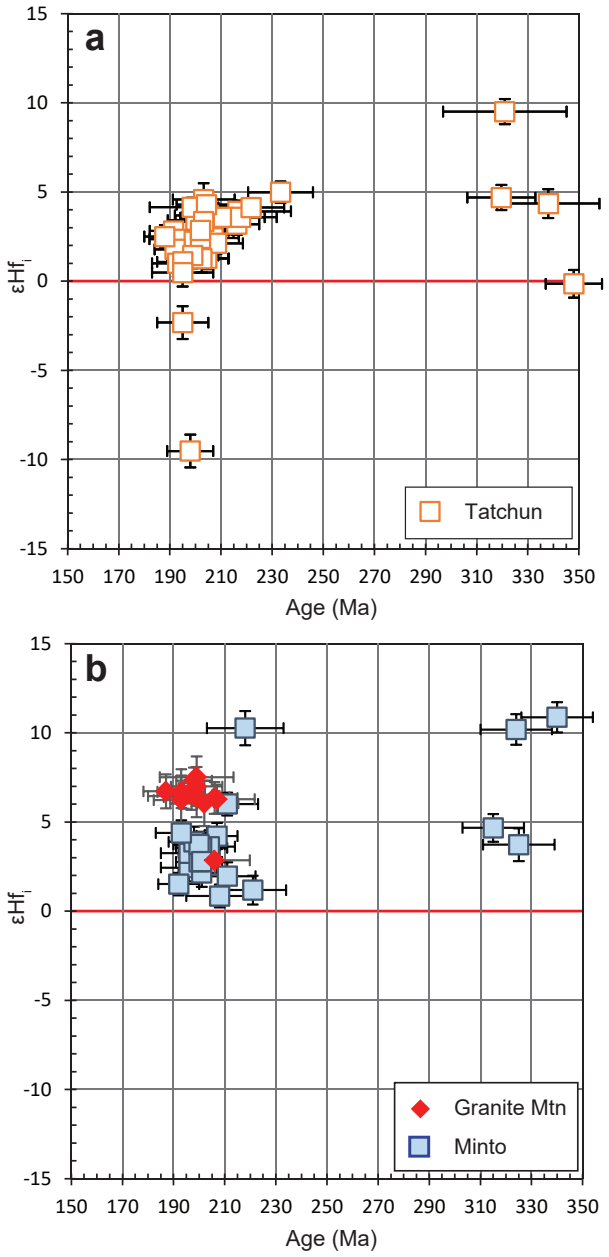


Figure 3-90. *Hf isotopic data for selected zircons from the Minto suite (Appendix 9).* ***(a)*** *Tatchun batholith;* ***(b)*** *Granite Mountain and Minto plutons. Error bars are 2σ.*

Figs. 3-41, 3-42, 3-74 and 3-75) that have generally more juvenile compositions than the Jurassic zircons (Figs. 3-88 and 3-89), and are consistent with incorporation of Mississippian arc rocks of the Yukon-Tanana terrane in these plutons (or Quesnellia in the case of the Tatchun batholith). A Late Triassic inherited zircon component (*ca.* 217–214 Ma; Figs. 3-22, 3-41 and 3-42) in samples from the Granite Mountain and Minto plutons further suggest incorporation of igneous rocks of Stikinia (Stikine or Pyroxene Mountain suites, and Povoas formation). This is consistent with locally abundant mafic xenoliths within these plutons (Fig. 3-15), some of which are dated at *ca.* 217–214 Ma (Fig. 3-19; Kovacs et al., 2020; Chapter 2, Fig. 2-54).

Plutons of the Minto suite were intruded at mid-crustal levels into greenschist to amphibolite facies metamorphic rocks of Yukon-Tanana or Quesnellia terranes (Figs. 3-1, 3-2 and 3-61). Pressure estimates from Al-in-hornblende geobarometry suggest crystallization between 5–6 kbar for the Granite Mountain and Minto plutons (~20 km emplacement depths; McCausland *et al.*, 2002; Tafti, 2005; this study, Appendix 5), and 6–7 kbar for the Tatchun batholith (~25 km emplacement depth; Appendix 5). Coarse magmatic epidote is a common occurrence in all Minto suite plutons (Figs. 3-11, 3-33, 3-48, 3-53, 3-57 and 3-71).

$^{40}Ar/^{39}Ar$ biotite cooling ages from the Granite Mountain and Minto plutons (*ca.* 187–182 Ma; Fig. 3-25; Appendices 1 and 6) suggest cooling below ~350°C within 8–14 m.y. of crystallization of the youngest phases of the granodiorite (*ca.* 196–194 Ma; Fig. 3-91). This corresponds to ≤10 km of exhumation following emplacement of these plutons at ~20 km depth (assuming geothermal gradients of 25–30°C/km, the 350°C isotherm corresponds to ~12–14 km crustal depth) and average exhumation rates of 0.7–1.3 mm/yr in the Early Jurassic for the area northwest of Carmacks (Fig. 3-1). East of the Teslin fault, the Tatchun batholith cooled more rapidly, within 2–7 m.y. of crystallization ($^{40}Ar/^{39}Ar$ biotite dates of 194–189 Ma; Fig. 3-79), and was more deeply exhumed (~15 km) at rates of ~2.1–7.5 mm/yr in the Early Jurassic.

The Minto and Granite Mountain plutons are host to economic Cu-Ag-Au mineralization at the Minto mine and Carmacks Copper deposit (Figs. 3-1 and 3-2). The mineralization is hosted in variably migmatized rafts and xenoliths of foliated intermediate to mafic meta-igneous rocks (Figs. 3-15, 3-16 and 3-30); and the detailed study of Kovacs (2018; Kovacs *et al.*, 2020) at the Carmacks Copper deposit shows that these are in part derived from Late Triassic protoliths (*ca.* 217 Ma) with affinity to Stikinia.

The degree of migmatization of the host xenoliths appears to be more advanced at the Minto mine (*e.g.* Fig. 3-35). Hypogene mineralization comprises mainly chalcopyrite and bornite that occurs as disseminated sulphides and foliaform stringers in the host xenoliths, or as coarse-grained, mesh-textured sulphides in more migmatized host rocks (Kovacs, 2018). Re-Os dating of molybdenite from the Minto and Carmacks Copper deposits shows a mix of ages between *ca.* 213 and 196 Ma (Figs. 3-19 and 3-39) as well, as two distinct textural associations of molybdenite: 1) an early phase of deformed, anhedral to subhedral molybdenite flakes; and 2) euhedral to subhedral grains intergrown with net-textured sulphides (Hood, 2012; Kovacs, 2018). The older Re-Os dates (*ca.* 213 Ma) are inferred to date the texturally older molybdenite and original Late Triassic mineralization in the host rafts, whereas the younger *ca.* 196 Ma dates likely record timing of migmatization and recrystallization of mesh-texture mineralization (Kovacs, 2018; Kovacs *et al.*, 2020). This indicates that mineralization at Carmacks Copper and Minto formed in the Late Triassic (*ca.* 217–213 Ma) prior to emplacement of the Early Jurassic Granite Mountain and Minto plutons at mid-crustal depths (*ca.* 200–195 Ma, 5–6 kbar), and that the younger granodiorite is therefore not genetically related to ore formation. The mineralization was probably originally of alkalic porphyry Cu-Au style (Tafti, 2005; Kovacs, 2018; Kovacs *et al.*, 2020), similar to Late Triassic deposits in British Columbia (Logan and Mihalynuk, 2014). It was subsequently deformed and metamorphosed during incorporation within the Early Jurassic plutons of the Minto suite in Yukon. Plutons of the Minto suite were emplaced too deep in the crust (~20–25 km) to form porphyry-style mineralization. Further exploration for Minto-style deposits should focus primarily on occurrences of Late Triassic xenoliths within Early Jurassic plutons (*see* Chapter 2 for further discussion of Late Triassic rocks and related mineral potential).

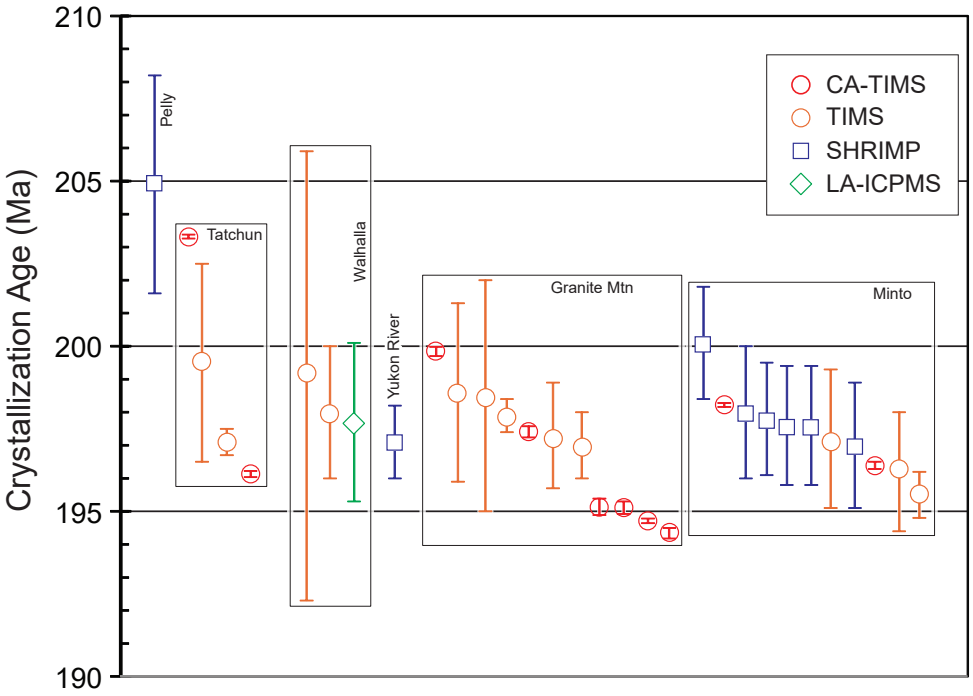


Figure 3-91. *Summary of interpreted U-Pb zircon crystallization ages for plutons of the Minto suite. Error bars are 2σ. Geochronological data is from compilation in Appendix 1.*

Chapter 4
Early Jurassic

Long Lake suite (188–183 Ma)
Bennett suite (178–175 Ma)
Lokken suite (195–184 Ma)

Summary

Early Jurassic plutons ranging in age from *ca.* 195 to 175 Ma intrude the Intermontane terranes in southern Yukon. The plutons are divided into three suites: the Long Lake and Bennett suites intrude the Stikinia–Yukon-Tanana boundary southwest of the Teslin fault and Whitehorse trough, whereas the Lokken suite intrudes Yukon-Tanana northeast of the fault. The Long Lake suite (188 to 183 Ma) comprises large plutons (350 to 3915 km²) including the Aishihik, Granite Mountain (southwest part) and Big Creek batholiths, all of which are west of the Klondike Highway between Whitehorse and Carmacks. The Bennett suite (178–175 Ma) comprises two smaller plutons, the Bennett batholith and Alligator Lake stock, that are west of Carcross and which may have originally been part of a single 600 km² batholith. Northeast of the Teslin fault, the Lokken suite (195–184 Ma) is more mafic and forms small plutons (<1 to ~200 km²) including the Lokken, Macmillan Range, Thirtymile Lake, Sawtooth, Englishman, Logjam and Swift River plutons. Similar plutons intrude the Yukon-Tanana terrane in the Finlayson Lake area northeast of the Tintina fault and are inferred to be part of the Lokken suite.

The Long Lake suite is mainly granodiorite in composition but ranges from syenite to diorite to tonalite. Plutons are oxidized, have magnetic susceptibility measurements of 5–10 × 10^{-3} SI units, are metaluminous to weakly peraluminous, and range from calcic to alkalic in composition. Trace element and isotopic compositions are consistent with continental arc magmatism containing a component of crustal contamination. Inherited zircon populations with Devonian–Mississippian, Late Triassic and minor Precambrian ages suggest incorporation of Yukon-Tanana and Stikinia rocks in the magma. The Long Lake plutons were mostly emplaced at mid-crustal depths during regional exhumation, with Al-in-hornblende pressures of 4.3–6 kbar (≥15 km), and $^{40}Ar/^{39}Ar$ dates from hornblende and biotite indicate relatively rapid cooling (2–6 m.y.).

The late Early Jurassic Bennett suite (178–175 Ma) occurs south of the Long Lake suite, west of Carcross, and consists of K-feldspar porphyritic granodiorite and equigranular monzodiorite phases. Bennett suite plutons are predominantly oxidized granodiorite to monzodiorite with magnetic susceptibilities between 5 and 10 x 10^{-3} SI units. They are magnesian, calc-alkalic, metaluminous, 'I-type' intrusions having trace element and isotopic compositions consistent with continental arc magmatism and significant crustal contamination. The Bennett suite plutons were emplaced at mid to upper crustal levels with Al-in-hornblende pressure estimates of ≤2 to 3.45 kbar.

The Lokken suite plutons are typically clinopyroxene-bearing and comprise mainly monzonite to monzodiorite and granodiorite. They are variably magnetic with susceptibilities ranging from 0.1–21.6 × 10^{-3} SI units. The plutons are metaluminous and calc-alkalic to alkali-calcic in composition. Trace element and isotopic compositions are consistent with continental arc magmatism with minor crustal assimilation. Inherited zircon components are only documented in the younger (*ca.* 186–184 Ma) plutons from this suite. The northern Lokken suite plutons (Lokken and Macmillan Range) were emplaced at mid to upper crustal levels, as recorded by Al-in-hornblende pressures of 2.6–3 kbar (≤10 km), and $^{40}Ar/^{39}Ar$ dates from hornblende and biotite indicate they cooled rapidly (≤2 m.y.).

Introduction

Early Jurassic plutons ranging from *ca.* 195 to 175 Ma intrude the Intermontane terranes in southern Yukon. They are divided into three suites, the Long Lake and Bennett suites are on the southwest side of the Teslin fault and Whitehorse trough, and the Lokken suite is on the northeast side (Fig. 4-1). The Long Lake (188 to 183 Ma) and Bennett (178–175 Ma) suites comprise large plutons (350 km² to 3915 km²) that intrude the boundary between Stikinia and Yukon-Tanana terranes. Long Lake suite plutons include the Aishihik, Granite Mountain (southwest part) and Big Creek batholiths, and the Bennett suite includes the Bennett batholith and the Alligator stock (Table 4-1). Smaller plutons of similar age and composition to the northwest of the Granite Mountain batholith intrude the Yukon-Tanana terrane (Gordey and Ryan, 2005; Colpron *et al.*, 2016b); these smaller bodies were not examined for this study. Plutons of the Long Lake and Bennett suites are mainly of granodiorite composition but range from syenite to diorite to tonalite (Fig. 4-2a). They are oxidized, and have magnetic susceptibility measurements of 5–10 × 10^{-3} SI units (Fig. 4-3a).

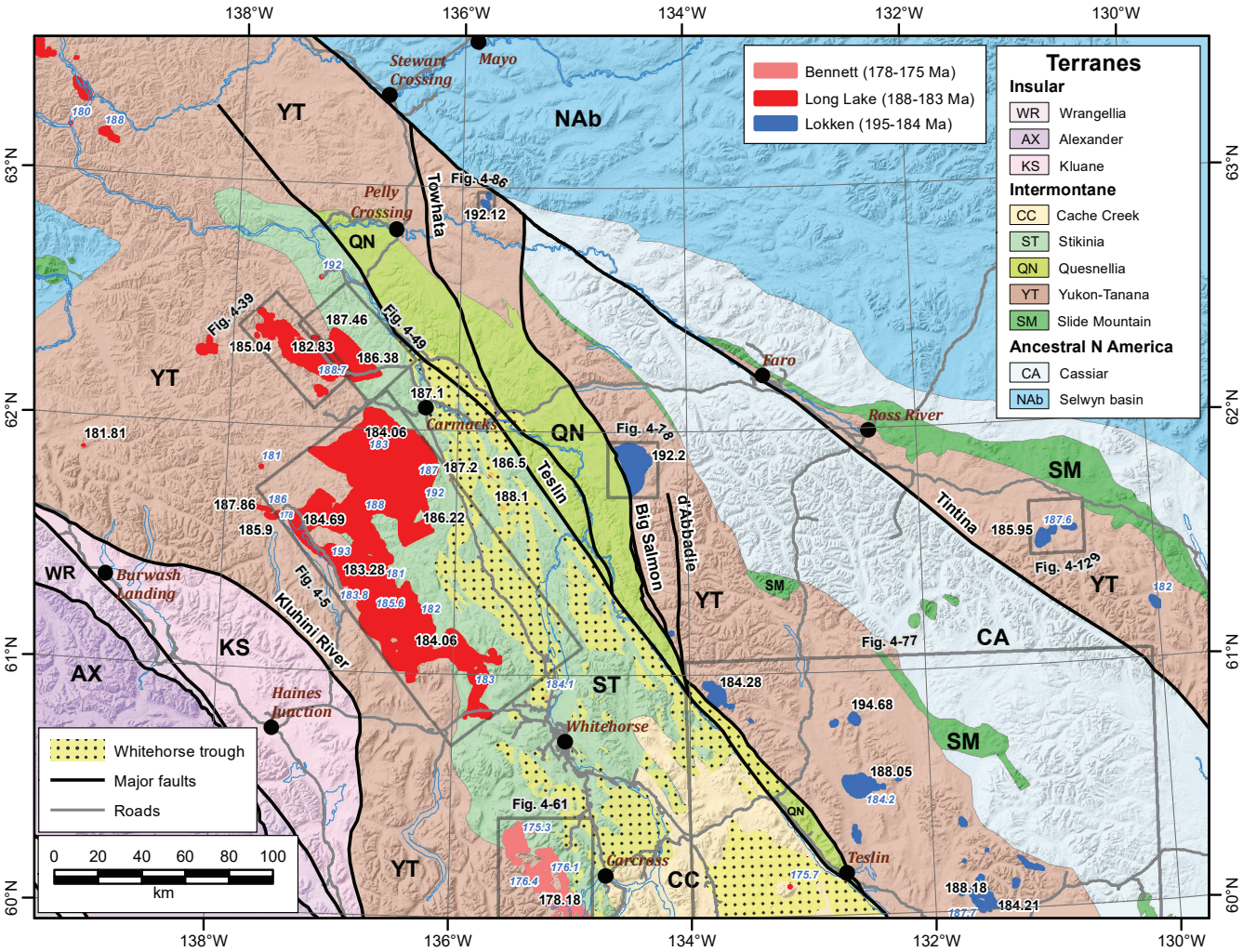


Figure 4-1. *Distribution of Early Jurassic plutons of the Long Lake, Bennett and Lokken suites in the Intermontane terranes of southern Yukon. U-Pb dates are indicated next to plutons–black numbers are zircon CA-TIMS ages (this study); blue, italicized numbers indicate samples dated by other U-Pb techniques from previous work (see Appendix 1 for geochronology compilation). Terrane map is modified after Colpron and Nelson (2011).*

Table 4-1. *Summary of characteristics for Early Jurassic plutons of the Long Lake, Bennett and Lokken suites in Yukon.*

Pluton	NTS	Area (km^2)	Terrane[1]	Rock[2]	Composition[3]	Oxidation state[4]	Age (Ma)[5]	Al-in-Hbl barometry (kbar)[6]	Ti-in-Zrn temp (°C)[7]	Isotopes[8]	Inheritance[9]	Comment	Reference
Long Lake suite													
Aishihik	105D/13, 105E/4, 115H/1–2, 7–11, 14–16, 115I/2	3915	ST/YT	Hbl-Bt granodiorite, tonalite, diorite; Bt ± Ms granite, Qz monzonite	Aishihik 1: calcic tc to alkali-calcic; peraluminous to metaluminous. Aishihik 2: calc-alkalic to alkalic; peraluminous	oxidized	186.22 ± 0.10 to 183.28 ± 0.07	2.3–6.0	550–760	εNd: -1.5 – -5.9 Sr_i: 0.7055–0.7065 $^{207/204}$Pb: 15.68–15.70 $εHf_{zrn}$: -5.8 – +6.4	2606, 1741, 571, 374, 353, 346, 326, 306, 275, 263, 250, 229, 209, 200, 196	BSU, CA-TIMS	this study
Big Creek	115I/3, 5–6	348	ST/YT	Kfs porphyritic syenite, monzonite; Bt ± Hbl granodiorite	alkali-calcic; metaluminous	oxidized	185.04 ± 0.06 182.83 ± 0.05	–	628–700	εNd: -2.8 Sr_i: 0.7051 $^{207/204}$Pb: 15.63 $εHf_{zrn}$: -3.6 – +1.7	324	BSU, CA-TIMS	this study
Granite Mountain (southwest)	115I/2, 6–7	220	ST/YT	Hbl ± Bt granodiorite; Kfs megacrystic Bt-Hbl granite	calc-alkalic; metaluminous	oxidized	187.46 ± 0.07 186.38 ± 0.07	4.33–4.73	590–750	εNd: -1.7 Sr_i: 0.7056 $^{207/204}$Pb: 15.68 $εHf_{zrn}$: -1.1 – +3.0	350, 204	BSU, CA-TIMS	this study
Bennett suite													
Bennett	105D/2–3, 6	208	ST/YT	Kfs porphyritic Hbl granodiorite; monzodiorite, diorite	calc-alkalic to alkali-calcic; metaluminous	oxidized	178.18 ± 0.06	3.45	620–770	εNd: -2.5 Sr_i: 0.7052 $^{207/204}$Pb: 15.64	–	BSU, CA-TIMS	this study
Alligator Lake	105D/5–6	86	ST/YT	Bt-Hbl monzodiorite, diorite; Kfs porphyritic Hbl granodiorite	calc-alkalic to calcic; metaluminous	oxidized to reduced	175.3 ± 1.9	≤2	–	εNd: -2.5 Sr_i: 0.7053 $^{207/204}$Pb: 15.64	–	UBC, ID-TIMS	Hart (1995)
Lokken													
Lokken	105E/15–16	203	YT	Hbl-Cpx-Bt granodiorite, monzodiorite, monzonite	calc-alkalic to alkali-calcic; metaluminous	oxidized	192.20 ± 0.06	3.06	699–818	εNd: -4.3 Sr_i: 0.7057	–	BSU, CA-TIMS	this study
Macmillan Range	105L/13	4.4	YT	Hbl-Cpx (Bt) Qz monzonite, granodiorite	calcic; metaluminous	oxidized	192.12 ± 0.07	2.62	–	–	–	BSU, CA-TIMS	this study
Thirtymile Lake	105C/15	15.3 + 1	YT	Hbl-Bt granodiorite; Cpx-Hbl-Bt monzonite	calc-alkalic; metaluminous	oxidized	194.67 ± 0.05	–	654–720	εNd: -2.5 Sr_i: 0.7059 $^{207/204}$Pb: 15.68 $εHf_{zrn}$: -1.0 – +3.8	–	BSU, CA-TIMS	this study

Table 4-1 continued. *Summary of characteristics for Early Jurassic plutons of the Long Lake, Bennett and Lokken suites in Yukon*

Pluton	NTS	Area (km^2)	Terrane[1]	Rock[2]	Composition[3]	Oxidation state[4]	Age (Ma)[5]	Al-in-Hbl barometry (kbar)[6]	Ti-in-Zrn temp (°C)[7]	Isotopes[8]	Inheritance[9]	Comment	Reference
Lokken suite continued													
Sawtooth	105C/13	54.3	YT	Hbl-Cpx-Bt diorite, monzodiorite	calc-alkalic; metaluminous	weakly oxidized	184.28 ± 0.07	–	660–770	εNd: -0.6 Sr_i: 0.7050 $^{207/204}$Pb: 15.65 $εHf_{zrn}$: +3.5 – +9.3	1698, 605, 232	BSU, CA-TIMS	this study
Englishman	105C/7, 9–10	98.8	YT	Hbl-Cpx-Bt monzonite, monzodiorite	calc-alkalic; metaluminous	oxidized	188.05 ± 0.05	–	690–775	εNd: -2.6 Sr_i: 0.7044 $^{207/204}$Pb: 15.67 $εHf_{zrn}$: +1.6 – +3.7	–	BSU, CA-TIMS	this study
Logjam	105B/4	12.8	YT	Hbl-Bt-Cpx monzodiorite; Kfs porphyritic monzonite; gabbro	alkali-calcic; metaluminous	oxidized	184.21 ± 0.05	–	670–817	–	2285, 348, 198	BSU, CA-TIMS	this study
Two Ladder	104O/13, 105B/4	12.4	YT	Hbl-Bt-Cpx monzodiorite; Kfs porphyritic monzonite, granodiorite	alkali-calcic; metaluminous	weakly oxidized	188.18 ± 0.05	–	650–710	εNd: -1.4 Sr_i: 0.7052 $^{207/204}$Pb: 15.69 $εHf_{zrn}$: -2.9 – +1.4	–	BSU, CA-TIMS	this study
Swift River	105B/3	7.9	YT	Hbl-Bt-Cpx diorite	calc-alkalic; metaluminous	reduced	–	–	–	–	–	–	–
Finlayson (Banana)	105G/7, 10	26.9 + 10.1	YT	Hbl-Cpx monzonite, syenite	calc-alkalic; metaluminous	oxidized to reduced	185.95 ± 0.05	–	650–730	–	200	BSU, CA-TIMS	this study

Notes:

[1] host terrane to intrusion. ST – Stikinia; YT – Yukon-Tanana

[2] rock types from Figs. 4-2, 4-136 and 4-139. Bt – biotite; Cpx – clinopyroxene; Hbl – hornblende; Kfs – K-feldspar; Qz – quartz

[3] composition from Figs. 4-138b and 4-141b

[4] oxidation state from Fig. 4-3

[5] best age for pluton, as discussed in text

[6] crystallization pressure estimates from Al-in-hornblende barometry, Appendix 5

[7] crystallization temperature from Ti-in-zircon thermometry, Appendix 3

[8] whole rock Nd and Sr data; K-feldspar Pb data (Appendix 9); Hf in zircon data (Appendix 10)

[9] inheritance determined from U-Pb LA-ICPMS analyses of zircon (Appendix 3)

Northeast of the Teslin fault, smaller, more mafic plutons (<1 to ~200 km²) intrude the Yukon-Tanana terrane and are assigned to the Lokken suite (195–184 Ma; Fig. 4-1; Table 4-1). They are typically clinopyroxene-bearing and comprise mainly monzonite to monzodiorite and granodiorite (Fig. 4-2b). They are variably magnetic with susceptibilities ranging from 0.1–21.6 × 10^{-3} SI units (Fig. 4-3b). These plutons were previously assigned to either the Minto or Long Lake suites (*e.g.,* Colpron *et al.*, 2016b; Aishihik suite of Gordey and Makepeace, 2001), but are grouped together here based on their distinct composition and distribution northeast of the Teslin fault. Monzonite and gabbro that intrude the Yukon-Tanana terrane in the Finlayson Lake district, northeast of the Tintina fault, are also assigned to the Lokken suite (Fig. 4-1; Table 4-1).

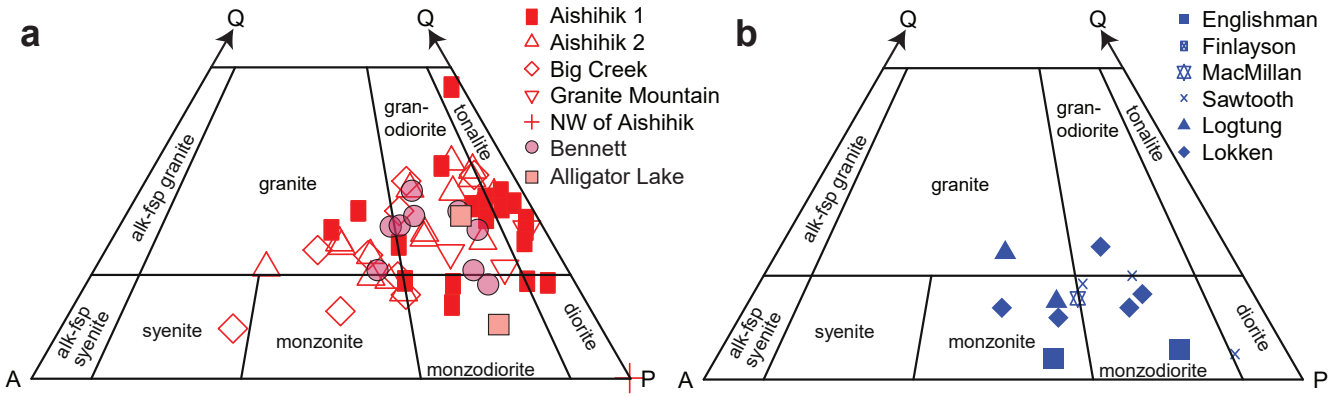


Figure 4-2. *Simplified quartz-alkali-feldspar-plagioclase (QAP) plot for Early Jurassic plutons in southern Yukon (Appendix 2; Le Bas and Streckeisen, 1991).* ***(a)*** *Long Lake and Bennett suites,* ***(b)*** *Lokken suite.*

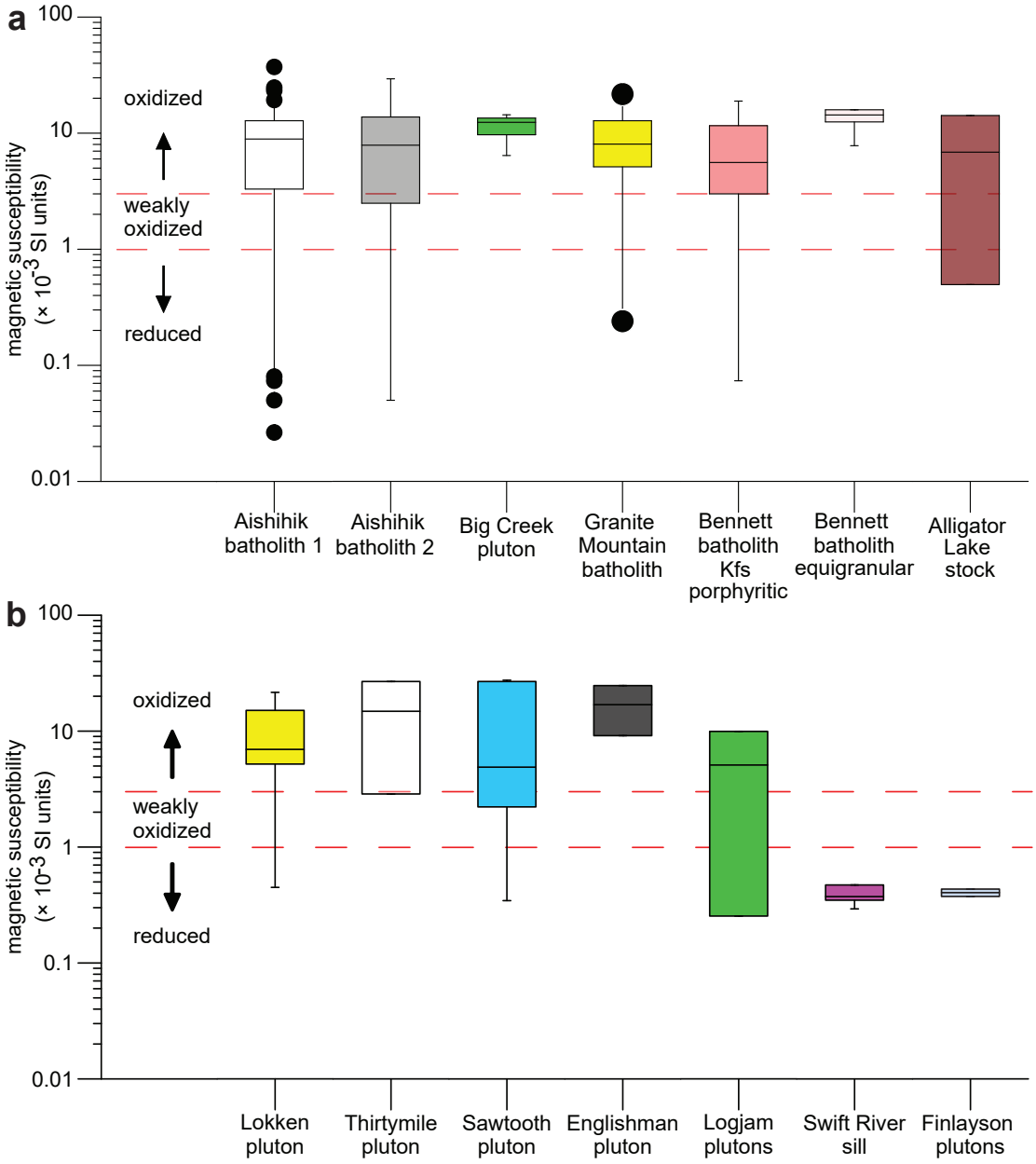


Figure 4-3. *Box and whisker plot of magnetic susceptibility measurements for each Early Jurassic pluton (Appendix 2).* ***(a)*** *Long Lake and Bennett suite plutons,* ***(b)*** *Lokken suite plutons. Divisions between reduced to weakly oxidized (1 × 10^{-3} SI units), and weakly oxidized to oxidized (3 × 10^{-3} SI units) are from Hart et al. (2004a,b). Ends of boxes are 75th and 25th percentile of data, white line within boxes indicate median (50th percentile) of data, whiskers 95th and 5th percentile.*

Long Lake suite

The Long Lake suite comprises the entire Aishihik and Big Creek batholiths and the southwestern portion of the Granite Mountain batholith (Fig. 4-1). The Early Jurassic Aishihik batholith and the southwestern portion of the Granite Mountain batholith have similar compositions. They are partially separated by Upper Cretaceous volcanic rocks of the Carmacks Group and are on opposing sides of the Big Creek fault (Fig. 4-4). In contrast, the Big Creek batholith is coarser grained and more alkalic than the Aishihik and Granite Mountain batholiths. It is separated from the Granite Mountain pluton by the Big Creek fault, and from the Aishihik batholith by Paleozoic metamorphic rocks of the Yukon-Tanana terrane (Fig. 4-4; Allan and Friend, 2018; Ryan *et al.*, 2016).

The Long Lake suite is a term that was applied to felsic, quartz monzonite to granite phases of the Aishihik batholith which were dated at *ca.* 186 Ma (pink quartz monzonite of Tempelman-Kluit, 1974a,b; Woodsworth *et al.*, 1991; Johnston and Erdmer, 1995a; Johnston *et al.*, 1996). The 'older' granodiorite that makes up more than 60% of the Aishihik batholith was assigned to the Aishihik plutonic suite (*ca.* 192–185 Ma; Johnston *et al.*, 1996), a name that was extended to similar granodiorite in the Granite Mountain, Minto and related plutons to the north (Gordey and Makepeace, 2001). These plutons are now known to be part of the older Minto suite (205–194 Ma; *see* Chapter 3; Colpron *et al.*, 2016b). Joyce *et al.* (2016) concluded that the entire Aishihik batholith represents a continuum of magmatism of the Long Lake suite, and proposed abandoning the term Aishihik suite.

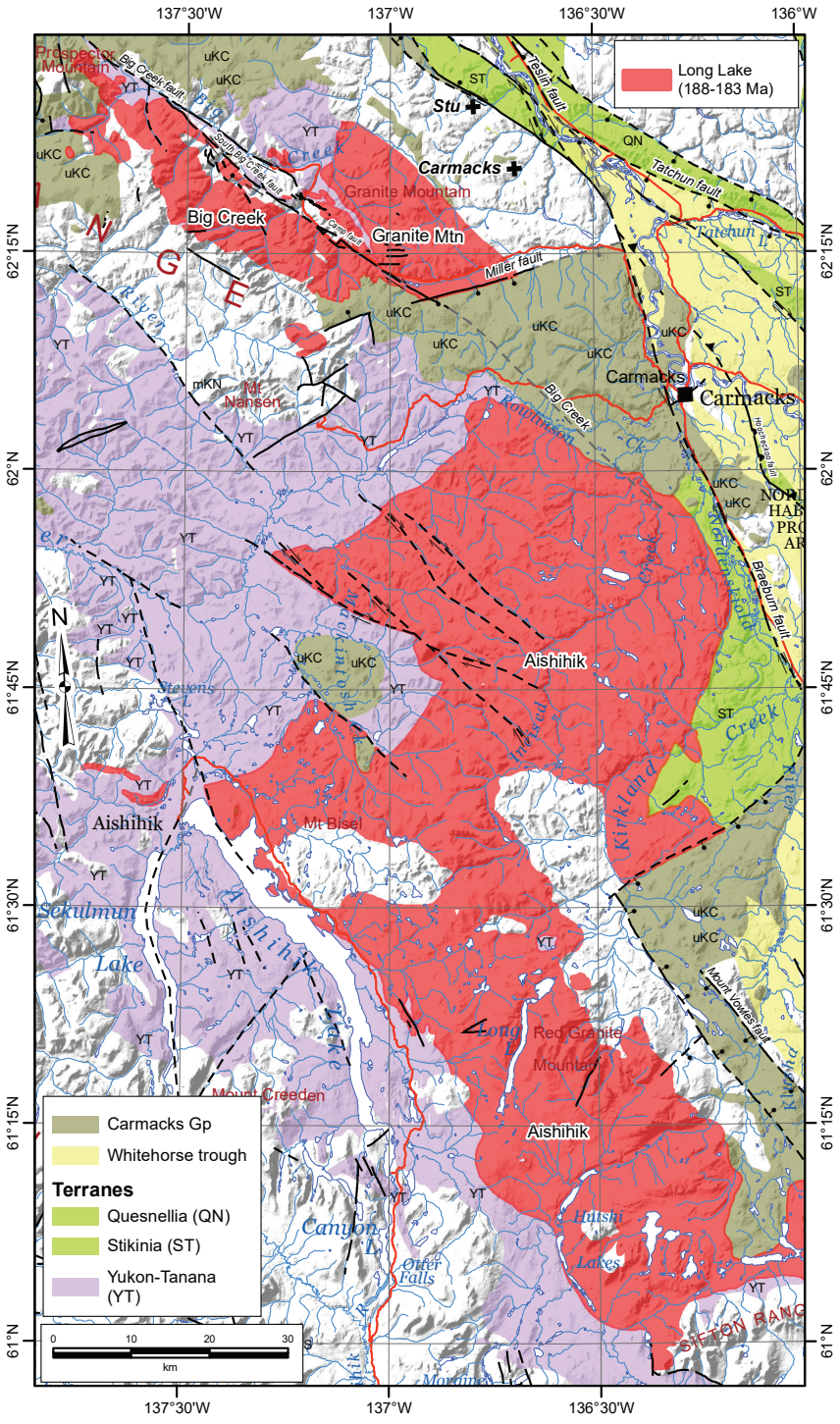


Figure 4-4. *Distribution of the main Early Jurassic plutons of the Long Lake suite (188–183 Ma) southwest of the Teslin fault, west of Carmacks. Exposures of the Aishihik and southwestern Granite Mountain plutons are separated by the Big Creek fault and overlapping younger volcanic rocks of the Upper Cretaceous Carmacks Group. Geology after YGS (2020a); fault symbology as in Figure 1-4.*

Aishihik batholith

The Aishihik batholith is the largest of the Late Triassic to Jurassic plutons in Yukon (Figs. 1-2 and 4-1). With a mapped area of 3915 km², it extends from near Whitehorse to the vicinity of Carmacks and intrudes the boundary between Stikinia (to the east) and Yukon-Tanana terranes (to the west; Figs. 4-1, 4-4 and 4-5; Table 4-1). The northeastern margin of the batholith intrudes augite-phyric basalt of the Povoas formation (Tempelman-Kluit, 1984; Colpron *et al.*, 2007b). Its southeastern margin intrudes weakly to strongly foliated greenschist and amphibolite of the Takhini assemblage, the upper Paleozoic part of Stikinia west of Whitehorse (Hart, 1997a). The majority of the eastern margin of the batholith is unconformably overlain by sedimentary and volcanic rocks including the Upper Jurassic to Lower Cretaceous Tantalus Formation (Allen and Weston, 2001), the Upper Cretaceous Carmacks Group, and the Paleogene Rhyolite Creek Group (Tempelman-Kluit, 1984). Mafic dikes that crosscut the batholith are common and are likely feeders to these younger volcanic rocks (Fig. 4-6). The western margin of the batholith intrudes rocks of the Yukon-Tanana terrane including metasedimentary rocks of the pre-Devonian Snowcap assemblage, metavolcanic rocks of the Devonian-Mississippian Finlayson assemblage and metaplutonic rocks of the Mississippian Simpson Range suite (Tempelman-Kluit, 1974a; Johnston and Timmerman, 1997; Joyce *et al.*, 2016; Ryan *et al.*, 2016; Israel *et al.*, 2017). The Aishihik batholith has been interpreted as a largely concordant body, possibly a lopolith (Johnston and Erdmer, 1995b). Three-dimensional inversion modelling of regional magnetic and gravity data show the base of the Aishihik batholith as a shallowly east to northeast dipping sheet with a steep eastern contact (Fig. 4-7; Mira Geoscience Ltd., 2014).

Much of the Aishihik batholith is exposed above treeline in a series of broad, smooth-topped ridges with mean elevation between 1200 and 1500 m (Fig. 4-8a) that are incised by deep, narrow valleys (Fig. 4-8b). The northern part of the Aishihik batholith lies beyond the limit of the late Pleistocene McConnell glaciation (Fig. 4-9), suggesting the Aishihik highland partially buttressed the St. Elias ice sheet from the west and the Cordilleran ice sheet from the east. Valleys within much of the Aishihik highland were filled by ice-dammed glacial lakes (Tempelman-Kluit, 1974b), as evidenced by multiple strand lines along hillsides that indicate past shorelines (Fig. 4-8c). These glacial lakes filled their valleys to different elevations; the more northerly ones were at lower levels than the southern ones (Tempelman-Kluit, 1974b). Exposure throughout the batholith consists of scattered outcrops and isolated tors on broad ridge tops, and steep cliffs along deeply incised valleys (Fig. 4-8).

The Aishihik batholith comprises granitoid rocks that range in composition from diorite to tonalite and granodiorite, to monzonite and granite (Fig. 4-10). Although the more intermediate units are generally older than felsic rocks, the various compositions are commonly intermixed and have gradational contacts suggesting they are in part coeval (Fig. 4-11; Tempelman-Kluit, 1974b, Johnston and Erdmer, 1995b; Johnston *et al.*, 1996), an interpretation consistent with the geochronological and geochemical data discussed below. We divide the Aishihik batholith into two main phases (Aishihik 1 and 2; Fig. 4-10) that are each dominant in parts of the batholith (Fig. 4-5). All phases are cut by late aplite and pegmatite dikes (Fig. 4-12).

Tonalite to granodiorite are the rock types in the older Aishihik 1 phase (Fig. 4-10). This phase is dominant in the central part of the batholith, between Long Lake and Macintosh Creek, and along its southern tail, southeast of Hutshi Lakes (Fig. 4-5). This phase is variably foliated, with a solid-state foliation more commonly developed near the margins of the batholith and generally subparallel to the intrusive contact. The Aishihik 2 phase comprises mainly monzonite, granodiorite and granite (Fig. 4-10) and is the dominant lithology in the northern part of the batholith and the Red Mountain area, east of Long Lake (Fig. 4-5).

The name Aishihik batholith was originally applied to areas dominantly underlain by granodiorite, and the two regions dominated by monzonite to granite were formerly assigned to the Carmacks and Long Lake batholiths respectively (Tempelman-Kluit, 1974b; Woodsworth *et al.*, 1991; Johnston and Erdmer, 1995a). More recently, the entire area underlain by Jurassic granitoid rocks has been called the Aishihik batholith (Gordey and Makepeace, 2001; Colpron *et al.*, 2016b), and this usage is followed here (Fig. 4-4).

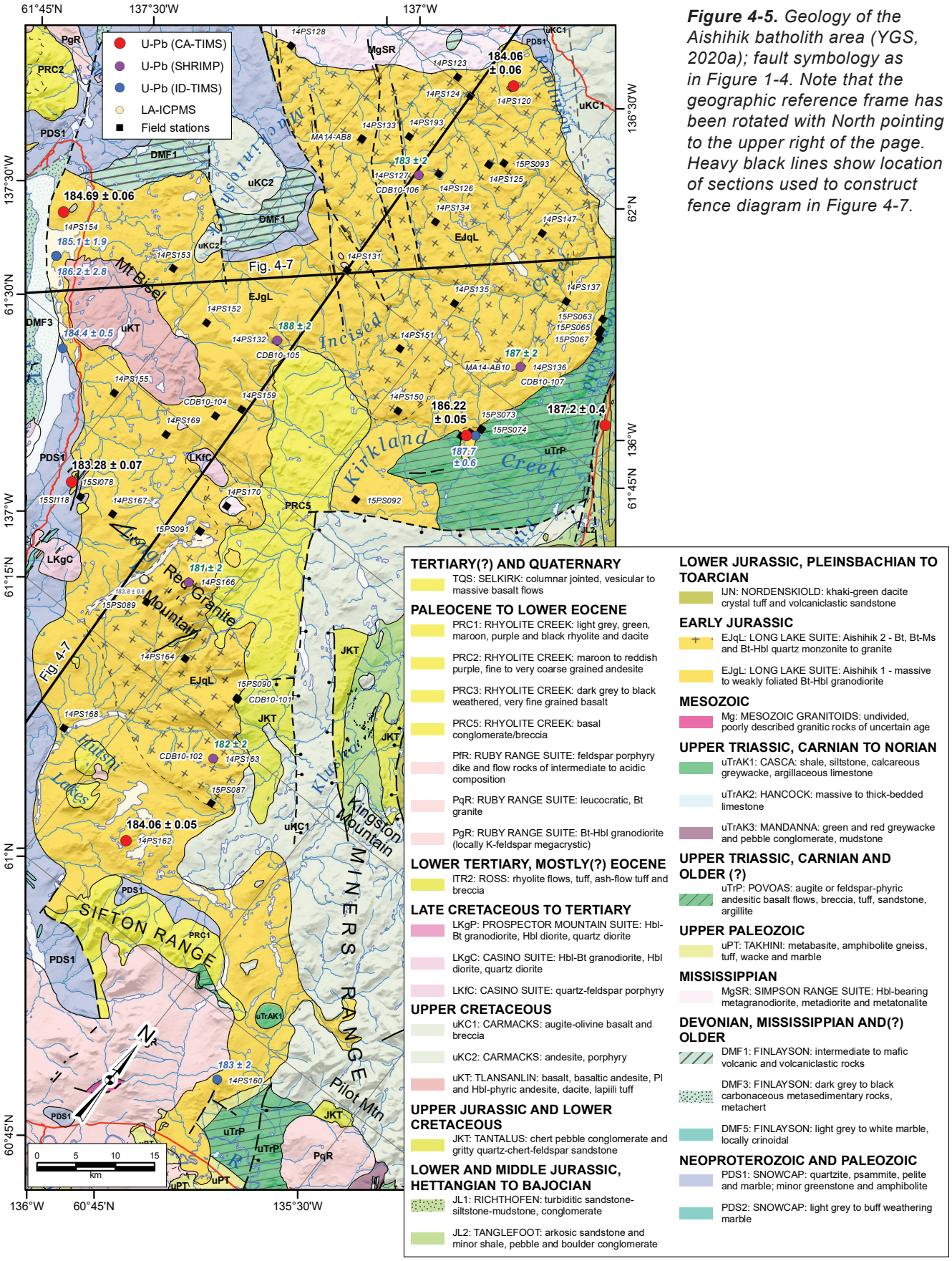


Figure 4-5. *Geology of the Aishihik batholith area (YGS, 2020a); fault symbology as in Figure 1-4. Note that the geographic reference frame has been rotated with North pointing to the upper right of the page. Heavy black lines show location of sections used to construct fence diagram in Figure 4-7.*

TERTIARY(?) AND QUATERNARY

TQS: SELKIRK: columnar jointed, vesicular to massive basalt flows

PALEOCENE TO LOWER EOCENE

PRC1: RHYOLITE CREEK: light grey, green, maroon, purple and black rhyolite and dacite

PRC2: RHYOLITE CREEK: maroon to reddish purple, fine to very coarse grained andesite

PRC3: RHYOLITE CREEK: dark grey to black weathered, very fine grained basalt

PRC5: RHYOLITE CREEK: basal conglomerate/breccia

PfR: RUBY RANGE SUITE: feldspar porphyry dike and flow rocks of intermediate to acidic composition

PqR: RUBY RANGE SUITE: leucocratic, Bt granite

PgR: RUBY RANGE SUITE: Bt-Hbl granodiorite (locally K-feldspar megacrystic)

LOWER TERTIARY, MOSTLY(?) EOCENE

lTR2: ROSS: rhyolite flows, tuff, ash-flow tuff and breccia

LATE CRETACEOUS TO TERTIARY

LKgP: PROSPECTOR MOUNTAIN SUITE: Hbl-Bt granodiorite, Hbl diorite, quartz diorite

LKgC: CASINO SUITE: Hbl-Bt granodiorite, Hbl diorite, quartz diorite

LKfC: CASINO SUITE: quartz-feldspar porphyry

UPPER CRETACEOUS

uKC1: CARMACKS: augite-olivine basalt and breccia

uKC2: CARMACKS: andesite, porphyry

uKT: TLANSANLIN: basalt, basaltic andesite, Pl and Hbl-phyric andesite, dacite, lapiili tuff

UPPER JURASSIC AND LOWER CRETACEOUS

JKT: TANTALUS: chert pebble conglomerate and gritty quartz-chert-feldspar sandstone

LOWER AND MIDDLE JURASSIC, HETTANGIAN TO BAJOCIAN

JL1: RICHTHOFEN: turbiditic sandstone-siltstone-mudstone, conglomerate

JL2: TANGLEFOOT: arkosic sandstone and minor shale, pebble and boulder conglomerate

LOWER JURASSIC, PLEINSBACHIAN TO TOARCIAN

lJN: NORDENSKIOLD: khaki-green dacite crystal tuff and volcaniclastic sandstone

EARLY JURASSIC

EJqL: LONG LAKE SUITE: Aishihik 2 - Bt, Bt-Ms and Bt-Hbl quartz monzonite to granite

EJgL: LONG LAKE SUITE: Aishihik 1 - massive to weakly foliated Bt-Hbl granodiorite

MESOZOIC

Mg: MESOZOIC GRANITOIDS: undivided, poorly described granitic rocks of uncertain age

UPPER TRIASSIC, CARNIAN TO NORIAN

uTrAK1: CASCA: shale, siltstone, calcareous greywacke, argillaceous limestone

uTrAK2: HANCOCK: massive to thick-bedded limestone

uTrAK3: MANDANNA: green and red greywacke and pebble conglomerate, mudstone

UPPER TRIASSIC, CARNIAN AND OLDER (?)

uTrP: POVOAS: augite or feldspar-phyric andesitic basalt flows, breccia, tuff, sandstone, argillite

UPPER PALEOZOIC

uPT: TAKHINI: metabasite, amphibolite gneiss, tuff, wacke and marble

MISSISSIPPIAN

MgSR: SIMPSON RANGE SUITE: Hbl-bearing metagranodiorite, metadiorite and metatonalite

DEVONIAN, MISSISSIPPIAN AND(?) OLDER

DMF1: FINLAYSON: intermediate to mafic volcanic and volcaniclastic rocks

DMF3: FINLAYSON: dark grey to black carbonaceous metasedimentary rocks, metachert

DMF5: FINLAYSON: light grey to white marble, locally crinoidal

NEOPROTEROZOIC AND PALEOZOIC

PDS1: SNOWCAP: quartzite, psammite, pelite and marble; minor greenstone and amphibolite

PDS2: SNOWCAP: light grey to buff weathering marble



Figure 4-6. *Basalt dike crosscutting K-feldspar porphyritic granodiorite in the southern part of the Aishihik batholith; 14PS160. Hammer 45 cm long. Inset shows K-feldspar porphyritic texture of the granodiorite.*

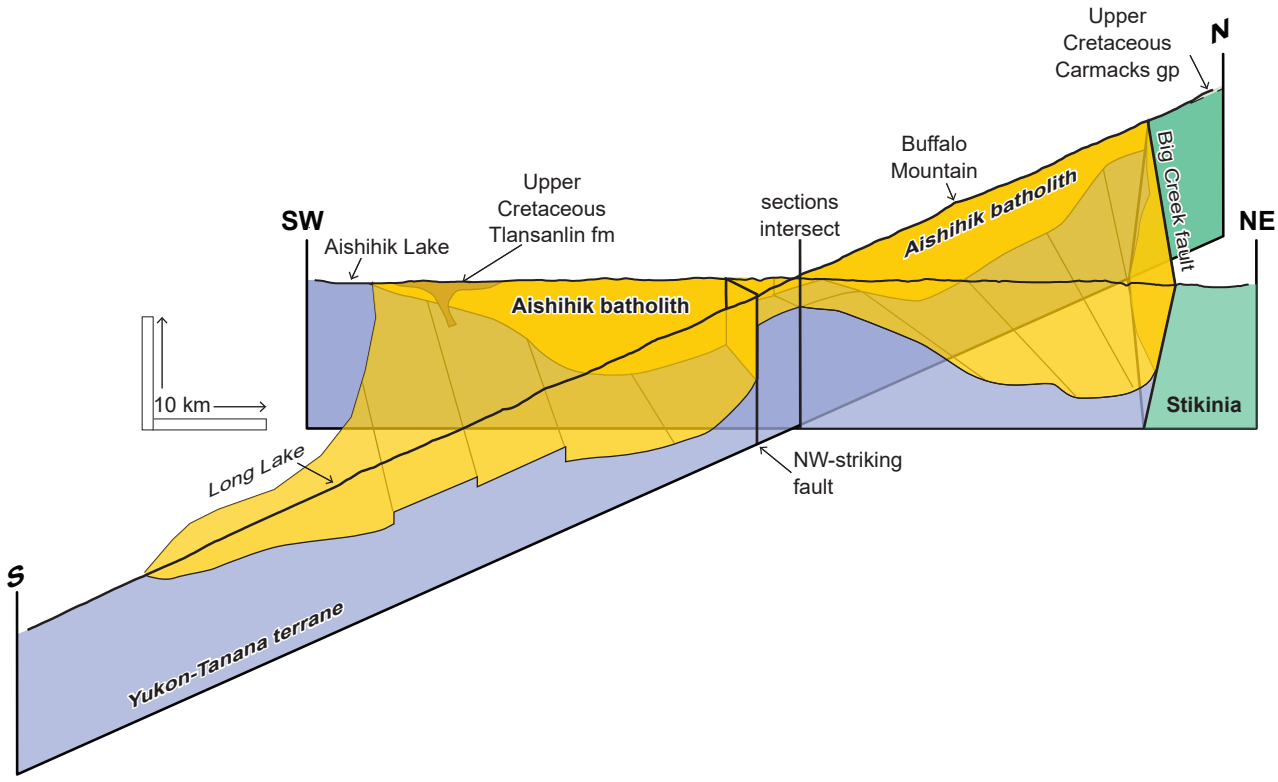


Figure 4-7. *Schematic fence diagram illustrating the interpreted geometry of the base of the Aishihik batholith. Surface geology from YGS (2020a). The base of the Aishihik batholith is modelled using 3D inversion of regional magnetic and gravity data (after Mira Geosciences, 2014). Lines of section used to construct the fence diagram are indicated on Figure 4-5. Note that the northern part of the batholith is modelled to be at shallower depth across a step that corresponds with a series of northwest-striking faults (see Fig. 4-5).*

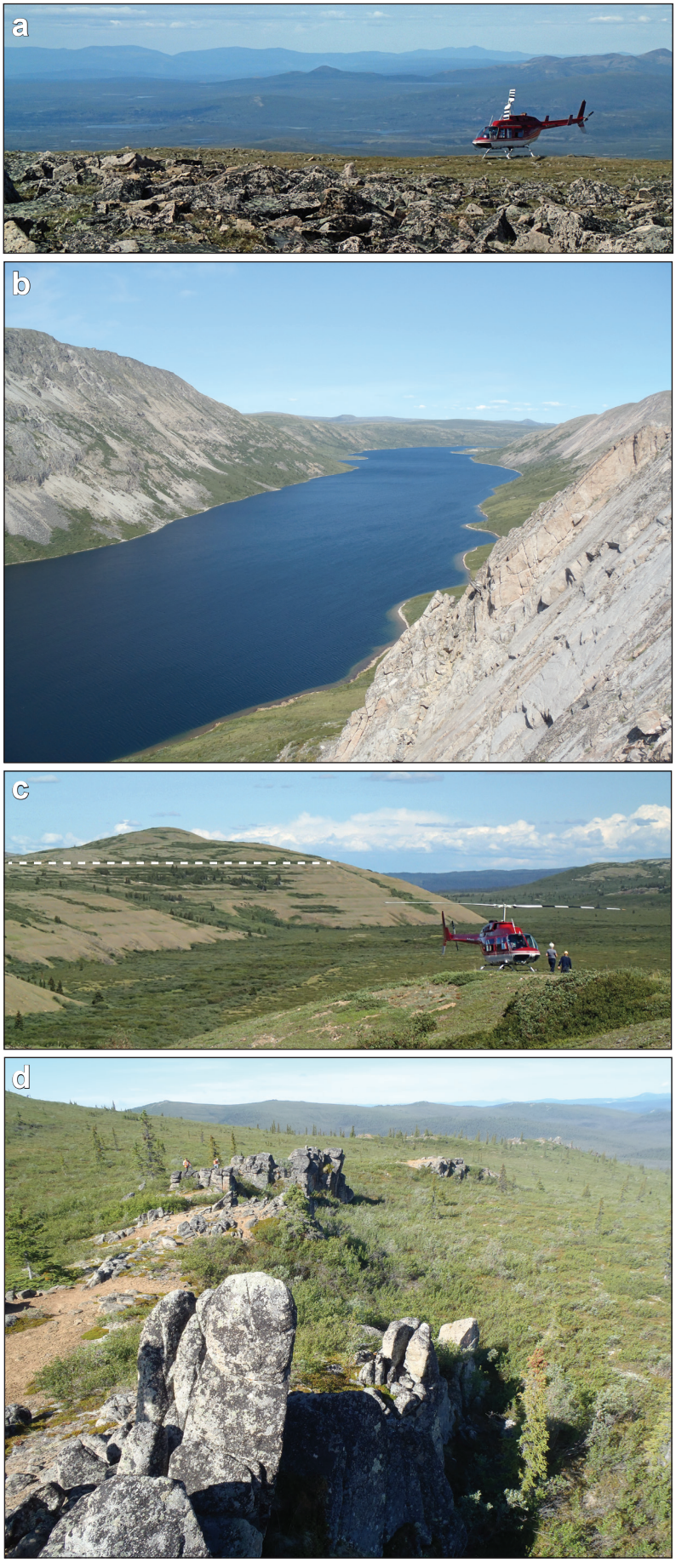


Figure 4-8. *Landscapes of the Aishihik batholith area.* ***(a)*** *View looking southwest from Red Granite Mountain showing gentle, rounded hills separated by broad valleys; 14PS166.* ***(b)*** *Looking north from central Long Lake where steep valley walls are nearly all outcrop; 14PS165.* ***(c)*** *Strand lines from glacial lake Champagne on the north side of Lake Terrace Creek in the central Aishihik batholith. Dashed white line showing highest elevation strand line; 14PS159.* ***(d)*** *Small, isolated tors near the northern margin of the batholith; 14PS120.*

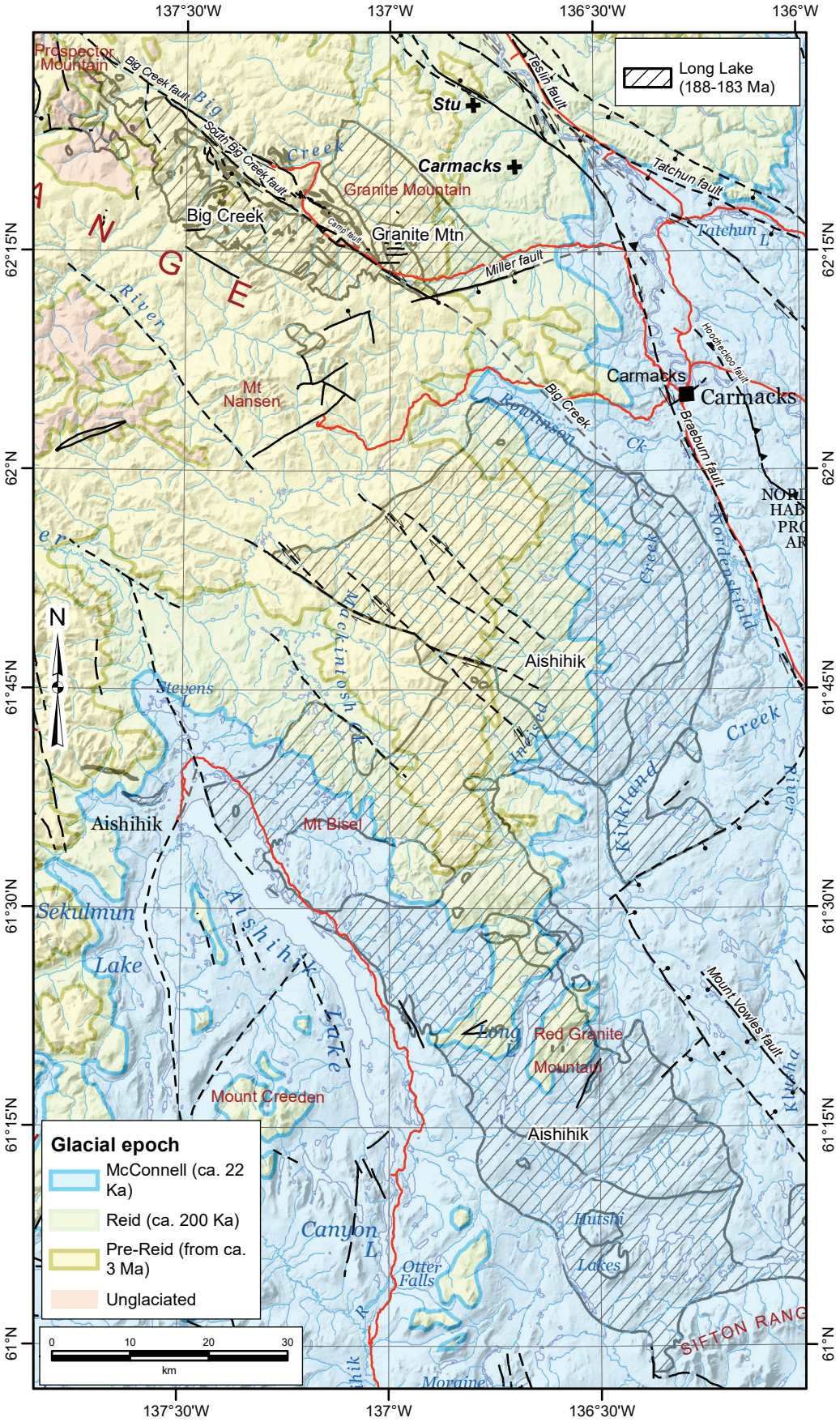


Figure 4-9. *Map of glacial limits for the Aishihik Lake–Carmacks area (after Duk-Rodkin, 1999). Much of the northern part of the Aishihik batholith (hatched area) escaped the late Pleistocene McConnell glaciation (ca. 22 Ka) and is only covered by a thin veneer of till from the Reid (ca. 200 Ka) and pre-Reid (≤3 Ma) glacial epochs. Distribution of Long Lake suite plutons (hatched areas) are after YGS (2020a); fault symbology as in Figure 1-4.*

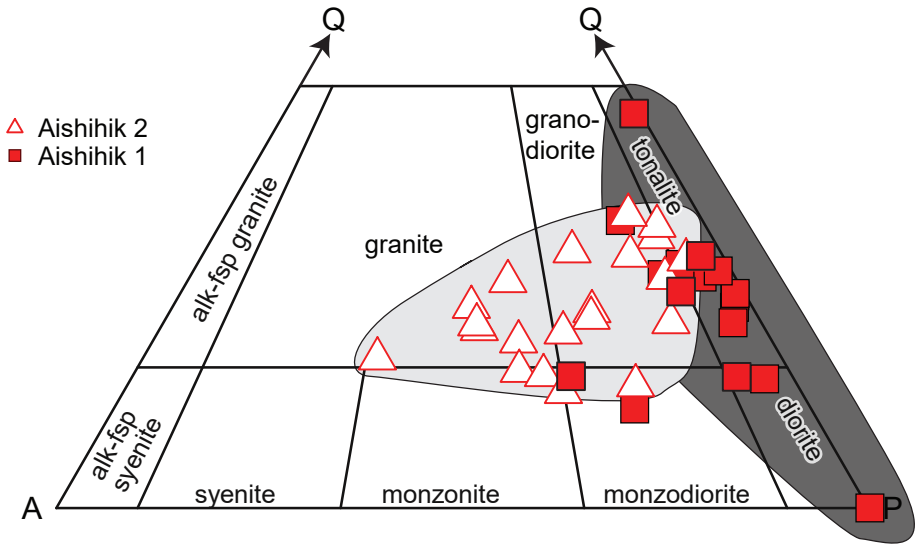


Figure 4-10. *Simplified quartz-alkali-feldspar-plagioclase (QAP) plot (Le Bas and Streckeisen, 1991) for samples from the Aishihik batholith (Appendix 2).*



Figure 4-11. *Crosscutting relationships showing the relative timing of phases near the northeast margin of the Aishihik batholith; 15PS067. 1 = foliated granodiorite, 2 = unfoliated granite, 3 = pegmatite dike. Hammer head is 13 cm across. Foliation in 1 is shown by dashed line and is oriented N035/65, batholith margin locally strikes ~N345.*



Figure 4-12. *Late aplite dikes in the Aishihik batholith.* ***(a)*** *Flat lying garnet-bearing aplite crosscutting the intermediate lithology of the Aishihik batholith near the Late Cretaceous Tahte occurrence [115H 038]; 14PS131. Hammer 45 cm long.* ***(b)*** *Small garnet and coarse-grained pocket within the aplite dike in (a).* ***(c)*** *Anastomosing aplite dikes near the northern margin of the Aishihik batholith; 14PS124.*

Petrography

Two granitoid phases make up most of the Aishihik batholith, an intermediate phase (Aishihik 1) and an intermediate to felsic phase (Aishihik 2; Fig. 4-10). Based on crosscutting relationships (*e.g.*, Fig. 4-11) and U-Pb zircon dating (*see* below) the Aishihik 1 phase is generally slightly older than the more felsic phase, but there is overlap between the two phases. The Aishihik 1 phase is fine to medium grained, equigranular to K-feldspar porphyritic, hornblende > biotite granodiorite-tonalite to diorite (Fig. 4-13). This lithology ranges from massive (Fig. 4-13a) to foliated (Fig. 4-13b), and is mostly located on the margins of the batholith (Fig. 4-5). Foliation, where present, is defined by the alignment of biotite and hornblende and elongate quartz (Fig. 4-14). The Aishihik 1 phase is either equigranular with interstitial K-feldspar and translucent, zoned plagioclase phenocrysts (Fig. 4-15) or has both white plagioclase and pink K-feldspar phenocrysts (Fig. 4-13). In comparison to the more felsic Aishihik 2 phase, these rocks are relatively K-feldspar-poor (Fig. 4-13), plotting near the granodiorite-tonalite and monzodiorite-diorite boundary on a modified QAP diagram (Fig. 4-10). They also have more hornblende than biotite, typically in a ratio of 2:1 or more, combining to ≤20 modal percent of the rock. Accessory minerals include minor titanite and epidote. Epidote occurs as a secondary alteration product, commonly associated with plagioclase. Plagioclase is weakly saussuritized to fresh and K-feldspar is weakly sericitized to fresh. Biotite is typically more chloritized than hornblende with intensity of chloritization in both phases varying from weak to moderate.

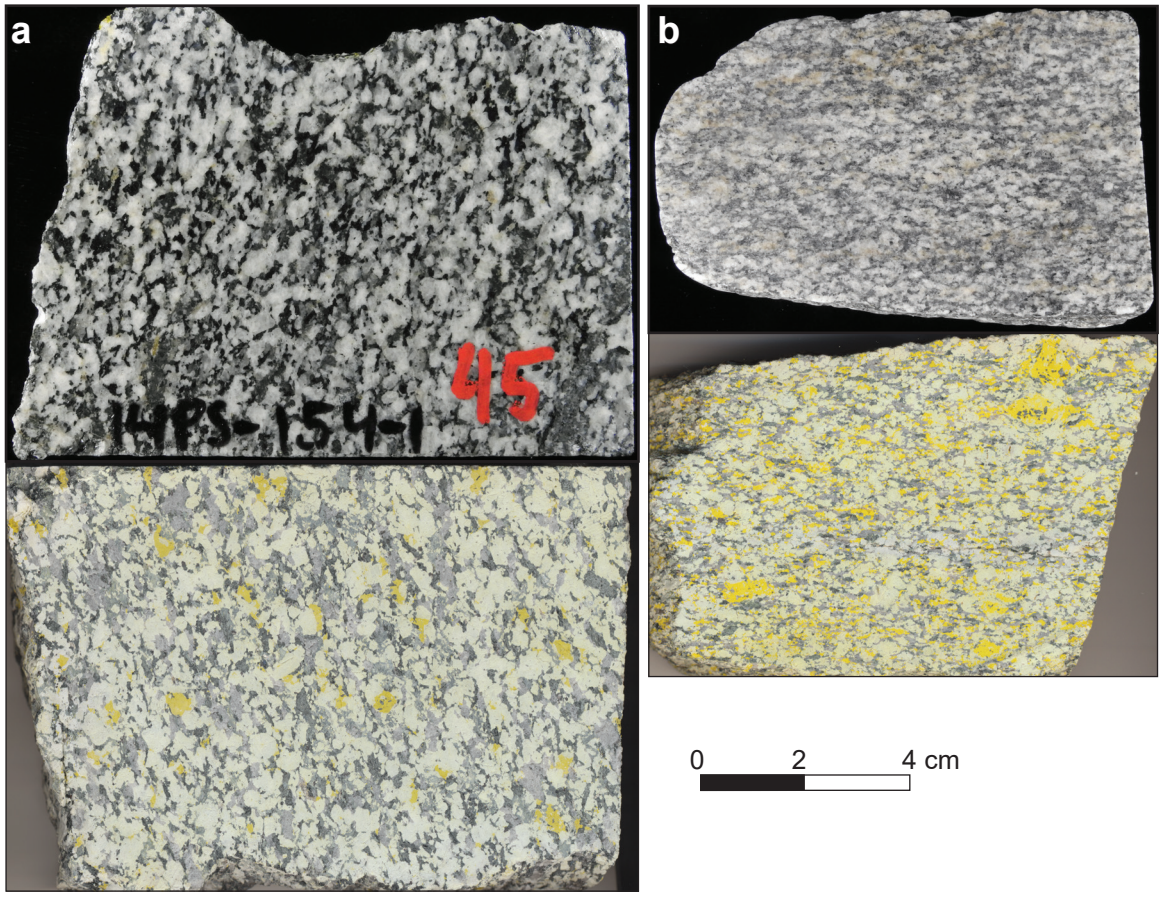


Figure 4-13. *Representative samples from phase 1 of the Aishihik batholith.* ***(a)*** *Unfoliated, medium to coarse-grained, equigranular tonalite from the northwestern corner of the batholith, 14PS154-1.* ***(b)*** *Foliated, medium-grained, equigranular to weakly K-feldspar porphyritic monzodiorite from the northern edge of the batholith, 14PS123-1. Foliation N045/40, batholith margin strikes N035. Fresh polished surface (upper) and a cobaltinitrite-stained surface (lower). Note K-feldspar is yellow.*

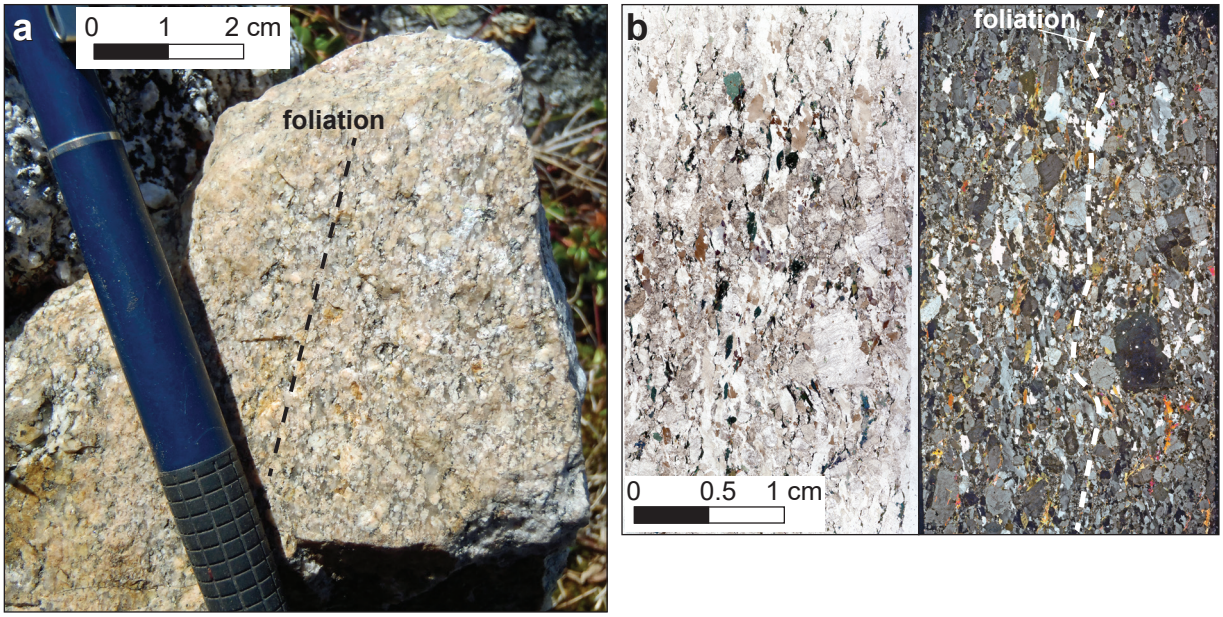


Figure 4-14. *Weakly foliated rocks from the Aishihik 1 phase; 14PS152-1.* ***(a)*** *Weathered float with weak foliation.* ***(b)*** *Thin section scans, plane polarized light (left) and cross-polarized light (right), of weak, anastomosing foliation defined by mafic minerals and elongate quartz and feldspar.*



Figure 4-15. *Equigranular diorite with trace amounts of interstitial K-feldspar (yellow) and abundant translucent, zoned plagioclase phenocrysts; 14PS131-1. Cobaltinitrite-stained surface.*

The younger and more felsic Aishihik 2 phase comprises granodiorite to granite and monzonite (Fig. 4-10). This phase is coarse grained with distinctive smoky quartz phenocrysts in hand sample (Fig. 4-16) that in thin section are quartz glomerocrysts (Fig. 4-17). The Aishihik 2 lithology varies from equigranular to K-feldspar porphyritic and compared to the Aishihik 1 phase is relatively mafic poor with ≤10 modal percent mafic minerals, and biotite > hornblende (Fig. 4-16). Hornblende is only a minor constituent locally. Muscovite is present in trace to minor amounts in approximately half of the localities we examined (Fig. 4-18). Titanite and epidote are ubiquitous accessory minerals; epidote is most commonly found as a secondary alteration product, but in a few instances may be a primary magmatic mineral (Fig. 4-19).

Late, coarse to very coarse grained K-feldspar-rich pegmatite and fine-grained aplite dikes commonly cut both phases of the batholith. In some instances, coarse-grained to pegmatitic material within the Aishihik 2 phase of the batholith is associated with recessive weathering features (Fig. 4-20). Features such as these have been interpreted as miarolitic cavities, and used as evidence of a shallow emplacement level for these rocks (*e.g.*, Johnston, 1993; Johnston *et al.*, 1996).

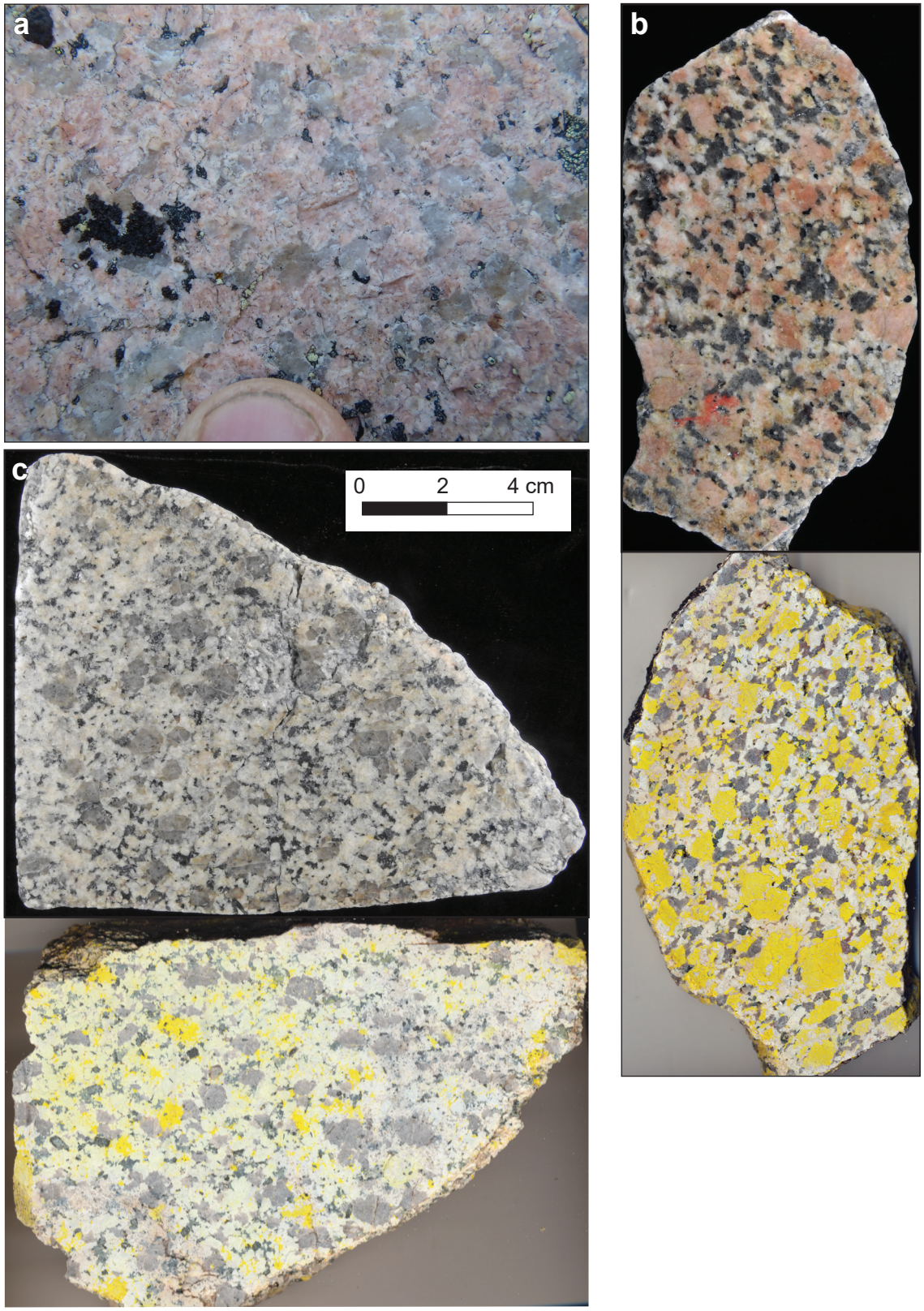


Figure 4-16. *Representative samples from the intermediate to felsic phase of Aishihik batholith.* ***(a)*** *Outcrop of medium-grained equigranular granite from the central felsic body; 14PS164. Fingertip for scale.* ***(b)*** *Coarse-grained, K-feldspar porphyritic monzonite from the central portion of the batholith, 14PS166-1.* ***(c)*** *Unfoliated, coarse-grained, equigranular granodiorite from the northern portion of the batholith with distinctive grey quartz phenocrysts; 14PS120-1. (b and c), fresh polished surface (upper) and a cobaltinitrite-stained surface (lower). Note K-feldspar is yellow, all images are same scale.*

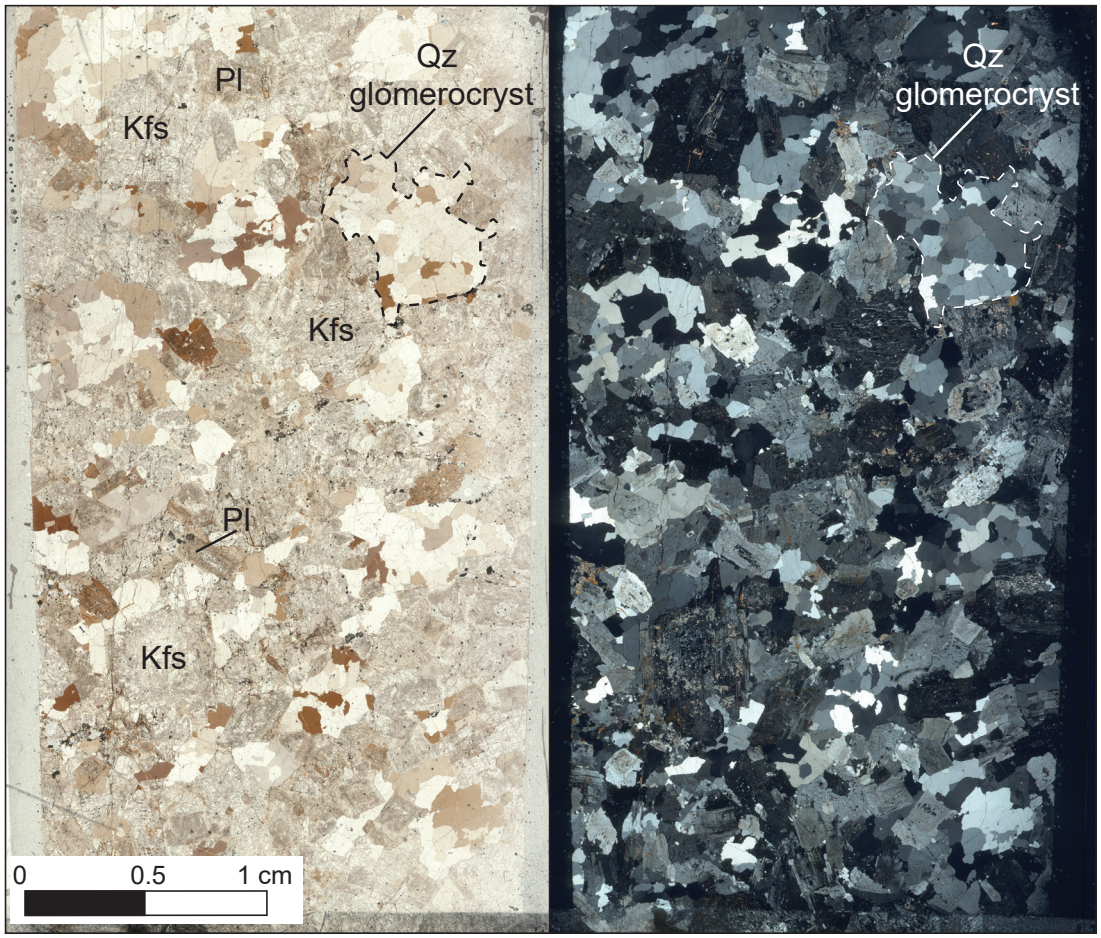


Figure 4-17. *Thin section scans, plane polarized light (left) and cross-polarized light (right), showing 5 to 10 mm quartz phenocrysts which in thin section are aggregates of optically discontinuous quartz crystals or glomerocrysts. From granite in the central felsic body of the Aishihik batholith; 14PS164-1.*

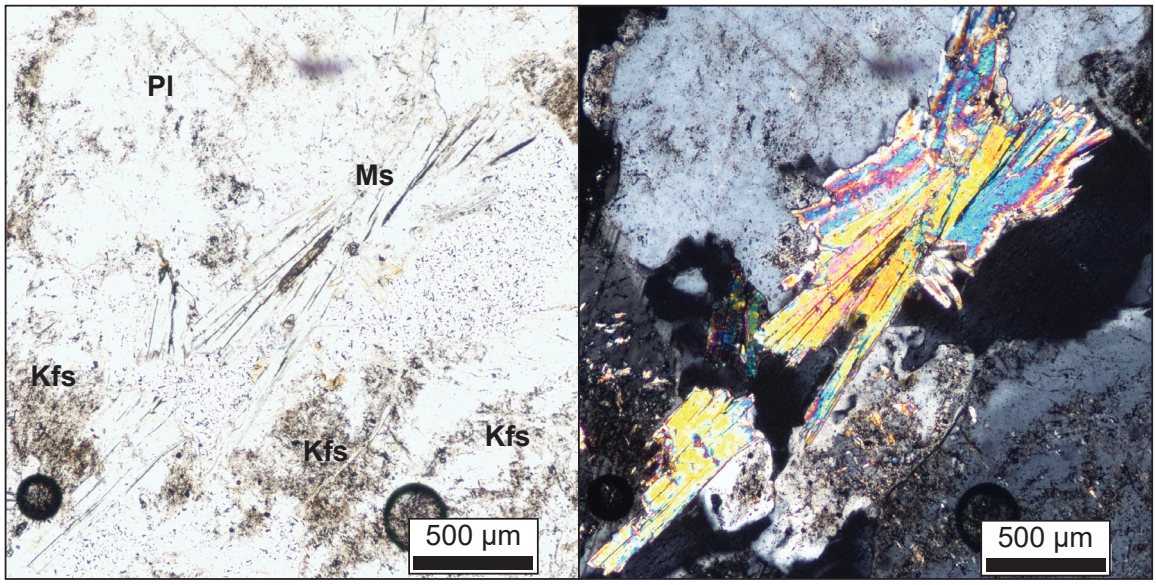


Figure 4-18. *Transmitted light photomicrographs from the Aishihik batholith showing euhedral magmatic muscovite from the northern felsic body; 14PS135-1. Plane polarized light (left) and cross-polarized light (right).*

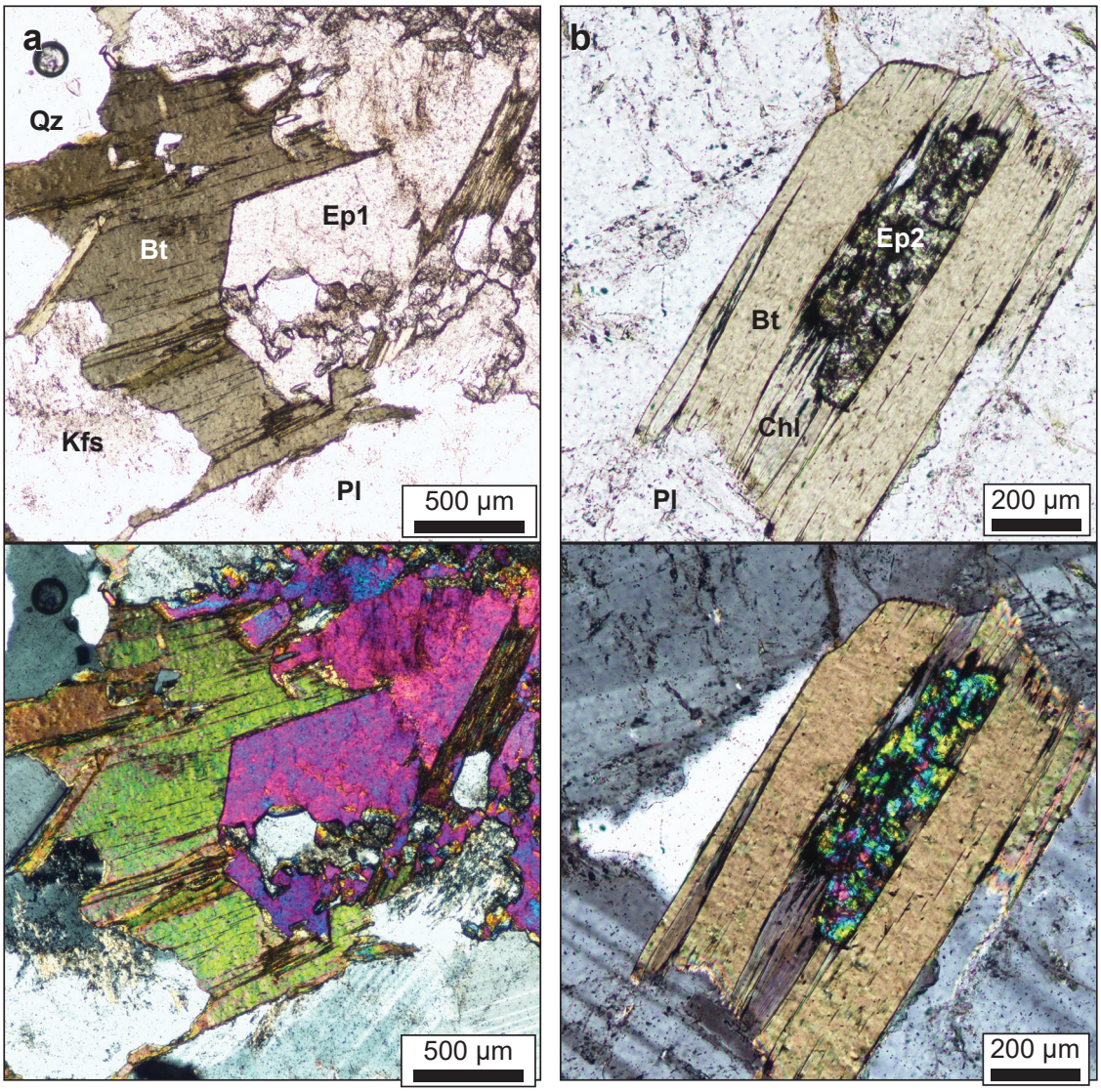


Figure 4-19. *Transmitted light photomicrographs of epidote from the Aishihik batholith; plane polarized light (upper) and cross-polarized light (lower).* ***(a)*** *Small, clean euhedral epidote intergrown with biotite suggesting a magmatic origin for the epidote; 14PS162-1.* ***(b)*** *Small, mottled subhedral epidote with biotite and chlorite. The presence of chlorite and the mottled, subhedral nature suggest a secondary origin for the epidote; 14PS148-1.*



Figure 4-20. *Recessive cavities within the felsic lithology of the Aishihik batholith.* ***(a** and **b)** Recessive feature within medium to coarse-grained granite from the central felsic body; 15PS089.* ***(c)*** *Cavities of recessively weathered pegmatite; 14PS169. Notebook 12 cm across.* ***(d)*** *Less weathered face of pegmatite associated with cavity in (c); 14PS169. Lens cap 4 cm across.* ***(e)*** *Recessive feature broadly associated with aplite dikes in the northern felsic body; 14PS124. Hammer handle 3 cm diameter.*

Oxidation state and mineral occurrences

All phases identified in the Aishihik batholith are oxidized and have magnetic susceptibilities ranging from 0.44 to 47.39 × 10^{-3} SI units (mean 13.5 × 10^{-3} SI units; n = 93; includes data from Tempelman-Kluit and Currie, 1978) for the intermediate Aishihik 1 phase and 0.05 to 56.28 × 10^{-3} SI units (mean 10.3 × 10^{-3} SI units; n = 93; includes data from Tempelman-Kluit and Currie, 1978) for the felsic to intermediate Aishihik 2 phase (Fig. 4-21). There is no appreciable difference in the magnetic susceptibility of foliated and unfoliated Aishihik 1 rocks (Fig. 4-21).

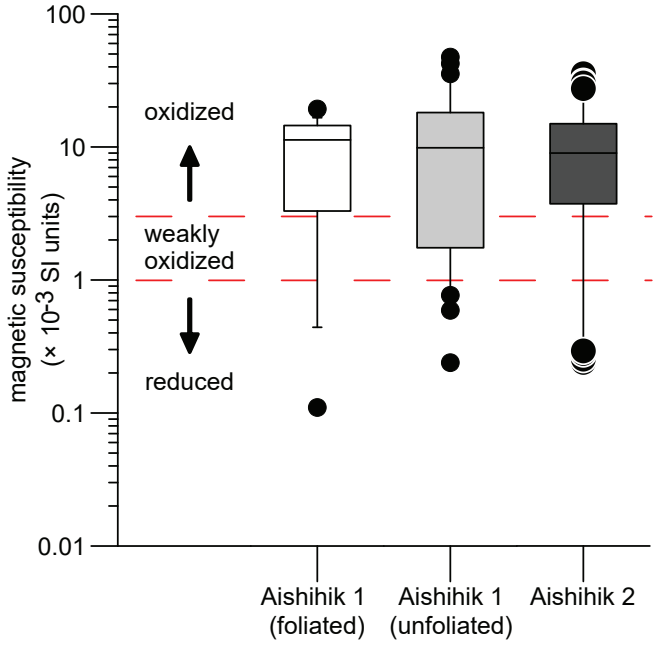


Figure 4-21. *Box and whisker plot of magnetic susceptibility measurements for each phase of the Aishihik batholith (Appendix 2). Divisions between reduced to weakly oxidized (1 × 10^{-3} SI units), and weakly oxidized to oxidized (3 × 10^{-3} SI units) are from Hart et al. (2004a,b). Ends of boxes are 75th and 25th percentile of data, white line within boxes indicate median (50th percentile) of data, whiskers 95th and 5th percentile.*

There are numerous MINFILE occurrences within, or near, the boundaries of the Aishihik batholith (Fig. 4-22; Table 4-2; YGS, 2020b). These occurrences are poorly understood and constrained. The occurrences that have been drilled and have known mineralization are related to Late Cretaceous intrusive rocks (*e.g.*, Tahte [115H 038] and Sato [115H 021]) and may be molybdenum ± copper intrusion-related systems (*i.e.*, porphyry or epithermal mineralization) similar to the Hopper occurrences [115H 019, 034] near the southwest margin of the batholith (Fig. 4-22). The Lascas occurrence [115H 052] has an historical resource for industrial grade quartz in veins that crosscut Early Jurassic quartz monzonite (YGS, 2020b).

Most of the occurrences hosted within the Aishihik batholith consist of minor molybdenum or copper mineralization or anomalies (Table 4-2). Very little work has been done on these occurrences, but they have been classified as porphyry occurrences because they are hosted by plutonic rocks and are anomalous in copper and molybdenum (YGS, 2020b).

The quality of stream sediment coverage in the Aishihik batholith area is poor, primarily because the area is located near the Pleistocene glacial limit (Fig. 4-9) and many of the valleys were melt water channels filled by glacial lakes (*e.g.*, Fig. 4-8; Hughes, 1990). The northern part of the batholith has several catchments with regional stream sediment anomalies >90th percentile in weighted sum model for porphyry Cu deposit types (Fig. 4-23); several of these anomalies are coincident with known occurrences associated with Late Cretaceous intrusive rocks, such as Sato and Tahte (Fig. 4-22).

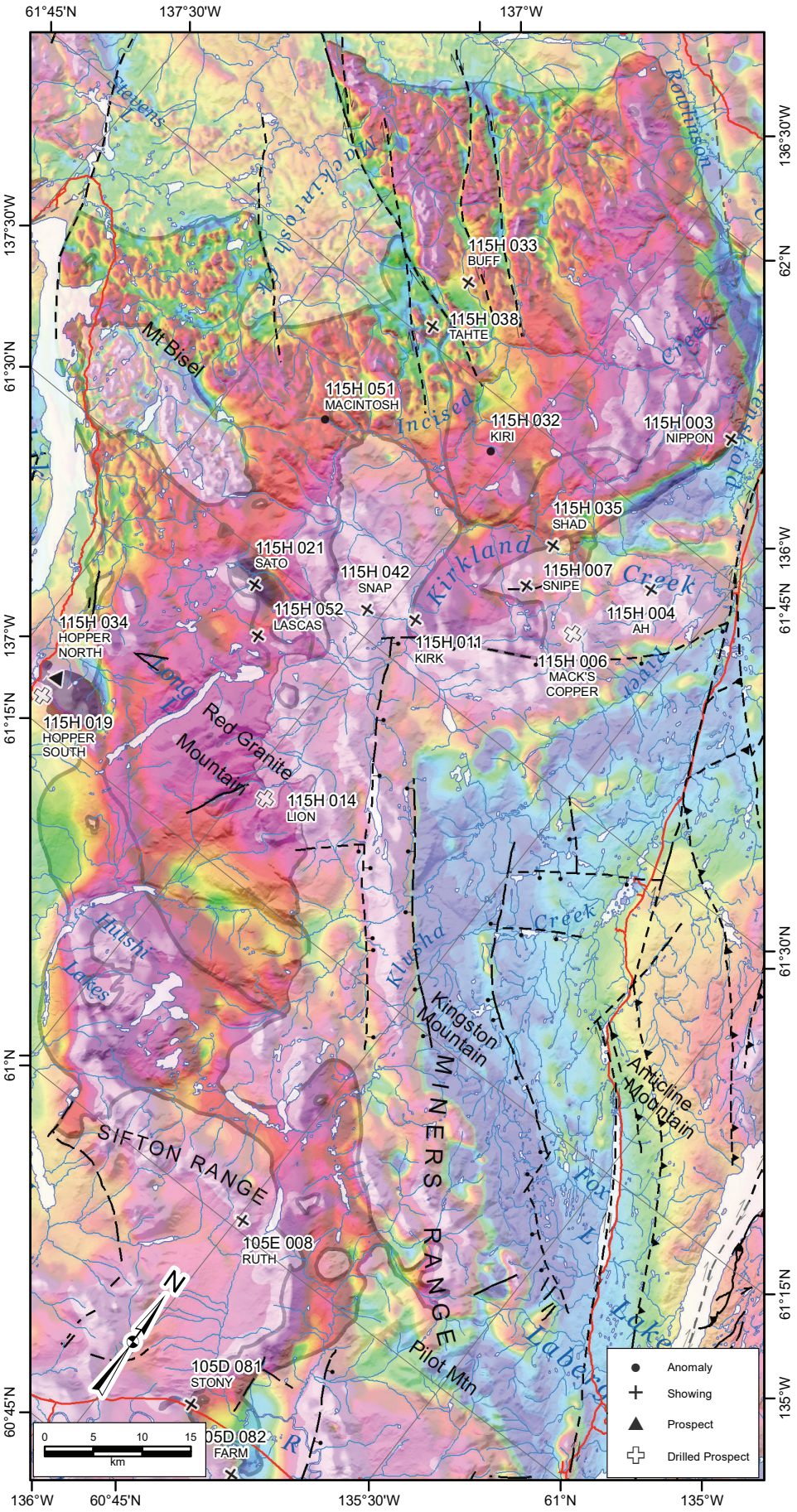


Figure 4-22. *Residual total field aeromagnetic map of the Aishihik batholith area (Hayward and Oneschuk, 2011) illustrating location of MINFILE occurrences (Table 4-2). Dark grey shaded areas indicate exposures of Late Cretaceous porphyritic intrusions. Note that the geographic reference frame has been rotated with North pointing to the upper right of the page. Fault symbology as in Figure 1-4.*

Table 4-2. *Summary of MINFILE occurrences near the Aishihik batholith (modified from YGS, 2020b).*

MINFILE number	Name	Latitude	Longitude	Deposit type	Deposit status	Commodities	Host unit	Host rock age	Comment
115H 042	SNAP	61.52222	-136.52972	Epithermal	Showing	unknown	Rhyolite Creek group	Paleogene	silicified and clay altered volcanics, cut by drusy or crustiform chalcedony and quartz veins with minor fluorite
115H 021	SATO	61.47583	-136.72750	Porphyry	Drilled Prospect	copper	Casino suite	Late Cretaceous	disseminated pyrite, magnetite, chalcopyrite and minor molybdenite in weakly altered and brecciated diorite, chargeability anomaly roughly coincides with a 900 by 300 m copper-in-soil anomaly which trends northwest; 789 m drilling
115H 038	TAHTE	61.76333	-136.77416	Porphyry	Drilled Prospect	copper, molybdenum, gold	Casino suite	Late Cretaceous	50 by 15 m altered zone coincident with a 250 by 150 m, northwest-trending low resistivity IP anomaly; 269 m drilling
115H 023	BISET	61.53611	-137.23388	Unknown	Anomaly	unknown	Tlansanlin fm	Late Cretaceous	300 gamma magnetic anomaly
115H 009	EMPRESS	61.56888	-136.30861	Unknown	Anomaly	unknown	Carmacks group	Late Cretaceous	
115H 032	KIRI	61.70694	-136.53361	Unknown	Anomaly	unknown	Long Lake suite	Early Jurassic	Cu stream sediment anomaly
115H 003	NIPPON	61.85305	-136.18305	Porphyry	Showing	unknown	Long Lake suite	Early Jurassic	coincident linear 150 gamma magnetic anomaly and disseminated chalcopyrite
115H 033	BUFF	61.81527	-136.77333	Porphyry	Showing	molybdenum	Long Lake suite	Early Jurassic	minor quartz veins with trace molybdenite
115H 014	LION	61.32805	-136.45583	Porphyry	Drilled Prospect	molybdenum, lead	Long Lake suite	Early Jurassic	minor pyrite, molybdenite and galena in narrow quartz veins associated with a 0.8 km long gossan in granodiorite; 117 m drilling
115H 039	TOSH	61.74111	-136.65277	Unknown	Unknown	unknown	Long Lake suite	Early Jurassic	
115H 051	MACINTOSH	61.63444	-136.82166	Vein Au-Quartz	Anomaly	unknown	Long Lake suite	Early Jurassic	gold stream sediment anomaly
115H 052	LASCAS	61.44055	-136.66166	Unknown	Showing	silica	Long Lake suite	Early Jurassic	industrial grade quartz vein in quartz monzonite

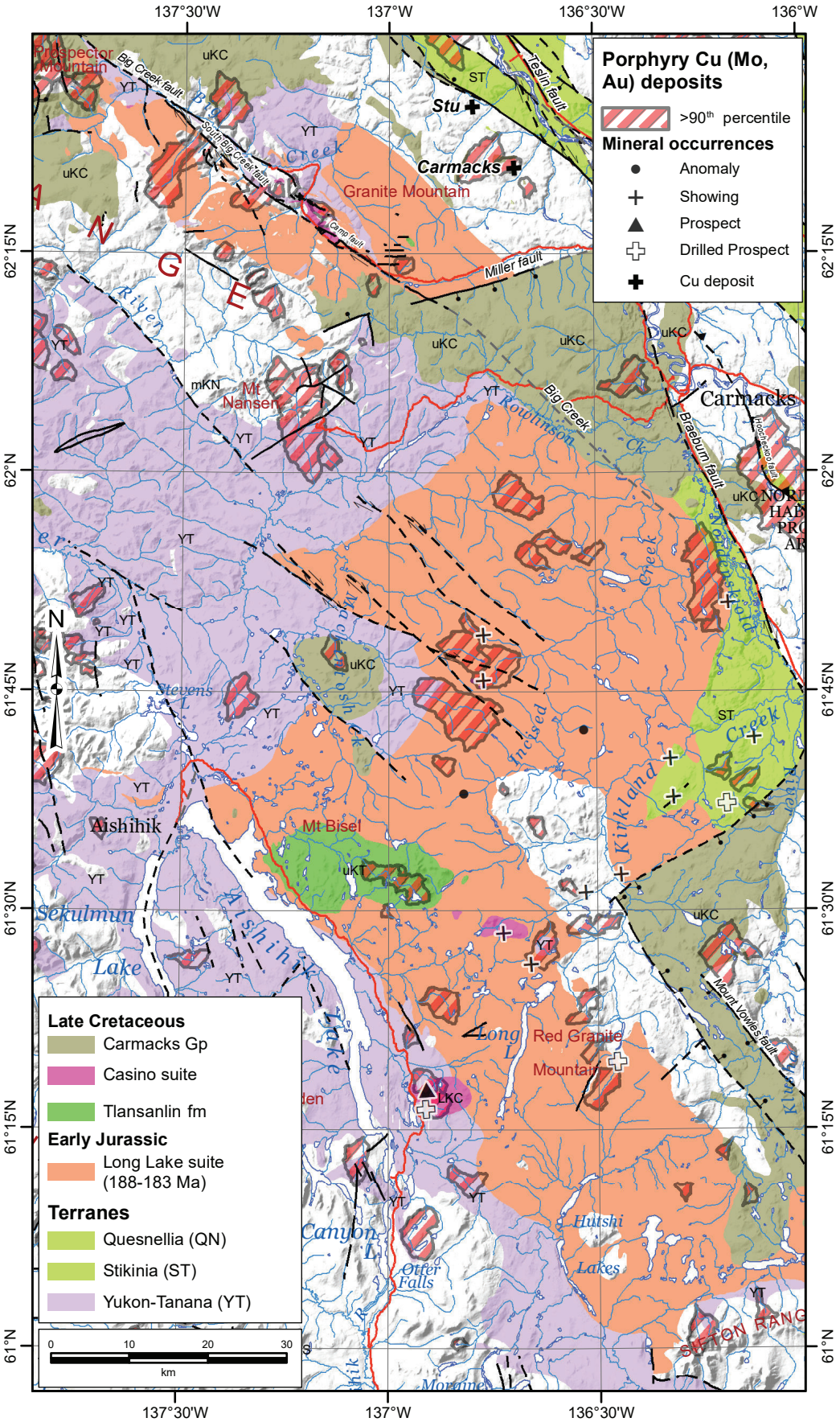


Figure 4-23. *Weighted sums models of regional geochemical stream sediment data. Red hatched catchment basins represent >90th percentile data when ranked by importance for porphyry Cu (Mo, Au) deposits in the respective NTS sheet (Mackie et al., 2016c,e). Weighted sums modelling and importance rankings for various deposit types are described in more detail in Mackie et al. (2015). Fault symbology as in Figure 1-4.*

Geochronology

The Aishihik batholith has been subject to a number of geochronological studies since the 1970s (Appendix 1; YGS, 2020c). Early attempts at dating this large batholith used the K/Ar and Rb/Sr methods on hornblende and biotite separates (LeCouteur and Tempelman-Kluit, 1976; Wanless *et al.*, 1978). Hornblende K/Ar dates of 175 ± 7 and 168.9 ± 7.0 Ma provided a minimum estimate for crystallization of the intermediate phases of the Aishihik batholith (Wanless *et al.*, 1978). Biotite K/Ar dates ranged from 169.9 ± 6.0 to 163.8 ± 6.0 Ma. A single biotite Rb/Sr date of *ca.* 144 Ma (LeCouteur and Tempelman-Kluit, 1976) is much younger than the biotite K/Ar date from the same sample and considered unreliable.

Johnston *et al.* (1996) produced the first U-Pb dates for the Aishihik batholith. These early samples were analyzed by ID-TIMS on multi-grain, air-abraded zircon fractions. A sample from the granodiorite phase (Aishihik 1) yielded two concordant fractions with a date of 186.2 ± 2.8 Ma, whereas a sample of quartz monzonite (Aishihik 2) yielded discordant results with a lower intercept from 5 fractions at 185.6 ± 2.4 Ma (Johnston *et al.*, 1996). Titanite from these two samples yielded slightly younger dates of 185.1 ± 1.9 and 179.1 ± 1.0 Ma, respectively. Hart (1997a) analyzed another sample of quartz monzonite from the southern part of the Aishihik batholith (Fig. 4-5; Appendix 1). The three zircon fractions analyzed yielded discordant results and a lower intercept of 183 ± 2 Ma (ID-TIMS, air-abraded multi-grain fractions). Inheritance was noted in all these samples.

To circumvent inheritance problems, Joyce *et al.* (2016) used a combination of imaging (CL and backscatter) to identify subgrain zircon domains and *in situ* analyses using the SIMS (GSC, Ottawa) on 5 samples from throughout the Aishihik batholith (Fig. 4-5; Appendix 1). Two samples of granodiorite from the Aishihik 1 phase yielded dates of 188 ± 2 and 187 ± 2 Ma, and the 3 samples from quartz monzonite, granite and granodiorite of the Aishihik 2 phase have consistently younger weighted mean dates between 183 ± 2 and 181 ± 2 Ma, but individual analyses show scatter to older dates (*ca.* 190–187 Ma) in most samples. A quartz monzonite from the northern part of the batholith was dated by LA-ICPMS at UBC as part of the same study (Joyce *et al.*, 2016). It yielded an older date of 186 ± 2 Ma which suggests that various phases of the Aishihik batholith may result from a continuum of magmatic activity between *ca.* 188–181 Ma. Core analyses from these samples indicate inherited components of Late Triassic–Early Jurassic (204–196 Ma), mid to late Paleozoic (361–316 Ma, and 260 Ma), and Paleoproterozoic ages (1866 Ma; Joyce *et al.*, 2016).

Joyce *et al.* (2016) also dated two samples of granodiorite gneiss from the western margin of the Aishihik batholith. Both samples show complex zircons with Mississippian igneous cores (*ca.* 345 Ma) and Early Jurassic metamorphic rims (*ca.* 193–187 Ma). This western orthogneiss was considered part of the sheared sole of the Aishihik batholith by Johnston and Erdmer (1995b). Joyce *et al.* (2016) show that the orthogneiss is part of the Mississippian Simpson Range plutonic suite (Yukon-Tanana terrane) that has been partially migmatized during intrusion of the Early Jurassic Aishihik batholith.

We present the results of combined LA-ICPMS and high-resolution CA-TIMS analyses from another 6 samples of Aishihik batholith (performed at BSU; Appendices 3 and 4). We also report the first $^{40}Ar/^{39}Ar$ analyses of hornblende and biotite from 9 samples of Aishihik batholith (Appendix 6).

U-Pb

Sample 14PS154-1 is massive, coarse-grained, equigranular tonalite (Aishihik 1 phase) from the northwest corner of the batholith near Aishihik Lake (Figs. 4-5 and 4-13a). It yielded stubby prismatic zircons with faint concentric zoning; a few grains have inherited cores (Fig. 4-24a). LA-ICPMS analyses of 41 zircons have $^{206}Pb/^{238}U$ dates between 571 and 177 Ma (Appendix 3). There are three inherited grains at *ca.* 571, 374 and 275 Ma, a xenocryst population (n = 6) with a weighted mean of 199.6 ± 3.1 Ma, and a majority of zircons (n = 31) with a weighted mean $^{206}Pb/^{238}U$ date of 187.2 ± 1.4 Ma (Fig. 4-24b; Appendix 3). Six zircon grains from this young population were analyzed by CA-TIMS. They yielded concordant $^{206}Pb/^{238}U$ dates that range from 184.92 ± 0.13 to 184.61 ± 0.12 Ma (Appendix 4) and have a weighted mean of 184.69 ± 0.06 Ma (MSWD = 1.44, n = 5; Fig. 4-24c).

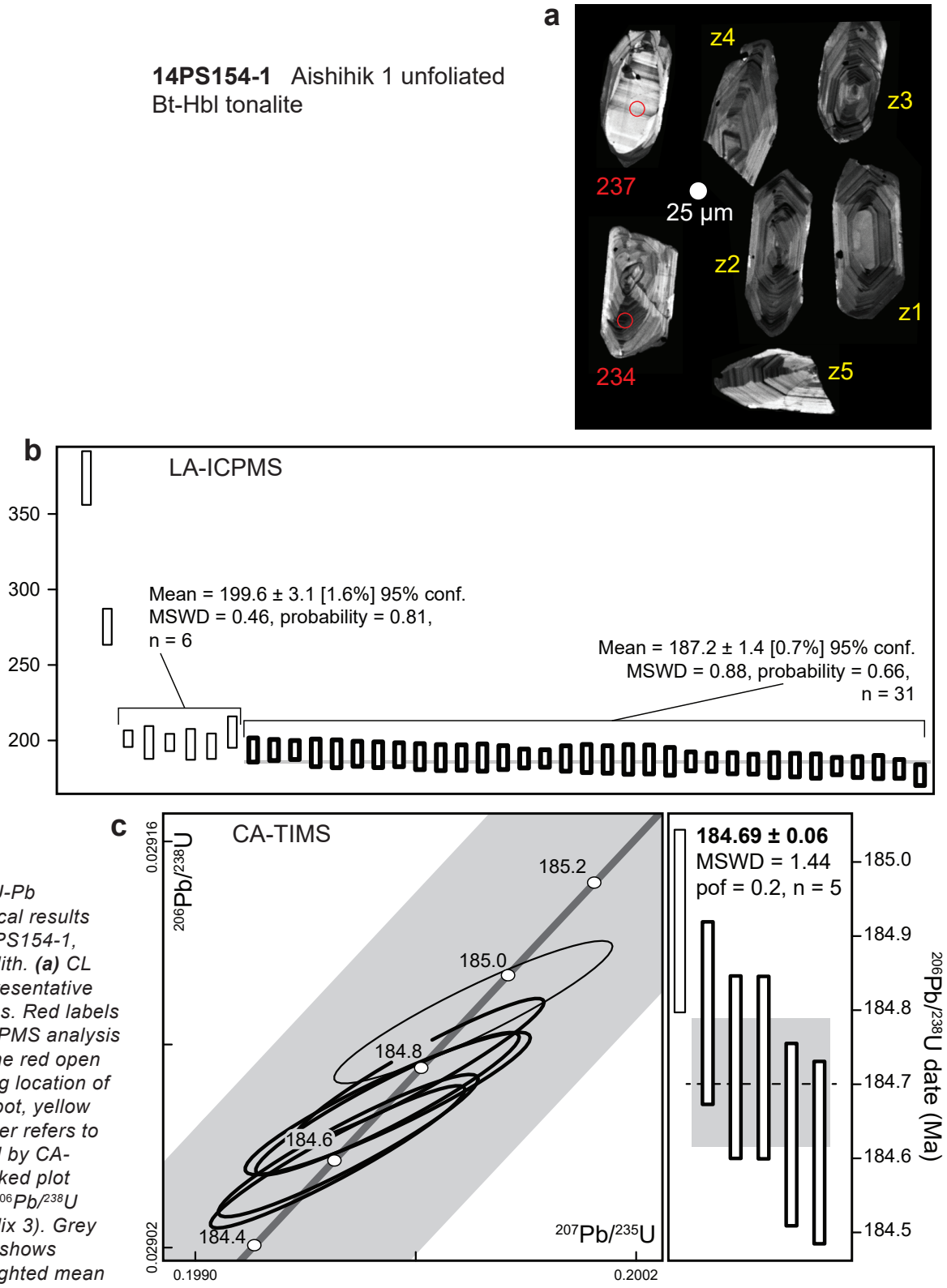


Figure 4-24. *U-Pb geochronological results for sample 14PS154-1, Aishihik batholith.* ***(a)*** *CL images of representative igneous zircons. Red labels indicate LA-ICPMS analysis number with the red open circle indicating location of the analysis spot, yellow analysis number refers to grain analyzed by CA-TIMS.* ***(b)*** *Ranked plot of LA-ICPMS $^{206}Pb/^{238}U$ dates (Appendix 3). Grey horizontal bar shows calculated weighted mean with errors.* ***(c)*** *Concordia diagram (left) and ranked $^{206}Pb/^{238}U$ dates (right) for zircons analyzed by CA-TIMS (Appendix 4). The light grey band around concordia (dark grey line) shows the decay constant uncertainties. Analyses included in weighted mean age (light grey horizontal bar) calculations are bold; analyses with thin lines are not used in calculations. Line-type designations are the same in all plots. Errors in all plots are at 2σ. MSWD = mean squared weighted deviation, pof = probability of fit, n = number of analyses included in age calculation.*

Sample 14PS162-1 is massive, medium-grained tonalite (Aishihik 1 phase) from the southern part of the batholith near Hutshi Lakes (Fig. 4-5). It yielded elongate zircons with a length to width ratio >3:1 and oscillatory zoning; a few grains have inherited cores (Fig. 4-25a). LA-ICPMS analyses of 46 zircons have $^{206}Pb/^{238}U$ dates between 378 and 175 Ma. Three inherited grains have a weighted mean of 377 ± 10 Ma, a xenocryst population of four grains has a weighted mean of 208.4 ± 6.1 Ma, and the youngest 39 grains have a weighted mean of 183.9 ± 1.5 Ma (Fig. 4-25b; Appendix 3). Two zircons with *ca.* 326 and 273 Ma dates are interpreted as inherited grains that may have undergone lead loss. Six zircon grains from the youngest population were analyzed by CA-TIMS and yielded concordant $^{206}Pb/^{238}U$ dates that range from 184.16 ± 0.13 to 183.91 ± 0.13 Ma (Appendix 4), with a weighted mean date of 184.06 ± 0.05 Ma (MSWD = 1.21, n = 6; Fig. 4-25c).

Sample 15PS071-1 is a medium-grained Bt-Hbl monzodiorite (Aishihik 1 phase) from the eastern edge of the batholith along Kirkland Creek (Fig. 4-5). It yielded stubby zircons with a length to width ratio of 2:1 and faint oscillatory zoning (Fig. 4-26a). LA-ICPMS analyses of 30 zircons have $^{206}Pb/^{238}U$ dates between 210 and 178 Ma. One inherited grain has a date of 209.5 ± 10.0 Ma; the remaining 29 grains have a weighted mean of 188.3 ± 1.5 Ma (Fig. 4-26b; Appendix 3). Six zircon grains analyzed by CA-TIMS yielded concordant $^{206}Pb/^{238}U$ dates that range from 186.35 ± 0.14 to 186.12 ± 0.13 Ma (Appendix 4), with a weighted mean date of 186.22 ± 0.10 Ma (MSWD = 2.28, n = 6; Fig. 4-26c).

Sample 15SI078-1 is a strongly foliated Hbl-Bt granodiorite (Aishihik 1 phase) from the western edge of the batholith, between Aishihik and Long Lakes (Fig. 4-5). It yielded stubby zircons with a length to width ratio of <2:1 and oscillatory zoning; a few grains have inherited cores (Fig. 4-27a). LA-ICPMS analyses of 30 zircons have $^{206}Pb/^{238}U$ dates between 346 and 178 Ma. Two inherited grains have dates of *ca.* 346 and 344 Ma, a xenocryst population of five grains has a weighted mean of 198.6 ± 3.2 Ma, and 21 of the 23 youngest grains have a weighted mean of 185.4 ± 1.5 Ma (Fig. 4-27b; Appendix 3). The two youngest grains have U >1700 ppm and are interpreted to have undergone minor Pb loss. Six zircon grains analyzed by CA-TIMS yielded concordant $^{206}Pb/^{238}U$ dates that range from 184.63 ± 0.13 to 183.22 ± 0.13 Ma (Appendix 4); the weighted mean date of the youngest three grains is 183.28 ± 0.07 Ma (MSWD = 2.66, n = 3; Fig. 4-27c).

Sample 14PS120-1 is a coarse-grained quartz porphyritic granodiorite (Aishihik 2 phase) from the northern tip of the Aishihik batholith (Fig. 4-5). It yielded elongate zircons with a length to width ratio of >3:1 and oscillatory zoning; a few grains have CL-bright cores (Fig. 4-28a). LA-ICPMS analyses of 44 zircons have $^{206}Pb/^{238}U$ dates between 2278 and 178 Ma (Fig. 4-28b; Appendix 3). Two inherited cores have Precambrian dates of *ca.* 2278 and 1453 Ma, and another four grains have Paleozoic dates, with two grains at *ca.* 351 and 343 Ma and two at *ca.* 264 and 250 Ma. A xenocryst population of three grains has a weighted mean of 199.1 ± 4.8 Ma, and the youngest 35 grains have a weighted mean of 185.6 ± 1.3 Ma. Six zircon grains from this youngest population were analyzed by CA-TIMS and yielded concordant $^{206}Pb/^{238}U$ dates that range from 184.16 ± 0.13 to 183.91 ± 0.13 Ma (Appendix 4), with a weighted mean date of 184.06 ± 0.05 Ma (MSWD = 1.21, n = 5; Fig. 4-28c).

Sample 14PS165-1 is coarse-grained granite (Aishihik 2 phase) from the central part of the batholith along Long Lake (Fig. 4-5). It yielded zircons with a length to width ratio of <2:1 and oscillatory zoning; CL-dark cores are visible in some grains (Fig. 4-29a). LA-ICPMS analyses of 52 zircons have $^{206}Pb/^{238}U$ dates between 374 and 171 Ma, with inherited populations at *ca.* 325 Ma (n = 4) and *ca.* 230 Ma (n = 2), xenocrysts at 208 and 209 Ma, and a xenocryst population at 196.5 ± 2.8 Ma (n = 7; Fig. 4-29b; Appendix 3). The largest population of analyses has a weighted mean date of 183.8 ± 0.6 Ma (n = 32); the five youngest analyses range from 175 to 171 Ma and are interpreted to have undergone minor Pb loss. Six zircon grains from the dominant population were analyzed by CA-TIMS (Appendix 4). Although all analyses are concordant, their $^{206}Pb/^{238}U$ dates are scattered between 184.68 ± 0.14 and 181.46 ± 0.13 Ma with no overlap in age between grains (Fig. 4-29c). Therefore, the LA-ICPMS date of 183.8 ± 0.6 Ma (MSWD = 1.3; n = 32; Fig. 4-29b) is considered the best estimate of crystallization age for this sample.

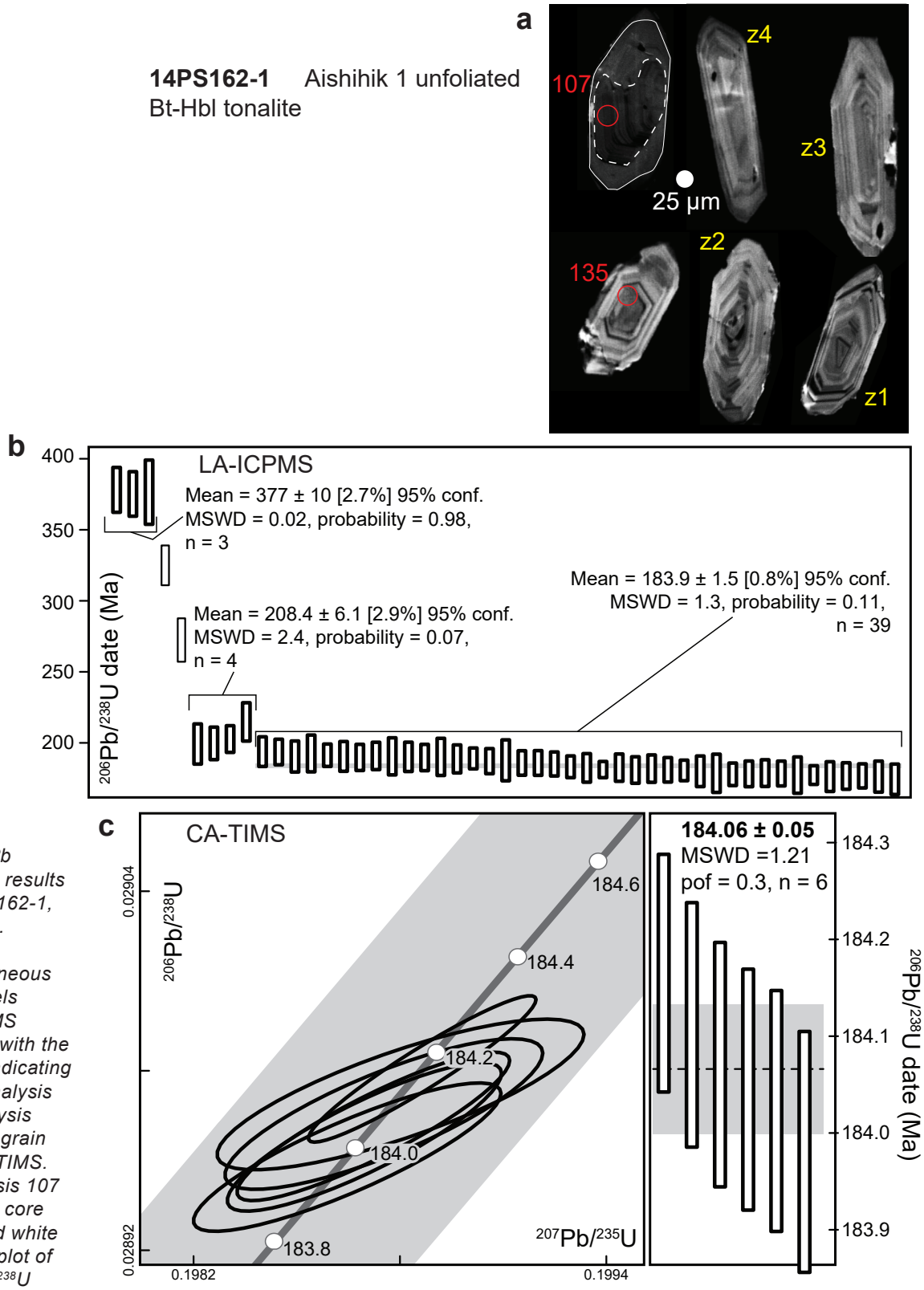


Figure 4-25. *U-Pb geochronological results for sample 14PS162-1, Aishihik batholith.* ***(a)*** *CL images of representative igneous zircons. Red labels indicate LA-ICPMS analysis number with the red open circle indicating location of the analysis spot, yellow analysis number refers to grain analyzed by CA-TIMS. LA-ICPMS analysis 107 from an inherited core outline by dashed white line.* ***(b)*** *Ranked plot of LA-ICPMS $^{206}Pb/^{238}U$ dates (Appendix 3). Grey horizontal bar shows calculated weighted mean with errors.* ***(c)*** *Concordia diagram (left) and ranked $^{206}Pb/^{238}U$ dates (right) for zircons analyzed by CA-TIMS (Appendix 4). The light grey band around concordia (dark grey line) shows the decay constant uncertainties. Analyses included in weighted mean age (light grey horizontal bar) calculations are bold; analyses with thin lines are not used in calculations. Line-type designations are the same in all plots. Errors in all plots are at 2σ. MSWD = mean squared weighted deviation, pof = probability of fit, n = number of analyses included in age calculation.*

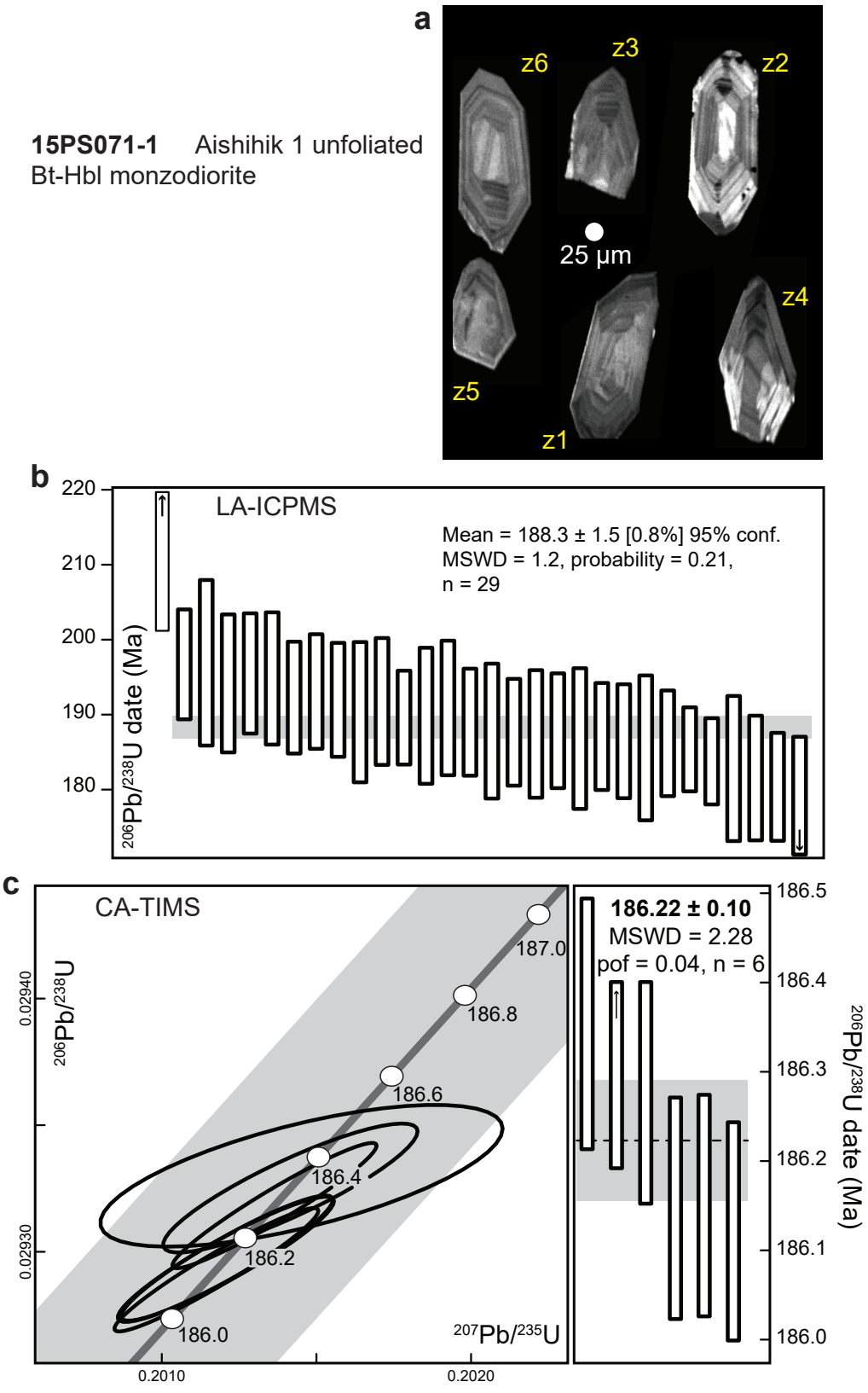


Figure 4-26. *U-Pb geochronological results for sample 15PS071-1, Aishihik batholith.* ***(a)*** *CL images of representative igneous zircons. Yellow analysis number refers to grain analyzed by CA-TIMS.* ***(b)*** *Ranked plot of LA-ICPMS $^{206}Pb/^{238}U$ dates (Appendix 3). Grey horizontal bar shows calculated weighted mean with errors.* ***(c)*** *Concordia diagram (left) and ranked $^{206}Pb/^{238}U$ dates (right) for zircons analyzed by CA-TIMS (Appendix 4). The light grey band around concordia (dark grey line) shows the decay constant uncertainties. Analyses included in weighted mean age (light grey horizontal bar) calculations are bold; analyses with thin lines are not used in calculations. Line-type designations are the same in all plots. Errors in all plots are at 2σ. Arrows indicate data extend beyond plot. MSWD = mean squared weighted deviation, pof = probability of fit, n = number of analyses included in age calculation.*

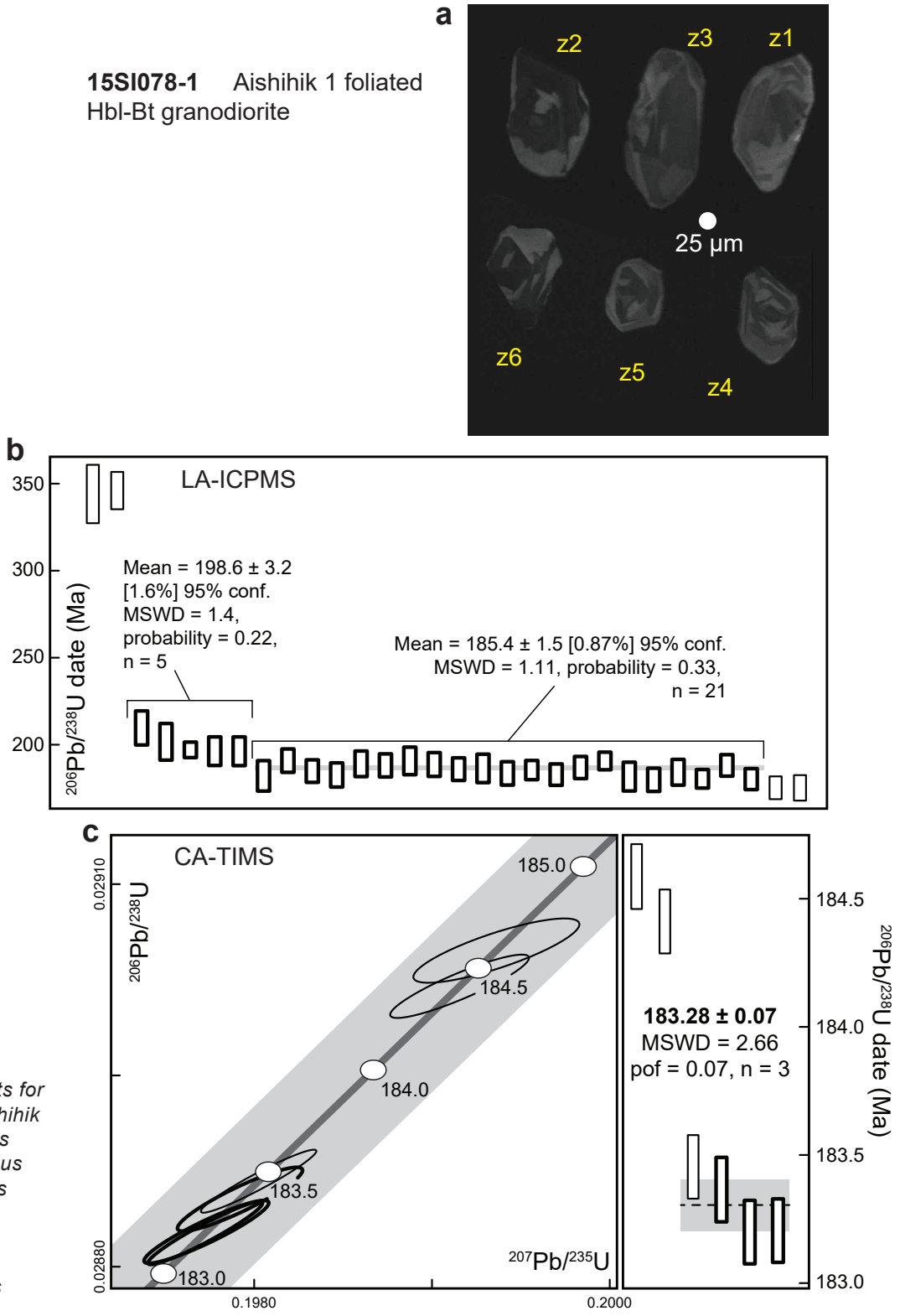


Figure 4-27. *U-Pb geochronological results for sample 15SI078-1, Aishihik batholith.* ***(a)*** *CL images of representative igneous zircons. Yellow analysis number refers to grain analyzed by CA-TIMS.* ***(b)*** *Ranked plot of LA-ICPMS $^{206}Pb/^{238}U$ dates (Appendix 3). Grey horizontal bar shows calculated weighted mean with errors.* ***(c)*** *Concordia diagram (left) and ranked $^{206}Pb/^{238}U$ dates (right) for zircons analyzed by CA-TIMS (Appendix 4). The light grey band around concordia (dark grey line) shows the decay constant uncertainties. Analyses included in weighted mean age (light grey horizontal bar) calculations are bold; analyses with thin lines are not used in calculations. Line-type designations are the same in all plots. Errors in all plots are at 2σ. MSWD = mean squared weighted deviation, pof = probability of fit, n = number of analyses included in age calculation.*

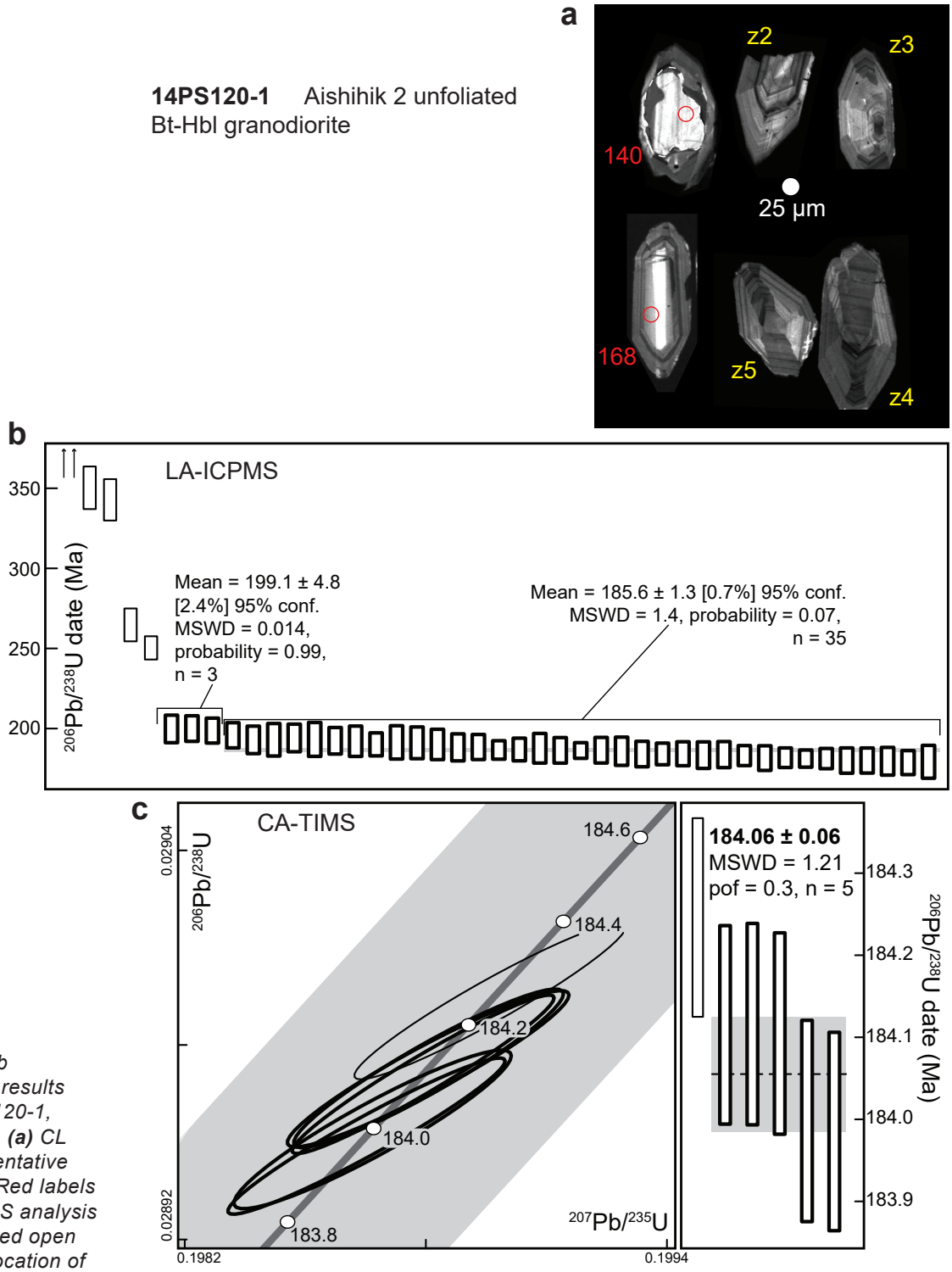


Figure 4-28. *U-Pb geochronological results for sample 14PS120-1, Aishihik batholith.* ***(a)*** *CL images of representative igneous zircons. Red labels indicate LA-ICPMS analysis number with the red open circle indicating location of the analysis spot, yellow analysis number refers to grain analyzed by CA-TIMS. LA-ICPMS analysis 140 from an inherited Paleozoic core outlined by dashed white line, 168 from a xenocryst core.* ***(b)*** *Ranked plot of LA-ICPMS $^{206}Pb/^{238}U$ dates (Appendix 3). Grey horizontal bar shows calculated weighted mean with errors.* ***(c)*** *Concordia diagram (left) and ranked $^{206}Pb/^{238}U$ dates (right) for zircons analyzed by CA-TIMS (Appendix 4). The light grey band around concordia (dark grey line) shows the decay constant uncertainties. Analyses included in weighted mean age (light grey horizontal bar) calculations are bold; analyses with thin lines are not used in calculations. Line-type designations are the same in all plots. Errors in all plots are at 2σ. Arrows indicate data extend beyond plot. MSWD = mean squared weighted deviation, pof = probability of fit, n = number of analyses included in age calculation.*

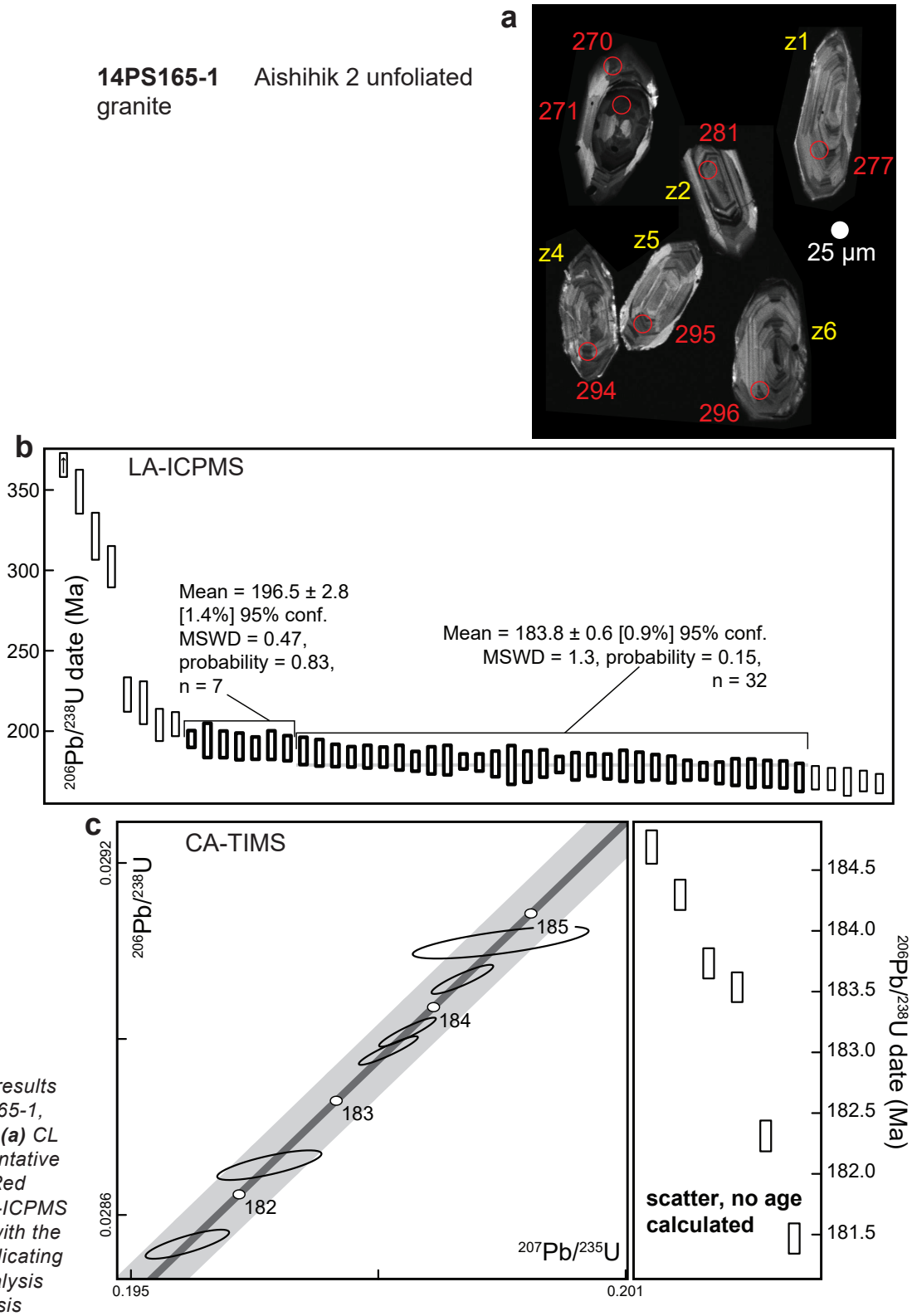


Figure 4.29. *U-Pb geochronological results for sample 14PS165-1, Aishihik batholith.* ***(a)*** *CL images of representative igneous zircons. Red labels indicate LA-ICPMS analysis number with the red open circle indicating location of the analysis spot, yellow analysis number refers to grain analyzed by CA-TIMS.* ***(b)*** *Ranked plot of LA-ICPMS $^{206}Pb/^{238}U$ dates (Appendix 3). Grey horizontal bar shows calculated weighted mean with errors.* ***(c)*** *Concordia diagram (left) and ranked $^{206}Pb/^{238}U$ dates (right) for zircons analyzed by CA-TIMS (Appendix 4). The light grey band around concordia (dark grey line) shows the decay constant uncertainties. Analyses are too scattered for an age calculation. Line-type designations are the same in all plots. Errors in all plots are at 2σ. Arrows indicate data extend beyond plot. MSWD = mean squared weighted deviation, pof = probability of fit, n = number of analyses included in age calculation.*

$^{40}Ar/^{39}Ar$

Mineral separates from nine samples of granitoid rocks from the Aishihik batholith were selected for $^{40}Ar/^{39}Ar$ analyses at the GSC laboratory in Ottawa (laser, step-heating; Appendix 6). Biotite was separated from all samples, but only eight contained hornblende. Six of these samples are from the Aishihik 1 phase, one foliated monzodiorite (14PS123-1) and five massive tonalite to monzodiorite (14PS131-1, 14PS153-1, 14PS159-1, 14PS162-1 and 14PS167-1), and three samples are granodiorite of the Aishihik 2 phase (14PS125-1, 14PS136-1 and 14PS150-1; Appendix 6).

Hornblende and biotite from the foliated Aishihik 1 sample (14PS123-1) yielded equivalent plateau ages at 180.5 ± 1.6 and 180.6 ± 1.2 Ma, respectively (Fig. 4-30a,c). Another aliquot of biotite yielded a slightly older plateau age at 183.7 ± 1.0 Ma (Fig. 4-30b). The five unfoliated samples yielded hornblende ages between 181.8 ± 1.5 and 179.9 ± 1.5 Ma, with broadly coeval to slightly younger biotite ages between 182.0 ± 3.0 and 177.8 ± 1.1 Ma (Figs. 4-31 to 4-33). Two samples of Aishihik 2 granodiorite from the northern part of the batholith, 14PS125-1 and 14PS136-1, have hornblende ages of 180.3 ± 1.4 and 184.0 ± 1.3 Ma, respectively (Fig. 4-34). Biotite from these samples yielded ages of 182.2 ± 1.1 and 181.4 ± 1.0 Ma, respectively. Another sample of Aishihik 2 granodiorite north of Kirkland Creek (14PS150-1) contains biotite that yielded a similar plateau age of 182.4 ± 1.2 Ma (Fig. 4-34e).

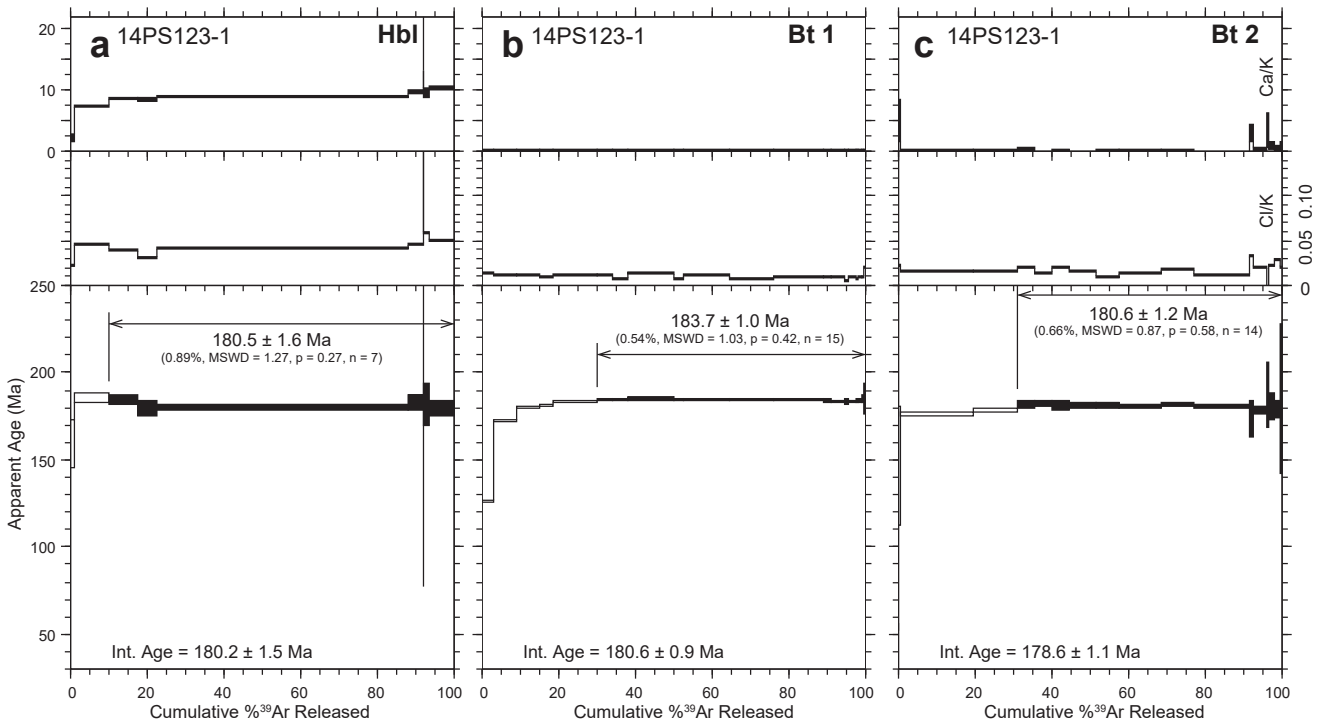


Figure 4-30. *$^{40}Ar/^{39}Ar$ age spectra for foliated sample of the intermediate phase (1a) from the northern margin of the Aishihik batholith.* ***(a)*** *Hornblende, 14PS123-1;* ***(b)*** *biotite, 14PS123-1;* ***(c)*** *biotite, 14PS123-1. Steps included in plateau are shown in black. Int. = integrated. Errors are 2σ.*

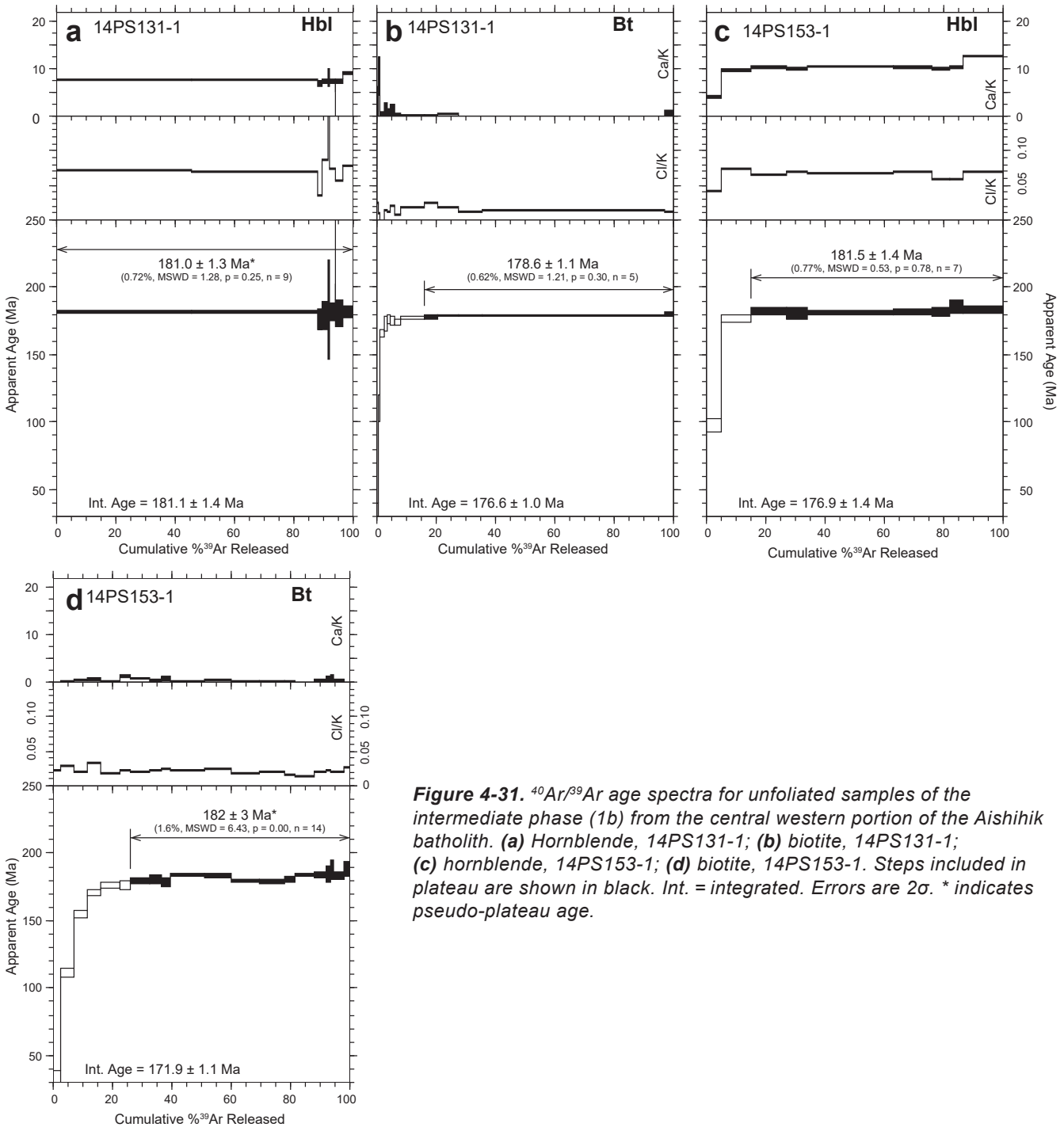


Figure 4-31. *$^{40}Ar/^{39}Ar$ age spectra for unfoliated samples of the intermediate phase (1b) from the central western portion of the Aishihik batholith.* ***(a)*** *Hornblende, 14PS131-1;* ***(b)*** *biotite, 14PS131-1;* ***(c)*** *hornblende, 14PS153-1;* ***(d)*** *biotite, 14PS153-1. Steps included in plateau are shown in black. Int. = integrated. Errors are 2σ. * indicates pseudo-plateau age.*

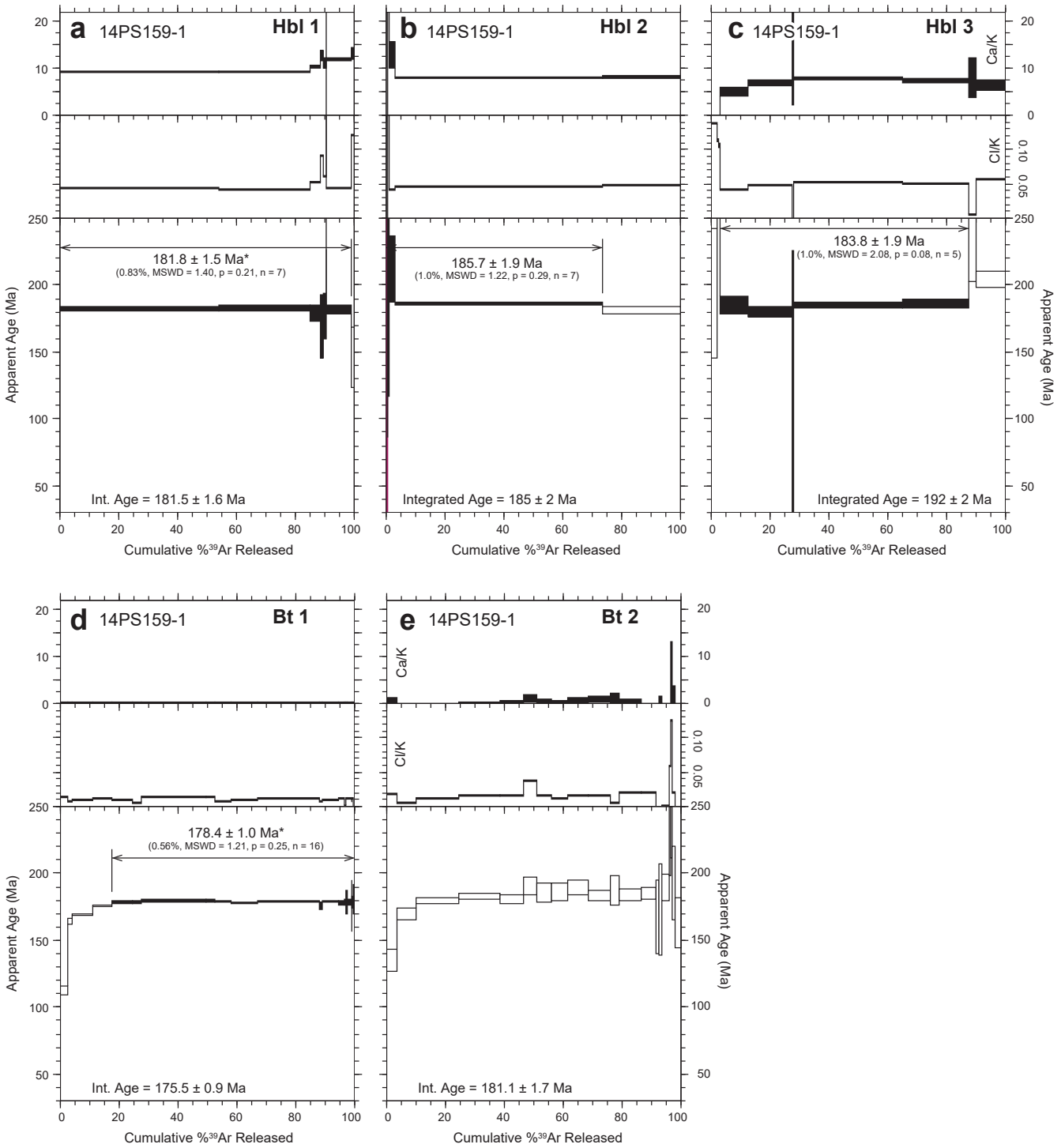


Figure 4-32. *$^{40}Ar/^{39}Ar$ age spectra for an unfoliated sample of the intermediate phase (1b) from the central western portion of the Aishihik batholith.* ***(a** to **c)** Hornblende, 14PS159-1; **(c** and **d)** biotite, 14PS159-1. Steps included in plateau are shown in black. Int. = integrated. Errors are 2σ. * indicates pseudo-plateau age.*

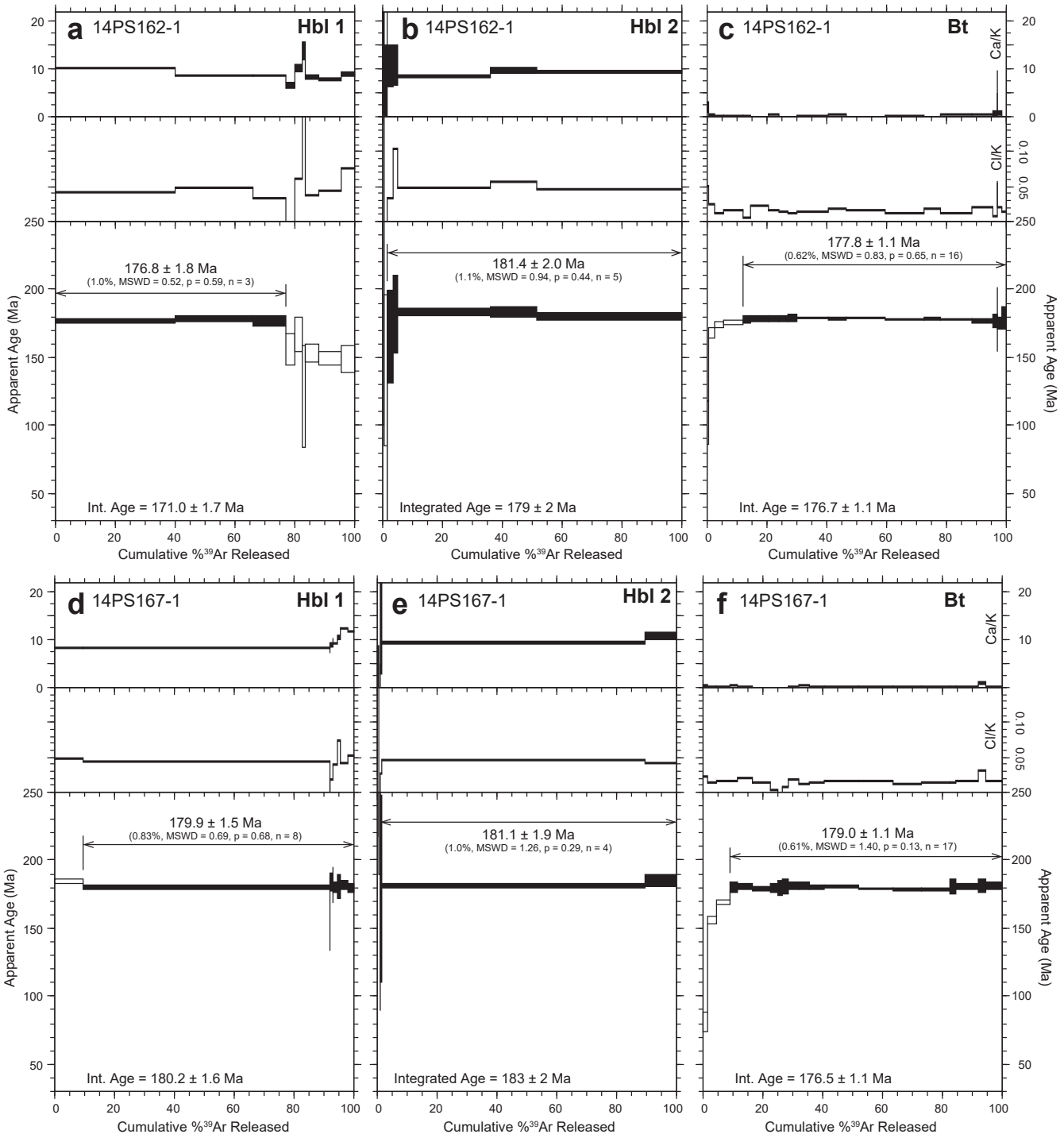


Figure 4-33. *$^{40}Ar/^{39}Ar$ age spectra for a samples of the intermediate phase (1b) from the southern portion of the Aishihik batholith.* ***(a)*** *and* ***(b)*** *Hornblende, 14PS162-1;* ***(c)*** *biotite, 14PS162-1;* ***(d)*** *and* ***(e)*** *hornblende, 14PS167-1;* ***(f)*** *biotite, 14PS167-1. Steps included in plateau are shown in black. Int. = integrated. Errors are 2σ.*

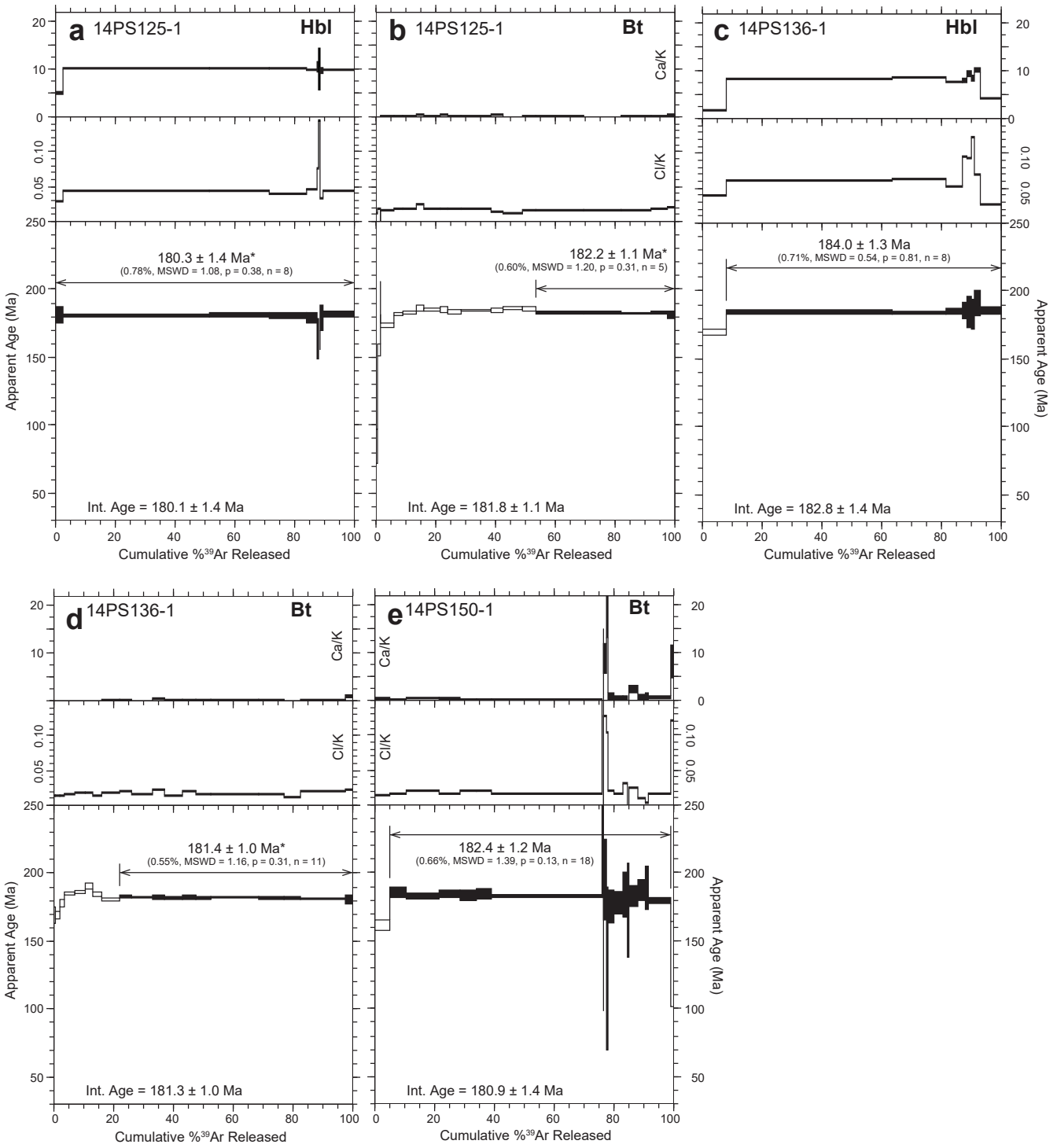


Figure 4-34. *$^{40}Ar/^{39}Ar$ age spectra for samples of the felsic to intermediate phase (2) from the northern portion of the Aishihik batholith.* ***(a)*** *Hornblende, 14PS125-1;* ***(b)*** *biotite, 14PS125-1;* ***(c)*** *hornblende, 14PS136-1;* ***(d)*** *biotite, 14PS136-1;* ***(e)*** *biotite, 14PS150-1. Steps included in plateau are shown in black. Int. = integrated. Errors are 2σ. * indicates pseudo-plateau age.*

Summary of geochronological results

Results of high-precision CA-TIMS dating of zircons from the Aishihik batholith indicate that it was intruded between *ca.* 186 and 183 Ma, and that both Aishihik 1 and 2 phases are broadly coeval (Fig. 4-35), as suggested by gradational contacts between them. The intermediate Aishihik 1 phase yielded slightly older dates up to 186.22 ± 0.10 Ma (Fig. 4-26), consistent with previous TIMS and SIMS dates from this phase (Fig. 4-25; Appendix 1; Johnston *et al.*, 1996; Joyce *et al.*, 2016), but overlaps with the felsic Aishihik 2 phase at *ca.* 184 Ma (Fig. 4-35). This is broadly consistent with previous TIMS and SIMS dates, although some SIMS results suggest the more felsic Aishihik 2 phase could extend as young as *ca.* 181 Ma (Fig. 4-35; Johnston *et al.*, 1996; Hart, 1997a; Joyce *et al.*, 2016). Additional CA-TIMS dating of the Aishihik 2 phase is required to test this hypothesis.

A few of the high-precision CA-TIMS dates presented here provide constraints on older, less precise multi-grain TIMS and single-grain SIMS analyses. Sample 15PS071-1 (186.22 ± 0.10 Ma; Fig. 4-26) was collected near locality QM-87-92 of Johnston *et al.* (1996) which yielded a date of 187.7 ± 0.6 Ma from two titanite fractions (Fig. 4-5). Our results confirm that this is an older portion of the Aishihik batholith but provide a more precise estimate of its crystallization. Sample 14PS120-1 (184.06 ± 0.05 Ma; Fig. 4-28) is from a granite of the Aishihik 2 phase in the northern part of the batholith similar to that of CDB10-106 of Joyce *et al.* (2016) which yielded a SIMS date of 183 ± 2 Ma. The more precise CA-TIMS date is considered the best estimate of the crystallization age of Aishihik 2 granite phase in the northern part of the batholith.

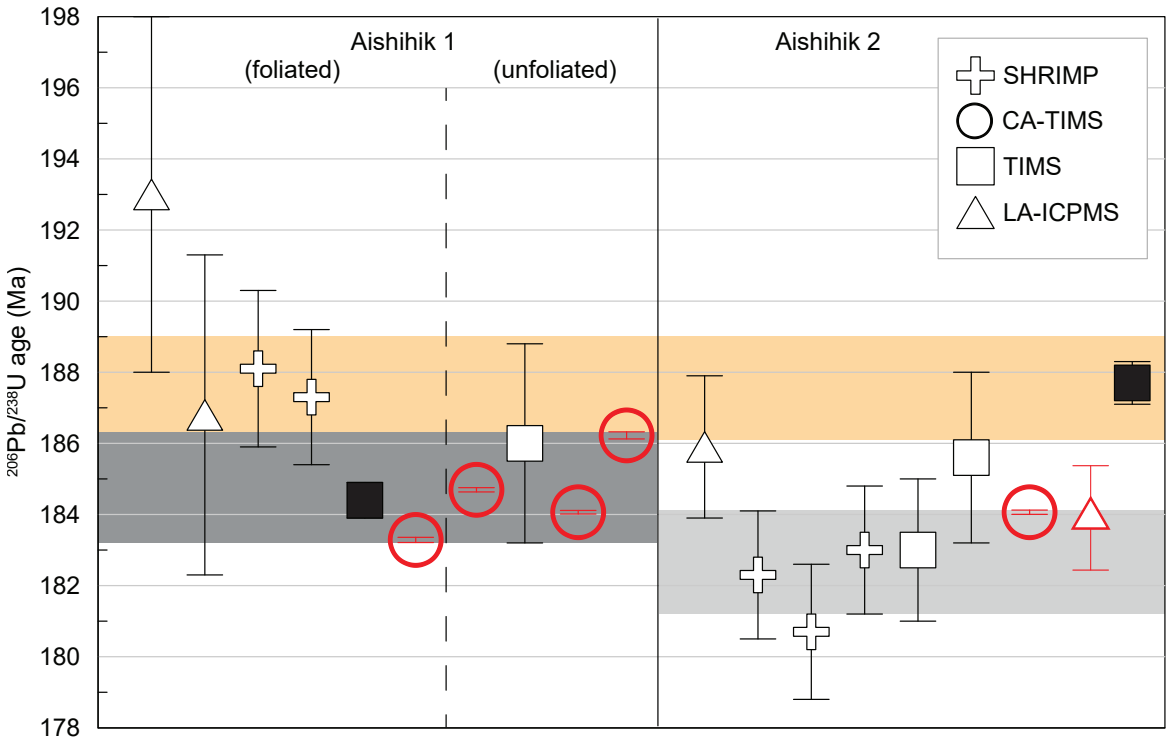


Figure 4-35. *Summary of U-Pb dates for granitoid samples of the Aishihik batholith (Appendix 1). All dates are shown with 2σ errors. SIMS zircon dates from Joyce et al. (2016); LA-ICPMS zircon dates from Joyce et al. (2016) and this study; TIMS multi-grain zircon (white square) from Hart (1997a) and Johnston et al. (1996), and titanite (black square) from Johnston et al. (1996); CA-TIMS dates are from this study (Appendix 4). Samples analyzed for this study are shown with red outlines. Orange interval in background indicates the range of dates from pyroclastic rocks in the Whitehorse trough (e.g., Nordenskiöld facies of the Laberge Group; Colpron and Friedman, 2008). Dark grey interval represents range of crystallization ages between 186 and 183 Ma for Aishihik 1 phase. Light grey represents range of crystallization ages between 184 and 181 Ma for Aishihik 2 phase.*

Sample 14PS165-1 failed to yield a precise CA-TIMS date, but its LA-ICPMS date of 183.8 ± 0.6 Ma (Fig. 4-29) is considered more reliable than discordant TIMS results of Johnston *et al.* (1996; sample STJ-86-82) collected at the same locality and yielding a lower-intercept date of 185.6 ± 2.4 Ma (Appendix 1). Our LA-ICPMS data are consistent with two SIMS dates (182 ± 2 and 181 ± 2 Ma) from the same granite body southeast of Long Lake (Fig. 4-5).

The new $^{40}Ar/^{39}Ar$ data indicate cooling of the Aishihik batholith shortly after intrusion of its two main phases, with hornblende dates of *ca.* 184–180 Ma and biotite between *ca.* 182 and 178 Ma (Fig. 4-36). These Early Jurassic cooling dates are consistently older than previous mid-Jurassic K-Ar dates (Wanless *et al.*, 1978). In general, $^{40}Ar/^{39}Ar$ biotite cooling ages appear to be older in the northern part of the Aishihik batholith and younger to the south (Figs. 4-37 and 4-38).

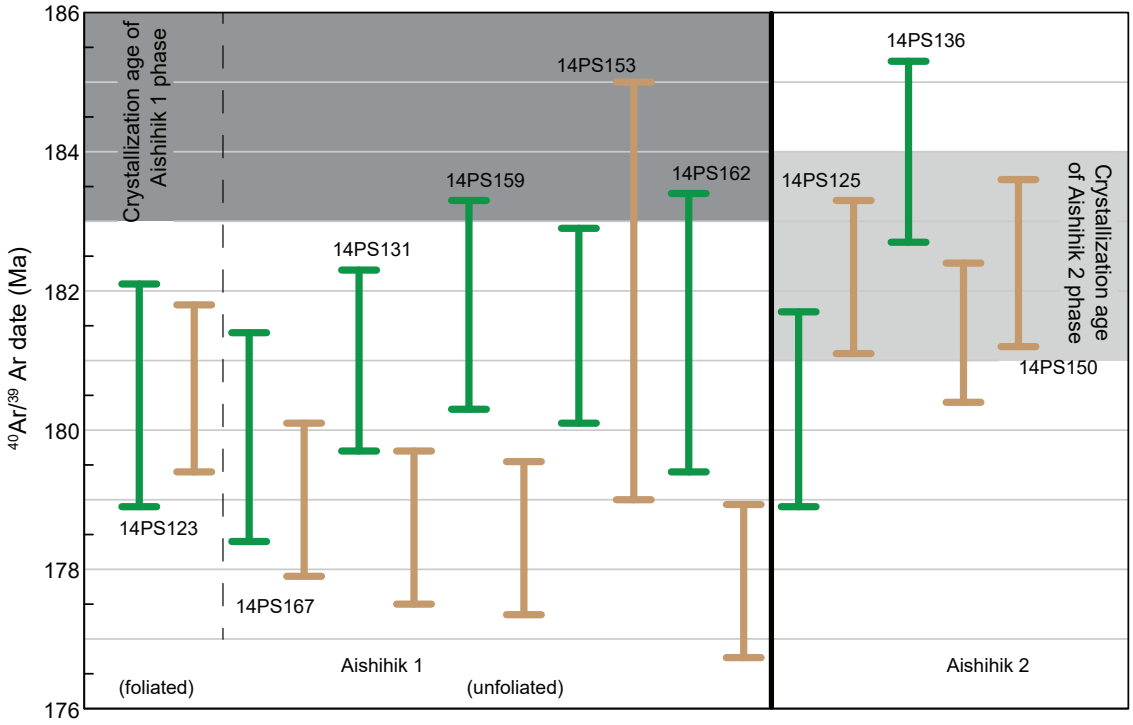


Figure 4-36. *Summary of $^{40}Ar/^{39}Ar$ dates from the Aishihik batholith. Dark grey band indicates range of U-Pb crystallization dates from the Aishihik 1 phase of the batholith (ca. 186 to 183 Ma Ma), light grey indicates range of U-Pb crystallization dates from the Aishihik 2 phase of the batholith (184 to 181 Ma). Errors are 2σ.*

Thermobarometry

Seven samples from the Aishihik batholith contain the suitable mineral assemblage for Al-in-Hbl geobarometry (Hammarstrom and Zen, 1986; Appendix 5); three of these (MA14-AB1, 8, 10) were first reported in Topham *et al.* (2016) and are recalculated here using a more straightforward approach to determining average hornblende composition in a given sample. These samples, and 15PS071-1, are from the northern portion of the batholith (Fig. 4-37). The three remaining samples are from the central and southern portions of the Aishihik batholith. Al^{TOT} in hornblende from the northern samples is 1.79–1.17 and cotectic plagioclase has X_{An} of 0.38 to 0.21, with crystallization pressure estimates of 4.16 ± 1.0 to 2.28 ± 1.25 kbar (Appendix 5; emplacement depths of 15.7 to 8.6 km) and solidus temperatures of 697–764°C. Al^{TOT} in hornblende from the central and southern samples are 2.13-1.75 and cotectic plagioclase has X_{An} of 0.33 to 0.27, indicating crystallization pressure estimates of 6.0 ± 1.0 to 4.52 ± 0.79 kbar (Appendix 5; emplacement depths of 22.7 to 17.1 km) and solidus temperatures of 731–739°C. The higher, 6 kbar pressure estimate is from a sample of Aishihik 1 granodiorite from the southern part of the batholith (14PS162-1; Figs. 4-5 and 4-37). This sample also contains magmatic epidote (Fig. 4-19) which is consistent with a deep emplacement depth and is dated at 184.06 ± 0.05 Ma (Fig. 4-25).

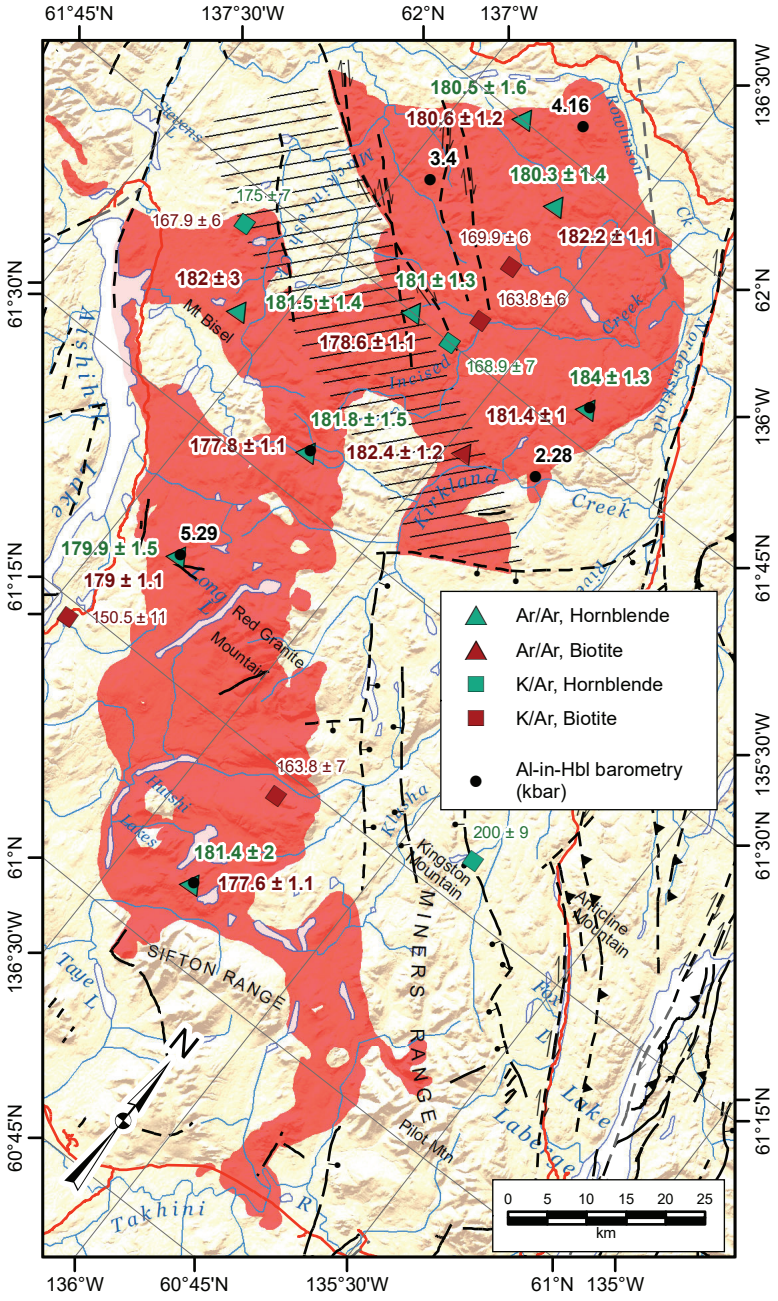


Figure 4-37. *Map of Aishihik batholith with Al-in-Hbl pressure estimates and hornblende (green) and biotite (brown) cooling ages. Hatched area indicates step in the floor of the batholith across a series of northwest-striking faults (Figs. 4-5 and 4-7), with the northern part of the batholith showing shallower depth to floor of the batholith. Note that the geographic reference frame has been rotated with North pointing to the upper right of the page. Fault symbology as in Figure 1-4.*

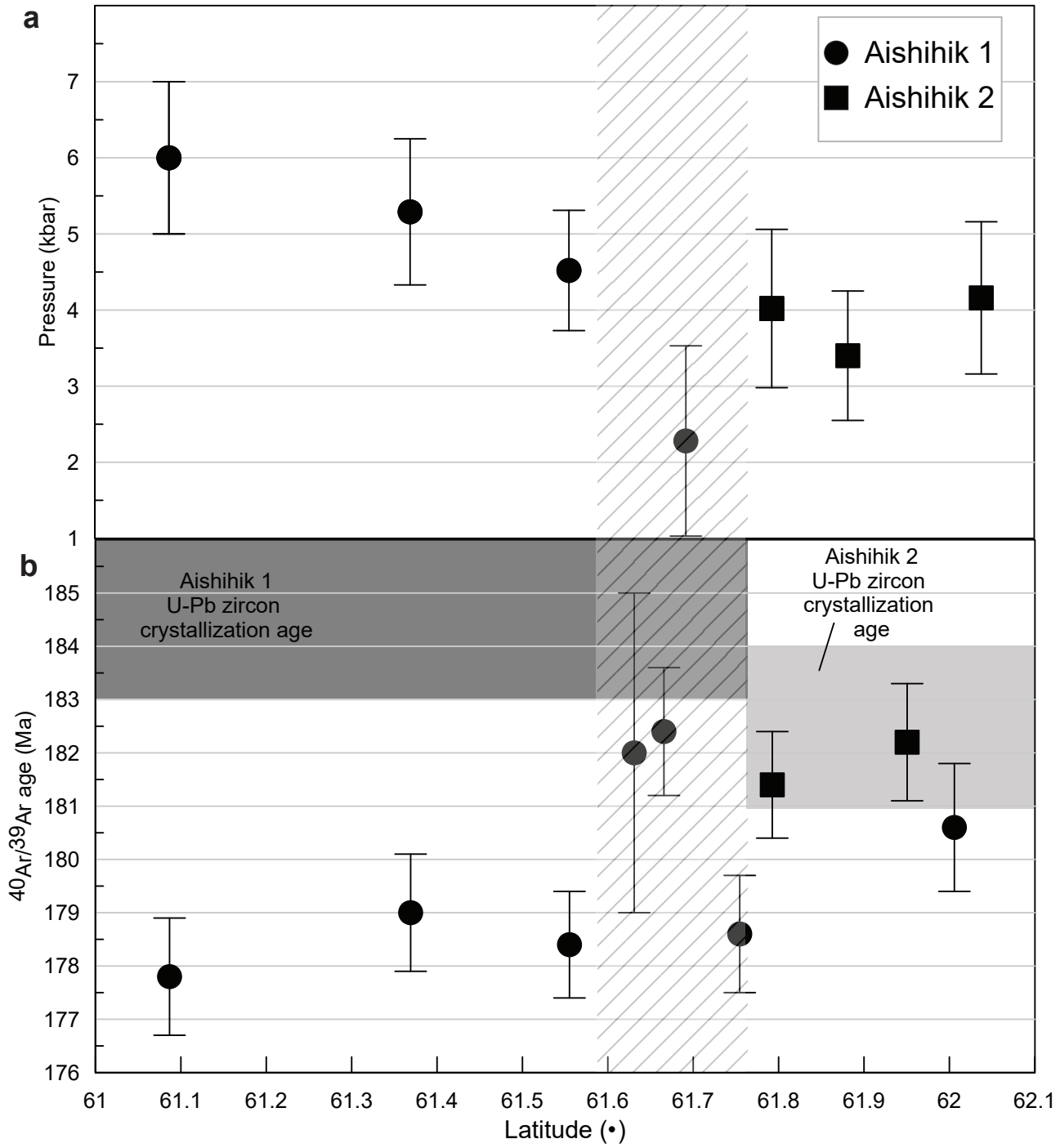


Figure 4-38. *Variation in Al-in-hornblende pressure estimates* ***(a)*** *and $^{40}Ar/^{39}Ar$ biotite cooling age* ***(b)*** *with latitude. Dark grey band indicates range of U-Pb crystallization dates from the Aishihik 1 phase of the batholith (ca. 186 to 183 Ma), light grey indicates range of U-Pb crystallization dates from the Aishihik 2 phase of the batholith (184 to 181 Ma). Errors are 2σ. Hatched area shows approximate latitudes where a step in the floor of the batholith is modelled (Fig. 4-7), with shallower depth in the north.*

Big Creek batholith

The Big Creek batholith is located 60 km northwest of Carmacks (Fig. 1) in the eastern Dawson Range, south of Big Creek. The batholith is a northwest elongate body with a mapped surface extent of 348 km² that is mostly located south of the Big Creek fault (Fig. 4-39; Table 4-1; Allan and Friend, 2018; Friend *et al.*, 2018). A series of small (≤10 km²) separate bodies, concordant with regional foliation and located north of the Big Creek fault, between the Big Creek and Granite Mountain batholiths, are of similar alkalic lithology (Allan and Friend, 2018) and are described here with the Big Creek batholith.

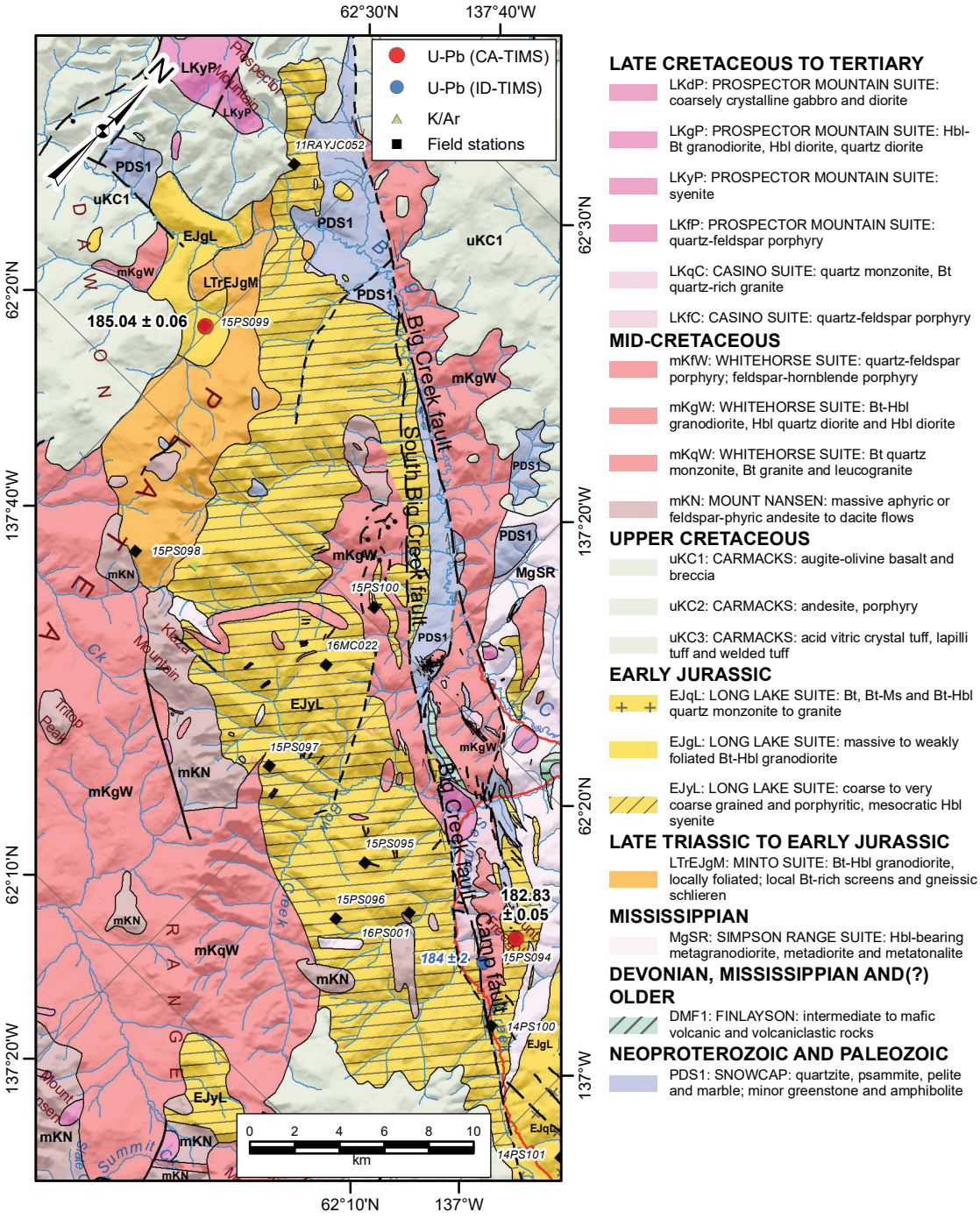


Figure 4-39. *Geology map of the Big Creek batholith area (YGS, 2020a); fault symbology as in Figure 1-4. Note that the geographic reference frame has been rotated with North pointing to the upper right of the page.*

The northern margin of the batholith intrudes Paleozoic metasedimentary rocks of the Snowcap assemblage and metaplutonic rocks of the Simpson Range suite, Yukon-Tanana terrane (Fig. 4-39; Allan and Friend, 2018). To the south, the batholith is intruded by younger biotite-hornblende granodiorite of the mid-Cretaceous Whitehorse suite and unconformably overlain by intermediate volcanic rocks of the mid-Cretaceous Mount Nansen Group (Carlson, 1987). The western and eastern margins are unconformably overlain by Upper Cretaceous basalt of the Carmacks Group (Tempelman-Kluit, 1984; Ryan *et al.*, 2013).

The area around the batholith lies outside Quaternary glacial limits and is deeply weathered (Fig. 4-9; Jackson, 1997a). The landscape consists of rounded hilltops with subdued outcrop or subcrop (Fig. 4-40a) dissected by over-steepened valleys. Outcrop is mostly found on ridges as tors and subcrop (Fig. 4-40b, c) and in stream and road cuts.

Petrography

Two phases are present within the Big Creek batholith. In the western part of the batholith (Fig. 4-39), and locally throughout, is a relatively minor granodiorite phase. The majority of the pluton is more alkalic, with composition ranging from syenite to monzonite to granite on the QAP classification determined primarily by modal abundance of K-feldspar phenocrysts (Fig. 4-2a). The granodiorite phase is medium grained, equigranular (Fig. 4-41), and containing more biotite than hornblende, totaling 10–20%. Biotite is commonly moderately to intensely altered to chlorite while hornblende, when present, is unaltered to weakly chlorite altered (Fig. 4-42a). Epidote is a ubiquitous accessory mineral and is present as a secondary mineral. Titanite is present in most, but not all samples of this phase. The granodiorite phase commonly has micrographic intergrowths of quartz and plagioclase (Fig. 4-42b) which may indicate simultaneous crystallization in the presence of a hydrous fluid phase (Barker, 1970).

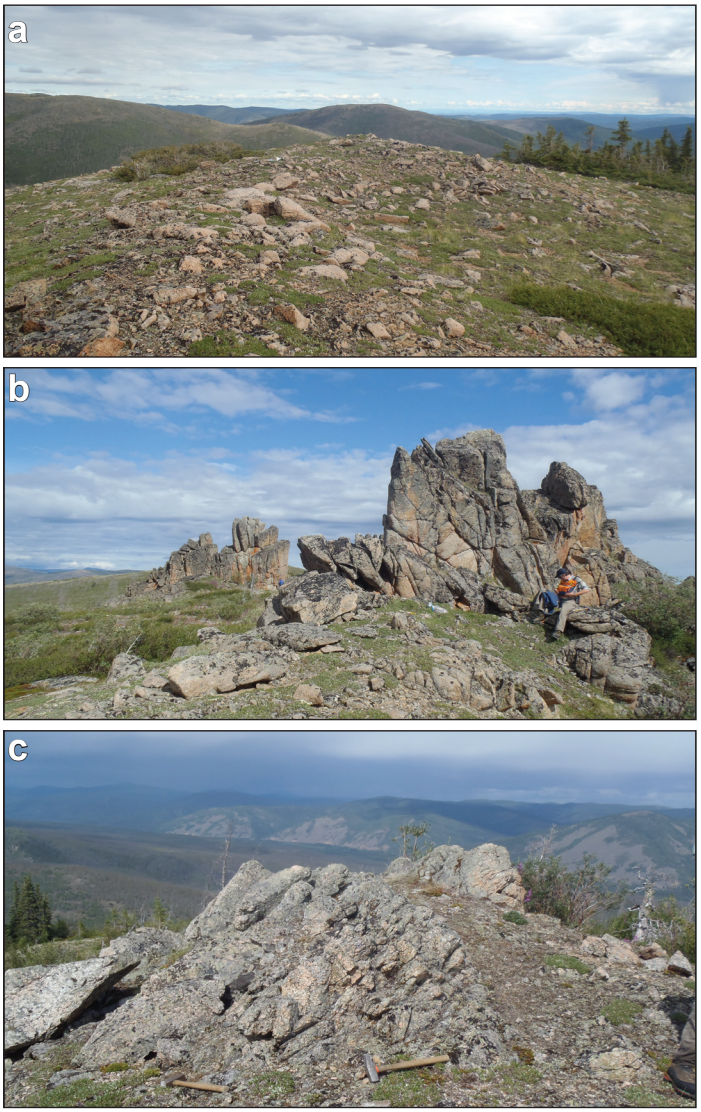


Figure 4-40. *Landscapes and outcrops in the Big Creek batholith area.* ***(a)*** *Weathered subcrop from the granodiorite phase west of Bow Creek in the southeastern portion of the batholith; 15PS097.* ***(b)*** *Granodiorite tors on the ridge above Caribou Creek, a tributary to Seymour Creek in the southeastern portion of the batholith; 15PS096.* ***(c)*** *Blocky weathering coarse-grained porphyritic granodiorite in the northwestern portion of the batholith; 15PS099.*

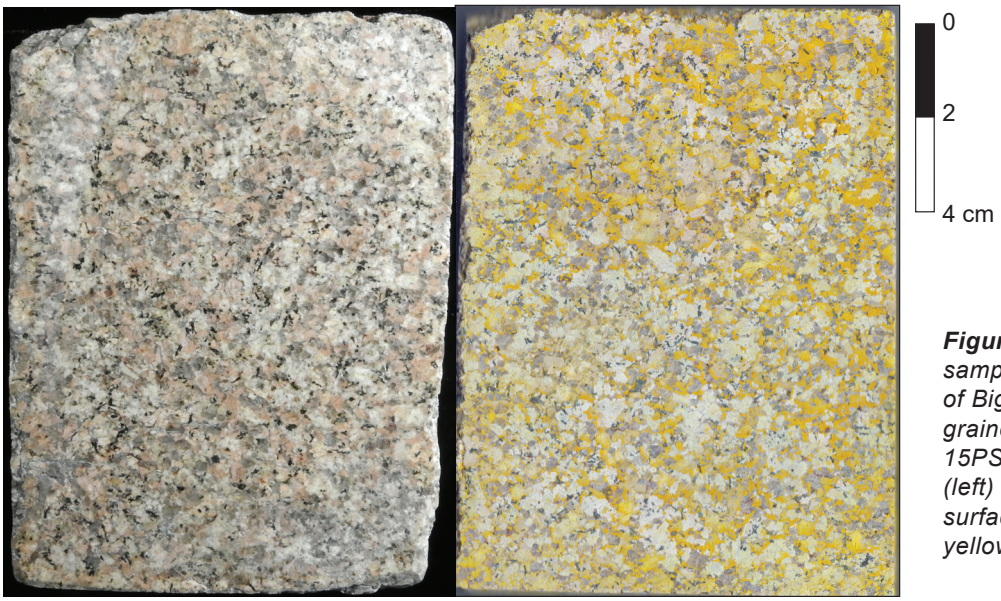


Figure 4-41. *Representative sample from the granodiorite phase of Big Creek batholith. Medium-grained equigranular granodiorite; 15PS097-1. Fresh polished surface (left) and a cobaltinitrite-stained surface (right). Note K-feldspar is yellow, both images are same scale.*

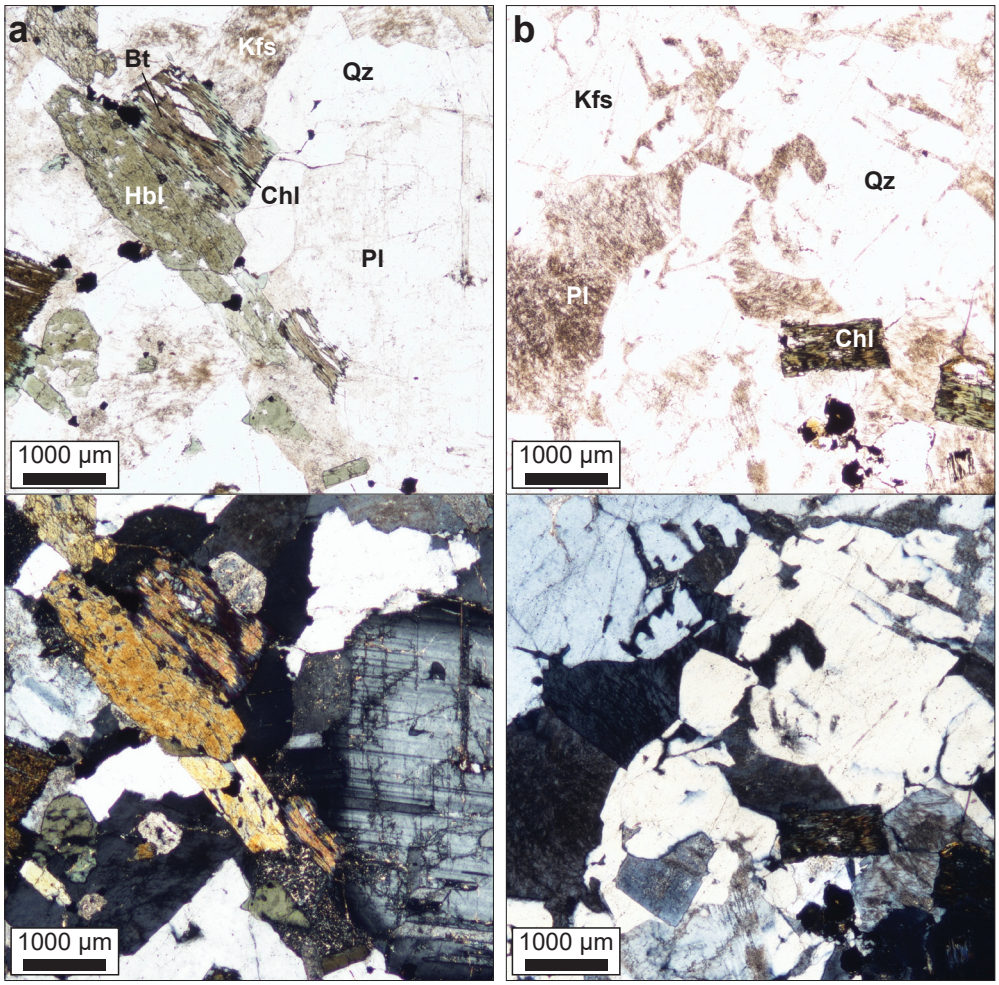


Figure 4-42. *Representative photomicrographs from the granodiorite phase of the Big Creek batholith; plane polarized light (upper) and cross-polarized light (lower).* ***(a)*** *Chlorite altered biotite and fresh hornblende; 15PS096-1.* ***(b)*** *Chlorite altered biotite and micrographic intergrowths of plagioclase with quartz and K-feldspar; 15PS097-1.*

The alkalic phase is distinct with its coarse-grained, equigranular to porphyritic texture and abundant K-feldspar phenocrysts ≤5 cm long (Figs. 4-43 and 4-44). Hornblende is the dominant mafic mineral with trace to absent biotite; hornblende is typically poikilitic (Fig. 4-45a,b). Plagioclase is weakly to moderately saussuritized and K-feldspar is fresh to weakly sericitized. Accessory minerals include titanite, magnetite, epidote and apatite; epidote is found with both feldspars and mafic minerals. All epidote is interpreted as secondary because the mafic minerals that are proximal to epidote are chlorite altered and the epidote is anhedral with a mottled appearance (Fig. 4-45c).

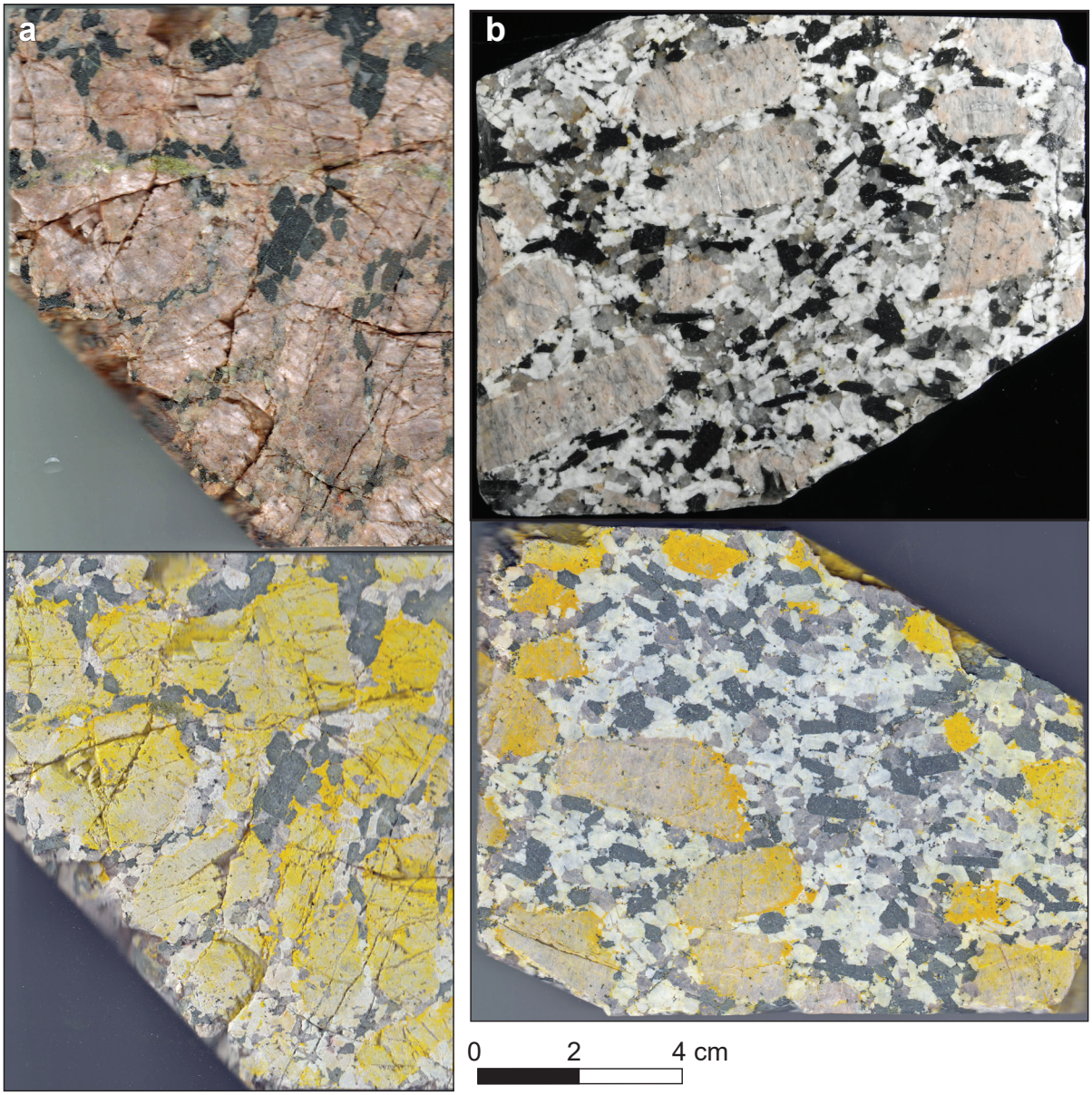


Figure 4-43. *Representative samples from the alkalic phase of Big Creek batholith.* ***(a)*** *Coarse-grained, porphyritic syenite from the largest body between Big Creek and Granite Mountain batholiths; 15PS094-1.* ***(b)*** *Coarse-grained, K-feldspar porphyritic granodiorite from the central portion of the Big Creek batholith, 15PS100-1. For both samples, fresh polished surface (upper) and a cobaltinitrite-stained surface (lower). Note K-feldspar is yellow, all images are same scale.*

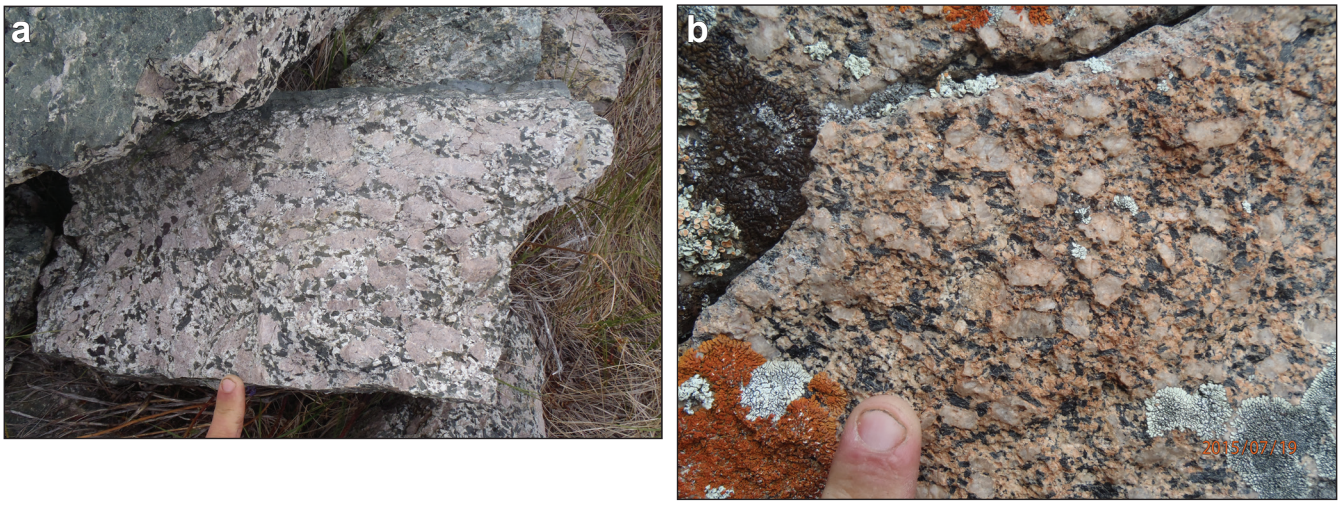


Figure 4-44. *Outcrops of the alkalic phase from the Big Creek batholith showing the distinct coarse grain size and pink K-feldspar crystals.* ***(a)*** *15PS094;* ***(b)*** *15PS099. Finger for scale.*

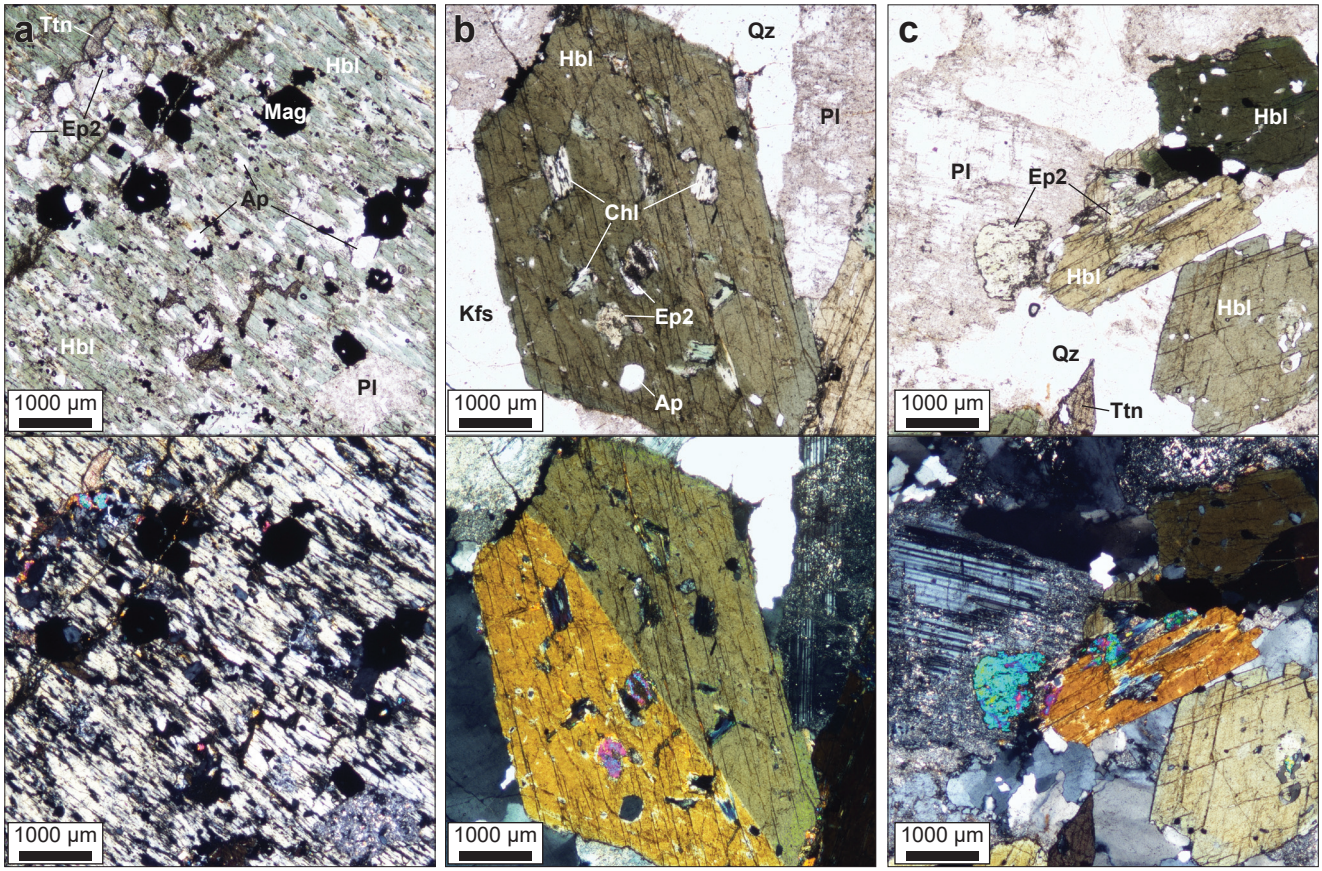


Figure 4-45. *Transmitted light photomicrographs of alkalic phase of Big Creek batholith; plane polarized light (upper) and cross-polarized light (lower).* ***(a)*** *Poikilitic hornblende phenocryst, larger than field of view, with abundant magnetite and apatite inclusions; 15PS094-1.* ***(b)*** *Twinned, poikilitic hornblende phenocryst with chlorite altered biotite and epidote inclusions.* ***(c)*** *Epidote with plagioclase and chlorite altered hornblende. (b) and (c) from 16PS001-1.*

Oxidation state and mineral occurrences

Both phases of the Big Creek batholith are oxidized with susceptibilities ranging from 6.4 to 12.1 × 10^{-3} SI units (mean 9.4 × 10^{-3} SI units; n = 3) for granodiorite and 12.7 to 40.5 × 10^{-3} SI units (mean = 31.3 × 10^{-3} SI units; n = 6) for the alkalic phase (Fig. 4-3a; Appendix 2). There are more than 20 mineral occurrences in the Big Creek area, including 4 porphyry deposits, 1 skarn deposit, two vein gold deposits, and 6 drilled occurrences (Fig. 4-46). All of the known occurrences appear to be related to mid-Cretaceous and younger magmatism (Allan and Friend, 2018). An Early Jurassic age (182.6 ± 2.4 Ma, CA-TIMS titanite) has been proposed for an early stage of skarn mineralization at the Nucleus deposit that was subsequently overprinted by *ca.* 76–75 Ma porphyry mineralization (Bineli Betsi *et al.*, 2016). However, the Early Jurassic Big Creek batholith (*ca.* 185–183 Ma; *see* below) is the host of the Late Cretaceous mineralization at Nucleus (Carlson, 1987; Allan and Friend, 2018), and titanite is a common accessory mineral of the Big Creek batholith as both inclusions in hornblende phenocrysts and as a primary igneous phase (*e.g.*, Fig. 4-45a,c, respectively). The textural evidence provided by Bineli Betsi *et al.* (2016, their fig. 14, p. 448) is ambiguous and it cannot be ruled out that titanite in their sample is inherited from the host Early Jurassic Big Creek batholith.

Geochronology

Stevens *et al.* (1982b) provided the first age constraints on the Big Creek batholith by dating hornblende separates using the K/Ar method which yielded dates ranging from 142 ± 10 to 184 ± 7 Ma. Hornblende from another sample of coarse-grained alkalic phase collected near the Big Creek fault yielded a slightly older Early Jurassic K/Ar date of 188.8 ± 3.8 Ma (Hunt and Roddick, 1991). Multi-grain zircon and titanite fractions from the same sample

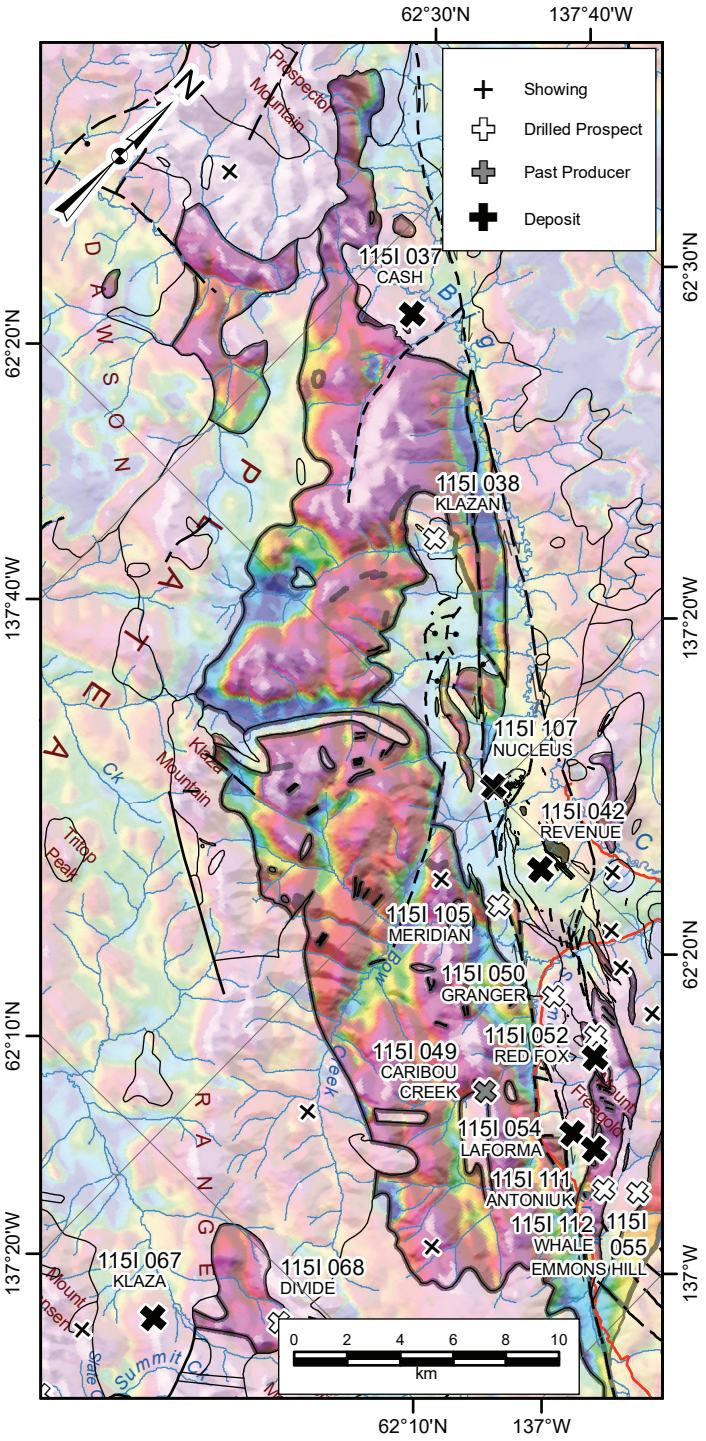


Figure 4-46. *Residual total field aeromagnetic map of the Big Creek batholith area (Hayward and Oneschuk, 2011) illustrating location of MINFILE occurrences. Note that the geographic reference frame has been rotated with North pointing to the upper right of the page. Fault symbology as in Figure 1-4.*

were analyzed by the TIMS method and yielded U-Pb dates of 197 ± 1 and 184 ± 2 Ma, respectively (J.K. Mortensen, unpublished data *in* YGS, 2020c; Fig. 4-39). We present CA-TIMS dates for both the granodiorite and syenite-monzonite phases of the Big Creek batholith.

Sample 15PS099-1 is from medium-grained granodiorite collected near the western edge of the batholith (Fig. 4-39). It yielded stubby zircons with a length to width ratio of <2:1 and oscillatory zoning; one grain has a xenocrystic core and one is an antecryst (Fig. 4-47a). LA-ICPMS analyses of 39 zircons resulted in $^{206}Pb/^{238}U$ dates between 216 and 173 Ma, and the youngest 37 grains yield a weighted mean date of 185.4 ± 1.5 Ma (Fig. 4-47b; Appendix 3). Six zircon grains analyzed by CA-TIMS yielded concordant $^{206}Pb/^{238}U$ dates that range from 185.27 ± 0.13 to 184.97 ± 0.13 Ma (Appendix 4); the youngest five grains have a weighted mean date of 185.04 ± 0.06 Ma (MSWD = 1.11, n = 5; Fig. 4-47c). This more precise date is considered the crystallization age of the granodiorite phase in the Big Creek batholith.

Sample 15PS094-1 is from coarse-grained syenite in an exploration trench on Mount Freegold, northeast of the Big Creek fault (Fig. 4-39). This lithology is typical of the majority of the Big Creek batholith (Fig. 4-43). This sample yielded elongate zircons with a length to width ratio of >3:1 and oscillatory zoning; one grain has an inherited core (Fig. 4-48a). LA-ICPMS analyses of 28 zircons have $^{206}Pb/^{238}U$ dates between 324 and 169 Ma. The oldest date of *ca.* 324 Ma is from an inherited core. Twenty-three of the youngest 27 grains have a weighted mean of 184.3 ± 2.0 Ma (Fig. 4-48b; Appendix 3). Six zircon grains analyzed by CA-TIMS yielded concordant $^{206}Pb/^{238}U$ dates that range from 182.91 ± 0.15 to 182.77 ± 0.13 Ma (Appendix 4), with a weighted mean date of 182.83 ± 0.05 Ma (MSWD = 0.81, n = 6; Fig. 4-48c). This more precise date is considered the crystallization age of the alkalic phase in the Big Creek batholith.

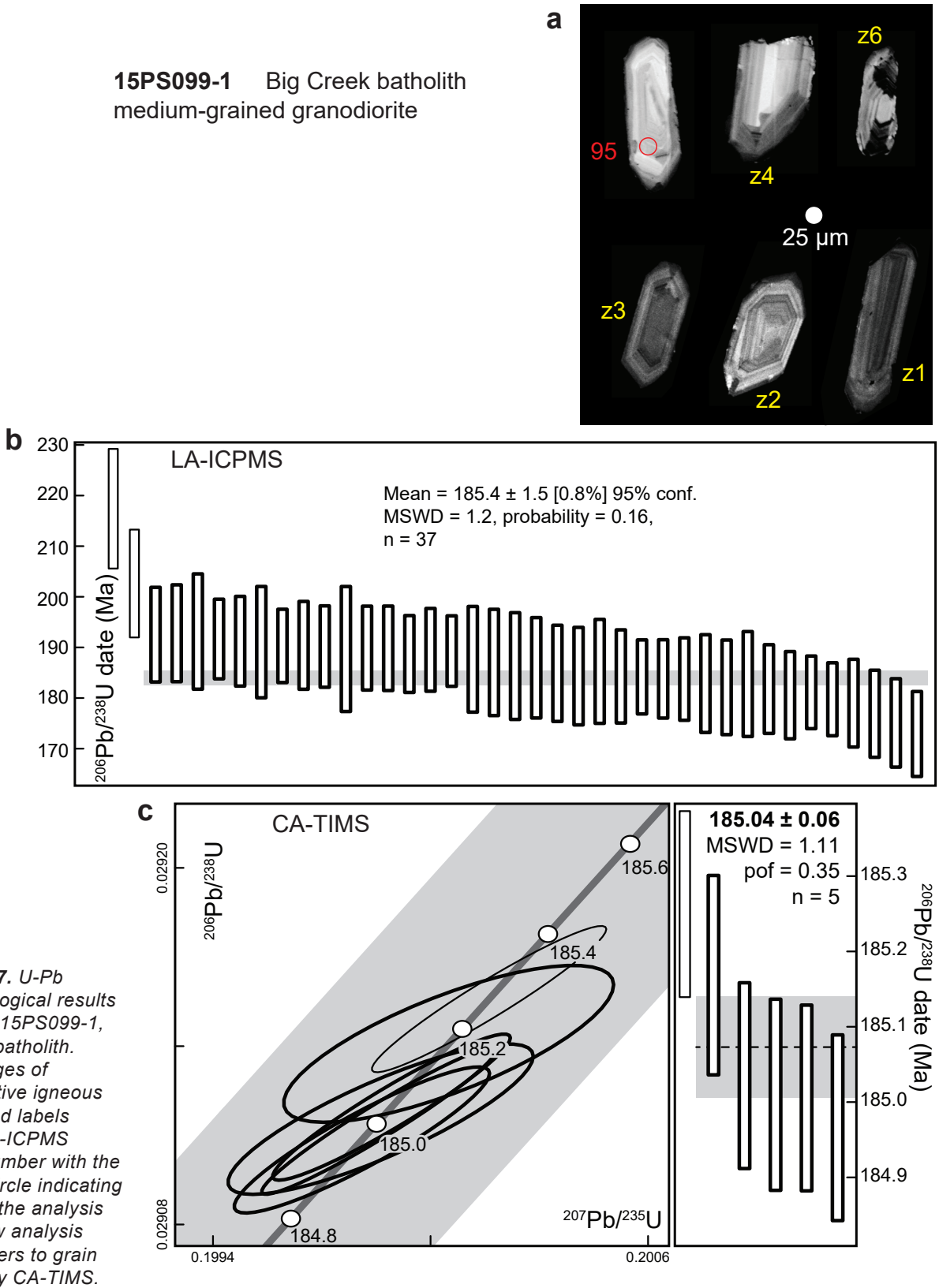


Figure 4-47. *U-Pb geochronological results for sample 15PS099-1, Big Creek batholith.* ***(a)*** *CL images of representative igneous zircons. Red labels indicate LA-ICPMS analysis number with the red open circle indicating location of the analysis spot, yellow analysis number refers to grain analyzed by CA-TIMS.* ***(b)*** *Ranked plot of LA-ICPMS $^{206}Pb/^{238}U$ dates (Appendix 3).* ***(c)*** *Concordia diagram (left) and ranked $^{206}Pb/^{238}U$ dates (right) for zircons analyzed by CA-TIMS (Appendix 4). The light grey band around concordia (dark grey line) shows the decay constant uncertainties. Analyses included in weighted mean age (light grey horizontal bar) calculations are bold; analyses with thin lines are not used in calculations. Line-type designations are the same in all plots. Errors in all plots are at 2σ. MSWD = mean squared weighted deviation, pof = probability of fit, n = number of analyses included in age calculation.*

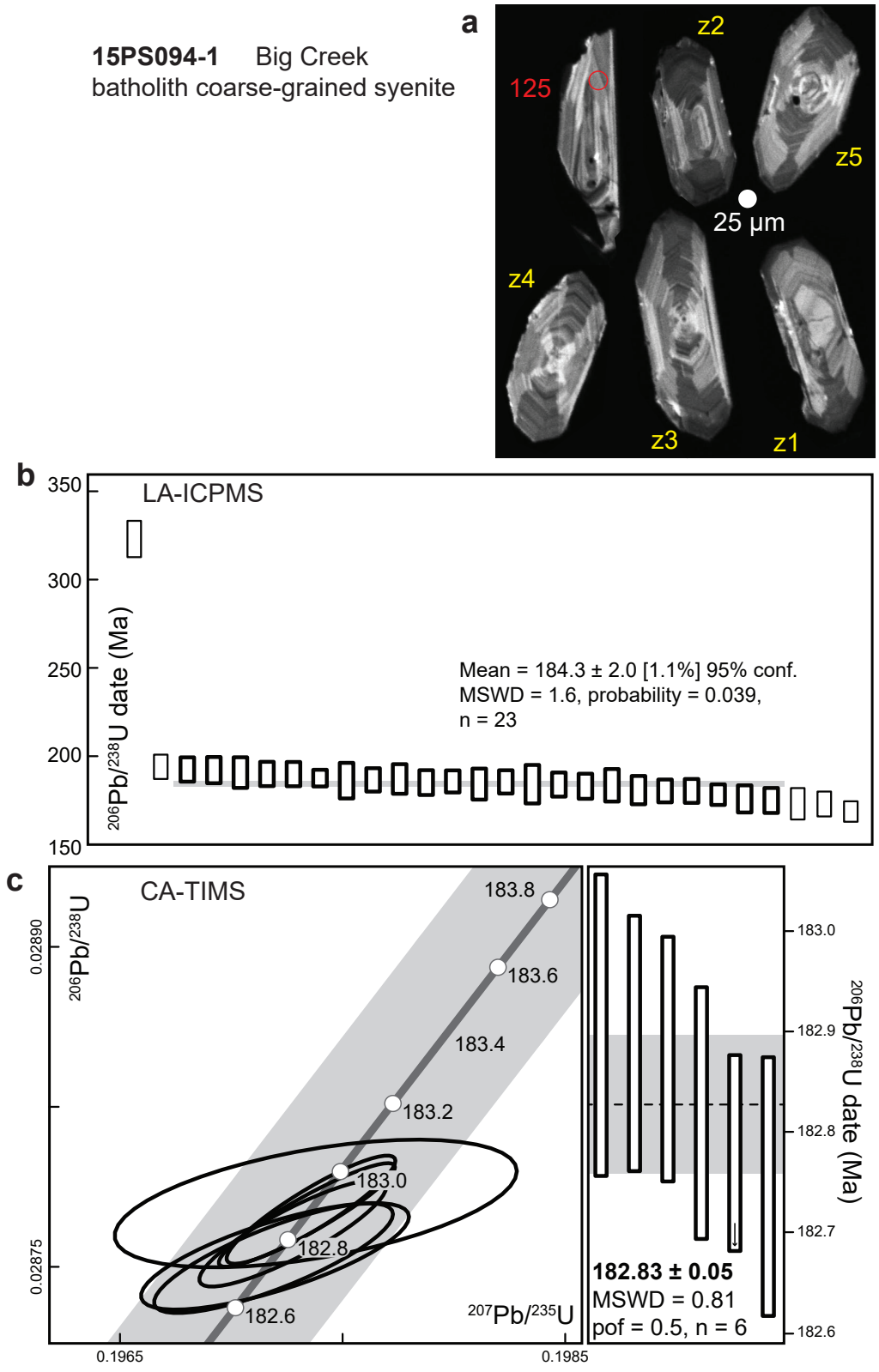


Figure 4-48. *U-Pb geochronological results for sample 15PS094-1, Big Creek batholith.* ***(a)*** *CL images of representative igneous zircons. Red labels indicate LA-ICPMS analysis number with the red open circle indicating location of the analysis spot, yellow analysis number refers to grain analyzed by CA-TIMS.* ***(b)*** *Ranked plot of LA-ICPMS $^{206}Pb/^{238}U$ dates (Appendix 3).* ***(c)*** *Concordia diagram (left) and ranked $^{206}Pb/^{238}U$ dates (right) for zircons analyzed by CA-TIMS (Appendix 4). The light grey band around concordia (dark grey line) shows the decay constant uncertainties. Analyses included in weighted mean age (light grey horizontal bar) calculations are bold; analyses with thin lines are not used in calculations. Line-type designations are the same in all plots. Errors in all plots are at 2σ. MSWD = mean squared weighted deviation, pof = probability of fit, n = number of analyses included in age calculation.*

Granite Mountain batholith

The composite Granite Mountain batholith is located ~30 km northwest of Carmacks (Fig. 4-1). It comprises an older northeastern portion assigned to the Minto plutonic suite (205–194 Ma), and a younger southwestern portion assigned to the Long Lake plutonic suite (188–183 Ma; Fig. 4-49). This section focuses on the younger, southwestern portion of the batholith; rocks of the older northeastern portion are described in Chapter 3. The batholith is elongate northwest and has a total mapped exposure of 720.6 km²; approximately 500 km² is assigned to the Minto suite and 220 km² to the Long Lake suite (Fig. 4-49). Two phases are recognized within the Long Lake suite portion of the Granite Mountain batholith, a main equigranular granodiorite body and a core of porphyritic monzonite exposed mainly south of Stoddart Creek (Fig. 4-49; Table 4-1; Allan and Friend, 2018).

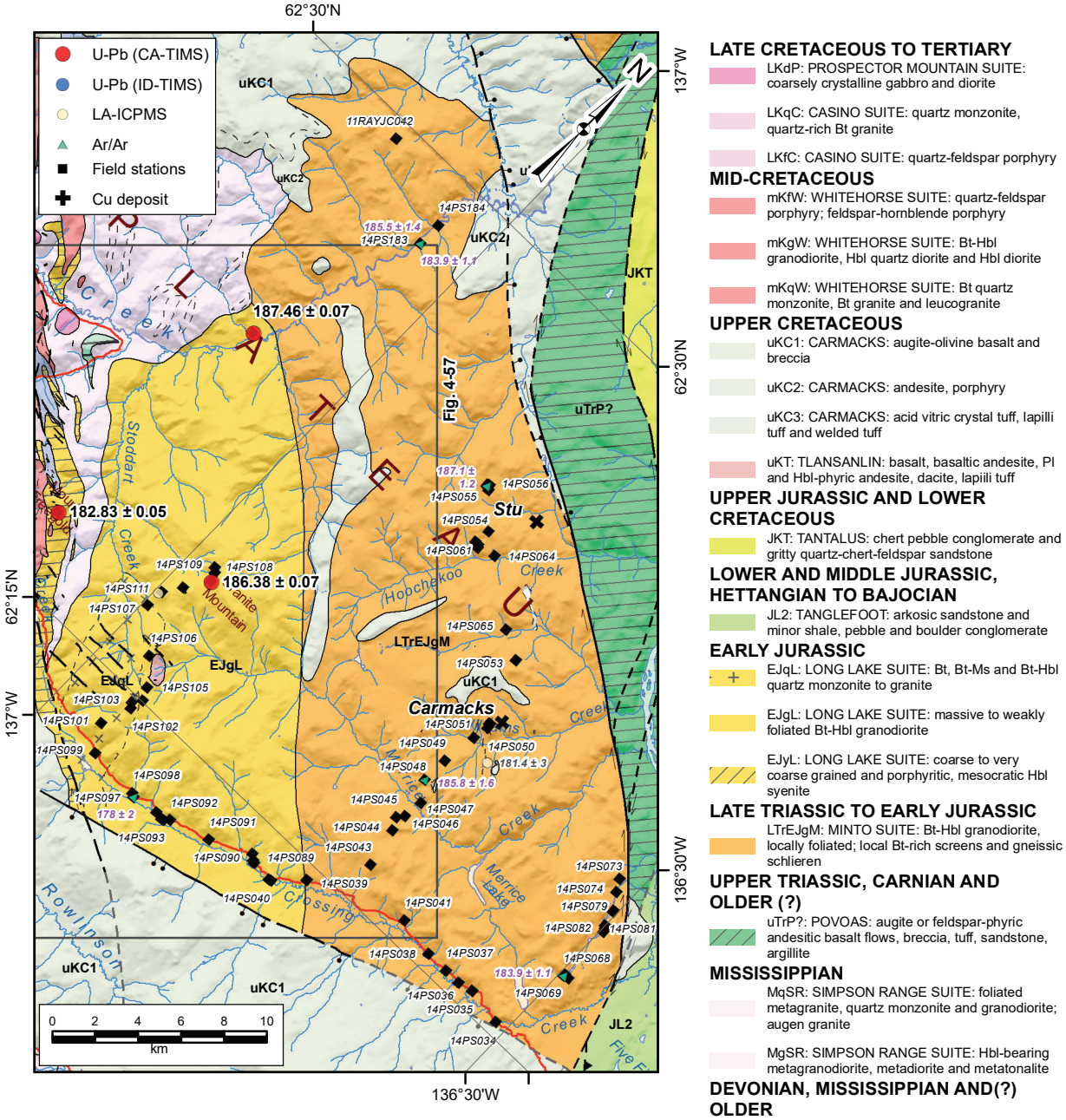


Figure 4-49. *Geology of the Granite Mountain batholith area. Geology from YGS (2020a); fault symbology as in Figure 1-4. Note that the geographic reference frame has been rotated with North pointing to the upper right of the page.*

The southwestern part of the Granite Mountain batholith intrudes Mississippian granodiorite-tonalite gneiss of the Yukon-Tanana terrane (Fig. 4-50; Simpson Range plutonic suite; Carlson, 1987; Allan and Friend, 2018). The exact nature of the contact between the Long Lake and Minto suite portions of the batholith is hindered by poor exposure but is inferred to be intrusive. Samples from the Minto suite part of the Granite Mountain batholith discussed in Chapter 3 show indication of a *ca.* 187–181 Ma reheating event based on $^{40}Ar/^{39}Ar$ hornblende cooling ages and Pb loss in zircon (*see* Figs. 3-19 and 3-25, in Chapter 3).

The southern margin of the batholith is defined by the Miller fault which down-drops the Upper Cretaceous Carmacks Group against both the Long Lake and Minto suite portions of the batholith (Tempelman-Kluit, 1984). Locally, dacite dikes related to the Lower Cretaceous Mt. Nansen Group intrude the batholith (Tempelman-Kluit, 1984) and Upper Cretaceous felsic volcanic rocks assigned to the Tlansanlin formation unconformably overlie the southwestern portion of the batholith (Fig. 4-49; Allan and Friend, 2018). Landscapes in the western Granite Mountain batholith are similar to the Big Creek batholith, with deeply weathered outcrops found mostly as isolated tors on ridges and in stream and road cuts (Fig. 4-51).

Petrography

The granodiorite phase is medium grained, equigranular, with hornblende greater than biotite (~2:1) and a total mafic content of 15 to 30 modal percent (Figs. 4-52 and 4-53); locally this phase is porphyritic with pink K-feldspar phenocrysts. In outcrop, this phase is smooth weathering and medium grey (Fig. 4-53). Plagioclase is weakly to moderately saussuritized and K-feldspar is white and weakly sericitized. Hornblende is fresh to weakly chlorite altered whereas biotite is moderately to intensely chlorite altered (Fig. 4-54a). Titanite and epidote are ubiquitous accessory minerals (Fig. 4-54b).

The more felsic biotite-hornblende monzonite to granite phase occurs in the southwestern portion of the Granite Mountain batholith, south of Stoddart Creek (Fig. 4-49; Allan and Friend, 2018). It crops out as prominent tors and subdued outcrops of white to pink weathered, sparsely K-feldspar porphyritic, medium-grained biotite-hornblende quartz monzonite to monzogranite (Fig. 4-55; Friend *et al.*, 2018). Potassium feldspar phenocrysts are typically tabular, opaque pink, and 1 to 4 cm in length.

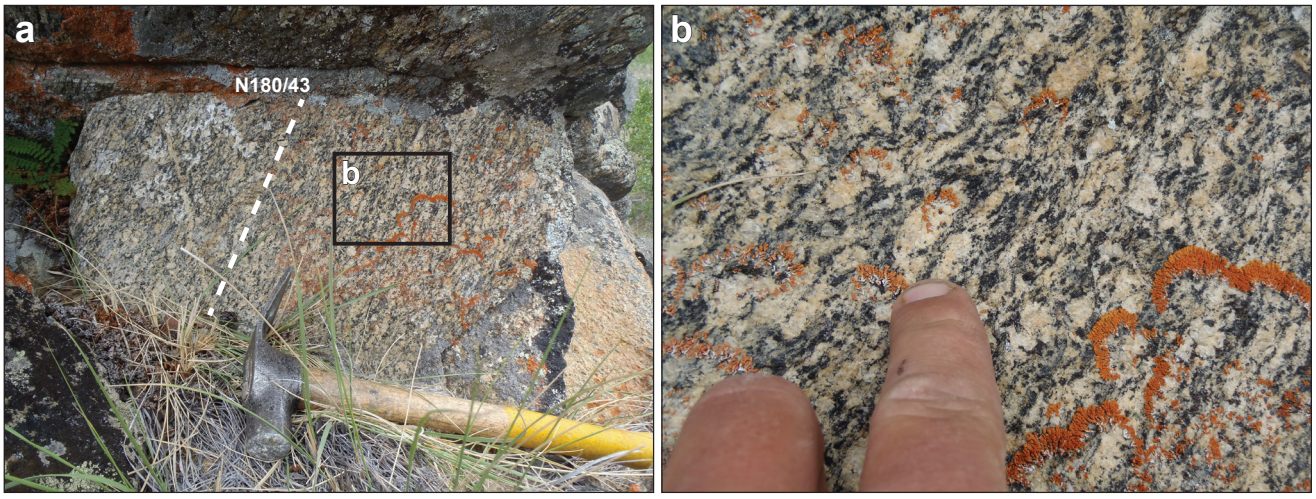


Figure 4-50. *Representative outcrop of Mississippian Simpson Range plutonic suite; 14PS117. Though this rock has a similar intermediate composition (e.g., granodiorite) to Early Jurassic plutonic rocks in the area, it can be distinguished in the field by the pervasive foliation.*

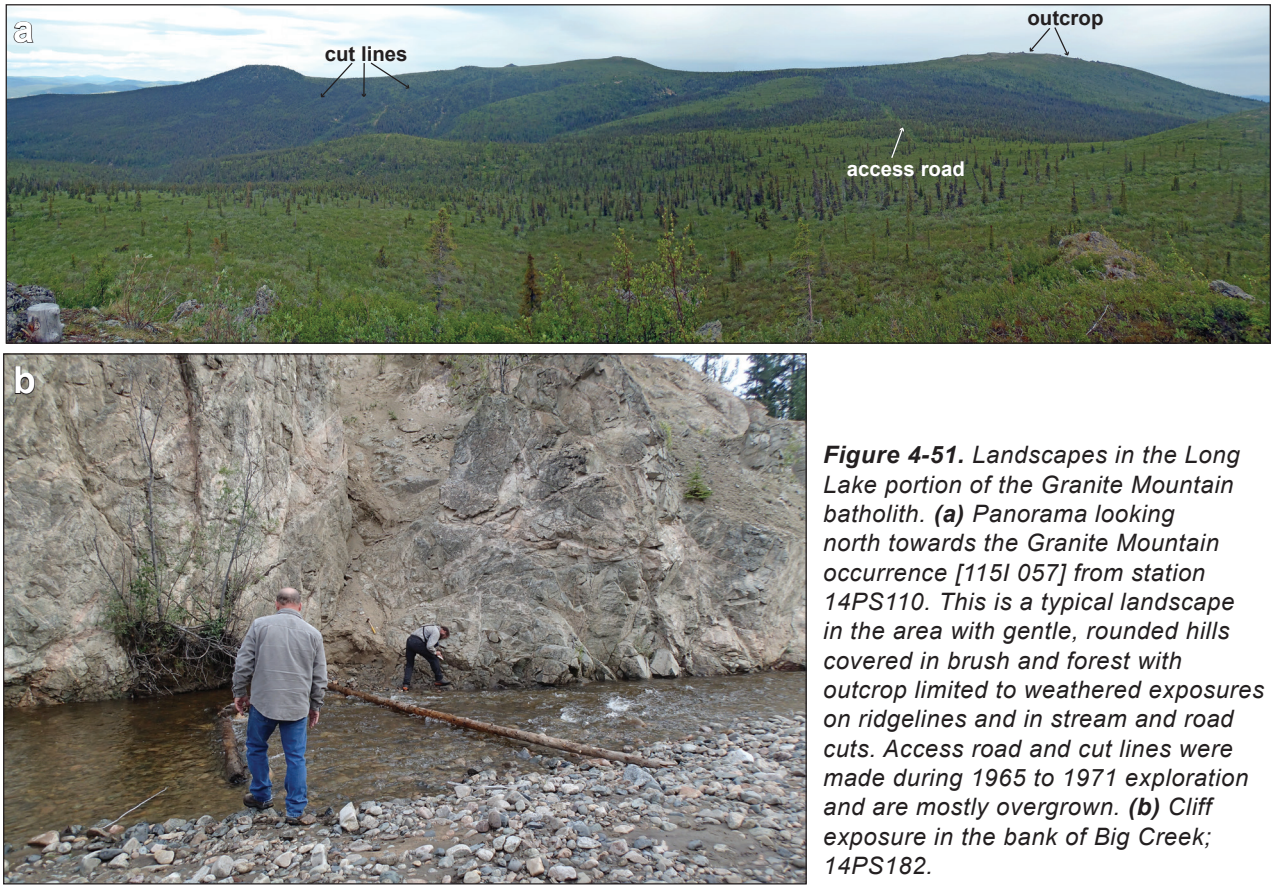


Figure 4-51. *Landscapes in the Long Lake portion of the Granite Mountain batholith.* ***(a)*** *Panorama looking north towards the Granite Mountain occurrence [115I 057] from station 14PS110. This is a typical landscape in the area with gentle, rounded hills covered in brush and forest with outcrop limited to weathered exposures on ridgelines and in stream and road cuts. Access road and cut lines were made during 1965 to 1971 exploration and are mostly overgrown.* ***(b)*** *Cliff exposure in the bank of Big Creek; 14PS182.*

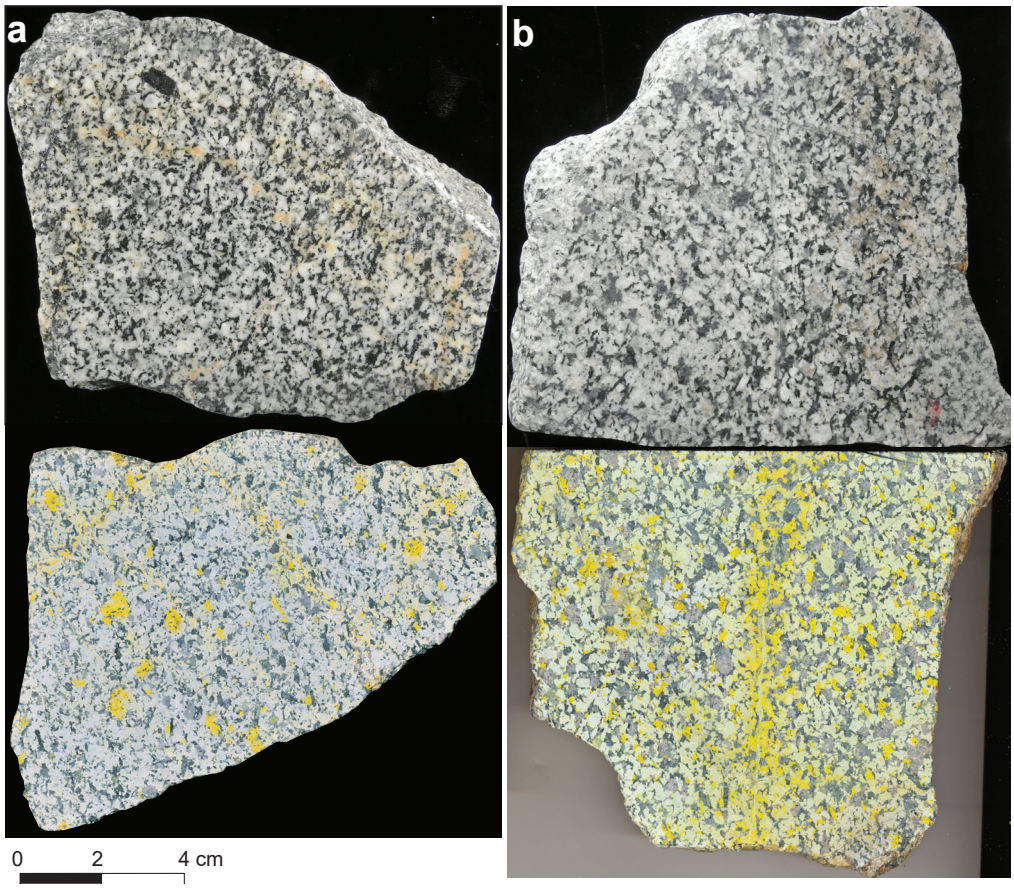


Figure 4-52. *Representative samples from the granodiorite phase in the southwestern portion of the Granite Mountain batholith; Allan and Friend (2018) map unit EJgL.* ***(a)*** *Medium-grained equigranular granodiorite from the northern portion of the Long Lake suite; 14PS182-1.* ***(b)*** *Medium-grained equigranular granodiorite from the central portion of the Long Lake phase with a hairline epidote vein and K-feldspar alteration halo; 14PS114-1. Fresh polished surface (upper) and a cobaltinitrite-stained surface (lower). Note K-feldspar is yellow; all images are same scale.*

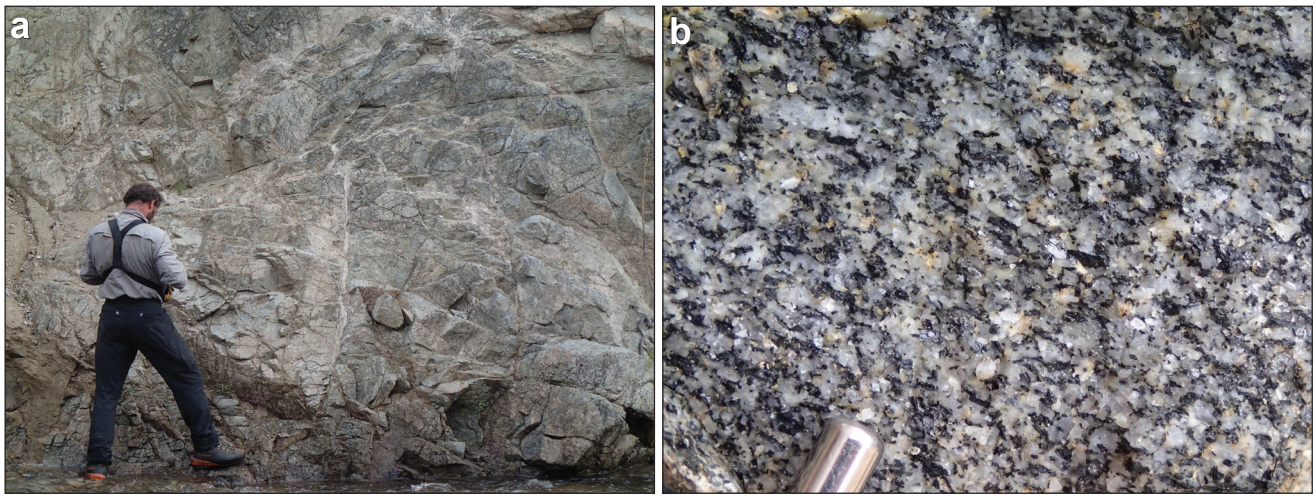


Figure 4-53. *Outcrop in the Long Lake portion of the Granite Mountain batholith; 14PS182.* ***(a)*** *Weathered creek bank exposure of medium-grained equigranular granodiorite on the west side of Big Creek.* ***(b)*** *Fresh broken surface of the same rock. Pencil tip for scale.*

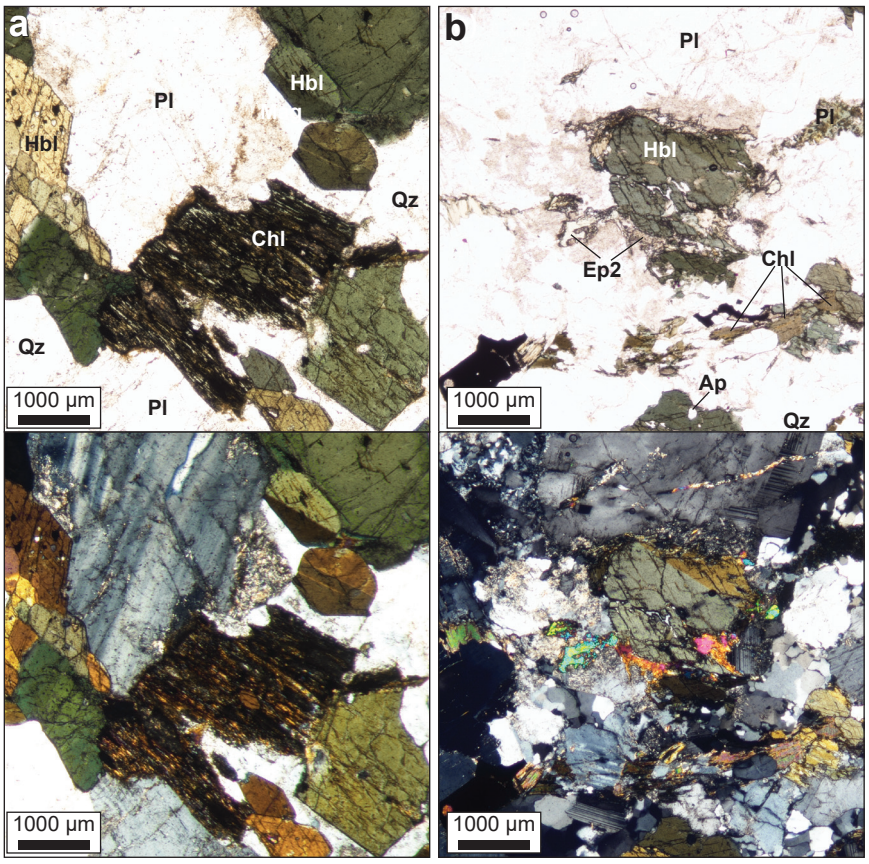


Figure 4-54. *Transmitted light photomicrographs of Long Lake phase of Granite Mountain batholith; plane polarized light (upper) and cross-polarized light (lower).*
(a) *Fresh hornblende and intensely chlorite altered biotite; 14PS114-1.*
(b) *Relatively fresh hornblende with small, anhedral and mottled epidote interpreted to be secondary, biotite is weakly chlorite altered; 14PS097-1.*

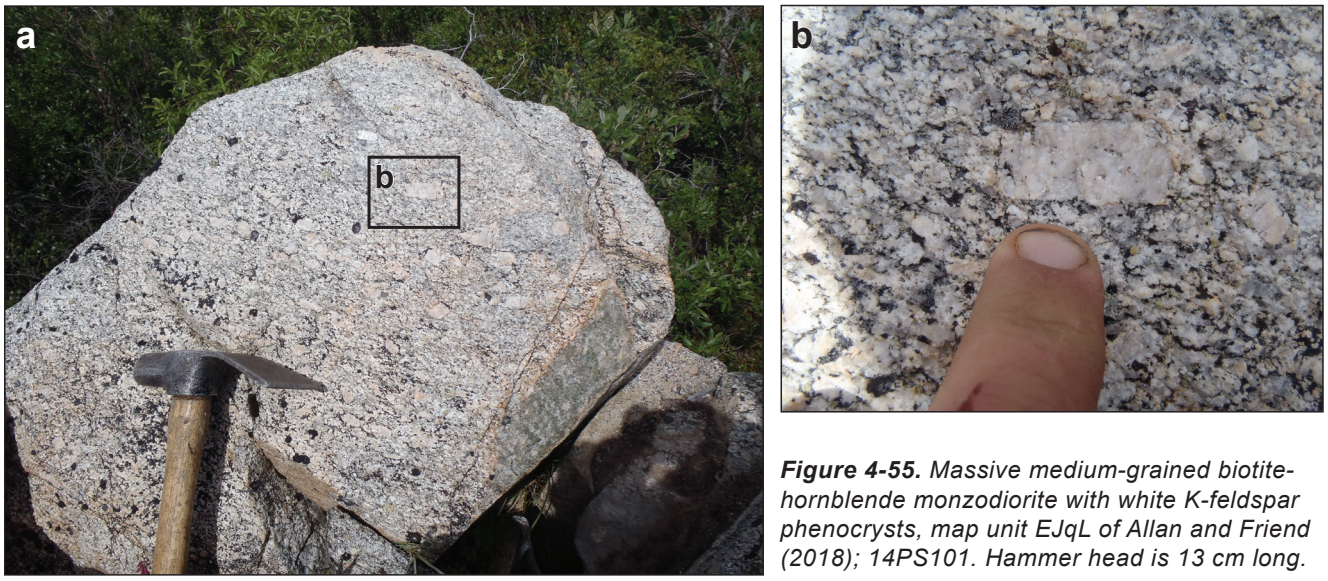


Figure 4-55. *Massive medium-grained biotite-hornblende monzodiorite with white K-feldspar phenocrysts, map unit EJqL of Allan and Friend (2018); 14PS101. Hammer head is 13 cm long.*

Oxidation state and mineral occurrences

The granodiorite phase of the Granite Mountain batholith is oxidized and magnetic susceptibilities range from 3.71 to 21.8 × 10^{-3} SI units (Fig. 4-56; mean 11.7 × 10^{-3} SI units; n = 23; includes data from Friend *et al.*, 2018). The more felsic phase of the Granite Mountain batholith is also oxidized but is slightly less magnetic than the granodiorite phase, with susceptibilities ranging from 3.7 to 13.3 × 10^{-3} SI units (Fig. 4-56; mean 8.5 × 10^{-3} SI units; n = 9; includes data from Friend *et al.*, 2018).

Seven mineral occurrences are hosted within the southwestern portion of the Granite Mountain batholith (Fig. 4-57). One of these, Tinta Hill [115I 058], is a polymetallic vein deposit with an inferred resource of 131 Koz Au, 3.8 Moz Ag, 12.9 Mlb Cu, 47.1 Mlb Pb, 67.1 Mlb Zn (Casselman, 2018). Mineralization at Tinta Hill has not been directly dated and is constrained to younger than the host monzonite (188.7 ± 1.2 Ma) and older than a 108.7 ± 0.4 Ma unaltered trachytic feldspar porphyry dike that crosscuts mineralization (Bineli Betsi and Bennett, 2010). Allan and Friend (2018) consider this deposit to be mid-Cretaceous and one of the older examples of mineralization in the Mt. Freegold district.

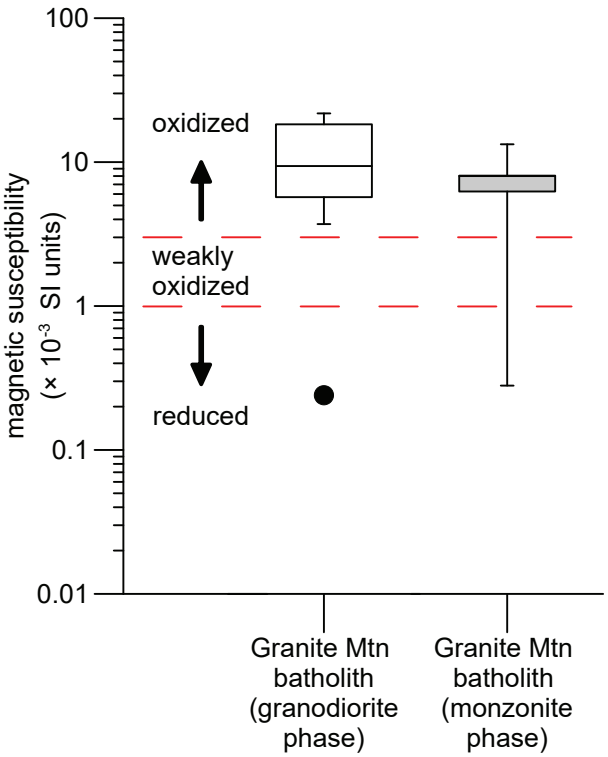


Figure 4-56. *Box and whisker plot of magnetic susceptibility measurements for each phase of the Long Lake suite portion of the Granite Mountain batholith (Appendix 2). Divisions between reduced to weakly oxidized (1 × 10^{-3} SI units), and weakly oxidized to oxidized (3 × 10^{-3} SI units) are from Hart et al. (2004a,b). Ends of boxes are 75th and 25th percentile of data, line within boxes indicate median (50th percentile) of data, whiskers 95th and 5th percentile. Data from the present study and Friend et al. (2018).*

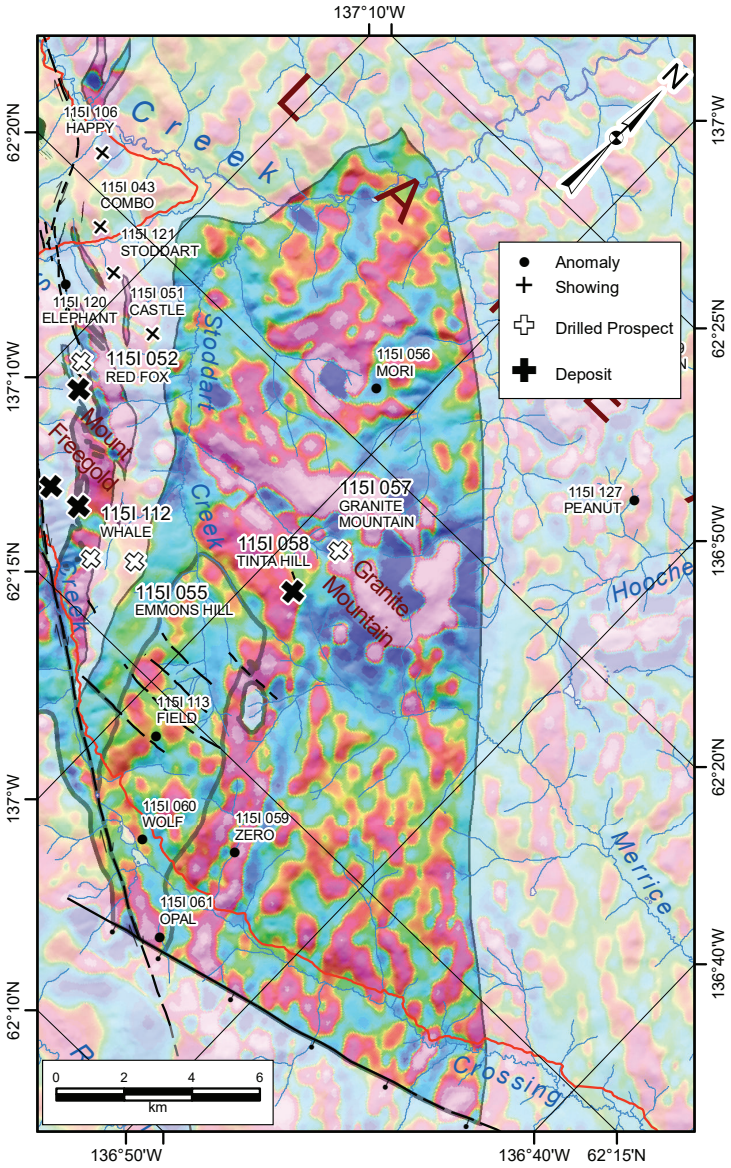


Figure 4-57. *Reduced to pole, first vertical derivative aeromagnetic map of the southwestern Granite Mountain batholith (Aurora Geosciences Ltd. and Bruce, 2017b) illustrating distribution of MINFILE occurrences. Note that the geographic reference frame has been rotated with North pointing to the upper right of the page. Fault symbology as in Figure 1-4.*

The Granite Mountain occurrence [115I 057] is located 2 km north of the Tinta Hill deposit (Fig. 4-57). It was first staked in 1965 and worked intensively until 1971 and discontinuously until the mid-1990s when Little Salmon-Carmacks First Nation selected it as Category A land in their self-government agreement (LSCFN, 1997). The Granite Mountain occurrence had 1244.5 m of diamond drilling in 10 holes and 274.3 m of rotary drilling in 2 holes in the early stages of exploration (Phillips, 1971). The property is underlain primarily by granodiorite of the Long Lake suite but detailed property-scale mapping shows quartz porphyry, breccia and aplite map units (Phillips, 1971), suggesting more variability than is captured on current regional geology maps (Fig. 4-49). Mineralization at the property consists of pyrite-chalcopyrite ± molybdenite in hairline fractures and disseminations; the highest-grade sample is from diamond drill hole 3 where the interval from 230 to 280 feet contains 0.28% Cu and 0.021% MoS_2 (Phillips, 1971). We interpret the mineralization at the Granite Mountain occurrence to be related to Cretaceous magmatism despite being hosted by the Early Jurassic Long Lake suite portion of the Granite Mountain batholith.

Two of the remaining five occurrences [115I 060 and 061] are anomalies located proximal to Upper Cretaceous Carmacks Group volcanic rocks and where reconnaissance soil sampling and prospecting occurred in the 1970s and 80s (YGS, 2020b). Results include weakly anomalous Au and As soil values and possible opal, consistent with high-level hydrothermal fluids likely related to local volcanism. No evidence of mineralization has been found at the remaining three occurrences [115I 056, 059, 113].

Geochronology

Previous age constraints for the Long Lake suite portion of the Granite Mountain batholith are from a monzonite sample collected in the adit of the Tinta Hill deposit [115I 058] which yielded a U-Pb zircon date (UBC, LA-ICPMS) of 188.7 ± 1.2 Ma (Fig. 4-49; J.K. Mortensen, unpublished data, 2011 *in* YGS, 2020c). We present two new U-Pb CA-TIMS dates for the granodiorite phase; the more felsic phase has not been re-dated by CA-TIMS for this study. We also report results of $^{40}Ar/^{39}Ar$ thermochronology for one sample from the southwestern part of the Granite Mountain batholith.

U-Pb

Sample 14PS182-1 is from medium-grained granodiorite collected near the northern tip of the Long Lake portion of the Granite Mountain batholith (Fig. 4-49). It yielded elongate zircons with a length to width ratio of ≥3:1 and oscillatory zoning; a few grains have cores (Fig. 4-58a). LA-ICPMS analyses of 47 zircons have $^{206}Pb/^{238}U$ dates between 352 and 173 Ma (Fig. 4-58b; Appendix 3). Two inherited cores have Mississippian dates of *ca.* 352 Ma and 9 cores are interpreted as Late Triassic xenocrysts with dates between 217 and 201 Ma. Thirty-five of the youngest 36 grains have a weighted mean of 186.7 ± 1.7 Ma. Six zircon grains from this population were analyzed by CA-TIMS (Appendix 4). They yielded concordant $^{206}Pb/^{238}U$ dates between 190.65 ± 0.13 and 187.39 ± 0.13 Ma, with the four youngest grains giving a weighted mean date of 187.46 ± 0.07 Ma (MSWD = 1.45, n = 4; Fig. 4-58c). The oldest grain (190.65 ± 0.13 Ma; Appendix 4) is interpreted as a xenocryst, and the next older (187.74 ± 0.13 Ma) is likely an antecryst.

Sample 14PS114-1 is also medium-grained granodiorite that was collected on Granite Mountain (Fig. 4-59). It yielded single growth stubby and elongate zircons with a length to width ratio between 2:1 and 3:1 and oscillatory zoning (Fig. 4-59a). LA-ICPMS analyses of 35 zircons have $^{206}Pb/^{238}U$ dates between 198 and 168 Ma (Fig. 4-59b; Appendix 3). The youngest zircon has likely undergone Pb-loss and the remaining 34 grains have a weighted mean of 186.1 ± 1.3 Ma. Six zircon grains analyzed by CA-TIMS yielded concordant $^{206}Pb/^{238}U$ dates that range from 186.96 ± 0.13 to 186.29 ± 0.13 Ma (Appendix 4). The three oldest grains are antecrysts and the youngest three grains are autocrysts which have a weighted mean date of 186.38 ± 0.07 Ma (MSWD = 2.38, n = 3; Fig. 4-59c). Collectively these two CA-TIMS dates indicate a crystallization age of 187–186 Ma for granodiorite of the Long Lake suite in the southwestern portion of the Granite Mountain batholith (Fig. 4-49).

Ar-Ar

Hornblende and biotite in sample 14PS097-1, granodiorite from the southern margin of the Granite Mountain batholith (Fig. 4-49), were analyzed by the $^{40}Ar/^{39}Ar$ method at the GSC laboratory in Ottawa (laser, step-heating; Appendix 6). Hornblende yielded a plateau age of 186 ± 2 Ma (Fig. 4-60a). Biotite shows evidence of argon loss in early steps and plateau-like regions in mid to high temperatures steps (178 ± 2 Ma; Fig. 4-60b). Another biotite aliquot yielded a disturbed age spectrum with an integrated age of 181 ± 3 Ma (Fig. 4-60c).

Thermobarometry

McCausland *et al.* (2002) provide results of Al-in-Hbl geobarometry for four granodiorite samples from the southwestern portion of the Granite Mountain batholith. They report that Al^{TOT} in hornblende ranges from 1.94 to 1.76 and cotectic plagioclase has X_{An} of 0.33 to 0.29, indicating crystallization pressure estimates of 4.73 ± 0.60 to 4.33 ± 0.15 kbar (emplacement depths of 17.3 to 14.6 km) and solidus temperatures of 745–769°C.

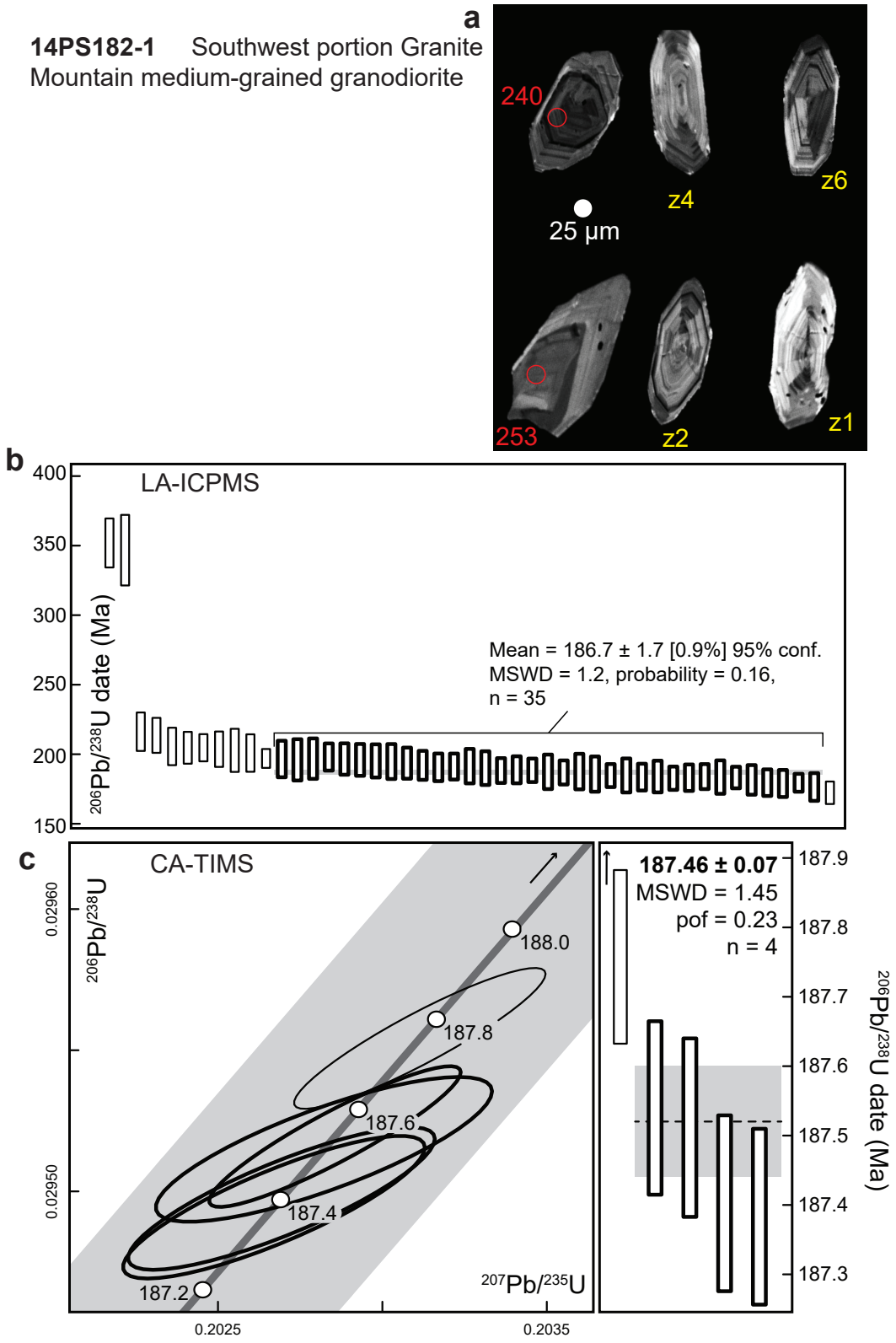


Figure 4-58. *U-Pb geochronological results for sample 14PS182-1, Granite Mountain batholith.* ***(a)*** *CL images of representative igneous zircons. Red labels indicate LA-ICPMS analysis number with the red open circle indicating location of the analysis spot, yellow analysis number refers to grain analyzed by CA-TIMS.* ***(b)*** *Ranked plot of LA-ICPMS $^{206}Pb/^{238}U$ dates (Appendix 3).* ***(c)*** *Concordia diagram (left) and ranked $^{206}Pb/^{238}U$ dates (right) for zircons analyzed by CA-TIMS (Appendix 4). The light grey band around concordia (dark grey line) shows the decay constant uncertainties. Analyses included in weighted mean age (light grey horizontal bar) calculations are bold; analyses with thin lines are not used in calculations. Arrows indicate data extend beyond plot. Line-type designations are the same in all plots. Errors in all plots are at 2σ. MSWD = mean squared weighted deviation, pof = probability of fit, n = number of analyses included in age calculation.*

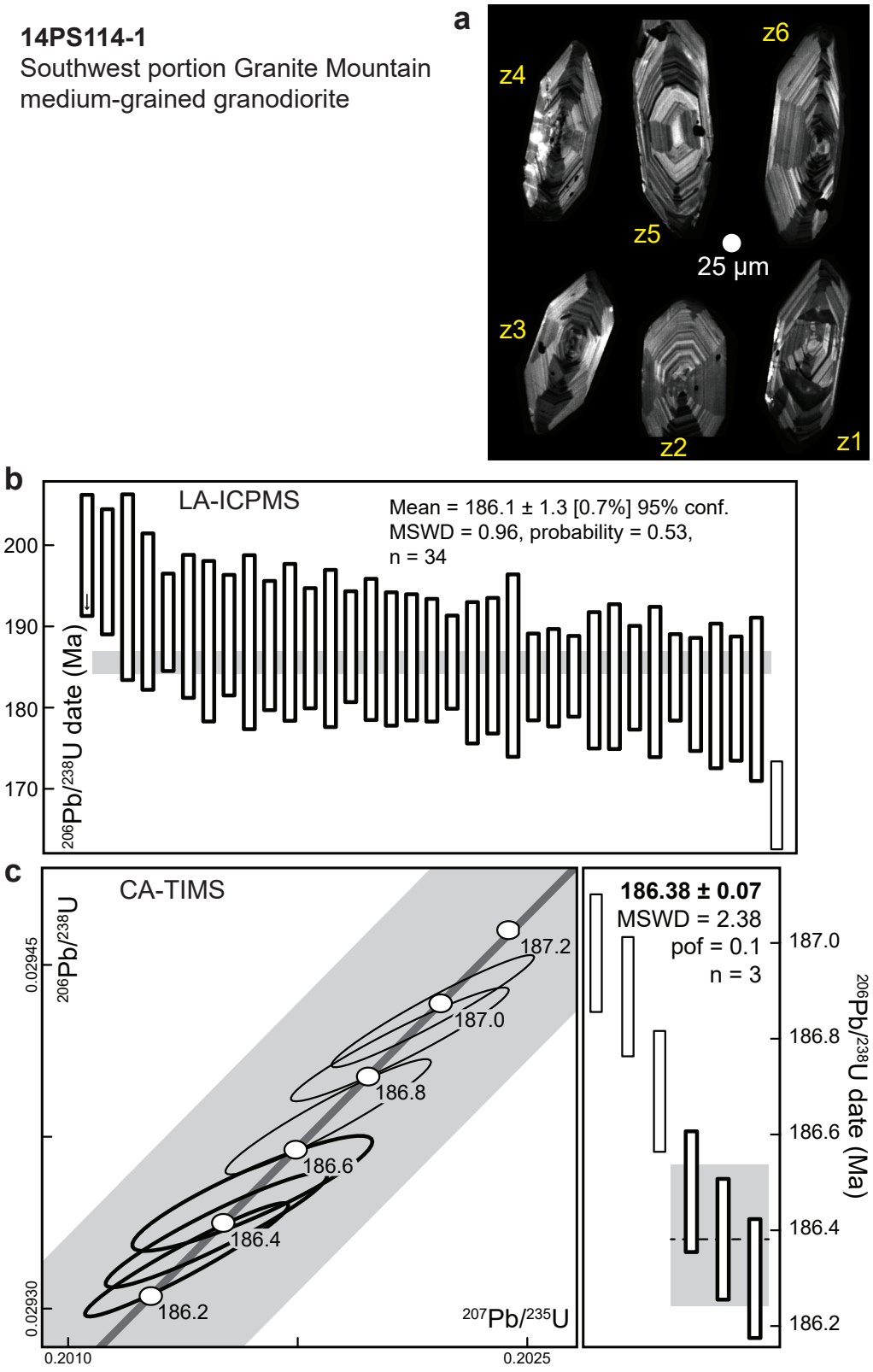


Figure 4-59. *U-Pb geochronological results for sample 14PS114-1, Granite Mountain batholith.* ***(a)*** *CL images of representative igneous zircons. Yellow analysis number refers to grain analyzed by CA-TIMS.* ***(b)*** *Ranked plot of LA-ICPMS $^{206}Pb/^{238}U$ dates (Appendix 3).* ***(c)*** *Concordia diagram (left) and ranked $^{206}Pb/^{238}U$ dates (right) for zircons analyzed by CA-TIMS (Appendix 4). The light grey band around concordia (dark grey line) shows the decay constant uncertainties. Analyses included in weighted mean age (light grey horizontal bar) calculations are bold; analyses with thin lines are not used in calculations. Arrows indicate data extend beyond plot. Line-type designations are the same in all plots. Errors in all plots are at 2σ. MSWD = mean squared weighted deviation, pof = probability of fit, n = number of analyses included in age calculation.*

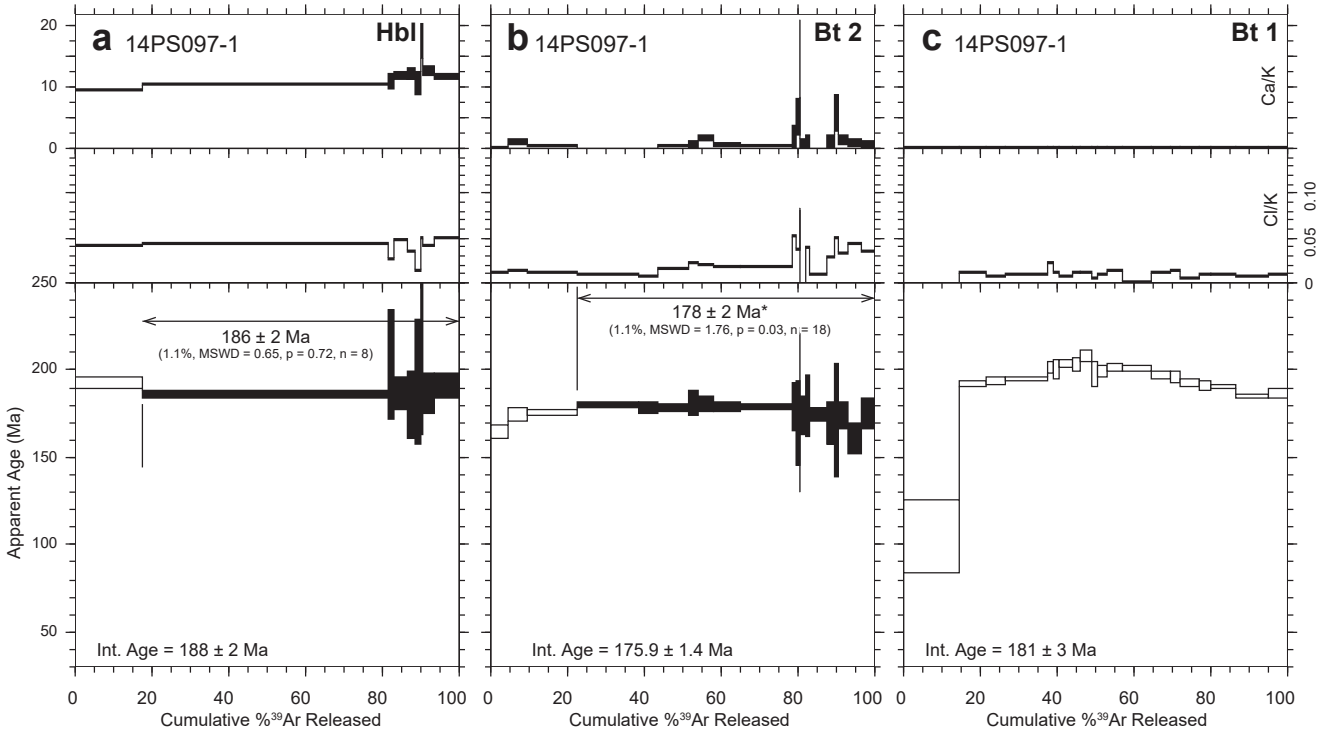


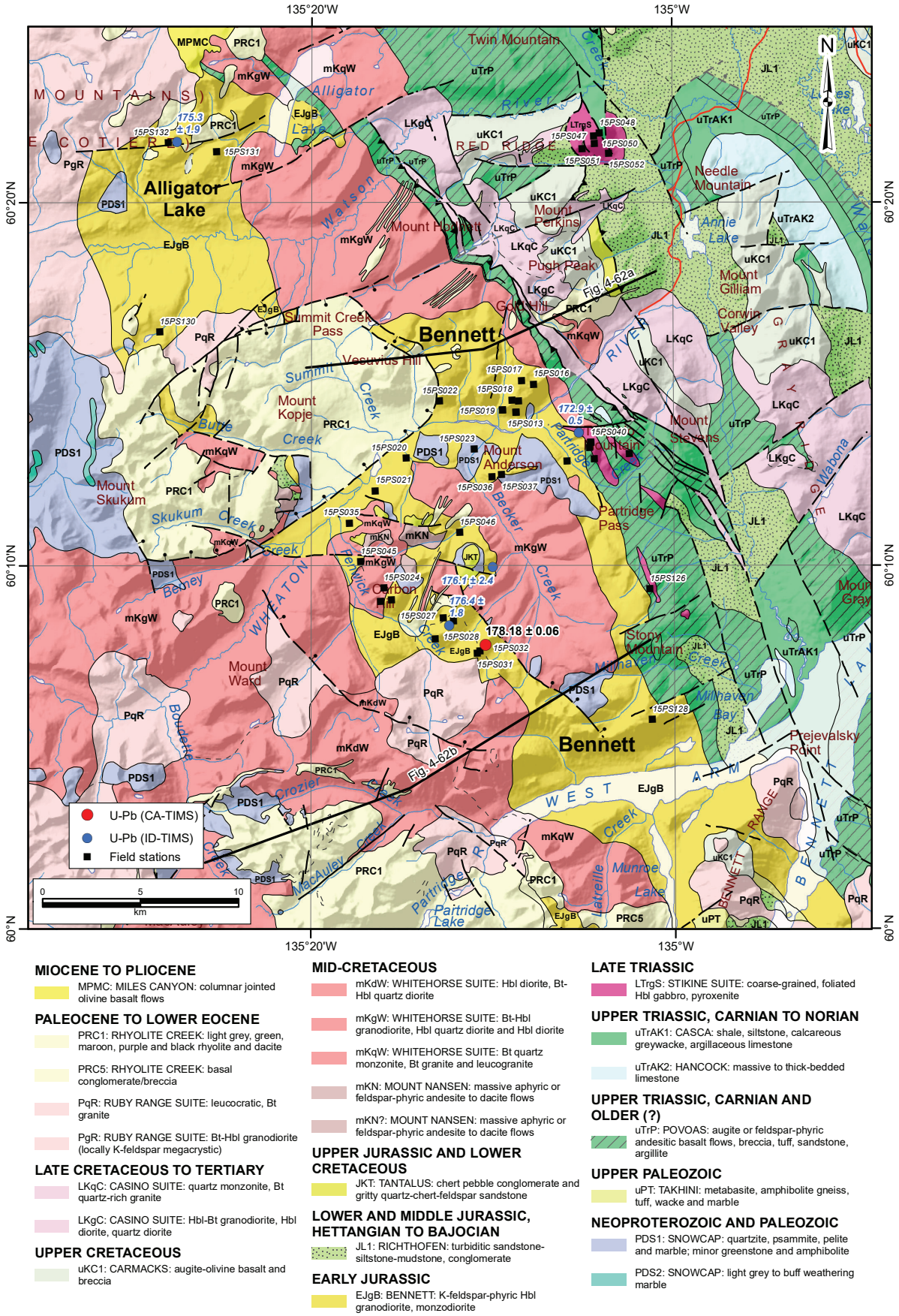
Figure 4-60. *$^{40}Ar/^{39}Ar$ age spectra for sample 14PS097-1 from the granodiorite phase of the Long Lake suite portion of the Granite Mountain batholith.* ***(a)*** *Hornblende,* ***(b*** *and* ***c)*** *biotite. Steps included in plateau are shown in black. Asterisk indicates plateau-like age calculation, as defined in Chapter 1. Int. = integrated. Errors are 2σ. * indicates pseudo-plateau age.*

Bennett suite

The late Early Jurassic Bennett and Alligator Lake plutons (178–175 Ma) are located 25 km west of Carcross and comprise the Bennett plutonic suite in Yukon (Fig. 4-1; Table 4-1), a northern extension of the Bennett suite in northern British Columbia (Mihalynuk, 1999). The Bennett batholith is bisected by Bennett Lake (West Arm) and the Wheaton River, while the Alligator Lake stock to the north is cut by the Watson River, and its northeastern tip underlies Alligator Lake (Fig. 4-61). The two plutons are separated by mid-Cretaceous and Paleogene intrusions and Paleogene volcanic rocks (Fig. 4-62; Hart and Radloff, 1990). Both plutons are composed of K-feldspar porphyritic granodiorite and equigranular monzodiorite phases (Fig. 4-2a) and are dated at *ca.* 178–175 Ma (Fig. 4-61; Table 4-1; Appendix 1). The combined Bennett–Alligator Lake batholith was probably elongate northwest with an original extent of ~600 km² (Hart, 1995). The present distribution of Bennett suite intrusive rocks is highly irregular between younger Cretaceous and Paleogene rocks and has a total mapped extent of only ~303 km² (Fig. 4-61).

The Bennett and Alligator Lake plutons intrude rocks of Stikinia and the Yukon-Tanana terrane (Fig. 4-1). However, the exact terrane relationships in the area are mostly obscured by intrusions of the Coast plutonic complex (Fig. 4-61; Hart and Radloff, 1990; Hart, 1995), a 1700 km long belt of Cretaceous to Paleogene plutonic rocks and older metamorphic inliers that intrude across the boundary between the Intermontane and Insular terranes of the northern Cordillera (Monger *et al.*, 1982). The metamorphic pendants of schist and gneiss within the plutonic rocks are locally ascribed to the Snowcap assemblage of the Yukon-Tanana terrane (Colpron, 2006). Between the Wheaton River and Bennett Lake, the eastern margin of the Bennett batholith intrudes foliated greenstone, amphibolite and gneiss assigned to the Upper Triassic Povoas formation that were deformed within the Tally-Ho shear zone (Figs. 4-61 and 4-62; Hart, 1995). Along this margin, the batholith is undeformed and contains xenoliths of foliated mafic rocks and small undeformed granodiorite dikes intrude the adjacent foliated greenschist, clearly indicating that it postdates deformation of the country rocks (Fig. 4-63; Hart, 1995). The Bennett and Alligator Lake plutons are mainly separated by Paleogene volcanic rocks of the Skukum Creek caldera complex (Rhyolite Creek Group; Fig. 4-61).

Two phases are observed within the Bennett plutonic suite: 1) a K-feldspar porphyritic granodiorite which corresponds to the Bennett granite of Hart and Radloff (1990); and 2) monzodiorite to diorite which corresponds to the Alligator quartz monzonite of Hart and Radloff (1990). Both phases are found in each pluton, but granodiorite is more common in the Bennett batholith and monzodiorite in the Alligator Lake stock (Hart and Radloff, 1990). The contact between the phases is variable, but typically is gradational over metres to tens of metres (Fig. 4-64). The K-feldspar porphyritic granodiorite phase is locally weakly foliated, particularly near the margins of the batholith and in local anastomosing shear bands; the monzodiorite phase is massive (Hart, 1995).



MIOCENE TO PLIOCENE

MPMC: MILES CANYON: columnar jointed olivine basalt flows

PALEOCENE TO LOWER EOCENE

PRC1: RHYOLITE CREEK: light grey, green, maroon, purple and black rhyolite and dacite

PRC5: RHYOLITE CREEK: basal conglomerate/breccia

PqR: RUBY RANGE SUITE: leucocratic, Bt granite

PgR: RUBY RANGE SUITE: Bt-Hbl granodiorite (locally K-feldspar megacrystic)

LATE CRETACEOUS TO TERTIARY

LKqC: CASINO SUITE: quartz monzonite, Bt quartz-rich granite

LKgC: CASINO SUITE: Hbl-Bt granodiorite, Hbl diorite, quartz diorite

UPPER CRETACEOUS

uKC1: CARMACKS: augite-olivine basalt and breccia

MID-CRETACEOUS

mKdW: WHITEHORSE SUITE: Hbl diorite, Bt-Hbl quartz diorite

mKgW: WHITEHORSE SUITE: Bt-Hbl granodiorite, Hbl quartz diorite and Hbl diorite

mKqW: WHITEHORSE SUITE: Bt quartz monzonite, Bt granite and leucogranite

mKN: MOUNT NANSEN: massive aphyric or feldspar-phyric andesite to dacite flows

mKN?: MOUNT NANSEN: massive aphyric or feldspar-phyric andesite to dacite flows

UPPER JURASSIC AND LOWER CRETACEOUS

JKT: TANTALUS: chert pebble conglomerate and gritty quartz-chert-feldspar sandstone

LOWER AND MIDDLE JURASSIC, HETTANGIAN TO BAJOCIAN

JL1: RICHTHOFEN: turbiditic sandstone-siltstone-mudstone, conglomerate

EARLY JURASSIC

EJgB: BENNETT: K-feldspar-phyric Hbl granodiorite, monzodiorite

LATE TRIASSIC

LTrgS: STIKINE SUITE: coarse-grained, foliated Hbl gabbro, pyroxenite

UPPER TRIASSIC, CARNIAN TO NORIAN

uTrAK1: CASCA: shale, siltstone, calcareous greywacke, argillaceous limestone

uTrAK2: HANCOCK: massive to thick-bedded limestone

UPPER TRIASSIC, CARNIAN AND OLDER (?)

uTrP: POVOAS: augite or feldspar-phyric andesitic basalt flows, breccia, tuff, sandstone, argillite

UPPER PALEOZOIC

uPT: TAKHINI: metabasite, amphibolite gneiss, tuff, wacke and marble

NEOPROTEROZOIC AND PALEOZOIC

PDS1: SNOWCAP: quartzite, psammite, pelite and marble; minor greenstone and amphibolite

PDS2: SNOWCAP: light grey to buff weathering marble

Figure 4-61. *Geology of the Bennett and Alligator Lake plutons area (YGS, 2020a); fault symbology as in Figure 1-4.*

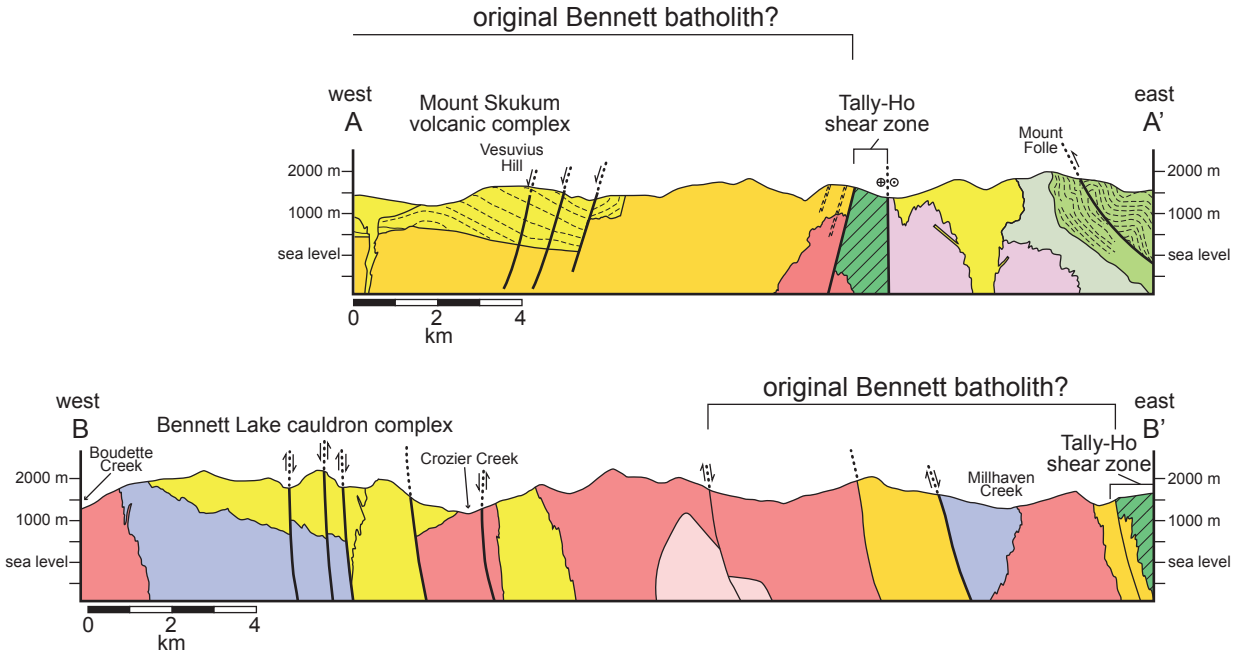


Figure 4-62. *Cross sections through the central (A-A') and southern (B-B') portions of the Bennett batholith. Modified from Hart and Radloff (1990). No vertical exaggeration. See Fig. 4-61 for location and legend.*

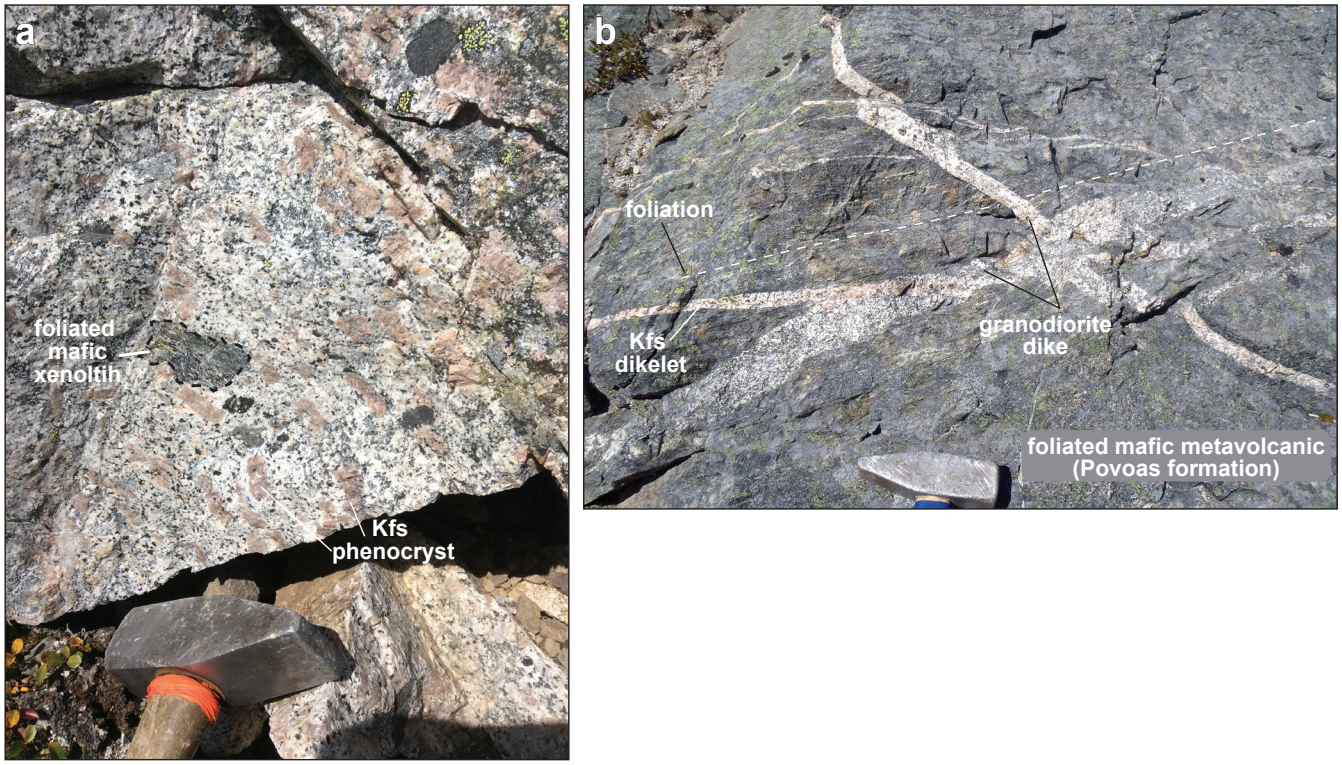


Figure 4-63. *Intrusive nature of contact between the Bennett batholith and Povoas formation; 15PS126.* ***(a)*** *Foliated mafic xenoliths within unfoliated K-feldspar porphyritic granodiorite of the Bennett batholith.* ***(b)*** *Undeformed, thin dikes of granodiorite and K-feldspar within foliated greenstone of the Povoas formation.*

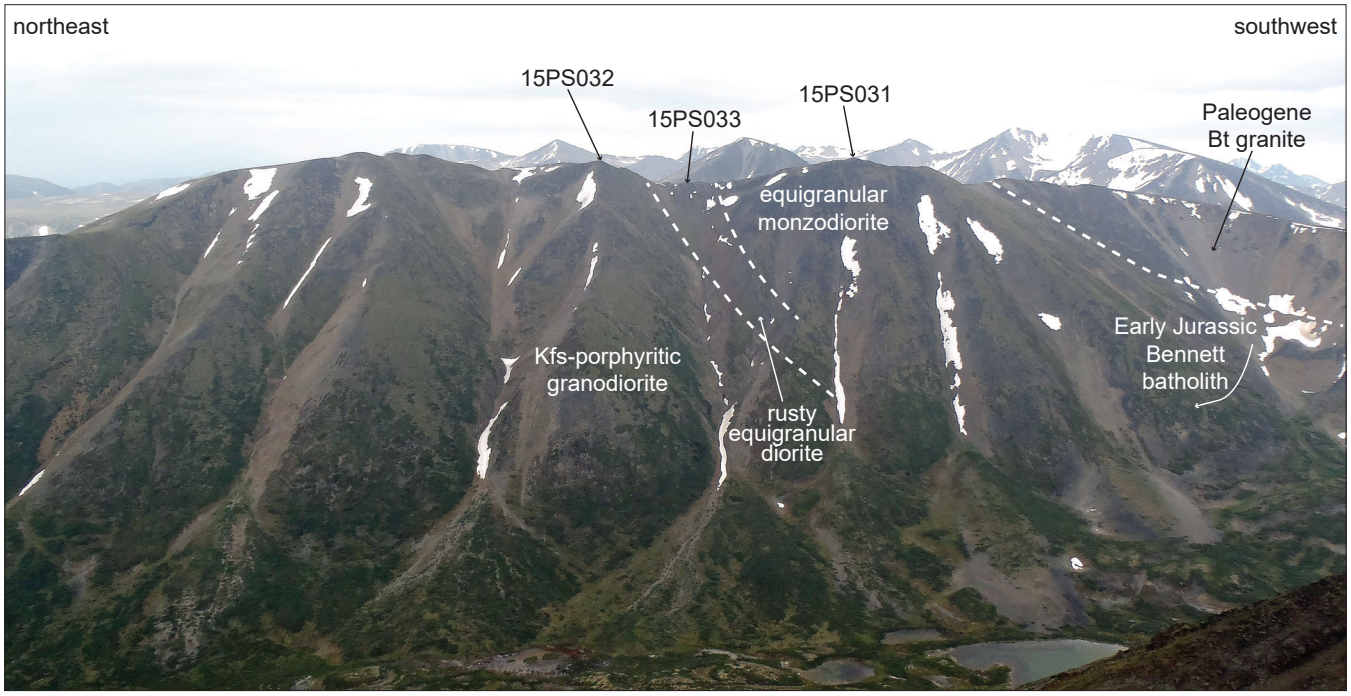


Figure 4-64. *View looking southeast from 15PS034. Local zonation in the Early Jurassic Bennett batholith from K-feldspar porphyritic hornblende-biotite granodiorite to equigranular hornblende diorite and monzodiorite. Mid-Cretaceous Whitehorse suite biotite (± hornblende) granodiorite is in normal fault contact with the Early Jurassic Bennett batholith (Hart and Radloff, 1990) immediately northeast of photo. Paleogene Ruby Range suite biotite granite intrudes the Early Jurassic Bennett batholith on the southwest margin (Hart and Radloff, 1990).*

Bennett batholith

The Bennett batholith comprises one large contiguous, but irregularly shaped, body with a mapped extent of 208 km² (Fig. 4-61); it includes the Bennett batholith and Fenwick Creek pluton of Hart (1995). The Bennett batholith intrudes Stikinia and the Yukon-Tanana terrane, the latter occurring as large pendants within the batholith near Mount Anderson and upper Millhaven Creek (Figs. 4-61 and 4-65). The core of the Bennett batholith, between Becker and Fenwick creeks, is intruded by mid-Cretaceous and Paleogene biotite (± hornblende) granite and granodiorite of the Whitehorse and Ruby Range suites (Fig. 4-64) and locally intruded and overlain by mid-Cretaceous andesite to dacite dikes and flows of the Mount Nansen Group (Fig. 4-66; Hart and Radloff, 1990). Two Paleogene volcanic complexes—the Bennett Lake cauldron complex, to the south, and the Mount Skukum caldera complex, to the north—were superposed onto the Bennett batholith, and the Skukum complex separates the Bennett and Alligator Lake plutons (Fig. 4-61; Hart and Radloff, 1990).

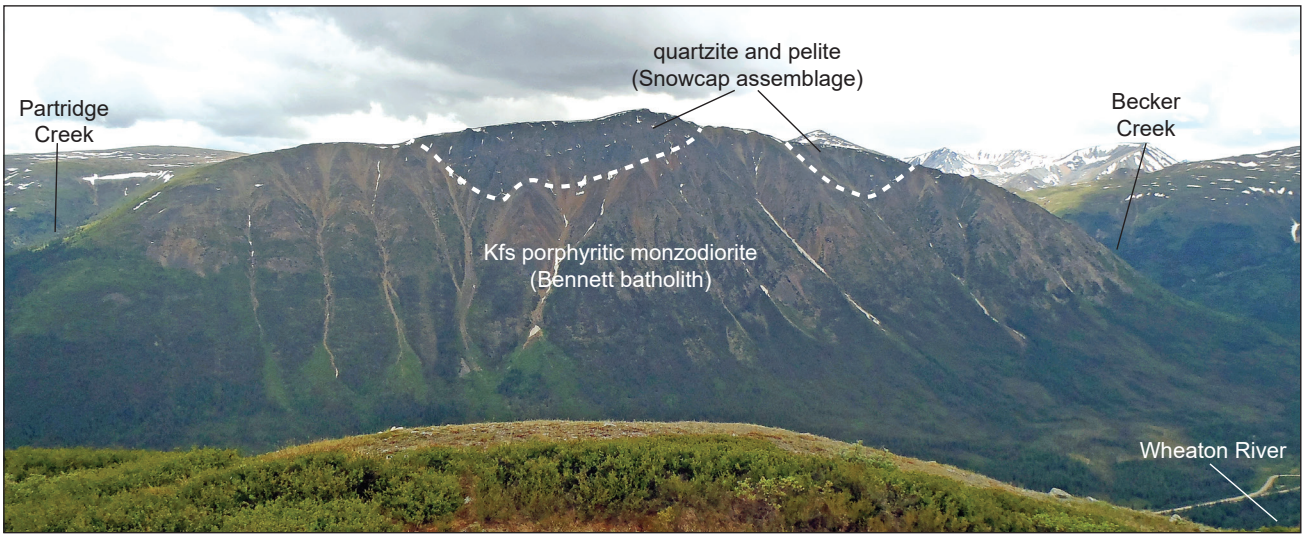


Figure 4-65. *Looking southeast towards Mount Anderson; 15PS015. Pendants of Snowcap assemblage metasedimentary rocks within the Bennett batholith.*

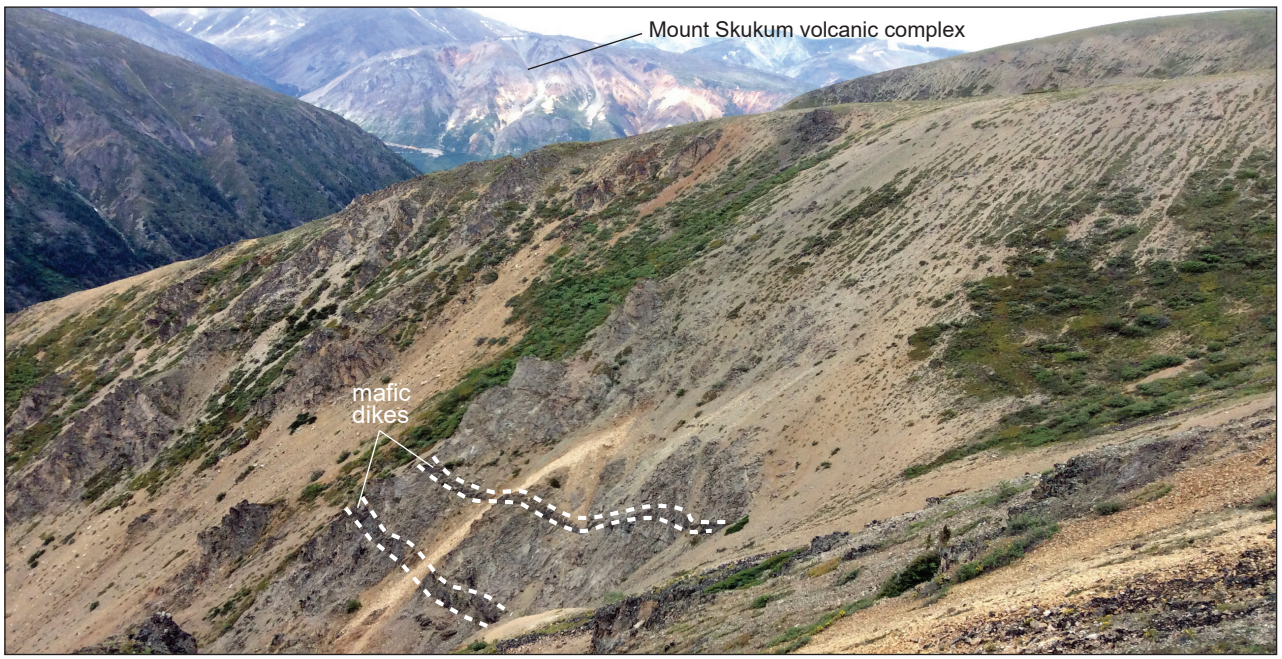


Figure 4-66. *Mafic dikes of the Mount Nansen Group intrude mid-Cretaceous Bt (± Hbl) granodiorite of the Whitehorse suite (Hart and Radloff, 1990). Note Paleogene Mount Skukum volcanic complex in the background. These rocks host the Skukum Creek epithermal deposits.*

Petrography

Two phases are recognized within the Bennett batholith, a variably K-feldspar porphyritic granodiorite to granite and a slightly more mafic and alkalic, equigranular monzodiorite to diorite (Figs. 4-67 and 4-68). The groundmass in the porphyritic phase is fine-grained, equant quartz (Fig. 4-69) that is slightly finer grained than a similar lithology in the *ca.* 188–183 Ma Aishihik batholith to the north (Long Lake Suite; *see* Figs. 4-16 and 4-17 for comparison); it commonly has granophyric to graphic textures near phenocrysts. These textures may be evidence of a shallow depth of emplacement and/or water-saturated magmatic conditions (Barker, 1970). The abundance and size of K-feldspar phenocrysts in the granodiorite is variable, making up to 70% of the rock locally, and phenocrysts up

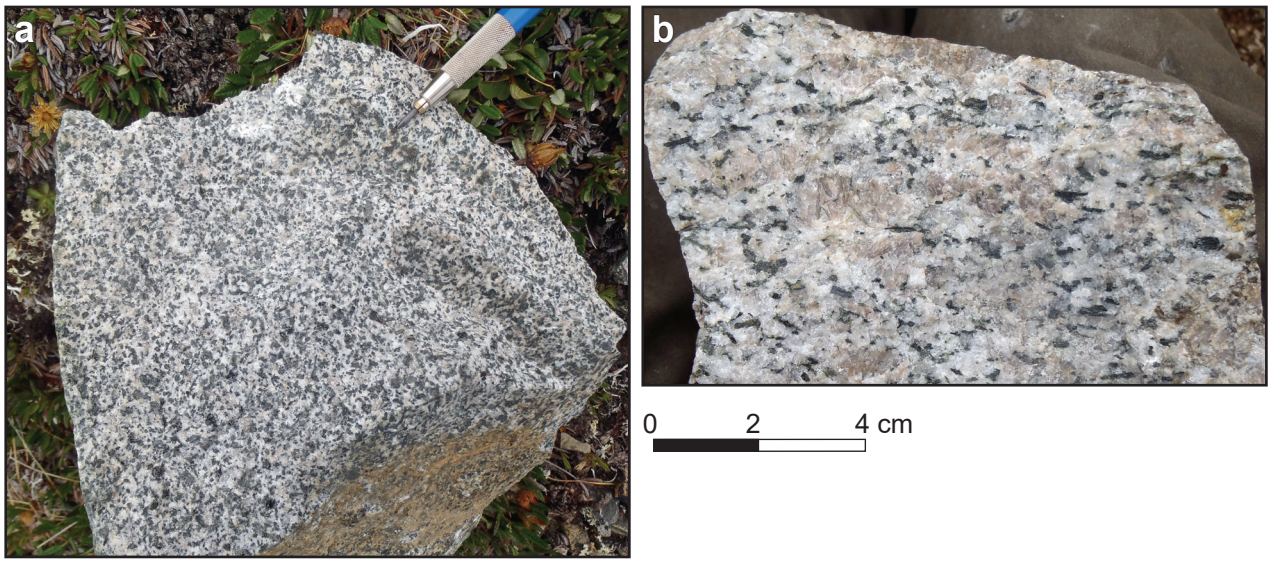


Figure 4-67. *Fresh broken surfaces of representative rocks of the Bennett batholith.* ***(a)*** *Equigranular, hornblende monzodiorite; 15PS027.* ***(b)*** *K-feldspar porphyritic hornblende-biotite granodiorite; 15PS032.*

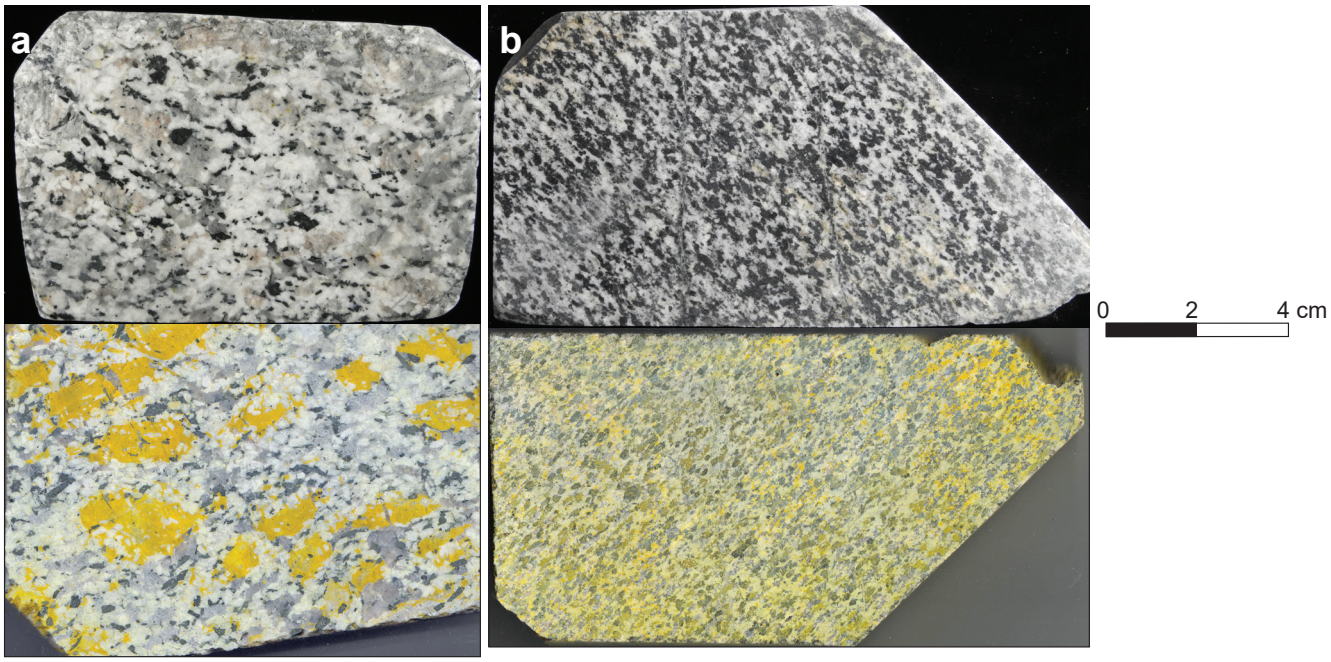


Figure 4-68. *Representative samples from the Bennett batholith.* ***(a)*** *K-feldspar porphyritic granodiorite; 15PS032-1.* ***(b)*** *Fine to medium-grained, equigranular monzodiorite; 15PS033-1. Fresh polished surface (upper) and a cobaltinitrite-stained surface (lower). Note K-feldspar is yellow, both images are same scale.*

to 5 cm in length (Hart, 1995). Typically, K-feldspar makes up 20% of the rock and is 1–3 cm in length (Fig. 4-68). In the monzodiorite phase, K-feldspar typically forms the groundmass to medium-grained (~2 mm) plagioclase and hornblende phenocrysts (Fig. 4-68). In both phases, K-feldspar is fresh and plagioclase is weakly to intensely saussuritized. Hornblende is fresh to moderately chlorite altered and more than twice as abundant as biotite, which is typically moderately to intensely chlorite altered (Fig. 4-69). Titanite, epidote and apatite are common, but not ubiquitous, accessory minerals; epidote is secondary in origin (Fig. 4-69).

Oxidation state and mineral occurrences

The K-feldspar porphyritic granodiorite phase of the Bennett batholith is variably oxidized and has magnetic susceptibilities ranging from 0.07 to 37.2 × 10^{-3} SI units (Fig. 4-3a; mean 8.82 × 10^{-3} SI units; n = 17; Appendix 2). The low magnetic susceptibility measurements in the northern Bennett batholith are within 1 km of pendants of metasedimentary rocks, including carbonaceous schist, that appear as a magnetic low near Mount Anderson in Figure 4-70. For example, station 15PS037 is 350 m from a pendant and the K-feldspar porphyritic granodiorite (Fig. 4-61) has a magnetic susceptibility of 0.07 × 10^{-3} SI units. The equigranular monzodiorite phase is more consistently oxidized and has slightly higher magnetic susceptibility values ranging from 6.59 to 23.3 × 10^{-3} SI units (Fig. 4-3a; mean 13.8 × 10^{-3} SI units; n = 8).

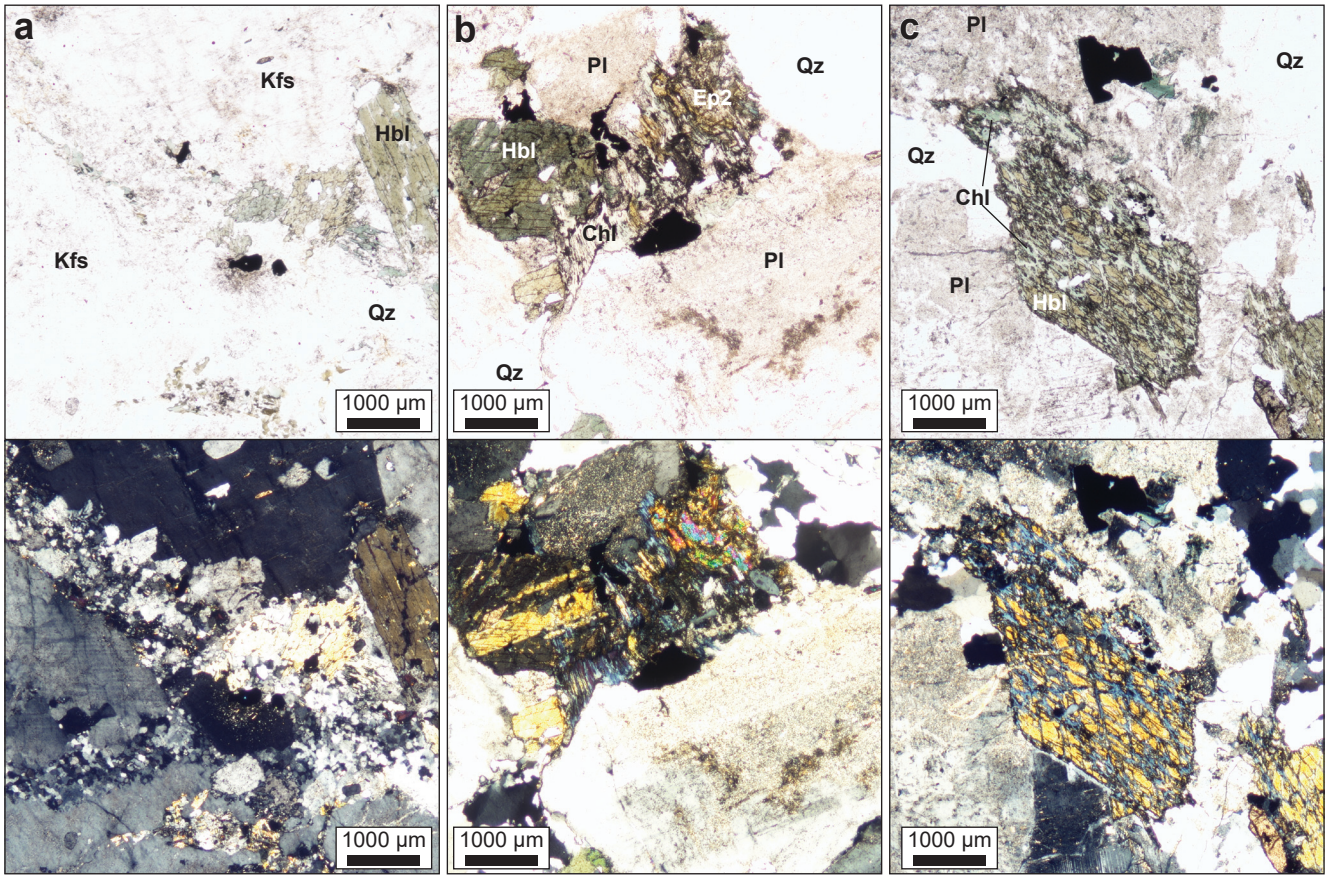


Figure 4-69. *Transmitted light photomicrographs from the Bennett batholith; plane polarized light (upper) and cross-polarized light (lower).* ***(a)*** *Fine-grained Qz-rich groundmass and K-feldspar phenocrysts within porphyritic granodiorite; 15PS043-1.* ***(b)*** *Relatively fresh hornblende next to chlorite altered biotite and secondary epidote and moderately saussuritized plagioclase; 15PS032-1.* ***(c)*** *Moderately saussuritized plagioclase and hornblende phenocryst altered to chlorite along cleavage planes; 15PS128-1.*

The Bennett batholith area contains more than 20 mineral occurrences, most of which are vein-hosted but a few are poorly developed porphyry-style examples (Fig. 4-70; Hart and Radloff, 1990). The most economically significant vein occurrences include the Paleogene Mount Skukum epithermal deposits (Hart and Radloff, 1990). Porphyry occurrences are exclusively associated with the mid-Cretaceous Whitehorse plutonic suite, which to the north is related to the Whitehorse Copper Belt (Hart and Radloff, 1990). Late Early Jurassic plutonic rocks only host a few poorly understood occurrences in the southern portion of the Bennett batholith, such as West Arm [105D 135], a U-Mo anomaly that had limited exploration in the late 1970s (YGS, 2020b).

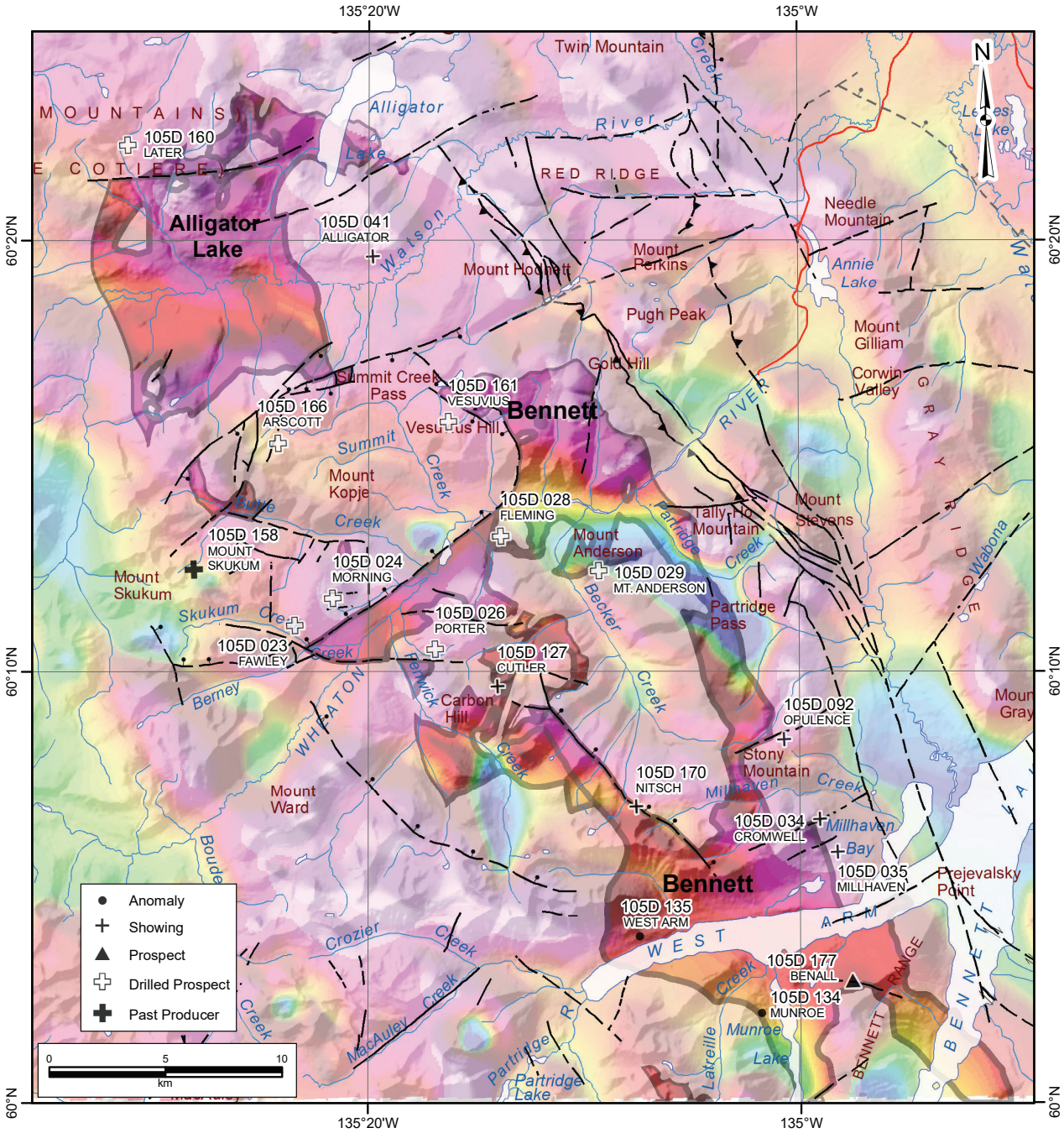


Figure 4-70. *Residual total field aeromagnetic map of the Bennett batholith and Alligator Lake pluton area (Hayward and Oneschuk, 2011) illustrating location of select MINFILE occurrences. Fault symbology as in Figure 1-4.*

Geochronology

The K-feldspar porphyritic granodiorite phase of the Bennett batholith was originally inferred to be Late Triassic based on preliminary U-Pb zircon dates (Hart and Radloff, 1990), but subsequent studies indicate these early results were derived from mixed zircon populations and thus are not representative of the crystallization age for this pluton (Hart, 1995). Better constraints were provided by ID-TIMS U-Pb analyses of multi-grain zircon fractions that yielded dates of 176.1 ± 2.4 Ma for the K-feldspar porphyritic phase (Mortensen and Hart, unpub. data *in* YGS, 2020c) and 176.4 ± 1.8 Ma for the equigranular monzodiorite to diorite phase of the Bennett batholith (Hart, 1995).

We collected one sample of K-feldspar porphyritic granodiorite from the central part of the batholith, in upper Becker Creek (Fig. 4-61), for combined LA-ICPMS and CA-TIMS analysis at BSU (Appendix 3 and 4). Sample 15PS032-1 yielded mostly stubby zircons with sector zoning (Fig. 4-71a). LA-ICPMS analyses of 28 zircons form a single population with $^{206}Pb/^{238}U$ dates between 186 and 173 Ma, and a weighted mean of 177.5 ± 1.1 Ma (Fig. 4-71b; Appendix 3). Seven zircon grains were analyzed by CA-TIMS and yielded concordant $^{206}Pb/^{238}U$ dates that range from 178.46 ± 0.12 to 178.09 ± 0.12 Ma (Appendix 4); the five youngest grains have a weighted mean of 178.18 ± 0.06 Ma (MSWD = 2.07, n = 5; Fig. 4-71c). This more precise date corresponds to the oldest range within error of the previous U-Pb dates of Hart (1995) and Mortensen and Hart (unpublished 1992, *in* YGS, 2020c) for the Bennett batholith (Fig. 4-72).

Thermobarometry

One sample of K-feldspar porphyritic granodiorite from the eastern Bennett batholith contains the suitable mineral assemblage for Al-in-Hbl geobarometry (15PS043-1; Hammarstrom and Zen, 1986; Appendix 5). Al^{TOT} in hornblende from this sample is 1.46 with cotectic plagioclase X_{An} of 0.21, indicating a crystallization pressure estimate of 3.45 ± 1.09 kbar (Appendix 5; emplacement depth of 13.0 ± 4.1 km km) and a solidus temperature of 718°C. Petrographic observations are consistent with batholith emplacement at the shallower end of this range.

Figure 4-71. *See next page.*

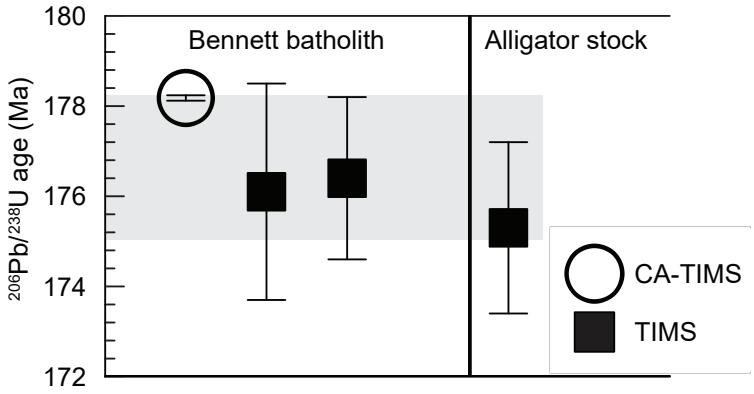


Figure 4-72. *Summary of geochronological data for Bennett suite. Light grey shaded box between ca.178 and 175 Ma defines zircon crystallization range. U-Pb zircon ages symbolized by analytical method. Data sources: this study; Hart (1995); Mortensen and Hart (unpublished data, in YGS, 2020c).*

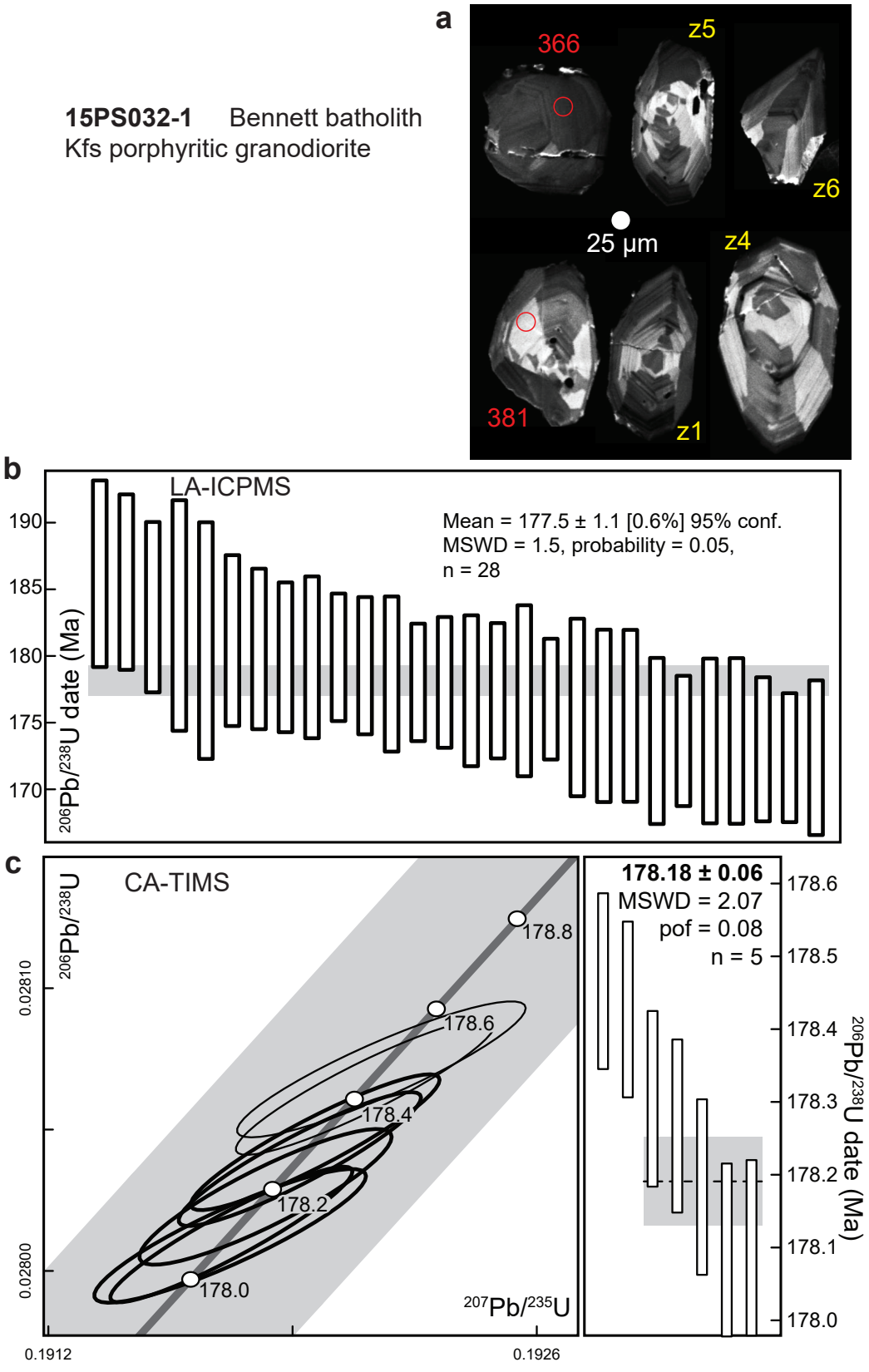


Figure 4-71. *U-Pb geochronological results for sample 15PS032-1, Bennett batholith.* ***(a)*** *CL images of representative igneous zircons. Red labels indicate LA-ICPMS analysis number with the red open circle indicating location of the analysis spot, yellow analysis number refers to grain analyzed by CA-TIMS.* ***(b)*** *Ranked plot of LA-ICPMS $^{206}Pb/^{238}U$ dates (Appendix 3).* ***(c)*** *Concordia diagram (left) and ranked $^{206}Pb/^{238}U$ dates (right) for zircons analyzed by CA-TIMS (Appendix 4). The light grey band around concordia (dark grey line) shows the decay constant uncertainties. Analyses included in weighted mean age (light grey horizontal bar) calculations are bold; analyses with thin lines not used in calculations. Line-type designations are the same in all plots. Errors in all plots are at 2σ. MSWD = mean squared weighted deviation, pof = probability of fit, n = number of analyses included in age calculation.*

Alligator Lake plutons

The Alligator Lake plutons comprise the Alligator Lake stock, with a mapped extent of 86 km², and a 0.8 km² plug east of Alligator Lake (Fig. 4-61; Table 4-1). The northeast margin of the Alligator Lake plutons intrude foliated metavolcanic rocks of the Povoas formation near southern Alligator Lake and are locally covered and intruded by Paleogene volcanic rocks (Fig. 4-73). The mid-Cretaceous Whitehorse suite intrudes the eastern margin of the stock and the western margin is intruded by the Paleogene Annie Ned batholith (Ruby Range suite; Fig. 4-61). Paleogene plutonic and volcanic rocks intrude and cover the southern margin of the stock. Two minor east to east-northeast faults cut the northern portion of the Alligator Lake stock (Fig. 4-61).

Petrography

Both K-feldspar porphyritic granodiorite and equigranular monzodiorite phases of the Bennett suite are present in the Alligator Lake stock (Hart and Radloff, 1990). For this study, only the more common monzodiorite phase of the Alligator Lake pluton was examined. The monzodiorite is medium grained, equigranular and contains equal amounts of biotite and hornblende (Fig. 4-74); K-feldspar is white (Fig. 4-75). Hornblende is typically fresh and biotite weakly to moderately chlorite altered (Fig. 4-76). Plagioclase is weakly to moderately saussuritized and K-feldspar fresh. The groundmass between phenocrysts is fine grained and quartz-rich (Fig. 4-76) giving the rock a pseudo-porphyritic texture in thin section. The fine-grained groundmass may be evidence of a shallow depth of emplacement. Titanite is uncommon but locally present (*e.g.*, 15PS130-1), epidote, apatite and zircon are ubiquitous accessory minerals. Epidote is secondary in origin.

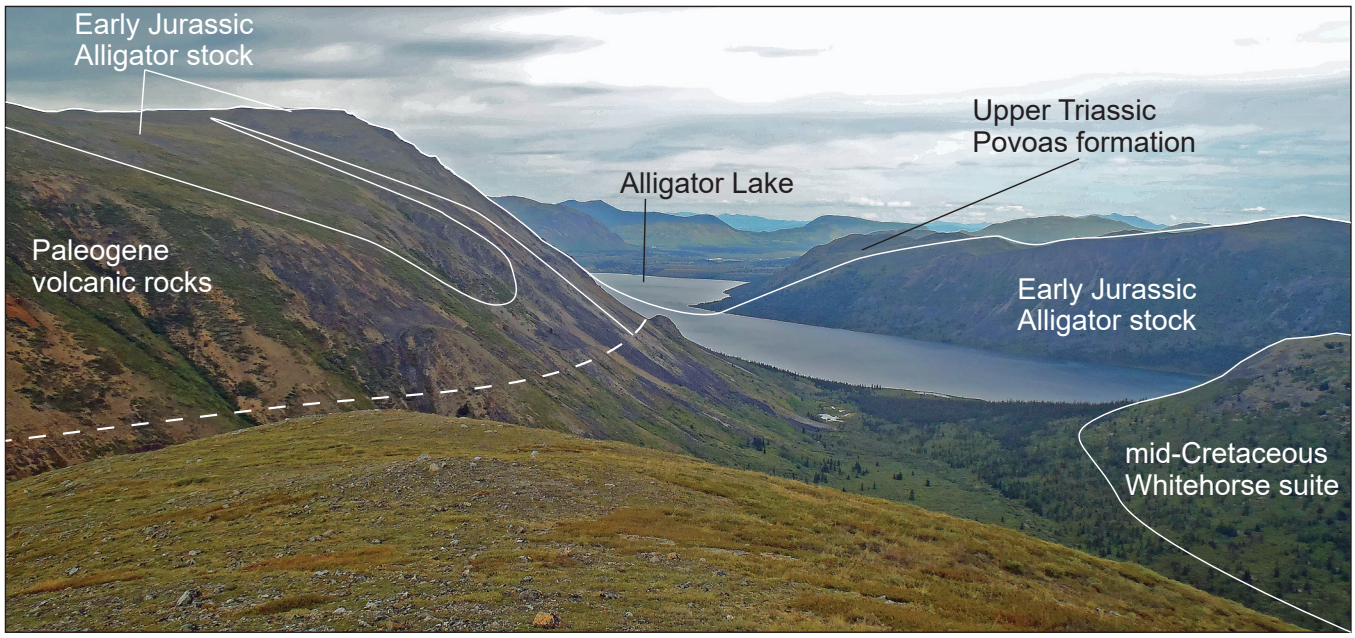


Figure 4-73. *Looking northeast from station 15PS131 showing the Alligator stock underlying Alligator Lake. Dashed line is a small fault of unknown type, solid lines are intrusive contacts (Hart and Radloff, 1990).*

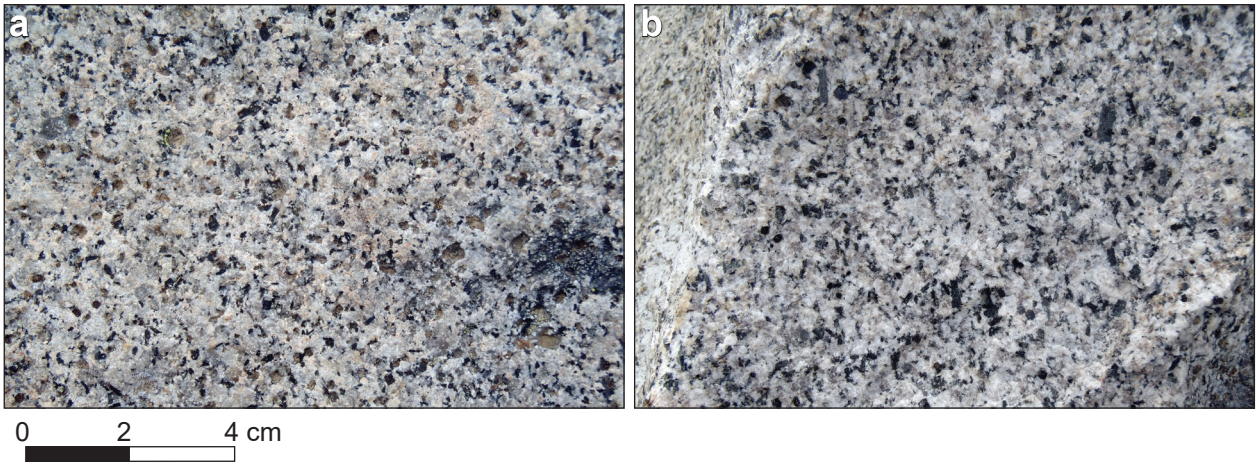


Figure 4-74. *Representative photos of equigranular monzodiorite outcrop in the Alligator stock; 15PS132.* ***(a)*** *Weathered surface with brown recessive hornblende.* ***(b)*** *Fresh broken surface. Scale same for both images.*

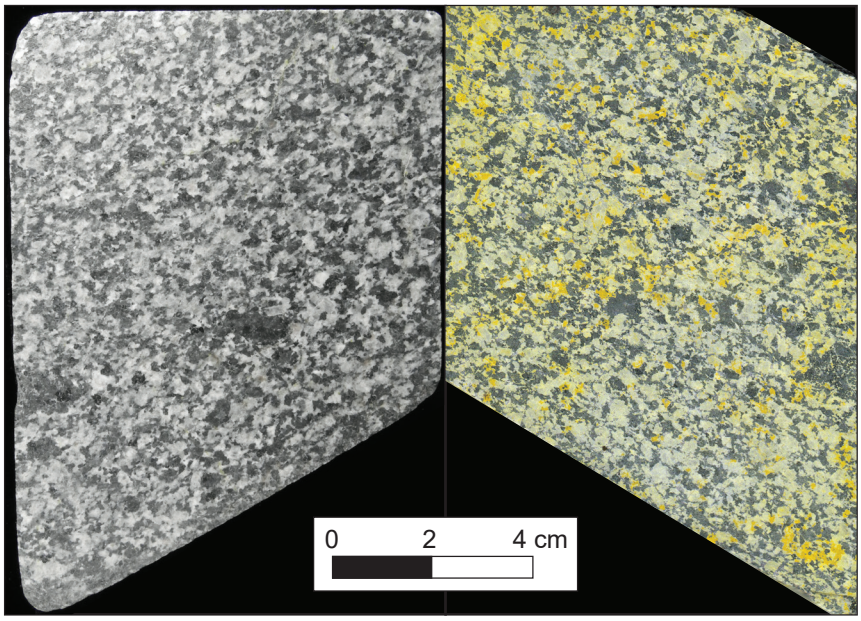


Figure 4-75. *Representative sample from the Alligator stock. Fine to medium-grained, equigranular monzodiorite; 15PS132-1. Fresh polished surface (left) and a cobaltinitrite-stained surface (right). Note K-feldspar is yellow, both images are same scale.*

Oxidation state and mineral occurrences

The equigranular monzodiorite phase of the Alligator Lake stock is mostly oxidized and magnetic susceptibility values are between 0.50 and 14.2×10^{-3} SI units (Fig. 4-3a; mean 7.19×10^{-3} SI units; n = 3). These measurements are consistent with the high aeromagnetic signature in the area (Fig. 4-70).

There are no mineral occurrences hosted in the late Early Jurassic rocks in the Alligator Lake area (YGS, 2020b). There are several vein occurrences associated with Paleogene volcanic rocks and one porphyry occurrence north of the Watson River within mid-Cretaceous Whitehorse suite rocks (YGS, 2020b).

Geochronology

As for the Bennett batholith, the age of the K-feldspar porphyritic granodiorite phase of the Alligator Lake stock was inferred to be Late Triassic based on preliminary U-Pb zircon dates from mixed zircon populations that are not representative of the crystallization age of the pluton (Hart and

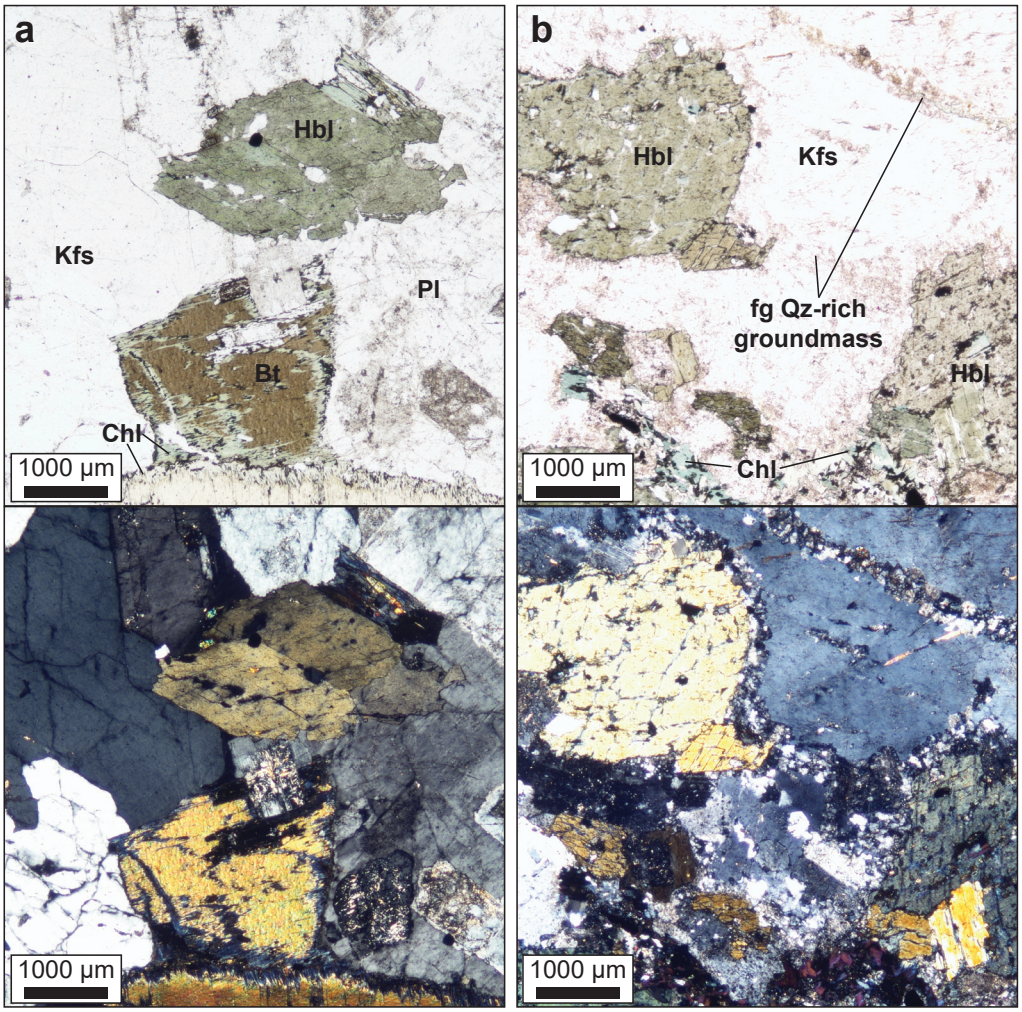


Figure 4-76. *Transmitted light photomicrographs from the Alligator stock; plane polarized light (upper) and cross-polarized light (lower).* ***(a)*** *Relatively fresh hornblende next to weakly chlorite altered biotite and secondary epidote and weakly saussuritized plagioclase; 15PS130-1.* ***(b)*** *Fine-grained Qz-rich groundmass within equigranular monzodiorite; 15PS132-1.*

Radloff, 1990; Hart, 1995). Hart (1995) dated the monzodiorite to diorite phase of the Alligator Lake pluton at 175.3 ± 1.9 Ma using U-Pb ID-TIMS on multi-grain zircon fractions (Fig. 4-72). The Alligator Lake pluton was not reanalyzed for this study.

Thermobarometry

One sample of K-feldspar porphyritic granodiorite from the western Alligator Lake pluton contains the suitable mineral assemblage for Al-in-Hbl geobarometry (15PS130-1; Hammarstrom and Zen, 1986; Appendix 5). Al^{TOT} in hornblende from this sample is 0.93 with cotectic plagioclase X_{An} of 0.24, resulting in a crystallization pressure estimate of 1.51 ± 1.47 kbar (Appendix 5; emplacement depths of 5.7 ± 5.6 km) and a solidus temperature of 649°C. Below ~2 kbar the temperature of final crystallization of calc-alkaline magma increases rapidly with decreasing pressure, making concentrations of Al in hornblende increasingly temperature-sensitive rather than pressure-sensitive (Hollister *et al.*, 1987). Although the pressure estimate of <2 kbar for the Alligator Lake pluton is not reliable, the low Al^{TOT} of hornblende in granodiorite is consistent with petrographic observations of granophyric to graphic textures that suggest emplacement at upper crustal levels.

Lokken suite

The series of approximately 30 small Early Jurassic plutons (<1 to 200 km²) that intrude metamorphic rocks of the Yukon-Tanana terrane east of the Teslin fault is assigned to the Lokken suite, named after the largest pluton in the suite in Yukon (Fig. 4-1; Table 4-1). These plutons occur mostly in the Teslin (105C) and Wolf Lake (105B) areas of southern Yukon, and as isolated plutons farther north in northwestern Glenlyon (105L; Macmillan Range plutons) and northeastern Lake Laberge (105E; Lokken batholith; Figs. 4-1 and 4-77). Early Jurassic plutons of this suite extend into northern British Columbia, where they form a large (>1620 km²) composite batholith including the Coconino, Simpson Peak and Nome Lake plutons (Massey *et al.*, 2005). Plutons of the Lokken suite in Yukon are typically mesocratic, medium-grained, equigranular, Hbl-Bt-Cpx-bearing monzonite, monzodiorite and granodiorite that range in age from 195–184 Ma. These plutons were previously assigned to the Aishihik suite (Gordey and Makepeace, 2001) and more recently to the Minto and Long Lake suites (Colpron *et al.*, 2016b). Here they are considered part of a distinct suite based on their different composition, the presence of clinopyroxene, and emplacement in the Yukon-Tanana terrane east of the Teslin fault (Figs. 4-1 and 4-77). Plutons of the Lokken suite (195–184 Ma) are slightly younger than the 205–195 Ma Minto suite to the west (*see* Chapter 3) and overlap in age with the 188–183 Ma Long Lake suite intruding Yukon-Tanana and Stikinia west of the Teslin fault.

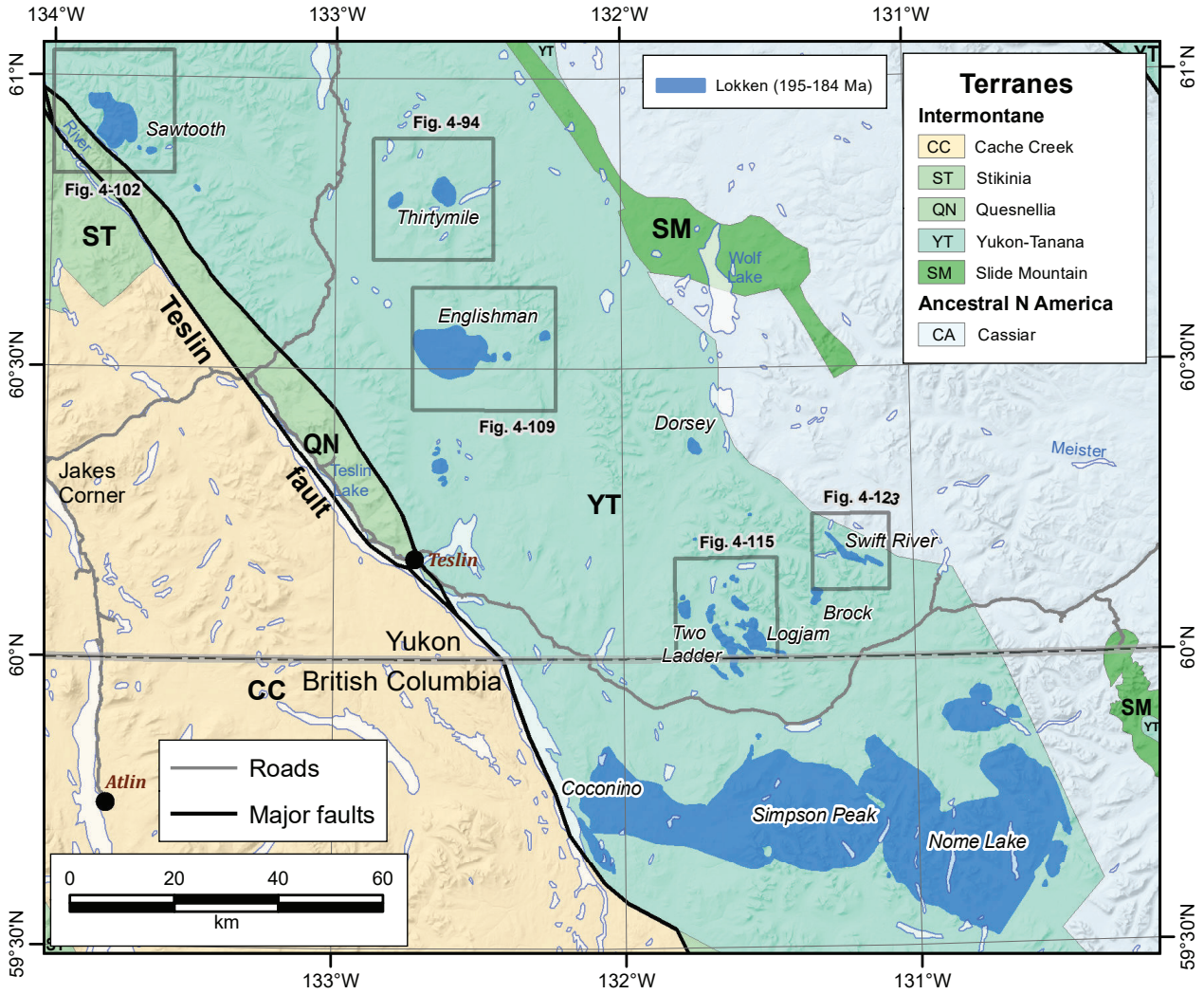


Figure 4-77. *Distribution of Early Jurassic plutons of the Lokken suite in southern Yukon and adjacent parts of northern British Columbia. Terranes from Colpron and Nelson (2011); Yukon plutons from YGS (2020a), British Columbia plutons from Massey et al. (2005).*

Lokken batholith

The Lokken batholith is the largest pluton of the Lokken suite in Yukon (Fig. 4-1). It is located ~90 km southeast of Carmacks and 25 km south of Little Salmon Lake. The pluton has a mapped extent of 203 km² (Fig. 4-78; Table 4-1). It intrudes Mississippian and older rocks of the Finlayson and Snowcap assemblages (Yukon-Tanana terrane; Colpron, 2006) and the Big Salmon fault juxtaposes it with the Devonian–Mississippian Moose formation (Quesnellia) along its southwestern edge (Fig. 4-78; Tempelman-Kluit, 1984b; Colpron, 2006). The pluton is mostly forest-covered and outcrop restricted to a few ridges above treeline, stream cuts at lower elevation, and local cliffs and small exposures within the forest (Fig. 4-79).

Petrography

The Lokken batholith comprises medium to coarse-grained, equigranular granodiorite, monzodiorite and monzonite (Figs. 4-2b and 4-80); the monzonite phase is locally red with green hornblende, about half of which have pyroxene cores. Plagioclase and K-feldspar are typically anhedral and weakly to intensely saussuritized and sericitized, respectively (Fig. 4-81). Mafic minerals make up 10 to 37% of the rock with hornblende and biotite present in similar proportions. Clinopyroxene is subordinate to hornblende and biotite and occurs as altered and embayed cores overgrown by relatively fresh hornblende (Fig. 4-82). Biotite is commonly altered to chlorite. Secondary (alteration) epidote is present in trace amounts.

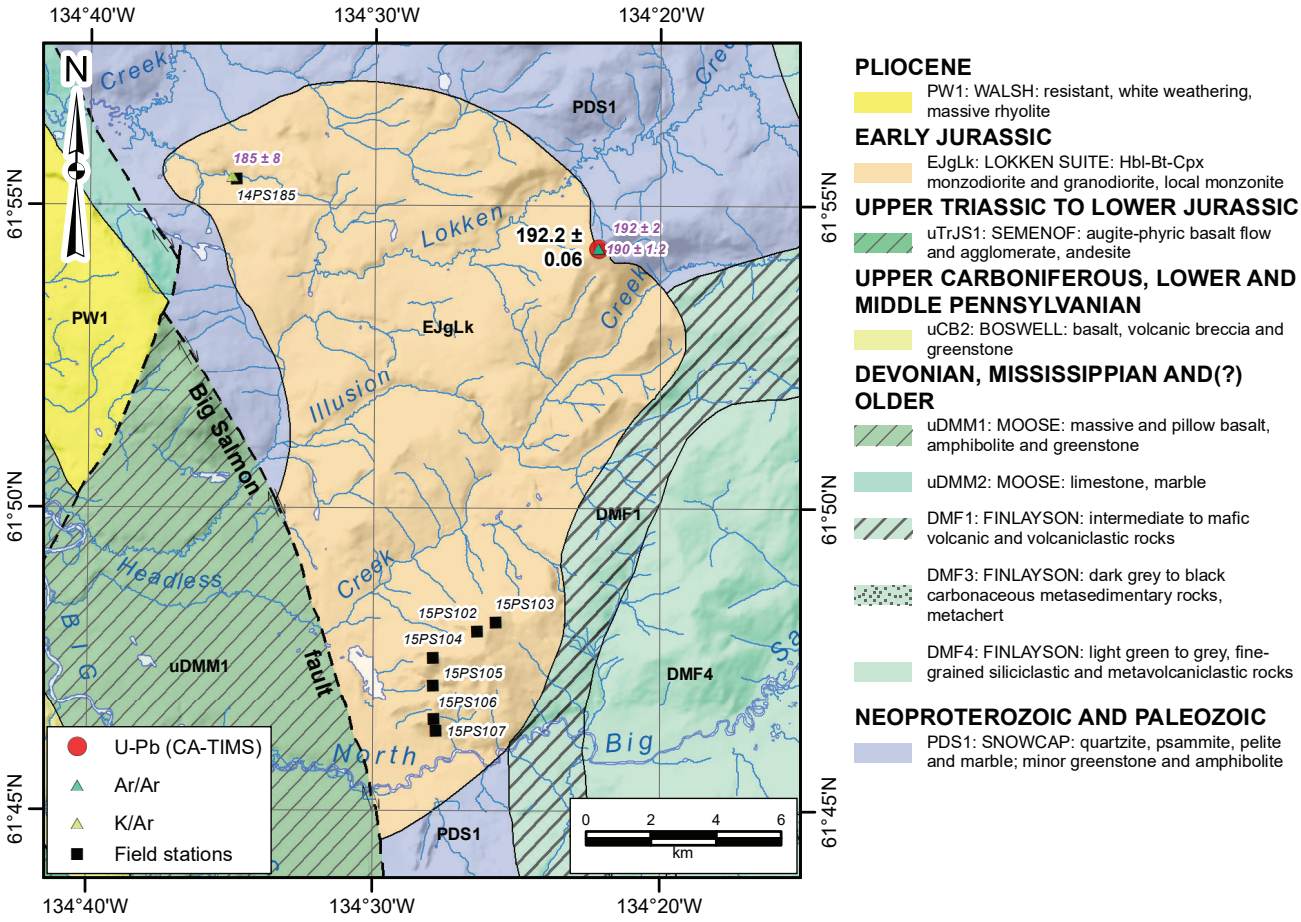


Figure 4-78. *Geology of the Lokken pluton area. Geology from YGS (2020a); fault symbology as in Figure 1-4.*



Figure 4-79. *Outcrops within the southern end of the Lokken pluton.* ***(a)*** *Cliff exposure 2.5 km north of the North Big Salmon River, 15PS105.* ***(b)*** *Rounded, weathered outcrop poorly exposed in a tight spruce forest, 15PS107.*

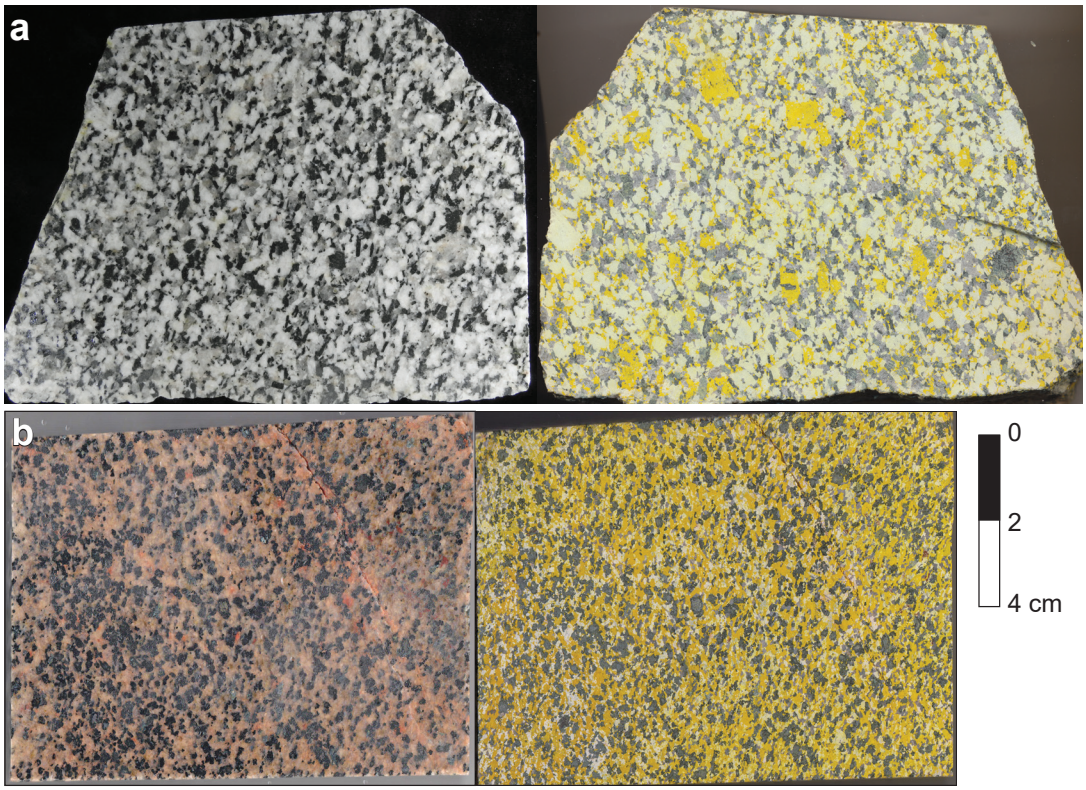


Figure 4-80. *Representative samples from the Lokken pluton. Fresh polished surface (left) and a cobaltinitrite-stained surface (right).* ***(a)*** *Medium-grained, equigranular to weakly K-feldspar porphyritic granodiorite, 14PS185-1.* ***(b)*** *Medium-grained, equigranular monzodiorite, 15PS105-1. Scale is the same for both samples; K-feldspar is stained yellow.*

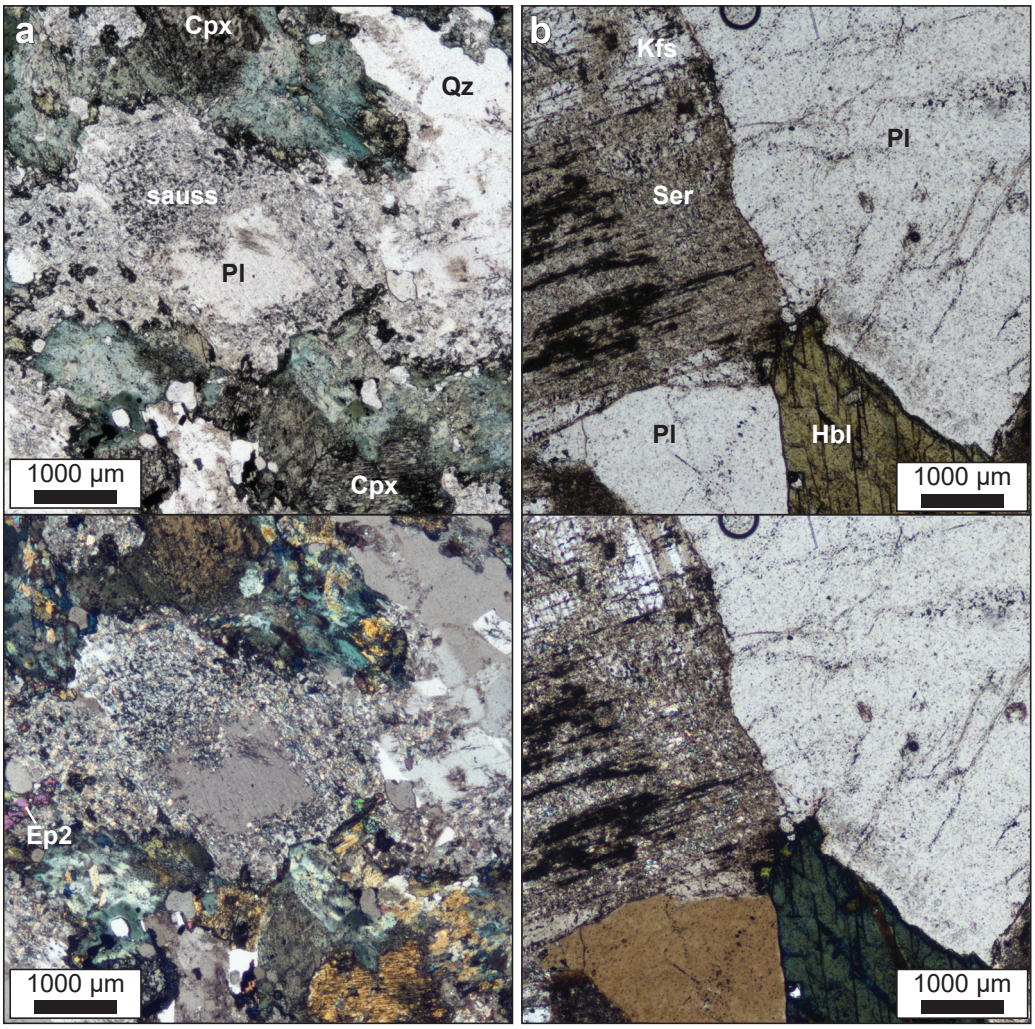


Figure 4-81. *Transmitted light photomicrograph pairs of feldspars from Lokken pluton; plane polarized light (upper) and cross-polarized light (lower).* ***(a)*** *Plagioclase with intensely saussuritized rims (sauss), 14PS184a-1. Clinopyroxene is rimmed by blueish green amphibole at top and bottom of view.* ***(b)*** *Intensely sericitized K-feldspar and relatively fresh plagioclase and hornblende, 14PS185-1.*

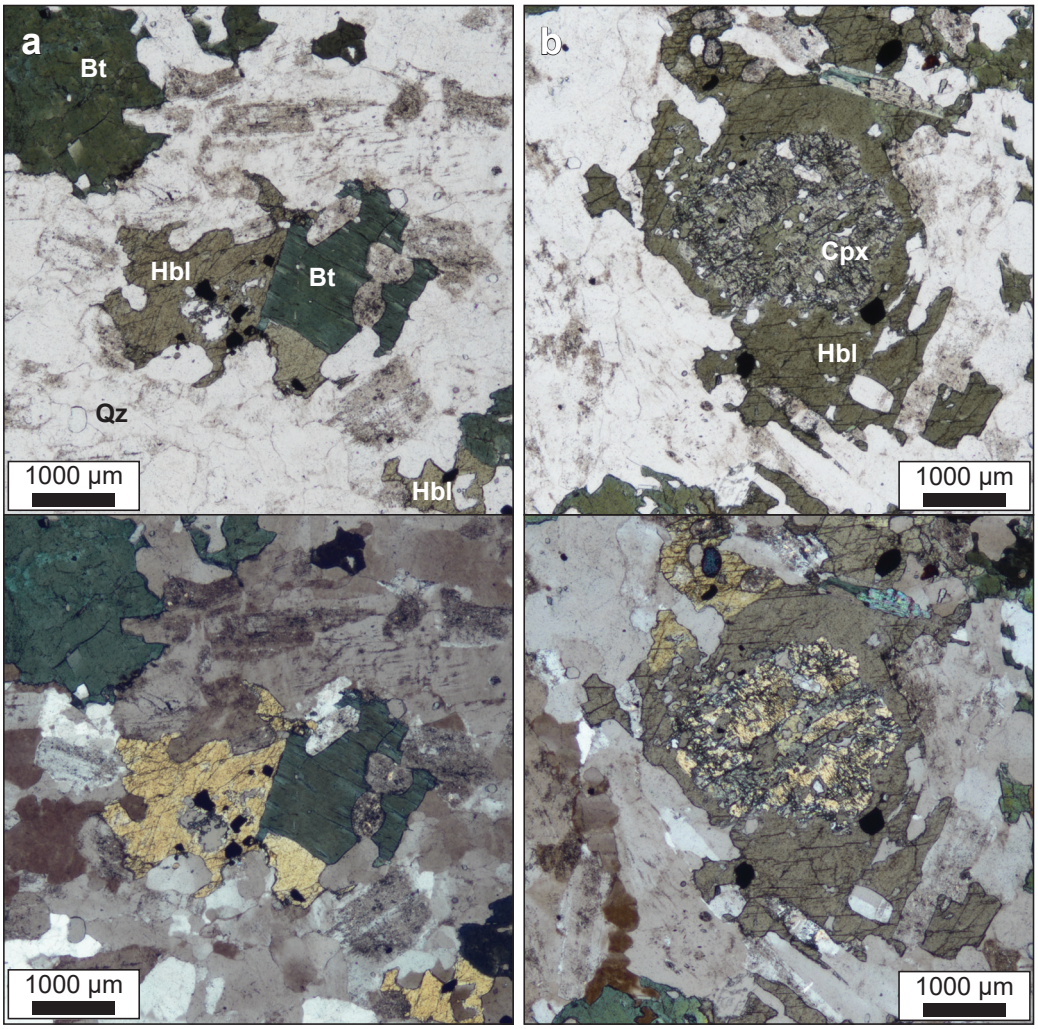


Figure 4-82. *Transmitted light photomicrograph pairs of mafic minerals within granodiorite of the Lokken batholith; plane polarized light (upper) and cross-polarized light (lower).* ***(a)*** *Unaltered, biotite and hornblende in quartz and plagioclase.* ***(b)*** *Embayed and altered clinopyroxene core overgrown by fresh, euhedral hornblende. (a) and (b) from 15PS107-1.*

Oxidation state and mineral occurrences

The Lokken batholith is magnetic (Fig. 4-83) with susceptibilities ranging from 0.45 to 21.60 × 10^{-3} SI units (mean 10.00 × 10^{-3} SI units; n = 9; Fig. 4-3b). An arsenic-antimony anomaly, the Fone occurrence [105E 059] is located approximately 1 km west of the pluton, in proximity to the Big Salmon fault (Fig. 83). It bears similarities, and is likely related to other Paleogene, structurally-controlled epithermal occurrences in the region, such as the Marble anomaly [105L 060], ~32 km to the northwest along the Big Salmon fault, or the Grew Creek deposit [105K 009], ~80 km to the east along the Tintina fault (YGS, 2020b).

Geochronology

The only previous age estimate for the Lokken batholith consists of a K-Ar hornblende date of 185 ± 8 Ma (Stevens *et al.*, 1982a) from the western part of the batholith. We collected a sample of monzodiorite along the eastern margin of the pluton (Fig. 4-78; Appendix 2). Sample 14PS184a yielded sharply faceted zircons with common twinning along the C-axis evident in CL images (Fig. 4-84a; Appendix 3). The zircons also commonly appear corroded with embayed margins and internal pits. No inherited cores are evident in CL images. The thirty-five LA-ICPMS spots analyzed yielded $^{206}Pb/^{238}U$ dates between 203 and 186 Ma, with a weighted

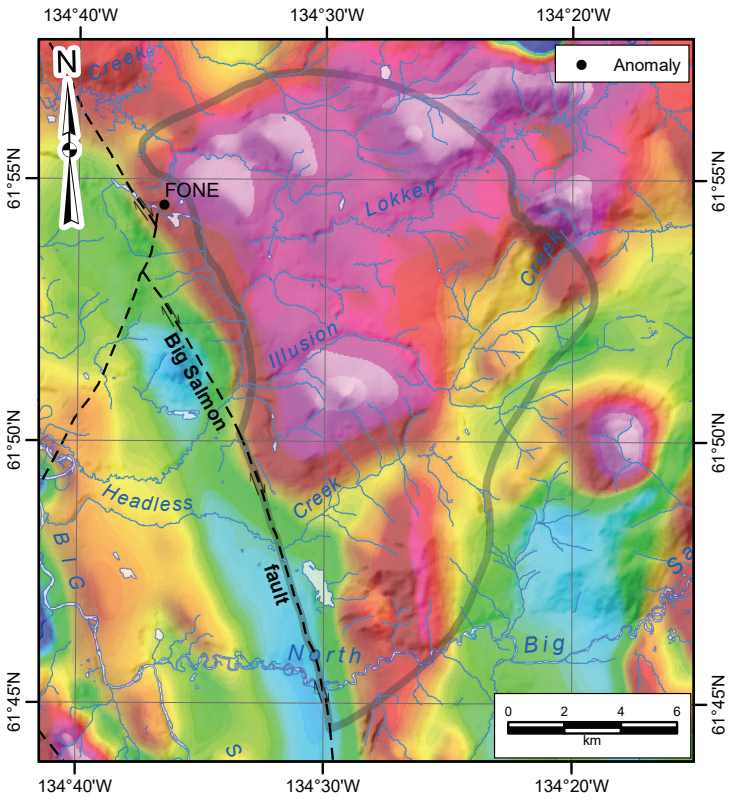


Figure 4-83. *Reduced to pole, residual total field aeromagnetic map of the Lokken batholith (Aurora Geosciences Ltd. and Bruce, 2017c) illustrating location of the Fone MINFILE occurrence along the Big Salmon fault. Fault symbology as in Figure 1-4.*

mean of 190.3 ± 1.2 Ma for 34 of 35 analyses (Fig. 4-84b). Seven zircons were selected for CA-TIMS analyses (Appendix 4). Their $^{206}Pb/^{238}U$ dates range from 192.52 ± 0.13 to 192.06 ± 0.13 Ma, with the youngest five grains yielding a weighted mean of 192.20 ± 0.06 Ma (MSWD = 1.93; Fig. 4-84c) that is interpreted as the crystallization age of this sample.

We also analyzed hornblende and biotite from the same sample by the $^{40}Ar/^{39}Ar$ method at the GSC laboratory in Ottawa (laser, step-heating; Appendix 6). Two aliquots of hornblende show evidence of excess ^{40}Ar in low temperature steps and saddle-shaped age spectra (Fig. 4-85a,b). The second aliquot levels out to a plateau at 192 ± 2 Ma in high temperature steps that is equivalent to the U-Pb zircon date for this sample (Fig. 4-84). An inverse isochron for both hornblende aliquots yields a range of regressions between 198 Ma and 193 Ma, and $^{40}Ar/^{36}Ar_i$ of 494 ± 11 (Fig. 4-85c). The biotite age spectrum for 14PS184-1 shows minor argon loss in low temperature steps and a well-defined plateau at 190.0 ± 1.2 Ma (91.5% of ^{39}Ar released; Fig. 4-85d) indicating cooling below ~350°C (Hodges, 2014) within 2 m.y. of crystallization for the Lokken batholith.

Thermobarometry

One sample from the Lokken pluton, 15PS107-1, contains the suitable mineral assemblage for Al-in-Hbl geobarometry (Hammarstrom and Zen, 1986; Appendix 5). Al^{TOT} in hornblende for this sample is 1.53 with cotectic plagioclase that has X_{An} of 0.27, indicating a crystallization pressure of 3.06 ± 0.85 kbar (Appendix 5; emplacement depth of 11.5 ± 3.2 km). The amphibole-plagioclase mineral thermometer suggests a crystallization temperature of ~759°C, which is slightly lower that the Ti-in-zircon temperature estimate of 773°C from sample 14PS184a-1 (Appendix 3; Watson *et al.*, 2006).

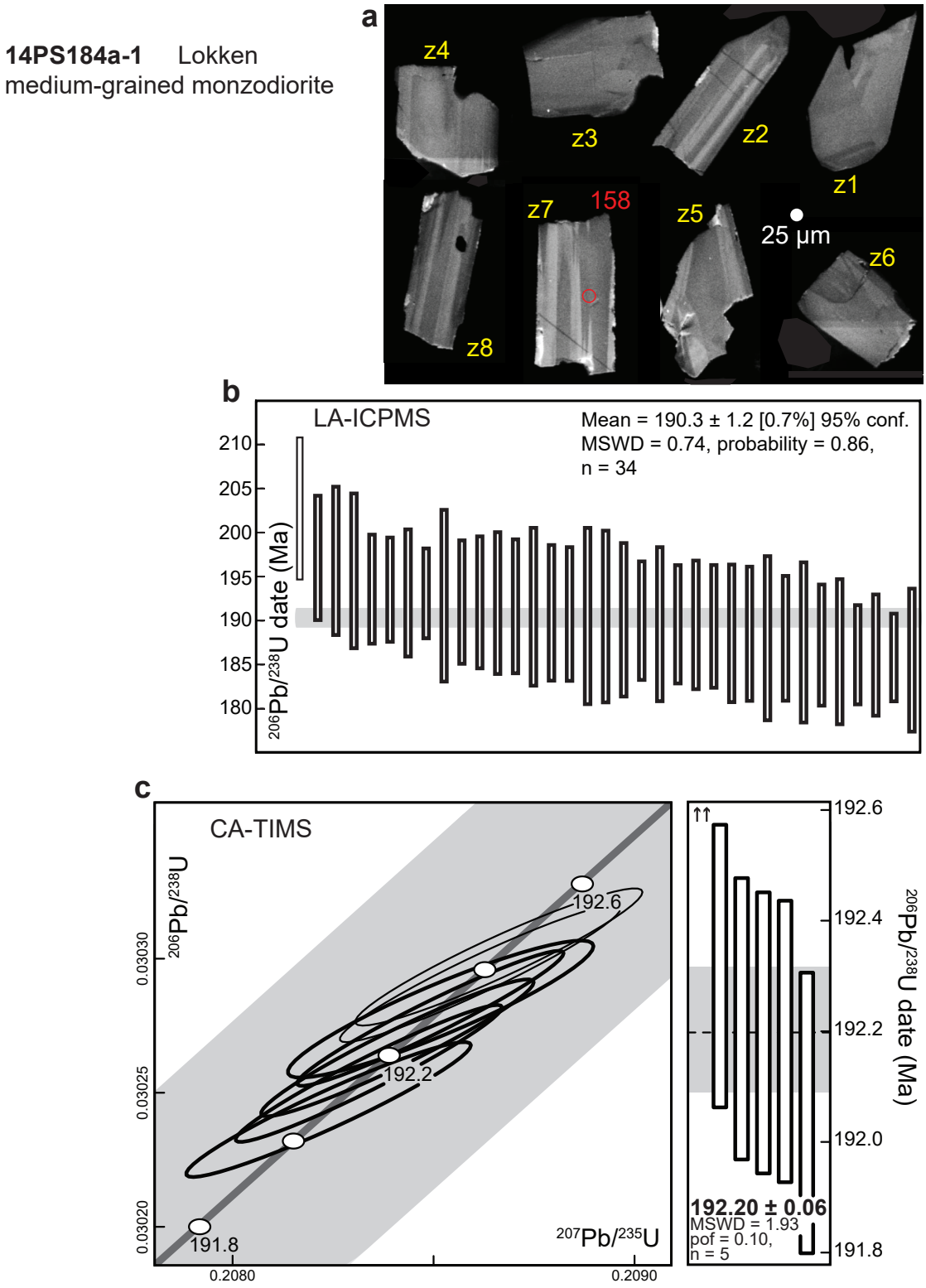


Figure 4-84. *U-Pb geochronological results for sample 14PS184a-1, Lokken batholith.* ***(a)*** *CL images of representative zircons. LA-ICPMS spot in red, analyses number of CA-TIMS analyses in yellow.* ***(b)*** *Ranked plot of LA-ICPMS $^{206}Pb/^{238}U$ dates (Appendix 3).* ***(c)*** *Concordia diagram (left) and ranked $^{206}Pb/^{238}U$ dates (right) for 7 zircons analyzed by CA-TIMS (Appendix 4). The light grey band around concordia (dark grey line) shows the decay constant uncertainties. Analyses included in weighted mean age (light grey horizontal bar) calculations are bold; analyses with thin lines are not used in calculations. Line-type designations are the same in all plots. Errors in all plots are at 2σ. MSWD = mean squared weighted deviation, pof = probability of fit, n = number of analyses included in age calculation.*

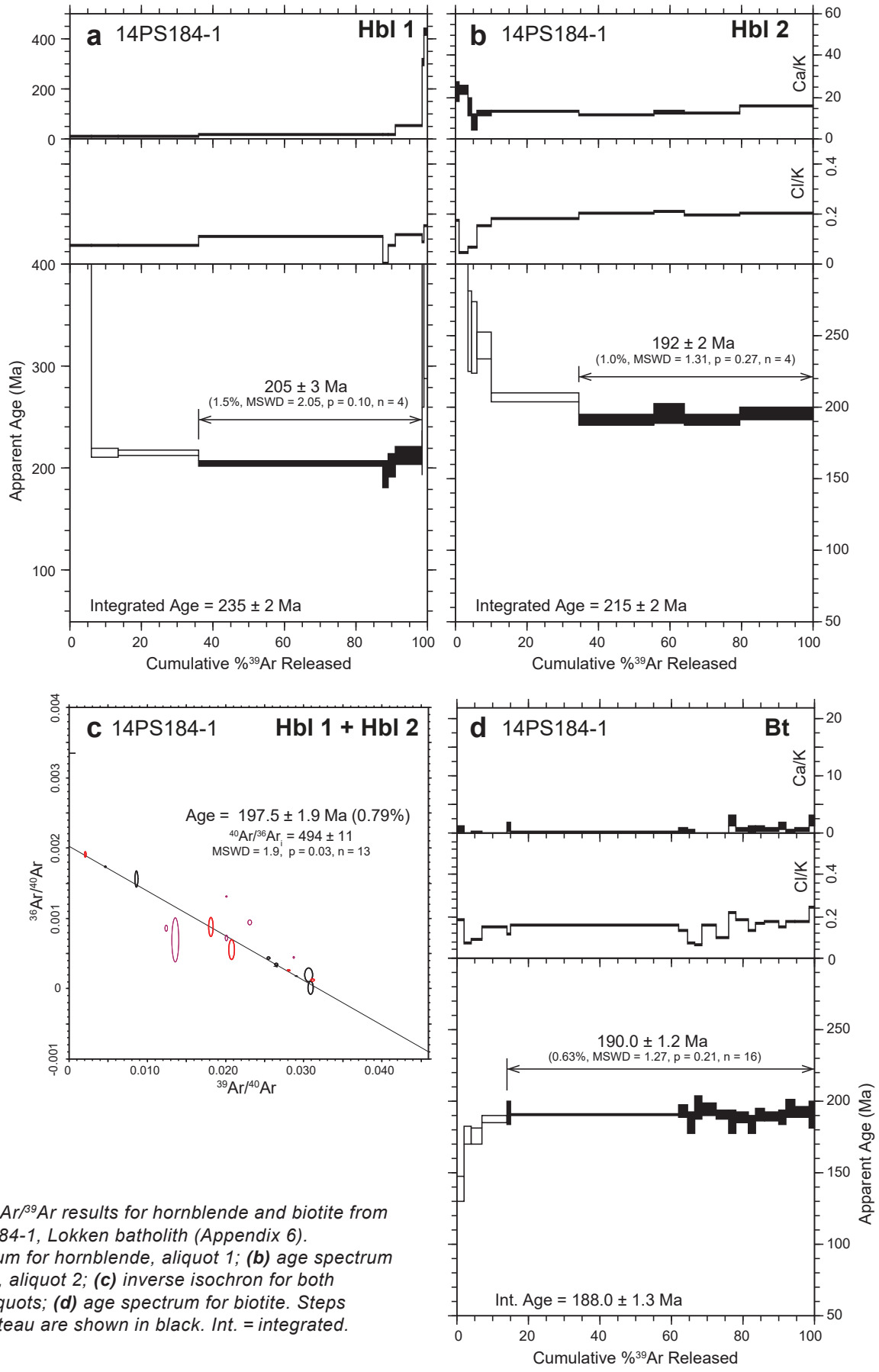


Figure 4-85. *$^{40}Ar/^{39}Ar$ results for hornblende and biotite from sample 14PS184-1, Lokken batholith (Appendix 6).* ***(a)*** *Age spectrum for hornblende, aliquot 1;* ***(b)*** *age spectrum for hornblende, aliquot 2;* ***(c)*** *inverse isochron for both hornblende aliquots;* ***(d)*** *age spectrum for biotite. Steps included in plateau are shown in black. Int. = integrated. Errors are 2σ.*

Macmillan Range plutons

Two small granodiorite to monzonite plutons assigned to the Lokken suite are exposed in the Macmillan Range, north of Macmillan River in northwestern Glenlyon (NTS 105L), approximately 42 km east-northeast of Pelly Crossing (Fig. 4-1). The main body (Cornolio pluton of Colpron, 1998, 1999) is exposed on the southern flank of the Macmillan Range and has a mapped extent of ~4.4 km^2 (Fig. 4-86; Table 4-1). It intrudes mainly quartzite and black phyllite of the Mississippian Pelmac formation (Finlayson assemblage, DMF4 on Fig. 4-86; Fig. 4-87); its northeastern tip intrudes meta-andesite and meta-rhyolite of the Mississippian Little Kalzas formation (both units are part of the Finlayson assemblage, Yukon-Tanana terrane; Colpron *et al.*, 2002, 2006b; Fig. 4-86). The pluton is generally massive (Fig. 4-88), although weak alignment of hornblende locally defines a magmatic foliation. The monzonite is locally cut by aplite dikes with diffuse margins (Fig. 4-88). Fluorite is locally present near the northern margin of the pluton. The northern margin of the pluton is marked by numerous dikes injected in pelitic metasedimentary rocks. A contact aureole with cordierite (± sillimanite) is present along the northern margin of the pluton (Colpron, 1999). A smaller body (~1.4 km^2) exposed along stream cuts approximately 2.5 km north of the main pluton is inferred to be related by Colpron (1998, 1999).

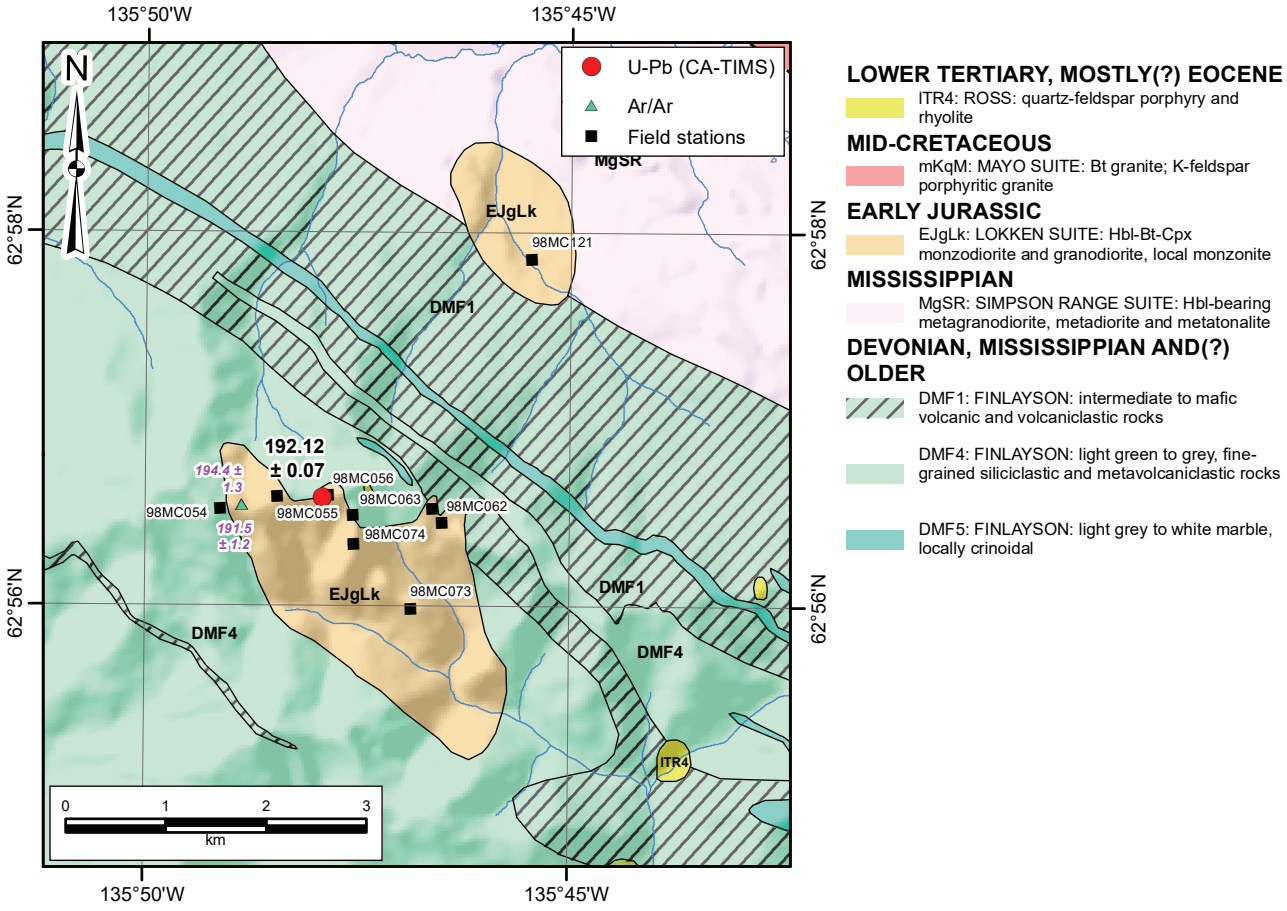


Figure 4-86. *Geology of the Macmillan Range plutons area. Geology from YGS (2020a); fault symbology as in Figure 1-4.*

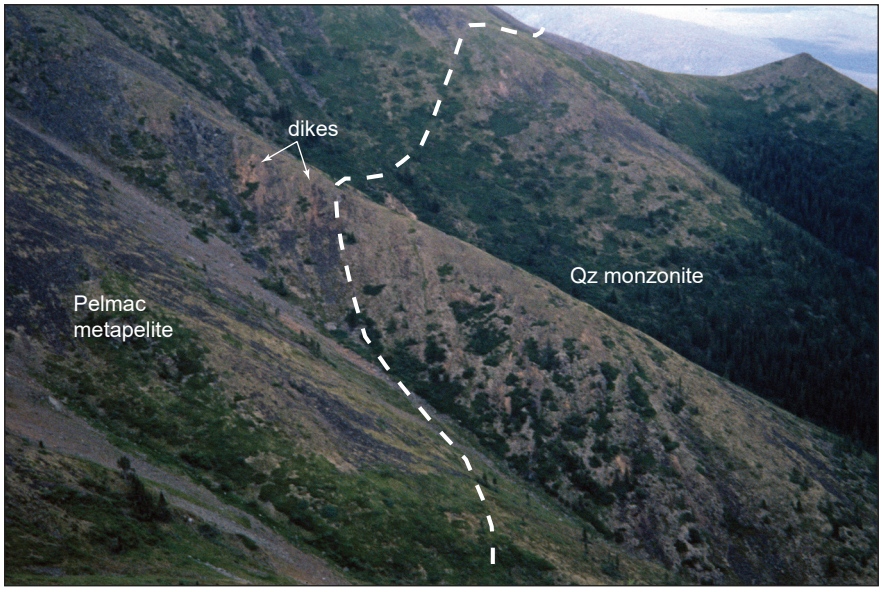


Figure 4-87. *Looking southeast along the northern contact of the Macmillan Range plutons. Contact outlined by white dashed line. The monzonite (right) intrudes black metapelite of the Pelmac formation (DMF4, Finlayson assemblage, Yukon-Tanana terrane).*

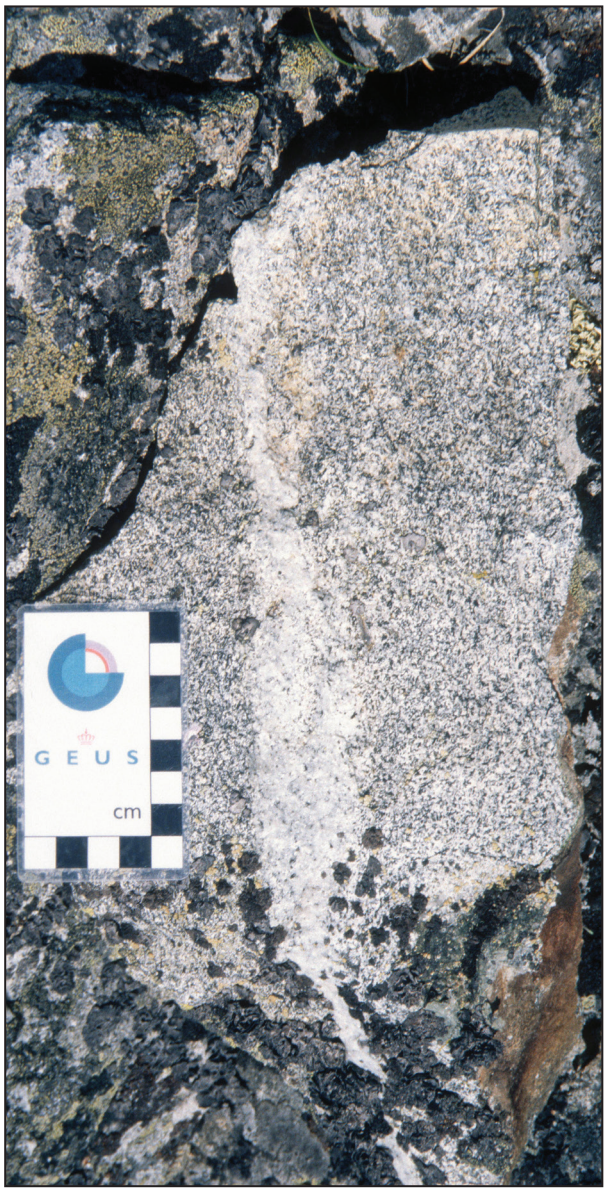


Figure 4-88. *Outcrop of monzonite cut by thin aplite dike, northern margin of Macmillan Range pluton.*

Petrography

The Macmillan Range pluton is fine to medium-grained, equigranular, mesocratic monzonite to granodiorite, with up to 15–30% modal quartz (Figs. 4-2b and 4-89). Plagioclase, K-feldspar and mafic minerals are subhedral to euhedral, quartz is anhedral and commonly interstitial between other minerals (Fig. 4-90). Hornblende is more abundant than biotite, and mafic minerals make up to 20–35% of the rock; clinopyroxene is less common but can represent as much as 10% of the rock. Clinopyroxene occurs both as tabular crystals (Fig. 4-91) and as cores in hornblende (Fig. 4-90a). Both hornblende and clinopyroxene are fresh, biotite is weakly to completely altered to chlorite (Fig. 4-90b). Epidote is present in trace amounts and mostly as alteration mineral. Plagioclase is moderately saussuritized (Fig. 4-90c), K-feldspar is sericitized. Titanite and magnetite are common accessory minerals making up to 5% of the rock (Fig. 4-91). A single sample (98MC121) from the small stock exposed north of Macmillan Range (Fig. 4-86) is strongly altered and includes clinozoisite, sericite groundmass, carbonate veining, intense saussuritization of plagioclase phenocrysts, and chloritization of hornblende.

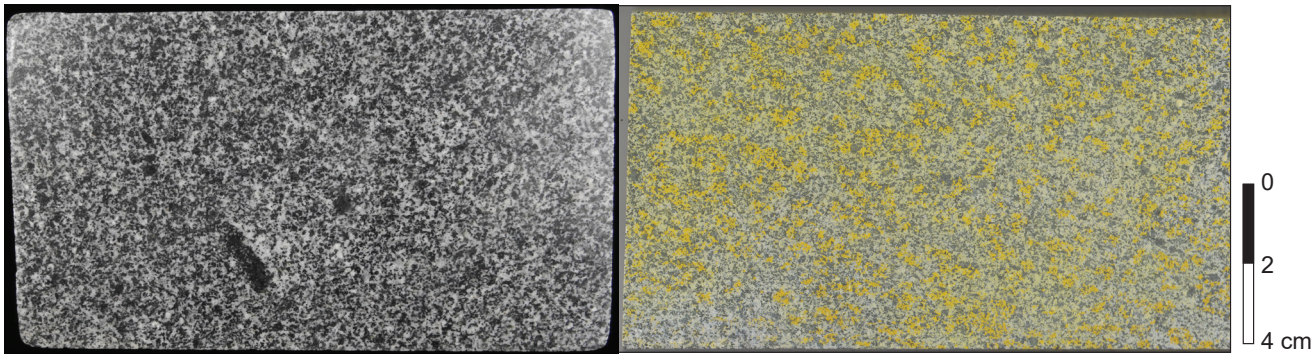


Figure 4-89. *Representative sample from the Macmillan Range pluton, 15MC003-1. Fresh polished surface (left) and a cobaltinitrite-stained surface (right). K-feldspar is stained yellow.*

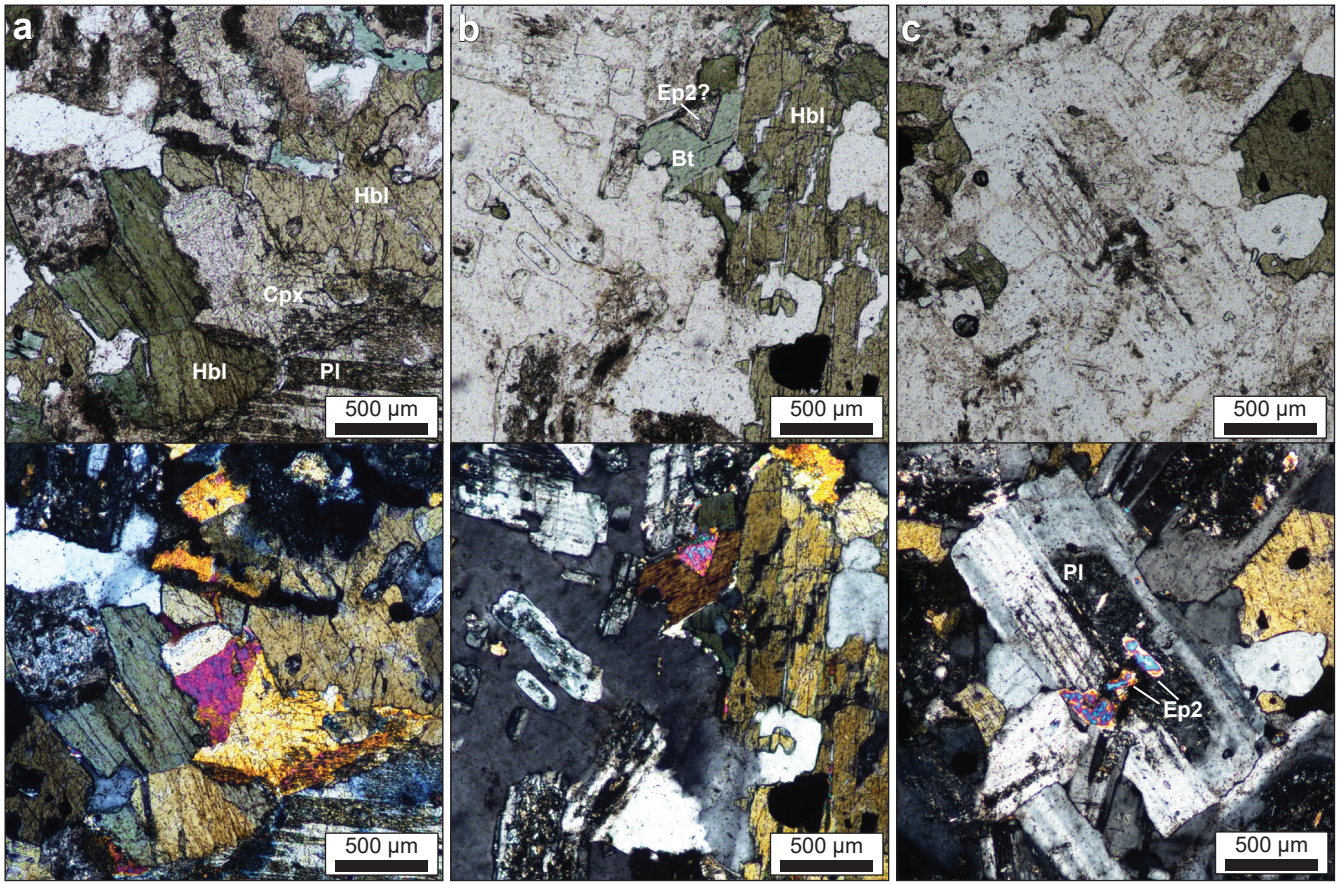


Figure 4-90. *Transmitted light photomicrograph pairs; plane polarized light (upper) and cross-polarized light (lower).* ***(a)*** *Clinopyroxene core overgrown on three sides by fresh hornblende.* ***(b)*** *Secondary epidote intergrown with chloritized biotite and hornblende.* ***(c)*** *Anhedral epidote in the centre of a saussuritized plagioclase phenocryst indicating a secondary origin for the epidote. All images from sample 15MC003-1.*

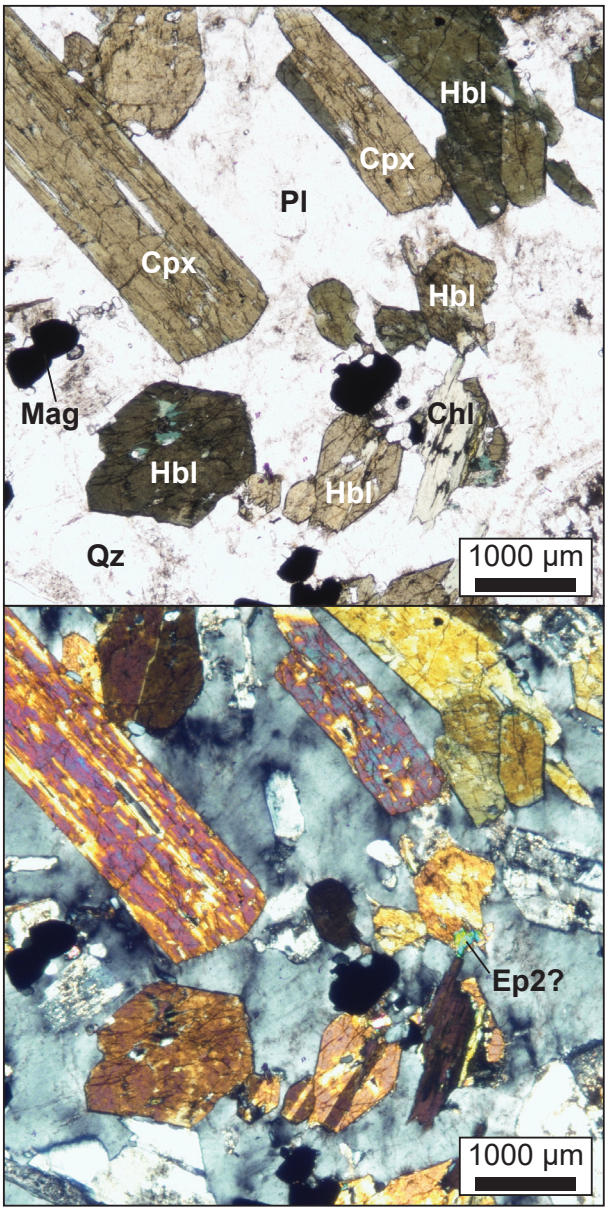


Figure 4-91. *Transmitted light photomicrograph pairs showing the mafic mineral assemblage of the Macmillan Range plutons, 98MC074-1; plane polarized light (upper) and cross-polarized light (lower). Fresh twinned hornblende is equant whereas clinopyroxene is tabular. Biotite completely altered to chlorite.*

Oxidation state and mineral occurrences

The main body of the Macmillan Range pluton is strongly magnetic (Fig. 4-92), whereas the northern stock is non-magnetic, possibly as result of the strong alteration observed in this rock or because it represents another magmatic phase unrelated to the larger pluton to the south. There are no known mineral occurrences associated with the Macmillan pluton. A single Au anomaly (132 ppb) in stream sediments ~3.5 km to the south, and a pair of Hg anomalies (302–571 ppb; Jackaman, 2015a) in proximity to the Macmillan Range plutons suggest potential for epithermal mineralization, but this could also be related to Eocene felsic plugs in the area (Fig. 4-86; Colpron, 1998, 1999).

Geochronology

A previous attempt at dating the Macmillan Range pluton by ID-TIMS on multi-grain zircon fractions yielded strongly discordant results, and a lower intercept of a three-point regression suggested a possible date of *ca.* 264 Ma (J.K. Mortensen, unpublished data, 1999). Hornblende from the western part of the pluton yielded a $^{40}Ar/^{39}Ar$ plateau date of 191.5 ± 1.2 Ma, while biotite from the same sample (98MC054) yielded disturbed age spectra with higher temperature steps from three aliquots suggesting a $^{40}Ar/^{39}Ar$ date of 194.4 ± 1.3 Ma (Joyce *et al.*, 2015).

A sample of Hbl-Bt monzonite (15MC003) was collected near the northern margin of the Macmillan Range pluton for U-Pb dating at Boise State University (Appendix 2; Fig. 4-86). It yielded a small amount of tiny zircon needles that were too small to mount for CL imaging and LA-ICPMS analyses. Five zircon needles were analyzed by CA-TIMS and yielded concordant $^{206}Pb/^{238}U$ dates between 192.22 ± 0.16 and 192.03 ± 0.15 Ma, and a weighted mean of 192.12 ± 0.07 Ma (MSWD = 1.09; Fig. 4-93; Appendix 4).

Thermobarometry

Sample 15MC003 from the Macmillan Range pluton contains the suitable mineral assemblage for Al-in-Hbl geobarometry (Hammarstrom and Zen, 1986; Appendix 5). Al^{TOT} in hornblende is 1.78 with cotectic plagioclase that has X_{An} of 0.48, indicating a crystallization pressure estimate of 2.62 ± 1.01 kbar (emplacement depth of 9.9 ± 3.8 km) and solidus temperatures of ~817°C. However, the high X_{An} content of plagioclase suggests this temperature estimate may be elevated.

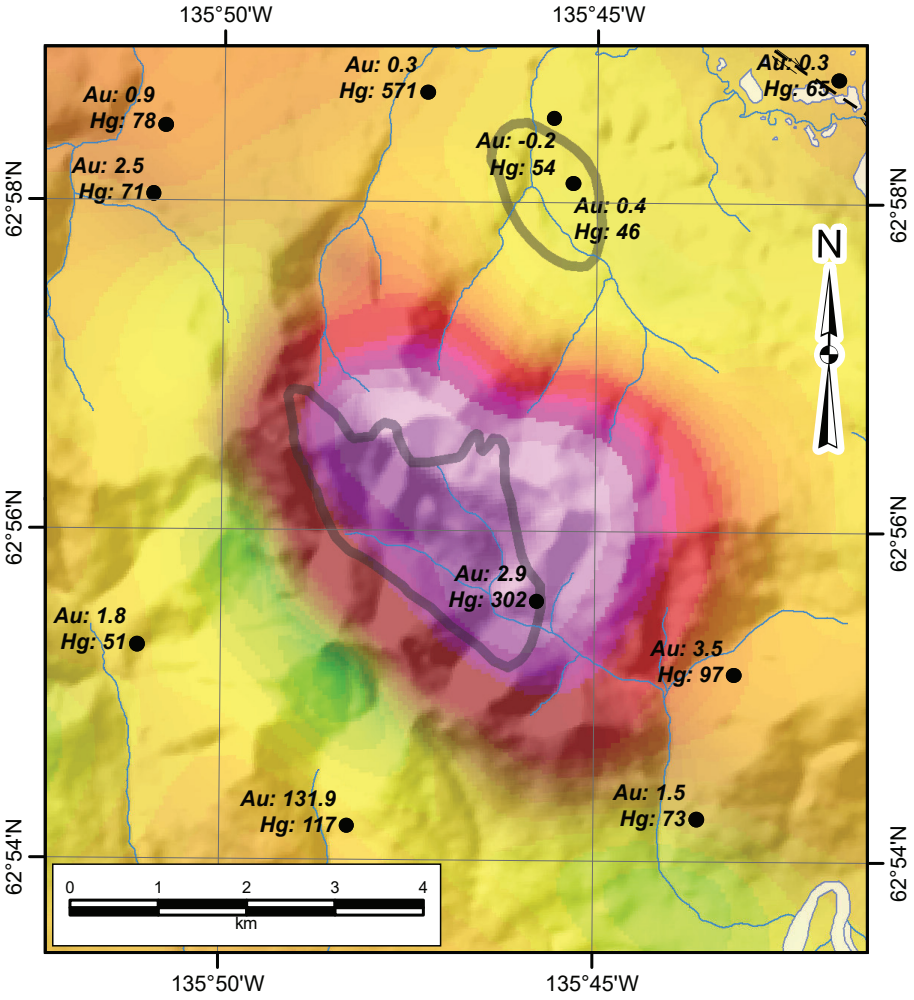


***Figure 4-92**. Reduced to pole, residual total field aeromagnetic map of the Macmillan Range plutons (Aurora Geosciences Ltd. and Bruce, 2017d). Concentrations of Au and Hg in stream sediments are indicated for samples collected in the vicinity of the Macmillan Range plutons (from Jackaman, 2015a).*

15MC003-1 Macmillan Range pluton monzonite

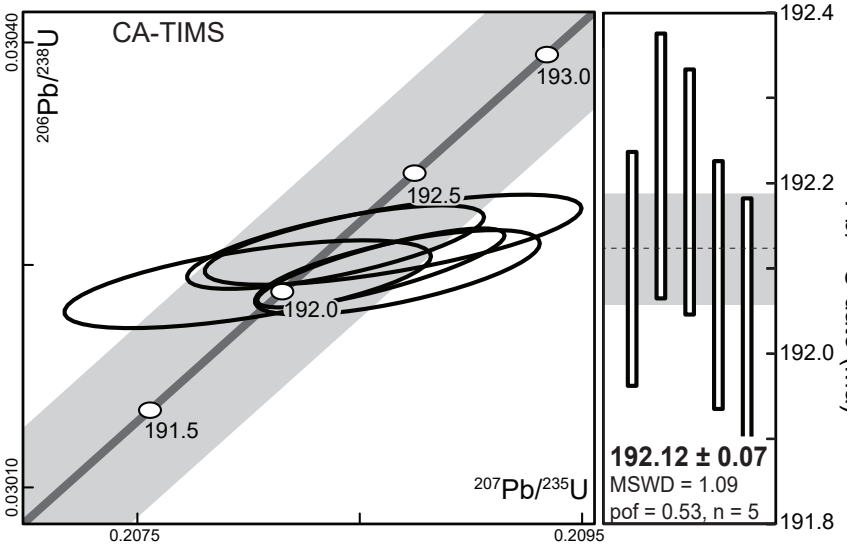


***Figure 4-93**. U-Pb geochronological results for sample 15MC003, Macmillan Range plutons. Concordia diagram (left) and ranked $^{206}Pb/^{238}U$ dates (right) for 5 zircons analyzed by CA-TIMS (Appendix 4). The light grey band around concordia (dark grey line) shows the decay constant uncertainties. Analyses included in weighted mean age (light grey horizontal bar) calculations are bold; analyses with thin lines are not used in calculations. Line-type designations are the same in all plots. Errors in all plots are at 2σ. MSWD = mean squared weighted deviation, pof = probability of fit, n = number of analyses included in age calculation.*

Thirtymile Lake plutons

Two small granodiorite plutons that intrude metasedimentary rocks of the Yukon-Tanana terrane west of Thirtymile Lake, approximately 75 km north of Teslin, are the oldest plutons of the Lokken suite in southern Yukon (Figs. 4-1, 4-77 and 4-94). The Thirtymile Lake plutons have a mapped extent of 15.3 km² for the eastern body, ~1 km west of Thirtymile Lake, and 4.6 km² for the western pluton (Table 4-1). Both plutons are mainly exposed along two subalpine ridges. These two plutons intrude a thrust-bound panel of marble and muscovite-chlorite phyllite (Gordey and Stevens, 1994), interpreted as part of the Devonian–Mississippian Finlayson assemblage (Yukon-Tanana terrane) by Colpron (2006; Fig. 4-94). Both plutons are dominantly granodiorite with subordinate pyroxene-porphyritic monzonite (Fig. 4-95; Table 4-1). The granodiorite is medium grained and equigranular, whereas the monzonite has clinopyroxene phenocrysts up to 1 cm long (Figs. 4-95 to 4-97).

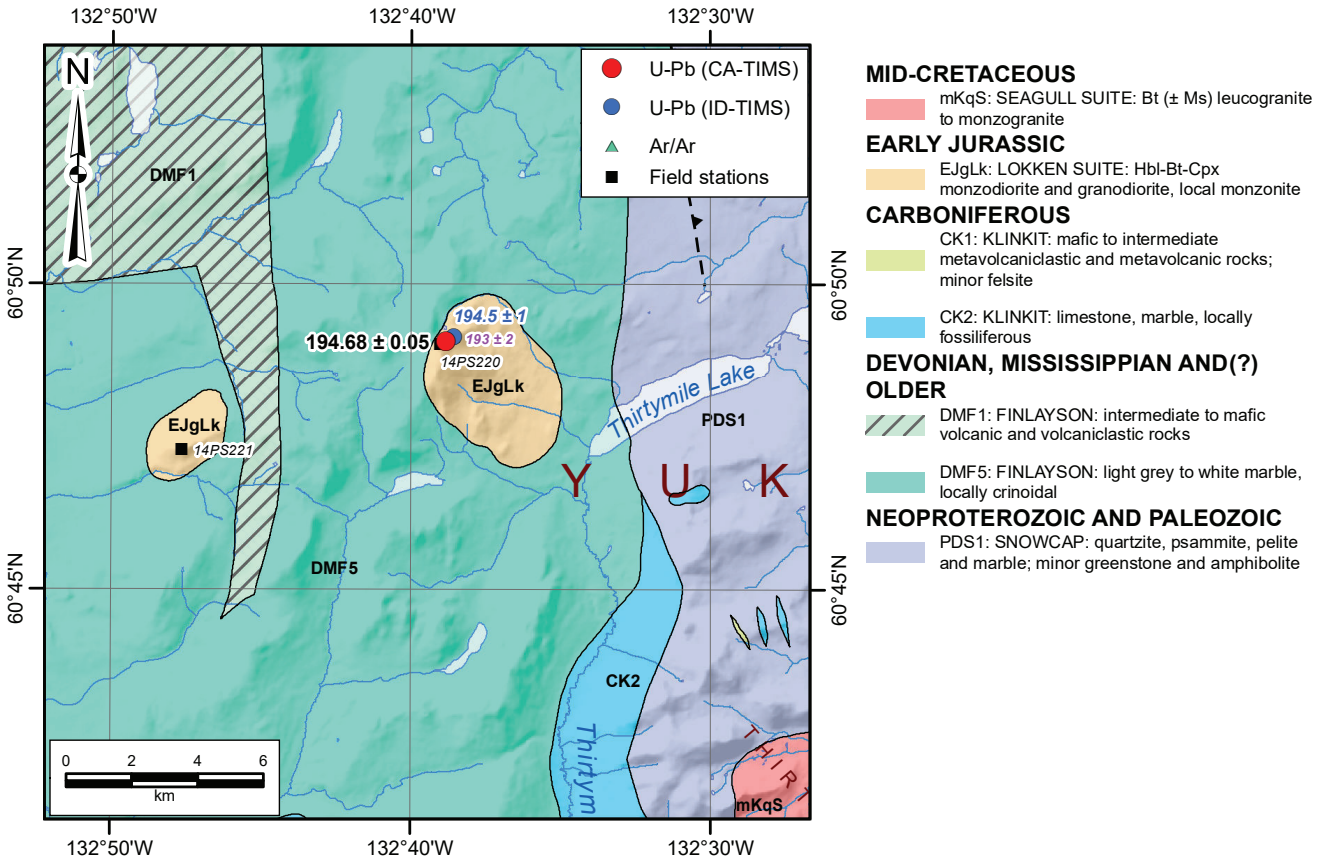


Figure 4-94. *Geology of Thirtymile Lake plutons area. Geology from YGS (2020a); fault symbology as in Figure 1-4.*

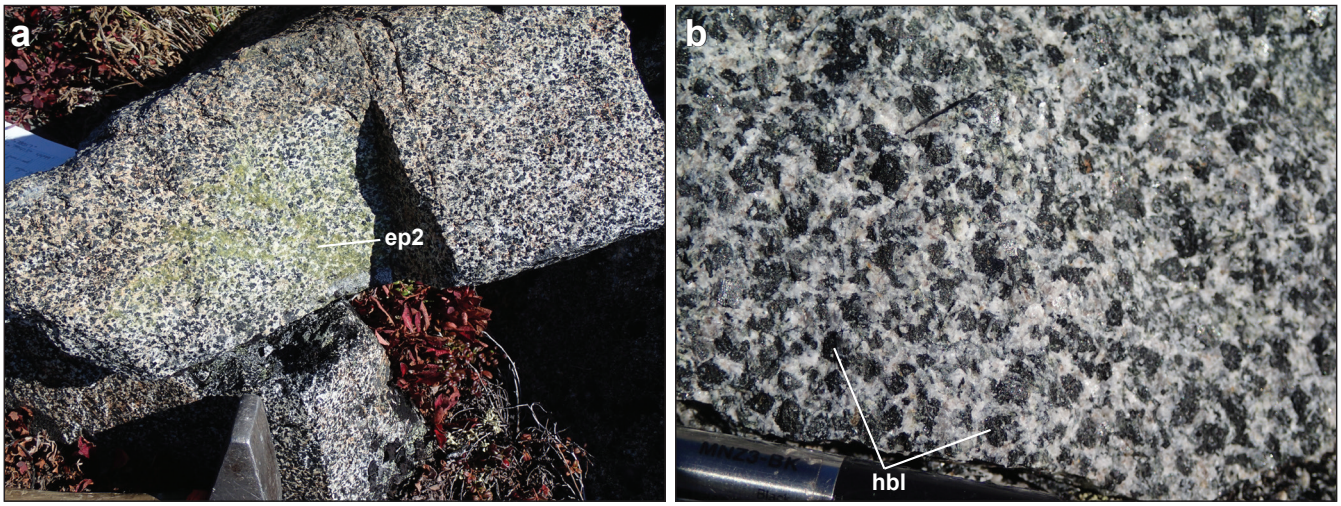


Figure 4-95. *Outcrop sample of western Thirtymile Lake body.* ***(a)*** *Monzodiorite with secondary epidote on fracture surface, hammer head at bottom is 4 cm.* ***(b)*** *Hornblende monzodiorite, pencil at bottom is 1 cm across. Both photos from station 14PS221.*

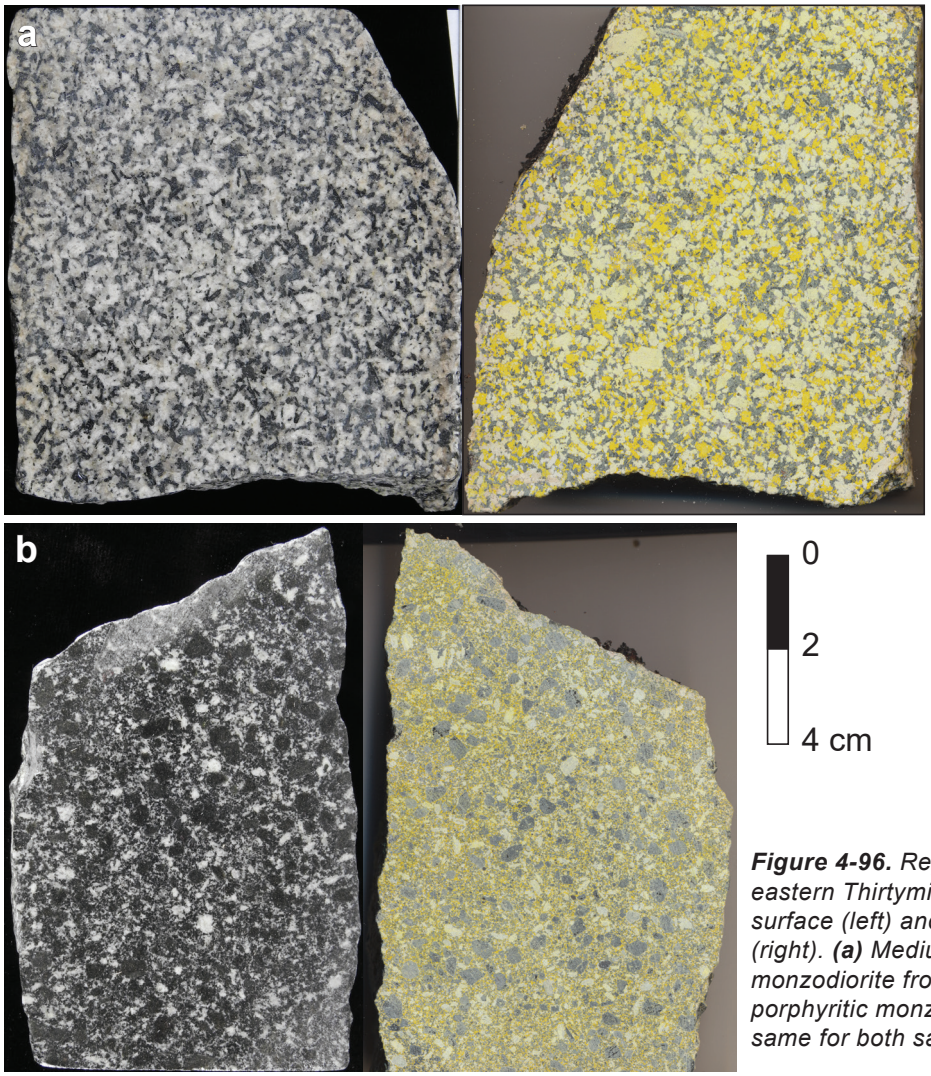


Figure 4-96. *Representative samples from the eastern Thirtymile Lake body. Fresh polished surface (left) and a cobaltinitrite-stained surface (right).* ***(a)*** *Medium-grained, equigranular monzodiorite from 14MC142-1,* ***(b)*** *pyroxene porphyritic monzonite from 14PS220-1. Scale is the same for both samples; K-feldspar is stained yellow.*

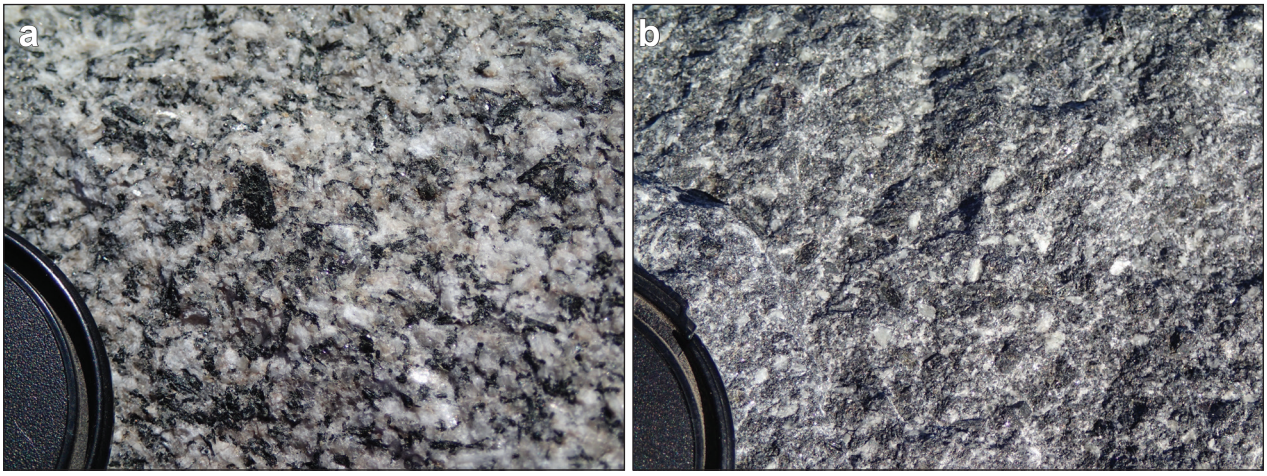


Figure 4-97. *Outcrop sample of the eastern Thirtymile Lake body.* ***(a)*** *Granodiorite lithology,* ***(b)*** *pyroxene monzonite lithology. Both photos from station 14MC142.*

Petrography

Hornblende and biotite are the main mafic phases in the granodiorite and hornblende often contains inclusions of chloritized biotite (Fig. 4-98a); plagioclase and K-feldspar are unaltered to weakly saussuritized and sericitized, respectively. Hornblende and biotite are both present in the monzonite, but crystals are generally ≤2 mm and part of the groundmass (Fig. 4-98b), whereas 1–10 mm clinopyroxene phenocrysts are the main mafic mineral and give the rock its porphyritic texture (Figs. 4-96b and 4-98c). The rims of clinopyroxene phenocrysts are locally altered to carbonate and chlorite (Fig. 4-98b,c). In the monzonite, plagioclase and K-feldspar have moderately to intensely saussuritized and sericitized cores, respectively (Fig. 4-99).

Oxidation state and mineral occurrences

The Thirtymile Lake plutons are magnetic (Fig. 4-100) with susceptibilities of 2.87 and 26.80 × 10^{-3} SI units for the western and eastern plutons, respectively (Fig. 4-3b). One minor occurrence, Nisutlin [105C 025], is located near the centre of the eastern body and consists of pyrite and arsenopyrite associated with a small porphyritic dike (YGS, 2020b). It is not known if this occurrence is genetically related to the Early Jurassic pluton or to a mid-Cretaceous pluton located ~15 km to the southeast (Figs. 4-94 and 4-100).

Geochronology

Monzodiorite of the Thirtymile Lake pluton was previously dated by ID-TIMS at the Geological Survey of Canada using multi-grain zircon and titanite fractions (Gordey *et al.*, 1998). Two nearly concordant zircon fractions yielded a weighted mean $^{206}Pb/^{238}U$ date of 194.8 ± 0.2 Ma, and two titanite fractions have overlapping $^{206}Pb/^{238}U$ dates at 194.5 ± 0.7 Ma. Gordey *et al.* (1998) interpreted a crystallization age of 194.5 ± 1.0 Ma from these data. Hornblende from the same sample yielded a $^{40}Ar/^{39}Ar$ date of 193 ± 2 Ma (Gordey *et al.*, 1998).

We collected a sample of granodiorite from the largest of the Thirtymile Lake plutons, ~250 m west of the site sampled by Gordey *et al.* (1998), for LA-ICPMS and CA-TIMS analyses at Boise State University (Appendix 2). Sample 14MC142 yielded abundant stubby, prismatic zircons with well-defined concentric igneous zoning (Fig. 4-101a). Thirty-three zircons were analyzed by LA-ICPMS and yielded $^{206}Pb/^{238}U$ dates between 199 and 175 Ma, with 30 spots having a weighted mean $^{206}Pb/^{238}U$ date of 188.4 ± 1.5 Ma (Fig. 4-101b; Appendix 3). Six zircons were selected for CA-TIMS analyses and yielded concordant $^{206}Pb/^{238}U$ dates between 194.74 ± 0.14 and 194.58 ± 0.13 Ma, and a weighted mean of 194.67 ± 0.05 Ma (MSWD = 0.83, n = 6; Fig. 4-101c; Appendix 4).

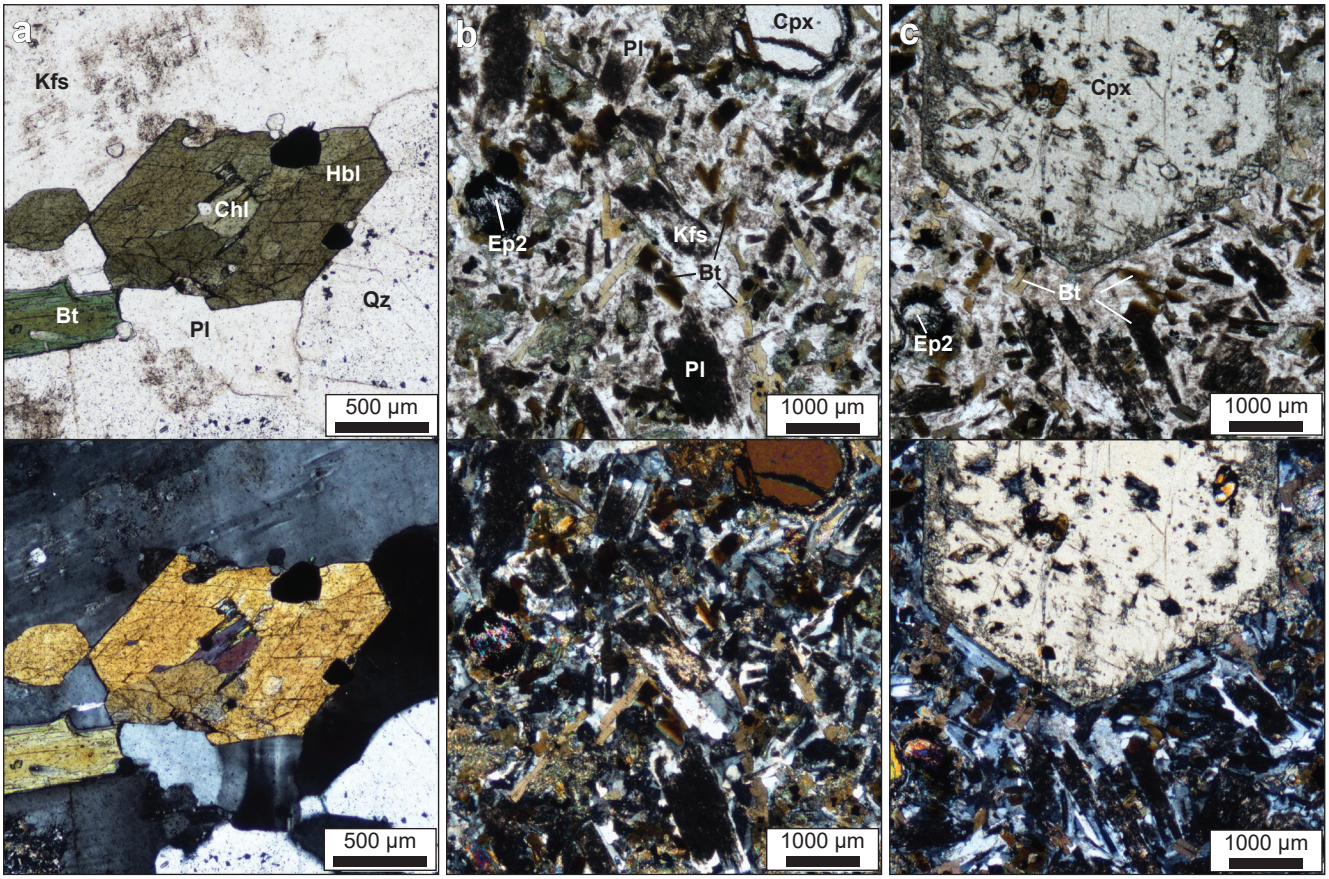


Figure 4-98. *Transmitted light photomicrograph pairs; plane polarized light (upper) and cross-polarized light (lower).* ***(a)*** *Medium-grained granodiorite with biotite inclusions (altered to chlorite) within hornblende and weak saussuritization of K-feldspar cores, 14MC142-1.* ***(b)*** *Biotite-rich fine-grained groundmass with porphyritic clinopyroxene; local secondary epidote.* ***(c)*** *Large clinopyroxene phenocryst with thin amphibole rim within fine-grained groundmass; local secondary epidote. (b) and (c) from station 14PS220.*

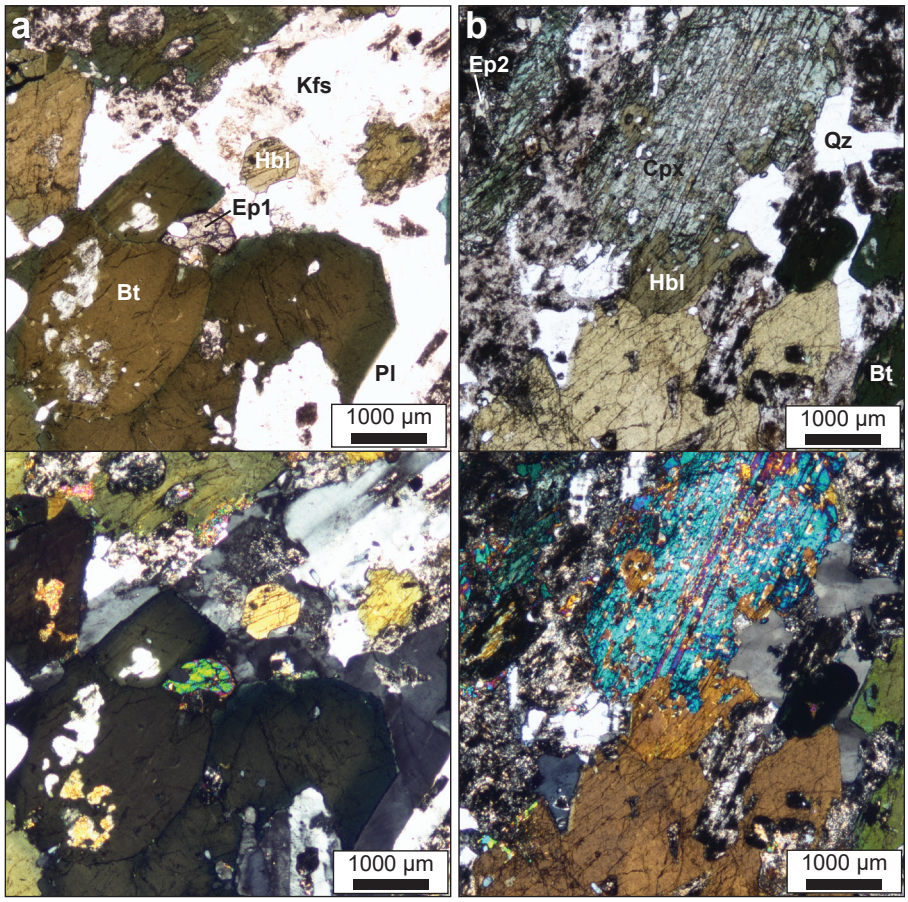


Figure 4-99. *Transmitted light photomicrograph pairs; plane polarized light (upper) and cross-polarized light (lower).* ***(a)*** *Epidote intergrown with biotite; weak saussuritization of K-feldspar.* ***(b)*** *Resorbed and altered clinopyroxene phenocryst intergrown with hornblende; local secondary epidote. Both from station 14PS221.*

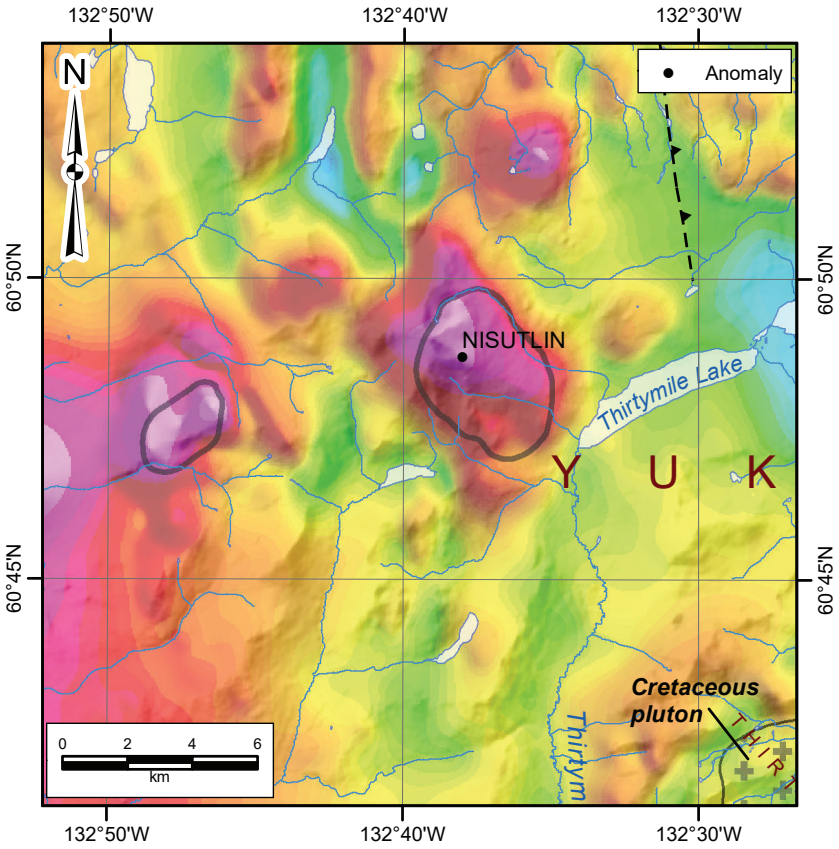


Figure 4-100. *Reduced to pole, residual total field aeromagnetic map of the Thirtymile Lake plutons (Aurora Geosciences Ltd. and Bruce, 2017e). Fault symbology as in Figure 1-4.*

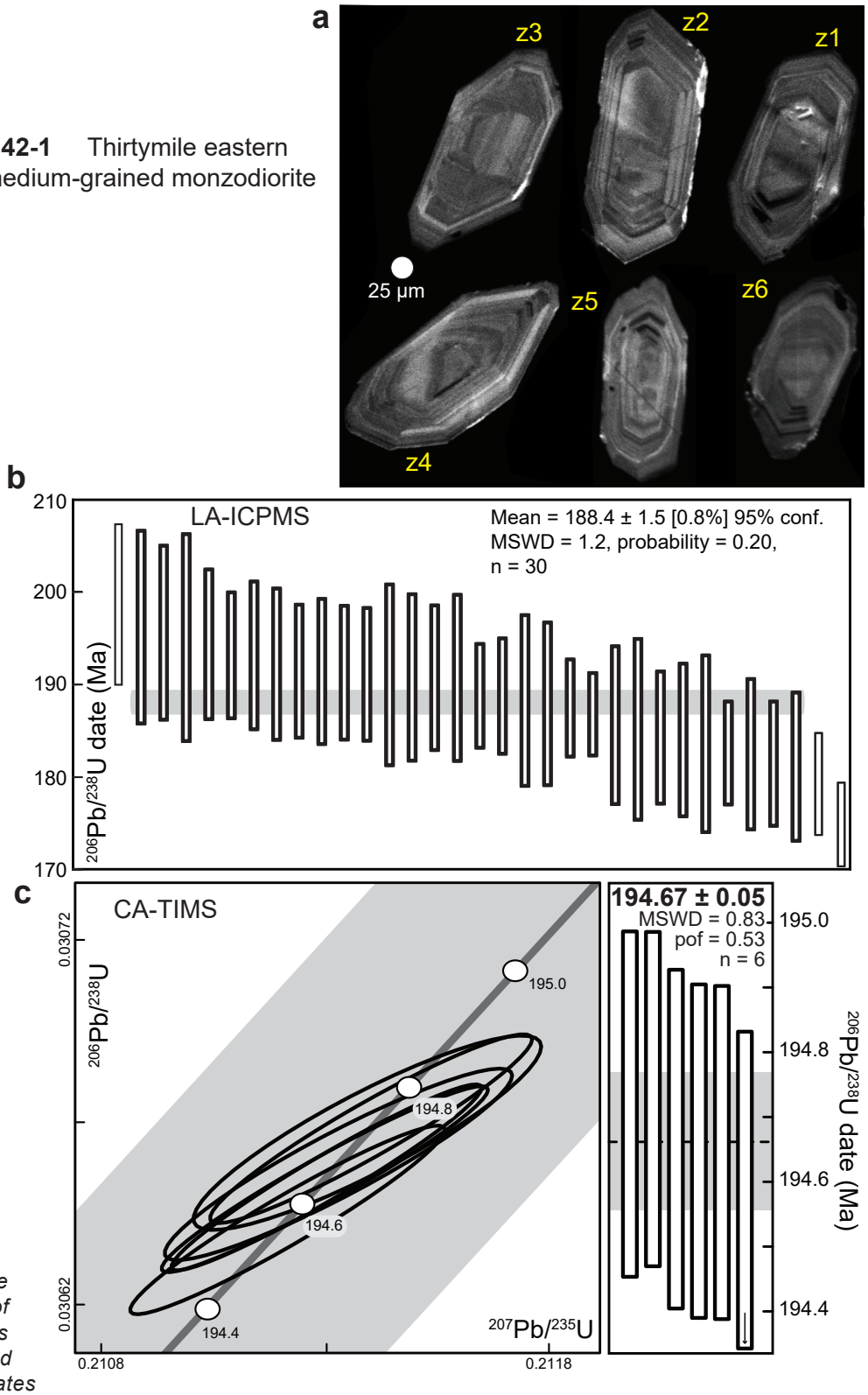


Figure 4-101. *U-Pb geochronological results for sample 14MC142-1, Thirtymile Lake plutons.* ***(a)*** *CL images of representative igneous zircons dated by CA-TIMS.* ***(b)*** *Ranked plot of LA-ICPMS $^{206}Pb/^{238}U$ dates (Appendix 3).* ***(c)*** *Concordia diagram (left) and ranked $^{206}Pb/^{238}U$ dates (right) for 6 zircons analyzed by CA-TIMS (Appendix 4). The light grey band around concordia (dark grey line) shows the decay constant uncertainties. Analyses included in weighted mean age (light grey horizontal bar) calculations are bold; analyses with thin lines are not used in calculations. Line-type designations are the same in all plots. Errors in all plots are at 2σ. Arrow indicates data extend off of plot. MSWD = mean squared weighted deviation, pof = probability of fit, n = number of analyses included in age calculation.*

Sawtooth plutons

The Sawtooth plutons are located 65 km north of Jakes Corner, the junction of the Alaska Highway and Tagish road (Fig. 4-77). The largest of the plutons is the Sawtooth stock with a mapped extent of 54.3 km²; two small plugs are located to the southeast and have mapped extents between 0.15 and 1.2 km² (Fig. 4-102; Table 4-1; Gordey and Stevens, 1994). Only the Sawtooth stock was visited for the present study. These plutons intrude Paleozoic metamorphic rocks of the Yukon-Tanana terrane, including quartz-mica schists of the Snowcap assemblage, and mafic metavolcanic rocks, mafic to ultramafic metaplutonic rocks and marble of the Finlayson assemblage (Gordey and Stevens, 1994; Colpron, 2006). The Teslin fault, ~1 km southwest of the margin of the Sawtooth stock, separates Richthofen formation sedimentary rocks of the Lower to Middle Jurassic Laberge Group and the Yukon-Tanana terrane (Figs. 4-1 and 4-77).

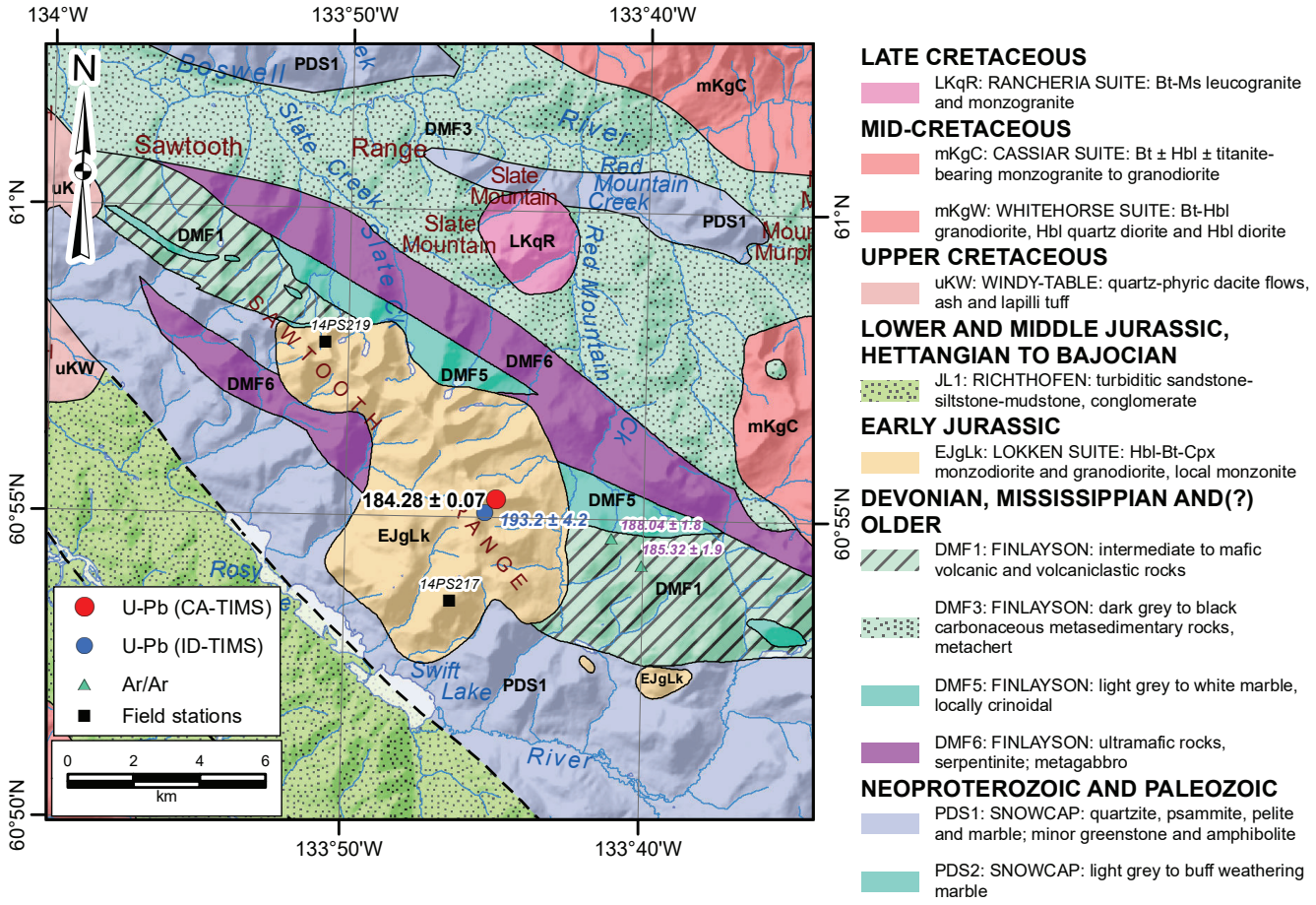


Figure 4-102. *Geology of Sawtooth plutons area. Geology from YGS (2020a); fault symbology as in Figure 1-4.*

Petrography

The Sawtooth stock forms jagged ridges and is the backbone of the Sawtooth Range (Figs. 4-102 and 4-103). The stock is mesocratic, medium grained and equigranular (Figs. 4-104 and 4-105). These rocks plot in the diorite to monzodiorite fields on a simplified QAP diagram (Fig. 4-2b). Mafic minerals are mostly hornblende with subordinate pyroxene and biotite. Hornblende is typically ≥1mm, fresh euhedral crystals (Fig. 4-106a). Clinopyroxene is present as corroded cores with hornblende overgrowths, good cleavage is rare, but where noted extinction angles are inclined (Fig. 4-106b). Biotite is commonly intensely chlorite altered. Plagioclase is present as euhedral laths that are intensely saussuritized (Fig. 4-106c) and K-feldspar is anhedral within the groundmass and is relatively fresh with sparse myrmekitic textures. Epidote and titanite are accessory phases; epidote is secondary in origin.



Figure 4-103. *Looking south into the cirque at the head of the central fork of Slate Creek. The Sawtooth stock makes up the entire field of view; 14PS219. Approximately 125 m of vertical relief.*

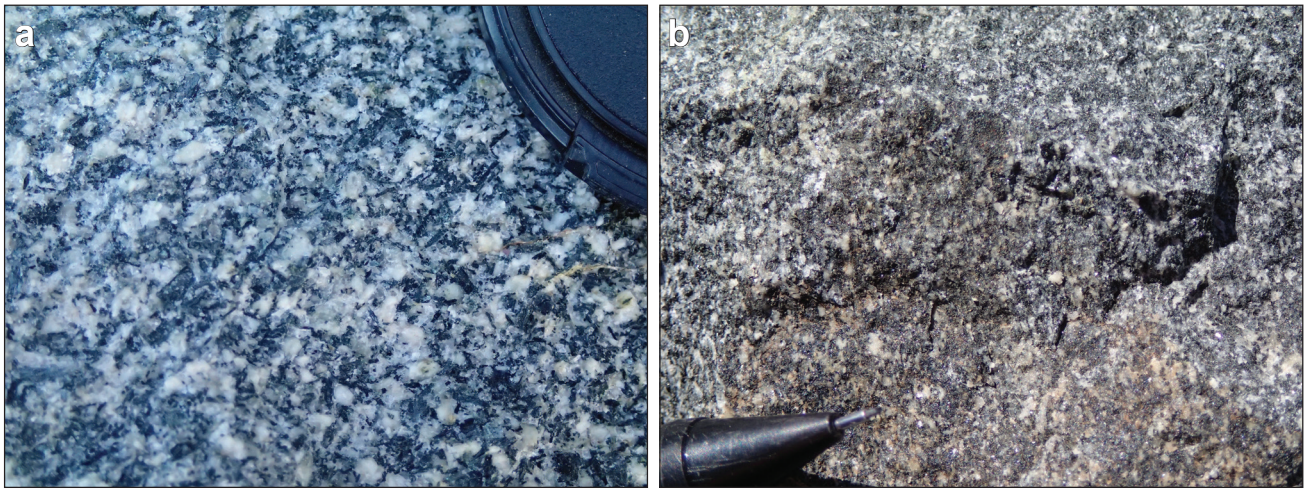


Figure 4-104. *Representative outcrop in the Sawtooth stock.* ***(a)*** *Hornblende-biotite-pyroxene monzodiorite; 14PS217. Lens cap 4 cm diameter.* ***(b)*** *Slightly more mafic and mesocratic, hornblende-pyroxene-biotite diorite; 14PS219.*

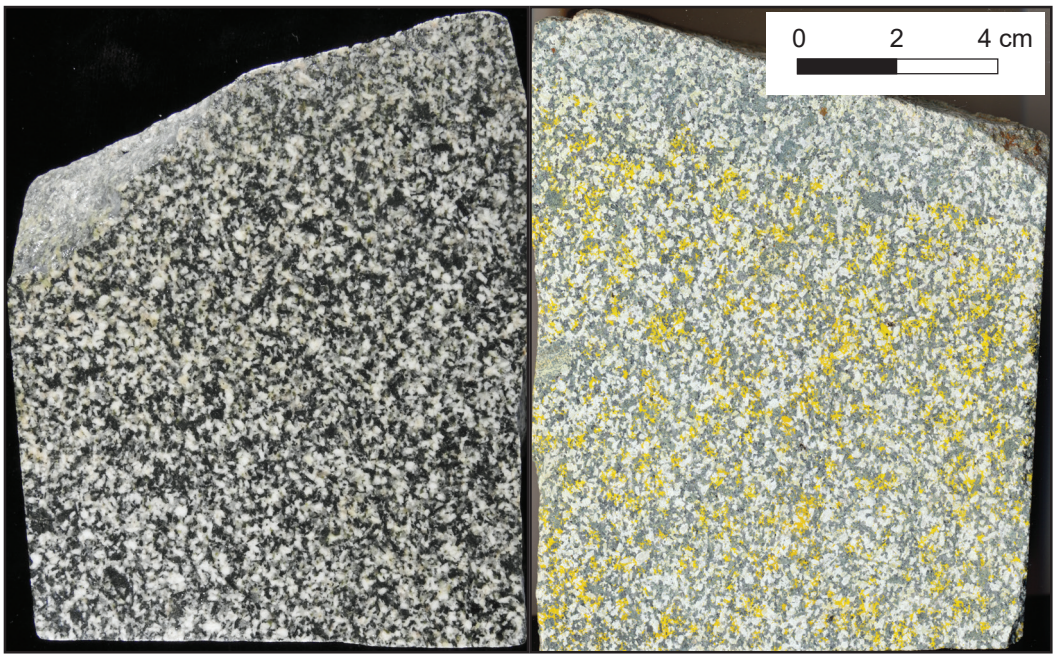


Figure 4-105. *Representative sample of monzodiorite from the Sawtooth stock; 14PS218-1. Fresh polished surface (left) and a cobaltinitrite-stained surface (right). Note K-feldspar is yellow, both images are same scale.*

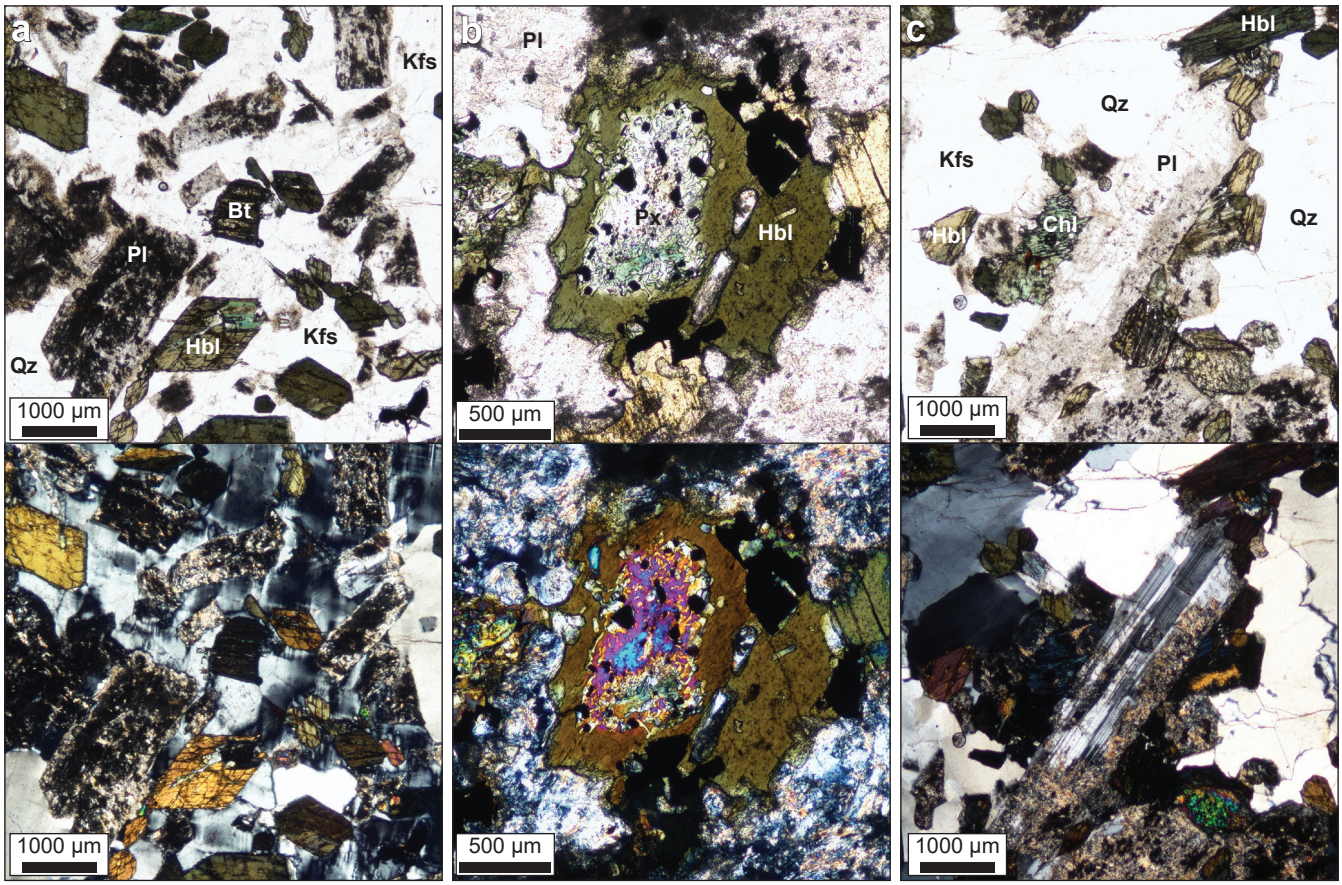


Figure 4-106. *Transmitted light photomicrographs from the Sawtooth stock; plane polarized light (upper) and cross-polarized light (lower).* ***(a)*** *Euhedral hornblende and intensely saussuritized plagioclase laths in a groundmass of K-feldspar and quartz.* ***(b)*** *Pyroxene core overgrown by hornblende; a and b from 14PS217-1.* ***(c)*** *Fresh hornblende and intensely chloritized biotite along with moderately to intensely saussuritized plagioclase; 14PS219-1.*

Oxidation state and mineral occurrences

The Sawtooth stock is weakly magnetic with susceptibilities ranging from 0.35 to 4.89 × 10^{-3} SI units (Fig. 4-3b; mean 2.5 × 10^{-3} SI units; n = 3). Two mineral occurrences, the Rosy [105C 024] and the Sawas [105C 047], are located near the margins of the Sawtooth stock (Fig. 4-107). Each of these occurrences has minor quartz-carbonate veins cutting metavolcanic rocks (YGS, 2020b) that are either rafts within the stock or are located outside the stock and may be unrelated to it. These occurrences and the Sawtooth stock are located 5–10 km south of the Red Mountain deposit [105C 009], a Late Cretaceous molybdenum porphyry deposit with an historic resource of 726.7 Mlb Mo (Casselman, 2018).

Geochronology

Previous constraints on the crystallization age of the Sawtooth stock are from a sample collected during regional mapping in 1991 which returned a U-Pb TIMS titanite date of 193.2 ± 4.2 Ma (Stevens *et al.*, 1993), and $^{40}Ar/^{39}Ar$ hornblende and biotite cooling ages of 179 ± 2 and 182 ± 2 Ma, respectively (Fig. 4-102; Appendix 1; Hunt and Roddick, 1993).

Sample 14PS218-1 is from medium-grained monzodiorite collected near the centre of the Sawtooth stock, approximately 500 m northeast of the site reported in Stevens *et al.* (1993) and Hunt and Roddick (1993). It yielded mostly elongate zircons with sector and concentric zoning; a few grains have inherited cores (Fig. 4-108a). LA-ICPMS analyses of 41 zircons returned $^{206}Pb/^{238}U$ dates between 605 and 164 Ma, and one grain has a $^{206}Pb/^{207}Pb$ date of 1698 Ma (Appendix 3). The two Proterozoic dates (1698 and 605 Ma) are from inherited cores, and two xenocrystic grains are Late Triassic at *ca.* 235 and 226 Ma. The weighted mean of the youngest population, including 37 of the 41 grains, is 179.5 ± 1.7 Ma (Fig. 4-108b). Six zircon grains analyzed by CA-TIMS yielded concordant $^{206}Pb/^{238}U$ dates that range from 266.66 ± 0.18 to 184.25 ± 0.13 Ma (Appendix 4). The youngest four grains have a weighted mean date of 184.28 ± 0.07 Ma (MSWD = 0.41, n = 4; Fig. 4-108c) which is considered the best estimate for crystallization of this monzodiorite.

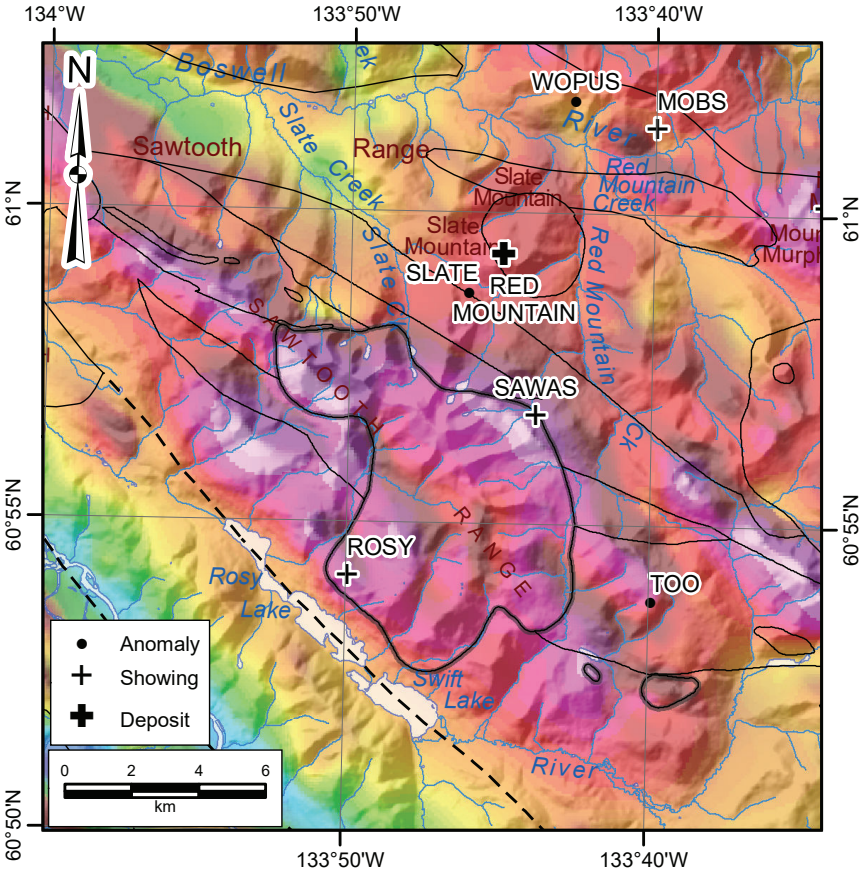


Figure 4-107. *Residual total field aeromagnetic of the Sawtooth plutons area (Hayward and Oneschuk, 2011) illustrating location of MINFILE occurrences. Fault symbology as in Figure 1-4.*

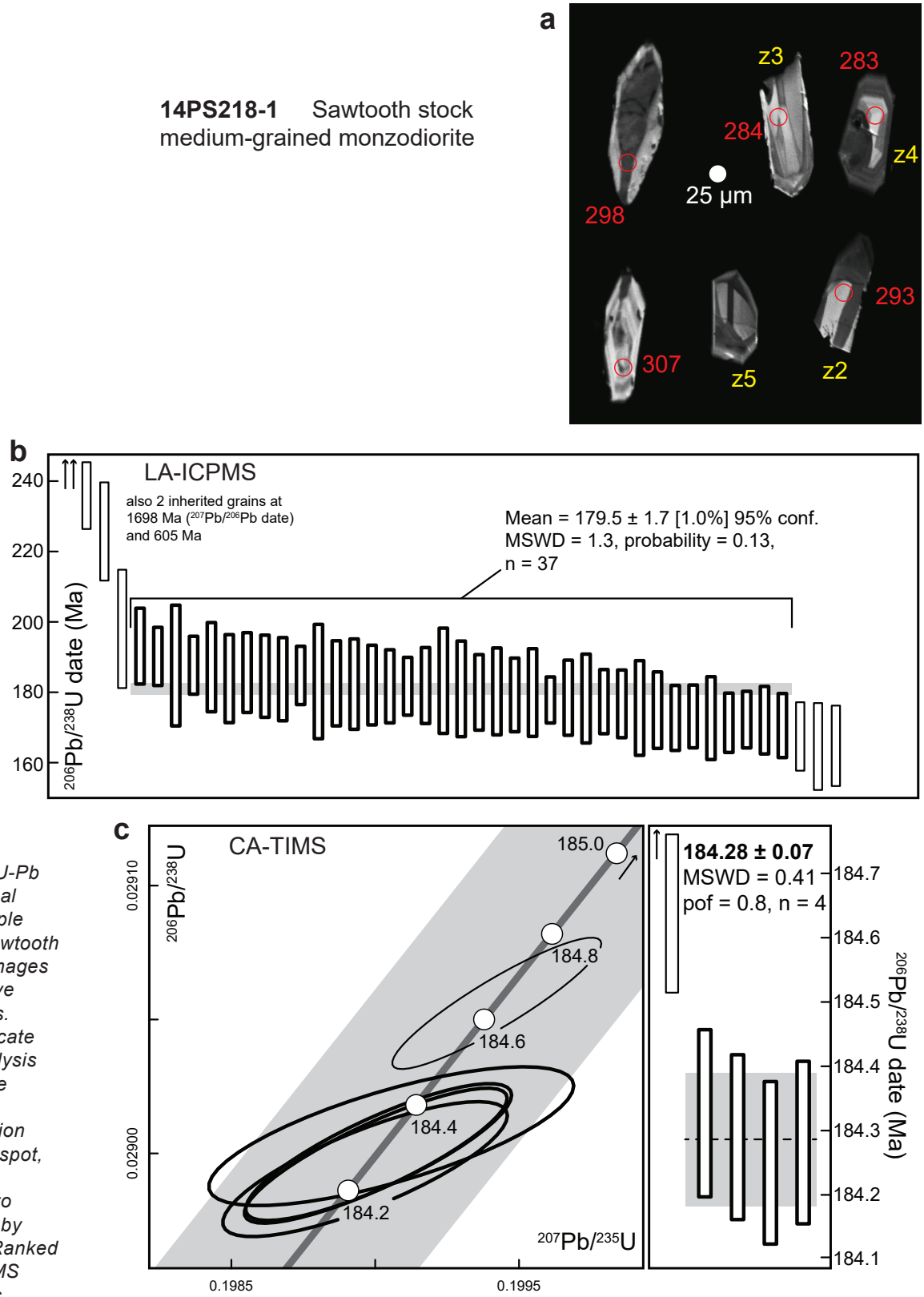


Figure 4-108. *U-Pb geochronological results for sample 14PS218-1, Sawtooth stock.* ***(a)*** *CL images of representative igneous zircons. Red labels indicate LA-ICPMS analysis number with the red open circle indicating location of the analysis spot, yellow analysis number refers to grain analyzed by CA-TIMS.* ***(b)*** *Ranked plot of LA-ICPMS $^{206}Pb/^{238}U$ dates (Appendix 3).* ***(c)*** *Concordia diagram (left) and ranked $^{206}Pb/^{238}U$ dates (right) for zircons analyzed by CA-TIMS, one inherited grain plots at 266.66 ± 0.18 Ma (Appendix 4). The light grey band around concordia (dark grey line) shows the decay constant uncertainties. Analyses included in weighted mean age (light grey horizontal bar) calculations are bold; analyses with thin lines not used in calculations. Line-type designations are the same in all plots. Errors in all plots are at 2σ. Arrows indicate data extend beyond plot. MSWD = mean squared weighted deviation, pof = probability of fit, n = number of analyses included in age calculation.*

Englishman plutons

The Englishman plutons are located 30 km east of the junction between the South Canol road and Alaska Highway (Figs. 4-1 and 4-77). The Englishman plutons consist of three bodies, the Englishman stock which has a mapped extent of 98.8 km² and two plugs to the east that are 1.1 and 2.0 km² in extent (Fig. 4-109; Table 4-1). The Englishman stock intrudes an overturned thrust fault that separates metasedimentary rocks of the Snowcap assemblage to the west from Carboniferous marble of the Klinkit Group and Triassic sedimentary rocks of the Teh formation (Colpron, 2006; note that Gordey and Stevens, 1994, previously assigned the metasedimentary rocks to the west to the Kootenay terrane, and the carbonate to the east to Cassiar terrane). The fault follows the Nisutlin River to the north and is clearly cut by the Englishman stock (Fig. 4-110), indicating a pre-Jurassic age for this structure. Only one locality in the Englishman stock and one in the plug immediately to the east were visited for this study.

Petrography

The Englishman plutons are weakly alkalic, plotting in the monzonite and monzodiorite fields of a simplified QAP diagram (Fig. 4-2b). The rock is medium grained and equigranular (Figs. 4-111 and 4-112). Mafic minerals are mostly hornblende with minor clinopyroxene and biotite, make up 20 to 30% of the rock, and are weakly altered to chlorite. Clinopyroxene is present as both relatively fresh, euhedral phenocrysts and as altered corroded cores with hornblende overgrowths (Fig. 4-113). Plagioclase are moderately saussuritized and K-feldspar is fresh. Titanite is a ubiquitous accessory mineral and epidote is variably distributed. When present, epidote is of secondary origin.

Oxidation state and mineral occurrences

The Englishman stock and plug are magnetic with susceptibilities of 24.70 and 9.14×10^{-3} SI units, respectively (Figs. 4-3b and 4-110). There are no MINFILE occurrences associated directly with the Englishman stock or plugs (YGS, 2020b). There are several W-Sn skarn occurrences within 10 km of the

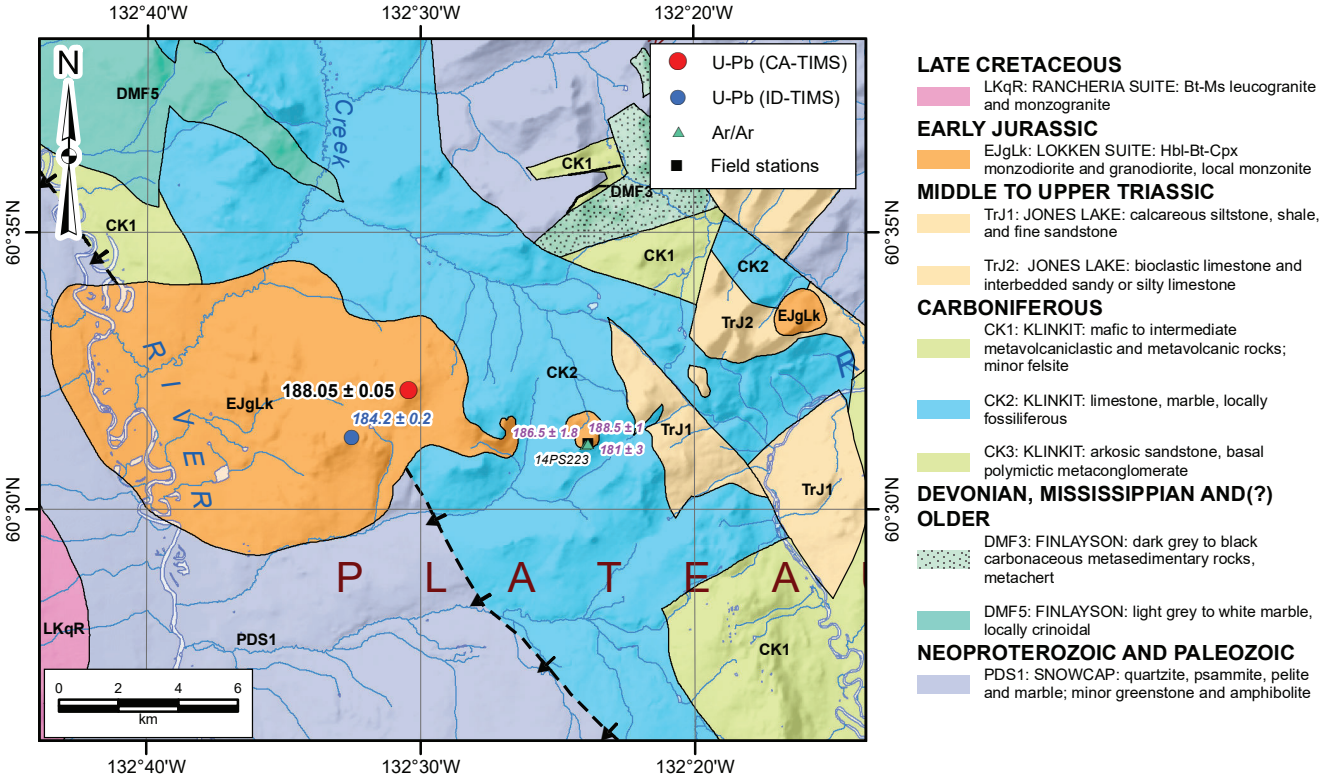


Figure 4-109. *Geology of Englishman plutons area. Geology from YGS (2020a); fault symbology as in Figure 1-4. The Englishman stock intrudes an overturned thrust fault shown with teeth pointing to hanging wall, and tick indicating dip of this surface.*

plugs, but these are more likely associated with the Late Cretaceous Seagull plutonic suite, also found in the area and known to host W-Sn occurrences (*e.g.*, Liverton *et al.*, 2005).

Geochronology

Two historical samples constrain the age of the Englishman stock and plugs. Sample GGAJ-94-19-11 D is from the Englishman stock and is a coarse-grained biotite syenite to monzonite that yielded a U-Pb zircon age of 184.2 ± 0.2 Ma (ID-TIMS, multi-grain fractions; Gordey *et al.*, 1998). Sample GGA-91-38-04C is from the plug immediately east of the Englishman stock and is a medium-grained, equigranular monzodiorite that yielded a $^{40}Ar/^{39}Ar$ hornblende date of 186.5 ± 1.8 Ma (Hunt and Roddick, 1994).

We collected sample 14PS222-1, a medium-grained monzonite (Figs. 4-111a and 4-112a) from the Englishman stock, approximately 2.5 km northeast from GGAJ-94-19-11 D (Fig. 4-109). It yielded mostly stubby zircons with sector zoning (Fig. 4-114a). LA-ICPMS analyses of 36 zircons form a single zircon population with $^{206}Pb/^{238}U$ dates between 205 and 178 Ma. Two xenocrystic Late Triassic grains are 205 and 203 Ma. The remaining zircon have a weighted mean date of 187.8 ± 1.5 Ma for 33 of 36 grains (Fig. 4-114b; Appendix 3). Six zircon grains analyzed by CA-TIMS yielded concordant $^{206}Pb/^{238}U$ dates that range from 188.15 ± 0.13 to 187.96 ± 0.13 Ma (Appendix 4), with a weighted mean date of 188.05 ± 0.05 Ma (MSWD = 1.27, n = 6; Fig. 4-114c).

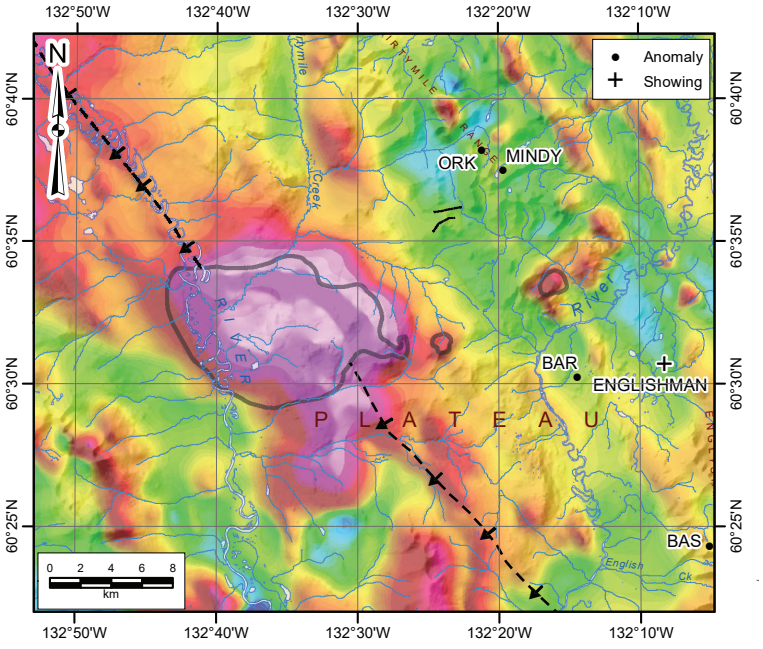


Figure 4-110. *Reduced to pole, residual total field aeromagnetic map of the Englishman plutons area (Aurora Geosciences Ltd. and Bruce, 2017e). Fault symbology as in Figure 1-4.*

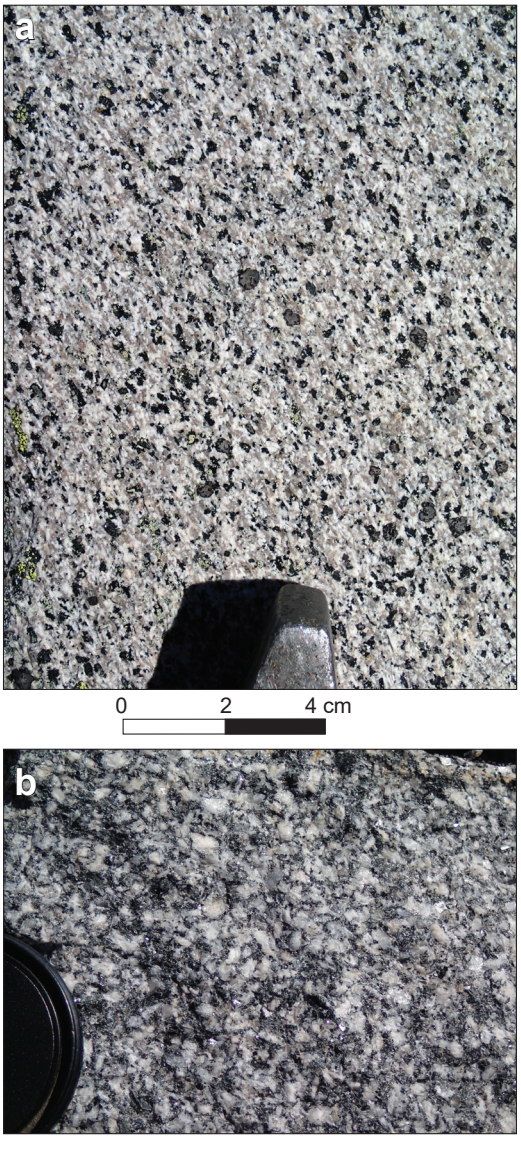


Figure 4-111. *Representative outcrop in the Englishman plutons.* ***(a)*** *Hornblende-pyroxene monzonite from the Englishman stock; 14PS222.* ***(b)*** *Slightly more mafic and mesocratic, hornblende-biotite-pyroxene monzodiorite from the plug immediately east of the stock; 14PS223.*

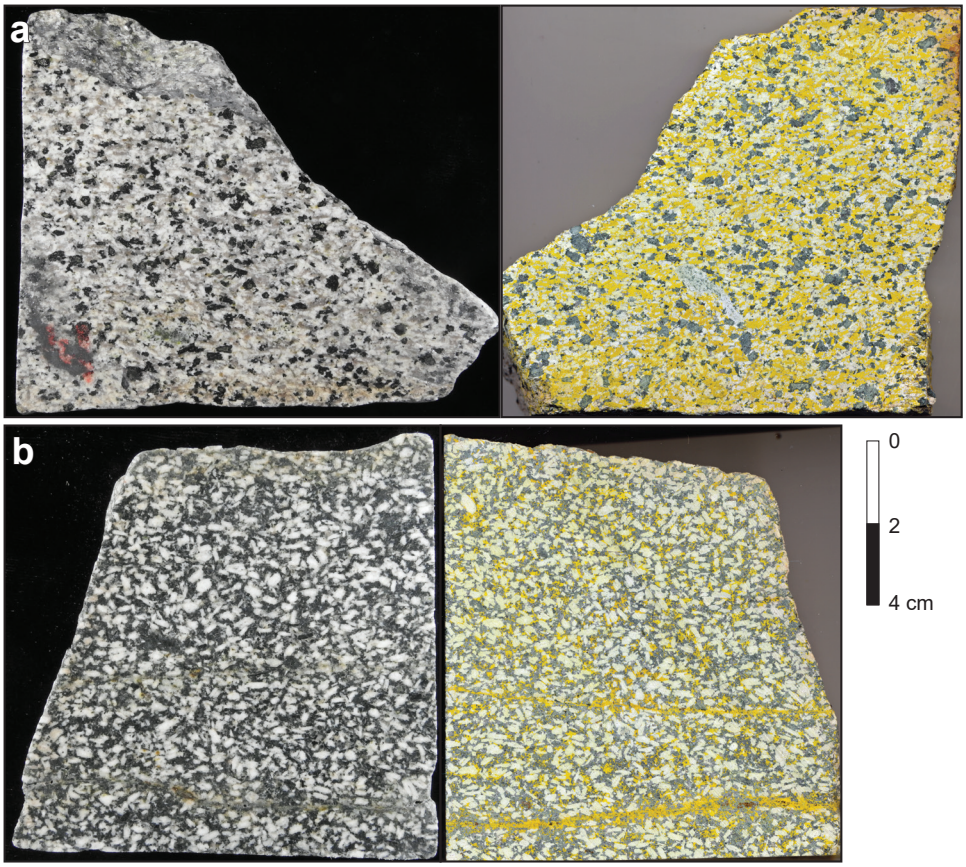


Figure 4-112. *Representative samples from the Englishman plutons.* ***(a)*** *Unfoliated, medium-grained, equigranular monzonite from the Englishman stock; 14PS222-1.* ***(b)*** *Medium-grained, equigranular monzodiorite from the plug immediately east of the Englishman stock; 14PS223-1. Fresh polished surface (left) and a cobaltinitrite-stained surface (right). Note K-feldspar is yellow.*

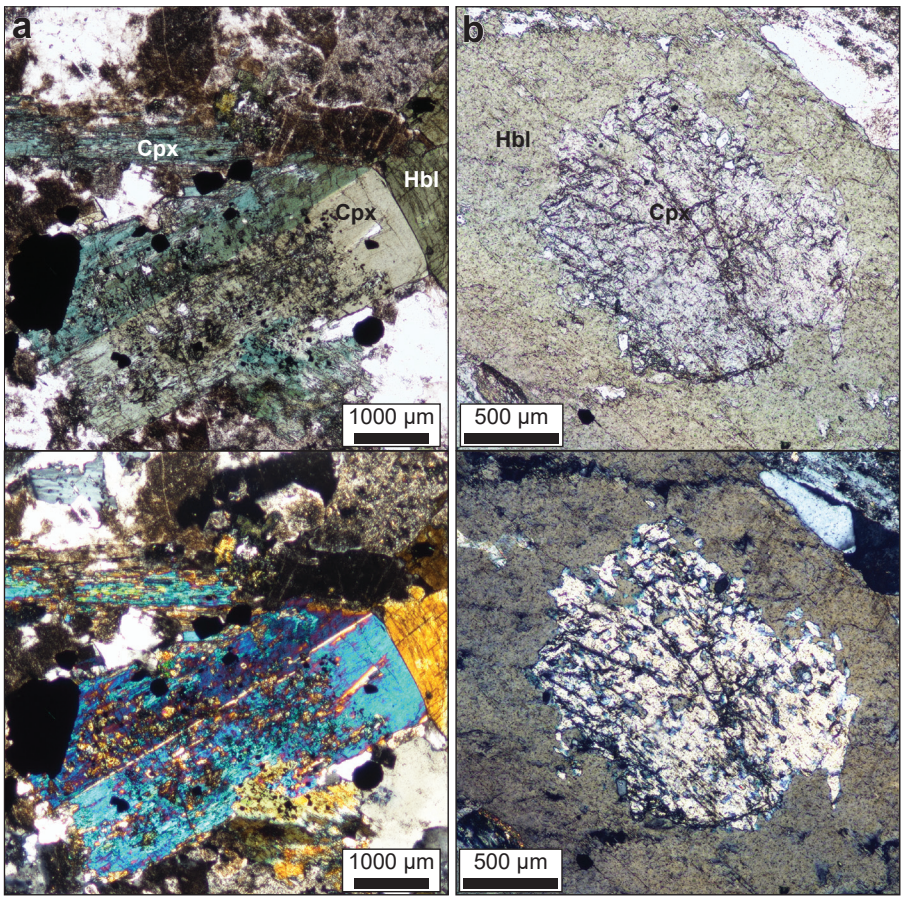


Figure 4-113. *Representative photomicrographs from the Englishman stock; plane polarized light (upper) and cross-polarized light (lower).* ***(a)*** *Relatively fresh euhedral clinopyroxene overgrown by hornblende; 14PS222-1.*
(b) *Anhedral mottled clinopyroxene overgrown by hornblende; 14PS222-1.*

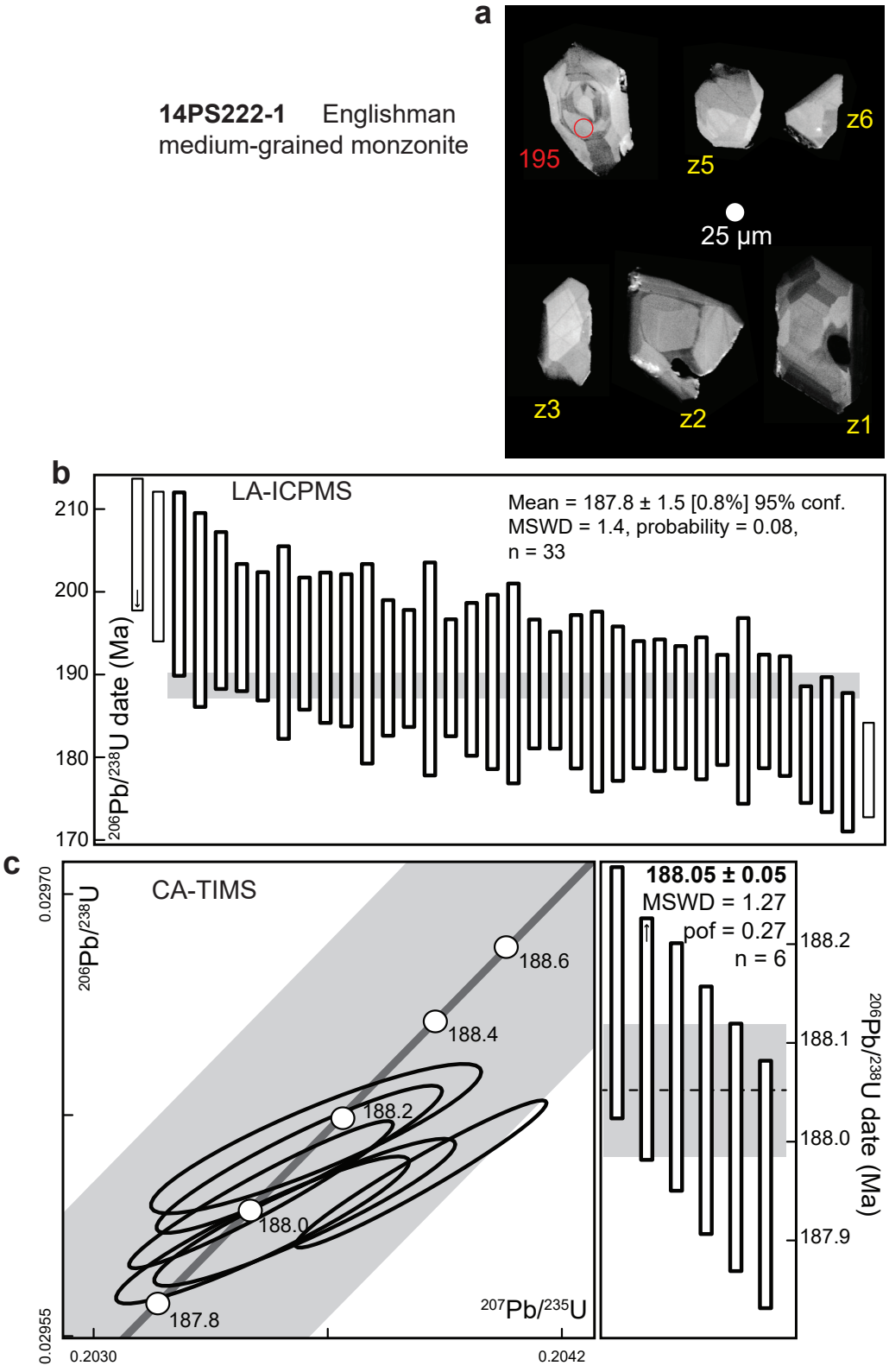


Figure 4-114. *U-Pb geochronological results for sample 14PS222-1, Englishman stock.* ***(a)*** *CL images of representative igneous zircons. Red labels indicate LA-ICPMS analysis number with the red open circle indicating location of the analysis spot, yellow analysis number refers to grain analyzed by CA-TIMS.* ***(b)*** *Ranked plot of LA-ICPMS $^{206}Pb/^{238}U$ dates (Appendix 3).* ***(c)*** *Concordia diagram (left) and ranked $^{206}Pb/^{238}U$ dates (right) for zircons analyzed by CA-TIMS (Appendix 4). The light grey band around concordia (dark grey line) shows the decay constant uncertainties. Analyses included in weighted mean age (light grey horizontal bar) calculations are bold; analyses with thin lines not used in calculations. Line-type designations are the same in all plots. Errors in all plots are at 2σ. Arrows indicate data extend beyond plot. MSWD = mean squared weighted deviation, pof = probability of fit, n = number of analyses included in age calculation.*

Logjam plutons

The Logjam plutons are a set of more than 15 composite and single-phase plutons spanning the British Columbia–Yukon border in the vicinity of the Smart River and Logjam Creek (Figs. 4-77 and 4-115; Roots *et al.*, 2004b). Three phases of Early Jurassic rocks are mapped in the area: 1) an intrusive ultramafic complex of gabbro with serpentinite and dunite; 2) a mafic phase of diorite to monzodiorite; and 3) a more felsic granodiorite, granite and monzonite phase (Roots *et al.*, 2004b). The Logjam plutons are generally northwest elongate stocks and plugs that intrude metavolcanic and metasedimentary rocks of the Yukon-Tanana terrane (Fig. 4-115; Roots *et al.*, 2004b). The plutons vary in mapped extent from 0.2 to 12.8 km². Two of the larger composite stocks were visited for this study, the Two Ladder Creek and Logjam Creek (Figs. 4-77 and 4-115). The Two Ladder Creek stock crosses the British Columbia–Yukon border and is an elongate, 10 km long by 1.5 km wide body with a mapped extent of 12.4 km² (Table 4-1). The Two Ladder Creek composite stock comprises mafic and felsic phases. The Logjam Creek stock is a similar size body with a mapped extent of 12.8 km² but is more equant with a 6 by 3 km distribution (Fig. 4-115; Table 4-1). The Logjam Creek stock comprises all three of the Early Jurassic phases described by Roots *et al.* (2004b).

The region is also intruded by plutons of the Early Cretaceous Seagull suite (Colpron *et al.*, 2016b). This suite includes the Seagull batholith associated with Sn mineralization (Liverton *et al.*, 2005) and the intrusion which hosts the Logtung W-Mo deposit ([105B 039]; Brand, 2008). Early Jurassic and Early Cretaceous plutons span a similar compositional and textural range but can be separated in the

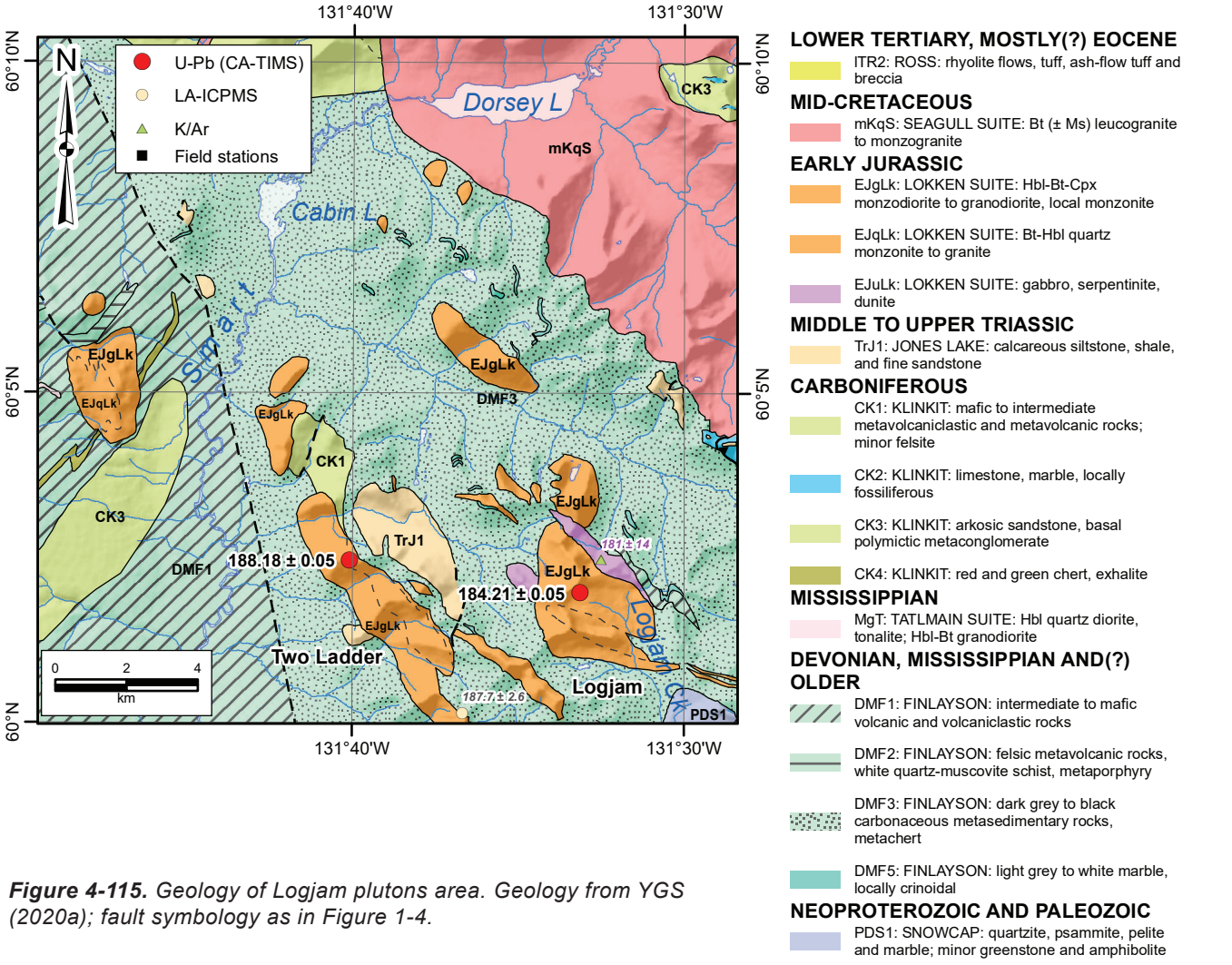


Figure 4-115. *Geology of Logjam plutons area. Geology from YGS (2020a); fault symbology as in Figure 1-4.*

field by hornblende ± pyroxene abundance. Hornblende ± pyroxene are the most common mafic minerals in the Early Jurassic plutons making up to 20% of the rock whereas the Early Cretaceous plutons have little to no hornblende and no pyroxene (Liverton *et al.*, 2005).

Petrography

Three phases of Jurassic plutons are mapped in the Logjam Creek area, a gabbro with serpentinite and dunite, a hornblende diorite to monzodiorite, and a granodiorite to monzonite (Fig. 4-115; Roots *et al.*, 2004a). The ultramafic rocks were not visited for the present study. The monzodiorite is medium grained and equigranular whereas the granite is medium grained and K-feldspar porphyritic (Figs. 4-116 and 4-117). The monzodiorite is mesocratic with 15% hornblende, 10% biotite and trace amounts of pyroxene (Figs. 4-117 and 4-118). Biotite is weakly chlorite altered and hornblende is fresh. Plagioclase is moderately saussuritized and K-feldspar is weakly sericitized. Titanite and epidote are present as accessory phases; epidote is secondary in origin (Fig. 4-118).

The monzonite is porphyritic with ~5 mm K-feldspar phenocrysts in a fine-grained felsic groundmass (Figs. 4-118 and 4-119). The rock contains 10% hornblende and 5% biotite; hornblende is fresh and biotite is fresh to intensely chlorite altered. Plagioclase is moderately saussuritized and K-feldspar is fresh. Titanite, epidote and apatite are present as accessory phases; epidote is secondary in origin.

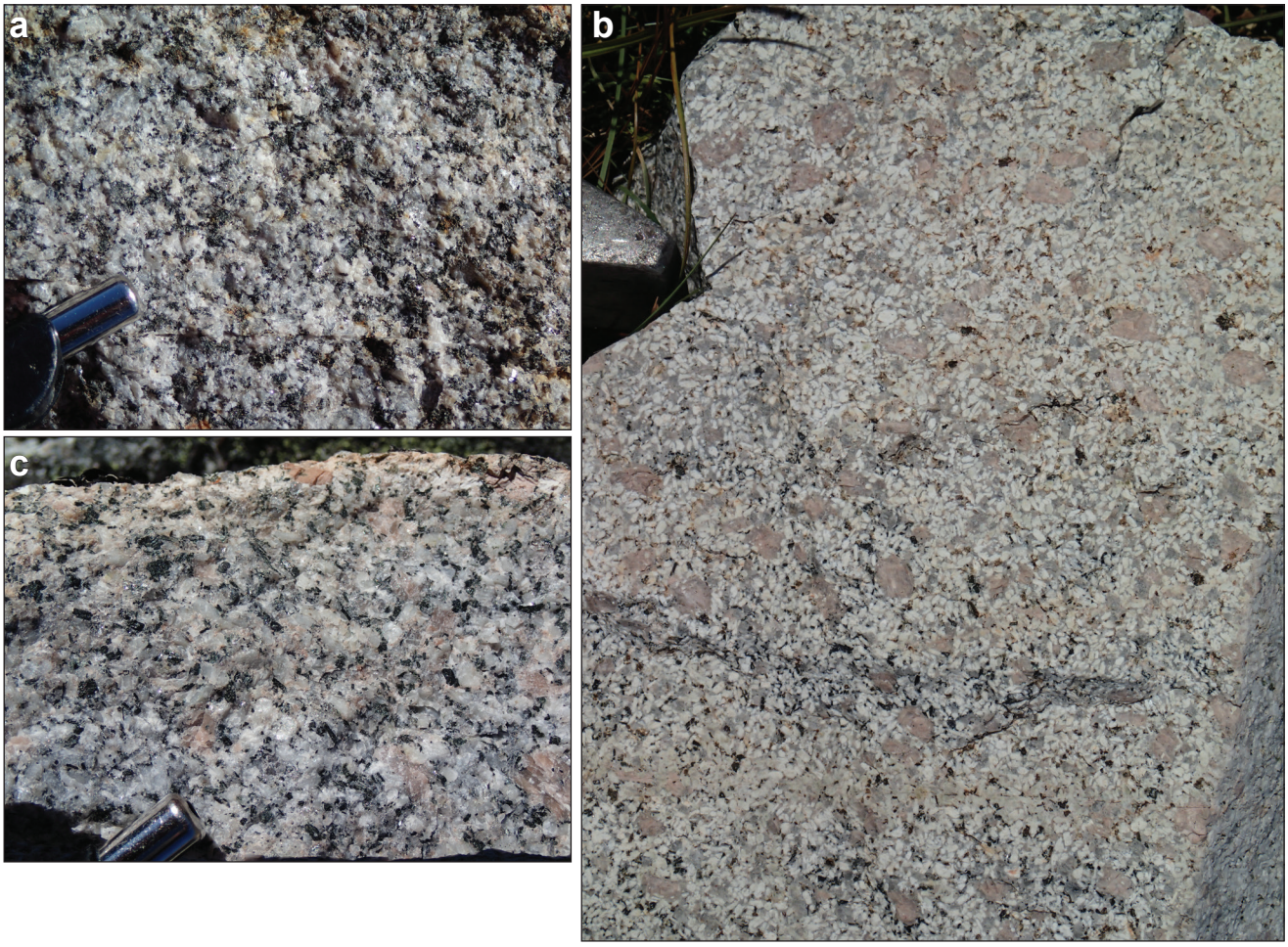


Figure 4-116. *Representative outcrop from the Logjam plutons.* ***(a)*** *Fresh broken surface of medium-grained, equigranular hornblende-biotite monzodiorite; 14PS226.* ***(b)*** *Weathered surface showing porphyritic texture with stubby pink K-feldspar phenocrysts and smaller, crowded white plagioclase phenocrysts in a groundmass of grey quartz; 14PS225.* ***(c)*** *Fresh broken surface of (b).*

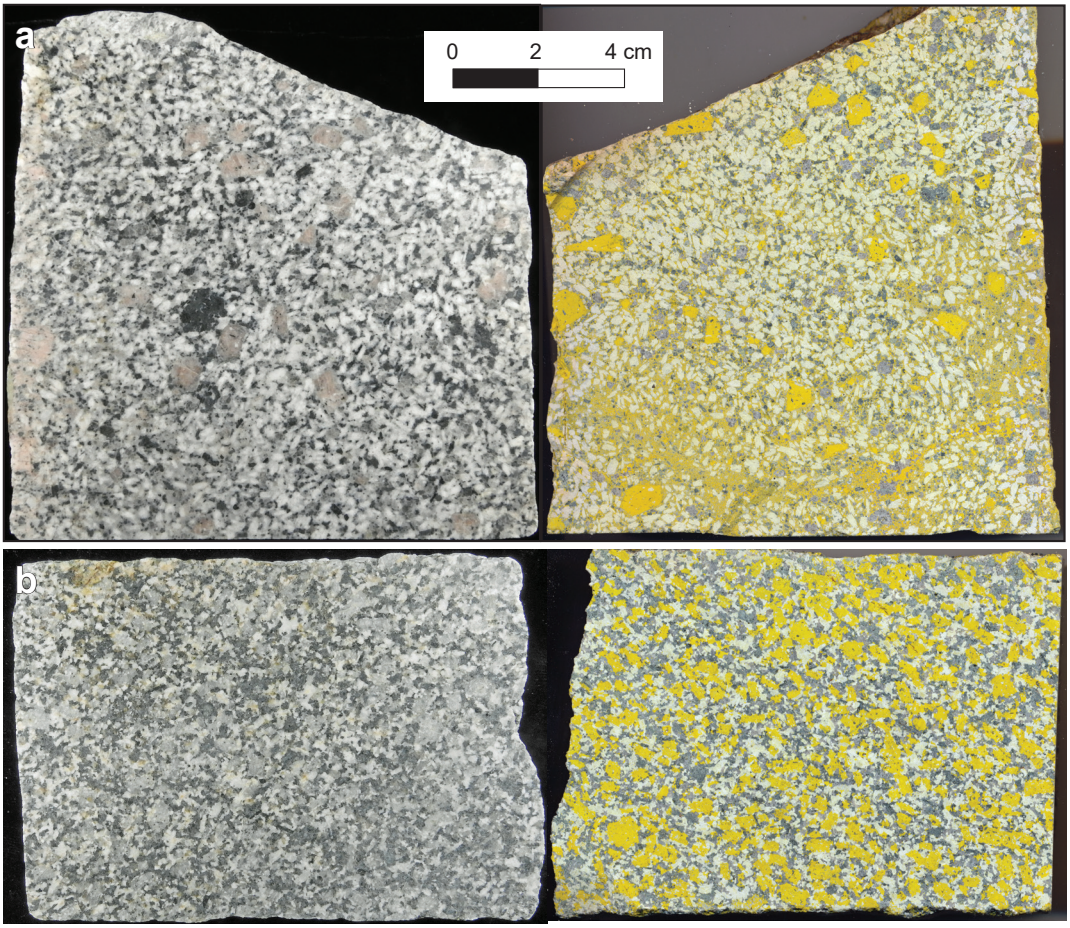


Figure 4-117. *Representative sample from the Logjam plutons.* ***(a)*** *K-feldspar porphyritic monzonite from an eastern stock; 14PS225-1.* ***(b)*** *Equigranular monzodiorite from a western body; 14PS226-1. Fresh polished surface (left) and a cobaltinitrite-stained surface (right). Note K-feldspar is yellow, both images are same scale.*

Oxidation state and mineral occurrences

The Logjam plutons are rimmed by aeromagnetic highs, but have reduced cores (Fig. 4-120). Our station in the Two Ladder Creek pluton has a relatively low magnetic susceptibility of 0.254×10^{-3} SI units, while the locality visited in the Logjam Creek stock has a relatively high magnetic susceptibility of 9.95×10^{-3} SI units (Fig. 4-3b).

There are five mineral occurrences, including two deposits, in the vicinity of the Logjam plutons in Yukon (Fig. 4-120). Two of these, Klinkit [105B 091] and Smart [105B 037] are anomalies of unknown type and significance (YGS, 2020b). Mineralization at the Cabin Lake occurrence [105B 044] consists of pyrite, chalcopyrite and other minor sulphide minerals as disseminated to massive bands in Devonian-Mississippian felsic metavolcanic rocks of Yukon-Tanana terrane (YGS, 2020b).

The Logtung deposit [105B 039] is an Early Cretaceous porphyry (Brand, 2008) that contains 425 Mt of ore at 0.1% WO_3 and 0.025% Mo (Casselman, 2018). The Logjam deposit [105B 038] has an historic resource of 70 000 tonnes of 3 g/t Au and 393 g/t Ag in quartz veins (Phendler, 1983). The age of mineralization at the Logjam deposit is not known, but there are similar Ag-Pb veins associated with the Logtung porphyry and it is likely that the Logjam veins are the distal expression of an Early Cretaceous system. Early Jurassic plutons in the area do not appear to be associated with mineralization.

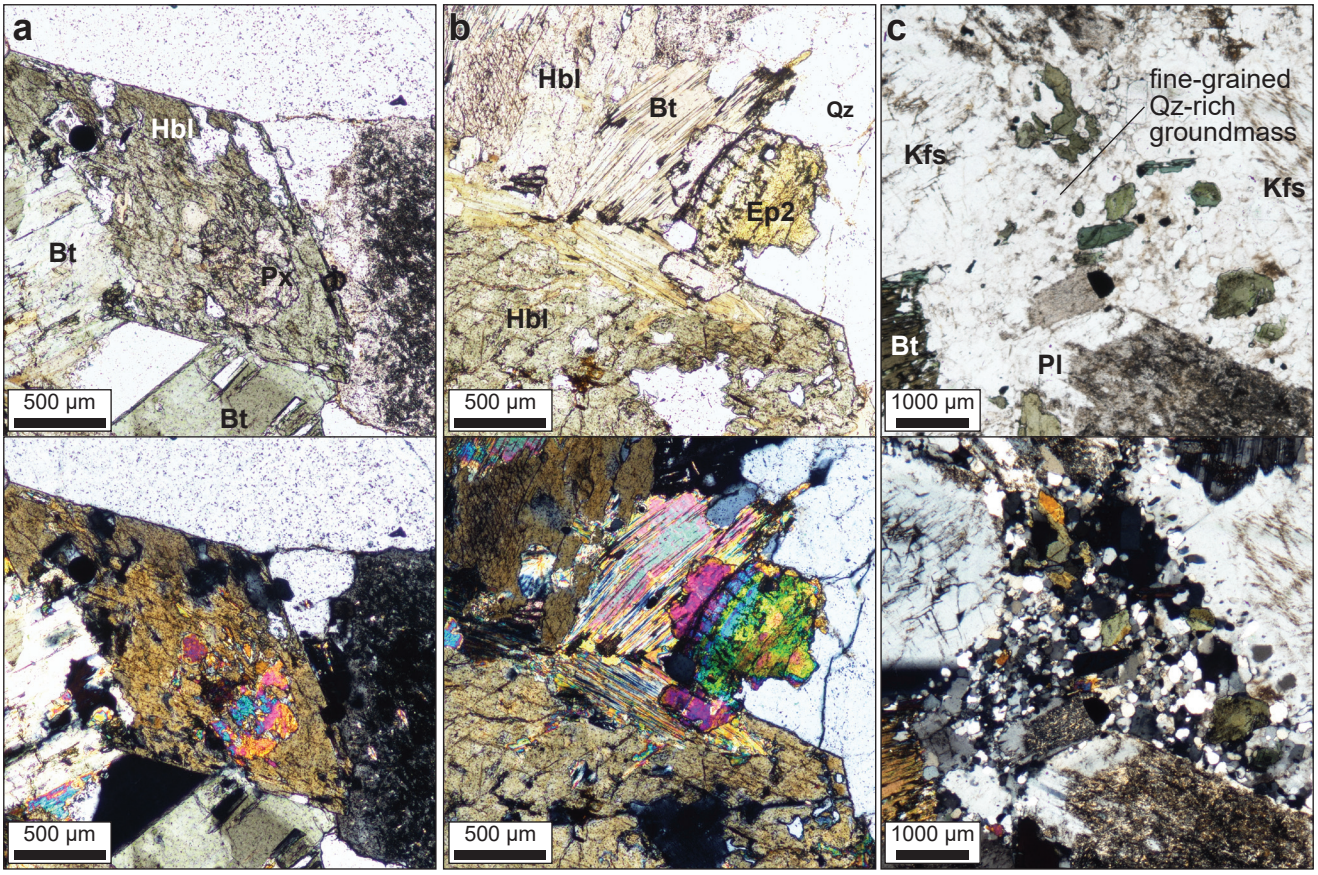


Figure 4-118. *Transmitted light photomicrographs from the Logjam plutons; plane polarized light (upper) and cross-polarized light (lower).* ***(a)*** *Rare pyroxene core overgrown by hornblende; 14PS226-1.* ***(b)*** *Subhedral epidote with chloritized biotite and fresh hornblende; 14PS226-1.* ***(c)*** *K-feldspar porphyritic monzonite with a fine-grained quartz and K-feldspar groundmass; 14PS225-1.*

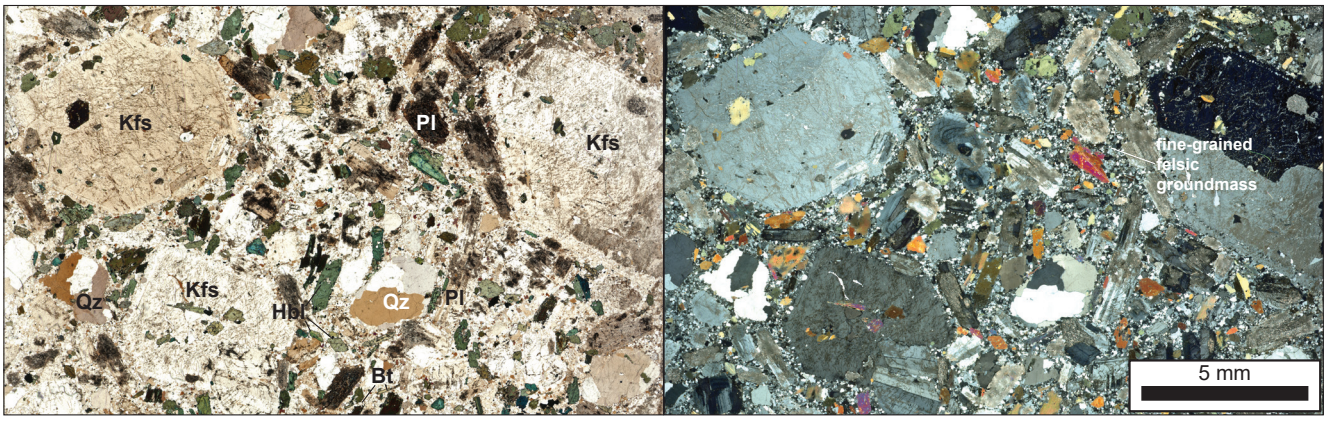


Figure 4-119. *Transmitted light thin section scans from 14PS225-1; plane polarized light (left) and cross-polarized light (right). Note K-feldspar porphyritic texture and fine-grained felsic groundmass of quartz and K-feldspar.*

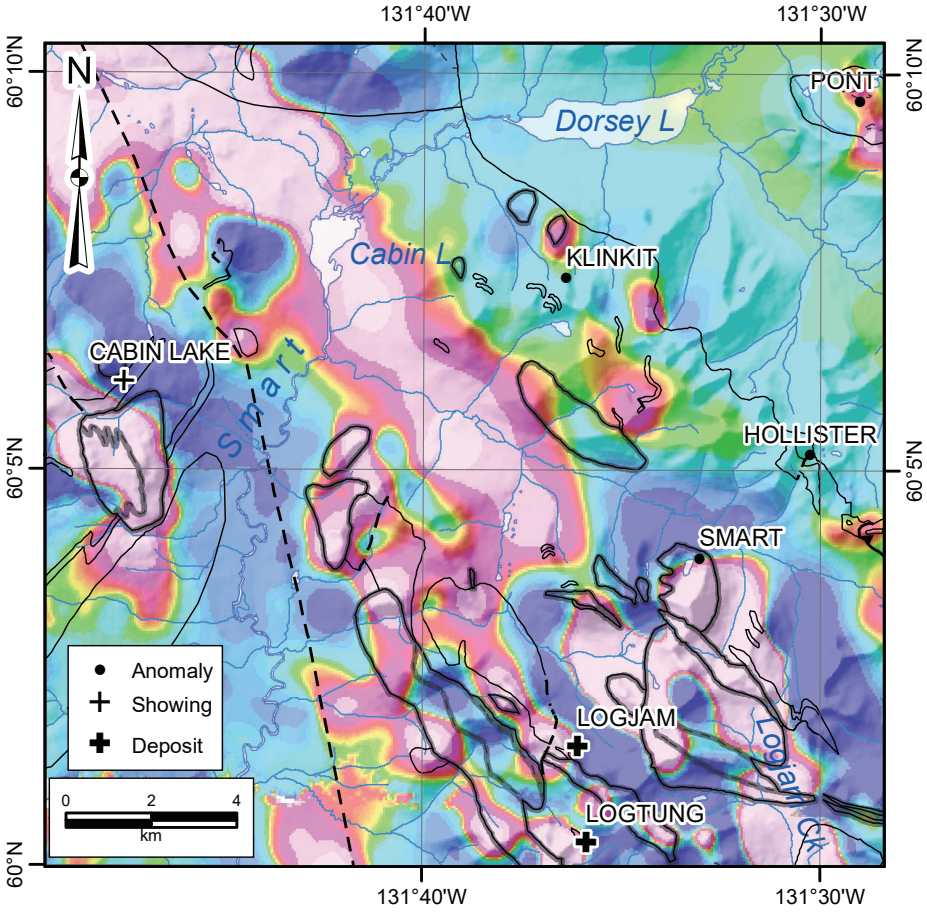


Figure 4-120. *Reduced to pole, residual total field aeromagnetic map of the Logjam plutons area (Aurora Geosciences Ltd. and Bruce, 2017f) illustrating locations of MINFILE occurrences in the region. Fault symbology as in Figure 1-4.*

Geochronology

Early Jurassic ages for these plutons were previously indicated by a hornblende K/Ar cooling age of 181 ± 14 Ma on the ultramafic phase of the Logjam Creek stock (Hunt and Roddick, 1987), and a U-Pb zircon date of 187.7 ± 2.6 Ma (LA-ICPMS, UBC) from a mafic phase of the Two Ladder Creek stock (Brand, 2008; Fig. 4-115; Appendix 1). We collected two samples for U-Pb zircon LA-ICPMS and CA-TIMS analyses at BSU (Fig. 4-115).

Sample 14PS226-1 is a medium-grained monzodiorite from the northern part of the Two Ladder Creek stock (Fig. 4-115). It yielded mostly elongate zircons with oscillatory zoning (Fig. 4-121a). LA-ICPMS analyses of 35 zircons form a single zircon population with $^{206}Pb/^{238}U$ dates between 198 and 170 Ma. Calculation of a weighted mean is not possible due to data scatter (Fig. 4-121b; Appendix 3). Six zircon grains analyzed by CA-TIMS yielded concordant $^{206}Pb/^{238}U$ dates that range from 188.24 ± 0.13 to 188.20 ± 0.13 Ma (Appendix 4), with a weighted mean date of 188.18 ± 0.05 Ma (MSWD = 0.72, n = 6; Fig. 4-121c).

Sample 14PS225-1 is a K-feldspar porphyritic granodiorite from the centre of the Logjam pluton (Fig. 4-115). It yielded mostly elongate zircons with sector and concentric zoning; a few grains have inherited cores (Fig. 4-122a). LA-ICPMS analyses of 45 zircons returned $^{206}Pb/^{238}U$ dates between 354 and 175 Ma, and one grain returned a $^{206}Pb/^{207}Pb$ date of 2285 Ma (Appendix 3). The Proterozoic and Mississippian (n = 2) grains are from inherited cores, and 3 grains with dates between 201 and 196 Ma are interpreted as xenocrysts. The 39 youngest dates form a population with a weighted mean date of 181.4 ± 1.2 Ma (Fig. 4-122b). Six zircon grains analyzed by CA-TIMS yielded concordant $^{206}Pb/^{238}U$ dates that range from 184.30 ± 0.18 to 184.11 ± 0.12 Ma (Appendix 4), with a weighted mean date of 184.21 ± 0.05 Ma (MSWD = 1.36, n = 6; Fig. 4-122c).

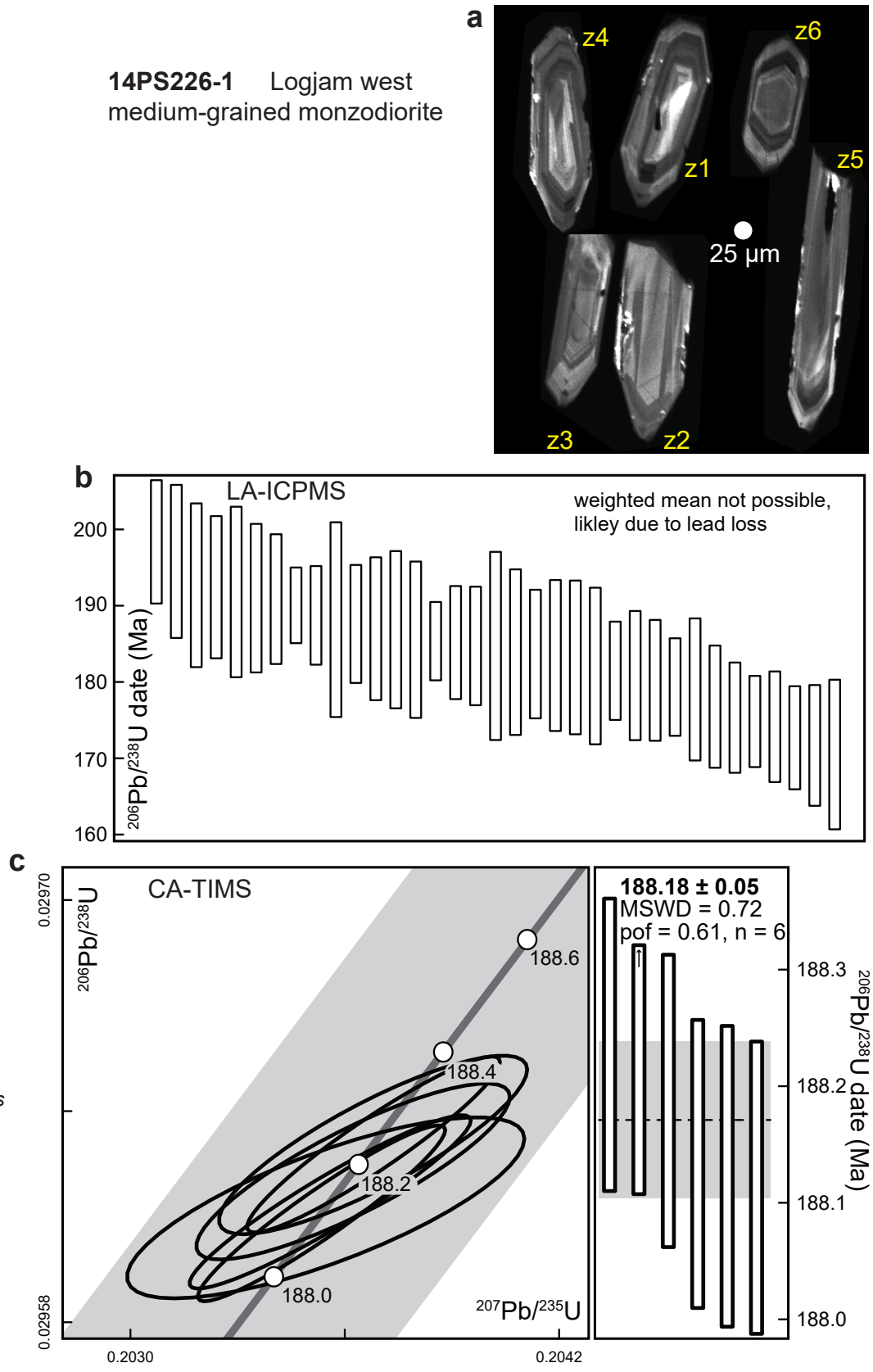


Figure 4-121. *U-Pb geochronological results for sample 14PS226-1, Logjam Creek stock.* ***(a)*** *CL images of representative igneous zircons. Yellow analysis number refers to grain analyzed by CA-TIMS.* ***(b)*** *Ranked plot of LA-ICPMS $^{206}Pb/^{238}U$ dates (Appendix 3).* ***(c)*** *Concordia diagram (left) and ranked $^{206}Pb/^{238}U$ dates (right) for zircons analyzed by CA-TIMS (Appendix 4). The light grey band around concordia (dark grey line) shows the decay constant uncertainties. Analyses included in weighted mean age (light grey horizontal bar) calculations are bold; analyses with thin lines not used in calculations. Line-type designations are the same in all plots. Errors in all plots are at 2σ. Arrows indicate data extend beyond plot. MSWD = mean squared weighted deviation, pof = probability of fit, n = number of analyses included in age calculation.*

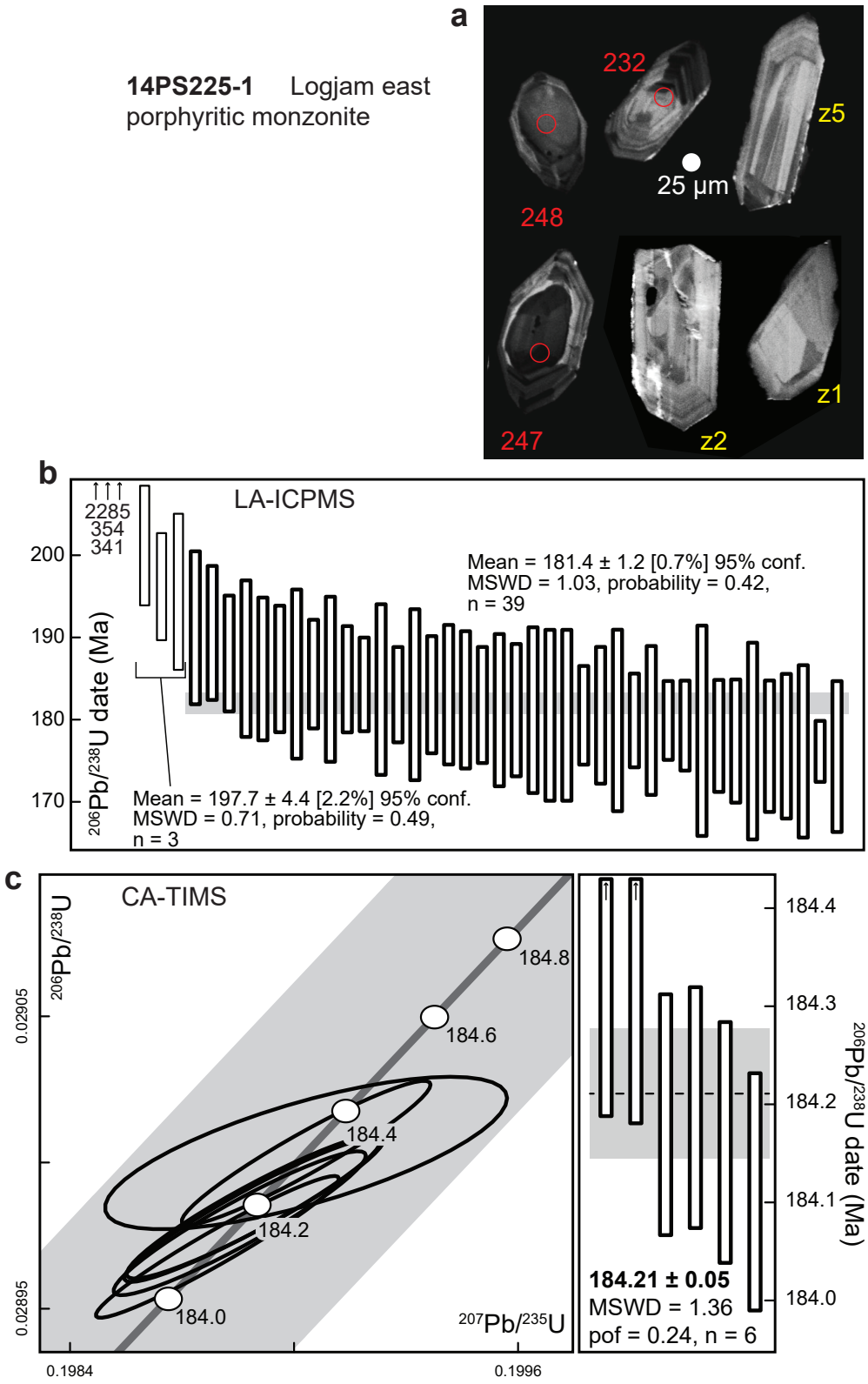
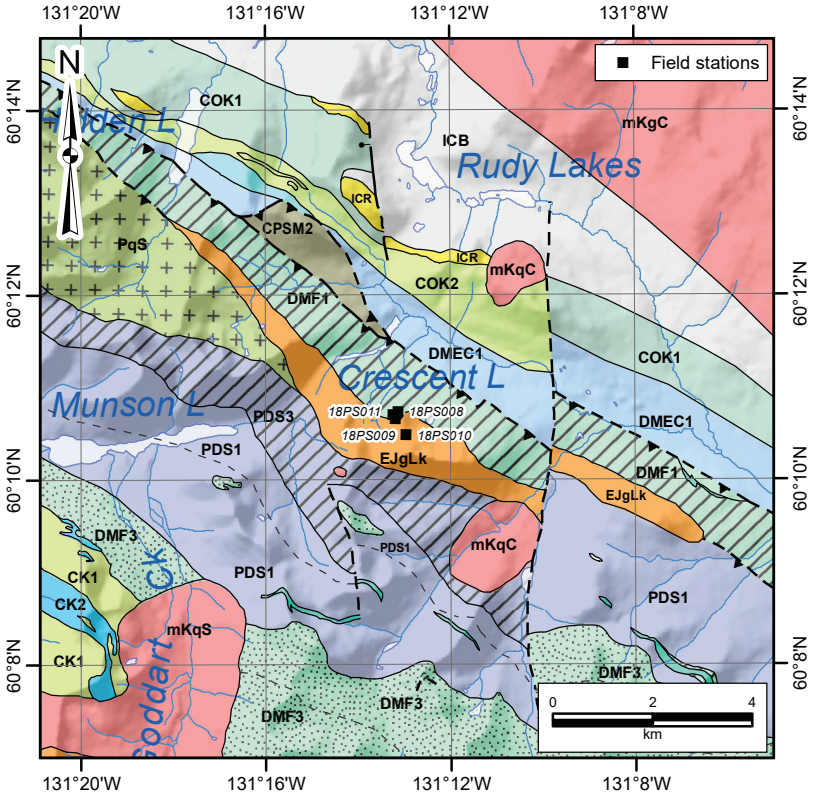


Figure 4-122. *U-Pb geochronological results for sample 14PS225-1, Two Ladder Creek stock.* ***(a)*** *CL images of representative igneous zircons. Red labels indicate LA-ICPMS analysis number with the red open circle indicating location of the analysis spot, yellow analysis number refers to grain analyzed by CA-TIMS.* ***(b)*** *Ranked plot of LA-ICPMS $^{206}Pb/^{238}U$ dates (Appendix 3). Arrows indicate three inherited analyses that plot beyond figure limit; Proterozoic date is calculated from $^{207}Pb/^{206}Pb$, Paleozoic dates are $^{206}Pb/^{238}U$.* ***(c)*** *Concordia diagram (left) and ranked $^{206}Pb/^{238}U$ dates (right) for zircons analyzed by CA-TIMS (Appendix 4). The light grey band around concordia (dark grey line) shows the decay constant uncertainties. Analyses included in weighted mean age (light grey horizontal bar) calculations are bold; analyses with thin lines not used in calculations. Line-type designations are the same in all plots. Errors in all plots are at 2σ. Arrows indicate data extend beyond plot. MSWD = mean squared weighted deviation, pof = probability of fit, n = number of analyses included in age calculation.*

Swift River sill

The Swift River sill is a northwest elongate body exposed over a 12 km length, is up to 1 km thick, and has a mapped extent of 7.9 km² (Fig. 4-123; Table 4-1; Roots *et al.*, 2004b). The sill is undeformed and intrudes the Hidden Lake thrust which places rocks of the Dorsey complex (Snowcap assemblage) on the Ram Creek complex (Finlayson assemblage) of the Yukon-Tanana terrane (Roots *et al.*, 2004b). The Dorsey complex rocks are higher metamorphic grade and include Upper Devonian and older schist, gneiss and amphibolite (Roots *et al.*, 2004b). Rocks of the Mississippian Ram Creek complex are greenschist facies mafic metavolcanic rocks (Roots *et al.*, 2004b). Xenoliths of mafic metavolcanic rocks that occur in diorite near the northern margin of the Swift River sill support an intrusive relationship (Fig. 4-124). The northern tip of the sill is in contact to the west with Permian monzonite of the Ram stock (Fig. 4-123; Sulphur Creek suite, Yukon-Tanana terrane). The Swift River sill is dissected by a north-trending fault with 1-3 km of apparent sinistral offset (Roots *et al.*, 2004b).



MID-CRETACEOUS

- mKgC: CASSIAR SUITE: Bt ± Hbl ± titanite-bearing monzogranite to granodiorite
- mKqC: CASSIAR SUITE: Bt ± Ms monzogranite and leucogranite
- mKqS: SEAGULL SUITE: Bt (± Ms) leucogranite to monzogranite

EARLY JURASSIC

- EJgLk: LOKKEN SUITE: Hbl-Bt-Cpx monzodiorite to granodiorite, local monzonite

MIDDLE TO LATE PERMIAN

- PqS: SULPHUR CREEK SUITE: variably foliated, K-feldspar augen granite, metaporphyry

CARBONIFEROUS

- CK1: KLINKIT: mafic to intermediate metavolcaniclastic and metavolcanic rocks; minor felsite
- CK2: KLINKIT: limestone, marble, locally fossiliferous

CARBONIFEROUS TO PERMIAN

- CPSM2: CAMPBELL RANGE: dark green to black basalt, greenstone, locally pillowed

MISSISSIPPIAN

- MgSR: SIMPSON RANGE SUITE: Hbl-bearing metagranodiorite, metadiorite and metatonalite

DEVONIAN, MISSISSIPPIAN AND(?) OLDER

- DMF1: FINLAYSON: intermediate to mafic volcanic and volcaniclastic rocks
- DMF3: FINLAYSON: dark grey to black carbonaceous metasedimentary rocks, metachert
- DMF4: FINLAYSON: light green to grey, fine-grained siliciclastic and metavolcaniclastic rocks
- DMF5: FINLAYSON: light grey to white marble, locally crinoidal

UPPER DEVONIAN TO LOWER MISSISSIPPIAN

- DMEC1: EARN - CASSIAR: black siliceous slate, quartz-chert greywacke, grit and conglomerate

MIDDLE SILURIAN TO MIDDLE DEVONIAN

- SDA2: ASKIN: dolostone, silty and sandy dolostone, limestone

UPPER CAMBRIAN AND ORDOVICIAN

- COK1: KECHIKA: thin-bedded, lustrous, calcareous, grey slate, phyllite, limestone
- COK2: KECHIKA: dark green and maroon amygdaloidal basalt flows and volcaniclastic rocks

LOWER CAMBRIAN

- ICR: ROSELLA: resistant, thick-bedded to massive, limestone and argillaceous limestone
- ICB: BOYA: quartz arenite, interbedded argillite, slate, siltstone, phyllite, minor limestone

NEOPROTEROZOIC AND PALEOZOIC

- PDS1: SNOWCAP: quartzite, psammite, pelite and marble; minor greenstone and amphibolite
- PDS2: SNOWCAP: light grey to buff weathering marble
- PDS3: SNOWCAP: amphibolite, commonly garnet-bearing; greenstone

Petrography

The Swift River sill was examined at four stations over 500 m, approximately 1.5 km south of Crescent Lake (Fig. 4-123). The Swift River sill in this area is altered and contains abundant veining (Fig. 4-125). The veins have two orientations, both steeply dipping (73 to 89°), striking either E–W or N–S. Mineralogy of the veins is dominantly chlorite with variable epidote and magnetite and a K-feldspar–carbonate alteration halo (Fig. 4-125). The sill is fine-grained equigranular diorite (Figs. 4-2b and 4-126). The diorite is mesocratic and mafic minerals make up 35 to 50% of the rock; hornblende comprises 30%, and biotite and pyroxene 5 to 10% each. Pyroxene is present as cores with hornblende rims (Fig. 4-127). Mafic minerals are moderately to intensely chlorite altered and plagioclase is intensely saussuritized (Fig. 4-127).

Figure 4-123. *Geology of Swift River pluton area. Geology from YGS (2020a); fault symbology as in Figure 1-4.*



Figure 4-124. *Scree downhill from the northern Swift River sill contact showing fine-grained mafic xenoliths within diorite of the Swift River sill; 18PS007. The xenoliths resemble mafic metavolcanic rocks of the Ram Creek complex. Hammer head is 13 cm.*



Figure 4-125. *Fine-grained diorite with chlorite-epidote vein oriented N182/87; 18PS009. White K-feldspar-carbonate alteration halo in diorite. Hammer handle is 4 cm across.*

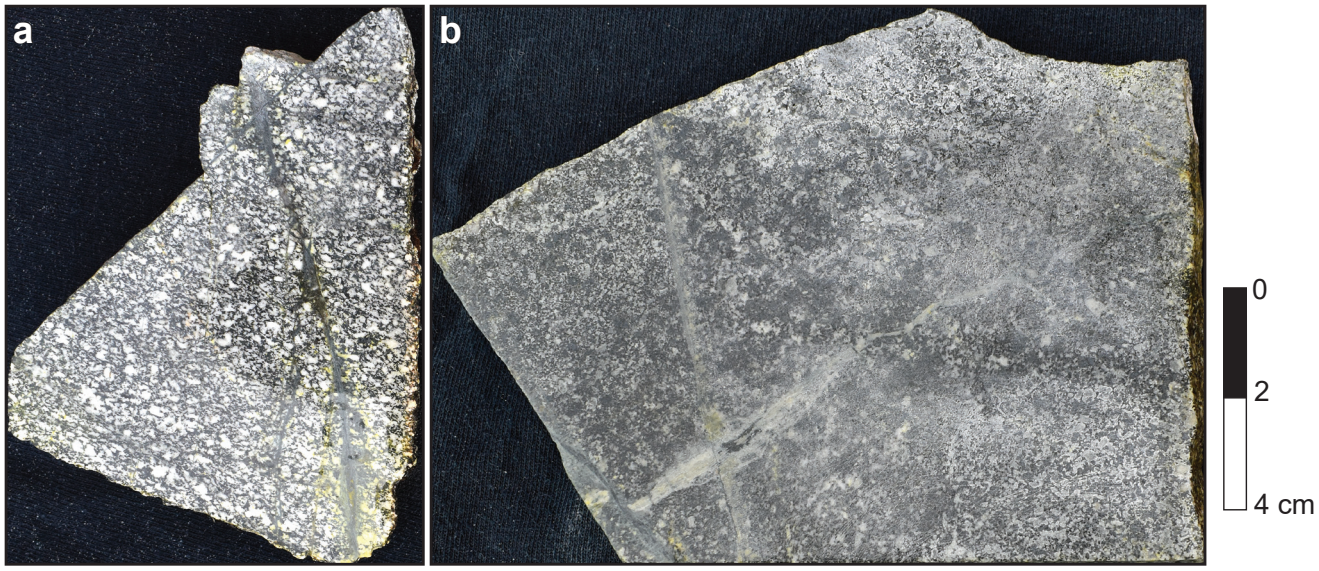


Figure 4-126. *Representative slabs from the Swift River sill.* ***(a)*** *Fine-grained equigranular diorite with chlorite-epidote hairline vein with K-feldspar alteration halo; 18PS008-1.* ***(b)*** *Patchy, fine-grained diorite with chlorite-epidote ± magnetite veins; 18PS010-1. Cobaltinitrite-stained surfaces. K-feldspar is yellow; both images are same scale.*

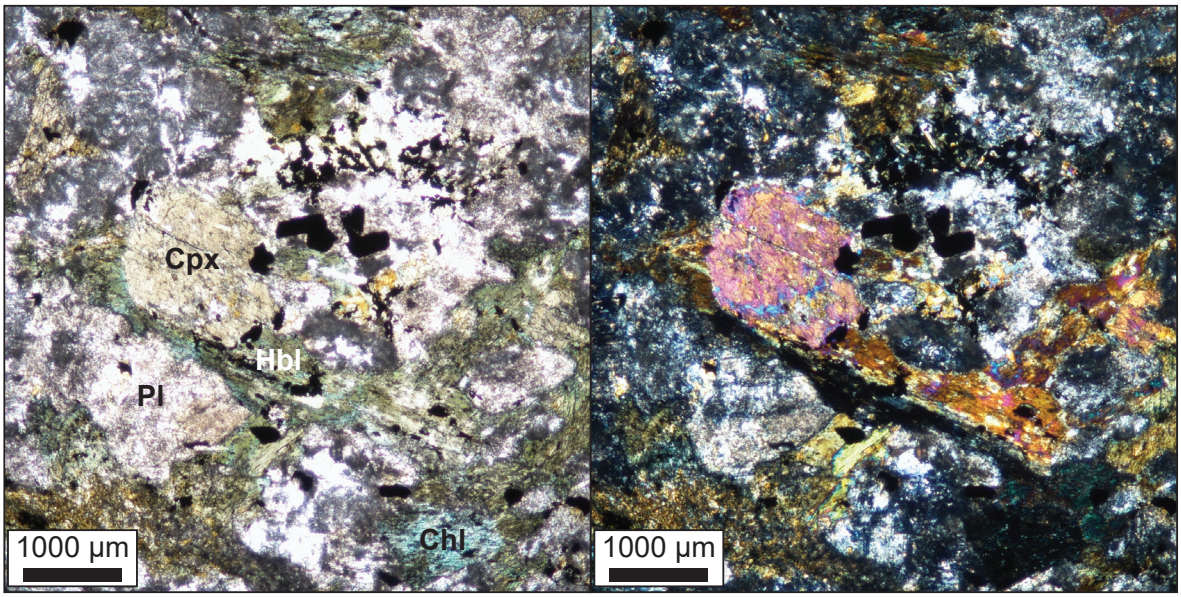


Figure 4-127. *Transmitted light photomicrographs from the Swift River sill; plane polarized light (left) and cross-polarized light (right). Intensely altered diorite with pyroxene overgrown by hornblende; 18PS008-1. Biotite is intensely chlorite altered, hornblende moderately. Plagioclase is intensely saussuritized.*

Oxidation state and mineral occurrences

The Swift River sill is generally non-magnetic (Fig. 4-128) and has magnetic susceptibilities between 0.29 and 0.47 × 10^{-3} SI units (mean = 0.38 × 10^{-3} SI units; n = 4; Fig. 4-3b). There are several mineral occurrences in mafic metavolcanic rocks of the Ram Creek complex to the north, including the Dan [105B 027] and Atom [105B 026], as well as within Dorsey complex rocks to the south, such as the MOD [105B 031] and TBMB [105B 029]. Mineralized rocks at these occurrences are metamorphosed semi-massive to massive stratiform sulphide (pyrrhotite, sphalerite, galena ± chalcopyrite) within a gangue of calc-silicate minerals (garnet-diopside-actinolite) and magnetite. The proximity to Early Jurassic and Early Cretaceous intrusions, calc-silicate mineralogy, and Pb isotopic composition of galena and pyrrhotite from the occurrences were used to interpret these occurrences as skarn mineralization related to the Mesozoic plutons (Bremner and Liverton, 1990; Mortensen and Gabites, 2002). D'el-Rey Silva *et al.* (2001) however have argued that the sulphides in these occurrences are deformed and thus predate intrusion of the post-tectonic Jurassic and Cretaceous plutons. Parts of the Permian Ram stock are deformed (Stevens, 1996) and could be related to older skarn mineralization, although it occurs several kilometres from these mineral occurrences (Fig. 4-123). Liverton and Casselman (2018) have proposed an alternative in which these occurrences are Mississippian syngenetic massive sulphides that were subsequently deformed and metamorphosed during intrusion of the Mesozoic plutons. Although the Early Jurassic Swift River sill may have metamorphosed some of these occurrences, it does not appear to be genetically related to mineralization.

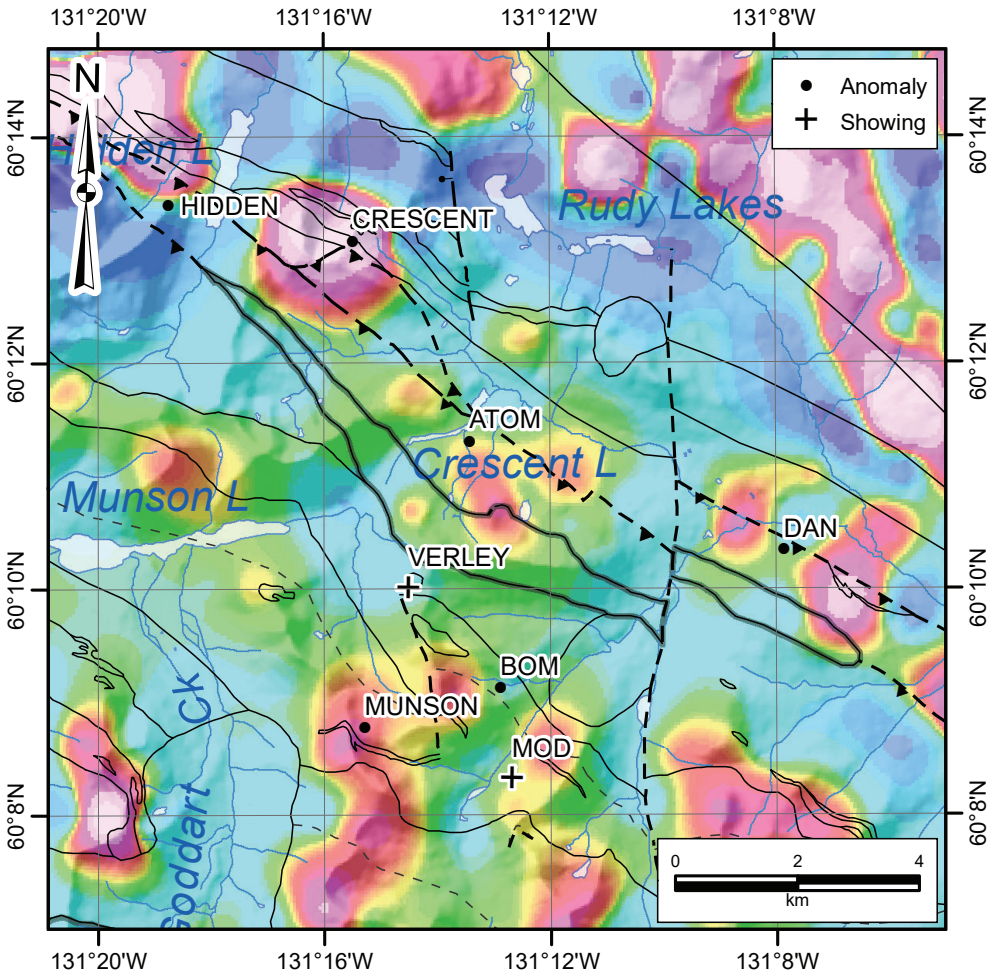
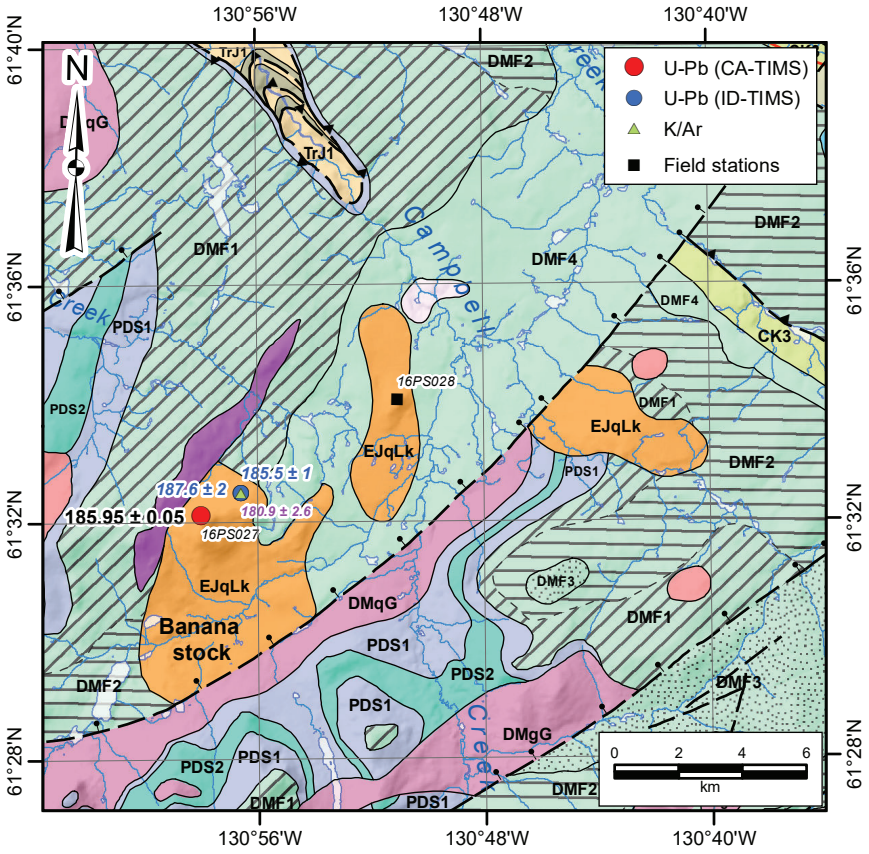


Figure 4-128. *Reduced to pole, residual total field aeromagnetic map of the Swift River pluton area (Aurora Geosciences Ltd. and Bruce, 2017f) illustrating locations of MINFILE occurrences in the region. Fault symbology as in Figure 1-4.*

Finlayson plutons

Early Jurassic plutons assigned to the Lokken suite also intrude rocks of the Yukon-Tanana terrane in the Finlayson Lake area, northeast of the Tintina fault (Fig. 4-1). The Early Jurassic plutons occur in two main areas. The northernmost exposures comprise three plutons in the upper reaches of Big Campbell Creek (Fig. 4-129), approximately 20 km southwest of Finlayson Lake. The largest pluton, the Banana stock, has a mapped extent of 26.9 km², whereas the other two are 10.1 and 10.7 km² in area (Fig. 4-129; Murphy *et al.*, 2001). All three stocks intrude rocks of Snowcap and Finlayson assemblages within the Big Campbell thrust sheet in the hanging wall of the Inconnu thrust (Murphy *et al.*, 2006). A northeast-striking normal fault separates the easternmost pluton from the Banana stock and its satellite pluton (Fig. 4-129). The Banana stock intrudes the contact between bimodal metavolcanic rocks and serpentinite of the Grass Lakes Group (Fire Lake and Kudz Ze Kayah formations) and metaclastic rocks of the overlying Wolverine Lake Group (Fig. 4-130). For this study, we visited two of the northern plutons (Fig. 4-129; Table 4-1). Another small stock, the Money plug (~11 km²), is exposed ~55 km to the southeast, approximately 25 km south of Wolverine Lake (Fig. 4-1).



MID-CRETACEOUS

mKqA: ANVIL SUITE: K-feldspar megacrystic, biotite ± muscovite monzogranite

EARLY JURASSIC

EJqLk: LOKKEN SUITE: Bt-Hbl quartz monzonite to granite

MIDDLE TO UPPER TRIASSIC

TrJ1: JONES LAKE: calcareous siltstone, shale, and fine sandstone

CARBONIFEROUS

CK1: KLINKIT: mafic to intermediate metavolcaniclastic and metavolcanic rocks; minor felsite

CK2: KLINKIT: limestone, marble, locally fossiliferous

CK3: KLINKIT: arkosic sandstone, basal polymictic metaconglomerate

CARBONIFEROUS TO PERMIAN

CPSM1: FORTIN CREEK: dark grey to black carbonaceous phyllite, chert and argillite

CPSM2: CAMPBELL RANGE: dark green to black basalt, greenstone, locally pillowed

CPSM4: SLIDE MOUNTAIN: brown weathering, variably serpentinized ultramafic rocks

MISSISSIPPIAN

MqSR: SIMPSON RANGE SUITE: foliated metagranite, quartz monzonite and granodiorite; augen granite

DEVONIAN, MISSISSIPPIAN AND(?) OLDER

DMF1: FINLAYSON: intermediate to mafic volcanic and volcaniclastic rocks

DMF2: FINLAYSON: felsic metavolcanic rocks, white quartz-muscovite schist, metaporphyry

DMF3: FINLAYSON: dark grey to black carbonaceous metasedimentary rocks, metachert

DMF4: FINLAYSON: light green to grey, fine-grained siliciclastic and metavolcaniclastic rocks

DMF6: FINLAYSON: ultramafic rocks, serpentinite; metagabbro

LATE DEVONIAN TO MISSISSIPPIAN

DMqG: GRASS LAKES SUITE; foliated, coarse-grained, K-feldspar-augen metagranite

DMgG: GRASS LAKES SUITE: fine to medium-grained, foliated granodiorite, granite, quartz monzonite

NEOPROTEROZOIC AND PALEOZOIC

PDS1: SNOWCAP: quartzite, psammite, pelite and marble; minor greenstone and amphibolite

PDS2: SNOWCAP: light grey to buff weathering marble

Figure 4-129. *Geology of the Finlayson Lake area in the vicinity of the northern cluster of Early Jurassic plutons, upper Big Campbell Creek. Geology from YGS (2020a); fault symbology as in Figure 1-4.*

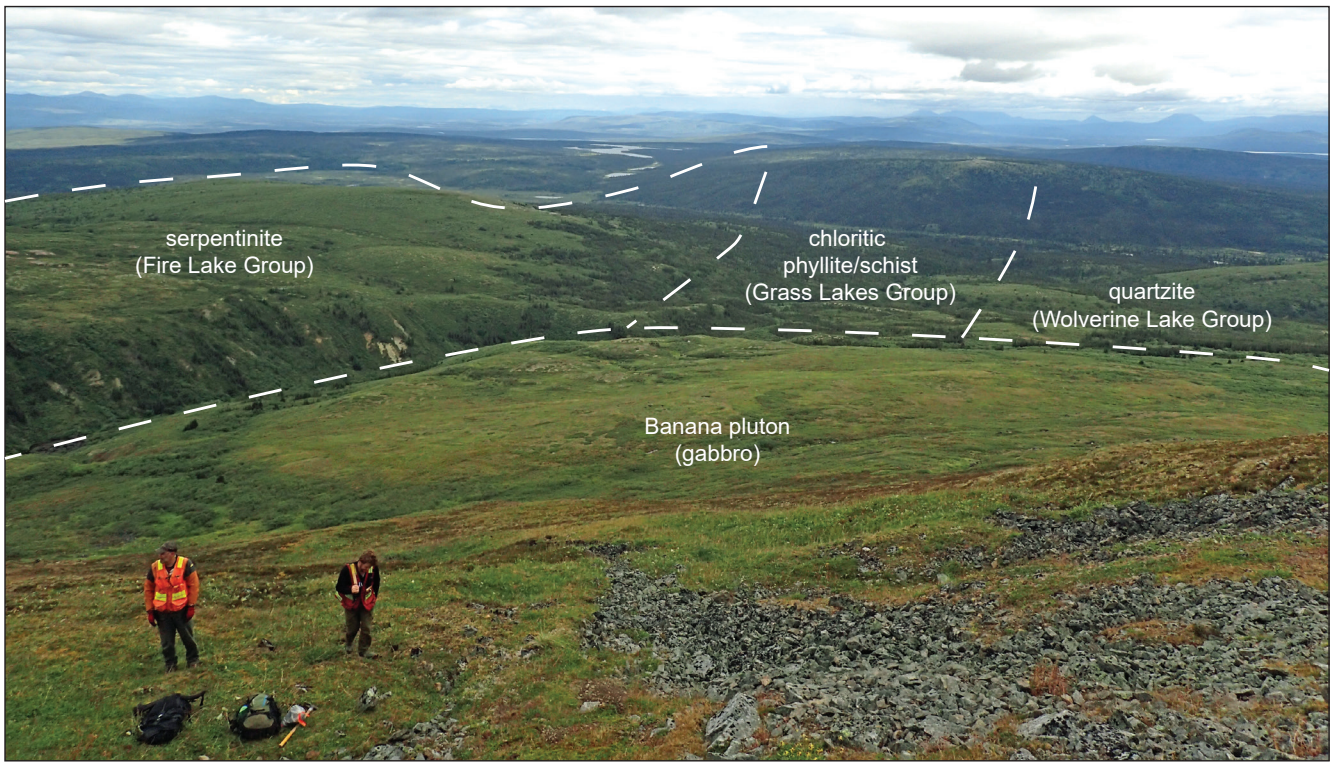


Figure 4-130. *View looking north from the Banana pluton, 16PS027. Rock units from Murphy et al. (2001; 2006).*

Petrography

The Finlayson plutons are fine to medium grained and weakly plagioclase-hornblende porphyritic to equigranular (Fig. 4-131). The syenite to monzonite composition of the rock (Fig. 4-2b) is primarily influenced by the ratio of plagioclase phenocrysts to groundmass K-feldspar (Figs. 4-131 and 4-132); monzonite composition is more common than syenite. The groundmass is primarily white K-feldspar (Fig. 4-132) and minor quartz (Fig. 4-133). The rock is mesocratic with 25% hornblende and 5% pyroxene. Both are relatively fresh, though hornblende commonly overgrows pyroxene (Fig. 4-133). Plagioclase is moderately saussuritized and K-feldspar is fresh (Fig. 4-133).

Oxidation state and mineral occurrences

The Finlayson stocks generally correspond with magnetic highs on regional maps (Fig. 4-134). However, the sites we visited have low magnetic susceptibilities of 0.375 and 0.434 × 10^{-3} SI units (mean = 0.405 × 10^{-3} SI units; n = 2; Fig. 4-3b); both localities are on the flank of high magnetic anomalies (Fig. 4-134). The only mineral occurrence proximal to the Early Jurassic stocks is the Copland ([105G 109]; YGS, 2020b). It was initially staked over the contact between quartz-carbonate and serpentinized ultramafic rocks and the Banana stock but no mineralization has been reported (YGS, 2020b). Other occurrences in the area are mostly related to Devonian–Mississippian syngenetic volcanogenic massive sulphide deposits of the Finlayson Lake district, including the Kudz Ze Kayah deposit ([105G 117]; Fig. 4-134).

Geochronology

The Banana stock was previously dated by U-Pb TIMS on multi-grain zircon and titanite fractions and are 187.6 ± 2.0 and 185.5 ± 1.0 Ma, respectively (J.K. Mortensen, unpublished *in* YGS, 2020c; Fig. 4-129; Appendix 1). Hornblende from the same locality yielded a K-Ar cooling age of 180.9 ± 2.6 Ma (Hunt and Roddick, 1992).

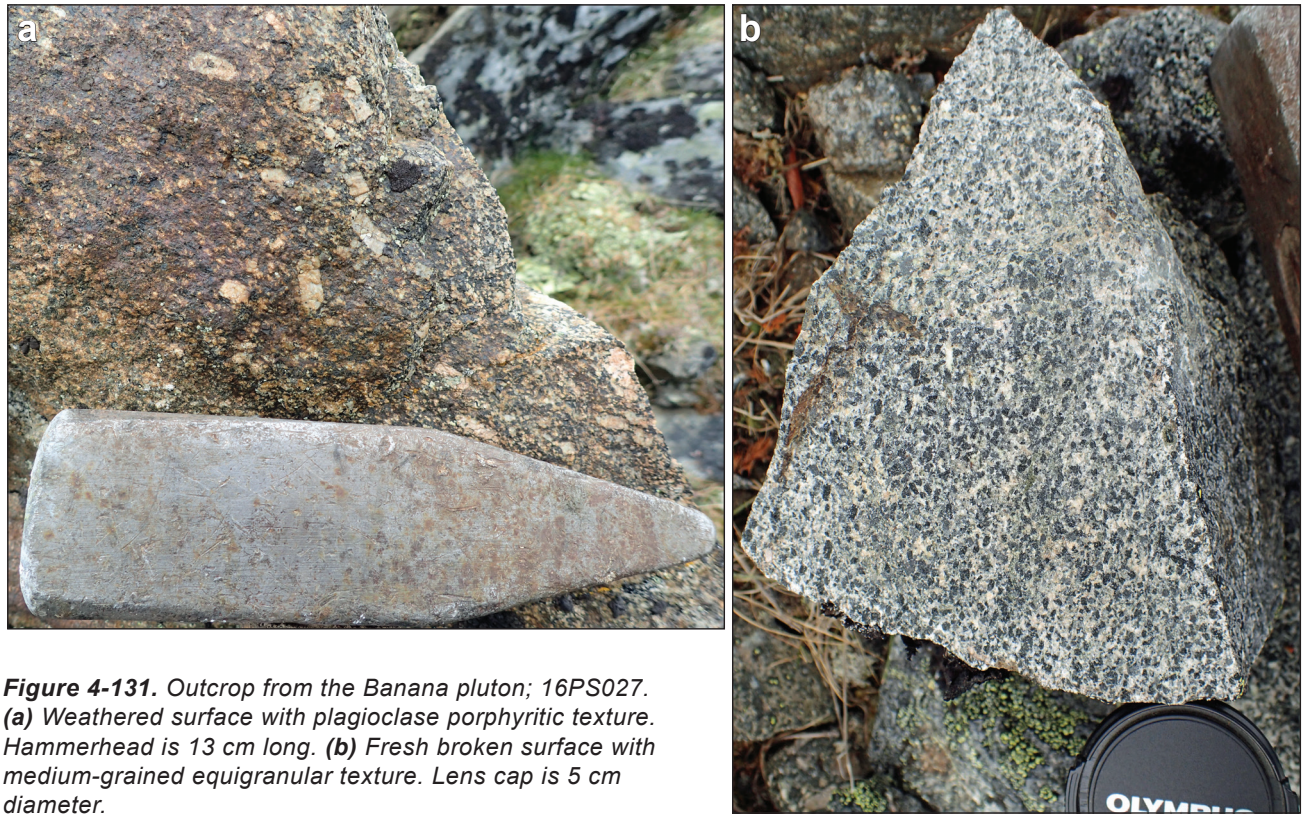


Figure 4-131. *Outcrop from the Banana pluton; 16PS027.* ***(a)*** *Weathered surface with plagioclase porphyritic texture. Hammerhead is 13 cm long.* ***(b)*** *Fresh broken surface with medium-grained equigranular texture. Lens cap is 5 cm diameter.*

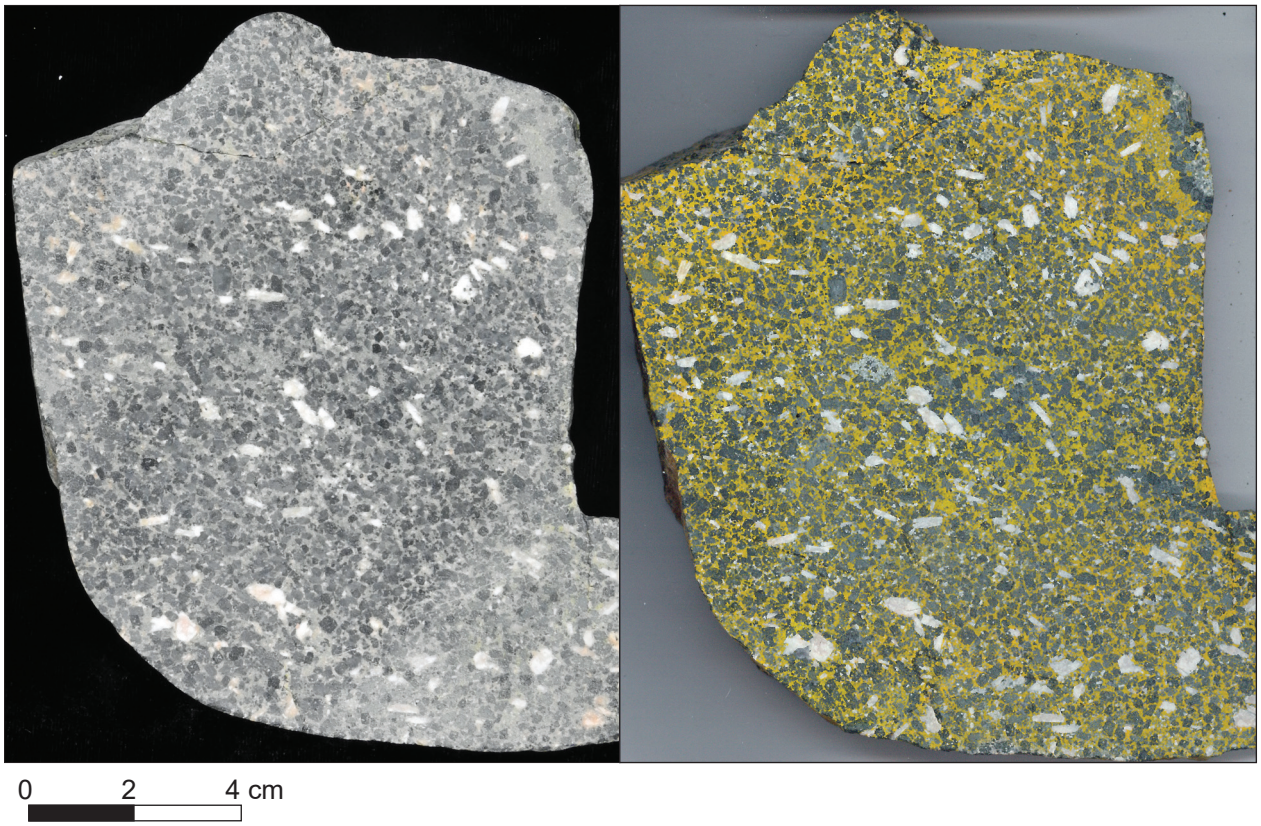


Figure 4-132. *Representative sample of syenite from the Finlayson plutons; 16PS028-1. Fresh polished surface (left) and a cobaltinitrite-stained surface (right). Note K-feldspar is yellow, both images are same scale.*

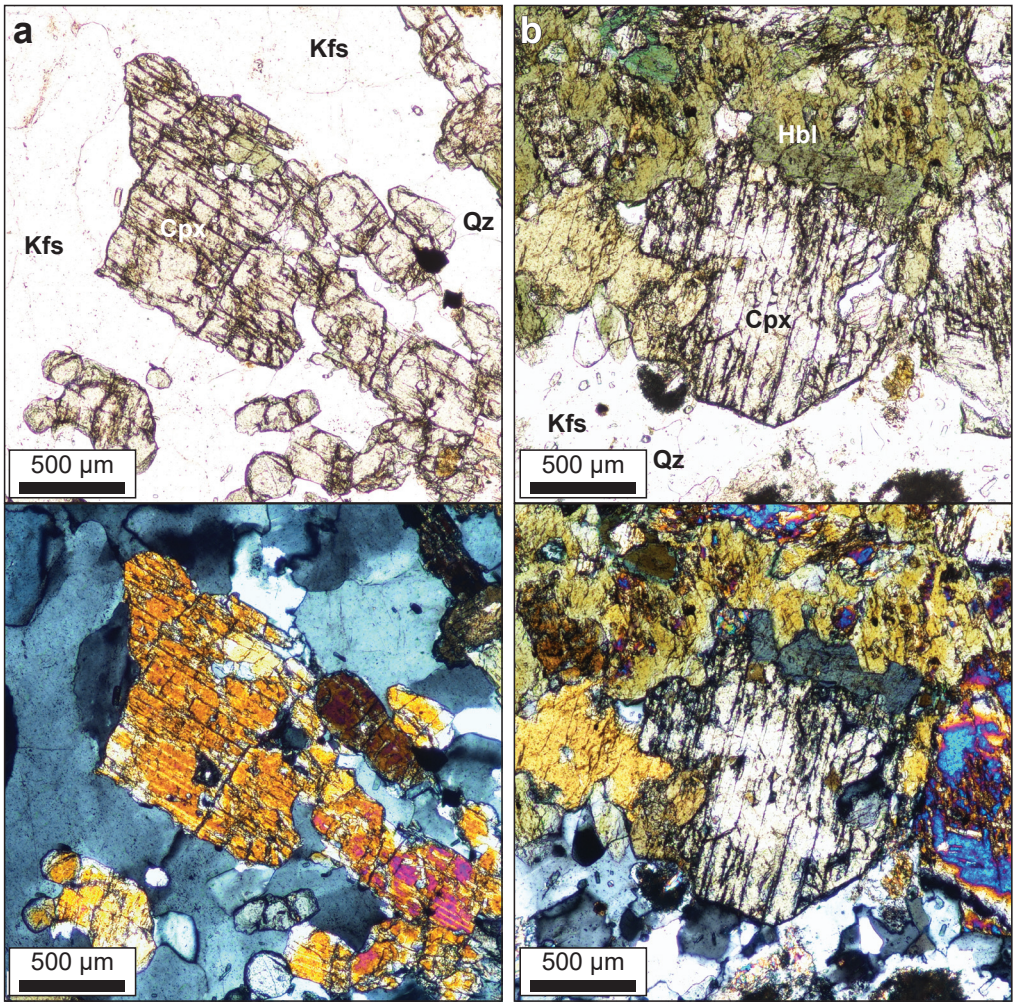


Figure 4-133. *Transmitted light photomicrographs from the Finlayson stocks; plane polarized light (upper) and cross-polarized light (lower).* ***(a)*** *K-feldspar groundmass with fine-grained clinopyroxene phenocryst; 16PS028-1.* ***(b)*** *Clinopyroxene core overgrown by hornblende; 16PS027-1.*

Sample 16PS027-1 is a medium-grained, equigranular Hbl-Cpx monzonite from the Banana stock collected ~1.5 km southwest of the previously dated locality (Fig. 4-129). It yielded stubby to elongate zircons with oscillatory and sector zoning (Fig. 4-135a). LA-ICPMS analyses of 38 zircons form a single zircon population with $^{206}Pb/^{238}U$ dates between 202 and 176 Ma. Three grains with dates of 202, 198 and 193 Ma are interpreted as xenocrysts. Another 32 grains have a weighted mean date of 185.2 ± 1.0 Ma (Fig. 4-135b; Appendix 3). Six zircon grains analyzed by CA-TIMS yielded concordant $^{206}Pb/^{238}U$ dates that range from 186.04 ± 0.13 to 185.88 ± 0.13 Ma (Appendix 4), with a weighted mean date of 185.95 ± 0.05 Ma (MSWD = 0.90, n = 6; Fig. 4-135c).

To the south, the Money stock (Fig. 4-1) was previously dated by U-Pb TIMS on multi-grain zircon and titanite fractions (J.K. Mortensen, unpublished *in* YGS, 2020c). The zircon fractions were discordant and provided a *ca.* 182 Ma date; a single concordant titanite fraction provides the best estimate of crystallization at 185.4 ± 1.0 Ma.

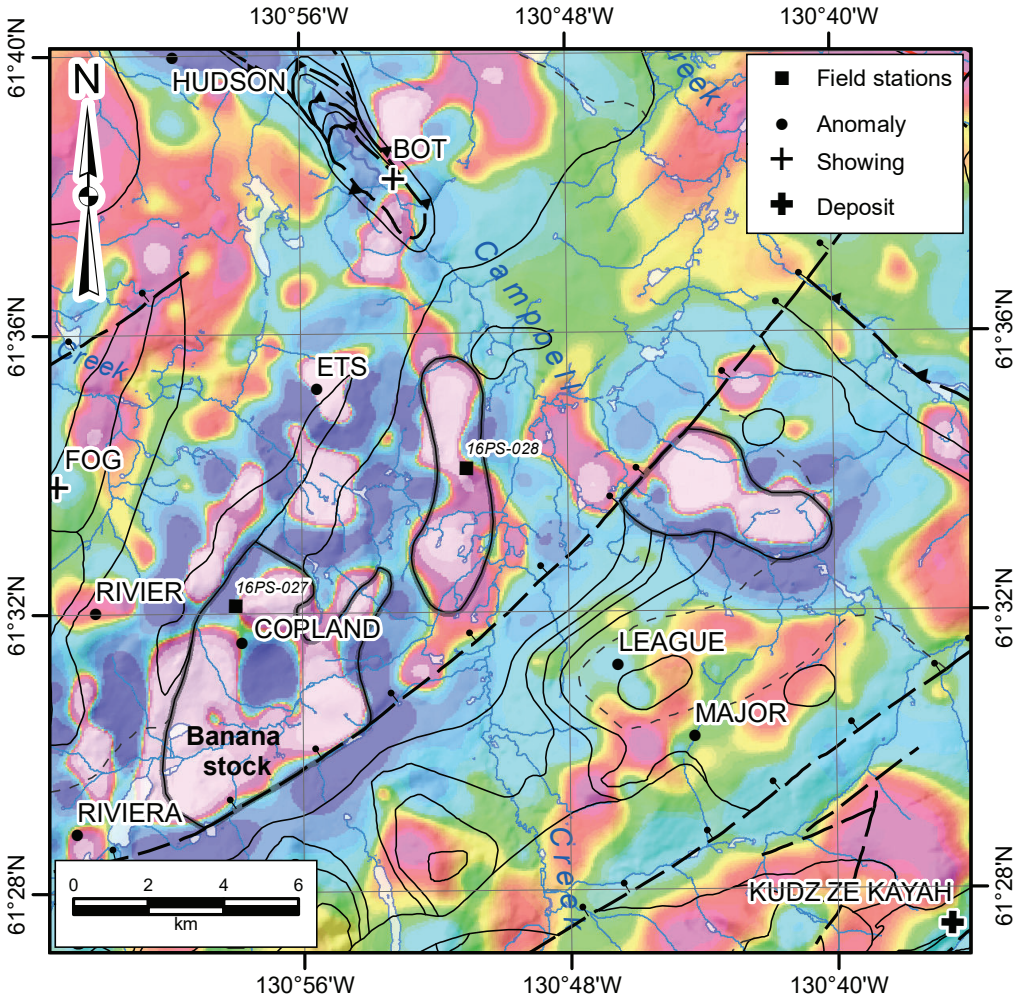


Figure 4-134. *Reduced to pole, residual total field aeromagnetic map of the Banana stock and surrounding area (Aurora Geosciences Ltd. and Bruce, 2017g) illustrating locations of MINFILE occurrences in the region. Fault symbology as in Figure 1-4.*

16PS027-1 Banana stock equigranular monzonite

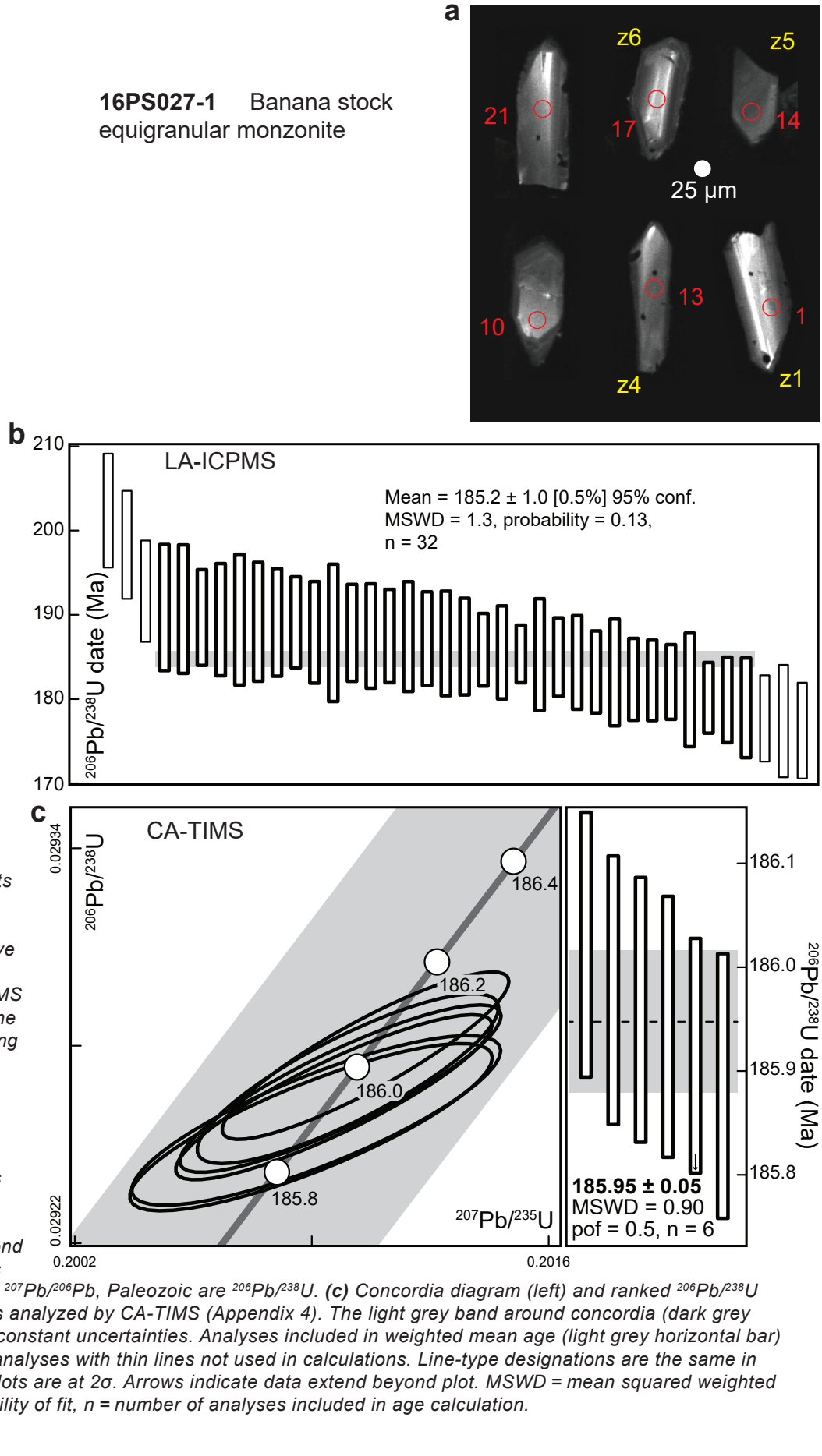


Figure 4-135. *U-Pb geochronological results for sample 16PS027-1, Banana stock.* ***(a)*** *CL images of representative igneous zircons. Red labels indicate LA-ICPMS analysis number with the red open circle indicating location of the analysis spot, yellow analysis number refers to grain analyzed by CA-TIMS.* ***(b)*** *Ranked plot of LA-ICPMS $^{206}Pb/^{238}U$ dates (Appendix 3). Arrows indicate three inherited analyses that plot beyond figure limit; Proterozoic date is calculated from $^{207}Pb/^{206}Pb$, Paleozoic are $^{206}Pb/^{238}U$.* ***(c)*** *Concordia diagram (left) and ranked $^{206}Pb/^{238}U$ dates (right) for zircons analyzed by CA-TIMS (Appendix 4). The light grey band around concordia (dark grey line) shows the decay constant uncertainties. Analyses included in weighted mean age (light grey horizontal bar) calculations are bold; analyses with thin lines not used in calculations. Line-type designations are the same in all plots. Errors in all plots are at 2σ. Arrows indicate data extend beyond plot. MSWD = mean squared weighted deviation, pof = probability of fit, n = number of analyses included in age calculation.*

Geochemistry

Fifty-six samples from plutons of the Long Lake suite were analyzed for whole-rock geochemistry: 39 from the Aishihik batholith (19 Aishihik 1 phase and 20 Aishihik 2), 10 from the Big Creek batholith, and 7 from the southwestern part of the Granite Mountain batholith (Appendix 8). Ten samples from the Bennett suite were analyzed. Most samples (n = 8) were collected in the northern part of the Bennett batholith between the Wheaton River and the Carbon Hill–Fenwick Creek area; two samples were collected in the Alligator Lake pluton north of the Skukum complex (Fig. 4-61). For plutons of the Lokken suite, 19 samples were analyzed: 5 from the Lokken batholith, 3 from Sawtooth, 2 each for the Thirtymile Lake, Englishman, Swift River, and Banana (Finlayson) plutons, and 1 each for the Logjam, Two Ladder and Macmillan Range plutons.

Major elements

Samples from the Long Lake suite have a total range in SiO_2 content between 58 and 72%, and samples from the Aishihik batholith span the entire range (Figs. 4-136a and 4-137). The more felsic Aishihik 2 phase typically has $SiO_2 > 66\%$, whereas the southwest Granite Mountain and Big Creek batholiths are generally $< 64\%$ SiO_2. Samples of Aishihik batholith plot mainly in subalkalic diorite to granite fields on classification diagrams, and a few samples show more alkalic affinities and monzonite to syenite composition (Fig. 4-136). The Granite Mountain samples cluster in the diorite field, and samples from the Big Creek batholith are consistently more alkalic with monzonite to syenite composition (Fig. 4-136). Some Big Creek samples are also distinguished from the rest of the Long Lake suite by their depleted Al_2O_3 and Na_2O content and elevated K_2O (Fig. 4-137). The Aishihik batholith spans the ferroan to magnesian fields and is generally calcic to alkali-calcic in composition, and again a few samples from the Aishihik 2 phase show alkalic tendencies (Fig. 4-138). Samples of the Aishihik 1 phase span the metaluminous to peraluminous fields of the Alumina Saturation Index of Maniar and Piccoli (1989), while those from Aishihik 2 are dominantly peraluminous (Fig. 4-138c). Both the Granite Mountain and Big Creek samples plot in the magnesian fields; the Granite Mountain samples cluster in the calc-alkalic field of the MALI diagram of Frost *et al.* (2001), and the Big Creek samples straddle the alkali-calcic to alkalic fields (Fig. 4-138a,b). Both the Big Creek and Granite Mountain batholith are metaluminous (Fig. 4-138c).

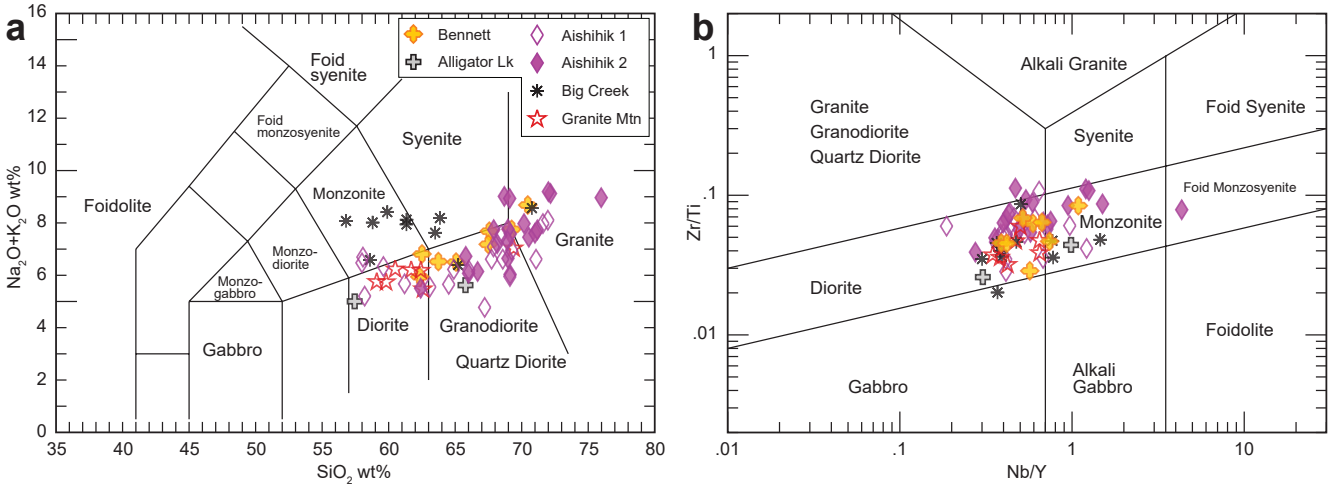


Figure 4-136. (a) *Total alkali-silica diagram for samples of the Long Lake and Bennett suites (adapted from Le Bas et al., 1986, for plutonic rocks).* ***(b)*** *Zr/Ti vs. Nb/Y classification diagram of Winchester and Floyd (1977) as modified by Pearce (1996).*

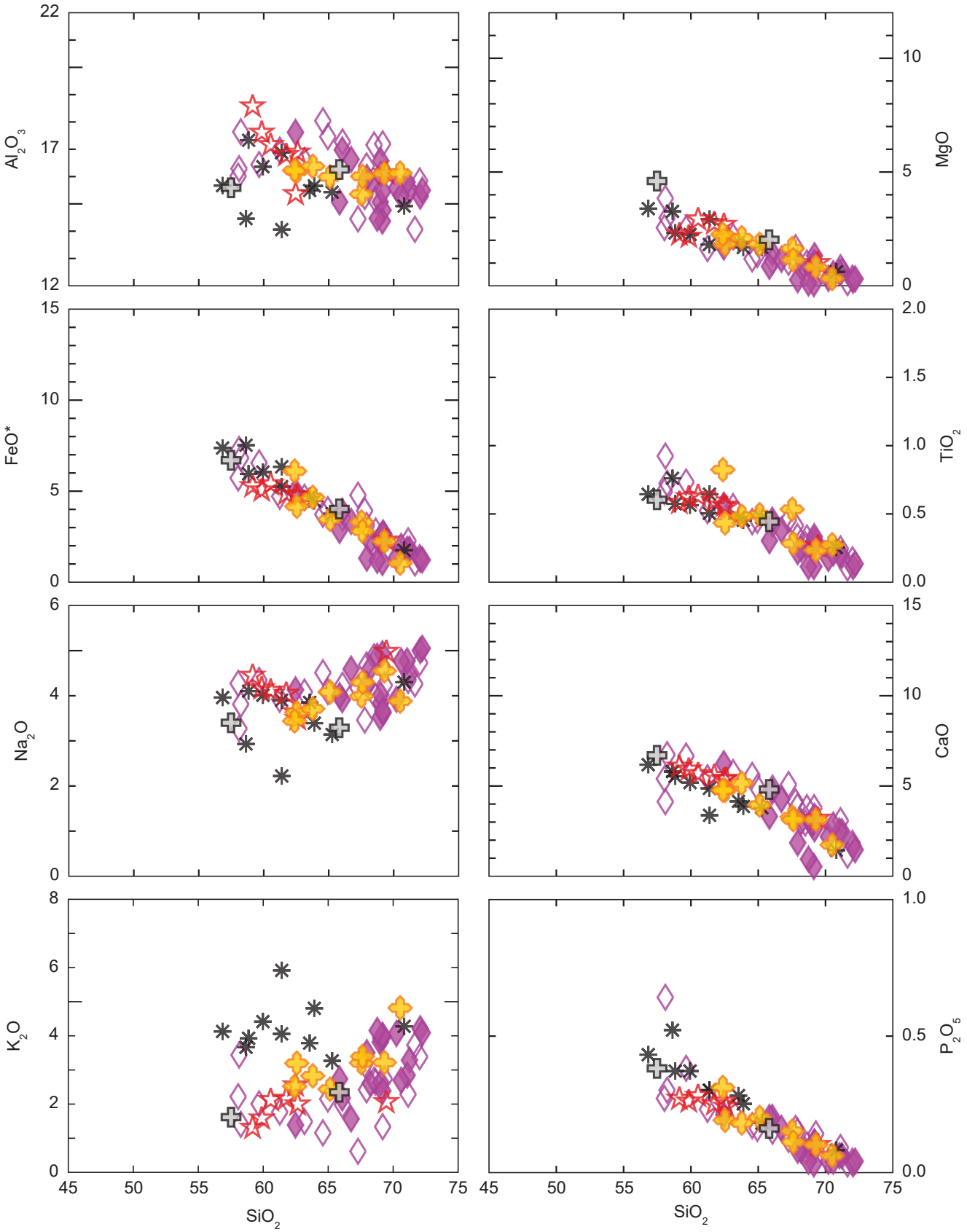
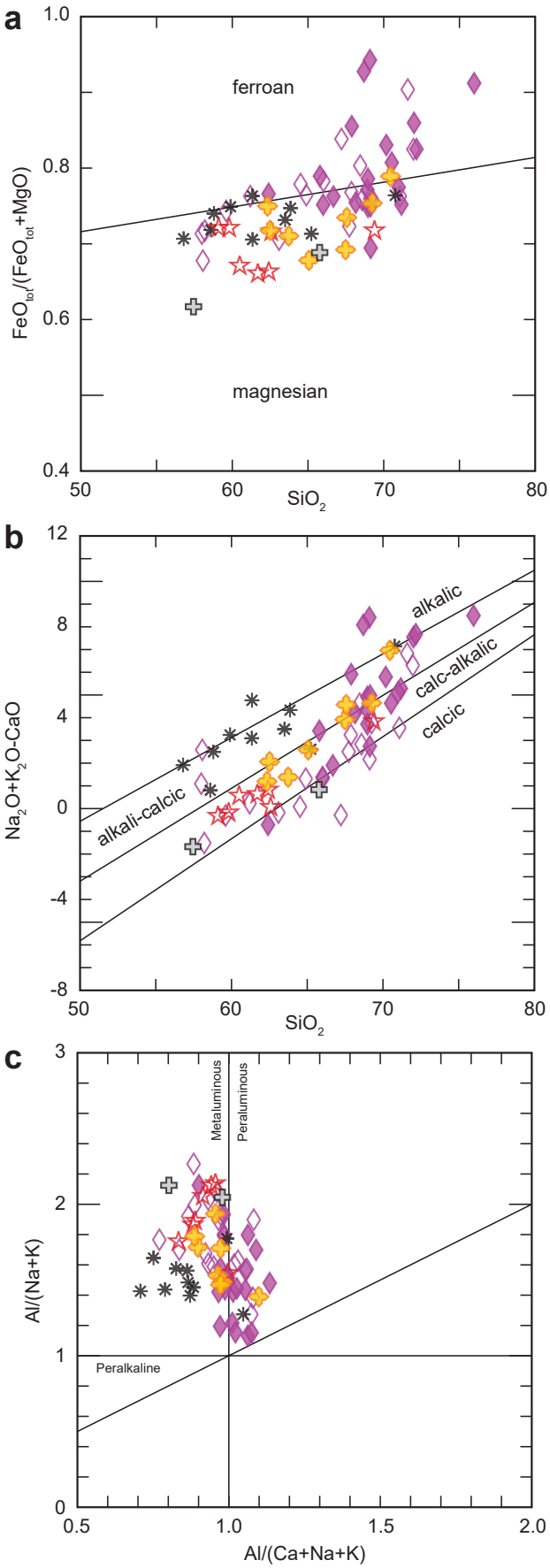


Figure 4-137. *Major elements vs. SiO_2 Harker plots for samples of the Long Lake and Bennett suites. Symbols as in Figure 4-136.*



Samples from the Bennett suite range in SiO_2 mostly between 62 and 70%, with a single sample from the Alligator Lake pluton having a lower SiO_2 content of 57.5% (Figs. 4-136 and 4-137). They are subalkalic to mildly alkalic, range from diorite to granite on composition diagrams, and show normal calc-alkaline differentiation trends on Harker diagrams. The Bennett suite samples are consistently magnesian, calc-alkalic to alkali-calcic, and metaluminous (Fig. 4-138).

Most samples from the Lokken suite have SiO_2 values between 54 and 64%, only the Logjam pluton has $SiO_2 > 64\%$ (Figs. 4-139 and 4-140). Samples from the Lokken and Englishman plutons have monzonite to diorite compositions, whereas the Sawtooth, Thirtymile Lake and Swift River plutons are bimodal with intermediate diorite-monzonite and mafic monzodiorite-monzogabbro end-members (Fig. 4-139a). Two samples from the Logjam pluton straddle the granodiorite to syenite fields. The Lokken suite plutons are subalkalic (Fig. 4-139b), with magnesian, calc-alkalic to alkali-calcic and metaluminous compositions (Fig. 4-141).

Plutons of the Long Lake and Bennett suites are predominantly of I-type character, and only a few samples of syenite from the Big Creek batholith show elevated K_2O and an S-type affinity (Fig. 4-142a). Most Lokken suite plutons also plot in the I-type field, and only samples from the Banana (Finlayson) stock and the Logjam pluton exhibit S-type character (Fig. 4-142b).

Figure 4-138. *Geochemical classification using criteria of Frost et al. (2001) for samples of the Long Lake and Bennett suites.* ***(a)*** *Fe-number,* ***(b)*** *modified alkali-lime index (MALI), and* ***(c)*** *alumina saturation index (ASI; after Maniar and Piccoli, 1989). Symbols as in Figure 4-136.*

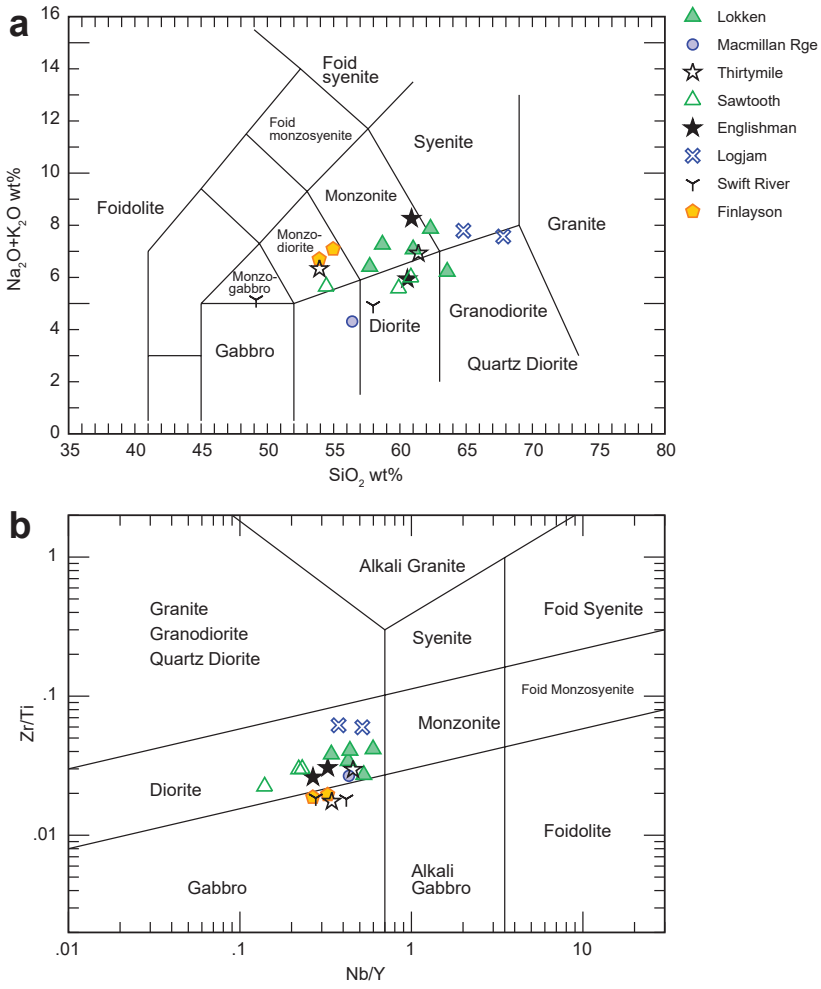


Figure 4-139. (a) *Total alkali-silica diagram for samples of the Lokken suite (adapted from Le Bas et al., 1986, for plutonic rocks).* ***(b)*** *Zr/Ti vs. Nb/Y classification diagram of Winchester and Floyd (1977) as modified by Pearce (1996).*

Trace elements

The trace element patterns for most samples of the Long Lake, Bennett and Lokken suites have negative Nb and Ti anomalies on primitive mantle normalized plots that are typical of continental crust or subduction-related magma (Figs. 4-143 to 4-145). The Long Lake samples have Th/Nb_N ratios of 2.6–11.7 and La/Yb_N of 4.4–14.6. The Bennett suite samples have relatively steep trace element patterns with La/Yb_N of 6.0–17.2 (average 10.2), Th/Nb_N of 3.8–12.9 (average 7.4), and Th enrichment 30–200 times those of primitive mantle (Fig. 4-144a). The Lokken samples have similar Th/Nb_N and La/Yb_N ratios of 4.1–11.1 and 3.9–9.8, respectively (Fig. 4-145). On upper continental crust normalized diagrams, samples from the Long Lake suite generally display flat trace element patterns that are slightly depleted relative to average upper continental crust (Fig. 4-143); the exception is the Big Creek batholith where trace element abundances are equal to slightly enriched relative to UCC and Zr depletion is more pronounced (Fig. 4-143f). Profiles on upper continental crust normalized plots of Bennett suite samples are relatively flat with trace element concentrations that are slightly depleted (Fig. 4-144b). Samples from the Lokken suite generally show slight depletion in LILE, positive Eu and Ti anomalies, and HREE comparable with UCC values (Fig. 4-145b,d). The two samples from the Banana stock (Finlayson) differ slightly with relative depletion of HREE and more depletion of Zr relative to Sm (Fig. 4-145f). All three suites plot in the arc (VAG) field of the Ta/Yb discrimination diagram of Pearce *et al.* (1984; Fig. 4-146).

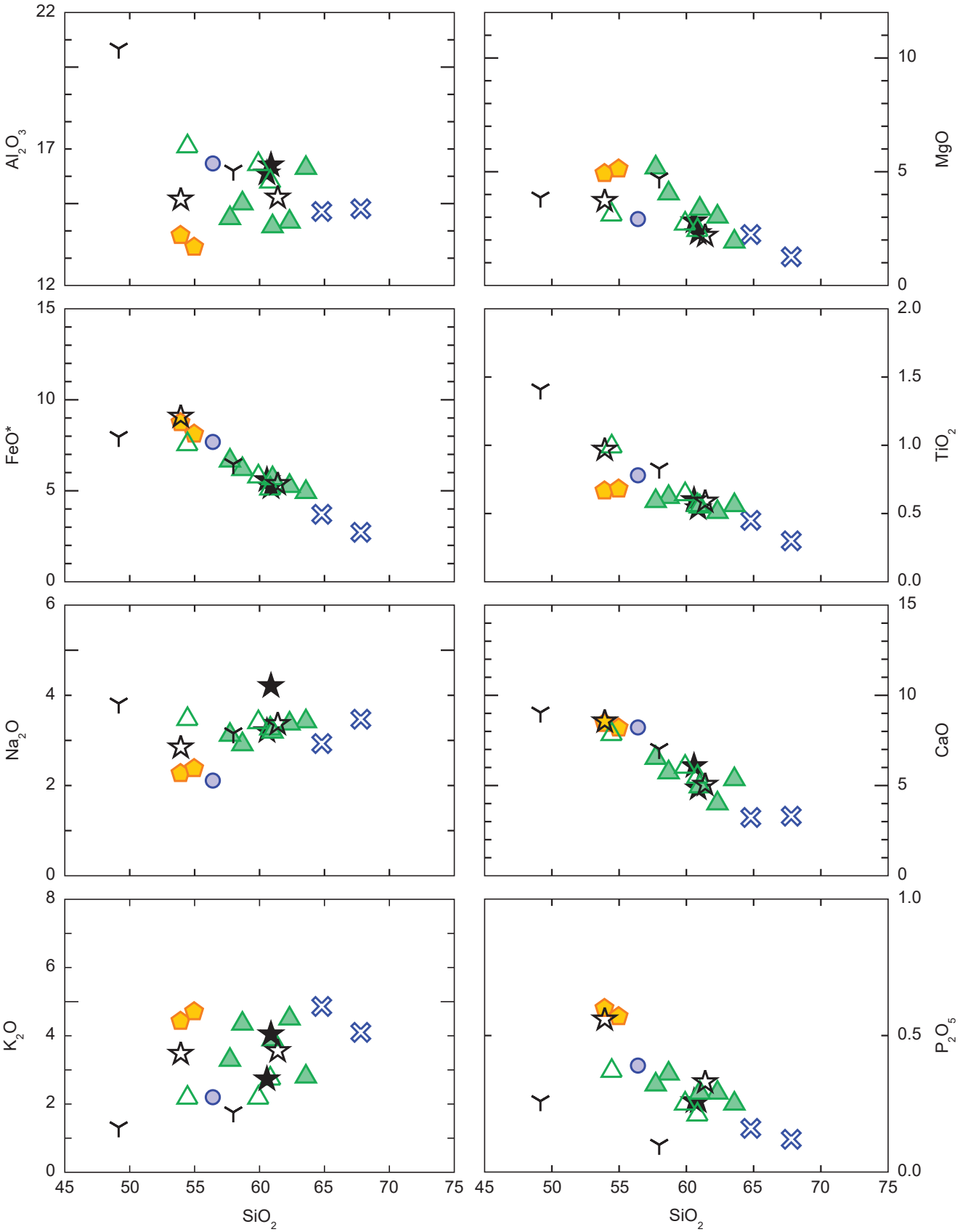


Figure 4-140. *Major elements vs. SiO_2 Harker plots for samples of the Lokken suite. Symbols as in Figure 4-139.*

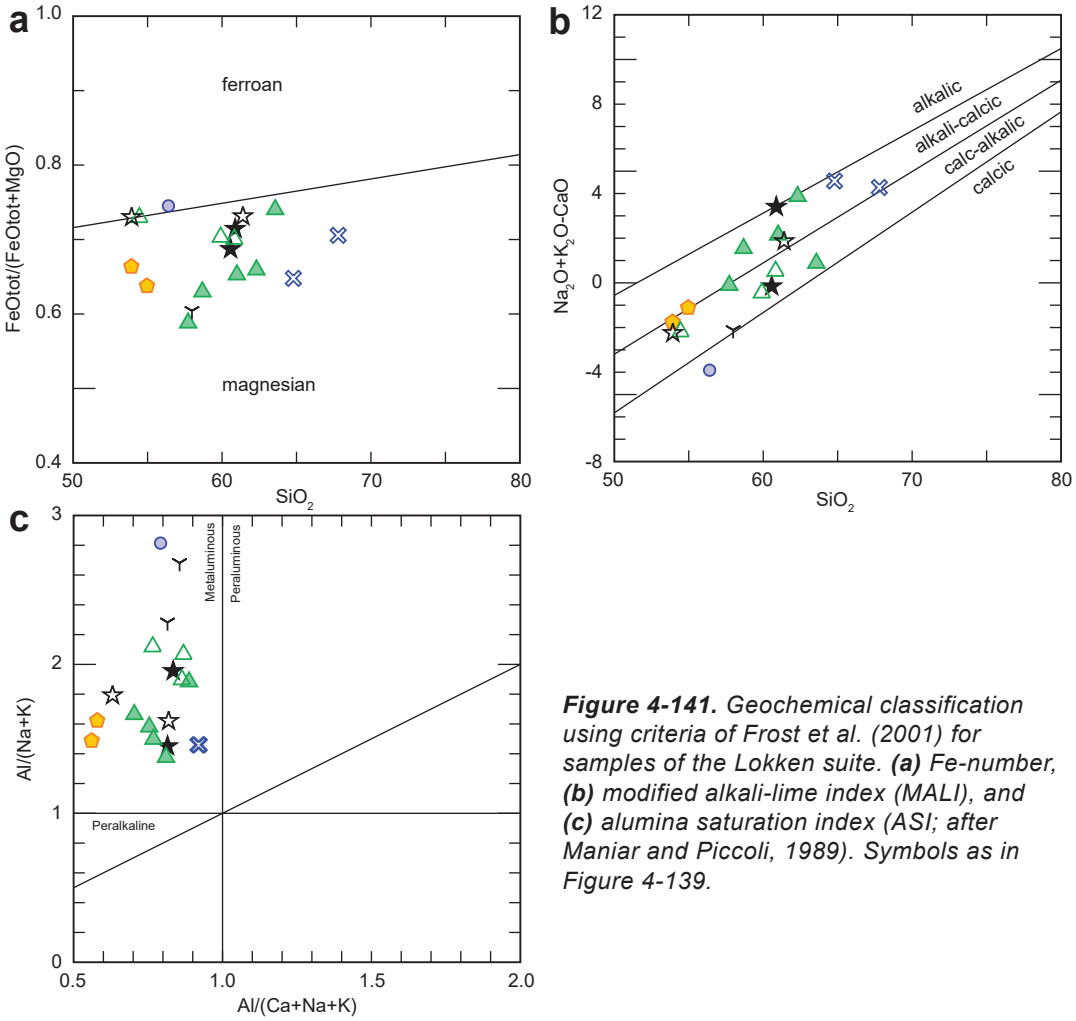


Figure 4-141. *Geochemical classification using criteria of Frost et al. (2001) for samples of the Lokken suite.* ***(a)*** *Fe-number,* ***(b)*** *modified alkali-lime index (MALI), and* ***(c)*** *alumina saturation index (ASI; after Maniar and Piccoli, 1989). Symbols as in Figure 4-139.*

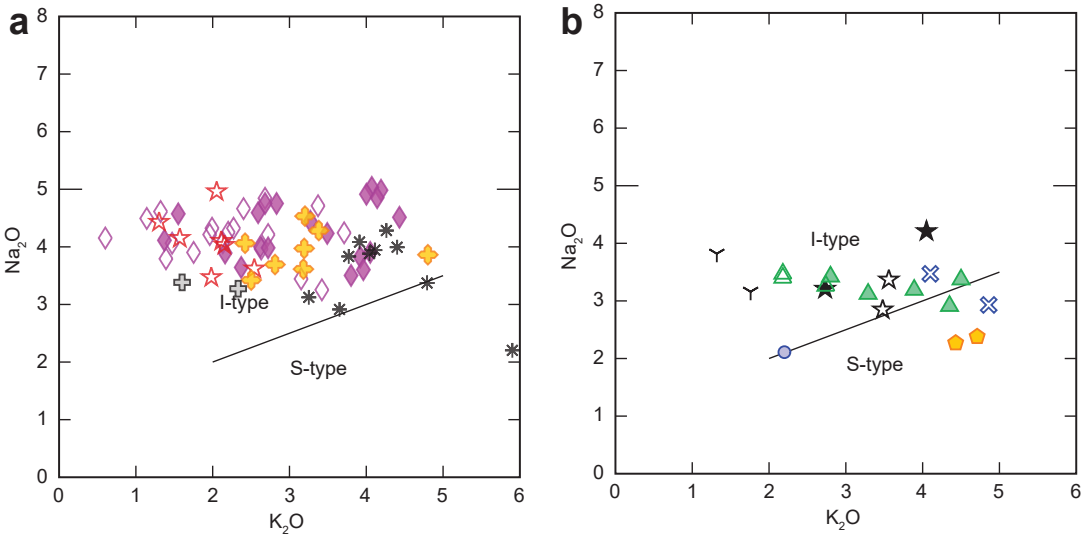


Figure 4-142. *Na_2O vs K_2O for samples of the* ***(a)*** *Long Lake and Bennett and* ***(b)*** *Lokken suites. The boundary between 'I-type' and 'S-type' granitoid rocks is from Chappell and White (1974). Symbols as in Figure 4-136 for Long Lake and Bennett suite Figure 4-139 for Lokken suite.*

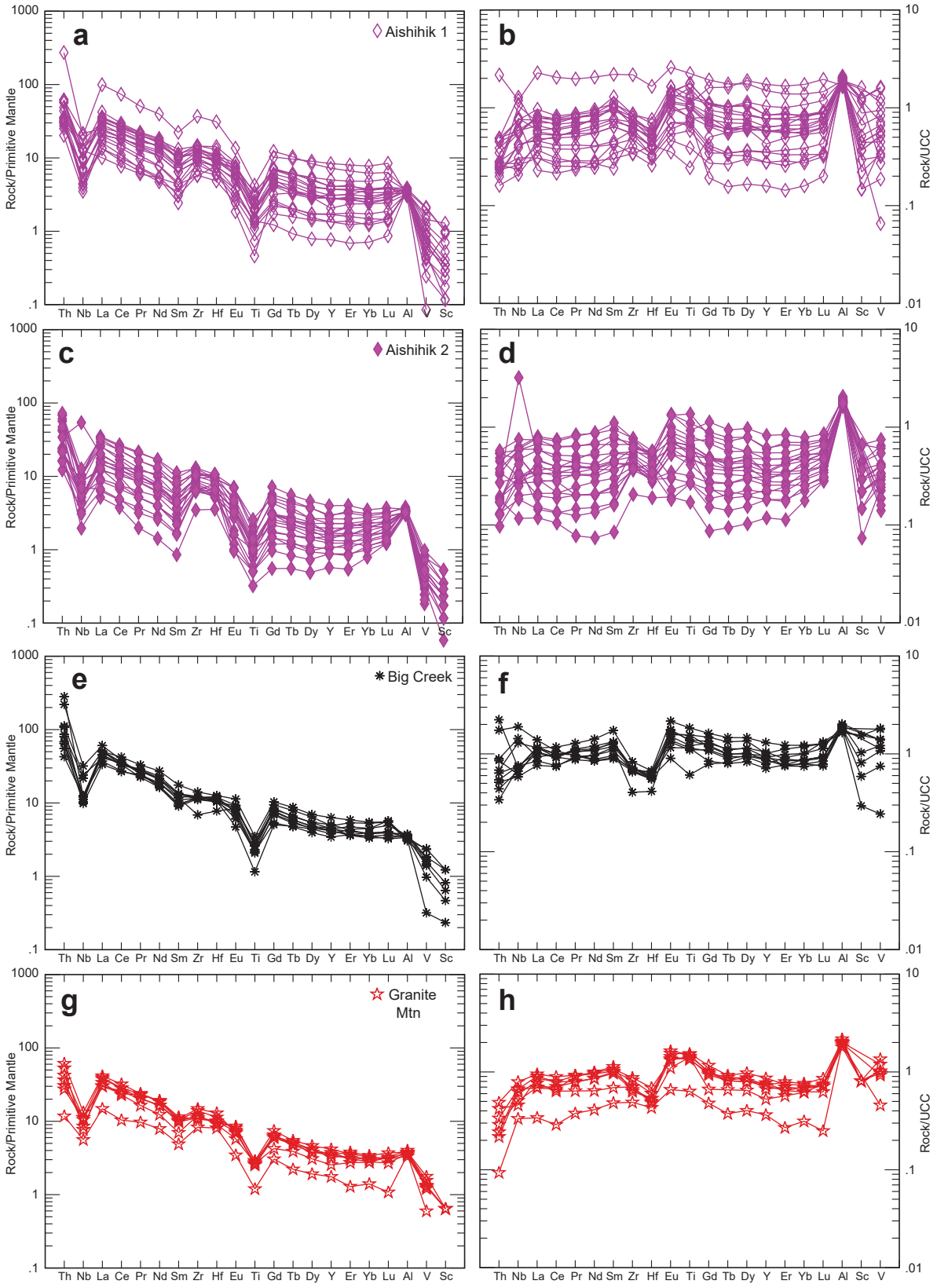


Figure 4-143. *Primitive mantle normalized (left; McDonough and Sun, 1995) and upper continental crust (UCC) normalized (right; McLennan, 2001) spider plots for samples of the Long Lake suite.* ***(a–d)*** *Aishihik batholith;* ***(e** and **f)*** *Big Creek batholith;* ***(g** and **h)*** *southwest Granite Mountain batholith.*

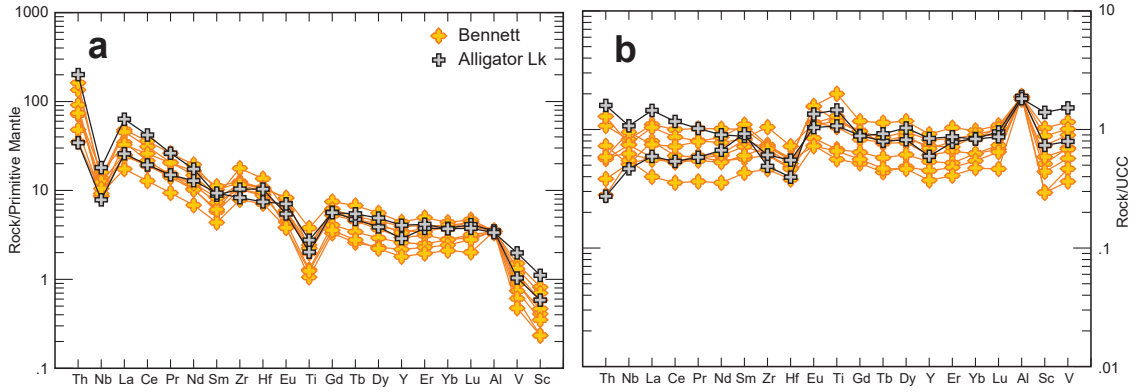


Figure 4-144. *(**a**) Primitive mantle normalized (McDonough and Sun, 1995) and (**b**) upper continental crust (UCC) normalized (McLennan, 2001) spider plots for samples of the Alligator Lake and Bennett plutons.*

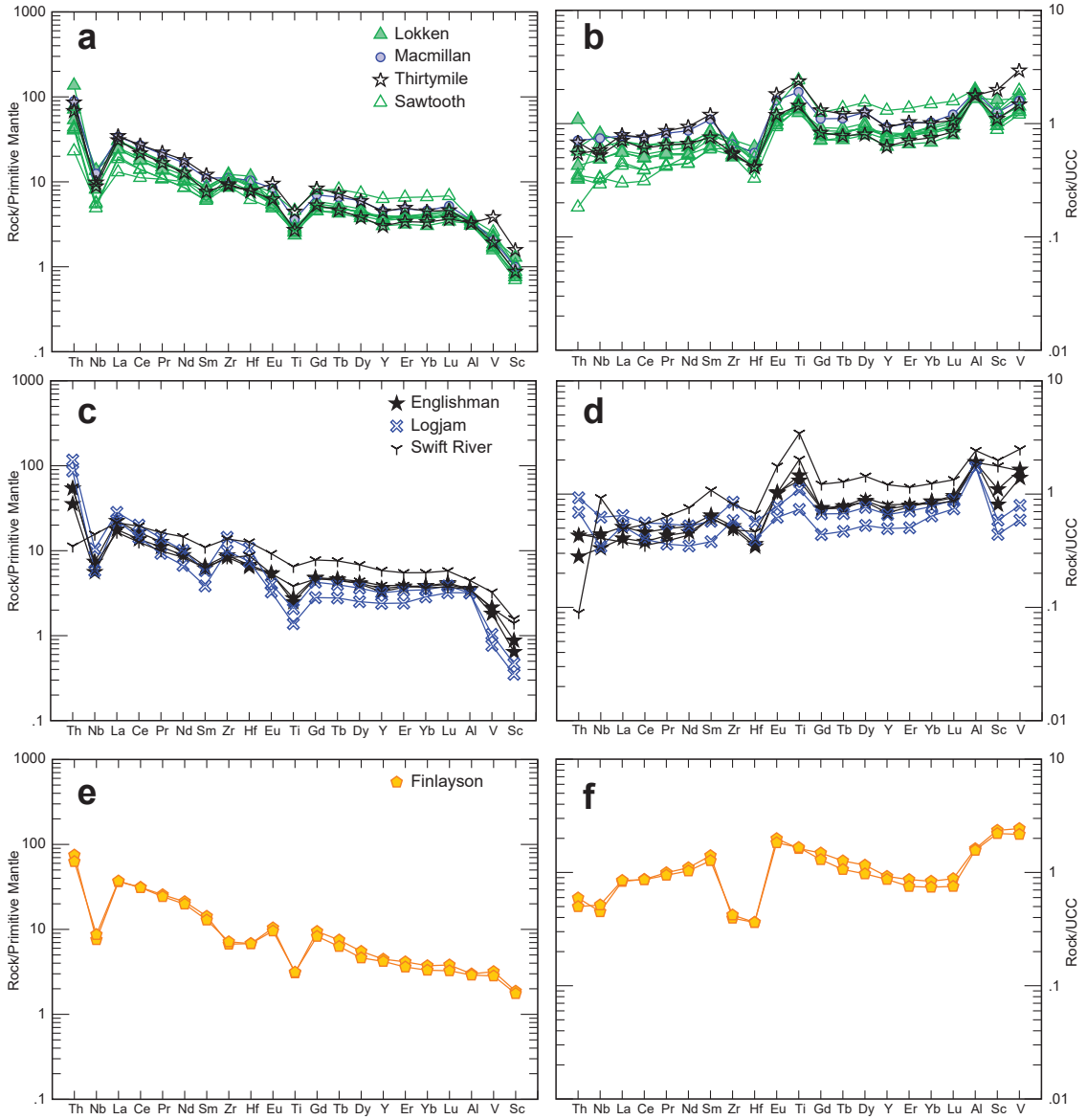


Figure 4-145. *Primitive mantle normalized (left; McDonough and Sun, 1995) and upper continental crust (UCC) normalized (right; McLennan, 2001) spider plots for samples of the Lokken suite. (**a** and **b**) Lokken, Macmillan Range, Thirtymile Lake and Sawtooth plutons; (**c** and **d**) Englishman, Logjam and Swift River plutons; (**e** and **f**) Finlayson (Banana) stock.*

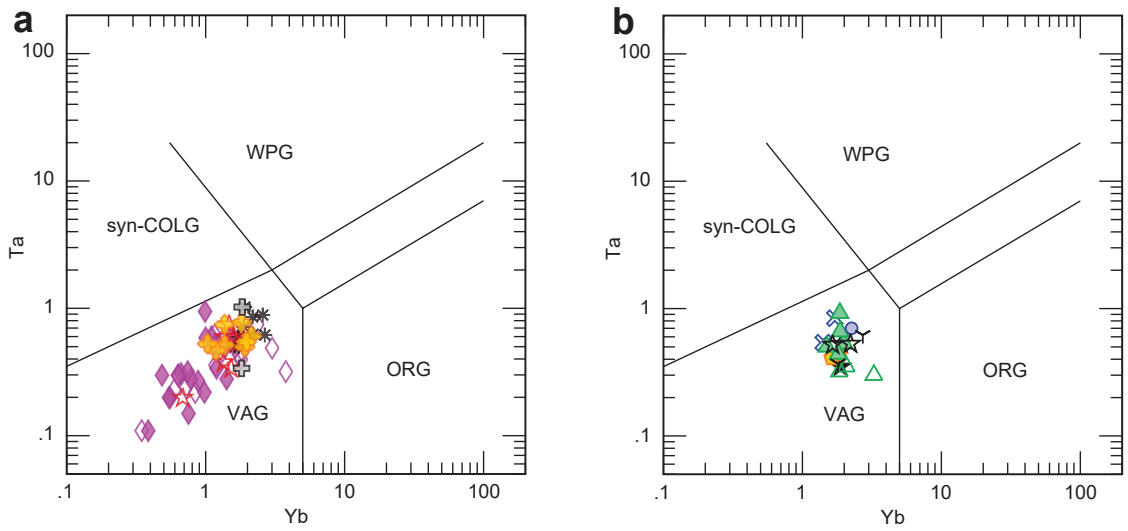


Figure 4-146. *Tectonic discrimination diagram for granites from Pearce et al. (1984).* ***(a)*** *Long Lake and Bennett suites;* ***(b)*** *Lokken suite. VAG = volcanic arc granite, ORG = ocean ridge granite, WPG = within plate granite and COLG = collisional granite. Symbols as in Figure 4-136 for Long Lake and Bennett suite Figure 4-139 for Lokken suite.*

Zircon chemistry

Trace element concentrations were measured in zircons from the Long Lake, Bennett and Lokken suites that were analyzed by LA-ICPMS at Boise State University (Appendix 3). Zircons from the Granite Mountain, Big Creek and Aishihik 2 phase have nearly identical compositions with Ti-in-zircon temperatures mainly clustered in the 600–700°C range that show little correlation with varying Hf contents (Fig. 4-147). Zircons from the Aishihik 1 phase have a greater range of Ti-in-zircon temperatures (550–760°C), and temperatures decrease with increasing Hf concentrations (Fig. 4-147a). Aishihik 1 zircons also show a wider range of mafic to intermediate arc compositions, and some zircons display strong fractionation with high U/Yb and low Gd/Yb (Fig. 4-147c,e). The Aishihik 2, Granite Mountain and Big Creek zircons are tightly clustered in the intermediate arc to post-collisional granitoid fields, with moderate U and Y concentrations and U/Yb ~1.

Zircons from the Bennett batholith show a range of Hf concentrations (~8500 to 12 400 ppm) and Ti-in-zircon temperatures between 620 and 770°C that decrease with increasing Hf concentration (Fig. 4-148a). Their trace elements are consistent with intermediate to mafic arc compositions with moderate U concentrations (100–440 ppm) and relatively low Gd/Yb of 0.01–0.06 (Fig. 4-148b,c).

Samples from the Lokken suite display a range of zircon compositions and each pluton has distinct characteristics (Fig. 4-149). The Lokken and Logjam plutons typically have the highest Ti-in-zircon temperatures of the suite, most values are between 720 and 817°C, but range as low as ~670°C for Logjam zircons with higher Hf concentrations. However, these two plutons show distinct ranges in Hf, the Lokken ranges from ~8400–11300 ppm, and zircons from the Logjam pluton have typically lower Hf concentration between ~7000 and 9000 ppm (Fig. 4-149a,b). On discriminant plots these plutons are distinct; the Logjam zircons have more mafic compositions with lower U concentrations than those from the Lokken batholith, and generally lower U/Yb (Fig. 4-149c–f).

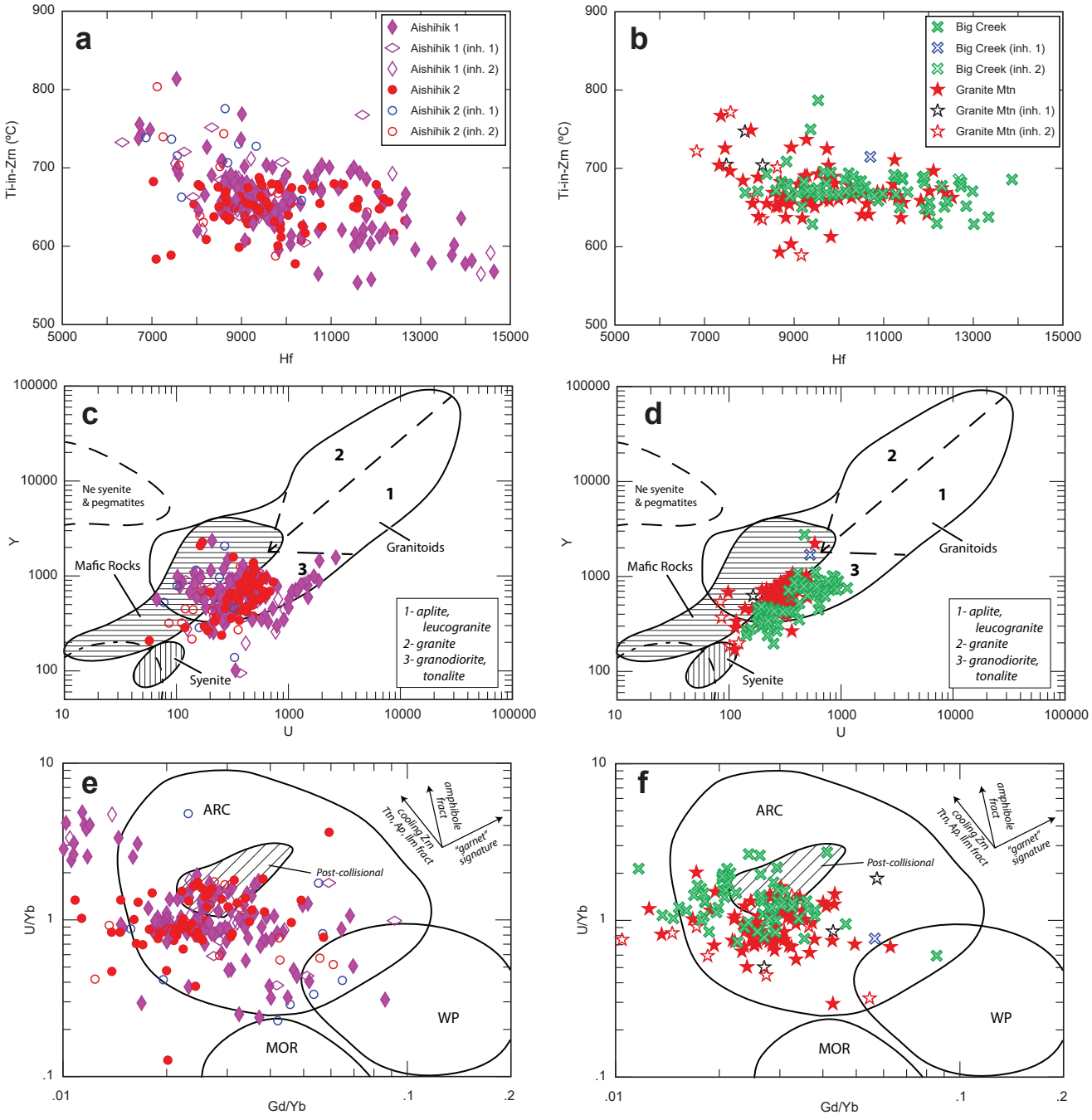


Figure 4-147. *Trace element zircon chemistry from LA-ICPMS analyses of samples from the Long Lake suite (Appendix 3).* ***(a** and **b)** Plots of crystallization temperature estimates (Ti-in-zircon) vs. Hf concentrations in zircons.* ***(c** and **d)** Y vs. U classification diagram of Belousova et al. (2002).* ***(e** and **f)** Discriminant diagram of Grimes et al. (2015). Fract = fractionation. Open symbols are analyses of inherited cores; two population of inherited zircons are documented in many samples with Inherited 1 representing Paleozoic and older grains and Inherited 2 from Late Triassic cores.*

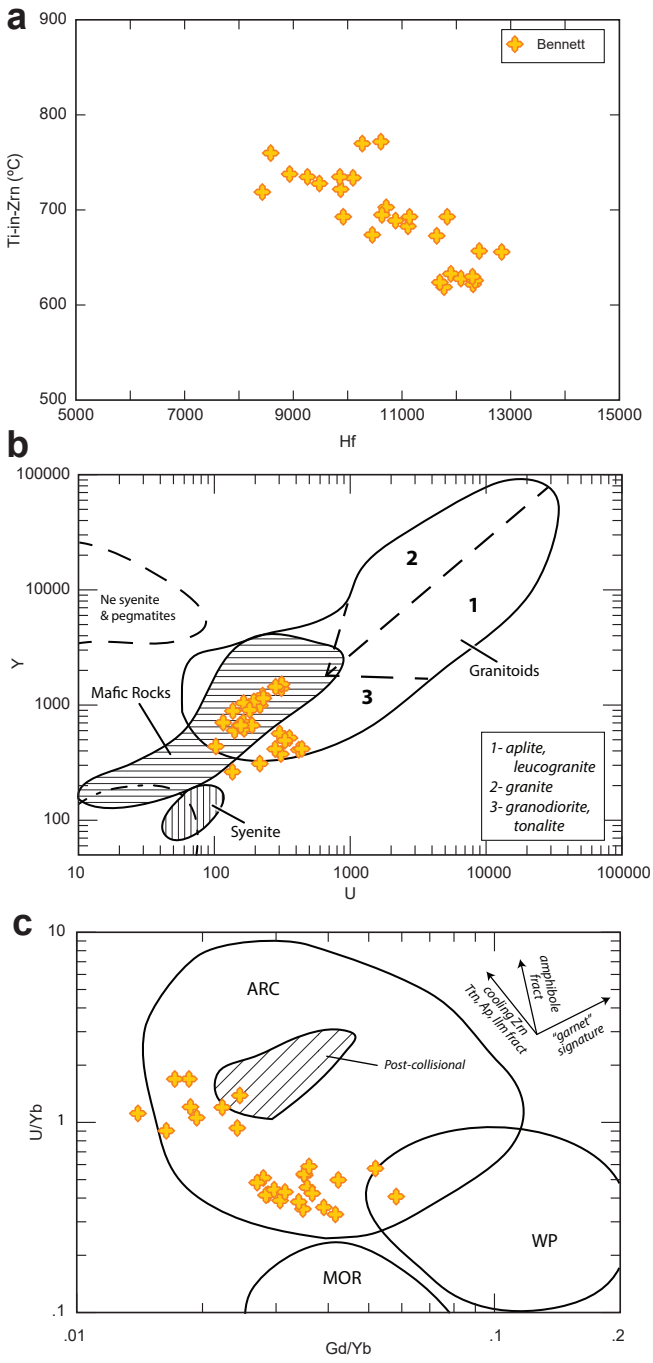


Figure 4-148. *Trace element zircon chemistry from LA-ICPMS analyses of samples from the Bennett suite (Appendix 3).* ***(a)*** *Plots of crystallization temperature estimates (Ti-in-zircon) vs. Hf concentrations in zircons.* ***(b)*** *Y vs. U classification diagram of Belousova et al. (2002).* ***(c)*** *Discriminant diagram of Grimes et al. (2015). Fract = fractionation.*

Zircons from the Englishman, Sawtooth and Thirtymile Lake plutons have overall similar range of Ti-in-zircon temperatures (~660–770°C) and Hf concentrations (~6700–9200 ppm; Fig. 4-149a). The Sawtooth zircons show a range from mafic to intermediate compositions, while zircons from the Englishman pluton overlap with the more mafic end-member (U/Yb <0.4) and those from the Thirtymile Lake plutons are more typical of intermediate arc granitoid rocks (U/Yb >0.5; Fig. 4-149 c,e).

Finally, zircons from the Two Ladder and Banana plutons have similar Ti-in-zircon temperatures (~650–730°C) but the Banana plug has lower Hf concentrations (~6100–9200 ppm) compared to the Two Ladder pluton (~8200–11800 ppm; Fig. 4-149b). Both the Banana and Two Ladder plutons have zircon compositions typical of intermediate arc granitoid rocks, and a few analyses from the Two Ladder pluton overlaps with the post-collisional granitoid field (Fig. 4-149d,f).

Isotopes

Seven samples from the Long Lake suite, one from the Bennett suite and five from the Lokken suite were analyzed for whole-rock Sr and Nd isotopes; K-feldspar from all but one sample of the Lokken suite were also analyzed for Pb isotopes (Appendix 9). Samples from all three suites show similar ranges of initial $^{87}Sr/^{86}Sr$ (0.7050–0.7065) and $^{143}Nd/^{144}Nd$ values (0.51210–0.51237; εNd_t = -0.6–-5.9; Fig. 4-150), and $^{207}Pb/^{204}Pb$ in feldspar ranging from 15.63–15.70, suggesting mixing with evolved crustal components. The sample from the Englishman pluton has lower initial $^{87}Sr/^{86}Sr$ of 0.7044 but εNd_t of -2.6 comparable to other plutons of the Lokken, Long Lake and Bennett suites.

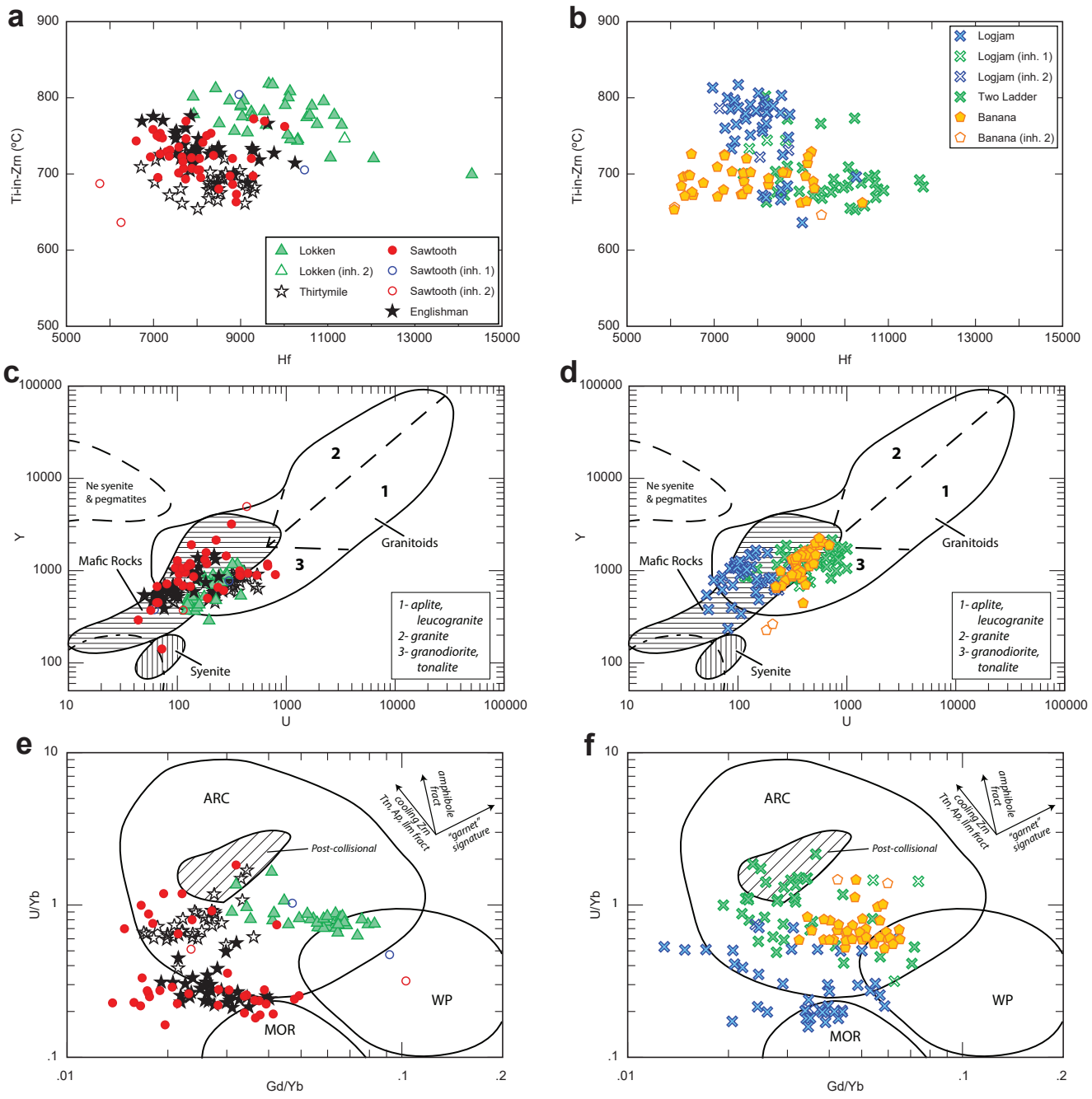


Figure 4-149. *Trace element zircon chemistry from LA-ICPMS analyses of samples from the Lokken suite (Appendix 3).* ***(a** and **b)** Plots of crystallization temperature estimates (Ti-in-zircon) vs. Hf concentrations in zircons.* ***(c** amd **d)** Y vs. U classification diagram of Belousova et al. (2002).* ***(e** and **f)** Discriminant diagram of Grimes et al. (2015).*
Fract = fractionation. Open symbols for the Lokken, Sawtooth, Logjam and Banana plutons are analyses of inherited cores; two population of inherited zircons are documented in samples from the Logjam and Sawtooth plutons with Inherited 1 representing Paleozoic and older grains and Inherited 2 from Late Triassic cores. Only Late Triassic inherited cores (Inh. 2) are documented in the Banana and Lokken plutons.

Zircons from five Long Lake suite samples and four samples from the Lokken suite were also analyzed for Lu-Hf by split-stream LA-ICPMS at Memorial University of Newfoundland (Appendix 10). Igneous zircons from the Long Lake suite plutons mostly have similar εHf_i values between -6.0 and +3.0, with a few zircons from the Aishihik 1 phase with more juvenile εHf_i values of +6.4 and +8.8 (Fig. 4-151). Late Triassic inherited zircons are generally more juvenile with εHf_i values between +3.0 and +10.1, although two analyses from the Aishihik batholith plot below CHUR at -3.1 and -3.8. Inherited zircons with Devonian–Mississippian dates have a wide range of εHf_i from -14.3 to +12.1, and 2 Permian zircons are most evolved at -15.3 (Appendix 10).

Zircons from the Lokken suite are generally more juvenile than those of the Long Lake suite with total range of εHf_i values from -3.6 to +9.0 (Fig. 4-151c). Zircons from the Logjam pluton are most evolved (εHf_i: -0.8 – +1.4), while those from the Englishman and Thirtymile Lake plutons have slightly more juvenile signatures (εHf_i: +1.4 – +3.8), and zircons from the Sawtooth pluton are the most juvenile of the Lokken suite (εHf_i: +3.7 – +9.0). Two Late Triassic zircons from the Sawtooth pluton are even more juvenile with εHf_i of +9.2 and +11.6 (Fig. 4-151c; Appendix 10).

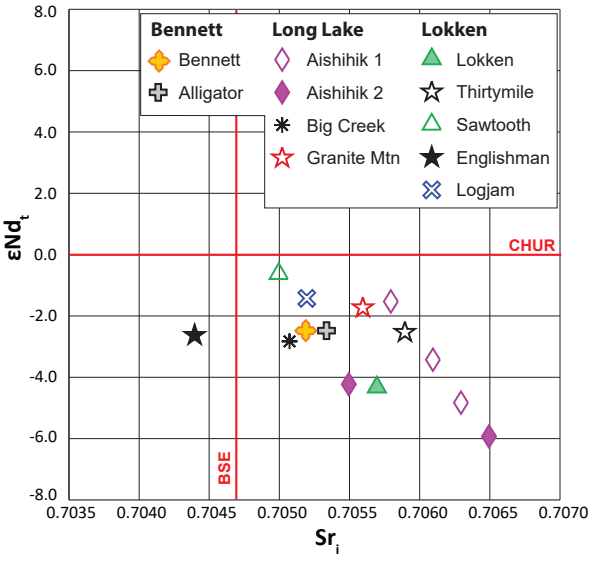


Figure 4-150. *Whole rock Nd and Sr isotopic data for the Long Lake, Bennett and Lokken suites (Appendix 9). Plot of εNdt vs. initial $^{87}Sr/^{86}Sr$. BSE = bulk silicate Earth; CHUR = chondrite uniform reservoir.*

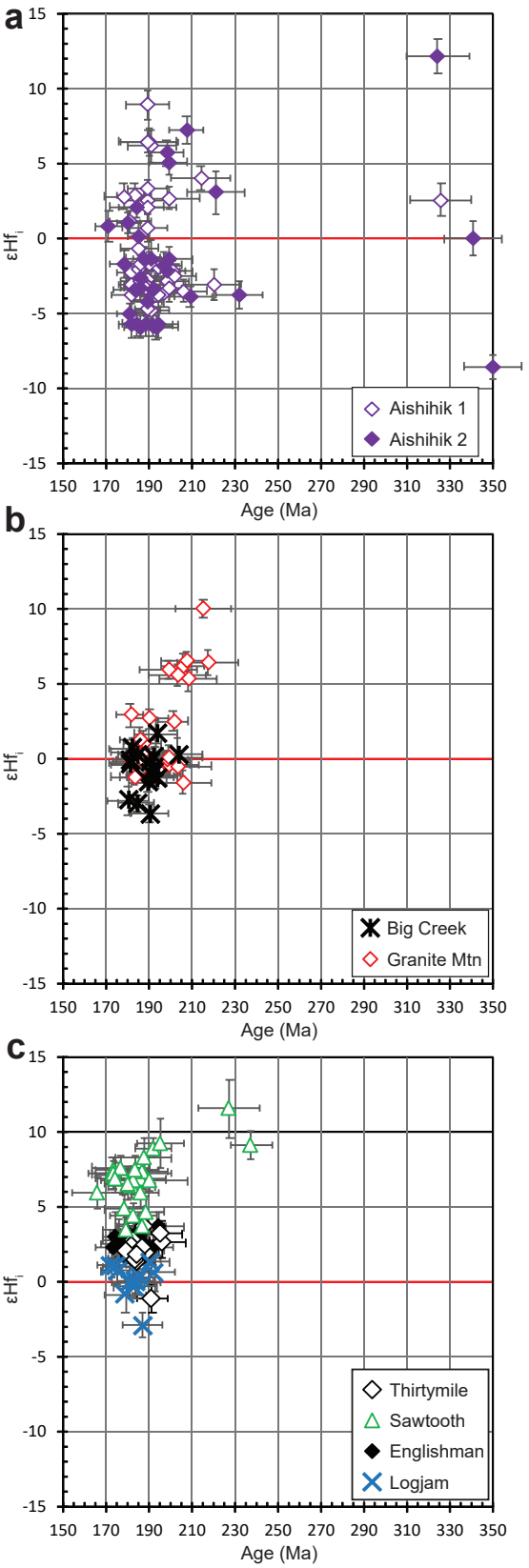


Figure 4-151. *Hf isotopic data for selected zircons from the Long Lake and Lokken suites (Appendix 10). **(a)** Aishihik batholith; **(b)** southwest Granite Mountain and Big Creek batholiths; and **(c)** Thirtymile Lake, Sawtooth, Englishman and Logjam plutons. Error bars are 2σ.*

Discussion

The Long Lake and Bennett suites are composed of arc granitoid rocks that mostly intrude the contact between Yukon-Tanana terrane and Stikinia southwest of the Whitehorse trough (Fig. 4-1). The Long Lake suite is tightly constrained to 188–183 Ma (Fig. 4-152; Table 4-1), and ranges from calc-alkalic to alkalic and is mostly metaluminous; phase 2 rocks of the Aishihik batholith are more ferroan (tholeiitic) and trend to weakly peraluminous (Figs. 4-138 and 4-146a). The late Early Jurassic Bennett suite plutons (178–175 Ma) are magnesian, calc-alkalic, metaluminous intrusions. Isotopic constraints for both suites (whole-rock Sr and Nd, K-feldspar Pb, and zircon Hf; Figs. 4-150 and 4-151) indicate a crustal component to the magma, though the Bennett suite is slightly more juvenile in composition than most of the Long Lake suite. Inherited zircon populations in Long Lake suite rocks demonstrate interaction between the magma and Devonian–Mississippian and Late Triassic rocks prior to emplacement of those plutons (Figs. 4-24 to 4-29; Table 4-1).

Geobarometry from the Aishihik and western Granite Mountain batholiths indicate emplacement at mid to lower crustal levels (3.5–6.0 kbar or 13–22 km; Fig. 4-38), consistent with lower greenschist to amphibolite facies metamorphism of the country rocks (Read *et al.*, 1991; Johnston and Erdmer,

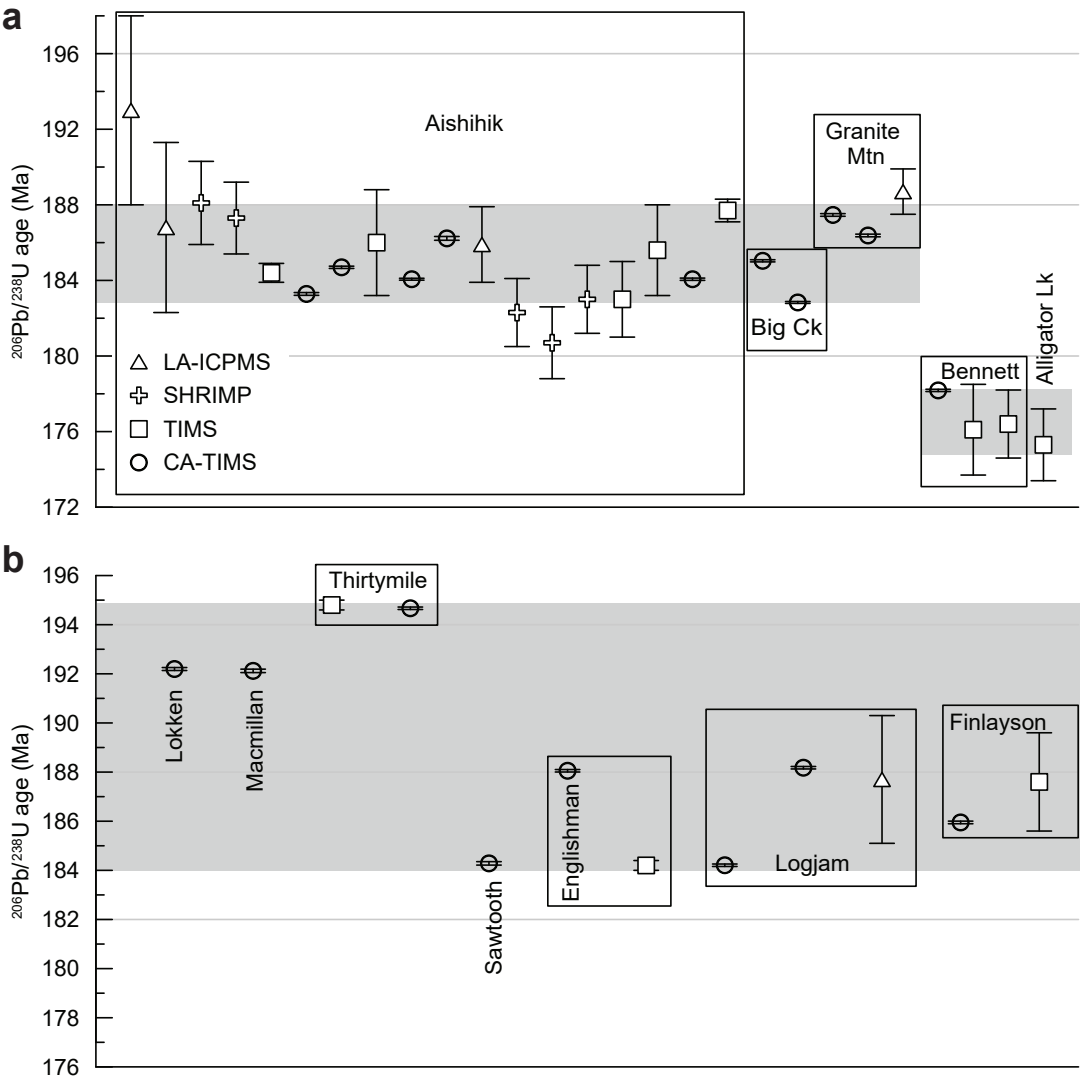


Figure 4-152. *Summary of U-Pb zircon geochronological data for* ***(a)*** *Long Lake and Bennett suite, and* ***(b)*** *Lokken suite plutons. Light grey shaded box defines zircon crystallization range for each suite. U-Pb zircon ages symbolized by analytical method.*

1995a; Johnston *et al.*, 1996; Clark, 2017). The Bennett suite plutons were emplaced at mid to upper crustal levels with Al-in-Hbl pressure estimates of 3.45 ± 1.09 kbar in the Bennett batholith and ≤2 kbar in the Alligator Lake stock.

In the Aishihik batholith, Al-in-Hbl pressure estimates show a systematic decrease from south to north (~6 to 3.5 kbar), and an inverse relationship with apparently younger biotite cooling ages in the southern part of the batholith (Fig. 4-38). The southern portion of the batholith crystallized at 6 to 4.5 kbar (~22–17 km) at *ca.* 184 Ma and cooled below the ~350°C closure temperature of Ar in biotite (Hodges, 2014; Table 1-6) between 182 and 178 Ma. This is consistent with thermobarometric estimates of 5–7 kbar and 640–650°C in the Early Jurassic (200–185 Ma) from regional metamorphic rocks west of Aishihik Lake (Clark, 2017). Similar P-T estimates (~7 kbar, 650–680°C) are documented in western Yukon for the Early Jurassic (197–188 Ma; Morneau, 2017) suggesting much of the Yukon-Tanana terrane was at mid to lower crustal levels in the Early Jurassic. Our data from the southern part of the Aishihik batholith suggest cooling rates between 305 and 153°C/Myr, and exhumation rates between 1.7 and 0.5 mm/year (assuming geothermal gradients of 25–30°C/km, the 350°C isotherm corresponds to ~12–14 km crustal depth). The northern portion of the batholith crystallized at 4 kbar (~15 km) at *ca.* 183 Ma and cooled below 350°C between 182 and 180 Ma, indicating more rapid cooling at 610–200°C/Myr and a slightly higher exhumation rate of 2.8–0.8 mm/year.

In all cases the results of Al-in-Hbl geobarometry indicate that the majority of the Aishihik batholith was emplaced at a depth of >15 km (Appendix 5) and therefore too deep to be favourable for porphyry systems (<10 km; Seedorff *et al.*, 2005). Topham *et al.* (2016) do suggest however that the northwest portion of the batholith may contain shallower, water-saturated rocks that could be prospective for magmatic-hydrothermal mineralization.

The oxidized state (Fig. 4-3a) and components of crustal contamination (Fig. 4-150) of the Long Lake suite suggests that metals such as tungsten, molybdenum and possibly copper would have been mobile in the magma (Fig. 4-153), and thus could have been transported to form deposits. Though the plutons were deeply emplaced, it remains possible that depth independent deposit types such as skarns could have formed in the vicinity of plutons of the Long Lake suite where they intrude calcareous country rocks.

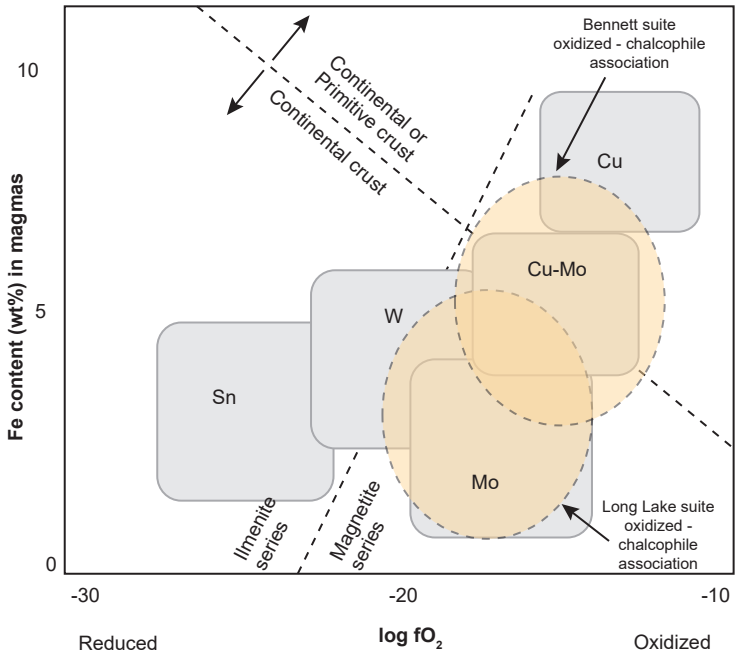


Figure 4-153. *Schematic plot of degree of fractionation, shown by the Fe content, vs. oxidation state (fO_2) for calc-alkalic to alkalic magmas associated with magmatic-hydrothermal mineralization (modified from Thompson et al., 1999). The generalized position of the Long Lake suite, with a potential Mo-W-Cu (siderophile) association and the Bennett suite with a potential Co-Mo (siderophile-chalcophile) association are shown by the orange ellipses. Boundary between the magnetite and ilmenite magma series is from Ishihara (1977).*

The Bennett suite plutons are oxidized (Fig. 4-3a) but slightly more juvenile than most of the Long Lake plutons suggesting copper and molybdenum would have been mobile in the magma (Fig. 4-153), and thus could have been transported to form deposits. The Bennett suite plutons were emplaced at middle to upper crustal levels, possibly at porphyry depths (<10 km; Seedorff *et al.*, 2008).

Small plutons of the Lokken suite intrude greenschist to amphibolite facies metamorphic rocks of the Yukon-Tanana terrane northeast of the Teslin fault (Fig. 4-1; Table 4-1). The Lokken suite spans a range of 195 to 184 Ma (Fig. 4-152) and is distinctly more mafic than the Long Lake suite, with predominance of clinopyroxene-bearing monzonite and monzodiorite plutons (Figs. 4-2b and 4-139). The Lokken suite is strongly magnetic, metaluminous, generally magnesian, and calc-alkalic to alkali-calcic in composition (Figs. 4-3b and 4-141). Whole-rock and zircon trace element and isotopic data are consistent with continental arc magma that show signs of minor crustal contamination (Figs. 4-145, 4-149, 4-150 and 4-151). Al-in-Hbl geobarometric estimates for the Lokken and Macmillan Range plutons, the northernmost plutons in the suite, indicate crystallization pressures of ~3 kbar (Appendix 5) and $^{40}Ar/^{39}Ar$ hornblende and biotite dates suggest relatively rapid cooling (≤2 m.y.; Appendices 1 and 6) consistent with emplacement at higher crustal levels (10–11 km) compared to the Long Lake suite to the west. The oxidized state of the Lokken suite (Fig. 4-3b) and indications of minor crustal contamination, particularly noted in *ca.* 185–184 Ma plutons (Fig. 4-150; Table 4-1), suggests that metals such as molybdenum and copper (Fig. 4-154) would have been mobile in the magma and thus could have been transported to form deposits. Though the emplacement level of these rocks is inferred to be at relatively high crustal level (≤10km depth), the lack of coeval volcanic rocks suggests the porphyry potential is low. As for the Long Lake suite, depth independent deposit models such as skarn, particularly proximal to calcareous rocks are possible. There are no known mineral occurrences directly associated with intrusions of the Lokken suite.

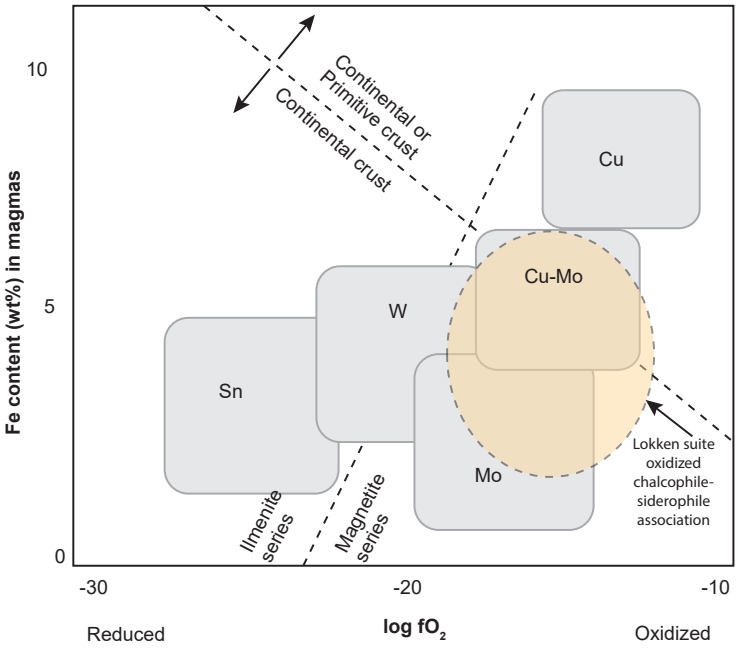


Figure 4-154. *Schematic plot of degree of fractionation, shown by the Fe content vs. oxidation state (fO_2) for calc-alkalic to alkalic magmas associated with magmatic-hydrothermal mineralization (modified from Thompson et al., 1999). The generalized position of the Lokken suite, with a potential Cu-Mo (chalcophile-siderophile) association is shown by the orange ellipse. Boundary between the magnetite and ilmenite magma series is from Ishihara (1977).*

Chapter 5
Middle Jurassic

Bryde suite (174–168 Ma)

Summary

Middle Jurassic (*ca.* 174–168 Ma) plutons are relatively small (≤60 km²) and sparse in southern Yukon but form large batholiths in northern British Columbia. These plutons intrude Stikinia and Cache Creek terranes, and the overlapping Early to Middle Jurassic Whitehorse trough. In Yukon, the Bryde suite is restricted to small, generally alkalic plutons east of Carcross and north of Whitehorse. These are the northern equivalents of the Fourth of July suite in northern British Columbia and include the northern tip of the Fourth of July batholith and the Mount Bryde, Michie and Teslin Crossing plutons.

The Bryde suite ranges in age from 174 to 168 Ma. It is a bimodal suite with two alkalic plutons, the Teslin Crossing and Michie stocks, and two more mafic plutons, the Mount Bryde stock and Fourth of July batholith. The plutons are hornblende-biotite bearing with lesser and variable amounts of clinopyroxene, typically as cores overgrown by hornblende. The alkalic plutons are titanite bearing, the more mafic plutons are not. The Teslin Crossing and Mount Bryde stocks are strongly magnetic, indicating oxidized magmatic conditions whereas the Michie and Fourth of July plutons are non-magnetic indicating reduced magmatic conditions. These plutons were likely all emplaced at high crustal levels (<2 kbar) based on weakly to unmetamorphosed country rock and small weakly metamorphosed pendants, hypabyssal textures in thin section, and Al-in-Hbl geobarometry from the Fourth of July batholith. The Teslin Crossing stock is a silica-saturated alkalic porphyry Cu-Au exploration target and is the only pluton in this suite to have significant associated mineral occurrences.

Introduction

Middle Jurassic plutons are relatively sparse in southern Yukon but form large batholiths in northern British Columbia (Fig. 5-1). They intrude Stikinia and Cache Creek terranes, and the overlapping Early-Middle Jurassic Whitehorse trough. These plutons postdate the Jurassic southwest-verging structural imbrication of these tectonic elements and stitch the Intermontane group of terranes (*e.g.*, Mihalynuk *et al.*, 2004; Bickerton *et al.*, 2020). In northern British Columbia, Mihalynuk (1999) assigned the Middle Jurassic plutons that intrude the Cache Creek terrane east of Atlin Lake to the Fourth of July suite (172–166 Ma; Fig. 5-1). In Yukon, Gordey and Makepeace (2001) assigned equivalent plutons to the Bryde suite, which in their definition included plutons of the Bennett suite (178–175 Ma) that intrude the western margin of Stikinia, west of Whitehorse trough, and which we describe in Chapter 4. In this report, the Bryde suite is restricted to the small, generally alkalic plutons (*ca.* 174–168 Ma) that intrude mainly the Cache Creek terrane and Whitehorse trough east of Carcross and north of Whitehorse (Fig. 5-1; Table 5-1). These are the northern equivalents of the Fourth of July suite of northern British Columbia and include the northern tip of the Fourth of July batholith and the Mount Bryde, Michie and Teslin Crossing plutons.

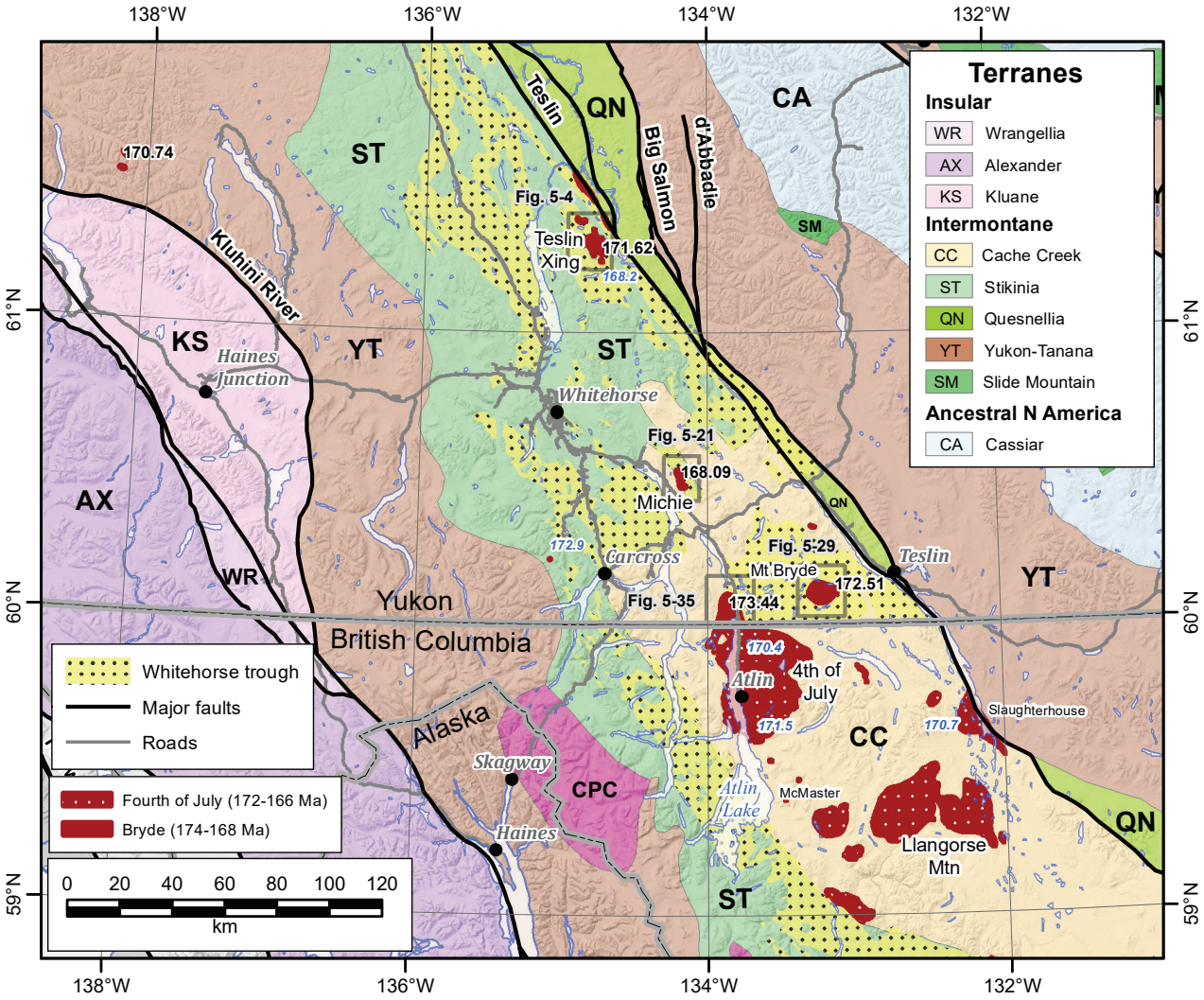


Figure 5-1. *Distribution of Middle Jurassic plutons of the Intermontane terranes in southern Yukon and northern British Columbia. U-Pb dates are indicated next to plutons–black numbers are zircon CA-TIMS ages (this study); blue, italicized numbers indicate samples dated by other U-Pb techniques from previous work (see Appendix 1 for geochronology compilation). Terrane map is modified after Colpron and Nelson (2011). CPC = Coast plutonic complex.*

Table 5-1. *Summary of characteristics for Middle Jurassic plutons of the Bryde suite in Yukon.*

Pluton	NTS	Area (km^2)	Terrane[1]	Rock[2]	Composition[3]	Oxidation state[4]	Age (Ma)[5]	Al-in-Hbl barometry (kbar)[6]	Ti-in-Zrn temp. (°C)[7]	Isotopes[8]	Inheritance[9]	Comment	Reference
Teslin Crossing	105E/7	36	WT	Hbl-Cpx-Bt syenite, monzonite	alkalic; metaluminous	oxidized	171.62 ± 0.05	–	720–788	εNd: +3.5 Sr_i: 0.7040 $^{207/204}$Pb: 15.64 εHf_{zrn}: +6.5 – +8.4	–	BSU, CA-TIMS	this study
Michie	105D/7	14	ST/WT	Hbl-Bt(Cpx) syenite, monzonite; locally pegmatitic	alkalic; metaluminous	reduced	168.09 ± 0.05	–	587–678	εNd: +0.5 Sr_i: 0.7050 $^{207/204}$Pb: 15.63 εHf_{zrn}: +0.8 – +3.8	–	BSU, CA-TIMS	this study
Mount Bryde	105C/3	60	CC	Hbl-Bt(Cpx) monzodiorite, granodiorite	calc-alkalic; metaluminous	oxidized	172.51 ± 0.05	–	750–804	εNd: +2.0 Sr_i: 0.7043 $^{207/204}$Pb: 15.64	–	BSU, CA-TIMS	this study
Fourth of July	105C/4	83 in Yukon (1121 total)	CC	Bt-Hbl-Cpx tonalite, diorite; (granodiorite, granite in BC)	calcic; metaluminous	reduced	173.44 ± 0.05	≤2	768–815	εNd: +2.3 Sr_i: 0.7045 $^{207/204}$Pb: 15.65 εHf_{zrn}: +4.7 – +7.0	215	BSU, CA-TIMS	this study

Notes:

[1] host terrane to intrusion. CC – Cache Creek; ST – Stikinia; WT – Whitehorse trough

[2] rock types from Figs. 5-2 and 5-44. Bt – biotite; Cpx – clinopyroxene; Hbl – hornblende; Kfs – K-feldspar

[3] composition from Fig. 5-46

[4] oxidation state from Fig. 5-3

[5] best age from pluton, as discussed in text

[6] crystallization pressure estimates from Al-in-hornblende barometry, Appendix 5

[7] crystallization temperature from Ti-in-zircon thermometry, Appendix 3

[8] whole rock Nd and Sr data; K-feldspar Pb data (Appendix 9); Hf in zircon data (Appendix 10)

[9] inheritance determined from U-Pb LA-ICPMS analyses of zircon (Appendix 3)

The Teslin Crossing and Michie stocks are composed of syenite and monzonite, whereas the Mount Bryde and Fourth of July plutons are mainly tonalite to diorite (Fig. 5-2). The Teslin Crossing and Mount Bryde stocks are strongly magnetic (39.8 to 0.55 × 10^{-3} SI units, mean = 15.1, n = 18), indicating oxidized magmatic conditions whereas the Michie and Fourth of July plutons are non-magnetic (0.45 to 0.16 × 10^{-3} SI units, mean = 0.29, n = 9) indicating reduced magmatic conditions (Fig. 5-3).

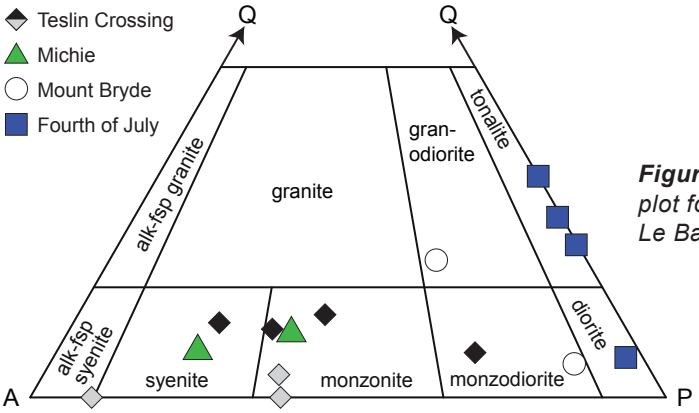


Figure 5-2. *Simplified quartz-alkali-feldspar-plagioclase (QAP) plot for Middle Jurassic plutons in southern Yukon (Appendix 2; Le Bas and Streckeisen, 1991).*

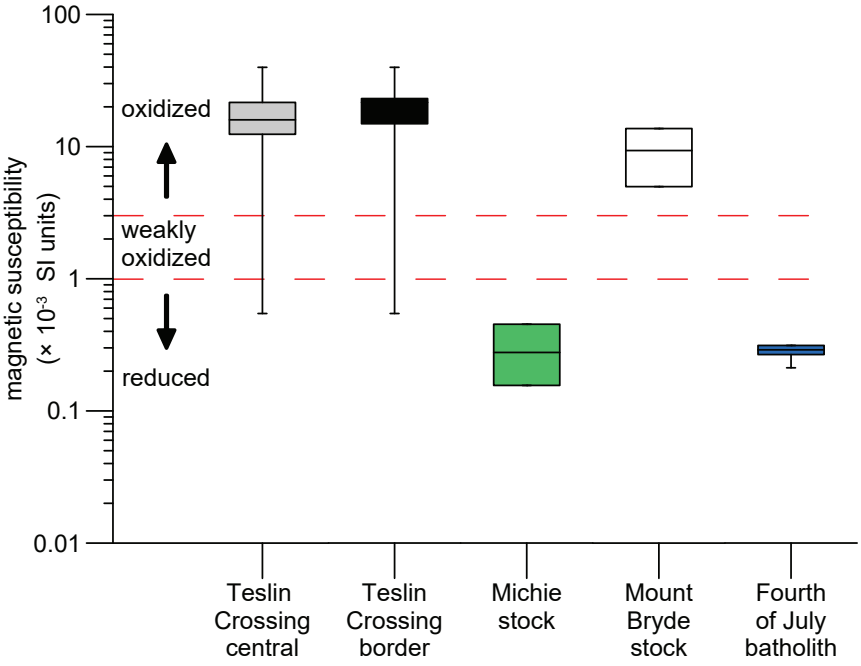


Figure 5-3. *Box and whisker plot of magnetic susceptibility measurements for each Middle Jurassic pluton (Appendix 2). Divisions between reduced to weakly oxidized (1 × 10^{-3} SI units), and weakly oxidized to oxidized (3 × 10^{-3} SI units) are from Hart et al. (2004a,b). Ends of boxes are 75th and 25th percentile of data, white line within boxes indicate median (50th percentile) of data, whiskers 95th and 5th percentile.*

Teslin Crossing stock

The Teslin Crossing stock is located 65 km north-northeast of Whitehorse between Lake Laberge and the Teslin River (Figs. 5-1 and 5-4; Table 5-1). The stock is located 10 km north-northwest of 'Teslin Crossing', where the Livingstone winter trail crosses the Teslin River. The stock forms a relatively high set of rounded ridges and knobby hills above treeline (Fig. 5-5; Hart, 1997c). The highest point is a rounded peak with an elevation of 1483 m, informally known as 'Windy Mountain' (Hart, 1997c). The Teslin Crossing stock intruded and metamorphosed mudstone and sandstone of the Richthofen formation, Laberge Group (Bordet *et al.*, 2019) and is bound on the eastern side by the Teslin Mountain and Chain Lake faults which juxtapose the stock with limestone of the Upper Triassic Aksala formation (Lewes River Group; Fig. 5-4; Tempelman-Kluit, 1984; Bordet, 2019). The stock has a mapped extent of 36 km² with irregular shaped intrusive contacts, and is centred on a larger, 75 km², strong positive magnetic anomaly (Fig. 5-6). A similar strong magnetic anomaly also occurs north of Miller Creek, beneath small porphyry exposures inferred to be related to the Teslin Crossing stock (Tempelman-Kluit, 1984).

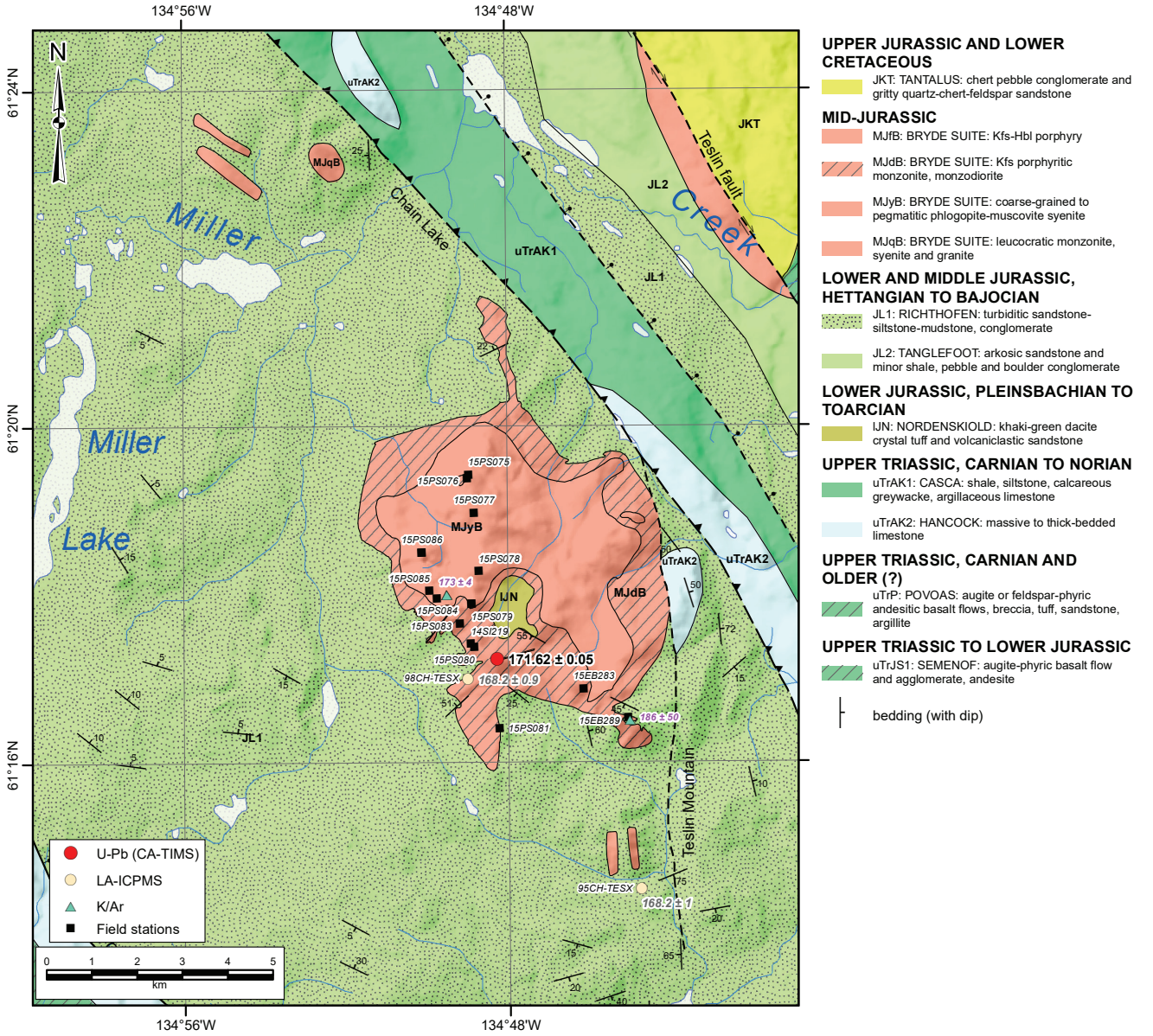


Figure 5-4. *Geology of the area surrounding the Teslin Crossing pluton (YGS, 2020a); fault symbology as in Figure 1-4.*

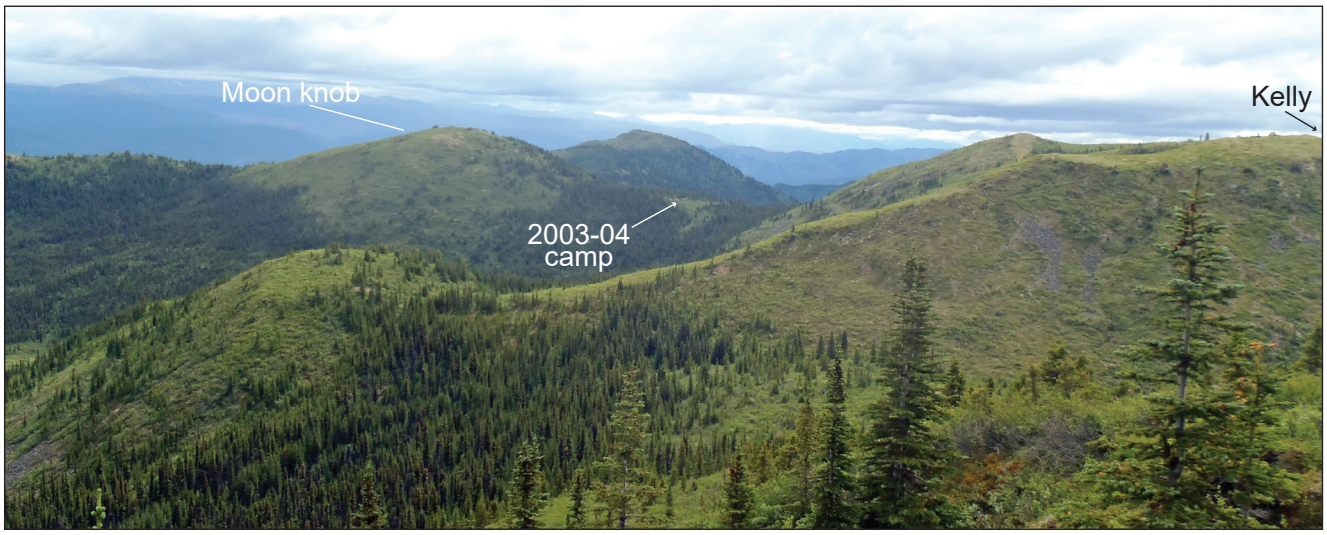


Figure 5-5. *Looking southeast from station 15PS083. Outcrop limited to weathered exposures near ridge tops. 2003-04 camp was where Saturn Minerals Inc. stored diamond drill core from holes M4-01 to 07.*

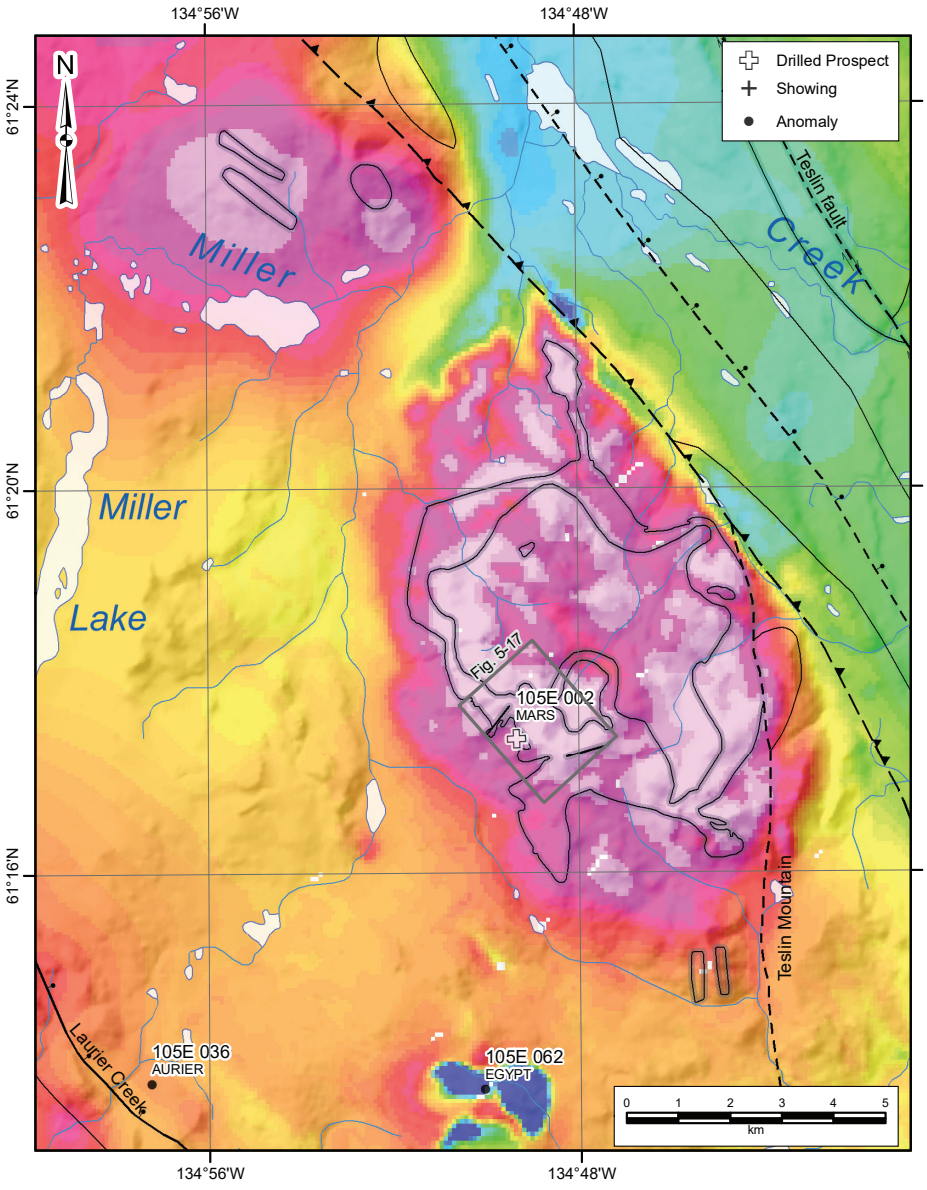


Figure 5-6. *Reduced to pole, residual total field aeromagnetic map of the Teslin Crossing pluton area (Aurora Geosciences Ltd. and Bruce, 2017c) illustrating distribution of Mars (TUV) occurrence. Fault symbology as in Figure 1-4. Area of Figure 5-17 is also indicated.*

Bedding regionally dips shallowly to the southwest or northeast (Tempelman-Kluit, 1984), but locally strata dip moderately to steeply away from the Teslin Crossing stock (Pangman, 1973), which suggests the pluton domed the local stratigraphy (Fig. 5-4). However, Hart (1997c) notes that the western pluton boundary is broadly concordant with topography and that exposures of the pluton are rare below 1225 m in the south and 1050 m in the north, possibly indicating a sill-like geometry. An area of poorly exposed fine-grained volcanic and sedimentary rock near the centre of the stock (Fig. 5-4) is contact metamorphosed and is likely a roof pendant of the Laberge Group (Nordenskïold facies; Lang and McClaren, 2004). Keyser (2001) suggested alternatively that these may represent volcanic rocks related to the stock itself.

Petrography

The central portion of the Teslin Crossing stock is pink, fine to medium-grained, generally equigranular monzonite to syenite (Figs. 5-7 and 5-8). Surrounding the central phase is a light grey-green, K-feldspar ± hornblende porphyritic monzonite to monzodiorite border phase (Fig. 5-9). The two phases grade into each other or have diffuse irregular contacts (Fig. 5-10) without chilled margins suggesting a comagmatic relationship. Xenoliths vary from mafic plutonic (*e.g.*, pyroxenite) to sedimentary (*e.g.*, siltstone) and are found in all phases (Fig. 5-11). Mafic xenoliths are more common in the central phase and sedimentary rocks in the border phase (Pangman, 1973). Both phases of the stock are cut by lamprophyres or leucocratic plagioclase porphyritic dikes (Pangman, 1973).

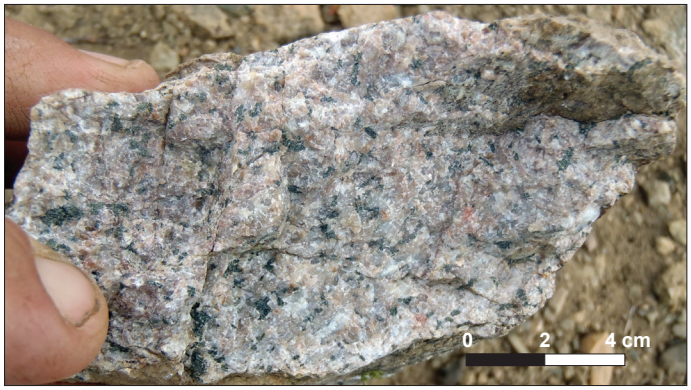


Figure 5-7. *Fresh, broken face of medium-grained equigranular monzonite from the central phase of the Teslin Crossing stock; 15PS086-1.*

The central syenite to monzonite varies from equigranular to weakly porphyritic, with white K-feldspar phenocrysts in a groundmass that weathers pink to red (Fig. 5-8). Clinopyroxene, hornblende and biotite are the main mafic minerals and make up <8% of the rock; they are weakly to intensely chlorite altered. Clinopyroxene has been identified by X-ray diffraction as diopside (Pangman, 1973). The majority of the rock in this phase is K-feldspar which has a distinct anhedral interlocking texture (Fig. 5-12). Minor quartz is present in the groundmass between K-feldspar grains. Plagioclase is weakly saussuritized.

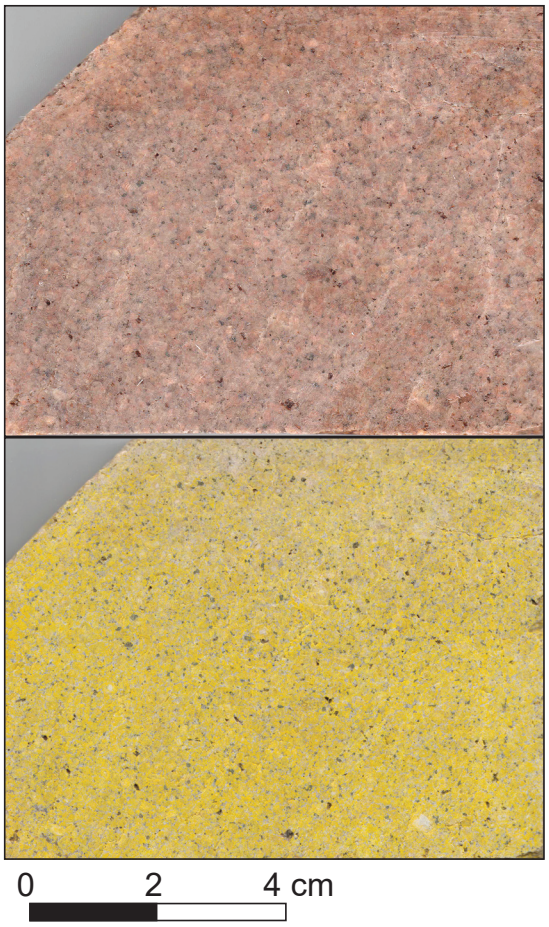


Figure 5-8. *Representative sample of the fine-grained equigranular syenite from the central phase of Teslin Crossing stock; 15PS078-1. Fresh polished surface (upper) and a cobaltinitrite-stained surface (lower). Note K-feldspar is yellow, both images are same scale.*

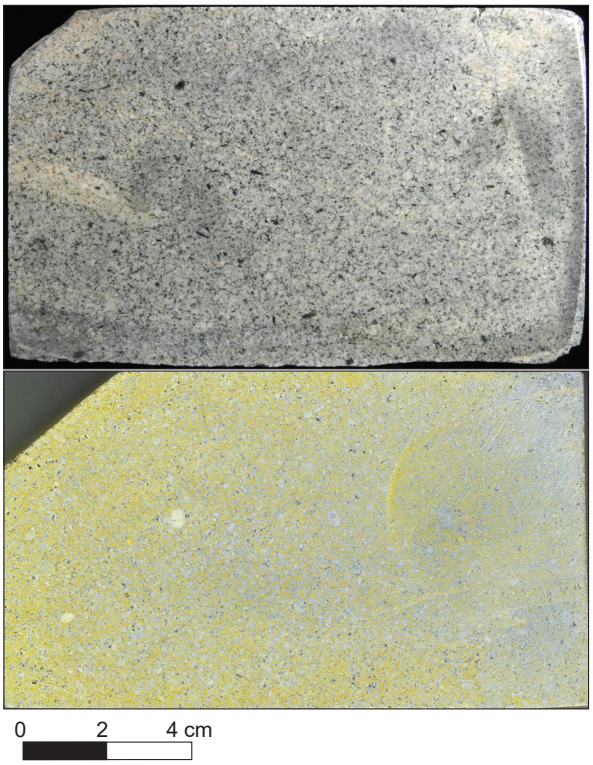


Figure 5-9. *Representative sample of the weakly porphyritic monzodiorite from the border phase of Teslin Crossing stock; 15PS082-1. Fresh polished surface (upper) and a cobaltinitrite-stained surface (lower). Note K-feldspar is yellow, both images are same scale.*

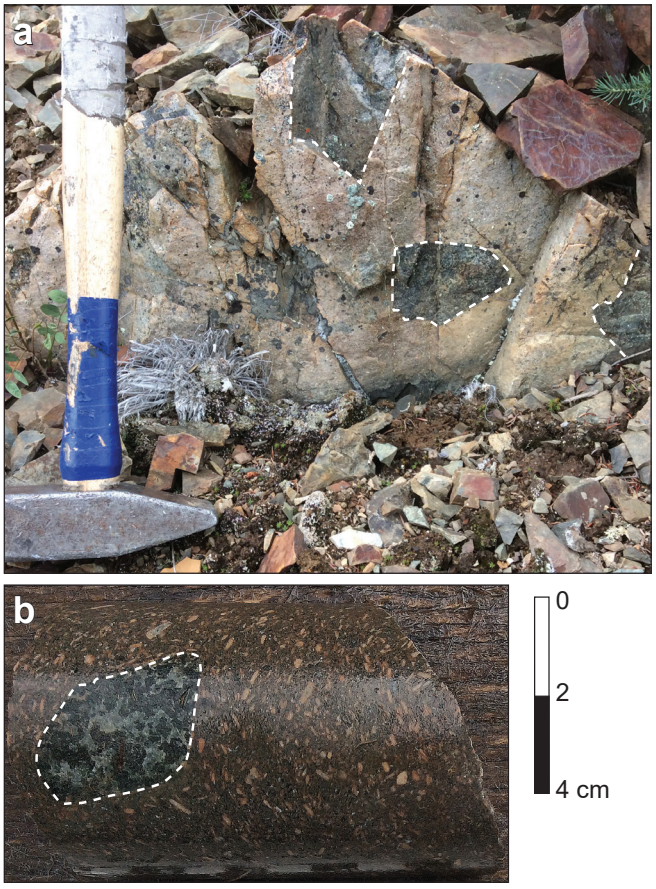


Figure 5-11. *Xenoliths (outlined in dashed white line) in the Teslin Crossing stock.* ***(a)*** *Siltstone xenoliths of the Lower to Middle Jurassic Richthofen Formation in the border phase of the stock; 15PS081.* ***(b)*** *Pyroxenite xenolith within the central phase of the stock; diamond drill hole M04-004 at 457.7 feet (139.50 m) depth.*

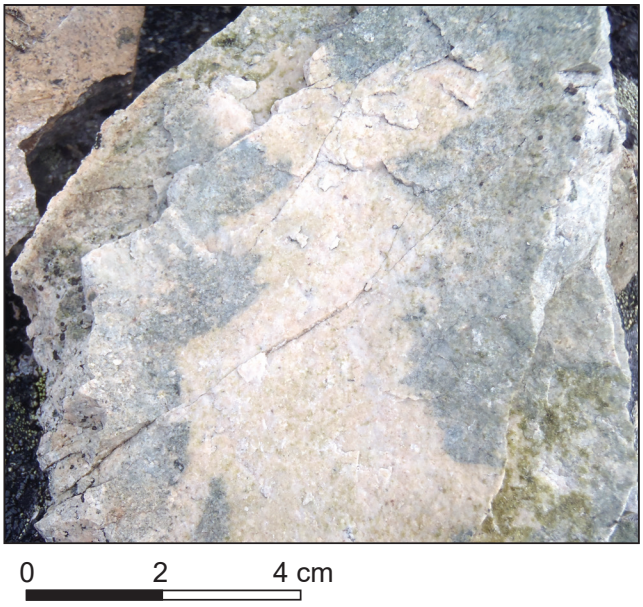


Figure 5-10. *Diffuse, irregular boundary between pink syenite and light grey-green monzodiorite phases of the Teslin Crossing stock; 15PS082. Scale below photo.*

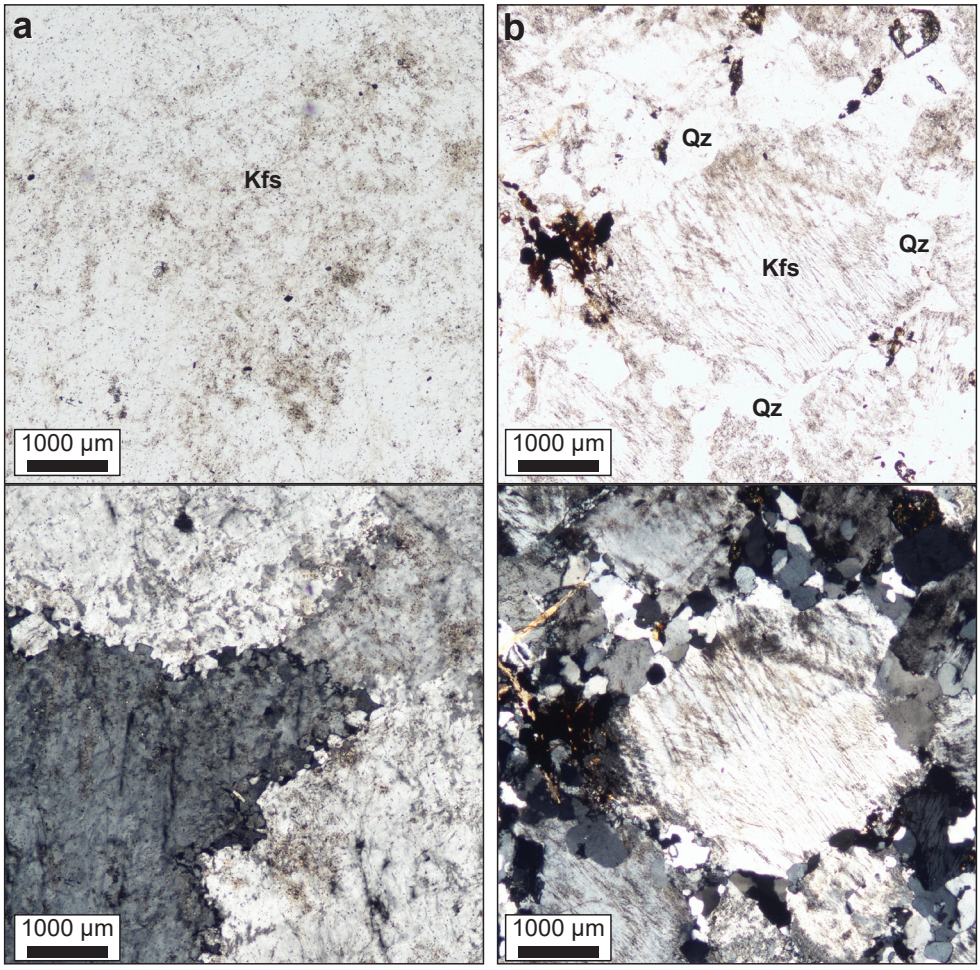


Figure 5-12. *Transmitted light photomicrographs of felsic minerals from the central phase of the Teslin Crossing stock. Plane polarized light (upper) and cross-polarized light (lower).* ***(a)*** *Coarse-grained K-feldspar with a distinct anhedral interlocking texture; 15PS086-2.* ***(b)*** *Medium-grained K-feldspar phenocryst within a relatively quartz-rich groundmass; 15PS078-1.*

The monzodiorite border phase is porphyritic with zoned K-feldspar, plagioclase, embayed quartz and acicular hornblende phenocrysts (Figs. 5-13 and 5-14). The fine-grained to cryptocrystalline groundmass is dominantly K-feldspar (Fig. 5-14; Pangman, 1973). Biotite and hornblende with lesser diopside are the mafic minerals (Pangman, 1973) and are fresh to weakly chlorite altered. The presence of minor quartz and abundance of K-feldspar in both phases demonstrate they formed from silica saturated alkalic magma.

Lamprophyre dikes, mostly found near the northern margin of the stock, contain 40 to 60% mafic minerals, diopside, hornblende and biotite (Pangman, 1973). Lamprophyres were not sampled for this study. Felsic dikes and plugs are found throughout the central phase; they are light pink and porphyritic (Fig. 5-15) to equigranular (Pangman, 1973). Accessory minerals in all intrusive rocks include titanite (Fig. 5-16), apatite and magnetite (Pangman, 1973); epidote is uncommon but where present is secondary.

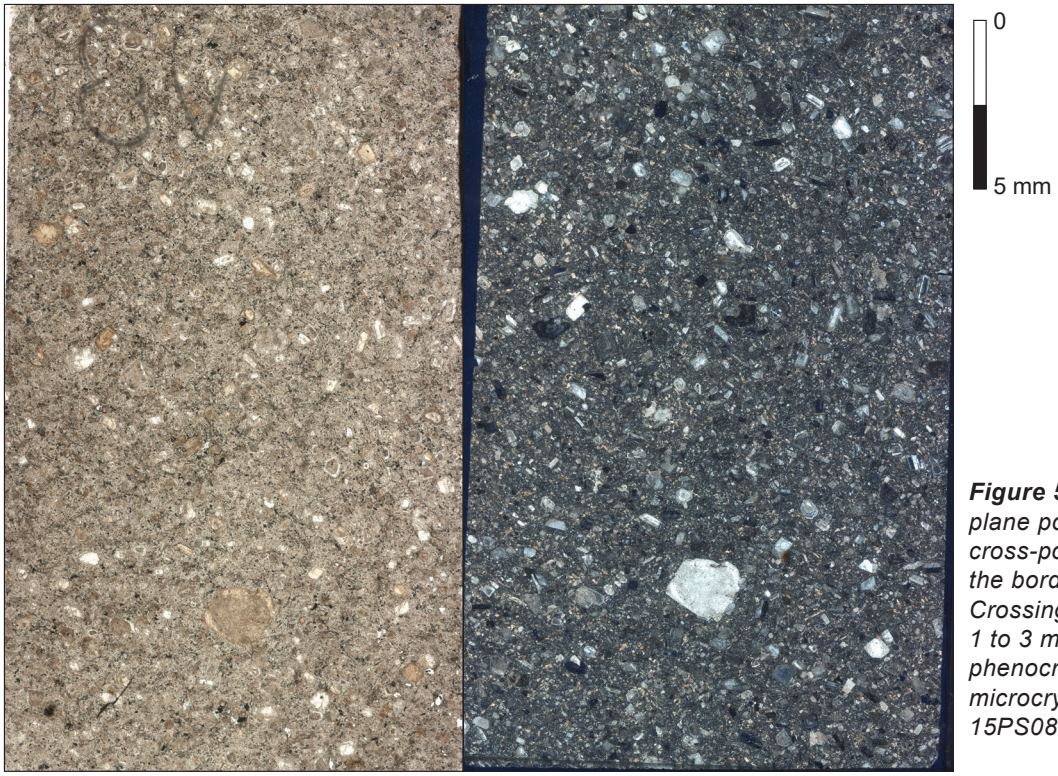


Figure 5-13. *Thin section scans, plane polarized light (left) and cross-polarized light (right), from the border phase of the Teslin Crossing stock showing 1 to 3 mm K-feldspar phenocrysts within a microcrystalline groundmass; 15PS081-1.*

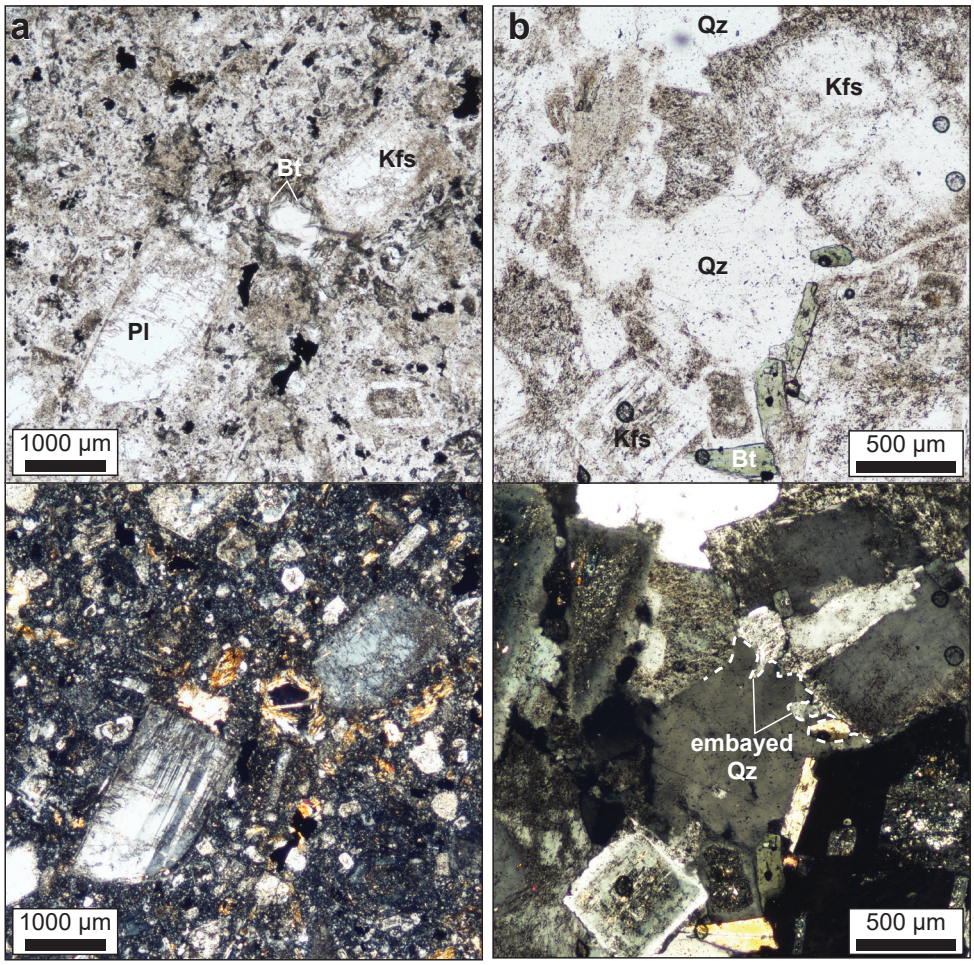


Figure 5-14. *Transmitted light photomicrographs of hypabyssal textures in the border phase of the Teslin Crossing stock. Plane polarized light (upper) and cross-polarized light (lower).* ***(a)*** *Weakly altered plagioclase and K-feldspar phenocrysts within a K-feldspar-rich groundmass; 15PS081-1.* ***(b)*** *Embayed quartz phenocrysts; 15PS082-1.*



Figure 5-15. *Weathered surface of K-feldspar porphyritic felsic dike intruding the border phase of the Teslin Crossing stock; 15PS083.*

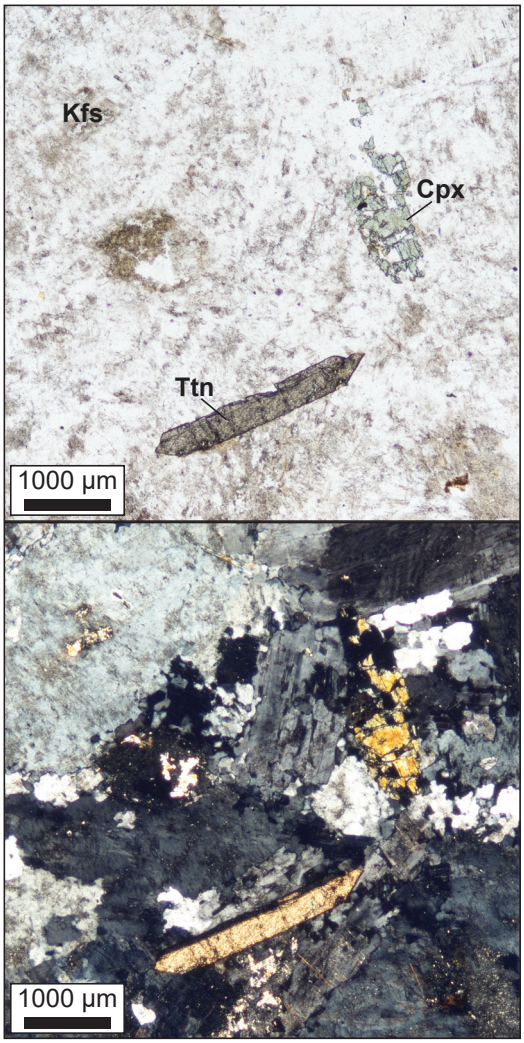


Figure 5-16. *Transmitted light photomicrographs of titanite and clinopyroxene (diopside) in the central phase of the Teslin Crossing stock; 15PS076-1. Plane polarized light (upper) and cross-polarized light (lower).*

Oxidation state and mineral occurrences

The central phase of the Teslin Crossing stock is oxidized with susceptibilities ranging from 2.1 to 23.1 × 10^{-3} SI units (Fig. 5-3; mean 14.0 × 10^{-3} SI units; n = 11). The border phase of the stock is slightly more oxidized with susceptibilities ranging from 14.9 to 39.8 × 10^{-3} SI units (Fig. 5-3; mean = 24.9 × 10^{-3} SI units; n = 4) except right at the contact with the sedimentary rocks where it is reduced (magnetic susceptibility = 0.55 × 10^{-3} SI units). The main mineral occurrence associated with the Teslin Crossing stock is Mars [105E 002], a Cu-Au alkalic porphyry target described by Hart (1997c) and Lang and McClaren (2003). A second occurrence, Egypt [105E 062], is located 7 km to the south and is thought to be a similar target based on reconnaissance prospecting (YGS, 2020b). However, its relationship to Bryde suite magmatism is unclear as it is associated with a negative magnetic anomaly, which is atypical of the suite in this area (Fig. 5-6).

Mars occurrence [105E 002]

The Mars occurrence [105E 002], also known as the TUV occurrence, is located on the southwest margin of the Teslin Crossing stock (Fig. 5-6). The occurrence was first staked in 1972 to cover anomalous stream sediment geochemistry; reconnaissance soil sampling, bedrock mapping and trenching were conducted in the following few years (YGS, 2020b). The property saw further work in 1996 and 1997, focusing on geophysical surveys, and most recently in 2003 and 2004 when seven holes

were diamond drilled (YGS, 2020b). Mineralized 'prospects', defined by the presence of quartz veins and silicification, define a northwest elongate 3 by 1.5 km area and include the Cliff, X, Kelly, Pluto, New, Windy Ridge South, Moon Knob, JL, Andrew and TA zones (Fig. 5-17; Lang and McClaren, 2003). This area also has discontinuous copper-in-soil values >100 ppm coincident with a core of sodic and magnetite-rich alteration surrounded by a more extensive calc-potassic alteration (Fig. 5-17; Lang and McClaren, 2003). Diamond drilling has occurred at the Moon Knob (3 holes; 454 m), Kelly (3 holes; 248 m) and Andrew zones (1 hole; 125 m; Lang and McClaren, 2004).

The following description of alteration assemblages and style is from Lang and McClaren (2004) and is based on outcrop and diamond drill core observations in the southwest portion of the stock. Alteration that is pervasive with variable intensity includes K-feldspar, albite and sericite. Alteration restricted to veins and fractures includes K-feldspar-actinolite-calcite, magnetite, quartz, epidote-albite and hematite-actinolite. Alteration associated with sulphides includes pervasive K-feldspar, magnetite veining, and quartz veining. Intensity is highest in areas such as the Cliff and Moon Knob zones where the pervasive K-feldspar assemblage includes pyrite and chalcopyrite. Lang and McClaren (2004) interpet the presence of a large hydrothermal system with sulphides based on reconnaissance diamond drilling. Copper assays were all <670 ppm, the highest Au and Mo assays are from intervals of hornfelsed metasedimentary rocks, 6.4 ppm Au over 15 feet from the Andrew zone, DDH M06-060' to 075'; and 1080 ppm Mo over 12.5 feet from the Moon Knob zone, DDH M04-314' to 326.5' (Lang and McClaren, 2004).

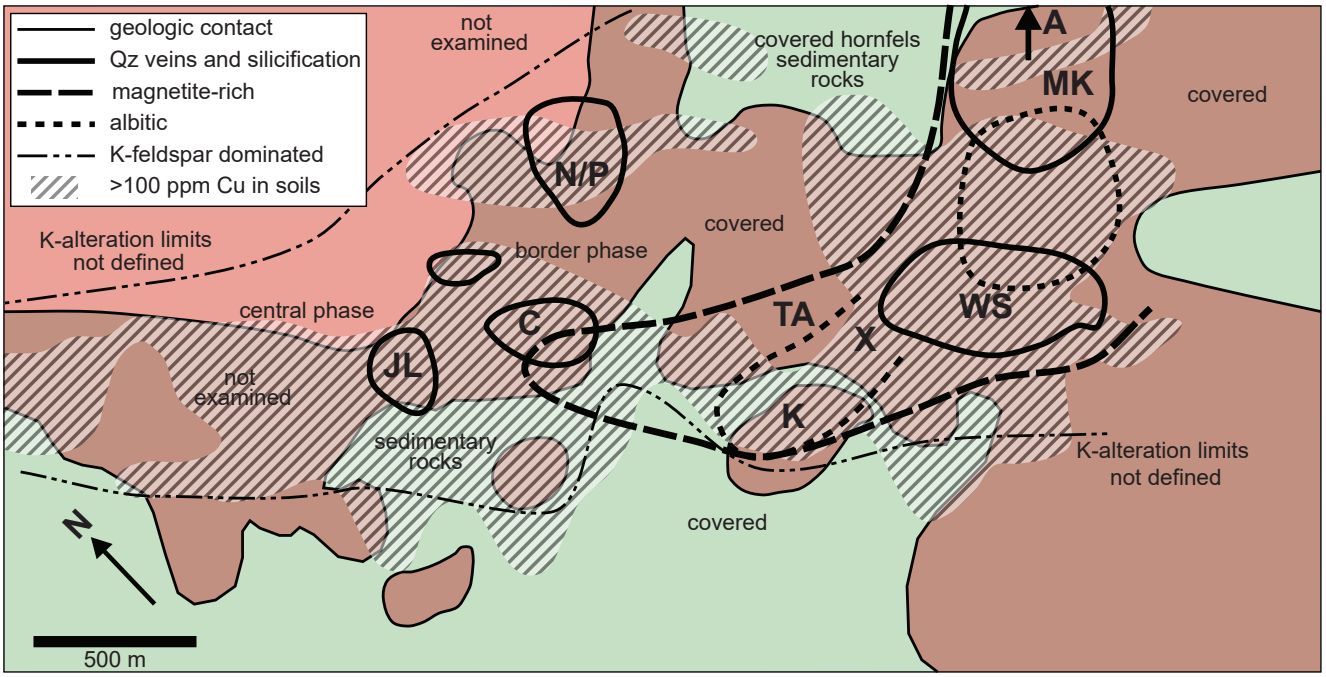


Figure 5-17. *Distribution of alteration assemblages in the Mars magmatic-hydrothermal system (Lang and McClaren, 2003). Boundaries for alteration zones are not fully defined. Geologic contacts from Wark (1998). Mineralized zones: JL = JL, C = Cliff, N/P = New Pluto, K = Kelly, TA = TA, X = X, WS = Windy Ridge south, MK = Moon Knob, A = Andrew. Location of this figure is shown as outline on Figure 5-6. Covered hornfels sedimentary rocks in the south inferred from uppermost bedrock logged in diamond drill core (Lang and McClaren, 2004). Note that the geographic reference frame has been rotated with North pointing to the upper left of the page.*

The alteration, mineralization and host rocks at the Mars occurrence are consistent with an alkalic porphyry model (Hart, 1997c; Lang and McClaren, 2003). The irregular pluton margins, porphyritic textures with cryptocrystalline groundmass, presence of dikes and sills into the surrounding low metamorphic grade sedimentary rocks are all consistent with a high-level of emplacement for the stock and associated dikes. However, the abundance of post-hydrothermal faults suggests that the system might contain structurally-bound domains that represent considerably different paleodepths in the hydrothermal system (Lang and McClaren, 2004). These faults may be related to >5 km linear low magnetic features that cross the stock in northwest and northeast orientations (Fig. 5-6).

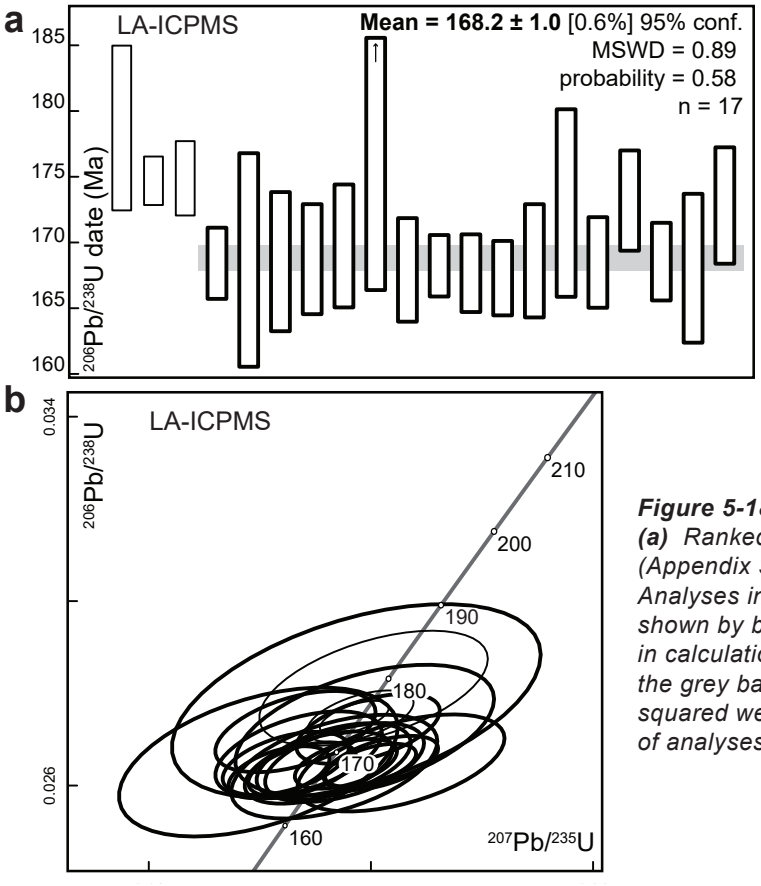
There are two other magnetic anomalies in the vicinity of the Teslin Crossing stock, one to the northwest and one to the southwest. The one to the northwest is a strong positive anomaly associated with mapped exposures of monzonite to syenite dikes (Tempelman-Kluit, 1984). The anomaly to the southwest is a small positive anomaly within a larger negative anomaly that does not have known plutonic rocks associated with it, but underlies the Egypt occurrence. Both anomalies likely represent intrusions at depth (Fig. 5-6). Neither of the magnetic anomalies are associated with >90% regional stream sediment anomalies in weighted sum modelling for porphyry Cu and epithermal deposits, though this could be the result of poor exposure and low relief as these anomalies are at lower elevations where there is extensive overburden.

Geochronology

The first indication of the Jurassic age of the Teslin Crossing stock was provided by K/Ar dates from two samples that yielded a hornblende date of 186 ± 5 Ma and two biotite dates of 181 ± 4 Ma and 173 ± 4 Ma (Fig. 5-4; Stevens *et al.*, 1982a; Tempelman-Kluit, 1984). Two samples were subsequently collected by Craig Hart in 1995 and 1998 for U-Pb zircon dating; these were analyzed by LA-ICPMS at UBC (95CH-TESX and 98CH-TESX). These previously unpublished results are presented here (Appendix 11).

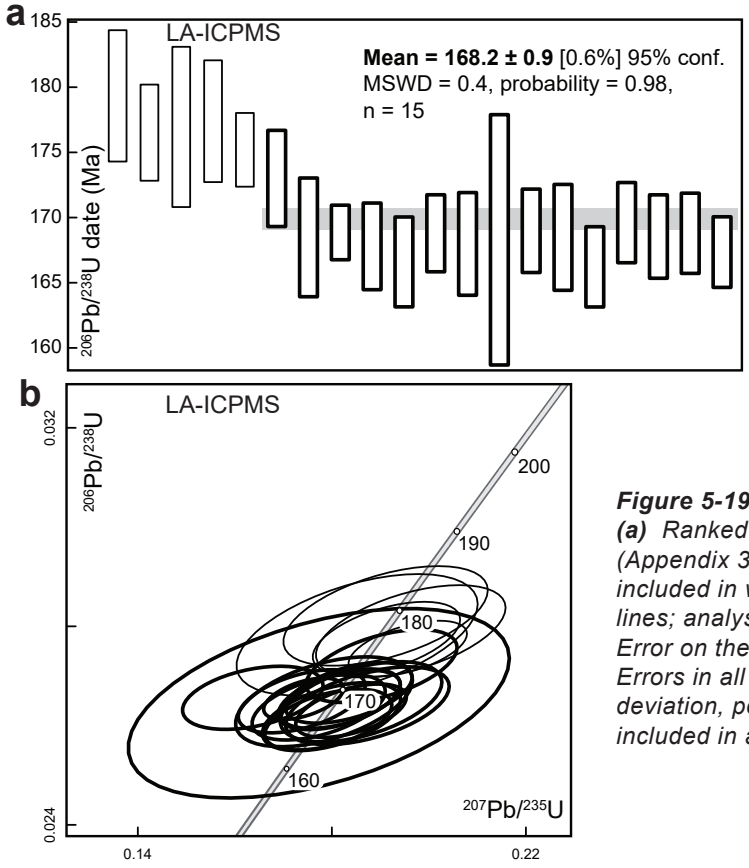
Sample 95CH-TESX was collected from the K-feldspar porphyritic monzodiorite border phase of the Teslin Crossing stock at the Mars property (Fig. 5-4). Twenty LA-ICPMS spot analyses from this sample yielded a range of $^{206}Pb/^{238}U$ dates between 179 and 167 Ma, with a weighted mean date of 168.2 ± 1.0 Ma (n = 17; Fig. 5-18). The other sample, 98CH-TESX, is from a porphyry dike intruding sedimentary rocks of the Laberge Group, approximately 6 km southeast of the Mars occurrence (Fig. 5-4). Twenty LA-ICPMS spot analyses from this sample yielded a range of $^{206}Pb/^{238}U$ dates between 179 and 166 Ma, with a weighted mean date of 168.2 ± 0.9 Ma (n = 15; Fig. 5-19).

We collected a sample of weakly porphyritic monzodiorite from the border phase of the Teslin Crossing stock for combined LA-ICPMS and CA-TIMS analyses at Boise State University (Sample 15PS082-1; Fig. 5-4; Appendices 3 and 4). It yielded faceted, concentrically or sector zoned zircons with <2:1 aspect ratio and no apparent inherited cores (Fig. 5-20a). Thirty-two LA-ICPMS spot analyses yielded $^{206}Pb/^{238}U$ dates between 178 and 163 Ma, and a weighted mean of 168.7 ± 1.2 Ma (n = 32; Fig. 5-20b). Six zircons from 15PS082-1 were analyzed by CA-TIMS and yielded equivalent $^{206}Pb/^{238}U$ dates ranging from 171.72 ± 0.12 to 171.56 ± 0.12 Ma, with a weighted mean of 171.62 ± 0.05 Ma (MSWD = 1.01, n = 6; Fig. 5-20c).



95CH-TESX
Teslin Crossing dike

Figure 5-18. *U-Pb zircon geochronology for 95CH-TESX.* ***(a)*** *Ranked plot of $^{206}Pb/^{238}U$ dates determined by LA-ICPMS (Appendix 3).* ***(b)*** *Concordia plot of LA-ICPMS dates. Analyses included in weighted mean date calculation are shown by bold lines; analyses with thin lines are not used in calculations. Error on the weighted mean date shown by the grey band. Errors in all plots are at 2σ. MSWD = mean squared weighted deviation, pof = probability of fit, n = number of analyses included in age calculation.*



98CH-TESX Teslin Crossing border phase

Figure 5-19. *U-Pb zircon geochronology for 98CH-TESX.* ***(a)*** *Ranked plot of $^{206}Pb/^{238}U$ dates determined by LA-ICPMS (Appendix 3).* ***(b)*** *Concordia plot of LA-ICPMS dates. Analyses included in weighted mean date calculation are shown by bold lines; analyses with thin lines are not used in calculations. Error on the weighted mean date shown by the grey band. Errors in all plots are at 2σ. MSWD = mean squared weighted deviation, pof = probability of fit, n = number of analyses included in age calculation.*

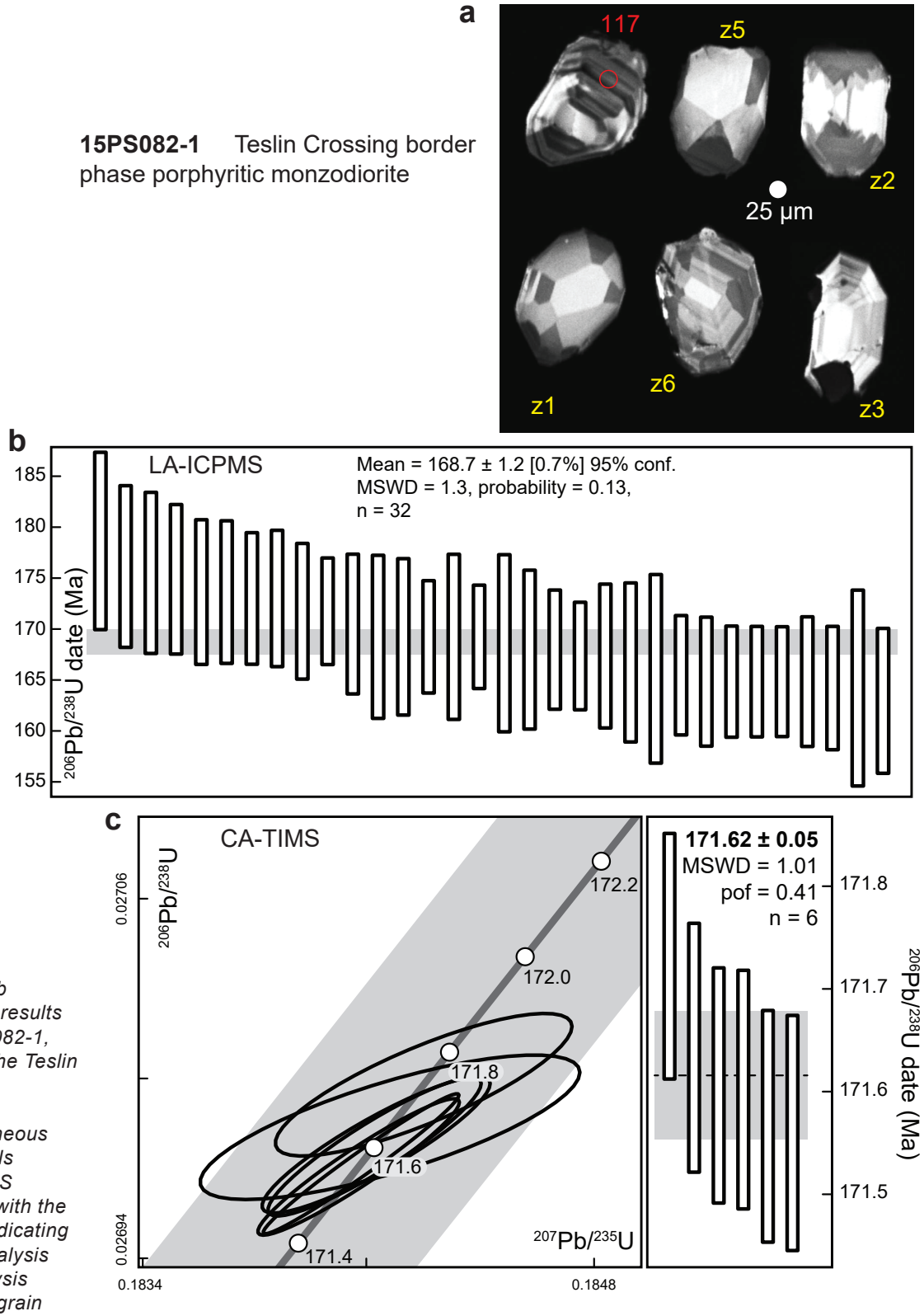


Figure 5-20. *U-Pb geochronological results for sample 15PS082-1, border phase of the Teslin Crossing stock.* ***(a)*** *CL images of representative igneous zircons. Red labels indicate LA-ICPMS analysis number with the red open circle indicating location of the analysis spot, yellow analysis number refers to grain analyzed by CA-TIMS.* ***(b)*** *Ranked plot of LA-ICPMS $^{206}Pb/^{238}U$ dates (Appendix 3). Grey horizontal bar shows calculated weighted mean with errors.* ***(c)*** *Concordia diagram (left) and ranked $^{206}Pb/^{238}U$ dates (right) for zircons analyzed by CA-TIMS (Appendix 4). The light grey band around concordia (dark grey line) shows the decay constant uncertainties. Analyses included in weighted mean age (light grey horizontal bar) calculations are bold; analyses with thin lines are not used in calculations. Line-type designations are the same in all plots. Errors in all plots are at 2σ. MSWD = mean squared weighted deviation, pof = probability of fit, n = number of analyses included in age calculation.*

Michie stock

The Michie stock is located 6 km east of Marsh Lake in southern Yukon and has a mapped extent of 14 km² (Fig. 5-21; Table 5-1). The Michie stock area is located near the northern termination of the Cache Creek terrane (Fig. 5-1), where there is a complex structural relationship between Cache Creek, Stikinia and the Whitehorse trough. Two phases of thrust imbrications are documented in the area; early (D_1) southwest-verging thrusting of the Cache Creek terrane over Stikinia and Whitehorse trough, and subsequent (D_2) eastward thrusting of Stikinia and Whitehorse trough (D_1 footwall) back over Cache Creek rocks (Figs. 5-21 and 5-22; Bickerton *et al.*, 2020). The Michie stock itself is poorly exposed and contact relationships with surrounding strata of Whitehorse trough (Richthofen formation, Laberge Group) and Stikinia (Casca member, Aksala formation, Lewes River Group) are poorly constrained. The stock is undeformed, although a weak magmatic alignment of feldspar crystals is locally noted (Fig. 5-23). The mapped extent of the Michie stock cuts stratigraphic contacts and fold structures (Fig. 5-21), and local hornfels development in adjacent sedimentary strata indicate that it intruded after initial deformation of Stikinia and Whitehorse trough (Bickerton, 2014a; Bickerton *et al.*, 2020).

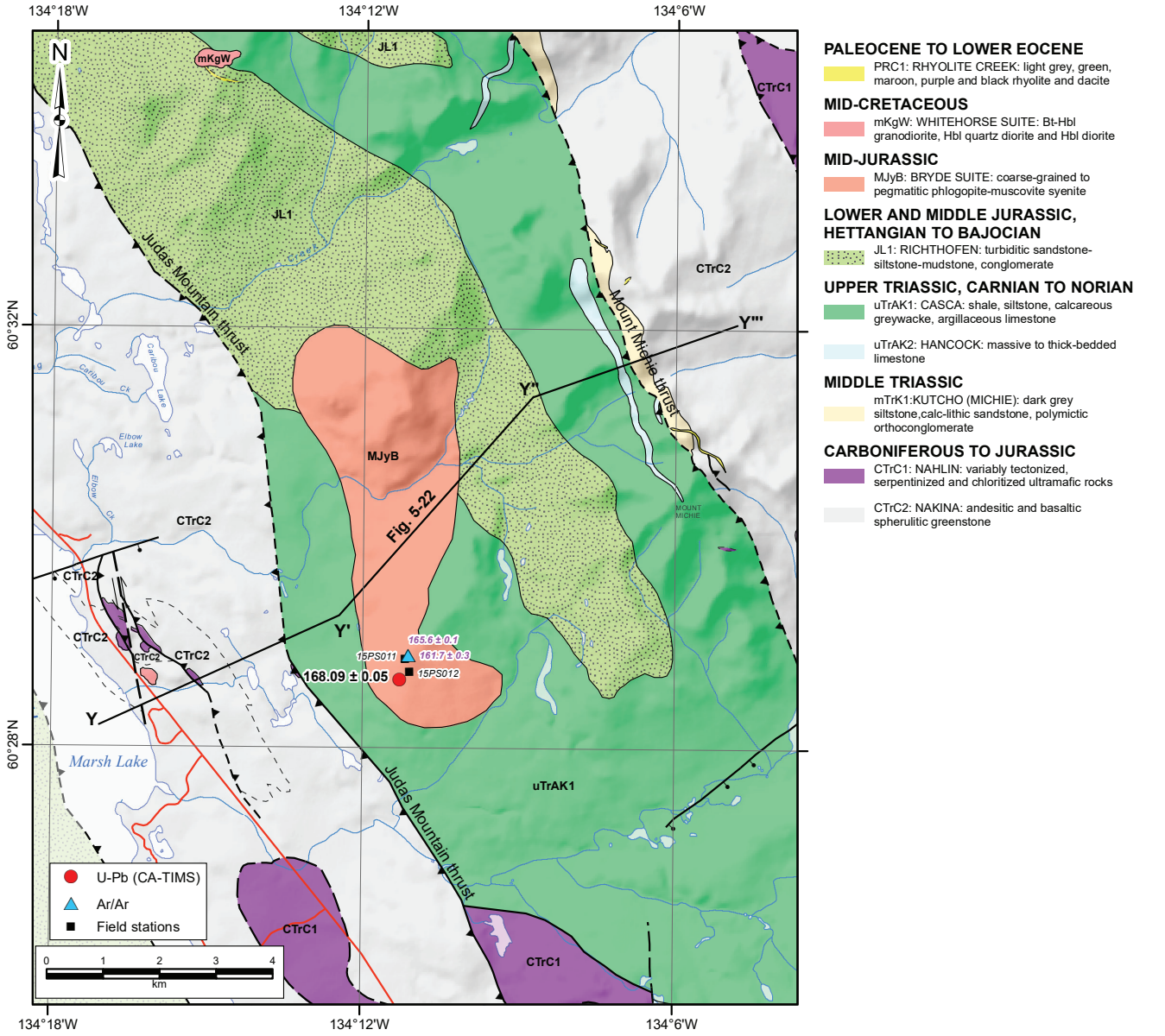


Figure 5-21. *Geology of the Michie pluton area (YGS, 2020a); fault symbology as in Figure 1-4. Location of Figure 5-22 shown.*

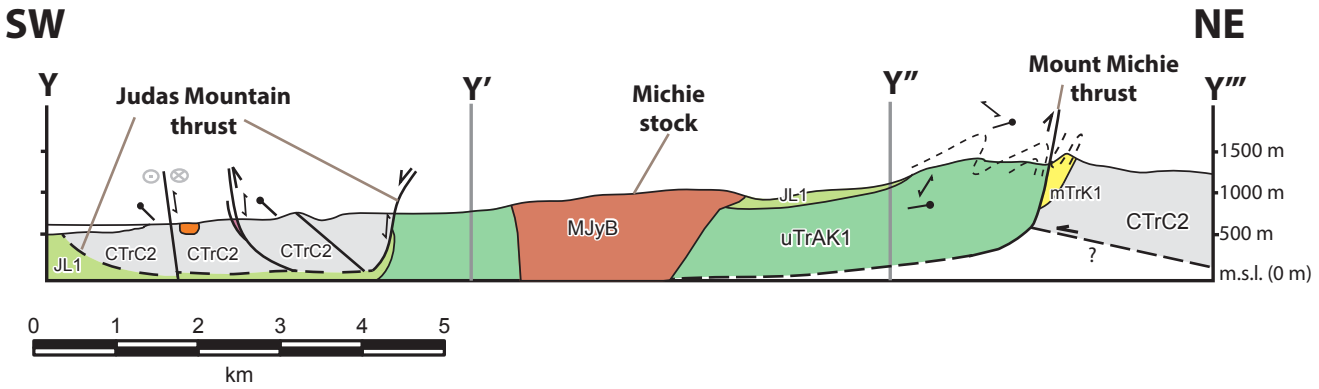


Figure 5-22. *Structural cross section for the Marsh Lake area modified from Bickerton et al. (2020); line of section and legend are shown on Fig. 5-21. Black pins present the apparent strike and dip of bedding in sedimentary rocks at surface, off of section. Note that Judas Mountain thrust is interpreted as a folded southwest-verging fault. The Michie stock has been extended at depth emphasizing the crosscutting geometry.*

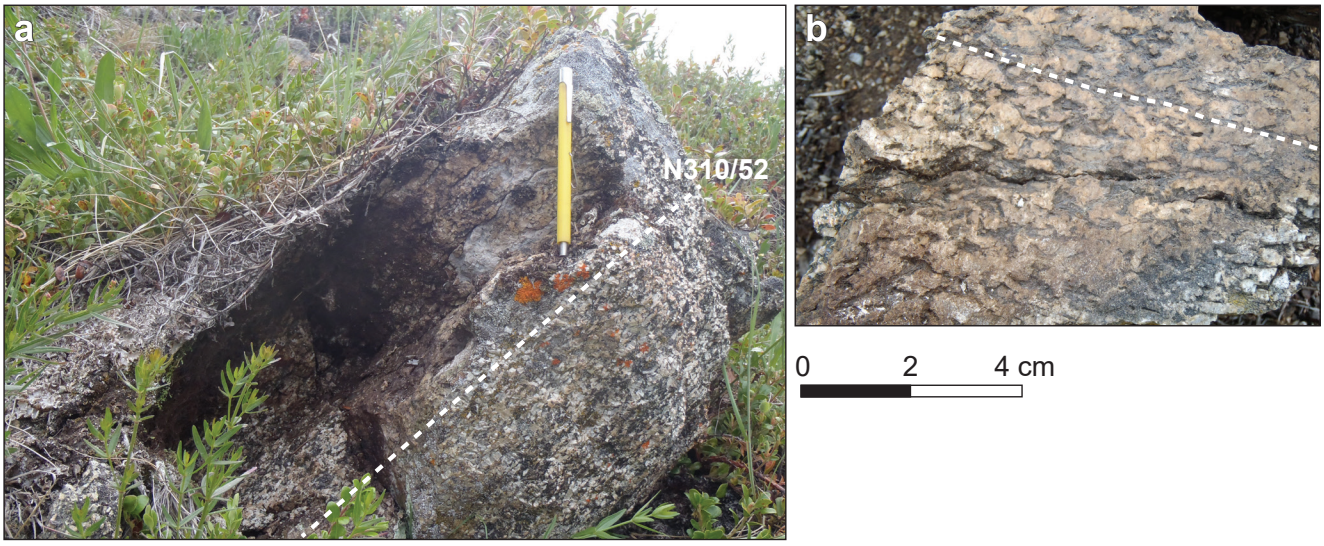


Figure 5-23. *Weak alignment of minerals in the Michie stock, interpreted as magmatic foliation; 15PS011.* ***(a)*** *Outcrop with weak mineral alignment and strike and dip shown. Magnet is 12 cm long.* ***(b)*** *Weathered surface with recessive mafic minerals and resistant K-feldspar highlighting the alignment of minerals. In both photo foliation is shown by dashed white line.*

Petrography

The Michie stock is equigranular and coarse grained to locally pegmatitic and weathers to a distinct 'knobbly' appearance (Fig. 5-24). The majority of the rock is made up of K-feldspar and compositionally straddles the syenite-monzonite boundary of a simplified QAP diagram (Fig. 5-2). K-feldspar is mostly light grey (Fig. 5-25), and correspondingly the rock weathers light pink to grey (Figs. 5-24 and 5-25). Fresh surfaces are mesocratic with mafic mineral content varying between 10 and 30%. Hornblende and biotite are the dominant mafic minerals and are present in equal proportions; clinopyroxene is present but rare (Fig. 5-26). Biotite is fresh and hornblende is weakly to moderately epidote altered (Fig. 5-26). Plagioclase is fresh to weakly saussuritized; epidote is minor and secondary. K-feldspar is moderately sericitized near grain boundaries. Muscovite has been noted in some samples (Bickerton, 2014a; Bickerton *et al.*, 2020).

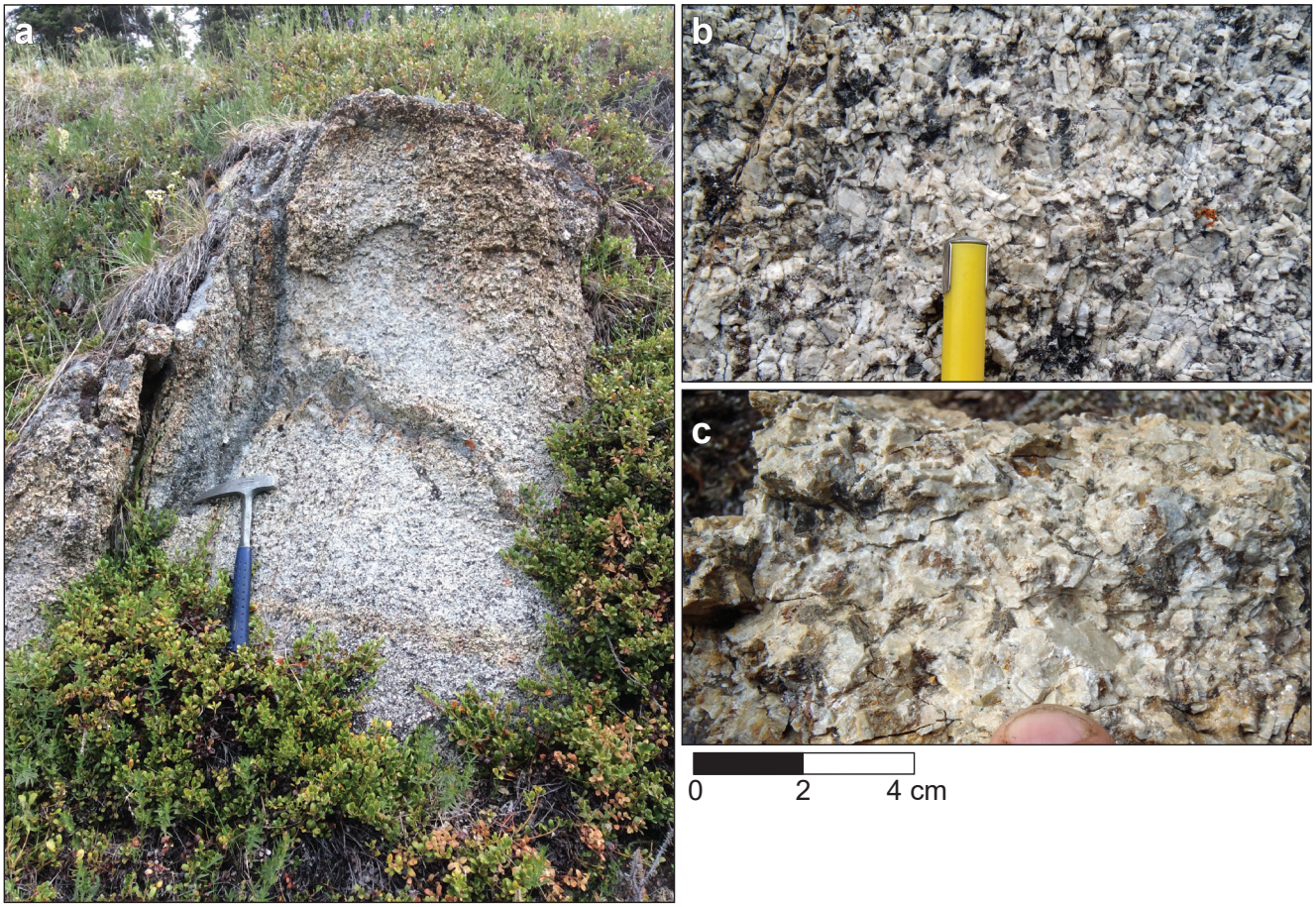


Figure 5-24. *Outcrop of the Michie stock.* ***(a)*** *Typical poor exposure with characteristic equigranular coarse-grained, 'knobbly' texture; 15PS011. Hammer is 30 cm long.* ***(b)*** *Photograph of 15PS011 outcrop displaying the coarse-grained equigranular texture of K-feldspar. Magnet diameter is 8 mm.* ***(c)*** *Fresh, broken face with coarse-grained to pegmatitic texture; 15PS010. Scale below photo.*

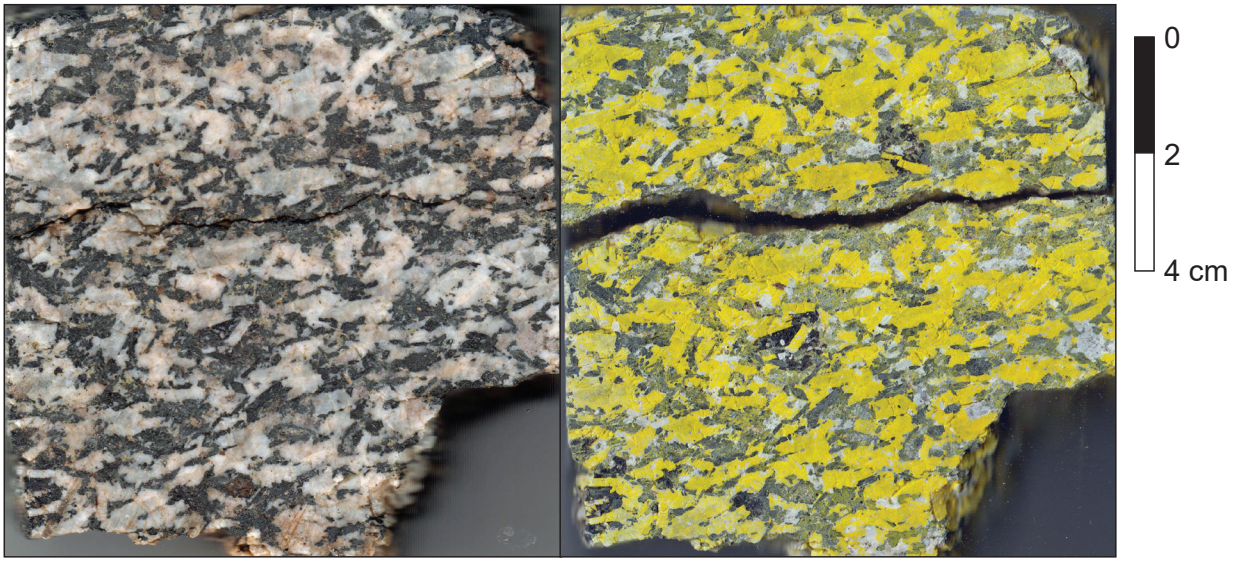


Figure 5-25. *Representative sample of the coarse-grained equigranular syenite from the Michie stock; 15PS011-1. Slightly oxidized polished surface (left) and a cobaltinitrite-stained surface (right). Note K-feldspar is yellow, both images are same the scale.*

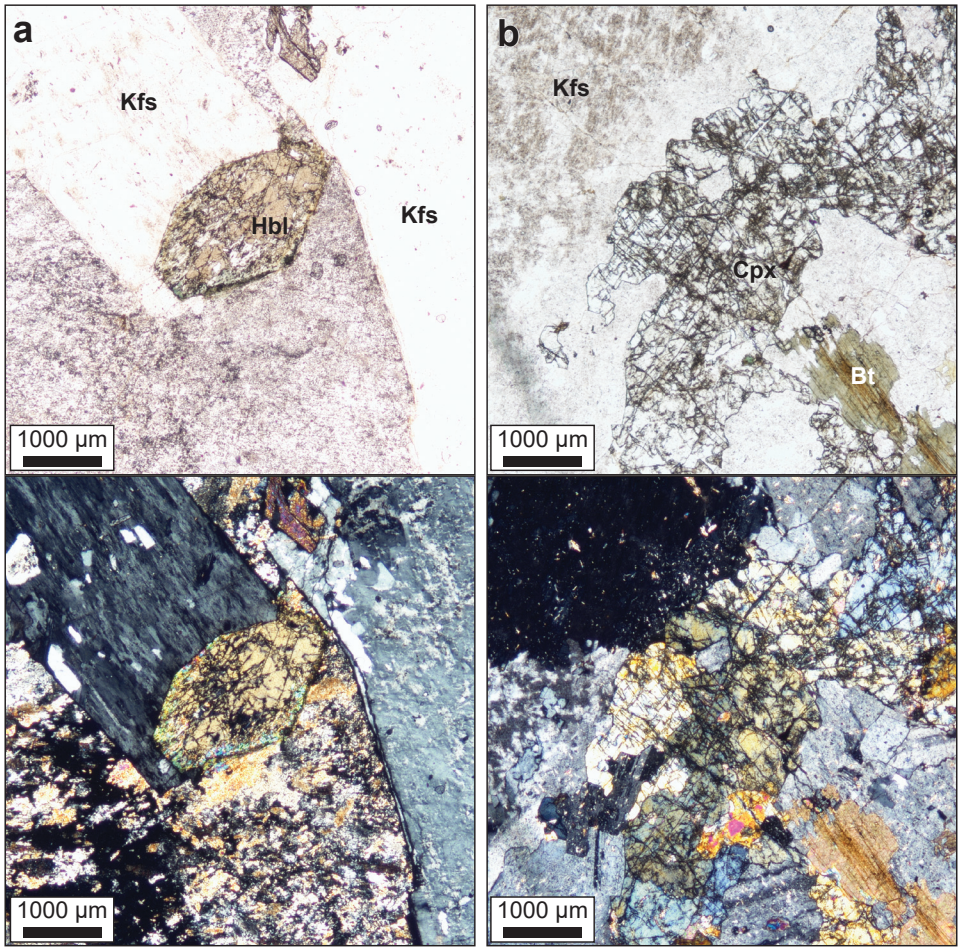


Figure 5-26. *Transmitted light photomicrographs of mafic minerals from the Michie stock. Plane polarized light (upper) and cross-polarized light (lower).* ***(a)*** *Coarse-grained K-feldspar with euhedral hornblende; 15PS010-1.* ***(b)*** *Anhedral K-feldspar with anhedral clinopyroxene and subhedral biotite; 15PS011-1.*

Oxidation state and mineral occurrences

The Michie stock is reduced and susceptibilities range from 0.16 to 0.45 × 10^{-3} SI units (Fig. 5-3; mean 0.30 × 10^{-3} SI units; n = 3). The pluton is rimmed to the north and west by a high magnetic anomaly which likely reflects in part its contact aureole (Fig. 5-27). The Bronco [105D 185] mineral occurrence occurs near the pluton margin at the southern end of this magnetic high. It consists of minor stockwork veining and could be related either to the Michie pluton or to mineralization associated with the Judas Mountain thrust (Bickerton, 2014b).

Geochronology

The Michie stock was originally inferred to be part of the mid-Cretaceous Whitehorse plutonic suite (Wheeler, 1961; Gordey and Makepeace, 2001), although its alkalic composition sets it apart from typical calc-alkaline plutons of this suite. The first indication of the Jurassic age of the Michie stock was provided by $^{40}Ar/^{39}Ar$ dating of muscovite and biotite from a pegmatitic syenite which yielded disturbed age spectra with pseudo-plateau segments at 165.6 ± 0.1 and 161.7 ± 0.3 Ma, respectively (Fig. 5-21; Bickerton *et al.*, 2020).

We collected sample 15PS010-1 approximately 500 m south of the locality dated by Bickerton *et al.* (2020) for combined LA-ICPMS and CA-TIMS analyses at Boise State University (Fig. 5-21; Appendices 3 and 4). It is from coarse-grained monzonite and yielded large, equant broken shards of zoned zircons without apparent inherited cores (Fig. 5-28a). Twenty-three LA-ICPMS spot analyses yielded $^{206}Pb/^{238}U$ dates between 172 and 143 Ma, and a weighted mean of 164.3 ± 2.0 Ma (n = 20; Fig. 5-28b). Six zircons from 15PS010-1 were analyzed by CA-TIMS and yielded equivalent $^{206}Pb/^{238}U$ dates ranging from 168.14 ± 0.12 to 168.09 ± 0.12 Ma, with a weighted mean of 168.09 ± 0.05 Ma (MSWD = 1.25, n = 6; Fig. 5-28c).

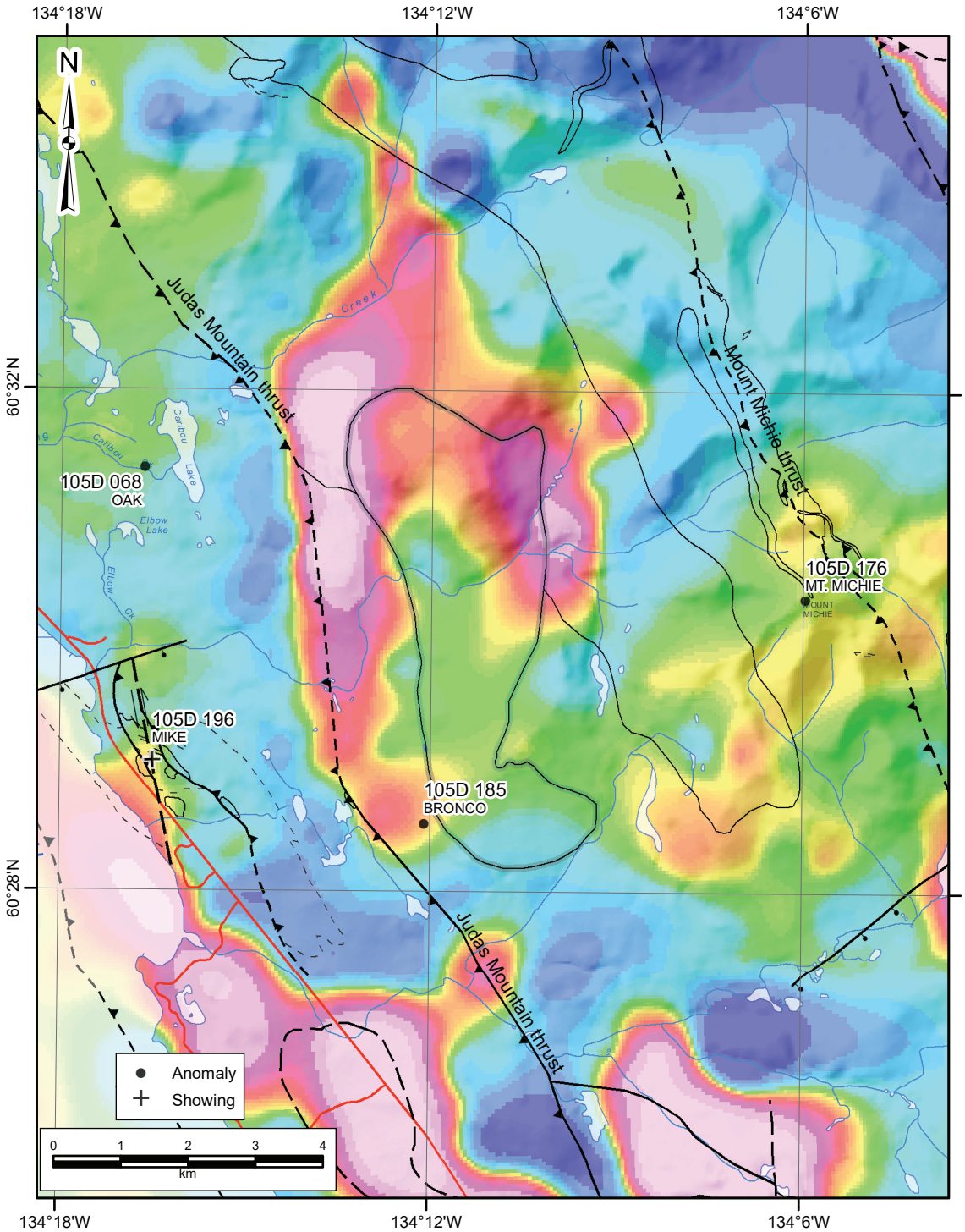


Figure 5-27. *Reduced to pole, first vertical derivative aeromagnetic map of the Michie stock area (Aurora Geosciences Ltd. and Bruce, 2017a) illustrating distribution of mineral occurrences. Fault symbology as in Figure 1-4.*

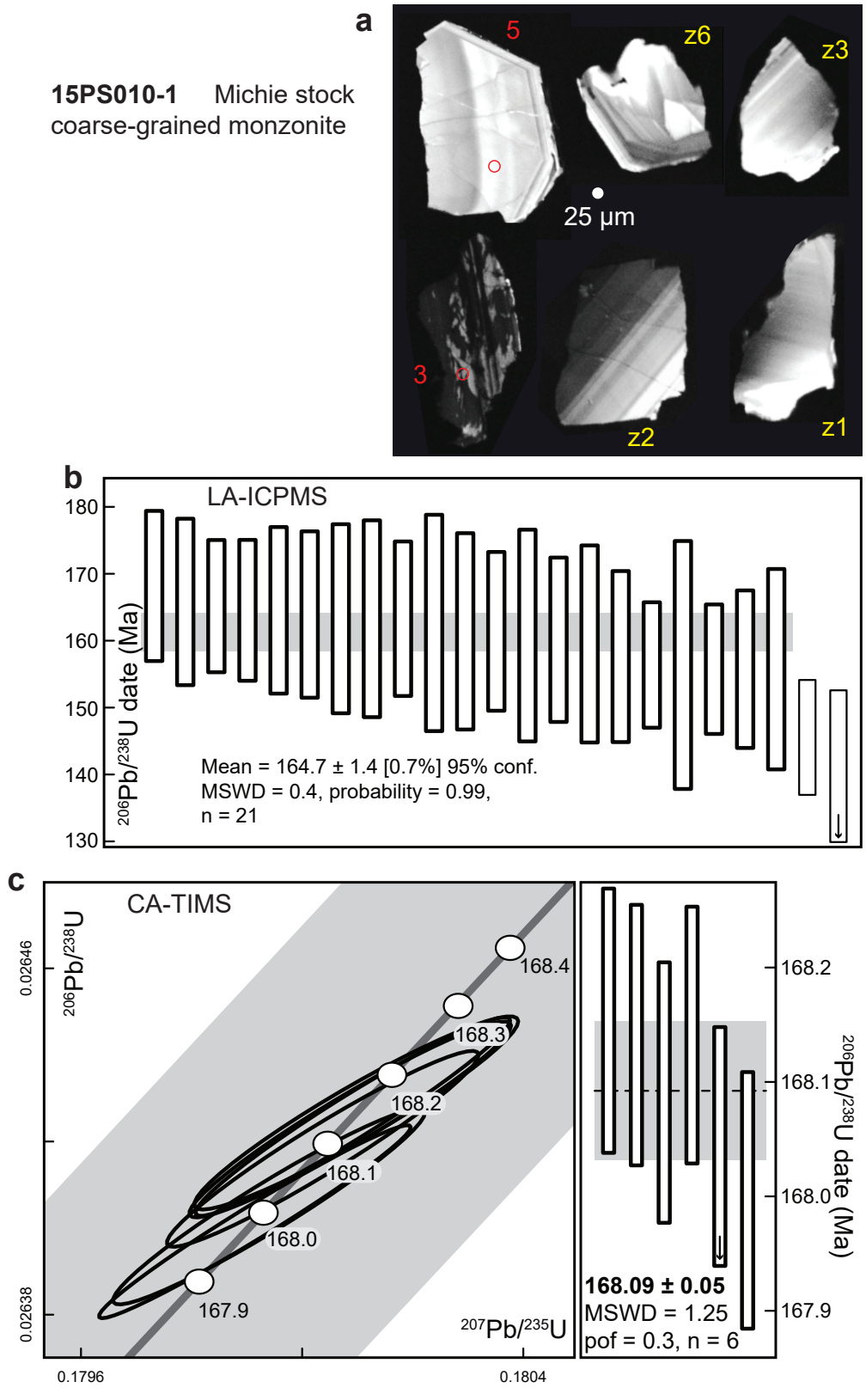


Figure 5-28. *U-Pb geochronological results for sample 15PS010-1, Michie stock.* ***(a)*** *CL images of representative igneous zircons. Red labels indicate LA-ICPMS analysis number with the red open circle indicating location of the analysis spot, yellow analysis number refers to grain analyzed by CA-TIMS.* ***(b)*** *Ranked plot of LA-ICPMS $^{206}Pb/^{238}U$ dates (Appendix 3). Grey horizontal bar shows calculated weighted mean with errors.* ***(c)*** *Concordia diagram (left) and ranked $^{206}Pb/^{238}U$ dates (right) for zircons analyzed by CA-TIMS (Appendix 4). The light grey band around concordia (dark grey line) shows the decay constant uncertainties. Analyses included in weighted mean age (light grey horizontal bar) calculations are bold; analyses with thin lines are not used in calculations. Arrows indicate data project off figure. Line-type designations are the same in all plots. Errors in all plots are at 2σ. MSWD = mean squared weighted deviation, pof = probability of fit, n = number of analyses included in age calculation.*

Mount Bryde stock

The Mount Bryde stock is circular with a mapped extent of 60 km², and is located 50 km south of Jakes Corner, the junction of the Atlin road and the Alaska Highway (Fig. 5-1; Table 5-1). The stock intrudes well-bedded grey to green ribbon chert, siltstone and greywacke of the Late Triassic–Early Jurassic Cache Creek Group (Fig. 5-29; Gordey and Stevens, 1994), part of the Cache Creek terrane. The stock is centred on the ridge system that includes Mount Bryde, its namesake peak. Topography of the stock consists of rounded ridges and peaks (Fig. 5-30) with elevations up to 1750 m; most outcrop is above 1350 m (Gordey and Stevens, 1994). There are two small pendants of Cache Creek Group rocks near the western margin of the stock (Fig. 5-29).

Petrography

The Mount Bryde stock is equigranular, medium-grained monzodiorite to granodiorite (Fig. 5-2). It is mesocratic with up to 30% mafic minerals (Fig. 5-31). Mafic minerals are equal amounts of hornblende and biotite; hornblende is locally cored by clinopyroxene (Fig. 5-32). Pyroxene mantled by hornblende or biotite is a diagnostic characteristic of the coeval Fourth of July plutonic suite in northern British Columbia (Mihalynuk, 1999). Mafic minerals are mostly fresh, with the exception of a few biotite that have been chlorite altered, commonly with secondary epidote (Fig. 5-32). Plagioclase is weakly to intensely saussuritized and K-feldspar is fresh. Apatite is a ubiquitous accessory mineral, titanite is not observed.

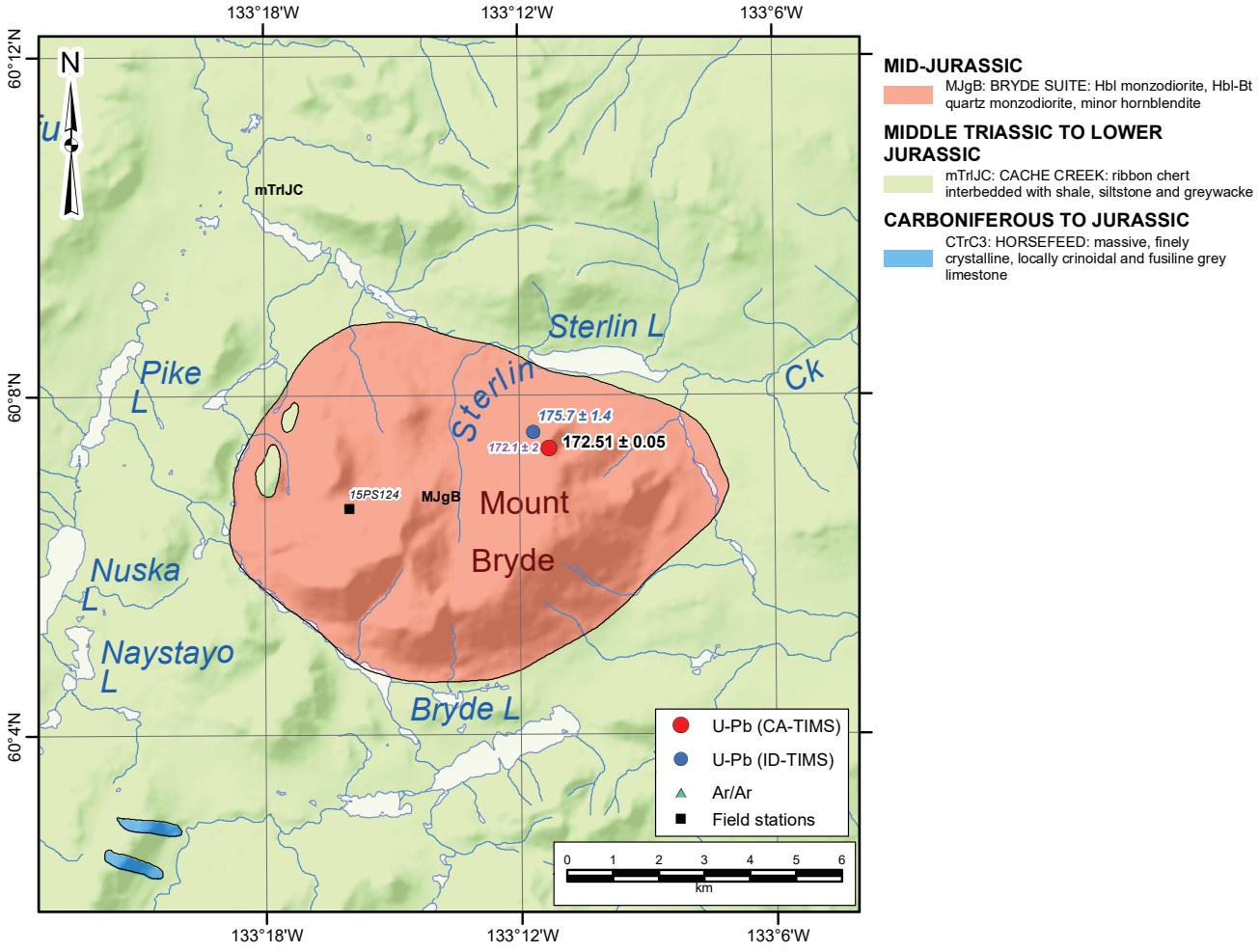


Figure 5-29. *Geology of the Mount Bryde pluton area (YGS, 2020a). L = lake; Ck = creek.*

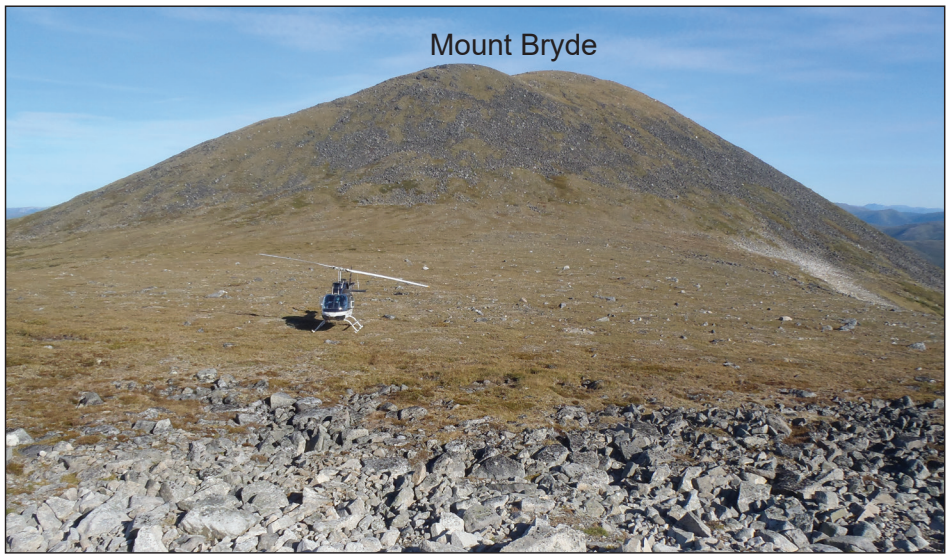


Figure 5-30. *Looking south from station 15PS123 towards Mount Bryde. This photo shows the amount and rubbly nature of outcrop on the ridges where the Mount Bryde pluton is best exposed.*

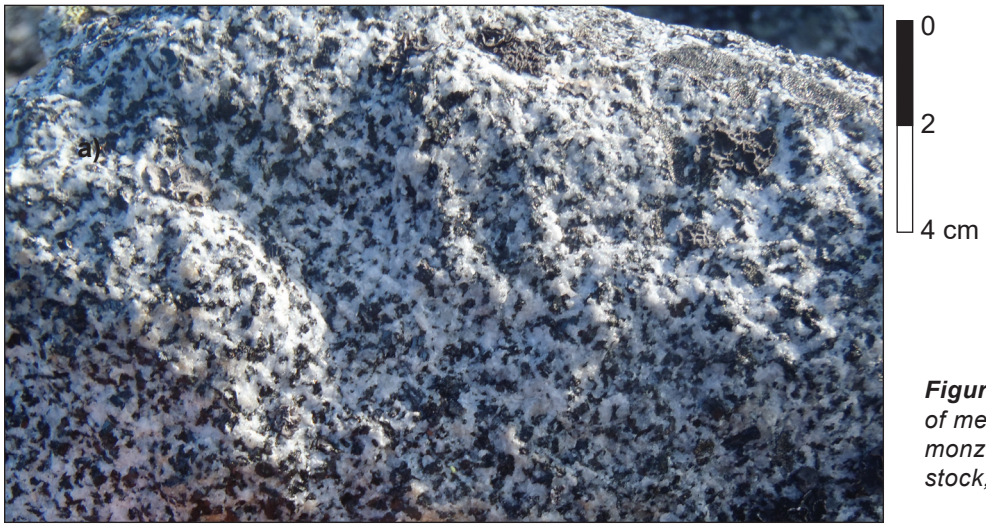


Figure 5-31. *Weathered surface of medium-grained equigranular monzodiorite in the Mount Bryde stock; 15PS123.*

Oxidation state and mineral occurrences

The Mount Bryde stock is oxidized and has magnetic susceptibilities of 5.0 and 13.7 × 10^{-3} SI units at the two sites we visited (Fig. 5-3). On the aeromagnetic map, the core of the Mount Bryde stock is strongly magnetic and rimmed by magnetic lows along its mapped edges (Fig. 5-33). There are no known mineral occurrences associated with the Mount Bryde stock, although stream sediment geochemical data modelled for epithermal deposits are >90th percentile to the west, near Nuska Lake (Mackie *et al.*, 2016g).

Geochronology

Gordey *et al.* (1998) previously reported a U-Pb zircon date of 175.7 ± 1.4 Ma (multi-grain ID-TIMS, GSC) from a medium-grained biotite-hornblende monzodiorite collected ~2 km north from the peak of Mount Bryde (Fig. 5-29). Hornblende and biotite from the same sample were also analyzed by the $^{40}Ar/^{39}Ar$ method and yielded cooling dates of 173 ± 3 and 169 ± 2 Ma, respectively (Hunt and Roddick, 1994).

We collected sample 15PS123-1, a medium-grained monzodiorite, approximately 500 m southeast of the locality sampled by Gordey *et al.* (1998) for combined LA-ICPMS and CA-TIMS analyses at Boise State University (Fig. 5-29; Appendices 3 and 4). It yielded mostly equant sector zoned zircons with a few elongate oscillatory zoned crystals, and no indications of inherited cores (Fig. 5-34a). Twenty-nine LA-ICPMS spot analyses yielded $^{206}Pb/^{238}U$ dates between 180 and 166 Ma, and a weighted mean of 171.8 ± 1.2 Ma (n = 29; Fig. 5-34b). Six zircons from 15PS123-1 were analyzed by CA-TIMS and yielded equivalent $^{206}Pb/^{238}U$ dates ranging from 172.55 ± 0.12 to 172.49 ± 0.12 Ma, with a weighted mean of 172.51 ± 0.05 Ma (MSWD = 0.23, n = 6; Fig. 5-34c).

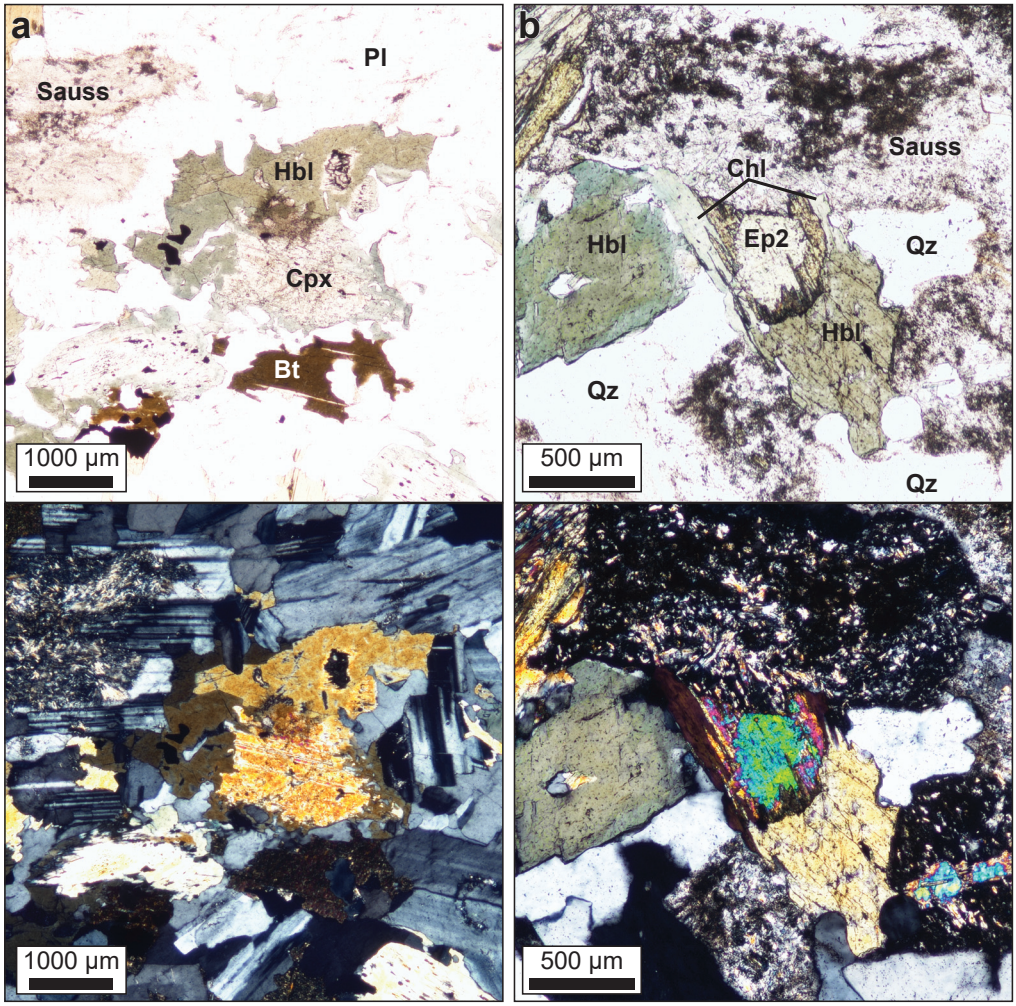


Figure 5-32. *Transmitted light photomicrographs from the Mount Bryde stock. Plane polarized light (upper) and cross-polarized light (lower).* ***(a)*** *Weakly saussuritized plagioclase with fresh biotite and hornblende overgrowing clinopyroxene; 15PS123-1.* ***(b)*** *Intensely saussuritized plagioclase with subhedral epidote surrounded by chlorite and hornblende; 15PS124-1.*

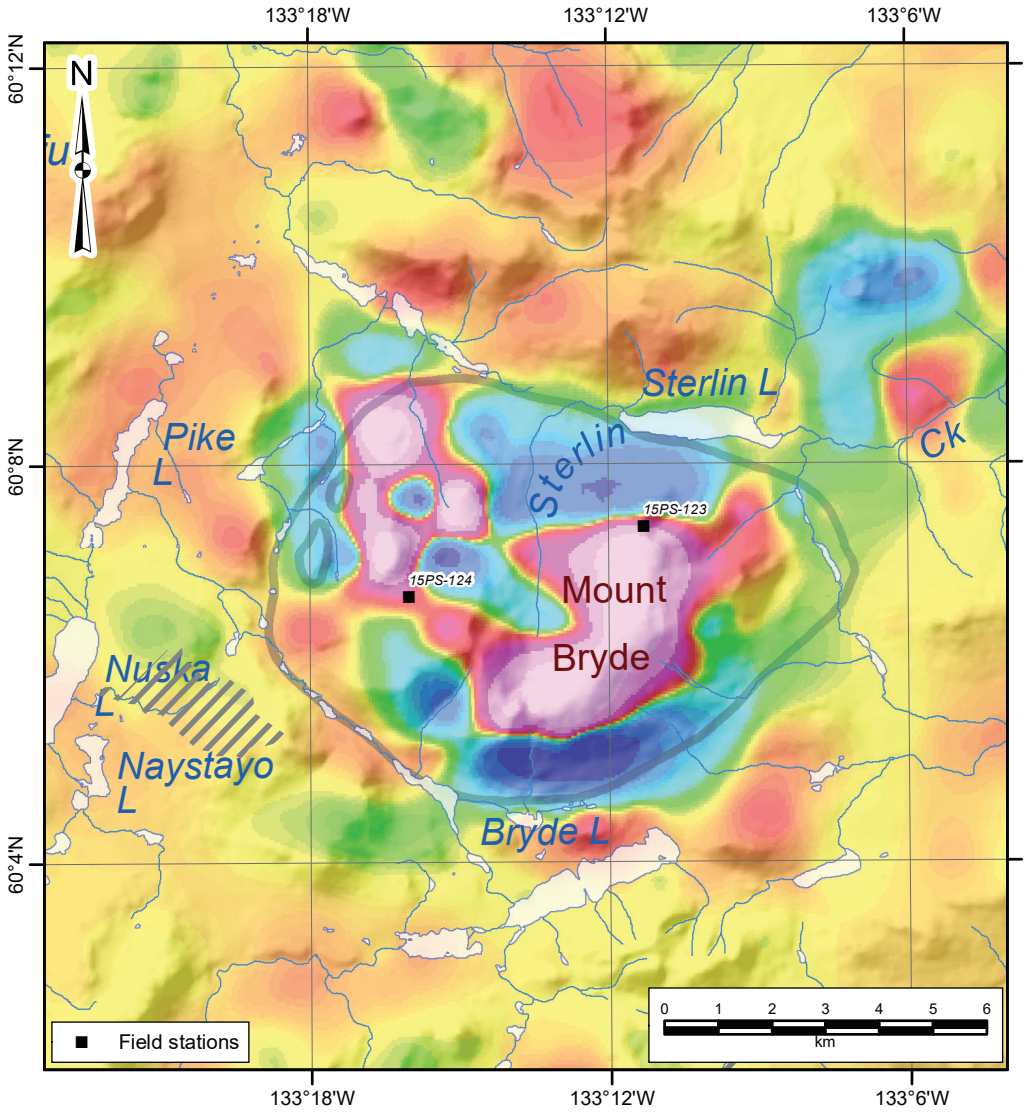


Figure 5-33. *Reduced to pole, first vertical derivative aeromagnetic map of the Mount Bryde stock area (Aurora Geosciences Ltd. and Bruce, 2017e) illustrating distribution of mineral occurrences and catchment area (hatched) near Nuska Lake with >90th percentile RGS data modeled for epithermal Au deposits (Mackie et al., 2016g). L = lake; Ck = creek.*

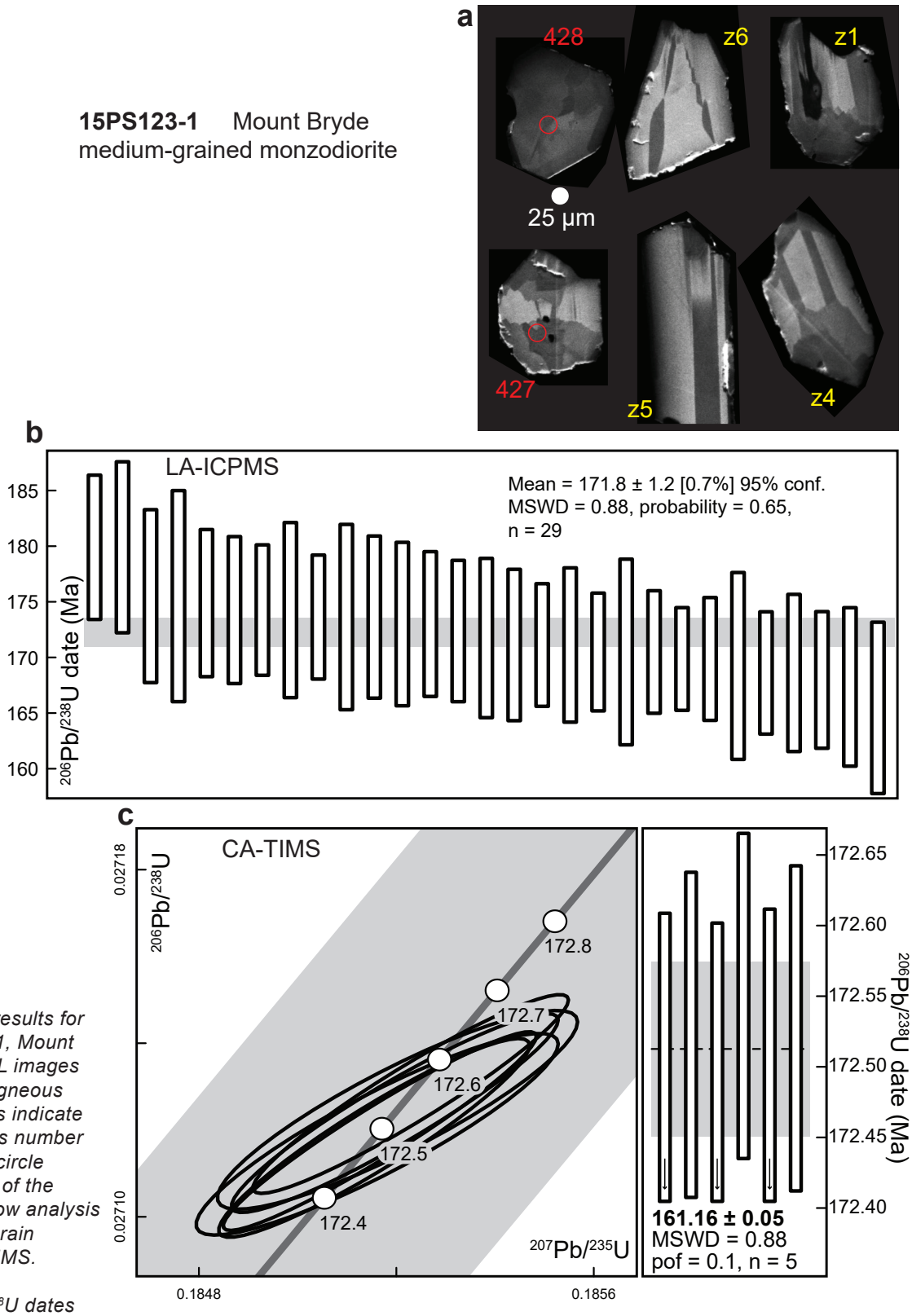


Figure 5-34. *U-Pb geochronological results for sample 15PS123-1, Mount Bryde stock.* ***(a)*** *CL images of representative igneous zircons. Red labels indicate LA-ICPMS analysis number with the red open circle indicating location of the analysis spot, yellow analysis number refers to grain analyzed by CA-TIMS.* ***(b)*** *Ranked plot of LA-ICPMS $^{206}Pb/^{238}U$ dates (Appendix 3). Grey horizontal bar shows calculated weighted mean with errors.* ***(c)*** *Concordia diagram (left) and ranked $^{206}Pb/^{238}U$ dates (right) for zircons analyzed by CA-TIMS (Appendix 4). The light grey band around concordia (dark grey line) shows the decay constant uncertainties. Analyses included in weighted mean age (light grey horizontal bar) calculations are bold; analyses with thin lines are not used in calculations. Arrows indicate data project off figure. Line-type designations are the same in all plots. Errors in all plots are at 2σ. MSWD = mean squared weighted deviation, pof = probability of fit, n = number of analyses included in age calculation.*

Fourth of July batholith

The Fourth of July batholith, with a mapped extent of 1121 km², is the largest Middle Jurassic pluton to intrude the northern Intermontane terranes (Fig. 5-1). The bulk of the batholith is located in northern British Columbia east of Atlin Lake; only its northernmost tip extends into southern Yukon where it has a mapped extent of 83 km² (Fig. 5-35; Table 5-1). The centre of the Yukon portion of the batholith is dissected by the Lubbock River and Atlin Lake valley (Fig. 5-36). The Fourth of July batholith intrudes late Paleozoic carbonate of the Horsefeed Formation to the west and early Mesozoic chert, siltstone and sandstone of the Cache Creek Group to the east, both constituents of the Cache Creek terrane, although the contact is concealed beneath younger cover in this region (Gordey and Stevens, 1994).

In British Columbia, the Fourth of July batholith is an undeformed, polyphase body composed of pink granite and granodiorite with a complex border phase that is more mafic in composition (Mihalynuk, 1999). Its northern tip in Yukon is composed of a relatively homogenous tonalite to diorite (Fig. 5-4) that is likely part of the border phase described by Mihalynuk (1999). The tonalite is locally cut by rare aplite dikes (Fig. 5-37). The best exposures of the northern tip of the batholith are along the shore of Atlin Lake (Fig. 5-38) and along the southern and eastern slopes of a series of forest-covered rounded hills to the northwest (Figs. 5-35 and 5-36). The medium-grained equigranular texture of the rock results in rounded 'bread loaf' shapes of weathered rock and the recessive margins are defined by joint surfaces (Fig. 5-38).

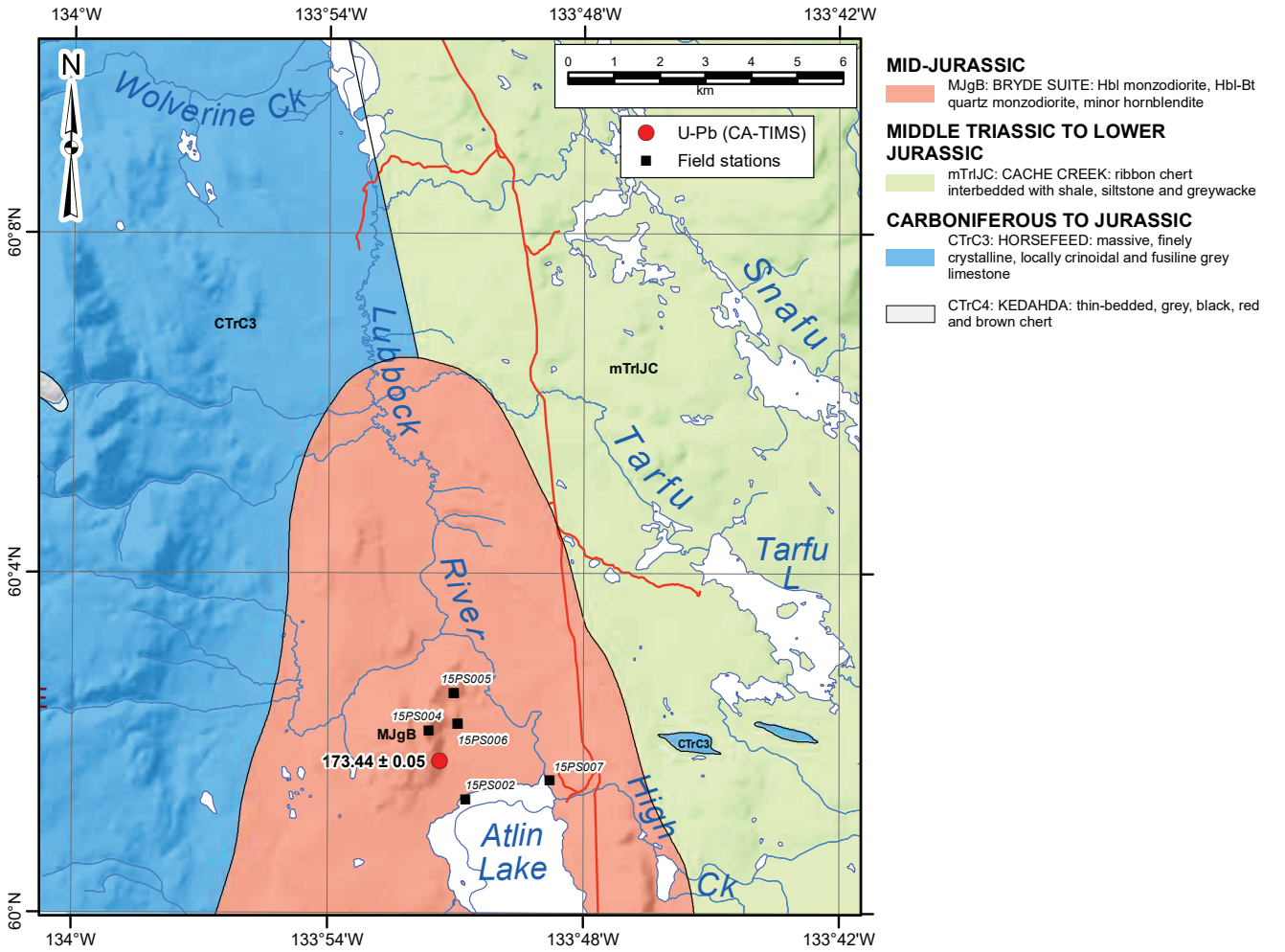


Figure 5-35. *Geology at the northern tip of the Fourth of July batholith in southern Yukon (after YGS, 2020a). L = lake; Ck = creek.*

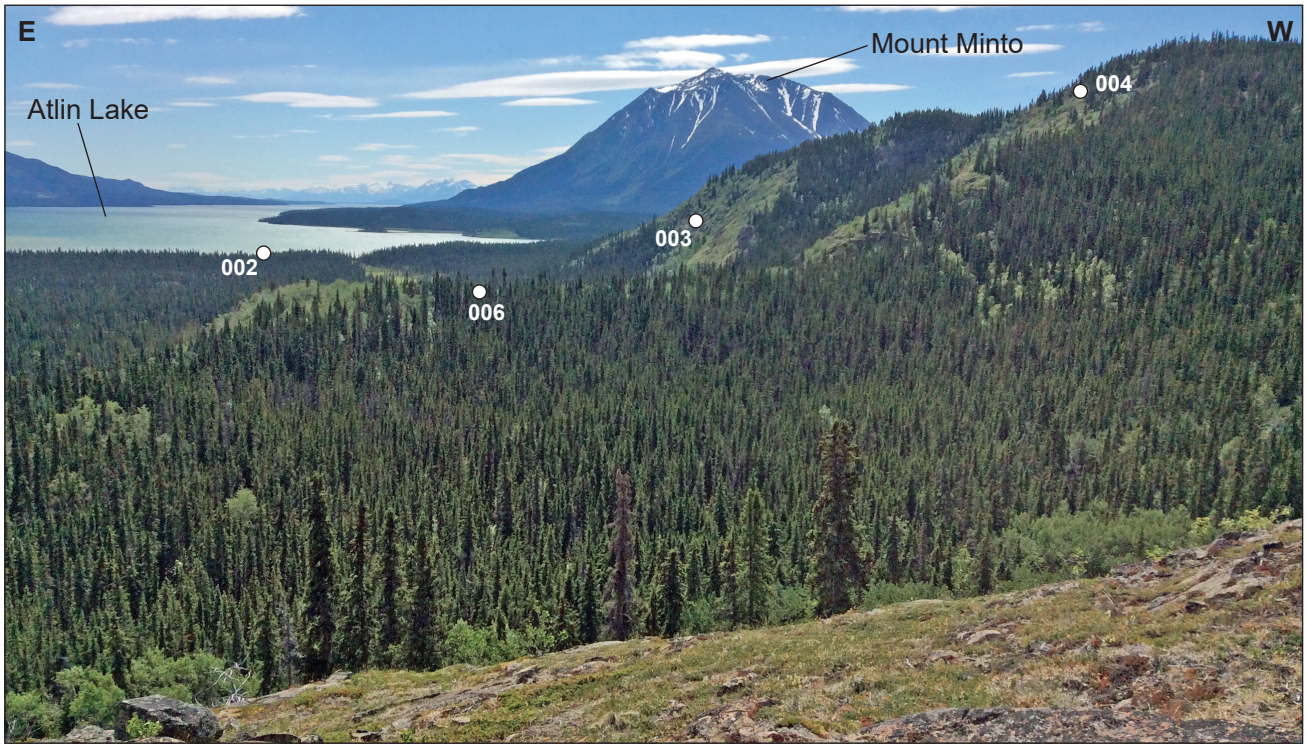


Figure 5-36. *Looking south from station 15PS005 towards Atlin Lake. Outcrop is mostly on the south and east sides of hills. Circles are approximate location of field stations, preceded by 15PS. Lubbock River just out the photo to the east.*



Figure 5-37*. Recessively weathered aplite dike within the Fourth of July batholith; 15PS005. Dike oriented N165/84. Hammer head to bottom right of dike is 13 cm across.*

Petrography

The Fourth of July batholith in Yukon is medium-grained and equigranular (Fig. 5-39). Fresh broken surfaces have abundant vitreous plagioclase (Fig. 5-40) and the rock has a tonalite to diorite composition (Fig. 5-2). The rock is mesocratic with mafic minerals making up 30–40% of the rock. Biotite is equal to, or more abundant than hornblende. Clinopyroxene is present in varying amounts between 1 and 20% of the rock and occurs primarily as cores mantled by hornblende or biotite (Fig. 5-41). Pyroxene mantled by hornblende or biotite is a diagnostic characteristic of the Fourth of July suite in northern British Columbia (Mihalynuk, 1999). Plagioclase, K-feldspar and mafic minerals are fresh. The majority of feldspars are plagioclase, but some grains have potassic cores; K-feldspar is fine grained and within the groundmass (Fig. 5-39). Epidote was only observed in one sample, 15PS002-1, and is secondary. Apatite is a ubiquitous accessory mineral and titanite is not observed.

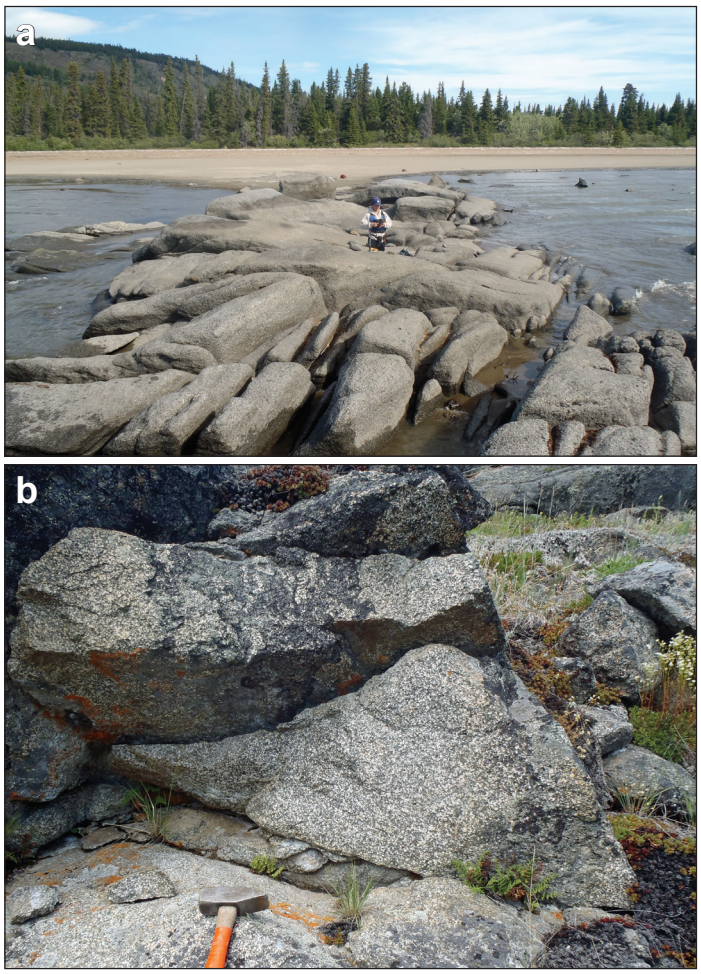


Figure 5-38. *Weathered outcrop in the Fourth of July batholith.* ***(a)*** *Rounded mesocratic diorite with recessively weathered jointing oriented N194/58; 15PS002.* ***(b)*** *Equigranular diorite displaying the mesocratic and equigranular nature of the northern tip of the batholith; 15PS003. Hammer head 13 cm across.*

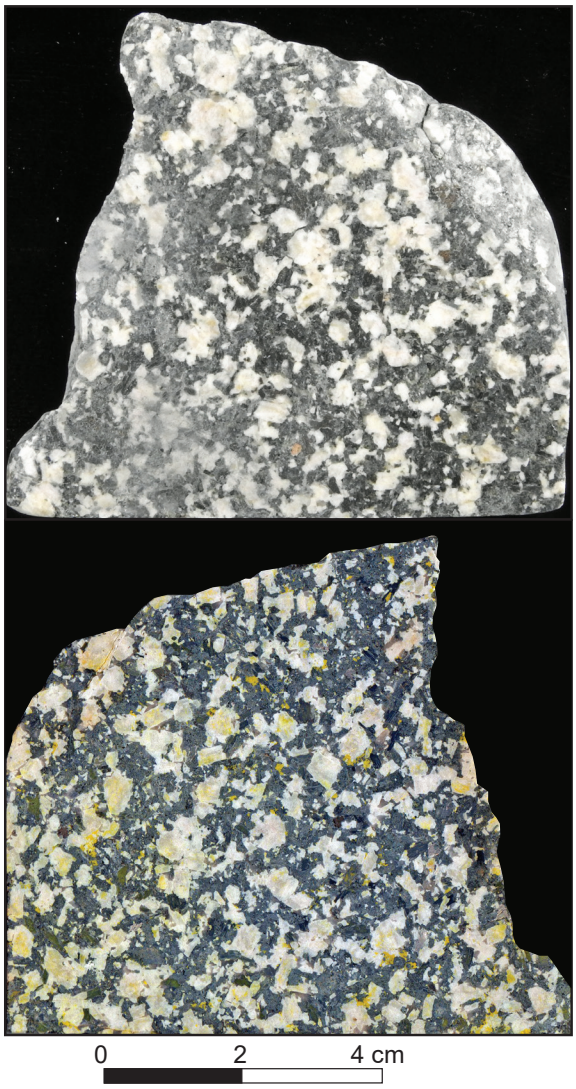


Figure 5-39. *Representative sample of the medium-grained equigranular diorite from the north end of the Fourth of July batholith; 15PS003-1. Slightly oxidized polished surface (upper) and a cobaltinitrite-stained surface (lower). Note K-feldspar is yellow, both images are same scale.*

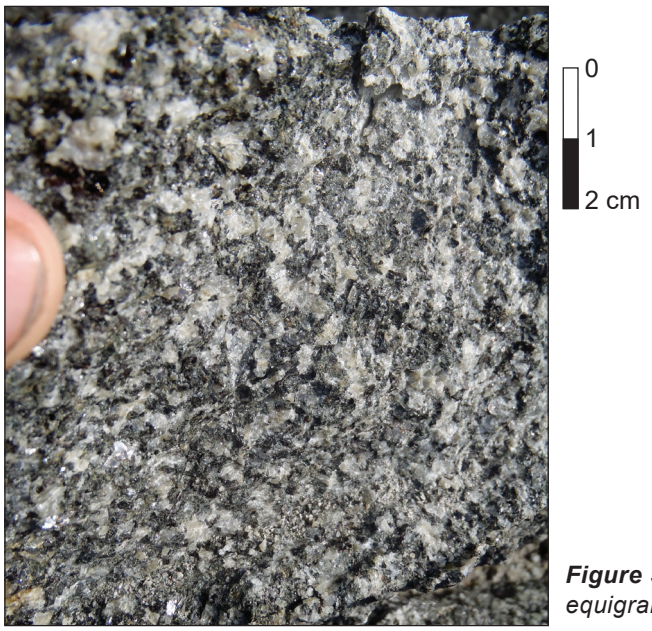


Figure 5-40. *Fresh broken face of medium-grained equigranular diorite; 15PS002.*

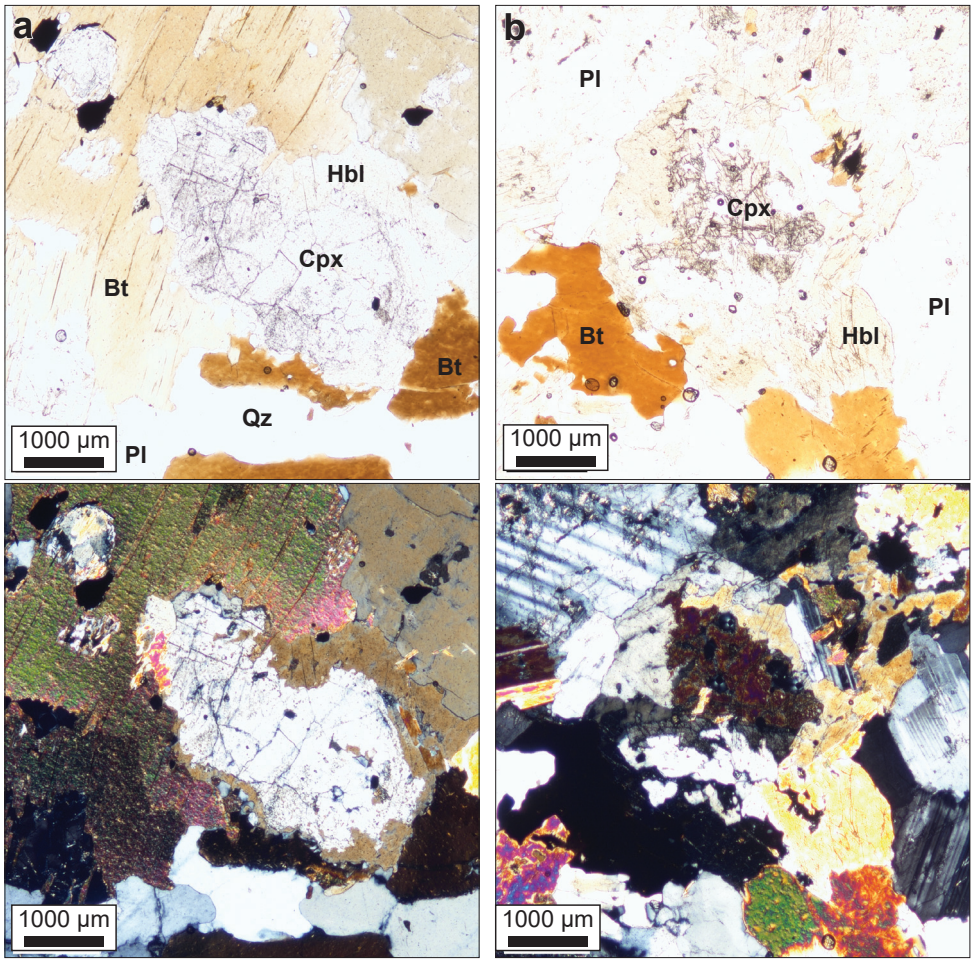


Figure 5-41. *Transmitted light photomicrographs from the Fourth of July batholith showing clinopyroxene mantled by hornblende and biotite. Plane polarized light (upper) and cross-polarized light (lower).* ***(a)*** *15PS002-1.* ***(b)*** *15PS003-1.*

Oxidation state and mineral occurrences

The Fourth of July batholith is reduced and magnetic susceptibilities range from 0.21 to 0.39 × 10^{-3} SI units (Figs. 5-3 and 5-42; mean 0.29 × 10^{-3} SI units; n = 6). The aeromagnetic map in this area closely mimics surficial features such as the Lubbock valley, which suggests the weak magnetic signature of the batholith is overwhelmed by surficial processes such as heavy mineral (*e.g.*, magnetite) concentration. There are no known mineral occurrences near the Fourth of July batholith in Yukon, nor are there significant mineral occurrences documented in the northern British Columbia portion of the batholith (Mihalynuk, 1999). However, quartz-molybdenite veins ~8 km southeast of Atlin have sericite alteration envelopes dated by K/Ar at 160 ± 2 Ma (Hunt and Roddick, 1988) which suggests possible association with the Middle Jurassic Fourth of July batholith (Mihalynuk, 1999).

Geochronology

Mihalynuk *et al.* (1992) reported U-Pb zircon dates from two samples of the Fourth of July batholith in northern British Columbia (multi-grains, TIMS, UBC; Fig. 5-1). Both samples yielded discordant results and ages were calculated from the upper intercept of isochrons anchored at zero. Diorite from the north-central portion of the Fourth of July batholith yielded an age of 170.4 ± 5.1 Ma, whereas a syenite from the southern end of the batholith has an age of 171.5 ± 3.4 Ma (Fig. 5-1). Hornblende and biotite from the Fourth of July batholith in northern British Columbia yielded $^{40}Ar/^{39}Ar$ cooling dates of *ca.* 173 and 165 Ma, respectively (Harris *et al.*, 2003; Hunt and Roddick, 1988).

Sample 15PS003-1 is a medium-grained diorite from the north end of the Fourth of July batholith in Yukon that was collected for combined LA-ICPMS and CA-TIMS analyses at Boise State University Fig. 5-35; Appendices 3 and 4). It yielded mostly elongate oscillatory zoned zircons with a few equant

sector zoned crystals, neither type with inherited cores (Fig. 5-43a). Thirty-five LA-ICPMS spot analyses yielded $^{206}Pb/^{238}U$ dates between 187 and 163 Ma, and a weighted mean of 176.1 ± 1.6 Ma (n = 34; Fig. 5-43b). Six zircons from 15PS003-1 were analyzed by CA-TIMS and yielded equivalent $^{206}Pb/^{238}U$ dates ranging from 173.53 ± 0.12 to 173.39 ± 0.12 Ma, with a weighted mean of 173.44 ± 0.05 Ma (MSWD = 0.86, n = 6; Fig. 5-43c).

Thermobarometry

Harris *et al.* (2003) provided Al-in-Hbl pressure estimates from the Fourth of July batholith near Atlin, British Columbia, that range from 0.7–3.1 kbar, with lowest pressure estimates mainly from the west side of Atlin Lake. Our sample 15PS002-1, collected along the shore of Atlin Lake in Yukon (Fig. 5-35), contains the suitable mineral assemblage for Al-in-Hbl geobarometry (Hammarstrom and Zen, 1986; Appendix 5). Al^{TOT} in hornblende for this sample is 0.70 and cotectic plagioclase that has X_{An} 0.41. Crystallization pressure estimates derived from these data are 0.33 ± 0.94 kbar (Appendix 5; emplacement depths <4.7 km). Solidus temperatures were calculated for two samples from the Fourth of July batholith using two different geothermometers. The amphibole-plagioclase geothermometer of Holland and Blundy (1994) was applied to sample 15PS002-1 and yielded an estimate of 672°C. The Ti-in-zircon geothermometer was applied to sample 15PS003-1 (collected ~1 km north of 15PS002-1) and yielded higher temperature estimates between 768 and 815°C (Watson *et al.*, 2006; Appendix 3).

Below ~2 kbar, the temperature of crystallization of calc-alkaline magma increases sharply as pressure drops. As a result, the concentration of Al in hornblende becomes increasingly temperature-sensitive at low pressure (Hollister *et al.*, 1987), making it an unreliable geobarometer. Nevertheless, we interpret the Fourth of July batholith to have been emplaced at a shallow crustal level given the consistently low pressure estimates from our sample and those of Harris *et al.* (2003).

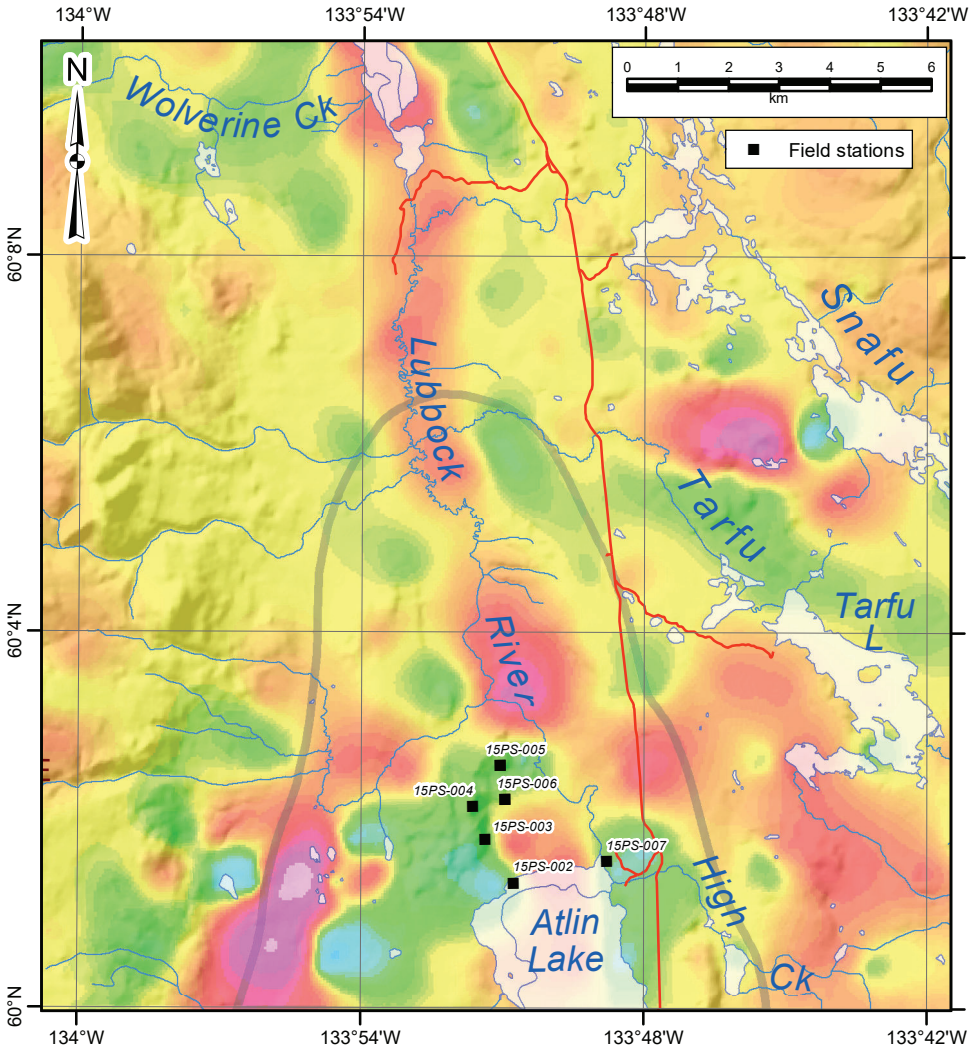


Figure 5-42. *Reduced to pole, first vertical derivative aeromagnetic map of the area around the northern tip of the Fourth of July batholith in Yukon (Aurora Geosciences Ltd. and Bruce, 2017e). L = lake; Ck = creek.*

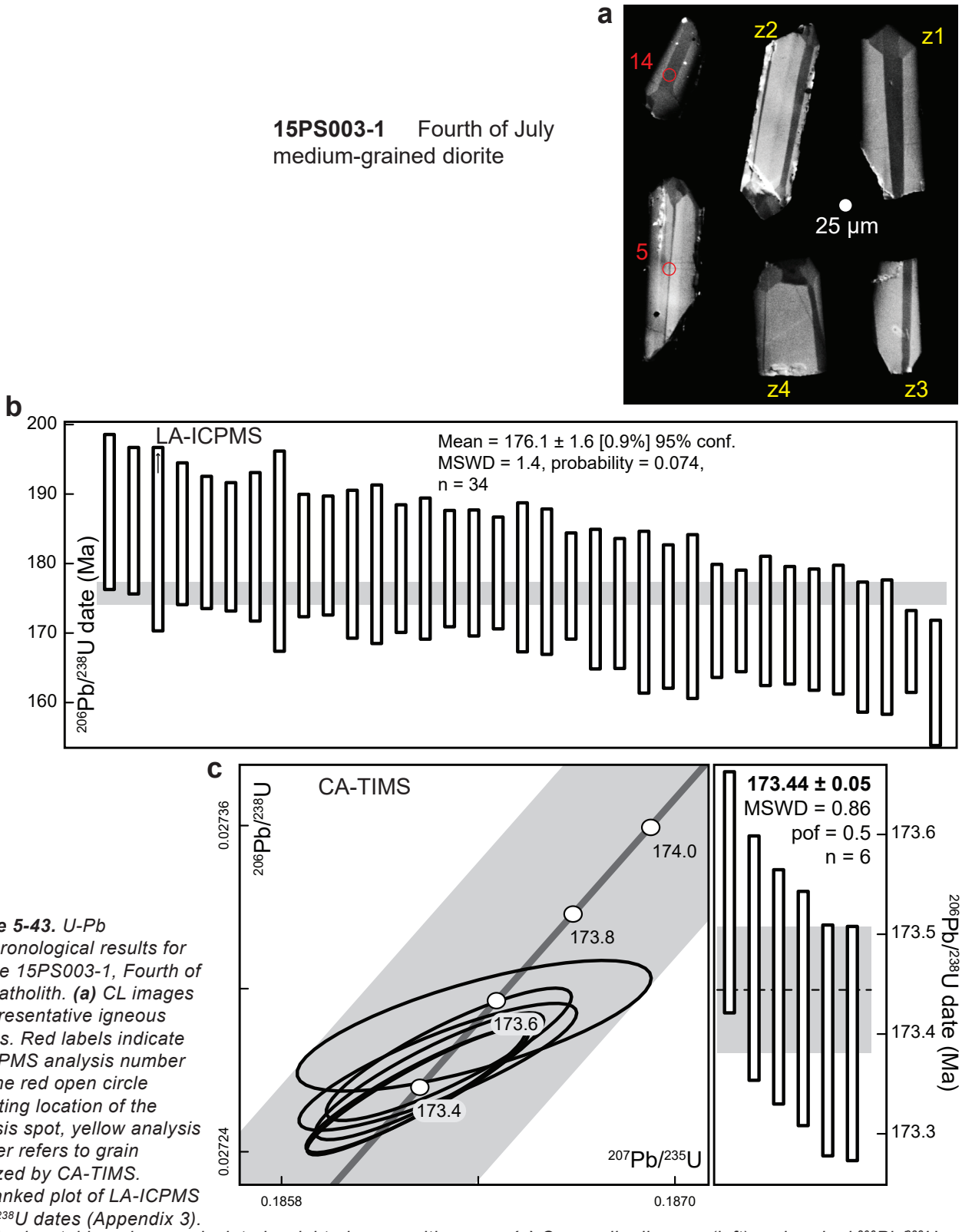


Figure 5-43. *U-Pb geochronological results for sample 15PS003-1, Fourth of July batholith.* ***(a)*** *CL images of representative igneous zircons. Red labels indicate LA-ICPMS analysis number with the red open circle indicating location of the analysis spot, yellow analysis number refers to grain analyzed by CA-TIMS.* ***(b)*** *Ranked plot of LA-ICPMS $^{206}Pb/^{238}U$ dates (Appendix 3). Grey horizontal bar shows calculated weighted mean with errors.* ***(c)*** *Concordia diagram (left) and ranked $^{206}Pb/^{238}U$ dates (right) for zircons analyzed by CA-TIMS (Appendix 4). The light grey band around concordia (dark grey line) shows the decay constant uncertainties. Analyses included in weighted mean age (light grey horizontal bar) calculations are bold; analyses with thin lines are not used in calculations. Arrows indicate data project off figure. Line-type designations are the same in all plots. Errors in all plots are at 2σ. MSWD = mean squared weighted deviation, pof = probability of fit, n = number of analyses included in age calculation.*

Geochemistry

Fifteen samples from plutons of the Bryde suite in Yukon were analyzed for whole-rock geochemistry (Appendix 8): 7 from the Teslin Crossing stock, 4 from the northern tip of the Fourth of July batholith, and 2 each from the Michie and Mount Bryde stocks.

Major elements

Plutons of the Bryde suite have SiO_2 ranging from 52.5–66.8% and show two distinct compositional trends, the Mount Bryde and Fourth of July samples plot in subalkalic, diorite to granodiorite fields and the Michie and Teslin Crossing stocks plot in the alkalic, monzodiorite to syenite fields (Fig. 5-44). Samples from the Teslin Crossing and Michie stocks are enriched in Al_2O3, Na_2O, K_2O, and generally have Nb/Y > 0.7 compared to the Fourth of July and Mount Bryde plutons (Figs. 5-44b and 5-45). The Fourth of July and Mount Bryde plutons are magnesian, metaluminous and calcic to calc-alkalic (Fig. 5-46). The Teslin Crossing samples straddle the magnesian to ferroan fields, are alkali-calcic to alkalic and mainly metaluminous. The two samples from the Michie stock are ferroan and strongly alkalic and straddle the metaluminous and peraluminous fields (Fig. 5-46). Plutons of the Bryde suite are all I-type in character (Fig. 5-47).

Trace elements

Trace element patterns for samples of the Bryde suite have negative Nb and Ti anomalies on primitive mantle normalized plots that are typical of continental crust or subduction-related magma (Fig. 5-48). Samples from the subalkalic rocks of the Bryde suite (Mount Bryde and Fourth of July plutons; Fig. 5-48a,b) have less pronounced slopes on primitive mantle normalized plots with La/Yb_N of 6.5–9.4 (average 8.0), and smaller Th enrichment indicated by Th/Nb_N ratios of 3.3–4.5 (average 4.0; Fig. 5-48a). On upper continental crust normalized plots, they have HREE concentrations near UCC and relatively depleted LREE and LILE (Fig. 5-48b). They show pronounced depletion of Hf relative to Eu.

The more alkalic rocks of the Teslin Crossing and Michie stocks show broader ranges of trace element concentrations, with many samples being more enriched in LREE and LILE than the Mount Bryde and Fourth of July plutons (Fig. 5-48c,d). On primitive mantle normalized plots they have relatively steep slopes with La/Yb_N of 5.8–16.5 (average 12) and pronounced Th enrichment (Th/Nb_N of 5.0–8.4, average 6.6). On continental crust normalized plots, samples from the Teslin Crossing and Michie stocks exhibit, for the most part, flat patterns equivalent or slightly depleted relative to UCC, with one sample from the Michie stock showing strong enrichment in overall trace elements, and another sample from the Teslin Crossing stock being strongly depleted relative to UCC (Fig. 5-48d). On the Ta *vs.* Yb tectonic discriminant diagram of Pearce *et al.* (1984), samples from the Bryde suite plot in the volcanic arc (VAG) field (Fig. 5-49).

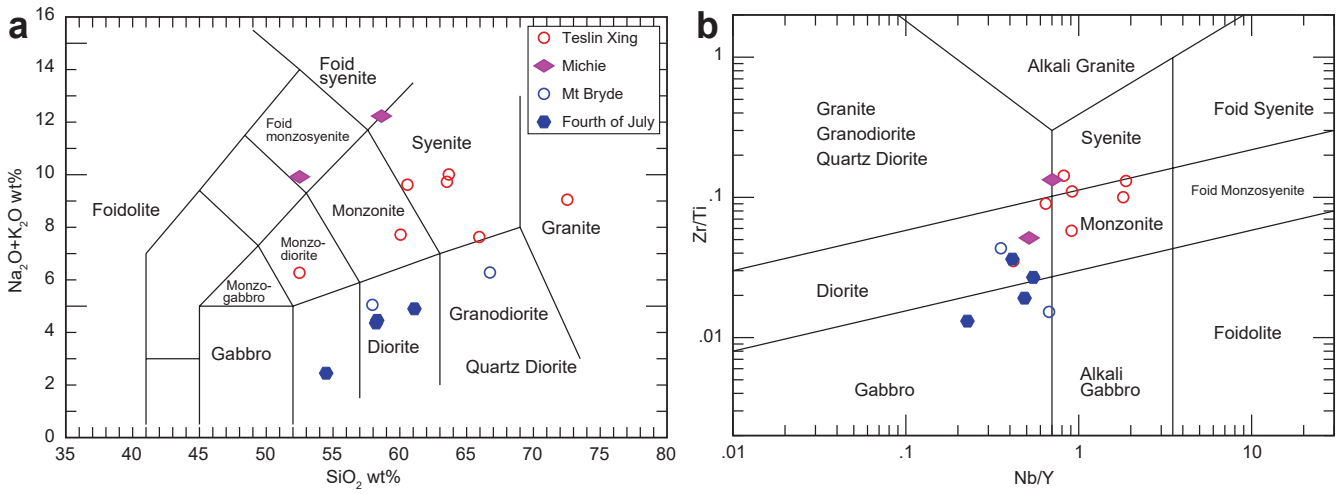


Figure 5-44. (a) *Total alkali-silica diagram for samples of the Bryde suite (adapted from LeBas et al., 1986, for plutonic rocks).* ***(b)*** *Zr/Ti vs. Nb/Y classification diagram of Winchester and Floyd (1977) as modified by Pearce (1996).*

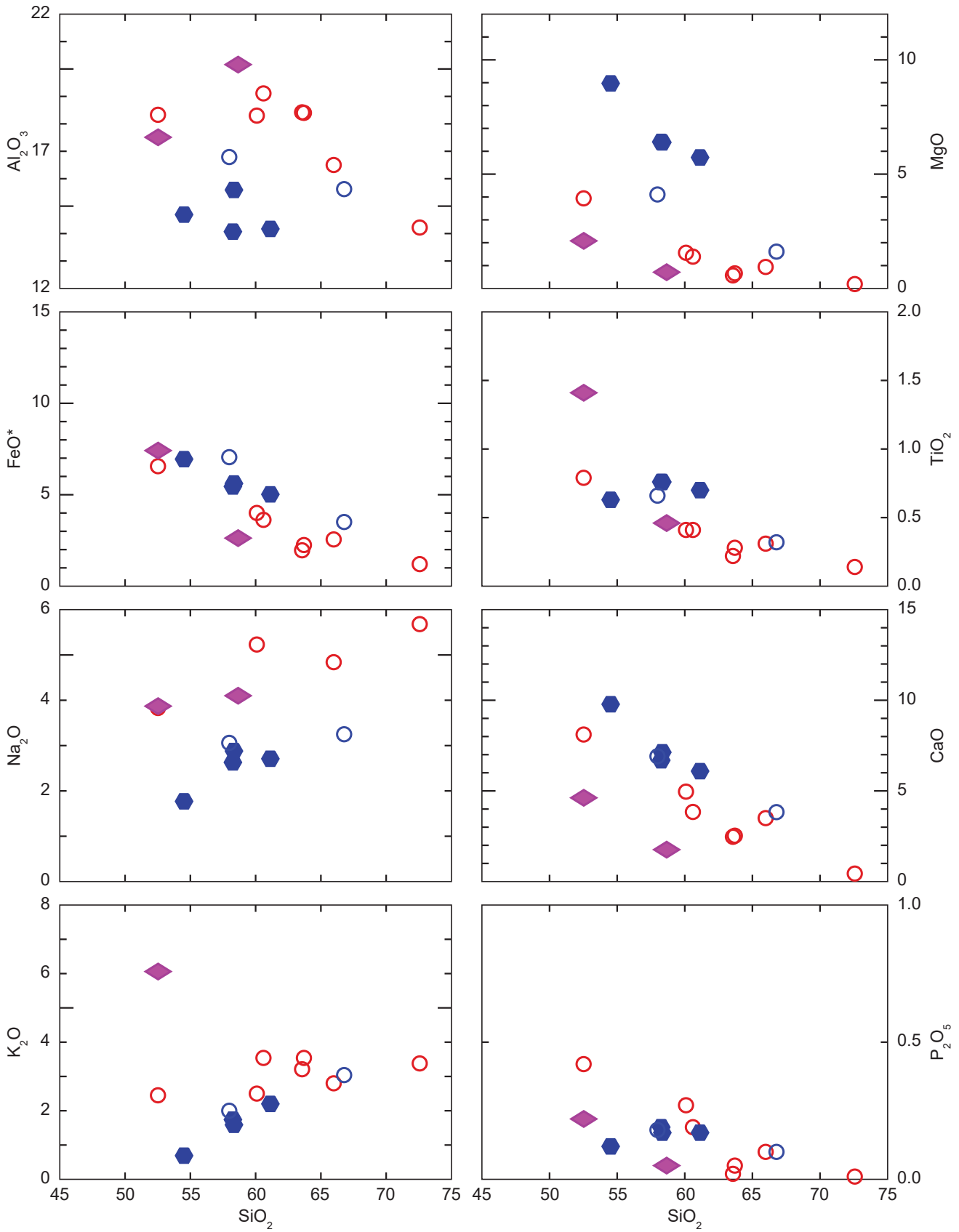


Figure 5-45. *Major elements vs. SiO_2 Harker plots for samples of the Bryde suite. Symbols as in Figure 5-44.*

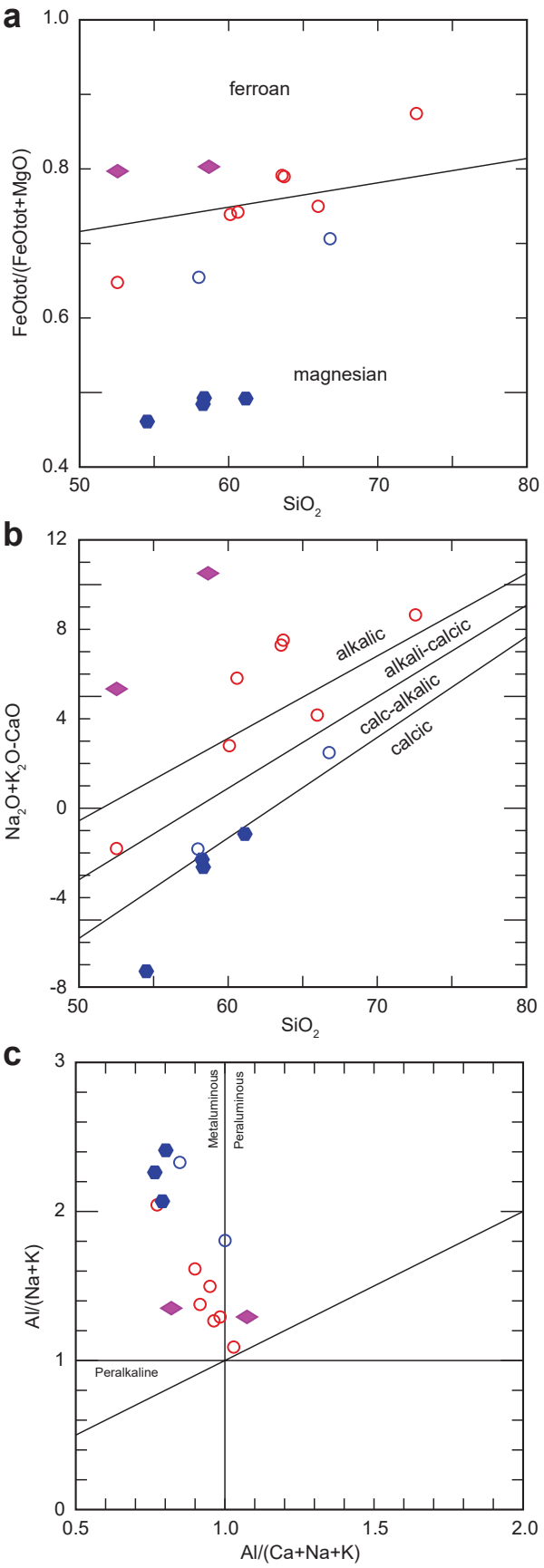


Figure 5-46. *Geochemical classification using criteria of Frost et al. (2001) for samples of the Bryde suite.* ***(a)*** *Fe-number,* ***(b)*** *modified alkali-lime index (MALI), and* ***(c)*** *alumina saturation index (ASI; after Maniar and Piccoli, 1989). Symbols as in Figure 5-44.*

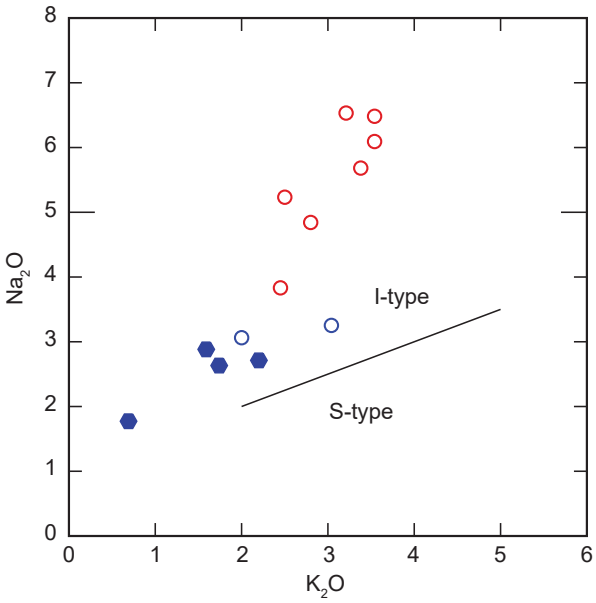


Figure 5-47. *Na_2O vs K_2O for samples of the Bryde suite. The boundary between 'I-type' and 'S-type' granitoid rocks is from Chappell and White (1974). Symbols as in Figure 5-44.*

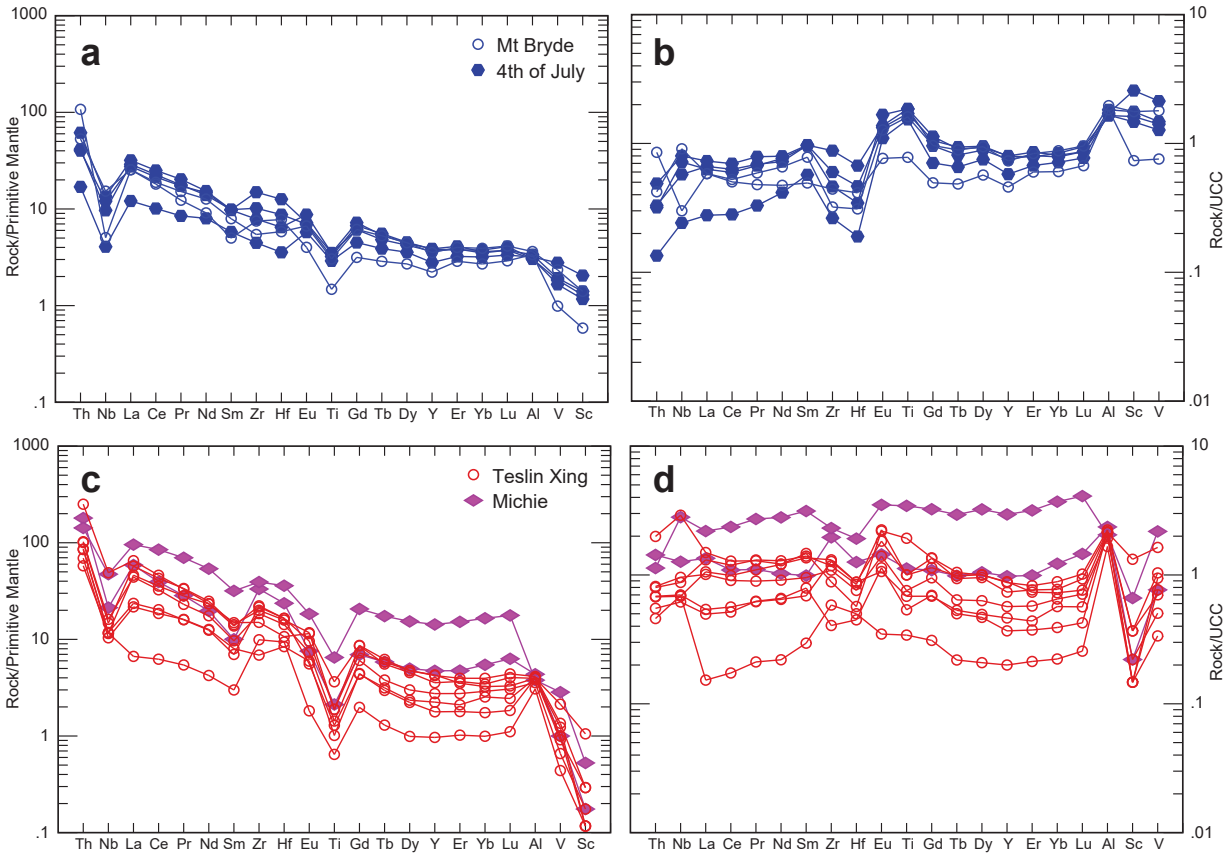


Figure 5-48. *Primitive mantle normalized (left; McDonough and Sun, 1995) and upper continental crust (UCC) normalized (right; McLennan, 2001) spider plots for samples of the Bryde suite.* ***(a*** *and* ***b)*** *Mount Bryde and Fourth of July plutons;* ***(c*** *and* ***d)*** *Teslin Crossing and Michie stocks. Symbols as in Figure 5-44.*

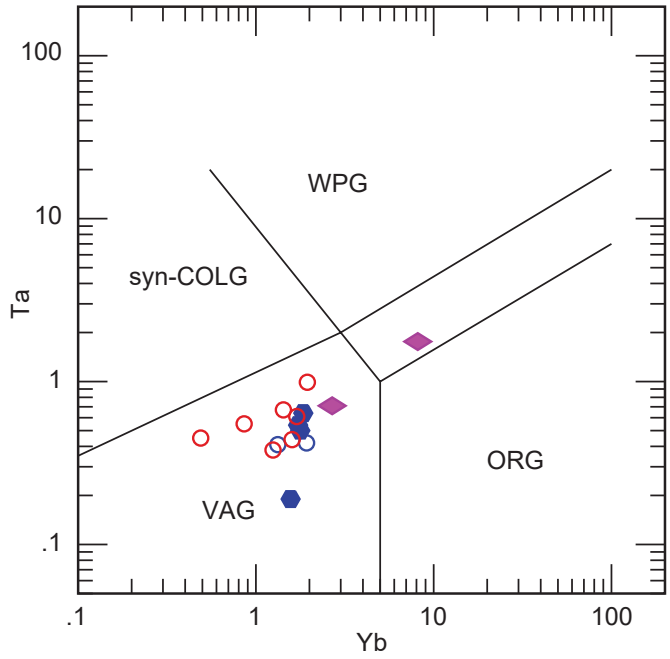


Figure 5-49. *Tectonic discrimination diagram for granites of the Bryde suite, from Pearce et al. (1984). VAG = volcanic arc granite, ORG = ocean ridge granite, WPG = within plate granite and COLG = collisional granite. Symbols as in Figure 5-44.*

Zircon chemistry

Trace element concentrations in zircons from the Bryde suite were analyzed by LA-ICPMS at Boise State University (Appendix 3). Plutons with subalkalic, diorite and granodiorite compositions (Mount Bryde and Fourth of July) have generally higher Hf concentrations (~8100–12 500 ppm) and Ti-in-zircon temperatures (750–815°C) than their alkalic counterparts in the suite (Fig. 5-50a). The Teslin Crossing zircons have the lowest range of Hf concentrations (~5500-7600 ppm) and Ti-in-zircon temperatures of 720–788°C. In the Michie stock, zircons have intermediate Hf values clustered between ~6500 and 8400 ppm and low Ti-in-zircon temperatures of 587–678°C (Fig. 5-50a).

With the exception of the Michie stock, zircons from plutons of the Bryde suite generally have moderate U and Y concentrations typical of more mafic arc magma (Fig. 5-50b), and zircons from the Fourth of July and Mount Bryde plutons straddle the within-plate field on the discriminant plot of Grimes *et al.* (2015; Fig. 5-50c). Zircons from the Teslin Crossing pluton are generally more intermediate and have slightly higher U concentrations. The Michie stock zircons are very distinct with high U (~1100 to 5170 ppm; Fig. 5-50b) and Gd/Yb generally >0.8; they plot off-scale in the Grimes *et al.* (2015) diagram (Fig. 5-50c).

Isotopes

A single sample from each pluton of the Bryde suite was analyzed for whole-rock Sr and Nd, and K-feldspar Pb isotopes (Appendix 9). Samples of the Bryde suite are generally juvenile with $^{87}Sr/^{86}Sr_i$ of 0.7040–0.7050, εNd_t of +0.5 – +3.5 and $^{207}Pb/^{204}Pb$ in feldspar of 15.63–15.65. Isotopic signatures are indicative of a small amount of mixing with evolved crustal components (Fig. 5-51).

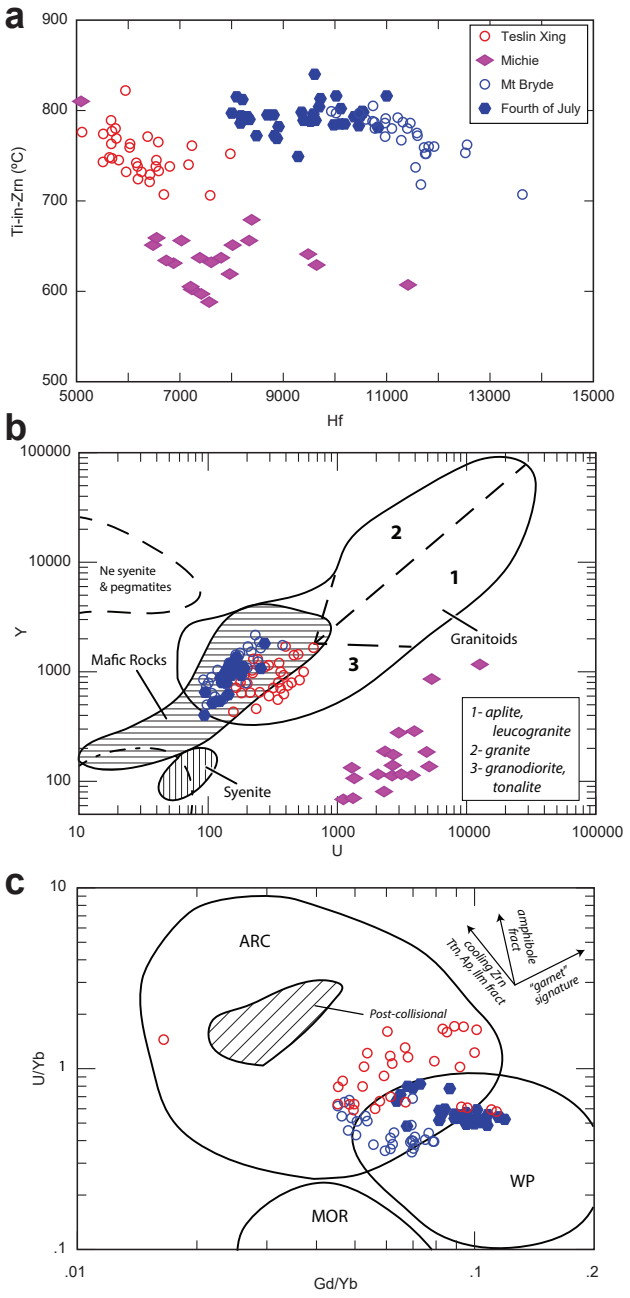


Figure 5-50. *Trace element zircon chemistry from LA-ICPMS analyses of samples from Bryde suite (Appendix 3).* ***(a)*** *Plots of crystallization temperature estimates (Ti-in-zircon) vs. Hf concentrations in zircons.* ***(b)*** *Y vs. U classification diagram of Belousova et al. (2002).* ***(c)*** *Discriminant diagram of Grimes et al. (2015).*

Zircons from three plutons of the Bryde suite (Teslin Crossing, Michie and Fourth of July) were also analyzed for Lu-Hf by split-stream LA-ICPMS at Memorial University of Newfoundland (Appendix 10). Hafnium isotopes in these zircons show similar trends as whole-rock isotopes from these plutons; zircons from the Teslin Crossing stock have higher (more juvenile) εHf_i values of +6.8 to +8.4, the Fourth of July batholith has slightly lower εHf_i of +4.7 to +7.0, and those from the Michie stock showing the lowest εHf_i values between +0.8 and +3.8 (Fig. 5-52).

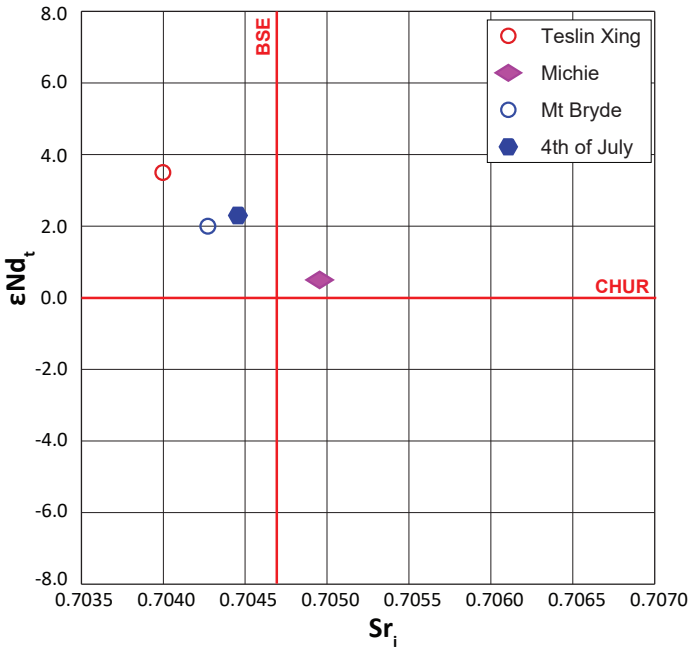


Figure 5-51. *Whole-rock Nd and Sr isotopic data for the Bryde suite (Appendix 9). Plot of εNdt vs. initial $^{87}Sr/^{86}Sr$. BSE = bulk silicate Earth; CHUR = chondrite uniform reservoir.*

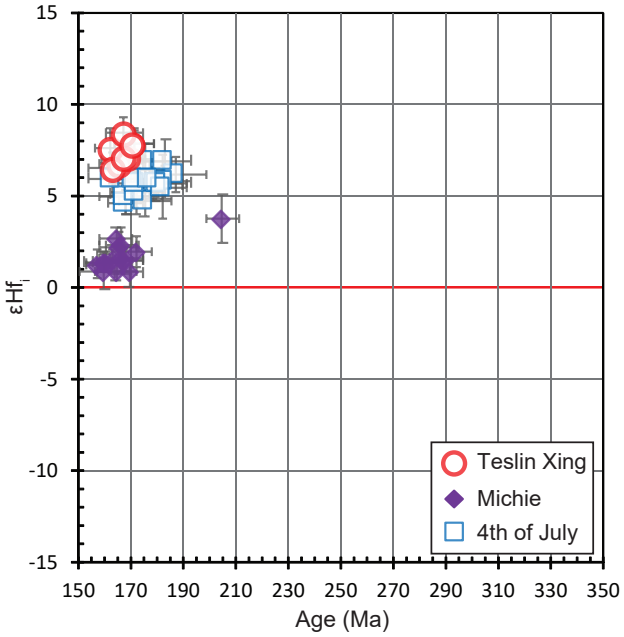


Figure 5-52. *Hf isotopic data for selected zircons from the Bryde suite (Appendix 10). Error bars are 2σ.*

Discussion

The Bryde suite comprises relatively juvenile, bimodal alkalic-mafic plutons that intrude Stikinia, the Cache Creek terrane and Whitehorse trough (Figs. 5-1, 5-4, 5-21, 5-29 and 5-35). Whole-rock and K-feldspar isotopic data suggest only minor assimilation of evolved crustal rocks (Fig. 5-51), an interpretation supported by the lack of inherited zircon in all Bryde suite plutons (Figs. 5-18 to 5-20, 5-28, 5-34 and 5-43; Table 5-1). The suite is well constrained to 174 to 168 Ma (Fig. 5-53; Table 5-1). All Bryde suite plutons are metaluminous with the Teslin Crossing and Michie plutons ferroan alkali-calcic to alkalic and the Fourth of July and Mount Bryde plutons magnesian, calc-alkalic to calcic (Fig. 5-46). The suite was likely emplaced at upper crustal levels based on small surface area, intricate geometry of plutons, very fine grained groundmass in porphyritic rocks (*e.g.*, Teslin Crossing), low regional metamorphic grade of country rocks (*e.g.*, Michie), and estimates of low pressure from the northern tip of the Fourth of July batholith (≤2 kbar). Both the Teslin Crossing and Michie stocks have metamorphic aureoles imposed on the surrounding sedimentary rocks of the Whitehorse trough (Laberge Group). All plutons of the Bryde suite are undeformed and cut regional structures, thus constraining the regional deformation to pre-173 Ma (Mihalynuk *et al.*, 2004).

The oxidized state (Fig. 5-3) and minor crustal contamination (Fig. 5-51) of the Bryde suite suggests that metals such as copper and possibly

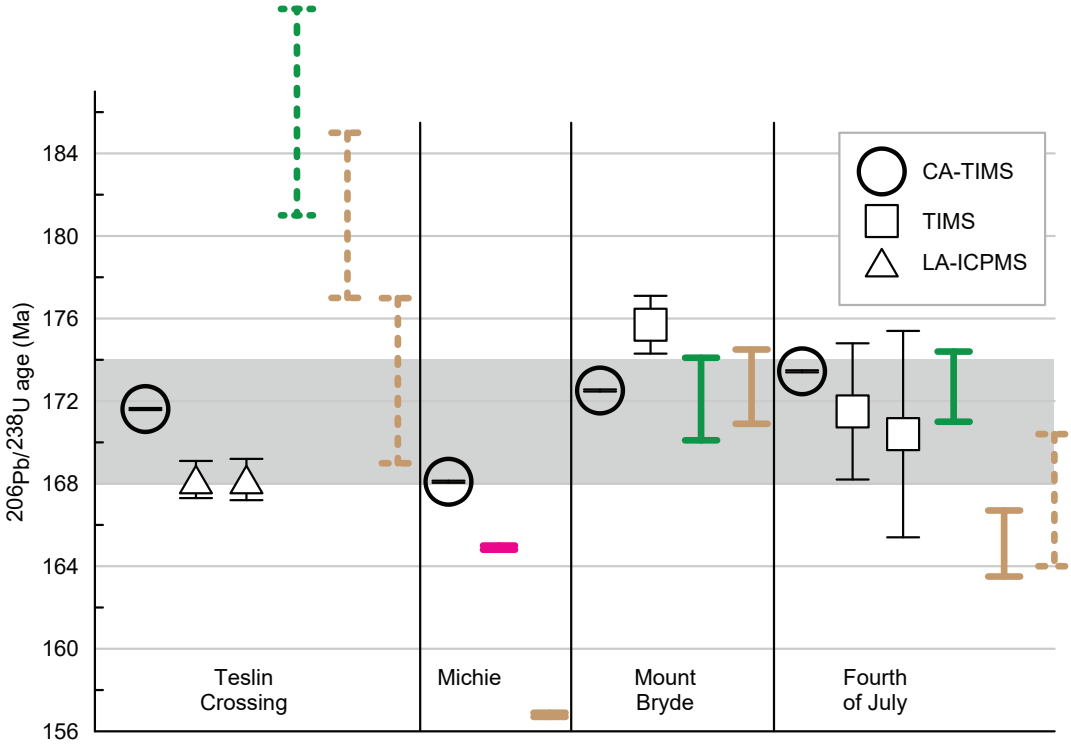


Figure 5-53. *Summary of geochronological data for Bryde suite plutons. Light grey shaded box between 174 and 168 Ma defines zircon crystallization range. U-Pb zircon ages symbolized by analytical method. Hornblende (green), biotite (brown) and muscovite (pink) are Ar/Ar ages; solid = step heating; dashed = total fusion. Data sources: this study; Stevens et al. (1982a); Mihalynuk et al. (1992); Harris et al. (2003), Hunt and Roddick (1994); Bickerton et al. (2020).*

molybdenum (Fig. 5-54) would have been mobile in the magma, and thus could have been transported to form deposits. As these plutons were likely emplaced at upper crustal levels, the confining pressure may have been low enough to allow formation of porphyry-epithermal systems (Seedorff *et al.*, 2005). The Teslin Crossing stock is an alkalic porphyry target with gold-rich mineralization (Hart, 1997c).

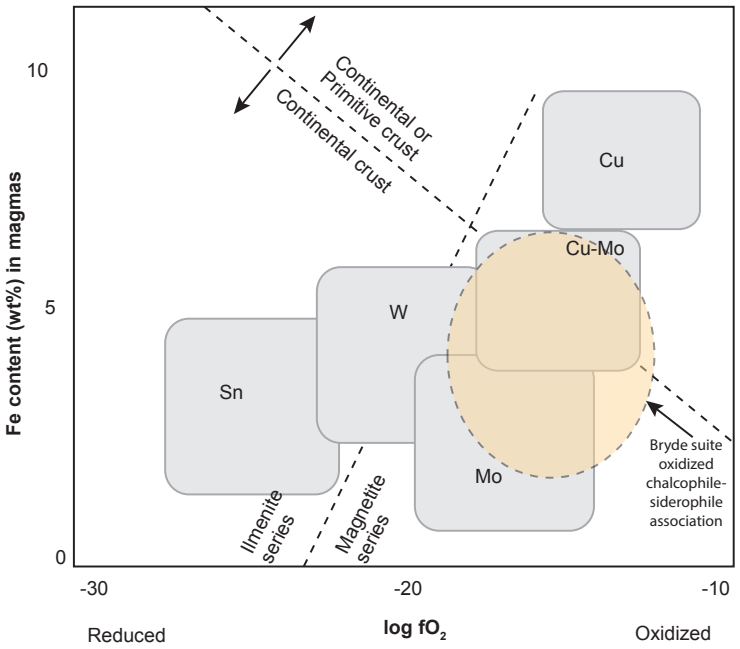


Figure 5-54. *Schematic plot of degree of fractionation, shown by the Fe content, versus oxidation state (fO_2) for calc-alkalic to alkalic magmas associated with magmatic-hydrothermal mineralization (modified from Thompson et al., 1999). The generalized position of the Bryde suite, with a potential Cu-Mo (chalcophile-siderophile) association is shown by the orange ellipse. Boundary between the magnetite and ilmenite magma series is from Ishihara (1977).*

Chapter 6
Late Jurassic

McGregor suite (163–146 Ma)

Summary

The McGregor batholith intrudes Quesnellia within a structural panel bound by the Teslin and Towhata faults in central Yukon. It comprises two phases: 1) a dominant, coarse-grained, equigranular to K-feldspar porphyritic, hornblende granodiorite; and 2) a fine to medium-grained, equigranular two-mica granodiorite, which occurs near the centre of the batholith and along its southwestern margin. The McGregor batholith is reduced and has a generally subdued aeromagnetic response except for a magnetic halo outlining the central body of two-mica granodiorite. The dominant hornblende granodiorite phase of the McGregor batholith is dated at 163.42 ± 0.05 and 161.16 ± 0.05 Ma. The age of the two-mica granodiorite phase is not as well constrained, with a scatter of U-Pb zircon and $^{40}Ar/^{39}Ar$ muscovite dates indicating crystallization at *ca.* 155–146 Ma. The McGregor batholith has the composition of calc-alkalic to mildly alkalic, 'I-type', peraluminous, ilmenite series granitoid rocks. Isotopic data are consistent with mixing of evolved crustal components into the magma. The hornblende granodiorite was emplaced at ~5 kbar, or ~18 km depth, and may be prospective for Au-W mineralization associated with skarn or possibly reduced intrusion-related gold systems. The McGregor batholith is unique in Yukon and one of the few Late Jurassic plutons to intrude the Intermontane terranes in the northern Canadian Cordillera.

Introduction

The Late Jurassic McGregor suite comprises a single pluton in Yukon, the McGregor batholith, which intrudes Quesnellia northeast of the Teslin fault, 40 km north of Carmacks (Fig. 6-1). The McGregor batholith is a composite pluton with an older, dominant phase of hornblende granodiorite (*ca.* 163–161 Ma) intruded by a younger phase of two-mica granodiorite near the centre and the southern margin of the batholith (poorly dated at ~155–146 Ma; Fig. 6-2; Table 6-1). Both phases of the McGregor batholith are primarily composed of granodiorite and minor monzodiorite (Fig. 6-3) and generally have low magnetic susceptibility (Fig. 6-4).

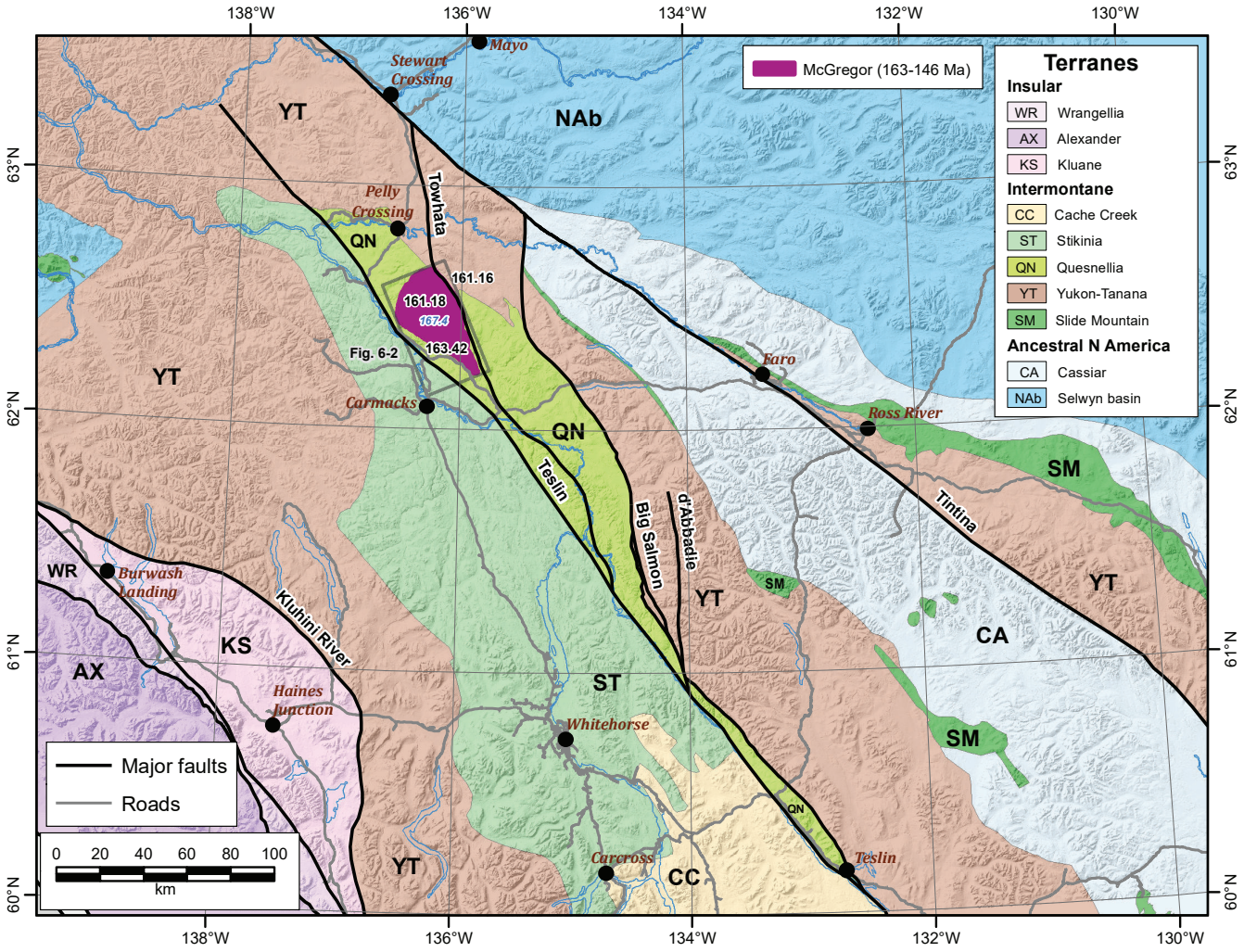


Figure 6-1. *Distribution of the Late Jurassic McGregor suite in southern Yukon. U-Pb dates are indicated next to plutons – black numbers are zircon CA-TIMS ages (this study); blue, italicized numbers indicate samples dated by other U-Pb techniques from previous work (see Appendix 1 for geochronology compilation). Terrane map is modified after Colpron and Nelson (2011).*

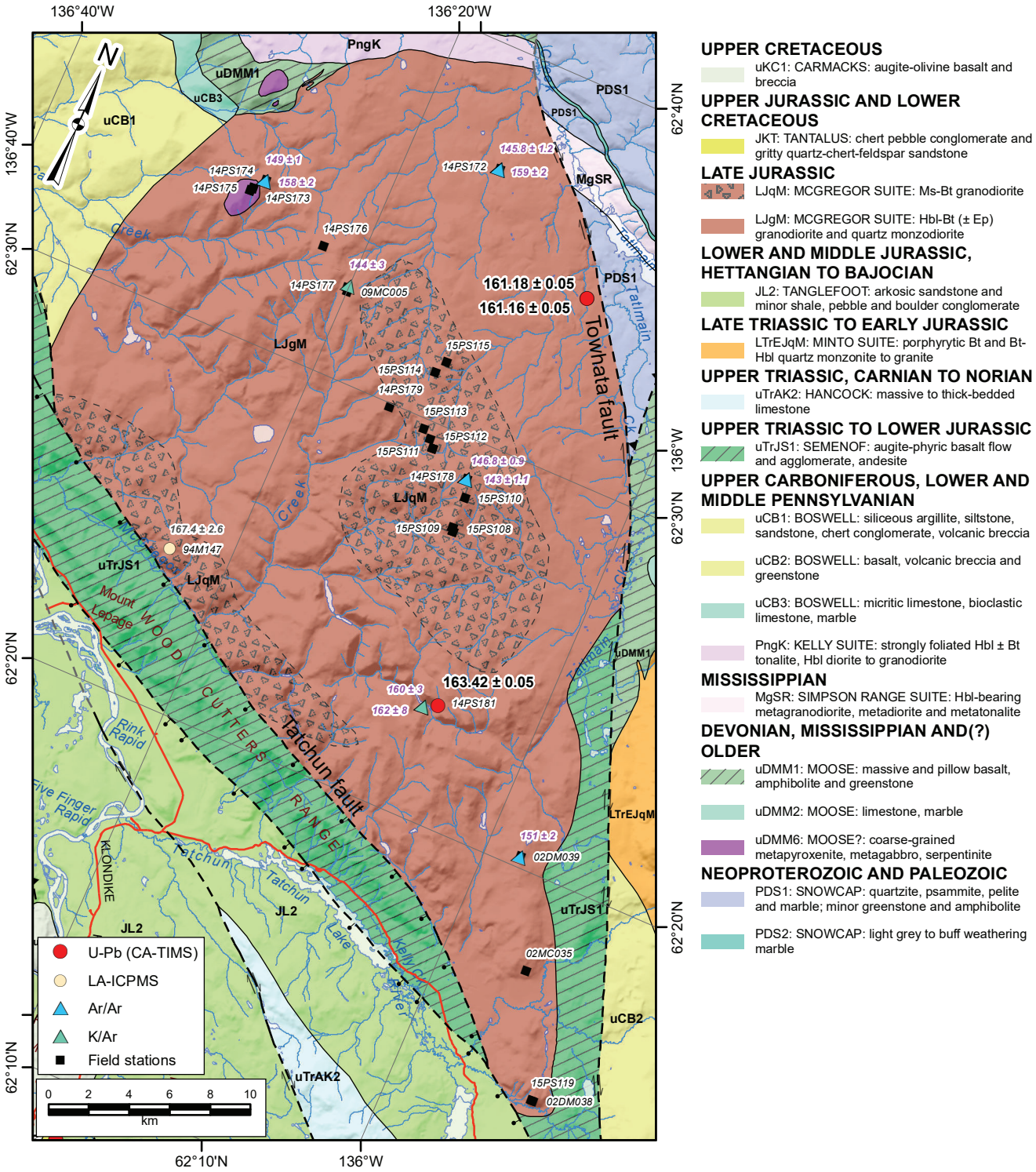


Figure 6-2. *Geology of the McGregor batholith (geology from YGS, 2020a); fault symbology as in Figure 1-4. Note that the geographic reference frame has been rotated with North pointing to the upper right of the page.*

Table 6-1. *Summary of characteristics for the Late Jurassic McGregor batholith.*

Pluton	NTS	Area (km²)	Terrane[1]	Rock[2]	Composition[3]	Oxidation state[4]	Age (Ma)[5]	Al-in-hbl barometry (kbar)[6]	Ti-in-zrn temp. (°C)[7]	Isotopes[8]	Inheritance[9]	Comment	Reference
Main phase	105L/5, 115I/8-9	686	QN	Hbl-Bt granodiorite	alkali-calcic to alkalic; peraluminous	reduced; weakly oxidized in aureole of younger phase	163.42 ± 0.05 161.16 ± 0.05	4.5–5.3	589–692	εNd: -0.1–0.7 Sr_i: 0.7055 $^{207/204}$Pb: 15.713 εHf_{zrn}: 0.8–4.2	318, 198 Ma	BSU, CA-TIMS	this study
Two-mica phase	115I/8-9	centre: 122 SW: 55	QN	Bt-Ms granodiorite, tonalite	calc-alkalic to alkali-calcic; peraluminous	reduced	≥ 147 Ma	–	590–807	–	–	GSC, Ar-Ar Ms	this study

Notes:

[1] host terrane to intrusion. QN – Quesnellia
[2] rock types from Figs. 6-3 and 6-23. Aug – augite; Bt – biotite; Hbl – hornblende; Qz – quartz
[3] composition from Fig. 6-25b
[4] oxidation state from Fig. 6-4
[5] best age from pluton, as discussed in text
[6] crystallization pressure estimates from Al-in-hornblende barometry, Appendix 5
[7] crystallization temperature from Ti-in-zircon thermometry, Appendix 3
[8] whole rock Nd and Sr data; K-feldspar Pb data (Appendix 9); Hf in zircon data (Appendix 10)
[9] inheritance determined from U-Pb LA-ICPMS analyses of zircon (Appendix 3)

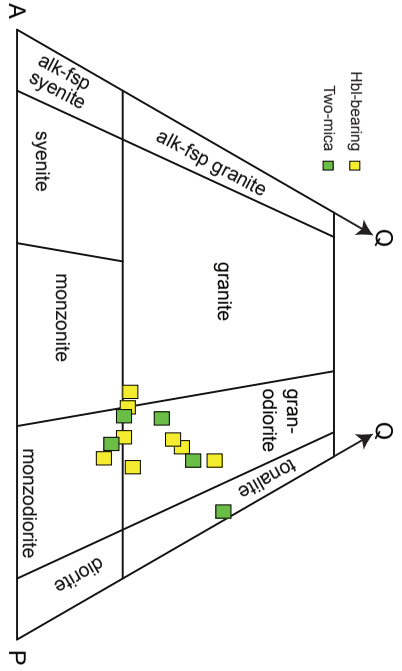


Figure 6-3. *Simplified quartz-alkali-feldspar-plagioclase (QAP) plot for samples of the McGregor batholith (after Le Bas and Streckeisen, 1991).*

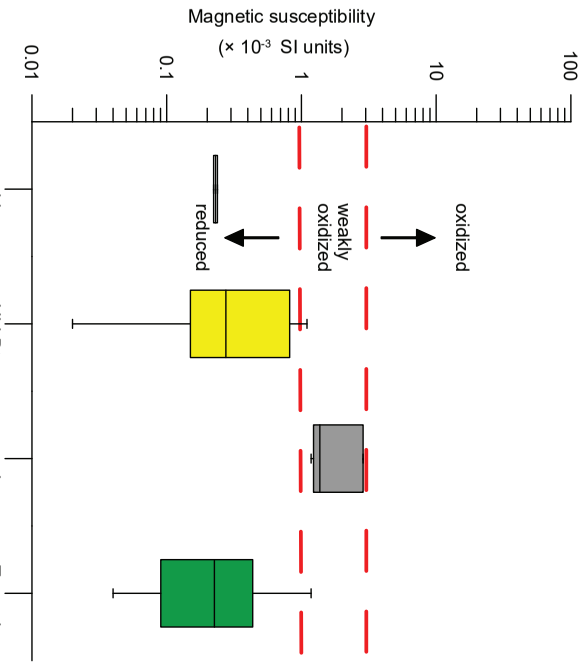


Figure 6-4. *Box and whisker plot of magnetic susceptibility measurements for the McGregor batholith (Appendix 2). Divisions between reduced to weakly oxidized (1 × 10^{-3} SI units), and weakly oxidized to oxidized (3 × 10^{-3} SI units) are from Hart et al. (2004a,b). Ends of boxes are 75th and 25th percentile of data, black line within boxes indicate median (50th percentile) of data, whiskers 95th and 5th percentile. Colours are as in Fig.6-3. Note the aureole (grey box) refers to measurements taken within the contact aureole between the two phases.*

McGregor batholith

The McGregor batholith underlies a poorly exposed area of 864 km² north of Tatchun Lake and the Wood Cutters Range in central Yukon (Figs. 6-1 and 6-2). The batholith is named for McGregor Creek which drains southwards from the centre of the pluton (Fig. 6-2). The landscape around the McGregor batholith consists mostly of sparse bedrock exposure on rounded ridges and a few outcrops in deeply eroded valleys (Fig. 6-5a,b). Although the majority of the McGregor batholith remained unglaciated during the most recent Cordilleran glaciation, the glacial limit of the McConnell ice sheet (*ca.* 22 Ka) cut across the eastern and southern edges of the pluton (Fig. 6-6). Much of the batholith is overlain by a thin veneer of till deposited during the Reid glaciation (*ca.* 200 Ka) and by locally thick glaciofluvial deposits (Jackson, 1997b,c). The erosive action of glacial melt water

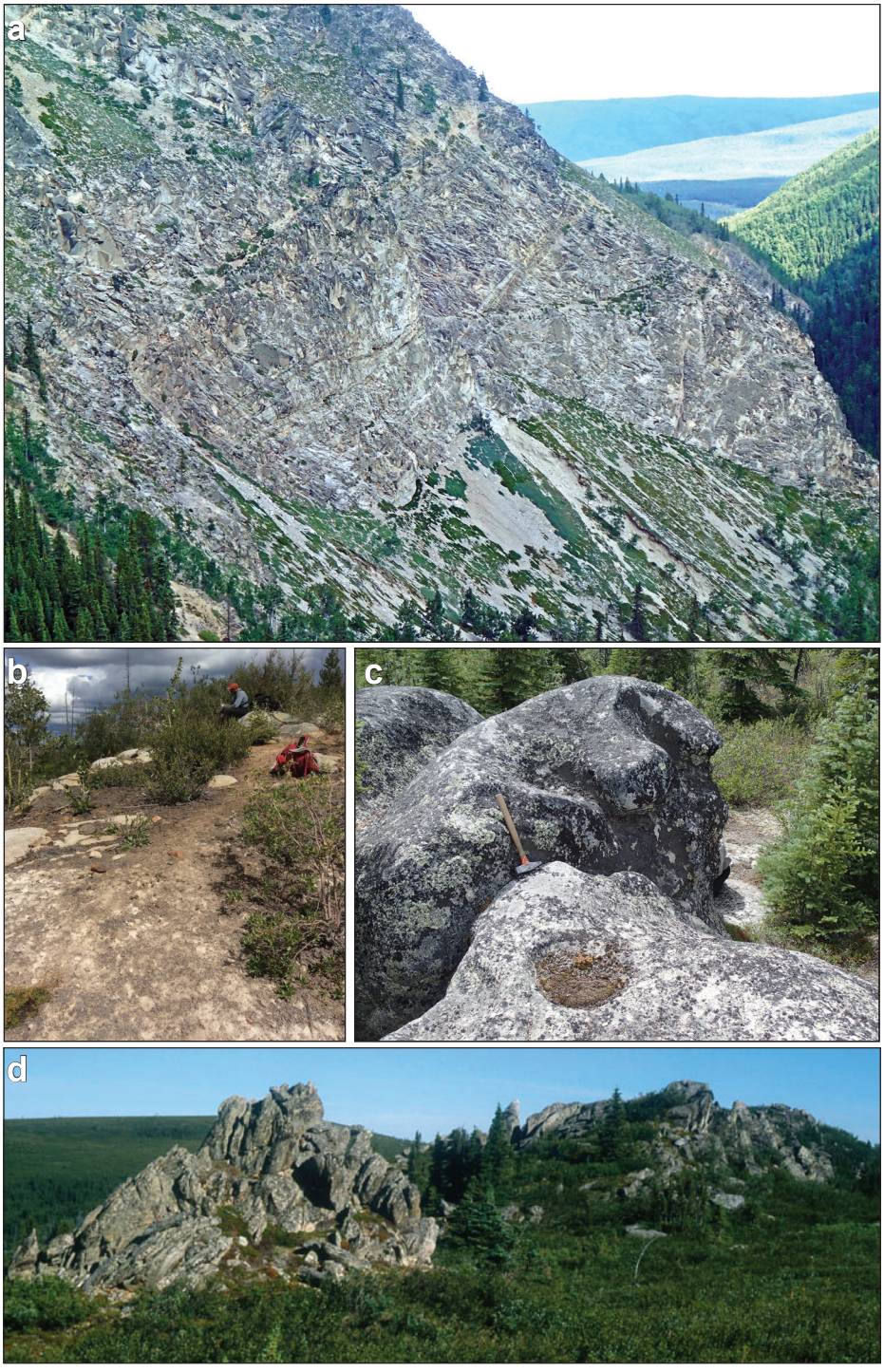


Figure 6-5. (a) *Deeply eroded valley on upper Tatlmain Creek in the main phase of the McGregor batholith.* ***(b)*** *Typical rounded, weathered outcrop from the centre of the McGregor batholith, 15PS110.* ***(c)*** *Potholes and polished surfaces characteristic of water erosion in the periglacial environment, 14PS178.* ***(d)*** *Tors in the west-central part of the McGregor batholith.*

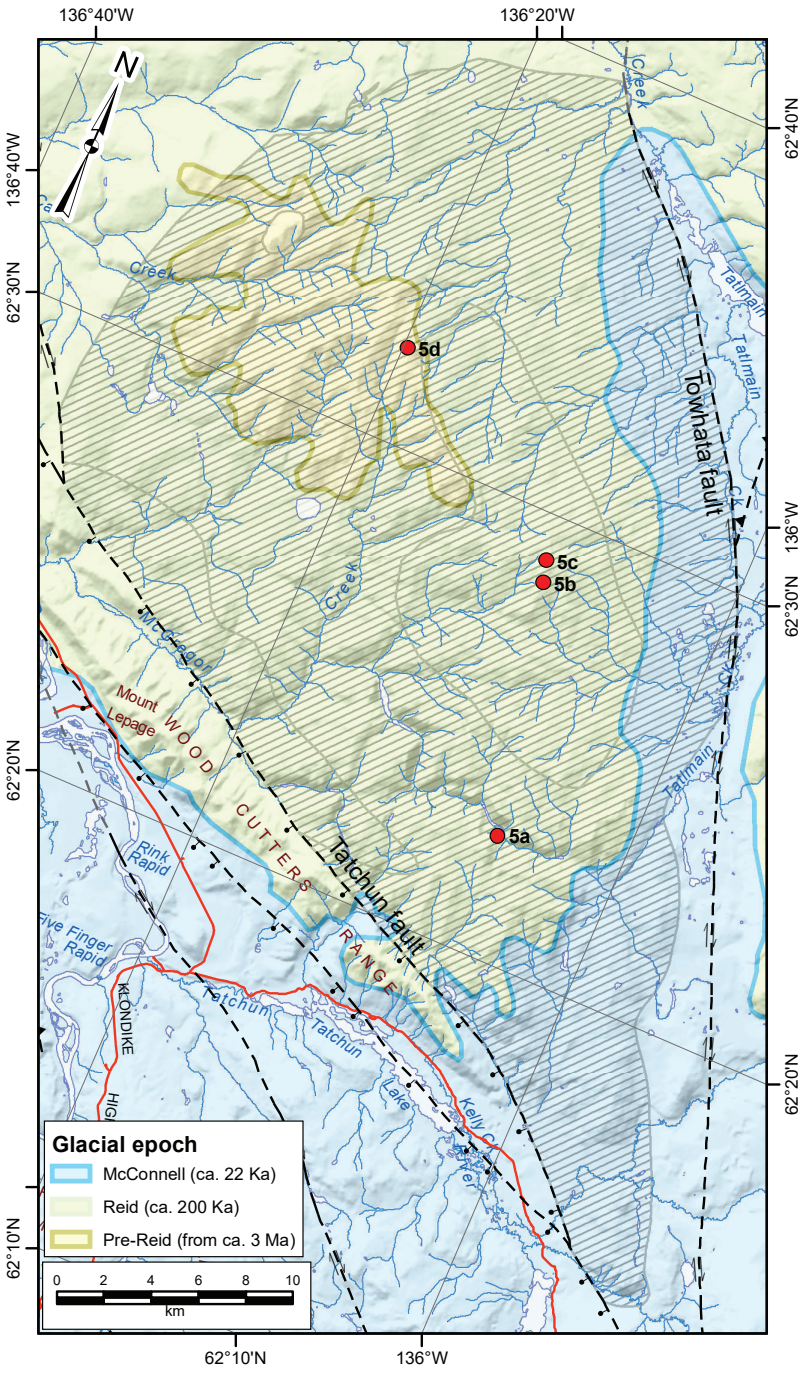


Figure 6-6. *Most of the McGregor batholith lies northwest of the maximum extent of the McConnell glaciation (ca. 22 Ka) and is covered mainly by a till veneer from the Reid glaciation (ca. 200 Ka) and glaciofluvial deposits related to both Reid and McConnell epochs (Jackson, 1997a,b). The headwaters of McGregor and McCabe creeks in the northwestern part of the batholith are more deeply weathered with landscape dating from the pre-Reid epoch (≤3 Ma). Glacial limits from Duk-Rodkin (1999). Hatched area shows extent of the Late Jurassic McGregor batholith. Red circles show location of photos in Fig. 6-5. Fault symbology as in Figure 1-4. Note that the geographic reference frame has been rotated with North pointing to the upper right of the page.*

is evident in the deeply incised valleys and local occurrence of potholes near the centre of the batholith (Fig. 6-5c). The northwestern part of the batholith is more deeply weathered, as shown by the local occurrence of tors near the headwaters of McGregor and McCabe creeks, a landscape dating back to the pre-Reid glacial epoch (≤3 Ma; Figs. 6-5d and 6-6).

The McGregor batholith intrudes Mississippian to Triassic arc rocks of Quesnellia within a structural panel bound by the Towhata fault to the northeast and the Tatchun fault to the southwest (Fig. 6-2). The northwestern portion of the batholith intrudes Carboniferous metasedimentary and metavolcanic rocks of the Moose and Boswell formations (Ryan *et al.*, 2010; Tempelman-Kluit, 1984) and metaplutonic rocks of the Kelly suite (Colpron *et al.*, 2002, 2016b). To the southwest, the batholith intrudes Upper Triassic basalt of the Semenof formation, a contact that is modified by the Tatchun fault along its southern margin (Colpron *et al.*, 2002; Colpron, 2011). The Towhata fault is a Cretaceous dextral strike-slip fault that juxtaposes the McGregor batholith with metasedimentary rocks of the Snowcap assemblage (Yukon-Tanana terrane; Colpron *et al.*, 2002; Figs. 6-1 and 6-2).

Tempelman-Kluit (1984) mapped the massive plutonic rocks in the McGregor Creek area as part of the Jurassic Tatchun batholith, a large, NW-elongate batholith approximately 85 km long by 25 km wide that was assigned by Gordey and Makepeace (2001) to the Aishihik plutonic suite. More detailed mapping by Colpron *et al.* (2002) showed that this large area of plutonic rocks actually represents two distinct batholiths separated by a thin band of Carboniferous to Upper Triassic mafic to intermediate metavolcanic rocks and a fault (Towhata fault; Fig. 6-2). Colpron *et al.* (2002)

considered both batholiths to be Early Jurassic based on their similar granodiorite composition and retained the name of Tatchun batholith for the southeastern (50 × 20 km) body; the 50 by 25 km northwestern body was named the McGregor batholith (Fig. 6-2; Colpron *et al.*, 2003). This study demonstrates that the two plutons are distinct in age and geochemistry, and the Tatchun batholith forms part of the Minto suite (205–194 Ma; *see* Chapter 3 for further discussion of the Tatchun batholith) and the McGregor batholith belongs to a *ca.* 163–146 Ma plutonic suite previously undocumented in Yukon (Fig. 6-7).

Petrography

The McGregor batholith is composed of two main phases of granodiorite: 1) a dominant hornblende-bearing phase that underlies most of the batholith; and 2) a two-mica granodiorite phase that occupies a central body near the core of the batholith and also occurs along its southwest margin just north of the Wood Cutters Range (Fig. 6-2). A smaller body of coarse-grained clinopyroxene-hornblende gabbro occurs near the northwest margin of the batholith (Fig. 6-8). This gabbro resembles rocks in the northern part of the Tatchun batholith to the east (Colpron *et al.*, 2002, 2003) and mafic intrusions of the Pyroxene Mountain suite to the west, and likely represents a xenolith of these older rocks within the McGregor batholith. It was not studied in detailed.

Although the contact relationships between the two phases of the McGregor batholith were not observed, the two-mica central phase is inferred to be younger and intrude the main hornblende-biotite granodiorite. A horseshoe-shaped magnetic high rims the northern portion of the central body of two-mica granodiorite and is inferred to mark a contact aureole into the older granodiorite (Fig. 6-9). Granodiorite of the McGregor batholith is generally massive and unfoliated, although alignment of mafic minerals locally defines a magmatic foliation (Fig. 6-10).

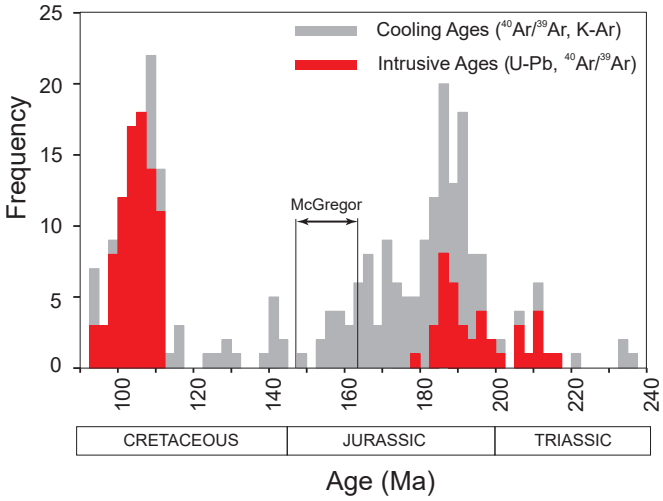


Figure 6-7. *Frequency distribution of Mesozoic intrusive and cooling ages for southern Yukon (modified after Allan et al., 2013). Major pulses of intrusive activity are in the Early Jurassic and Early Cretaceous. The Late Jurassic McGregor batholith falls within a range that previously appeared to mark a magmatic lull in Yukon.*

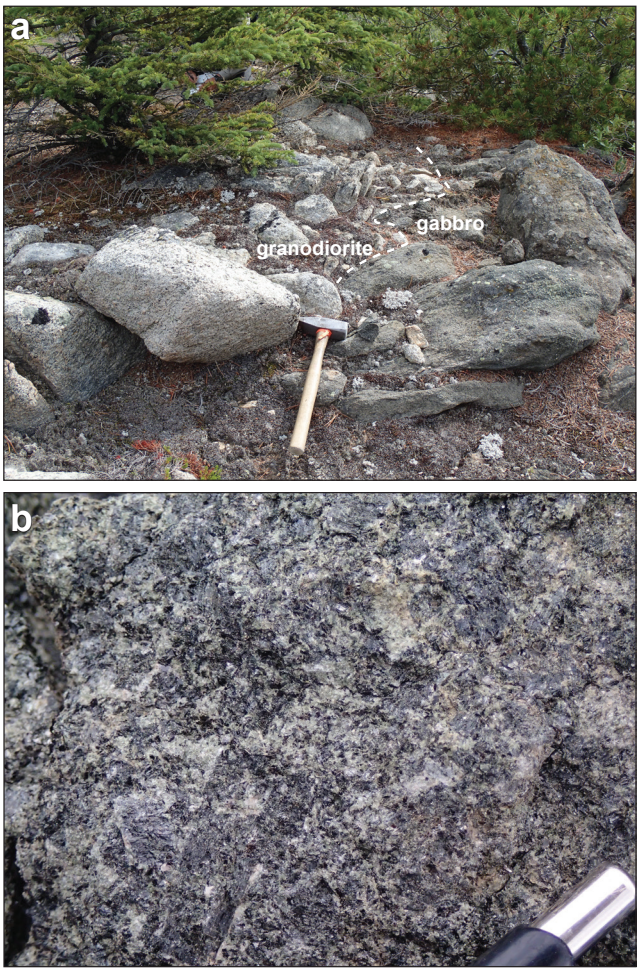


Figure 6-8. ***(a)*** *Outcrop of round weathering gabbro (dark rock), 14PS174.* ***(b)*** *Fresh gabbro surface with coarse-grained pyroxene, 14PS175.*

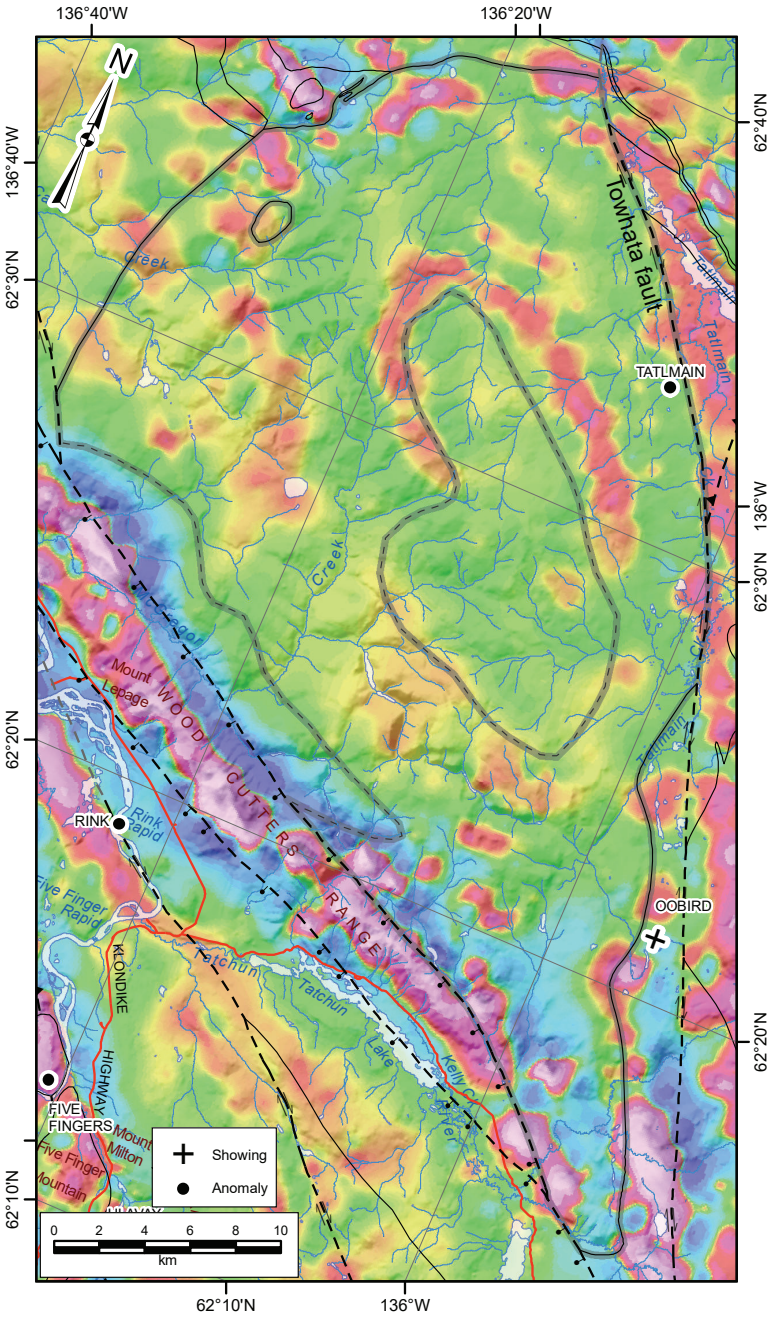


Figure 6-9. *First vertical derivative aeromagnetic map of the McGregor batholith (Hayward and Oneschuk, 2011) illustrating distribution of MINFILE occurrences and anomalies. Fault symbology as in Figure 1-4. Note that the geographic reference frame has been rotated with North pointing to the upper right of the page.*

The main hornblende-bearing phase of the McGregor batholith ranges from granodiorite to monzodiorite (Fig. 6-3). It is mostly medium to coarse grained and porphyritic (Fig. 6-11a,b) and less commonly medium grained and equigranular. Fine-grained leucocratic dikes that locally intrude the coarse-grained, porphyritic granodiorite have irregular margins suggesting comagmatic emplacement (Fig. 6-12). K-feldspar phenocrysts in the porphyritic phase are typically white, with lesser pink colours (Fig. 6-11); hornblende and biotite occur in equal proportions and represent ≤10% modal abundance. Primary accessory minerals include epidote and titanite; epidote is commonly euhedral and intergrown with biotite (Fig. 6-13).

The two-mica phase ranges from tonalite to monzodiorite, and most samples plot in the granodiorite field of the QAP diagram (Fig. 6-3). It is generally fine to medium grained, equigranular to locally porphyritic (Fig. 6-14), and contains biotite and muscovite (Fig. 6-15), with accessory epidote (primary and secondary) and rare hornblende. Aplite and pegmatite dikes locally intrude all phases of the McGregor batholith (Fig. 6-16).

Oxidation state and mineral occurrences

The McGregor batholith is generally reduced with magnetic susceptibilities of 0.12 to 1.10 × 10^{-3} SI units (avg. = 0.43; n = 8) for the main phase, and 0.04 and 1.65 × 10^{-3} SI units (avg. = 0.24; n = 10) for the two-mica granodiorite (Fig. 6-4). The magnetic high that highlights the contact aureole around the central body of the two-mica granodiorite has a slightly higher magnetic susceptibility measurement between 1.18 and 2.87 × 10^{-3} SI units (avg. = 1.70; n = 4; Figs. 6-4 and 6-9). The gabbro raft in the northwestern part of the batholith has magnetic susceptibilities of 0.238 and 0.223 × 10^{-3} SI units.



Figure 6-10. *Local alignment of mafic minerals in the dominant hornblende granodiorite phase of the McGregor batholith, 14PS176.*

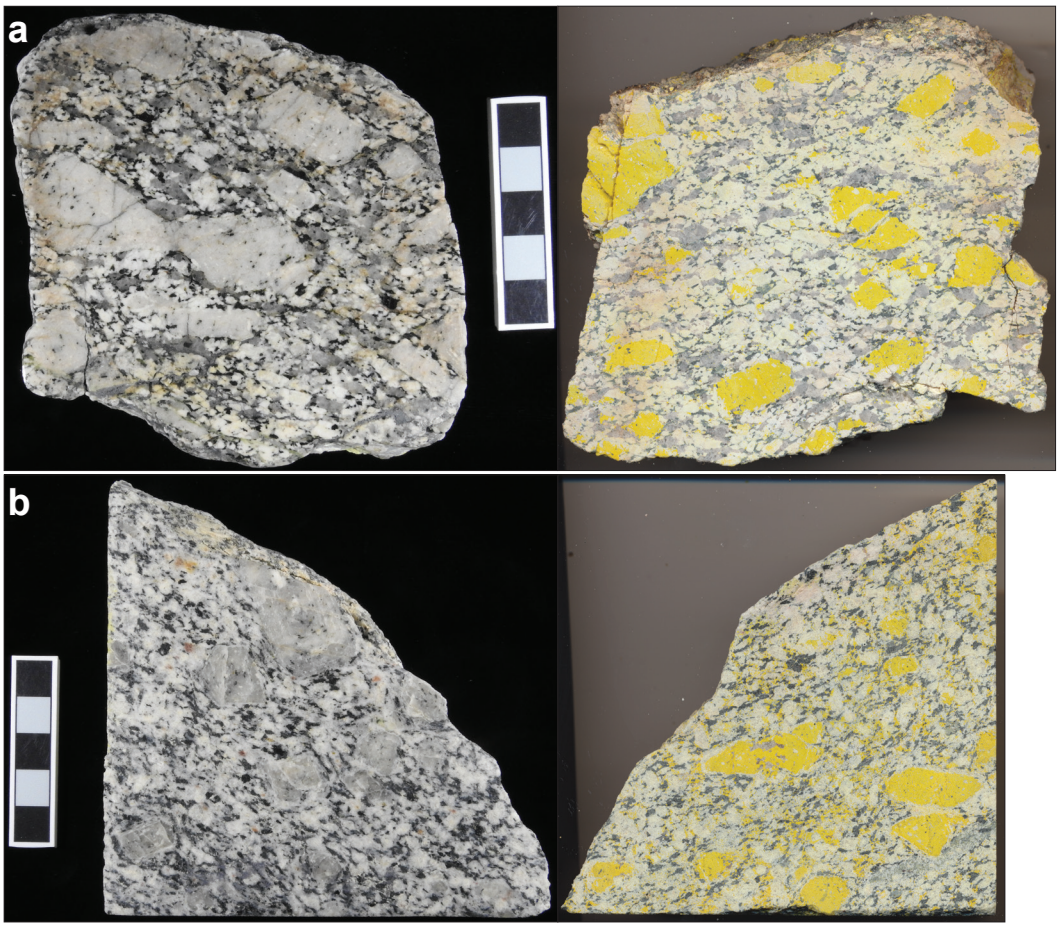


Figure 6-11. *Representative samples of the main, hornblende granodiorite phase of the McGregor batholith. Each sample shown with a fresh polished surface (left) and a cobaltinitrite-stained surface (right). Note K-feldspar is yellow stained mineral.* ***(a)*** *14PS181-1,* ***(b)*** *14PS171-1.*

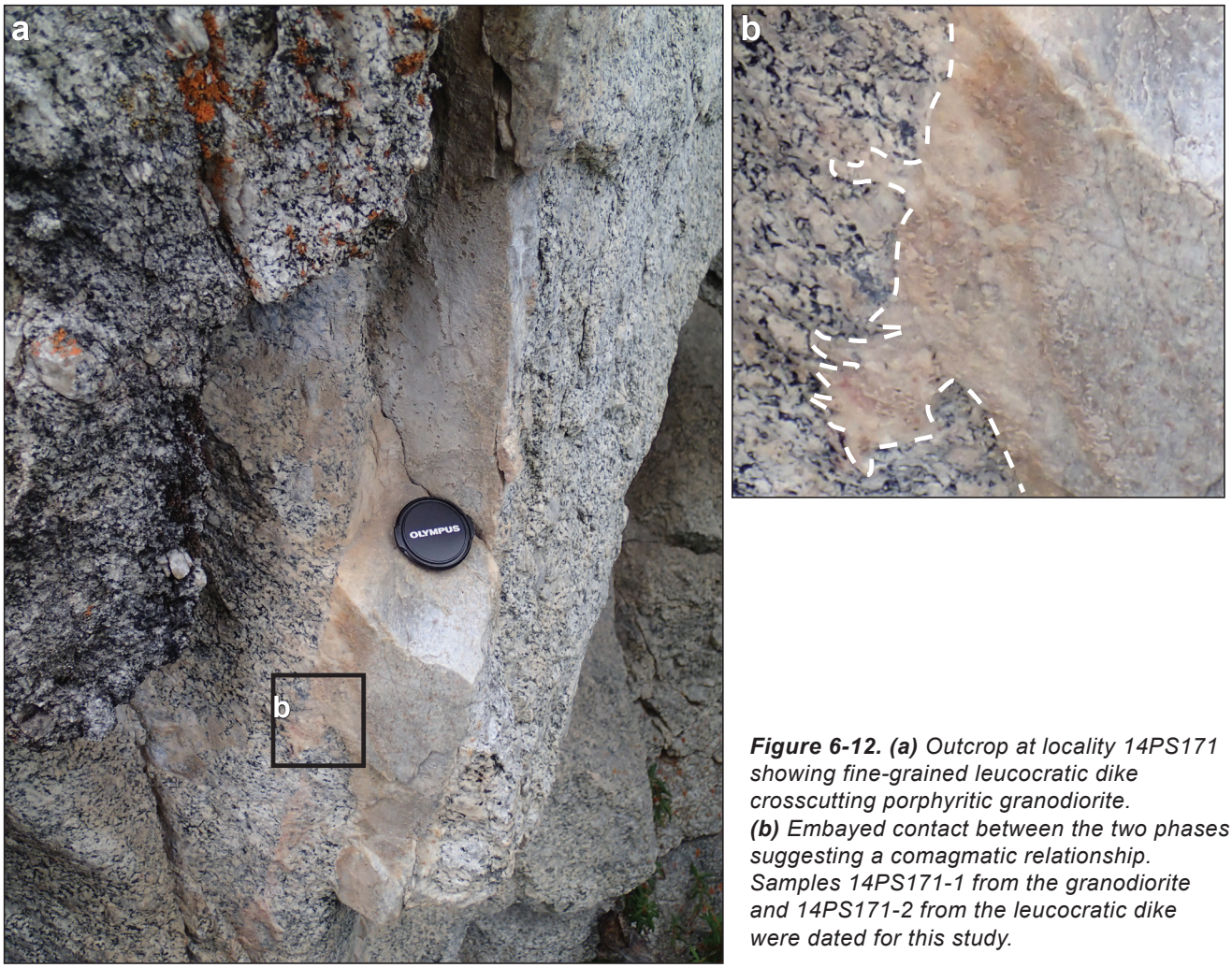


Figure 6-12. (a) *Outcrop at locality 14PS171 showing fine-grained leucocratic dike crosscutting porphyritic granodiorite.* ***(b)*** *Embayed contact between the two phases suggesting a comagmatic relationship. Samples 14PS171-1 from the granodiorite and 14PS171-2 from the leucocratic dike were dated for this study.*

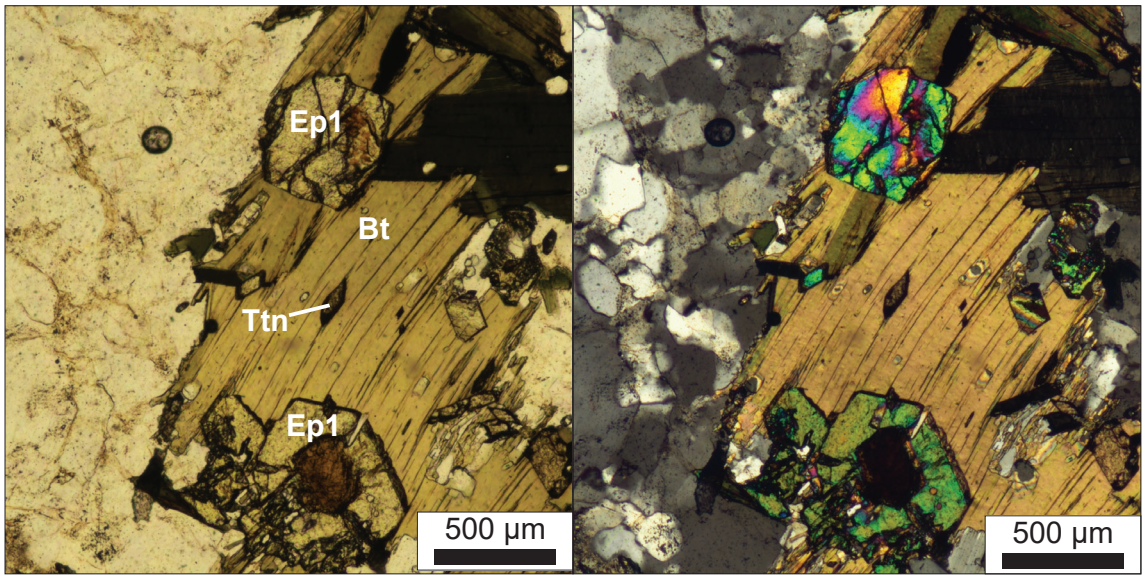


Figure 6-13. *Transmitted light photomicrograph pair from the main hornblende granodiorite phase of the McGregor batholith; plane polarized light (left) and cross-polarized light (right). Note euhedral epidote intergrown with biotite and accessory titanite, 02MC035-1.*

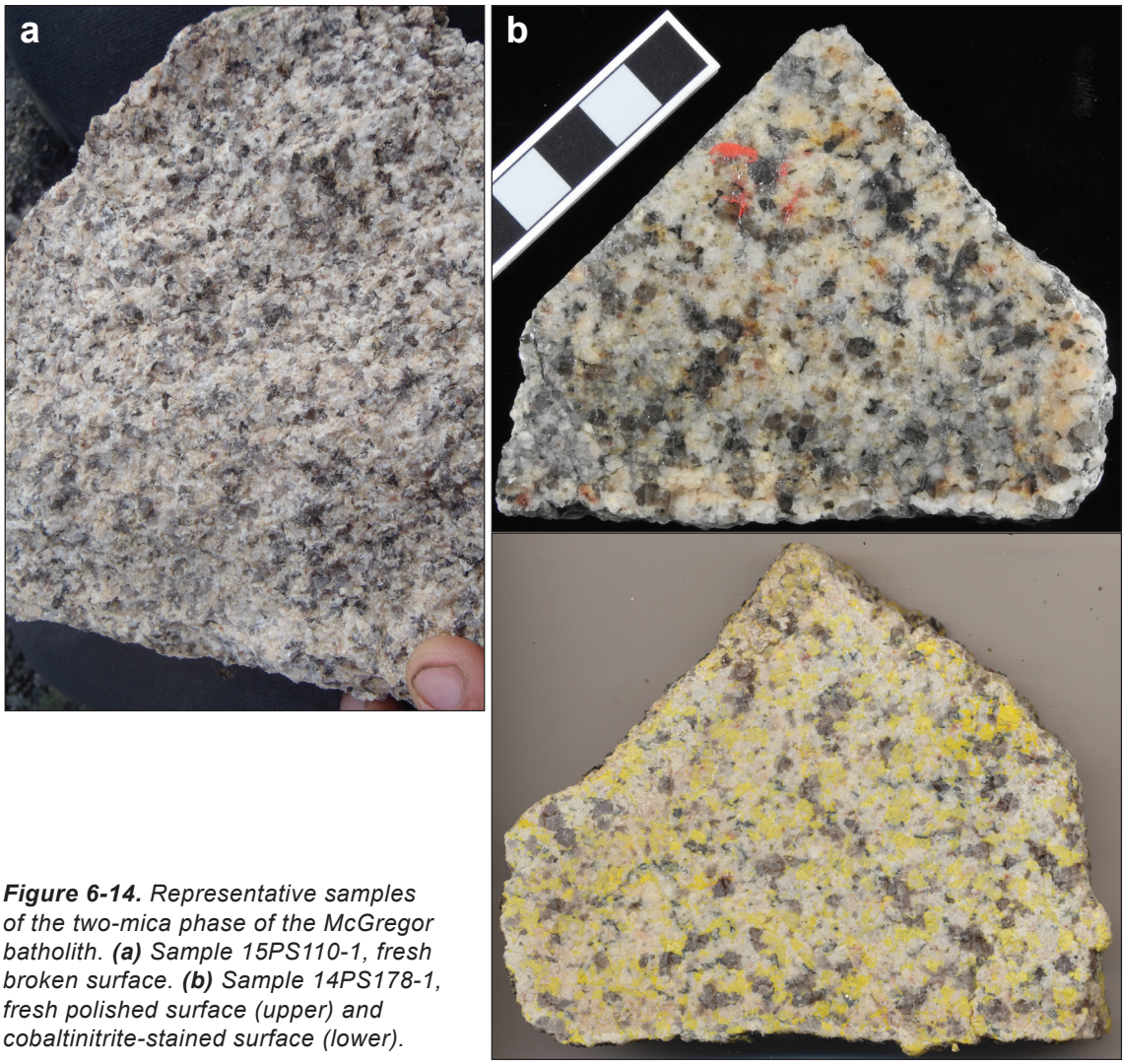


Figure 6-14. *Representative samples of the two-mica phase of the McGregor batholith.* ***(a)*** *Sample 15PS110-1, fresh broken surface.* ***(b)*** *Sample 14PS178-1, fresh polished surface (upper) and cobaltinitrite-stained surface (lower).*

Two mineral occurrences are documented in the vicinity of the McGregor batholith (Fig. 6-9). The Tatlmain [115I 114] was staked on a multi-element stream sediment anomaly near the northeastern margin of the pluton. The Oobird [105L 061], located just off the southeastern edge of the pluton, consists of traces of chalcopyrite and bornite and 5 to 20% pyrrhotite and pyrite on the margin of a quartz-feldspar porphyry dike cutting mafic volcanic rocks of the Upper Triassic Semenof formation; a similar dike to the north is dated at *ca.* 207 Ma and forms part of the Late Triassic Headless suite (*see* Chapter 2). Exploration at both occurrences was focused on Cu (± Au) and only consisted of cursory follow-up work. The last recorded work was in 1986 on the Tatlmain occurrence (YGS, 2020b).

Geochronology

Stevens *et al.* (1982a) provided the first age constraints on the McGregor batholith in the form of hornblende (160 ± 3 Ma) and biotite (162 ± 8 and 144 ± 3 Ma) K-Ar dates from the main hornblende-biotite granodiorite phase (Appendix 1). Older geological maps (*e.g.*, Gordey and Makepeace, 2001; Colpron *et al.*, 2002) inferred these to represent cooling ages, and the McGregor batholith was considered Early Jurassic because it has a similar lithology to that of the Tatchun batholith which has U-Pb zircon dates of 203–197 Ma (*see* Chapter 3). We present here the first U-Pb zircon dates for the McGregor batholith (Appendices 3, 4 and 11). We also report new $^{40}Ar/^{39}Ar$ dates from four samples of the McGregor batholith (Appendix 6).

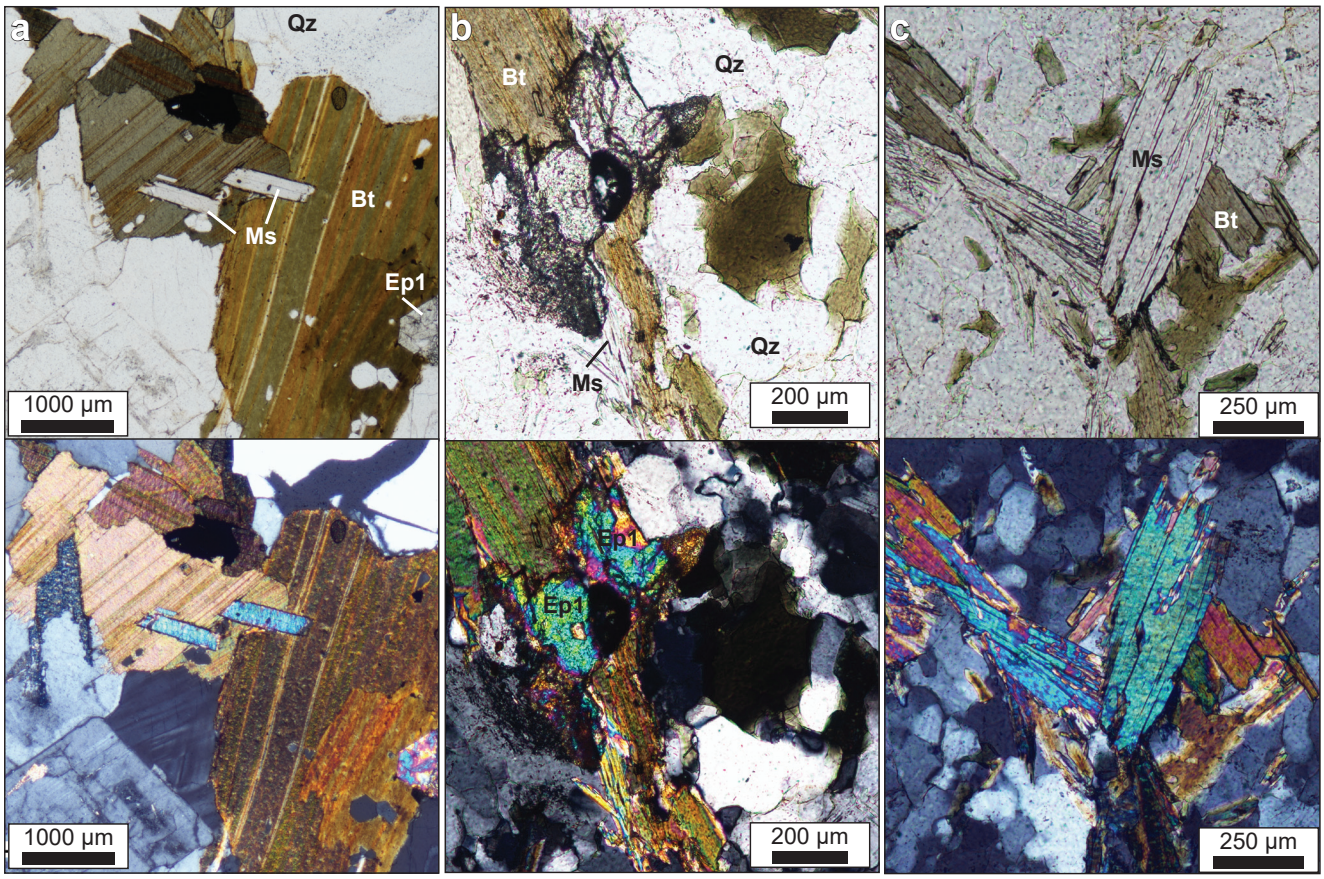


Figure 6-15. *Transmitted light photomicrograph pairs from the two-mica granodiorite phase of the McGregor batholith; plane polarized light (upper) and cross-polarized light (lower).* ***(a)*** *Euhedral muscovite and epidote intergrown with biotite, central body, 15PS110-1.* ***(b)*** *Euhedral to subhedral epidote and muscovite intergrown with biotite, southwestern body, 94M147.* ***(c)*** *Euhedral muscovite and biotite in the southwestern body, 94M147.*

U-Pb

Three samples from the main phase of hornblende-biotite granodiorite were analyzed using a combination of LA-ICPMS and CA-TIMS methods at Boise State University. Sample 14PS181-1 is a K-feldspar porphyritic hornblende granodiorite collected in the southern portion of the batholith (Fig. 6-2). Our sample was collected ~750 m east of one of the sites analyzed by Stevens *et al.* (1982a). It yielded nicely faceted, concentrically zoned zircons with 3:1 aspect ratio and no apparent inherited cores (Fig. 6-17a). Twenty-eight LA-ICPMS spot analyses yielded $^{206}Pb/^{238}U$ dates between 174 and 156 Ma, and a weighted mean of 165.8 ± 1.9 Ma (n = 28; Fig. 6-17b). Six zircons from 14PS181-1 were analyzed by CA-TIMS and yielded equivalent $^{206}Pb/^{238}U$ dates ranging from 163.50 ± 0.11 to 163.33 ± 0.11 Ma, with a weighted mean of 163.42 ± 0.05 Ma (MSWD = 1.45, n = 6; Fig. 6-17c).

Two samples were collected at locality 14PS171 in the northeastern part of the batholith, near Tatlmain Creek and the Towhata fault (Fig. 6-2). Sample 14PS171-1 is coarse-grained, hornblende granodiorite characteristic of the main phase of the McGregor batholith. It is intruded by a fine-grained, equigranular leucocratic dike from which 14PS171-2 was collected (Fig. 6-12). Both samples yielded stubby, prismatic zircons with 2:1 aspect ratio (Figs. 6-18a and 6-19a). Zircons in sample 14PS171-1 commonly have cores with sector zoning, surrounded by concentrically zoned rims (Fig. 6-18a). In 14PS171-2, CL bright cores are present in a number of grains (Appendix 3). Twenty-eight spots were analyzed by LA-ICPMS from 14PS171-1; they yielded $^{206}Pb/^{238}U$ dates between 160 and 152 Ma, and a weighted mean age of 160.9 ± 1.2 Ma (n = 28; Fig. 6-18b). Six zircons from 14PS171-1 were analyzed by CA-TIMS (Appendix 4). Five of these yielded equivalent



Figure 6-16. ***(a)*** *Aplite dike intruding gabbro near the northwestern margin of the McGregor batholith (14PS175);* ***(b)*** *aplite dike in two-mica granodiorite from the centre of the batholith (15PS108).* ***(c)*** *Fresh broken surface of pegmatite that intrudes the two-mica granodiorite, 15PS108.*

$^{206}Pb/^{238}U$ dates between 161.23 ± 0.11 and 161.09 ± 0.11 Ma and a weighted mean date of 161.16 ± 0.05 Ma (MSWD = 1.87, n = 5; Fig. 6-18c). An older grain (z5) with a $^{206}Pb/^{238}U$ date of 162.63 ± 0.11 Ma is interpreted as an antecryst.

Forty-three spots were analyzed by LA-ICPMS from 14PS171-2 (Appendix 3). They yielded $^{206}Pb/^{238}U$ dates between 322 ± 13 and 150 ± 5 Ma, and a weighted mean date of 154.5 ± 1.0 Ma for the 27 youngest analyses (Fig. 6-19b). Two distinct populations of inherited cores are also documented in this sample at *ca.* 198 Ma (n = 12) and *ca.* 318 Ma (n = 4; Fig. 6-19b). Six of the youngest zircons from 14PS171-2 were also analyzed by CA-TIMS (Appendix 4). They yielded $^{206}Pb/^{238}U$ dates between 161.27 ± 0.11 and 161.07 ± 0.11 Ma and a weighted mean date of 161.18 ± 0.05 Ma (MSWD = 1.73, n = 6; Fig. 6-19c). Both samples from locality 14PS171 yielded equivalent dates that are consistent with textural relationship that suggest they are comagmatic (Fig. 6-12).

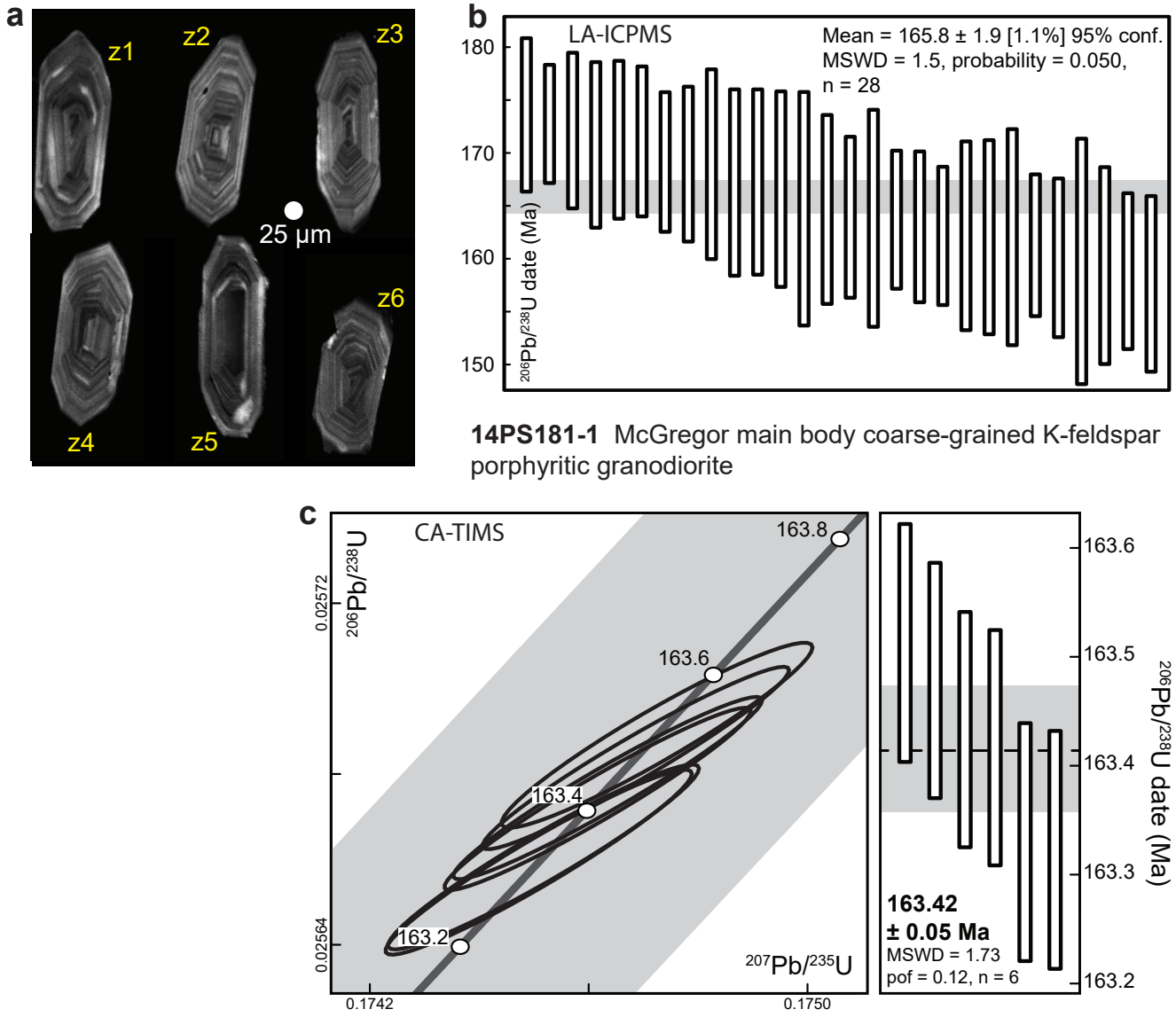


***Figure 6-17**. U-Pb zircon geochronology results for 14PS181-1. **(a)** Cathodoluminescence images of zircon analyzed by CA-TIMS, with analysis label. **(b)** Ranked plot of $^{206}Pb/^{238}U$ dates determined by LA-ICPMS (Appendix 3). **(c)** Concordia plot of CA-TIMS dates (Appendix 4). Analyses included in CA-TIMS weighted mean date calculation are shown by bold ellipses; ellipses with thin lines are not used in calculation. The light grey band around concordia (dark grey line) illustrates the decay constant uncertainties. Ranked $^{206}Pb/^{238}U$ dates plot is to the right of the concordia plot, with the weighted mean date shown by the grey band. Line-type designations are the same as the concordia plot. Errors in all plots are at 2σ. MSWD = mean squared weighted deviation, pof = probability of fit, n = number of analyses included in age calculation.*

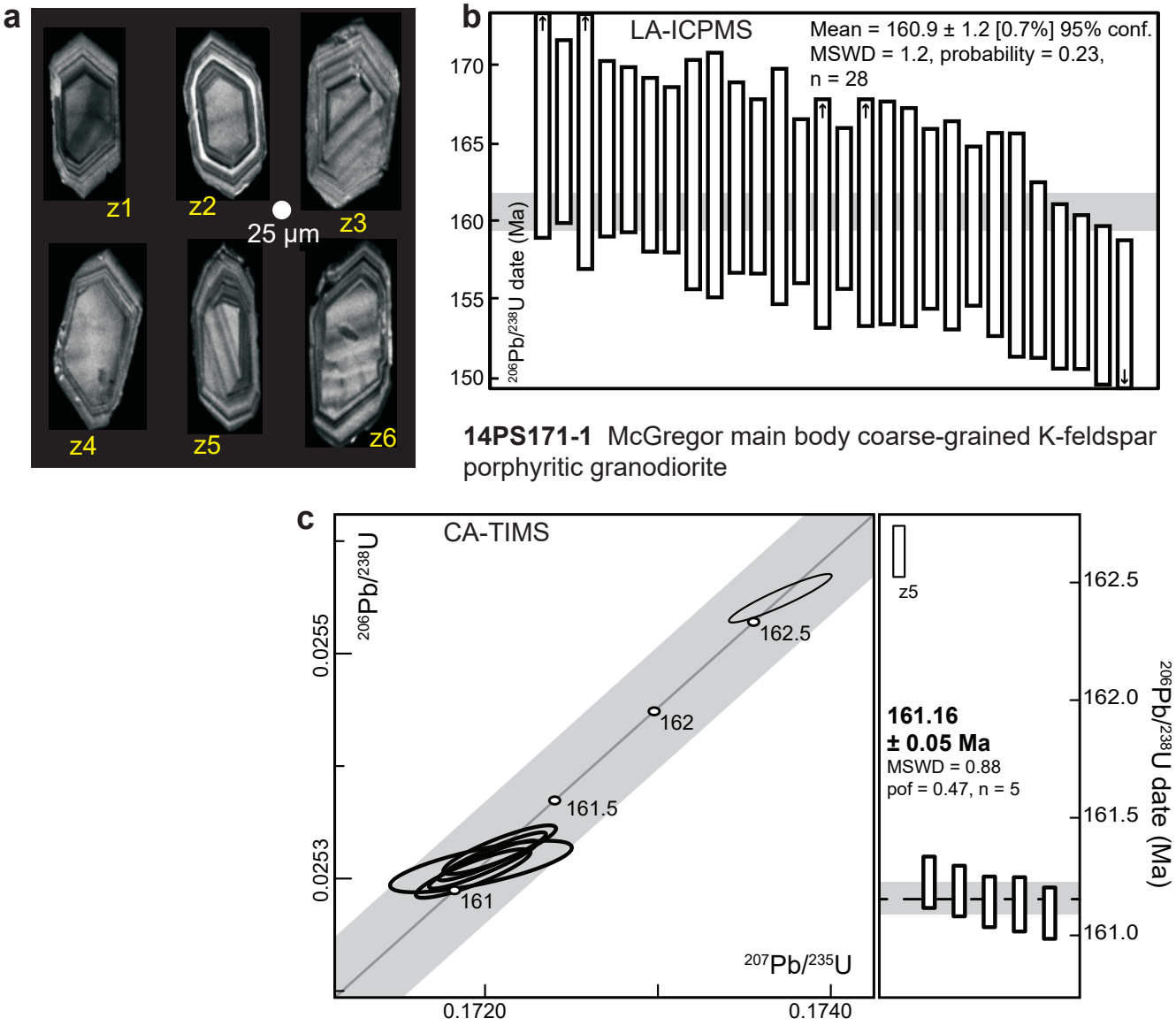


Figure 6-18. *U-Pb zircon geochronology for 14PS171-1.* ***(a)*** *Cathodoluminescence images of zircon analyzed by CA-TIMS, with analysis label.* ***(b)*** *Ranked plot of $^{206}Pb/^{238}U$ dates determined by LA-ICPMS (Appendix 3).* ***(c)*** *Concordia plot of CA-TIMS dates (Appendix 4). Analyses included in CA-TIMS weighted mean date calculation are shown by bold ellipses; ellipses with thin lines are not used in calculation. The light grey band around concordia (dark grey line) illustrates the decay constant uncertainties. Ranked $^{206}Pb/^{238}U$ dates plot is to the right of the concordia plot, with the weighted mean date shown by the grey band. Line-type designations are the same as the concordia plot. Errors in all plots are at 2σ. MSWD = mean squared weighted deviation, pof = probability of fit, n = number of analyses included in age calculation. Arrow indicates data extend off of plot.*

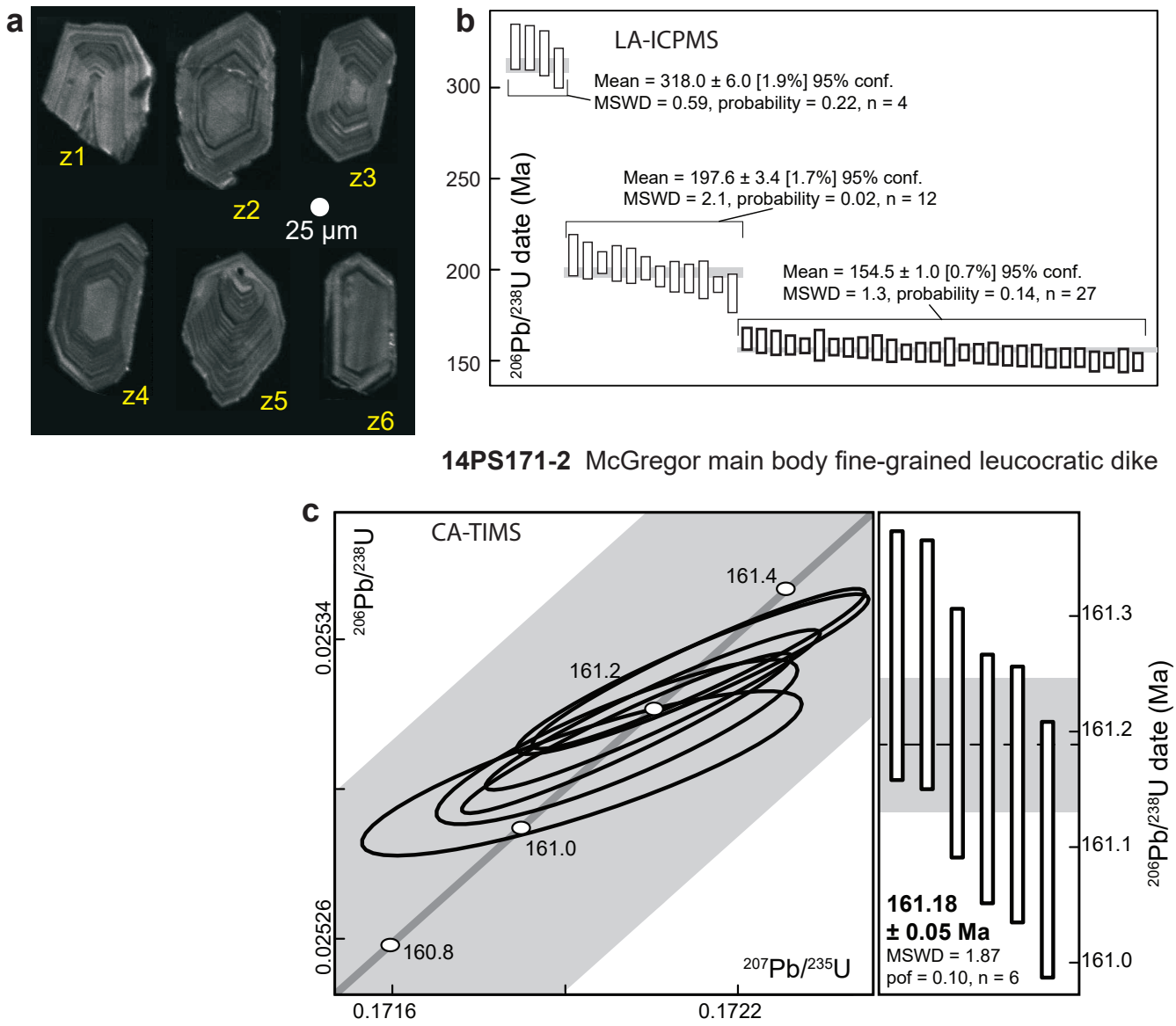


Figure 6-19. *U-Pb zircon geochronology for 14PS171-2.* ***(a)*** *Cathodoluminescence images of zircon analyzed by CA-TIMS, with analysis label.* ***(b)*** *Ranked plot of $^{206}Pb/^{238}U$ dates determined by LA-ICPMS (Appendix 3).* ***(c)*** *Concordia plot of CA-TIMS dates (Appendix 4). Analyses included in CA-TIMS weighted mean date calculation are shown by bold ellipses; ellipses with thin lines are not used in calculation. The light grey band around concordia (dark grey line) illustrates the decay constant uncertainties. Ranked $^{206}Pb/^{238}U$ dates plot is to the right of the concordia plot, with the weighted mean date shown by the grey band. Line-type designations are the same as the concordia plot. Errors in all plots are at 2σ. MSWD = mean squared weighted deviation, pof = probability of fit, n = number of analyses included in age calculation.*

We attempted to date two samples from the central body of two-mica granodiorite (14PS178-1, 15PS115-1; Fig. 6-2). Zircons with a range of morphologies were recovered from both samples, zoned needles are dominant, and their LA-ICPMS analyses yielded a scatter of dates (Appendix 3). In sample 14PS178-1 nineteen LA-ICPMS spot analyses have $^{206}Pb/^{238}U$ dates between 172 and 136 Ma (Fig. 6-20). The youngest three zircons have $^{206}Pb/^{238}U$ dates of 143–136 Ma, a high U concentrations (1371–3974 ppm; Appendix 3), and have likely undergone Pb loss due to internal α radiation damage. The next three youngest zircons have moderate U concentrations (266–881 ppm) and equivalent dates at *ca.* 146 Ma that provide a minimum estimate for crystallization of this sample. Nine LA-ICPMS spots were analyzed from 15PS115-1 and yielded $^{206}Pb/^{238}U$ dates between 175 and 152 Ma (Fig. 6-20). The youngest four analyses have moderate U concentrations (158–757 ppm) and provide a minimum estimate of *ca.* 155 Ma for this samples. Because of their scatter of LA-ICPMS $^{206}Pb/^{238}U$ dates, no attempt was made to date these samples by CA-TIMS.

A sample of two-mica granodiorite was collected by J.K. Mortensen in 1994 and analyzed by LA-ICPMS at UBC (94M147; Appendix 11). It yielded a range of $^{206}Pb/^{238}U$ dates between 1600 and 159 Ma, with two clusters of dates at *ca.* 260 and 167 Ma (Fig. 6-20). Three of the youngest 4 grains have a weighted mean date of 167.4 ± 2.6 Ma that provides the best estimate for the crystallization age of this sample, slightly older than the CA-TIMS dates for the hornblende-biotite granodiorite phase (*ca.* 163–161 Ma).

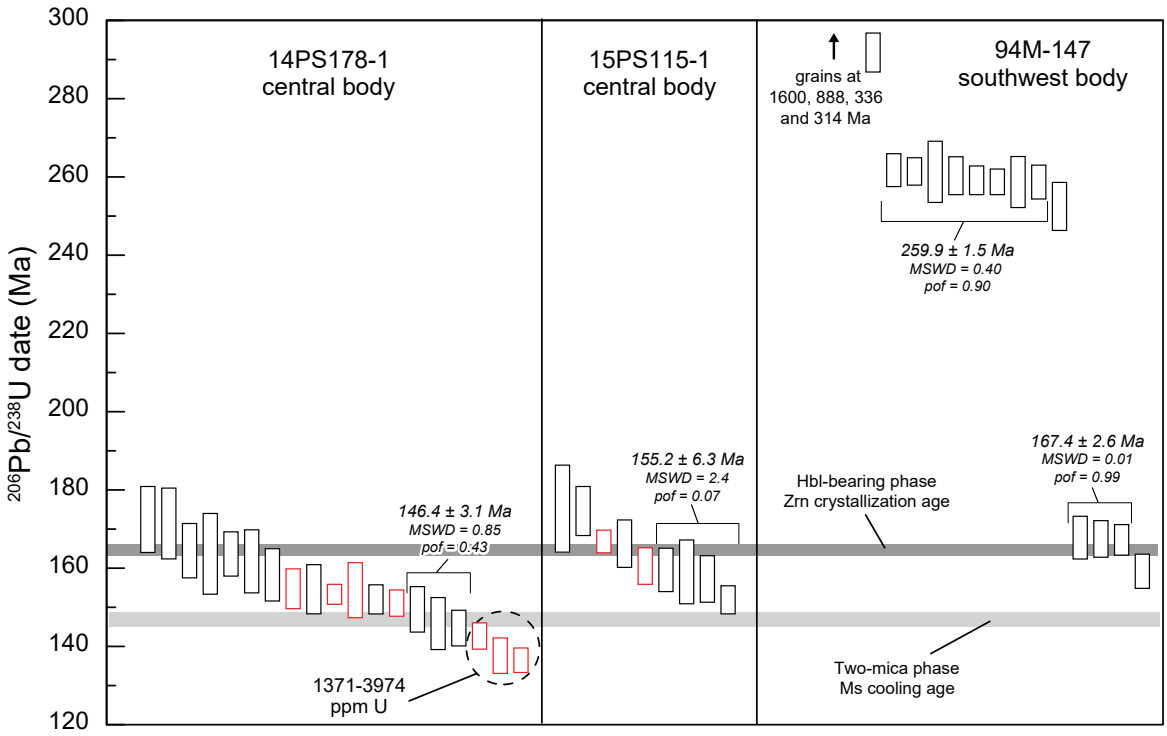


Figure 6-20. *Zircon LA-ICPMS $^{206}Pb/^{238}U$ dates for three samples of the two-mica phase, McGregor batholith. 14PS178-1 and 15PS115-1 are from the central body (Appendix 3), and 94M-147 is from the southwestern margin of the batholith (Appendix 11). Analyses with U concentration >1000 ppm are shown in red. Errors are at 2σ. MSWD = mean squared weighted deviation, pof = probability of fit.*

Ar-Ar

Four samples from the McGregor batholith, three from the main phase of hornblende granodiorite (14PS172-1, 14PS173-1 and 02DM039-1) and one from the central body of two-mica granodiorite (14PS178-1), were analyzed using $^{40}Ar/^{39}Ar$ step heating of hornblende, muscovite and biotite (GSC, Ottawa; Appendix 6). Sample 14PS172-1 is from the northern part of the batholith and was collected ~7.5 km northwest of locality 14PS171 where two samples were dated at *ca.* 161 Ma by U-Pb zircon (*see* above; Figs. 6-2, 6-18 and 6-19). Hornblende in 14PS172-1 yielded a multistep plateau age of 159 ± 2 Ma (Fig. 6-21a; 100% of the ^{39}Ar gas released in 11 steps, MSWD = 1.13); biotite shows Ar loss in the low temperature steps climbing to a plateau at 145.8 ± 1.2 Ma (Fig. 6-21b; 67% of the ^{39}Ar gas released in 15 steps, MSWD = 1.13).

Sample 14PS173-1 is from the northwestern part of the batholith (Fig. 6-2). Hornblende from this sample yielded a plateau age of 157.8 ± 1.1 Ma (Fig. 6-21d; 76% of the ^{39}Ar gas released in 7 steps, MSWD = 1.73); the lower temperature step is slightly younger and may indicate minor Ar loss. Biotite from 14PS173-1 shows Ar loss and thermal disturbance across most of the heating steps and a small pseudo-plateau occurs at 148.9 ± 1.2 Ma (Fig. 6-21e; 31% of the ^{39}Ar gas released in 9 steps, MSWD = 1.3).

Sample 02DM039-1 is from the southeastern 'tail' of the McGregor batholith (Fig. 6-2). Only biotite was analyzed from this sample (Appendix 6). The odd composition of this separate, with Ca/K up to 5 and overall low ^{39}Ar gas released suggests this is an impure biotite aliquot. Nonetheless, this aliquot yielded a well-defined plateau at 151 ± 2 Ma (Fig. 6-21c; 96.2% of ^{39}Ar released in 14 steps; MSWD = 1.46) that is consistent with other results from this phase of the McGregor batholith.

Sample 14PS178-1 is a two-mica granodiorite from the centre of the batholith (Figs. 6-2 and 6-14). Muscovite from this sample shows some evidence of disturbance in low temperature steps, but yielded a plateau at 146.8 ± 0.9 Ma in mid to high temperature steps (Fig. 6-22a; 65% of the ^{39}Ar gas released in 11 steps, MSWD = 1.48). A biotite aliquot shows evidence of Ar loss in low temperature steps climbing to a plateau at 143.0 ± 1.1 Ma in mid to high temperatures (Fig. 6-22b; 66% of the ^{39}Ar gas released in 15 steps, MSWD = 0.87). In light of the inconclusive results from U-Pb zircon dates in this phase of the McGregor batholith, the *ca.* 147 Ma $^{40}Ar/^{39}Ar$ muscovite cooling age from sample 14PS178-1 is considered to provide a minimum age for the two-mica granodiorite phase. These results are further discussed below.

Thermobarometry

Two samples from the hornblende-biotite granodiorite phase of the McGregor batholith contain the suitable mineral assemblage for Al-in-Hbl geobarometry (14PS171-1 and 14PS173-1; Hammarstrom and Zen, 1986; Appendix 5). Al^{TOT} in hornblende for these samples is 1.71 and 1.54 with cotectic plagioclase that has X_{An} 0.17 and 0.12, respectively. Crystallization pressure estimates derived from these data are 5.25 ± 1.08 and 4.46 ± 1.47 kbar (Appendix 5; emplacement depths between 19.8 and 16.8 km). Solidus temperatures of 659 and 664°C derived using the amphibole-plagioclase thermometer of Holland and Blundy (1994) are comparable to Ti-in-zircon temperature estimates of 589 to 692°C for zircon in samples 14PS171-1, 14PS171-2 and 14PS181-1 (Watson *et al.*, 2006; Appendix 3).

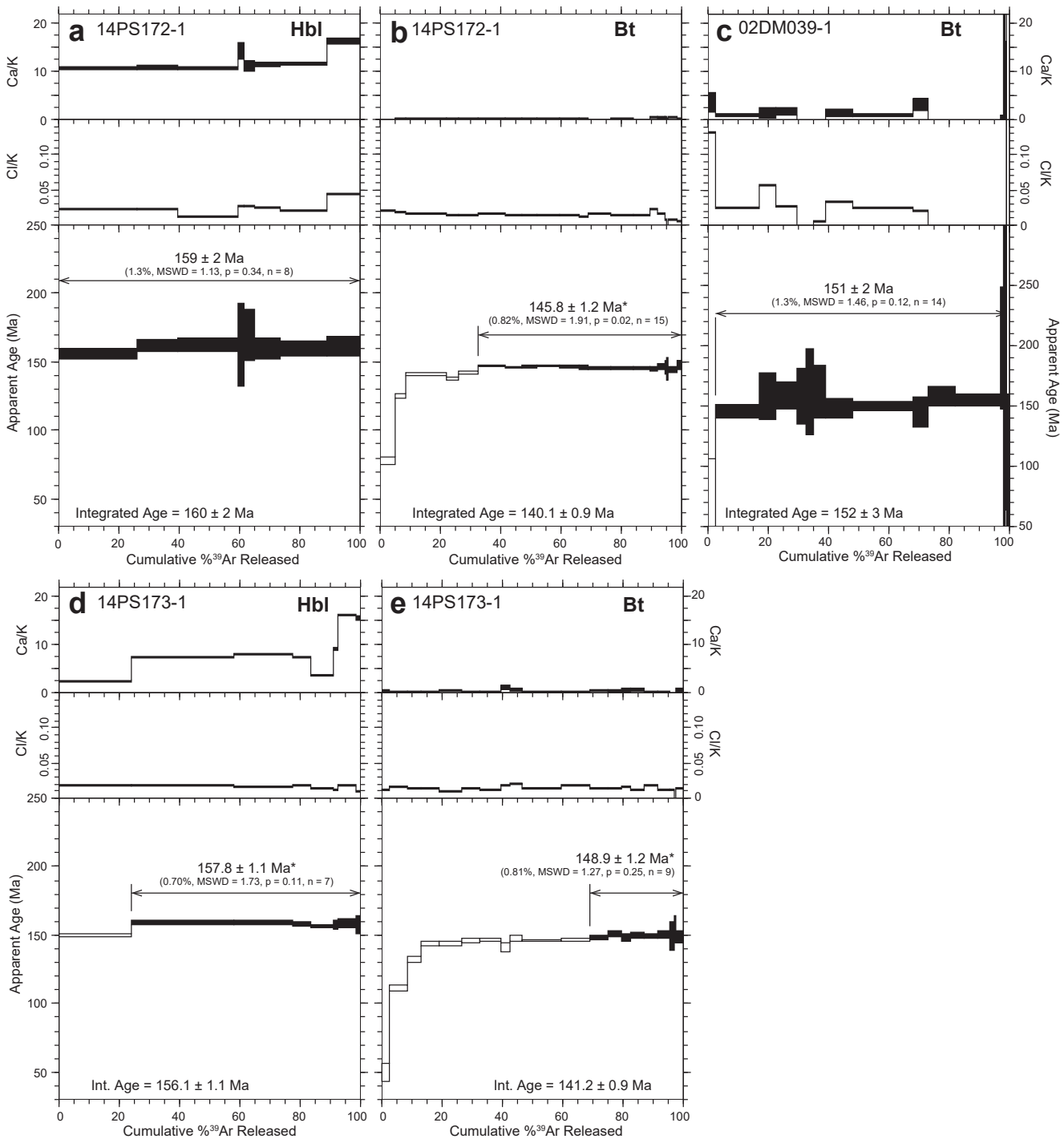


Figure 6-21. *$^{40}Ar/^{39}Ar$ age spectra for samples from the dominant phase of hornblende-biotite granodiorite, McGregor batholith.* ***(a)*** *Hornblende, 14PS172-1;* ***(b)*** *biotite, 14PS172-1;* ***(c)*** *biotite, 02DM039-1;* ***(d)*** *hornblende, 14PS173-1; and* ***(e)*** *biotite, 14PS173-1. Steps included in plateau are shown in black. MSWD = mean squared weighted deviation, p = probability of fit, n = number of steps included in age calculation. * indicates pseudo-plateau age.*

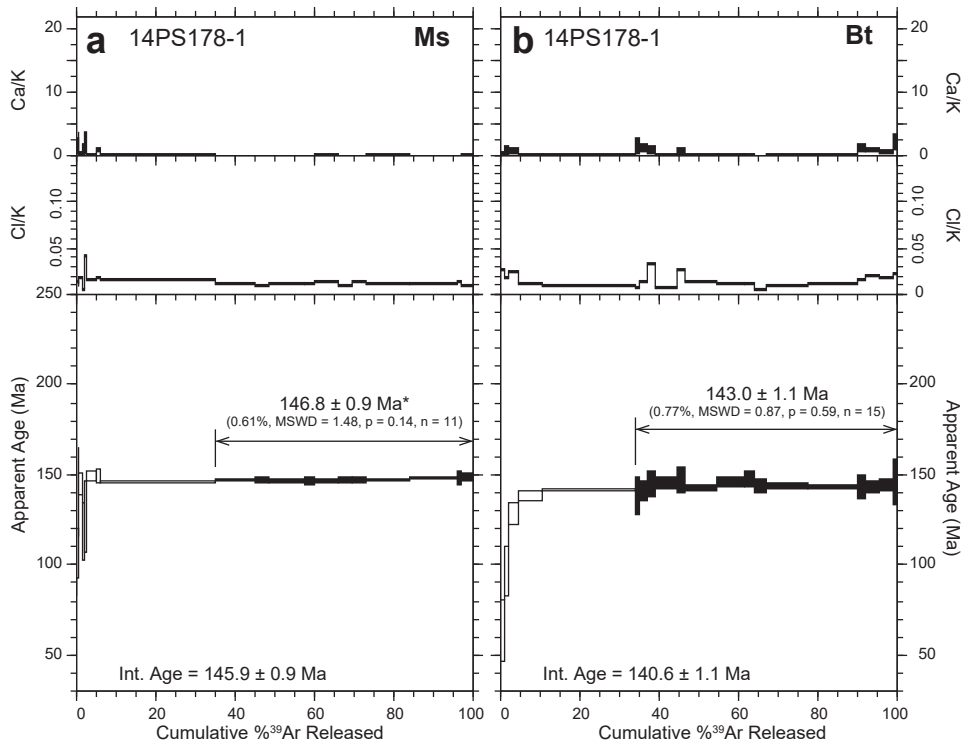


Figure 6-22. *$^{40}Ar/^{39}Ar$ age spectra for a sample two-mica granodiorite from the centre of the McGregor batholith.* ***(a)*** *Muscovite, 14PS178-1; and* ***(b)*** *biotite, 14PS172-1. Steps included in plateau are shown in black. MSWD = mean squared weighted deviation, p = probability of fit, n = number of steps included in age calculation. * indicates pseudo-plateau age.*

Geochemistry

Nineteen samples from the McGregor batholith were analyzed for whole-rock geochemistry: 13 from the main phase of hornblende granodiorite, and 6 from the two-mica granodiorite phase. These samples are unaltered and considered representative of the batholith, although only one sample was analyzed for the southwestern body of two-mica granodiorite.

Major elements

The main hornblende-bearing phase of the McGregor batholith has an SiO_2 content of 61 to 71%, whereas the two-mica phase has slightly higher SiO_2 ranging from 68 to 74% (Fig. 6-23a; Appendix 8). The main body has ferric/ferrous Fe ratios between 1.0 and 0.6; the central body has a larger range with values between 2.5 and 0.6. This range of ferric/ferrous Fe is near the transition between ilmenite and magnetite series granites (Ishihara, 1977), consistent with reduced to weakly oxidized magmatic conditions (Fig. 6-4; Hart *et al.*, 2004a,b). On most major element variation diagrams, both phases plot along a fractionation trend with the two-mica granodiorite phase showing lower Al_2O_3, MgO, $Fe_{(total)}$, TiO_2, Na_2O, CaO, and P_2O_5 with increasing SiO_2 (Fig. 6-24). Both phases have a similar K_2O content of 2-4%, and no apparent variation in SiO_2 content. The hornblende-bearing granodiorite is dominantly magnesian, alkalic to alkali-calcic, and weakly peraluminous (Fig. 6-25), consistent with the modal abundances of 1–13% combined biotite and hornblende in these samples (Appendix 2). The two-mica granodiorite straddles the magnesian-ferroan fields, is alkali-calcic to calc-alkalic, and peraluminous (Fig. 6-25). Both phases are sodic and plot in the 'I-type' field of Chappell and White (2001; Fig. 6-26).

Trace elements

On primitive mantle and upper continental crust normalized spider plots, the McGregor batholith is enriched in large ion lithophile elements (LILE) and light rare earth elements (LREE) suggesting significant fractionation (Pearce, 1996; Fig. 6-27). The hornblende-bearing phase is enriched in Rb, Ba, Th, U, has Th, La, Ce, Pr values up to 400 times those of primitive mantle, and La/Yb_N of ~36.9 (Fig. 6-27a; Appendix 8). It shows strong negative Nb and Ti anomalies and Th/Nb_N of ~13.3. The hornblende-bearing phase is enriched in LILE and LREE relative to upper continental crust, with marked negative Nb and positive Eu anomalies (Fig. 6-27b). The two-mica granodiorite phase shows variably enriched LILE and LREE values 7–200 times relative to primitive mantle and La/Yb_N ratios of 9.7 to 56.8 (average of 24.4; Fig. 6-27c; Appendix 8). It is generally slightly depleted relative to upper continental crust with flatter trace element patterns and variable Nb and Eu values (Fig. 6-27d). Samples from both phases plot in the volcanic arc field of the Ta/Yb tectonic discrimination diagram of Pearce *et al.* (1984; Fig. 6-28).

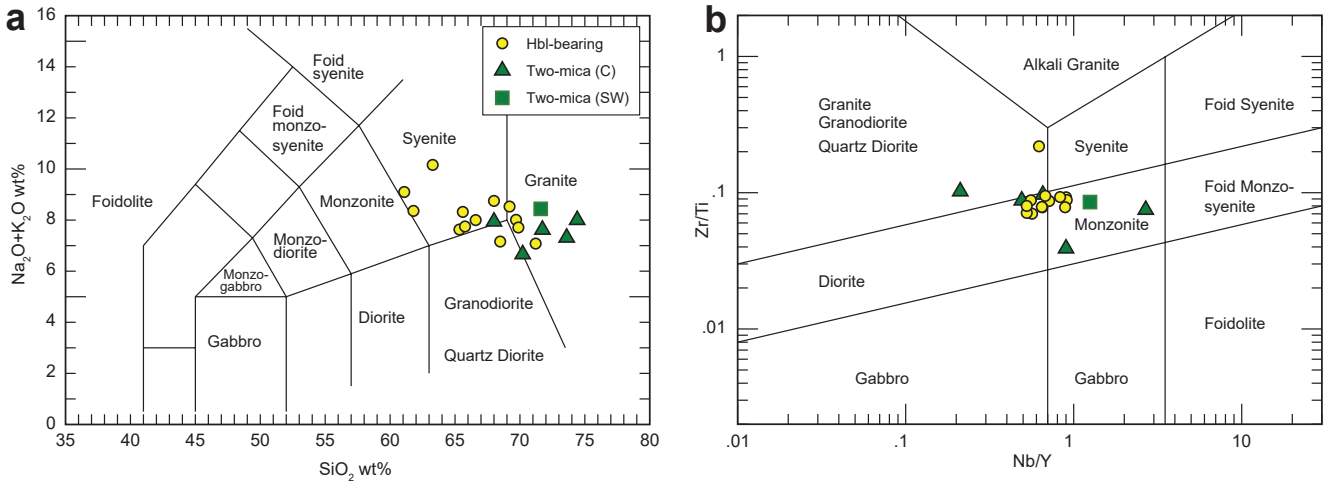


Figure 6-23. (a) *Total alkali-silica diagram for samples of the McGregor batholith (adapted from Le Bas et al., 1986, for plutonic rocks).* ***(b)*** *Zr/Ti vs. Nb/Y classification diagram of Winchester and Floyd (1977) as modified by Pearce (1996), adapted here for plutonic rocks.*

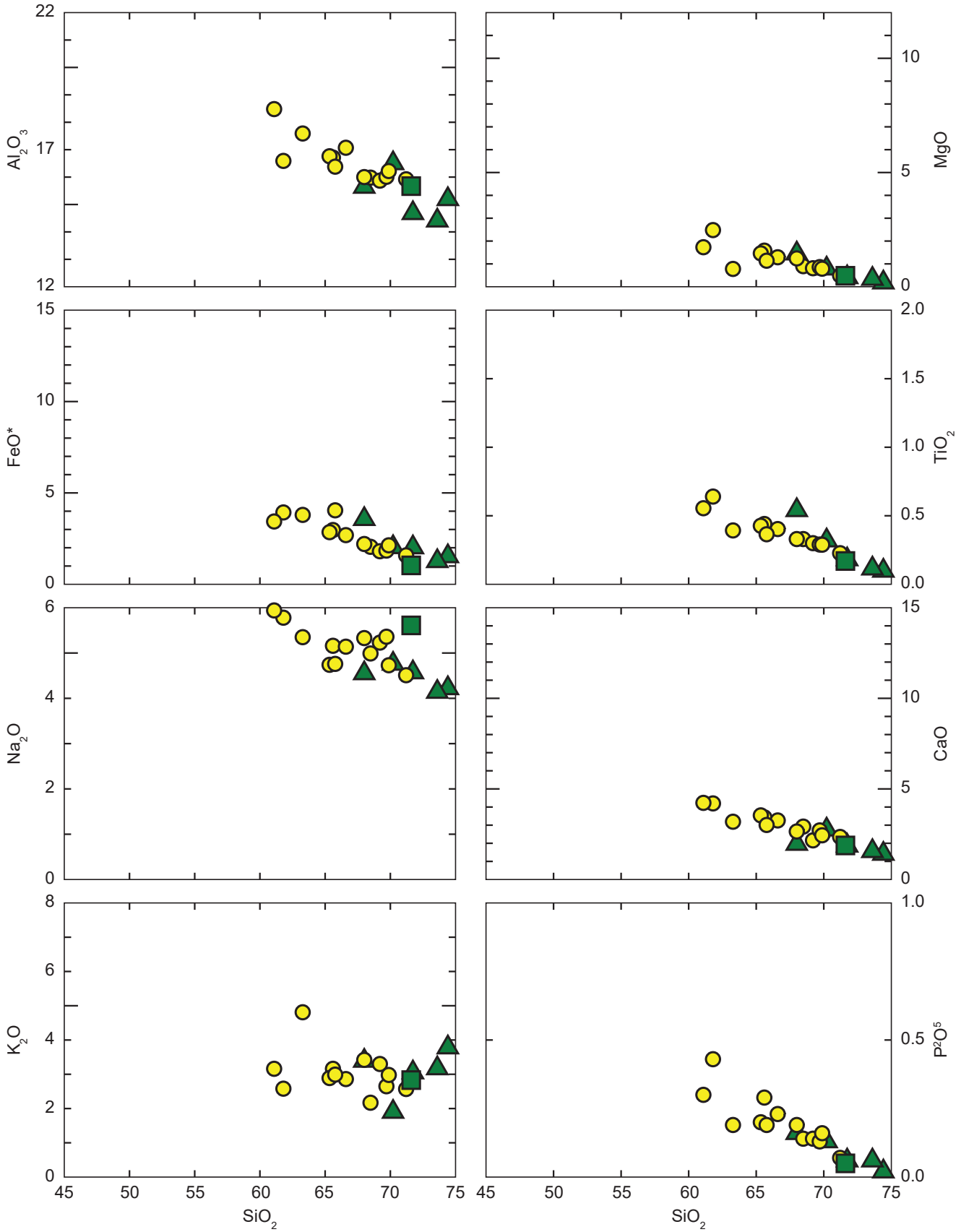
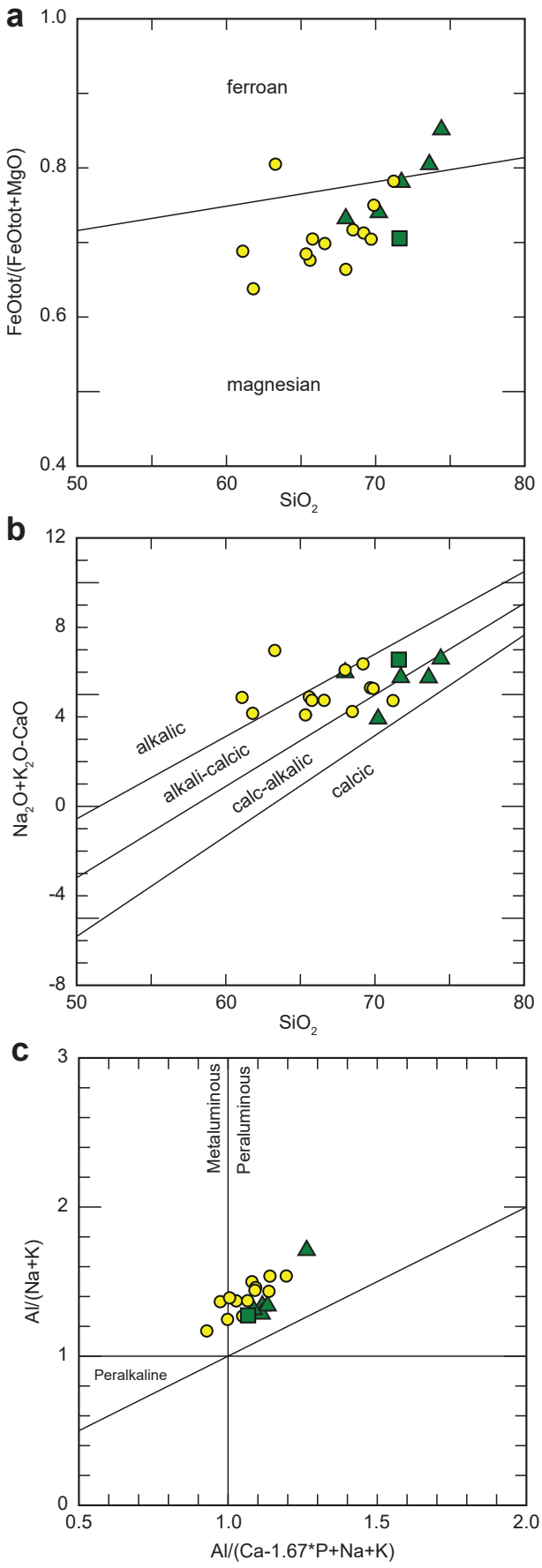


***Figure 6-24**. Major elements vs. SiO_2 Harker plots for the McGregor batholith. Symbols as in Fig.6-23.*



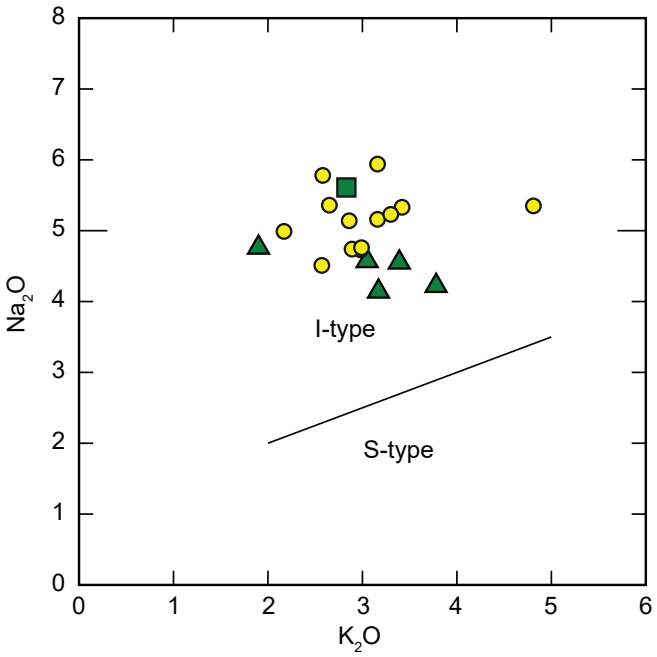


Figure 6-26. *Na_2O vs K_2O for samples of the McGregor batholith. The boundary between 'I-type' and 'S-type' granitoid rocks is from Chappell and White (1974). Symbols as in Fig.6-23.*

Figure 6-25. *Geochemical classification using criteria of Frost et al. (2001).* ***(a)*** *Fe-number,* ***(b)*** *modified alkali-lime index (MALI), and* ***(c)*** *alumina saturation index (ASI). Symbols as in Fig.6-23.*

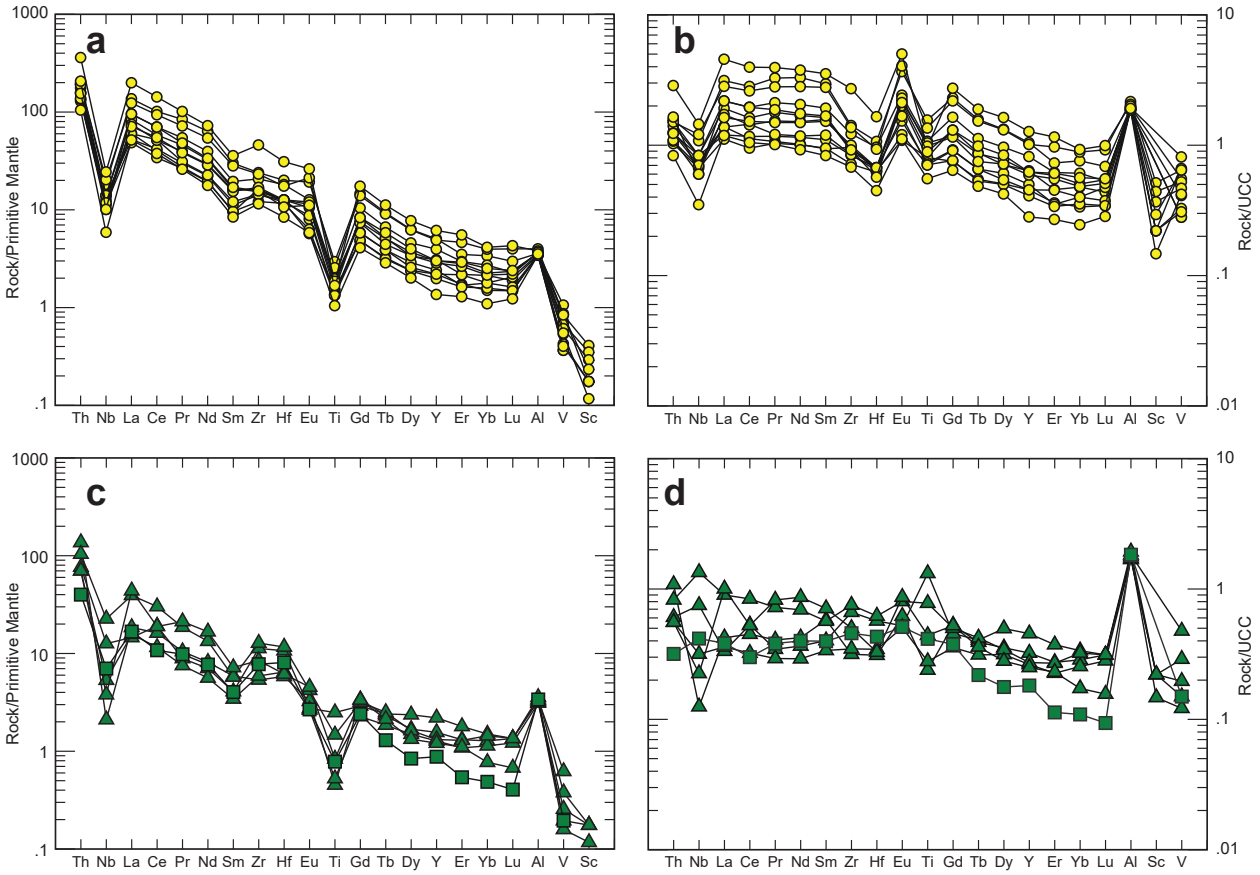


Figure 6-27. *Primitive mantle normalized spider plots using values (left; McDonough and Sun, 1995). Upper continental crust (UCC) normalized spider plots using values (right; McLennan, 2001).* ***(a*** *and* ***b)*** *Hornblende-bearing granodiorite;* ***(c*** *and* ***d)*** *two-mica granodiorite.*

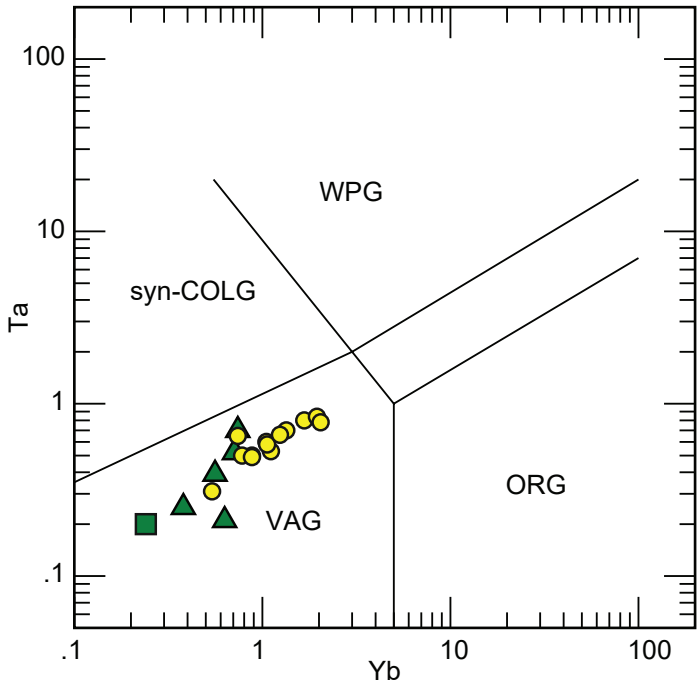


Figure 6-28. *Ta-Yb tectonic discrimination diagram for granites from Pearce et al. (1984). VAG = volcanic arc granite, ORG = ocean ridge granite, WPG = within plate granite and syn-COLG = syn-collisional granite. Symbols as in Fig.6-23.*

Zircon chemistry

Trace element concentrations were measured by LA-ICPMS analyses (Boise State University) on zircons from three samples of the dominant hornblende granodiorite phase (14PS171-1, 14PS171-2 and 14PS181-1) and two from the two-mica granodiorite phase (14PS178-1 and 15PS115-1; Appendix 3). Zircons from the hornblende-bearing phase have generally lower Ti-in-zircon temperatures varying from 589–692°C (average of 544°C); a few spots with low Hf concentrations having temperatures up to 863°C (Fig. 6-29a). However, the bulk of analyses for the hornblende-bearing phase do not show systematic variation in Ti-in-zircon temperature with respect to Hf values. Inherited components in sample 14PS171-2 have slightly elevated Ti-in-zircon temperatures relative to most zircons in the hornblende-bearing phase; Early Jurassic zircons show a range of 672–716°C (Inherited 1) and Mississippian zircons 692–760°C (Inherited 2; Fig. 6-29a). The two-mica granodiorite phase has more variable Ti-in-zircon temperatures between 590 and 807°C and shows a trend of decreasing temperature with increasing Hf content (Fig. 6-29a).

Zircons from the hornblende-bearing phase have elevated U values (560–1845 ppm, average of 1007 ppm; Appendix 3), U/Yb ratios of 2.0–6.5 and Gd/Yb > 0.03 indicative of highly fractionated post-collisional granitoid rocks (Fig. 6-29b,c). Both inherited components in sample 14PS171-2 have lower U contents (100–215 ppm), U/Yb < 1, and are more typical of mafic arc magma. Zircons from the two-mica granitoid phase show more variations with U values ranging from 158–3900 ppm, U/Yb ratios of 1–5, and a wider range of Gb/Yb ratios (0.03–0.5; Fig. 6-29) that also suggest strong fractionation of the parent magma.

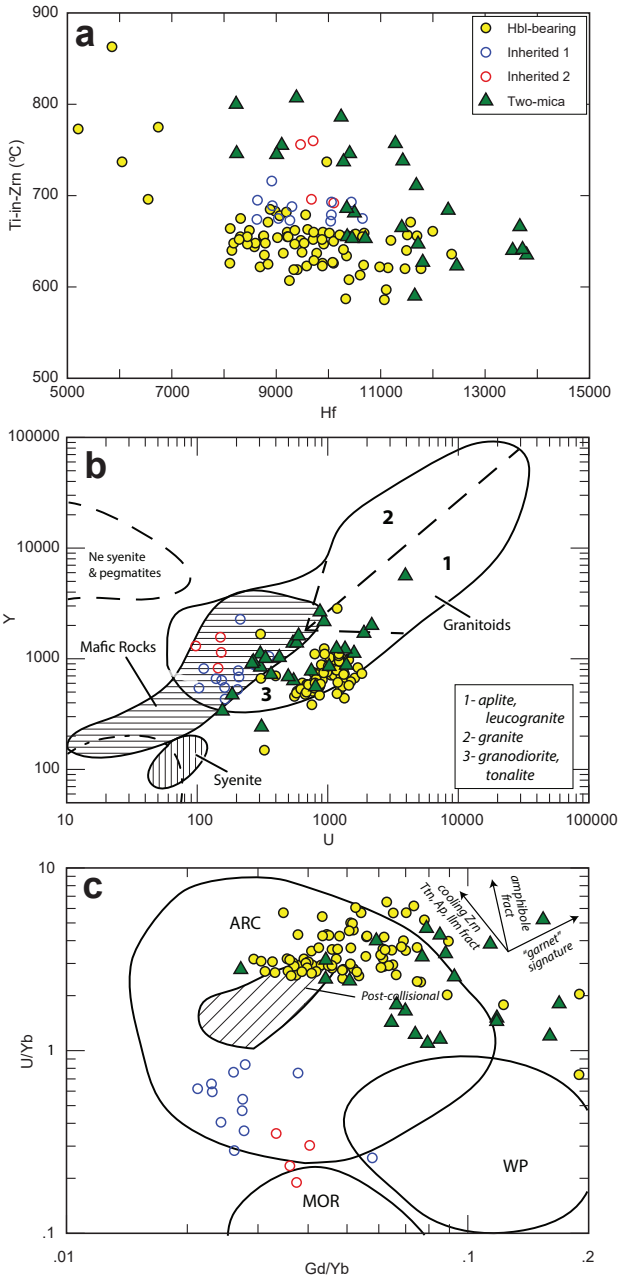


Figure 6-29. *Trace element zircon chemistry from LA-ICPMS analyses of samples from the McGregor batholith (Appendix 3).* ***(a)*** *Plot of crystallization temperature estimates (Ti-in-zircon) versus Hf concentrations in zircon.* ***(b)*** *Y vs. U classification diagram of Belousova et al. (2002).* ***(c)*** *Discriminant diagram of Grimes et al. (2015). Open symbols for sample 14PS171-2 are analyses of inherited cores; Inherited 1 are Early Jurassic zircons; Inherited 2 are Mississippian (see Fig. 6-19).*

Isotopes

Two samples from the main phase of hornblende granodiorite were analyzed for whole-rock Sr and Nd isotopes (14PS171-2 and 14PS181-1; Appendix 9). K-feldspar separates from 14PS181-1 were also analyzed for Pb isotopes. Initial $^{87}Sr/^{86}Sr$ (Sr_i) values for these samples are 0.7054–0.7055 and initial $^{143}Nd/^{144}Nd$ values are 0.512407–0.512448 (εNd_t = -0.1 – +0.7). $^{207}Pb/^{204}Pb$ in K-feldspar from 14PS181-1 is 15.713. These isotopic ratios are all consistent with some degree of mixing of evolved crustal material in the magma (Armstrong, 1988).

Zircons from these samples were also analyzed for Lu-Hf by split-stream LA-ICPMS at Memorial University (14PS181-1; Appendix 10). Sampled spots were chosen to match U-Pb LA-ICPMS analyses from Boise State University (Appendix 3). The Late Jurassic zircons in both samples have εHf_i values of +0.8 – +4.2 (Fig. 6-30) that are consistent with slightly evolved whole-rock isotopic values for these samples (Appendix 9). The inherited zircon components have more juvenile values with εHf_i of +2.6 – +8.2 for Early Jurassic zircons and εHf_i of +7.0 – +11.1 in Mississippian zircons (Fig. 6-30). This is consistent with the more mafic compositions of these zircons (Fig. 6-29). The two-mica granodiorite phase has not been characterized isotopically.

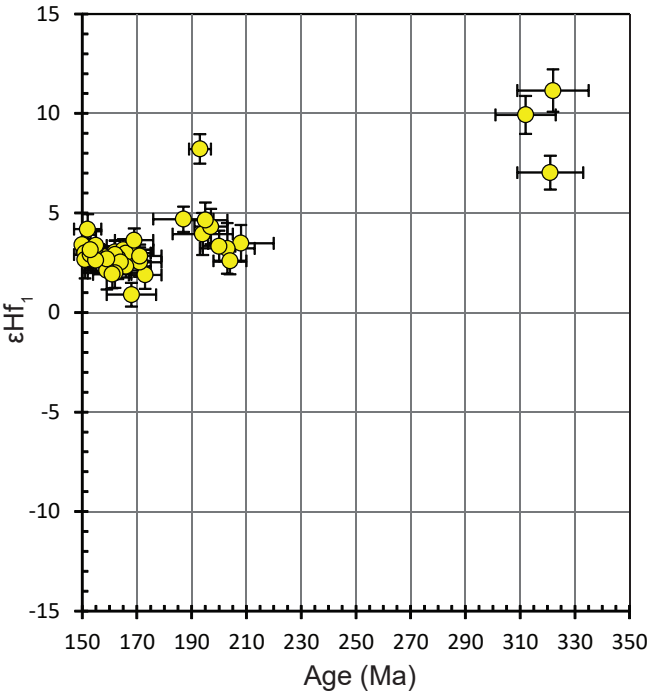


Figure 6-30. *Hf isotopic data for selected zircons from the McGregor batholith (Appendix 10). Error bars are 2σ.*

Discussion

The McGregor batholith intrudes metamorphosed rocks of Quesnellia within a structural panel bounded by the Towhata and Tatchun faults (Figs. 6-1 and 6-2). The McGregor batholith as described here was originally considered to be the northwestern extension of the Early Jurassic Tatchun batholith (Tempelman-Kluit, 1984; Gordey and Makepeace, 2001). More detailed mapping by Colpron *et al.* (2002) has shown that the McGregor and Tatchun batholiths are actually distinct plutons separated by a thin band of mafic to intermediate metavolcanic rocks and the Towhata fault (Fig. 6-2). The Tatchun batholith, east of the Towhata fault, is dated at *ca.* 203–196 Ma (*see* Chapter 3). Because both batholiths are dominantly composed of hornblende-biotite granodiorite, the McGregor was also assumed to be Early Jurassic (Colpron *et al.*, 2002; Colpron, 2011). It was assumed that the Late Jurassic K/Ar dates from the McGregor batholith (Stevens *et al.*, 1982a) were unreliable and likely recorded slow cooling and/or resetting of hornblende and biotite. We present here the first U-Pb zircon dates for the McGregor batholith that show that it is indeed part of a distinct Late Jurassic plutonic suite (Fig. 6-31; Table 6-1; Appendices 3 and 4).

The McGregor batholith comprises two distinct phases: 1) a hornblende-biotite granodiorite; and 2) a two-mica granodiorite (Fig. 6-2). The main hornblende granodiorite phase is well-constrained by three samples with $^{206}U/^{238}Pb$ dates of 163.42 ± 0.05 and 161.16 ± 0.05 Ma (Figs. 6-17 to 6-19, and 6-31). This clearly demonstrates that the McGregor batholith is the product of a distinct pulse of magmatism more than 35 m.y. younger than intrusion of Minto suite plutons, such as the Tatchun batholith. The hornblende-bearing phase of the McGregor batholith was emplaced at 4-5 kbar (depth of ~18 km; Appendix 5) into greenschist to amphibolite facies rocks of Quesnellia. This phase is reduced (Figs. 6-4 and 6-9), weakly peraluminous, alkali-calcic to alkalic (Fig. 6-25), and has trace element and isotopic compositions indicating significant fractionation and interaction of the parent magma with evolved crustal material (Figs. 6-27, 6-29 and 6-30; Appendices 3 and 8-10).

The two-mica granodiorite phase occurs as a central pluton that apparently intrudes the hornblende granodiorite, and as a southwestern border phase to the McGregor batholith (Fig. 6-2). The key evidence indicating that the two-mica phase is younger and intrudes the dominant hornblende granodiorite phase is the weak magnetic halo surrounding the central body, interpreted to mark a contact aureole (Fig. 6-9). However, the geochemistry of the two-mica granodiorite suggests it may represent a more highly fractionated component of the older hornblende granodiorite, with higher SiO_2 but lower Al_2O_3 - Na_2O - CaO - TiO_2 - P_2O_5 - Fe_T and REE abundances (Figs. 6-23, 6-24 and 6-27). The two-mica phase is more strongly peraluminous and calc-alkalic in composition (Fig. 6-25).

Dating of the two-mica granodiorite is proving more challenging. Zircons from three samples analyzed by LA-ICPMS yield a scatter of $^{206}U/^{238}Pb$ dates that suggest mixing of different age components and possible Pb loss, particularly in high U analyses (Fig. 6-20). Sample 94M147 from the southwestern margin of the batholith contains inherited components at *ca.* 260 Ma and older, and its best crystallization estimate at *ca.* 167 Ma is slightly older than the main phase hornblende granodiorite it is inferred to intrude (Fig. 6-31). Both samples from the central body of

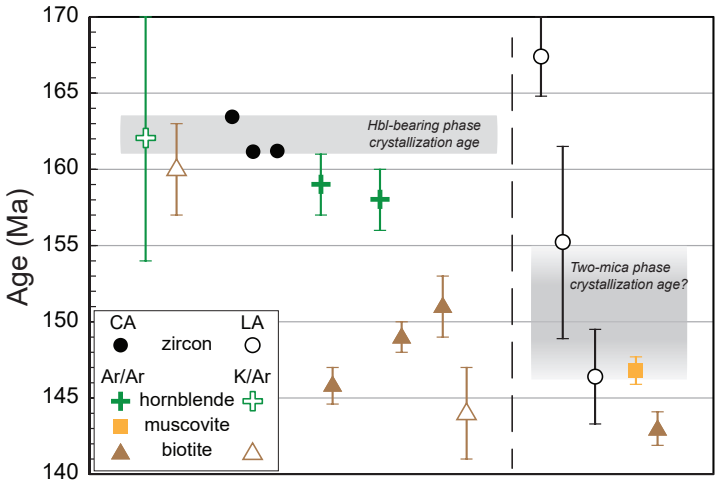


Figure 6-31. *Summary of geochronological results for the McGregor batholith (dates from Appendix 1). Older K/Ar dates are from Stevens et al. (1982a); all other dates are from this study (Appendices 3, 4, 6, and 11). All errors are 2σ.*

two-mica granodiorite yield younger estimates of *ca.* 155–146 Ma based on the youngest zircon analyses with U concentrations <1000 ppm (Figs. 6-20 and 6-31), consistent with the intrusive relationship indicated by the aeromagnetic data (Fig. 6-9).

A muscovite $^{40}Ar/^{39}Ar$ date of *ca.* 147 Ma from the central body further constrains the age of the two-mica granodiorite phase (Figs. 6-22 and 6-31). It records cooling below the 490°C closure temperature for Ar in muscovite (Hodges, 2014; Table 1-6), and matches the youngest reliable zircon analyses in this sample (14PS178-1; Figs. 6-20 and 6-31). Biotite from this sample is slightly younger at *ca.* 143 Ma (Figs. 6-22 and 6-31). It is notable that biotite $^{40}Ar/^{39}Ar$ cooling ages from the older phase of hornblende granodiorite yield disturbed age spectra with plateau segments at *ca.* 151–146 Ma (Figs. 6-21 and 6-31), suggesting either slow cooling after crystallization at *ca.* 161 Ma, or more likely resetting following intrusion of the younger two-mica granodiorite phase between 155 and 146 Ma. A biotite K/Ar date of 144 ± 3 Ma from the 'contact aureole' of the central body (Figs. 6-2 and 6-9) is consistent with the *ca.* 143 Ma biotite $^{40}Ar/^{39}Ar$ date within this central phase (Fig. 6-31). Hornblende from the main phase granodiorite have $^{40}Ar/^{39}Ar$ dates of *ca.* 159–158 Ma (Fig. 6-21) that suggest rapid cooling below ~550°C within ~2 m.y. from crystallization at temperatures of ~590–690°C (Ti-in-zircon; Table 6-1; Appendix 3), and that reheating related to intrusion of the younger two-mica phase was not sufficient to affect Ar retention in hornblende.

From these data, we take the range of youngest reliable zircon $^{206}U/^{238}Pb$ dates and the muscovite $^{40}Ar/^{39}Ar$ date to indicate *ca.* 155–146 Ma as the most probable age of emplacement of the two-mica granodiorite phase of the McGregor batholith. In this context, the *ca.* 167 Ma estimate for similar two-mica granodiorite along the southwest margin of the batholith (94M147; Figs. 6-2 and 6-20) likely represents an inherited component from the older phase of hornblende granodiorite.

The McGregor batholith is the only Late Jurassic pluton to intrude the Intermontane terranes in Yukon (Fig. 6-7). Late Jurassic plutons are a rare occurrence in the Intermontane terranes of the northern Cordillera (Fig. 6-32).The only other known occurrences of Late Jurassic granitoid rocks north of the 54th parallel are the Snowdrift Creek and McBride River plutons near Dease Lake, in northern British Columbia (van Straaten and Gibson, 2017; van Straaten and Bichlmaier, 2018). Both plutons are medium-grained hornblende-biotite granodiorite and the Snowdrift Creek pluton is dated by U-Pb zircon at 160.43 ± 0.16 Ma (CA-TIMS, UBC; van Straaten and Gibson, 2017). Late Jurassic plutons are more common in the Intermontane terranes of southern British Columbia, where they intrude mainly Quesnellia (Fig. 6-32). However, they are most common in the Coast plutonic complex where they intrude mainly into the Insular terranes and encroach into western Stikinia south of Prince Rupert.

The McGregor batholith has a low magnetic response and low ferric/ferrous Fe ratios indicating reduced to weakly oxidized magmatic conditions (Figs. 6-4 and 6-9). Geochemical data and the presence of local pegmatite and aplite indicate the pluton is strongly fractionated. These attributes suggest magmatic conditions that are favourable for Au, W ± Sn mineralization (Fig. 6-33). Al-in-hornblende geobarometry indicates that the hornblende granodiorite phase of the McGregor batholith was emplaced at 4–5 kbar (~18 km depth), well below the 6–9 km maximum depth at which porphyry deposits form (Seedorff *et al.*, 2005). The emplacement depth of the younger, two-mica granodiorite phase is not well constrained, but presumably somewhat shallower than that of the hornblende-bearing phase. In general, deep, or depth independent, deposit models such as skarns or possibly reduced intrusion-related gold systems are probably more appropriate exploration models for the McGregor batholith.

The western part of the McGregor batholith remained unglaciated during the last glaciation (*ca.* 22 Ka), with advance of the McConnell ice sheet only covering the easternmost edge of the pluton (Fig. 6-6). Valleys over much of the batholith area are filled with thick glaciofluvial deposits of the Reid and McConnell epochs which could result in more subdued geochemical response in stream sediment samples. Despite this potential for dilution, 17 of 94 stream sediment samples collected over the McGregor batholith have >10 ppb Au (Fig. 6-34; Table 6-2). A sample from the catchment which encompasses the Tatlmain occurrence [115I 114] has 141 ppb Au, 120 ppm As, 1.7 ppm W and 48 ppb Hg.

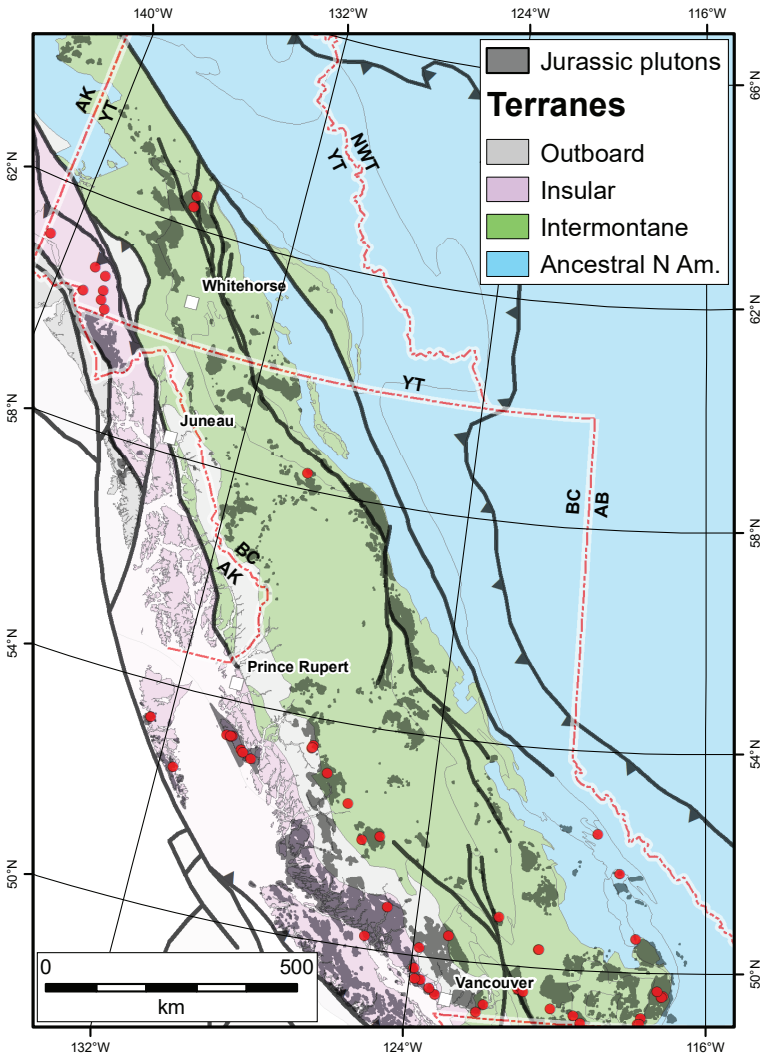


Figure 6-32. *Distribution of Late Jurassic plutons in the Cordillera of British Columbia and Yukon (red dots; U-Pb crystallization ages of 165–145 Ma; Canadian Geochronology Knowledgebase, 2013; YGS, 2020c; van Straaten and Gibson, 2017; this study). Grey areas show distribution of all Jurassic plutons (~200–145 Ma) in the Canadian Cordillera (Cui et al., 2017; YGS, 2020a). Simplified terrane map from Colpron and Nelson (2011).*

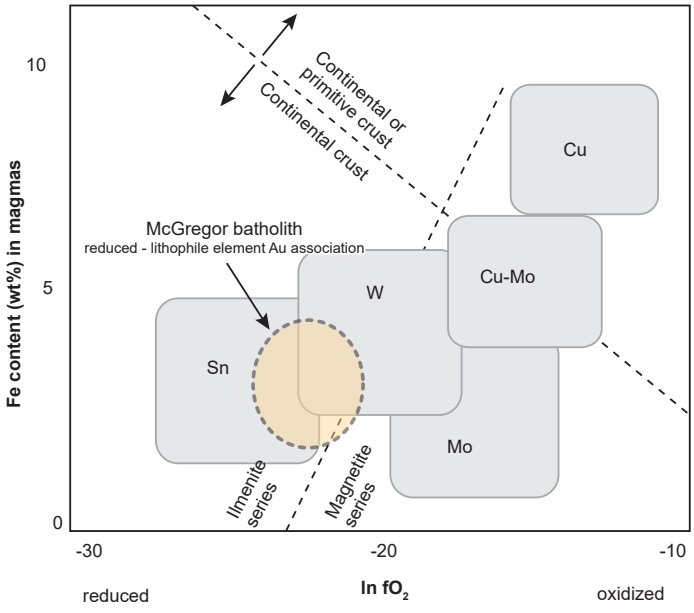


Figure 6-33. *Schematic plot of degree of fractionation, shown by the Fe content of magmas, versus oxidation state (fO_2) for calc-alkaline to alkaline magmas associated with magmatic-hydrothermal mineralization (modified from Thompson et al., 1999). The generalized position of the McGregor batholith, with a potential tin (lithophile) and tungsten (partial lithophile) and gold association, is shown and compared to the position of more typical copper-gold (chalcophile) systems. Boundary between the magnetite and ilmenite-series magmas from Ishihara (1977).*

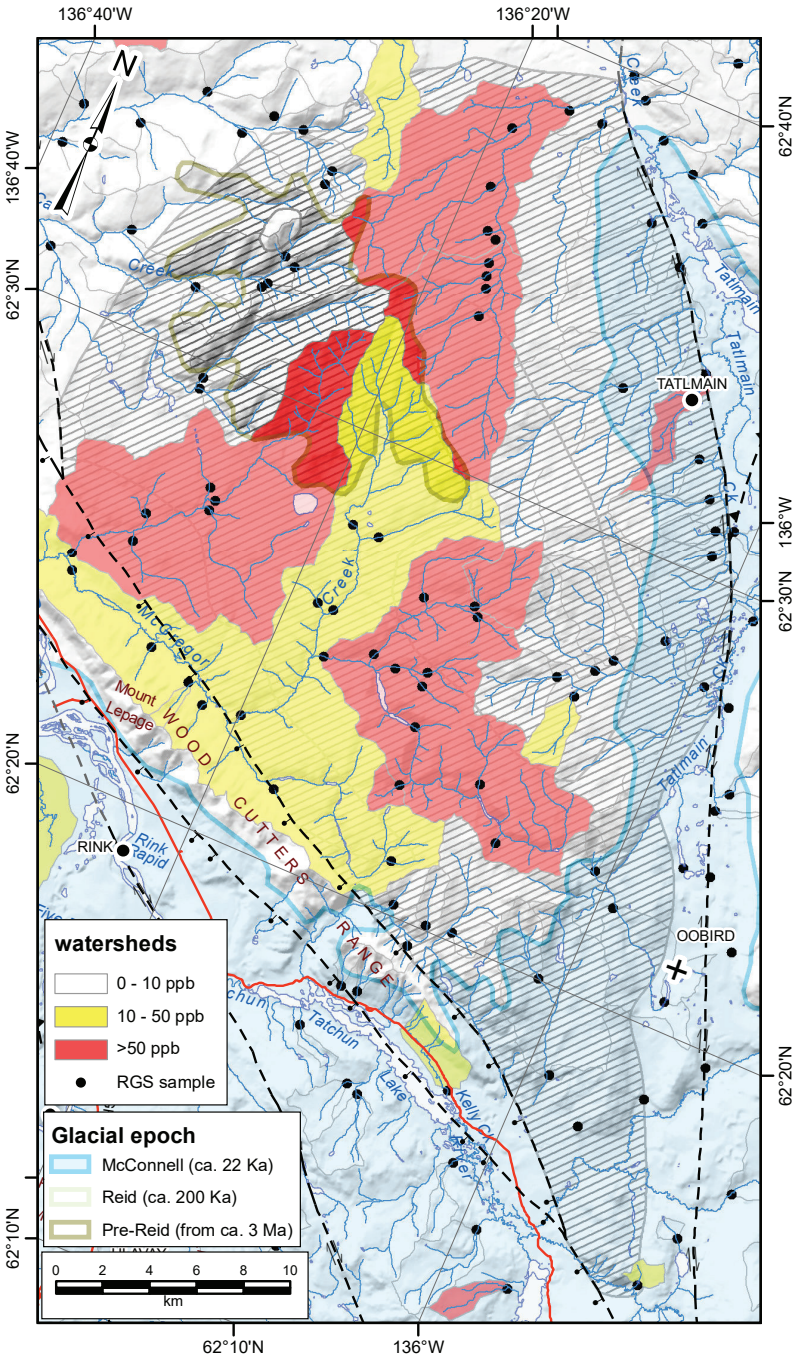


Figure 6-34. *Catchment basins in the McGregor batholith area with ≥10 ppb Au. Gold value used is highest from original data in Héon (2003) and re-analysis by Jackaman (2015b). Glacial limits after Duk-Rodkin (1999). Hatched area shows extent of the Late Jurassic McGregor batholith. Fault symbology as in Figure 1-4.*

Table 6-2. *Summary of select RGS data with >10 ppb Au[1] in the McGregor batholith area.*

		Ag	As	Au[1]	Bi	Hg	Te	W
McGregor batholith area n = 17	min	25	1.8	10.2	0.03	18	BD	BD
	max	640	119.8	145	3.03	81	0.1	1.7
	90th percentile threshold[2]	200	11.7	4.8	NA	92	NA	3

[1] Due to the 'nugget effect' of gold in stream sediment samples (Mackie et al., 2017), Au values quoted here are the highest out of the original analysis, rerun analysis or INAA analysis from Heon (2003) or reanalysis from Jackaman (2015b)

[2] from Heon (2003) calculations for Intermontane terranes

all values in ppm except Ag and Au which are ppb

References

Abbott, J.G., 1971. Geology of the Williams Creek prospect. BSc thesis, University of British Columbia, 53 p.

Allan, M.M. and Friend, M., 2018. Bedrock geological map of the Mount Freegold district, Dawson Range (NTS 115I/6 and parts of 115I/2, 3, 5, 7, 10, 11, 12). Yukon Geological Survey, Open File 2018-2, scale 1:50000.

Allan, M.M., Mortensen, J.K., Hart, C.J.R., Bailey, L.A., Sánchez, M.G., Ciolkiewicz, W., McKenzie, G.G. and Creaser, R.A., 2013. Magmatic and metallogenic framework of west-central Yukon and eastern Alaska. *In*: Tectonics, Metallogeny, and Discovery: The North American Cordillera and Similar Accretionary Settings, M. Colpron, T. Bissig, B.G. Rusk and J.F.H. Thompson (eds.), Society of Economic Geologists, Inc., Special Publication Number 17, p. 111–168.

Allen, T.L. and Weston, L.H., 2001. Preliminary geological map of Division Mountain area (105E/5-West Half and 115 H/8 East Half), central Yukon. Exploration and Geological Services Division, Yukon Region, Indian and Northern Affairs Canada, Open File 2001-3, scale 1:50 000.

Anderson, J.L. and Smith, D.R., 1995. The effects of temperature and f_{O_2} on the Al-in hornblende barometer. American Mineralogist, vol. 80, p. 549–559.

Armstrong, R.L., 1988. Mesozoic and early Cenozoic magmatic evolution of the Canadian Cordillera. Geological Society of America Special Papers, vol. 218, p. 55–92.

Aurora Geosciences Ltd. and Bruce, J.O., 2017a. Reprocessing of Yukon magnetic data for NTS 105D. Yukon Geological Survey, Open File 2017-12, scale 1:250 000.

Aurora Geosciences Ltd. and Bruce, J.O., 2017b. Reprocessing of Yukon magnetic data for NTS 115I. Yukon Geological Survey, Open File 2017-38, scale 1:250 000.

Aurora Geosciences Ltd. and Bruce, J.O., 2017c. Reprocessing of Yukon magnetic data for NTS 105E. Yukon Geological Survey, Open File 2017-13, scale 1:250 000.

Aurora Geosciences Ltd. and Bruce, J.O., 2017d. Reprocessing of Yukon magnetic data for NTS 105L. Yukon Geological Survey, Open File 2017-20, scale 1:250 000.

Aurora Geosciences Ltd. and Bruce, J.O., 2017e. Reprocessing of Yukon magnetic data for NTS 105C. Yukon Geological Survey, Open File 2017-11, scale 1:250 000.

Aurora Geosciences Ltd. and Bruce, J.O., 2017f. Reprocessing of Yukon magnetic data for NTS 105B. Yukon Geological Survey, Open File 2017-10, scale 1:250 000.

Aurora Geosciences Ltd. and Bruce, J.O., 2017g. Reprocessing of Yukon magnetic data for NTS 105G. Yukon Geological Survey, Open File 2017-15, scale 1:250 000.

Barker, D.S., 1970. Composition of granophyre, myrmekite and graphic granite. Geological Society of America Bulletin, vol. 81, p. 3339–3350.

Belousova, E.A., Griffin, W.L., O'Reilly, S.Y. and Fisher, N., 2002. Igneous zircon: trace element composition as an indicator of source rock type. Contributions to Mineralogy and Petrology, vol. 143, no. 5, p. 602–622.

Bickerton, L., 2014a. The northern Cache Creek terrane: a record of Middle Triassic arc activity and Jurassic-Cretaceous terrane imbrication. MSc thesis, Simon Fraser University, 94 p.

Bickerton, L., 2014b. Geological map of Michie Creek (NTS 105D/9) and parts of Tagish (NTS 105D/8) areas. Yukon Geological Survey, Open File 2014-11, scale 1:50 000.

Bickerton, L., Colpron, M., Gibson, H.D., Thorkelson, D.J. and Crowley, J.L., 2020. The northern termination of the Cache Creek terrane in Yukon: Middle Triassic arc activity and Jurassic-Cretaceous structural imbrication. Canadian Journal of Earth Sciences, vol. 57, p. 227–248.

Bineli Betsi, T. and Bennett, V., 2010. New U-Pb age constraints at Freegold Mountain: Evidence for multiple phases of polymetallic mid to Late Cretaceous mineralization *In*: Yukon Exploration and Geology 2009, K.E. MacFarlane, L.H. Weston and L.R. Blackburn (eds.), Yukon Geological Survey, p. 57–84.

Bineli Betsi, T., Lentz, D. and McFarlane, C., 2016. The Nucleus deposit: Superposed Au–Ag–Bi–Cu mineralization systems at Freegold Mountain, Yukon, Canada. Resource Geology, vol. 66, no. 4, p. 419–454.

Bond, J.D. and Plouffe, A., 2003. Yukon Targeted Geoscience Initiative, Part 2: Glacial history, till geochemistry and new mineral exploration targets in Glenlyon and eastern Carmacks map areas, central Yukon. *In*: Yukon Exploration and Geology 2002, D.S. Emond and L.L. Lewis (eds.), Exploration and Geological Services Division, Yukon Region, Indian and Northern Affairs Canada, p. 109–134.

Bordet, E., 2019. Bedrock geology map of the eastern Lake Laberge area (parts of NTS 105E/2, 3, 6, 7 and 105D/15, 16). Yukon Geological Survey, Geoscience Map GM2019-1, scale 1:50 000, 2 sheets.

Bordet, E., Crowley, J.L. and Piercey, S.J., 2019. Geology of the eastern Lake Laberge area (105E), south-central Yukon. Yukon Geological Survey, Open File 2019-1, 120 p.

Brand, A.A., 2008. Mineralogy, geochemistry, and geochronology of the Northern Dancer tungsten-molybdenum deposit, Yukon and British Columbia. MSc thesis, University of British Columbia, 256 p.

Breitsprecher, K. and Mortensen, J.K. (compilers), 2004. Yukon age 2004: A database of isotopic age determinations for rock units from Yukon Territory, Canada. Yukon Geological Survey, CD-ROM.

Bremner, T.J. and Liverton, T., 1990. Crescent, Dan (property descriptions). *In*: Yukon Exploration and Geology 1990, Exploration and Geological Services Division, Yukon Region, Indian and Northern Affairs Canada, p. 25–30.

British Columbia Geological Survey, 2019. BC MINFILE - A database of mineral occurrences. British Columbia Geological Survey, https://www2.gov.bc.ca/gov/content/industry/mineral-exploration-mining/british-columbia-geological-survey/mineralinventory [accessed October, 2019].

Calvert, A.J., Hayward, N., Vayavur, R. and Colpron, M., 2017. Seismic and gravity constraints on the crustal architecture of the Intermontane terranes, central Yukon. Canadian Journal of Earth Sciences, vol. 54, no. 7, p. 798–811.

Canadian Geochronology Knowledgebase, 2013. Geological Survey of Canada, Earth Science Sector, Natural Resources Canada, https://www.nrcan.gc.ca/earth-sciences/geography/atlas-canada/canadian-geochronology-knowledgebase/18211 [accessed November 2019].

Carlson, G.G., 1987. Geology of Mount Nansen (115-I/3) and Stoddart Creek (115-I/6) map areas Dawson Range, central Yukon. Exploration and Geological Services Division, Yukon Region, Indian and Northern Affairs Canada, Open File 1987-2, 194 p.

Casselman, S.G., 2008. Carmacks Copper project, 2007 assessment report. Yukon Energy, Mines and Resources, Assessment Report 094996, 184 p.

Casselman, S., 2018. Yukon mineral deposits summary 2018. Yukon Geological Survey 30 p.

Chappell, B.W. and White, J.R., 1974. Two contrasting granite types. Pacific Geology, vol. 8, p. 173–174.

Chappell, B.W. and White, J.R., 2001. Two contrasting granite types: 25 years later. Australian Journal of Earth Sciences, vol. 48, p. 489–499.

Clark, A.D., 2017. Tectonometamorphic history of mid-crustal rocks at Aishihik Lake, southwest Yukon. MSc thesis, Simon Fraser University, 153 p.

Colpron, M., 1998. Preliminary Geological Map of Little Kalzas Lake, Central Yukon (NTS 105L/13). Exploration and Geological Services Division, Yukon Region, Indian and Northern Affairs Canada, Open File 1998-3(G), scale 1:50 000.

Colpron, M., 1999. Glenlyon project: Preliminary stratigraphy and structure of Yukon-Tanana Terrane, Little Kalzas Lake area, central Yukon (105L/13). *In*: Yukon Exploration and Geology 1998, C.F. Roots and D.S. Emond (eds.), Exploration and Geological Sciences Division, Yukon Region, Indian and Northern Affairs Canada, p. 63–71.

Colpron, M. (compiler), 2006. Tectonic assemblage map of Yukon-Tanana and related terranes in Yukon and northern British Columbia. Yukon Geological Survey, Open File 2006-1, scale 1:1 000 000.

Colpron, M. (complier), 2011. Geological compilation of Whitehorse trough – Whitehorse (105D), Lake Laberge (105E), and part of Carmacks (115I), Glenlyon (105L), Aishihik Lake (115H), Quiet Lake (105F) and Teslin (105C). Yukon Geological Survey, Geoscience Map 2011-1, 3 maps, legend and appendices, scale 1:250 000.

Colpron, M., Crowley, J.L., Gehrels, G., Long, D.G.F., Murphy, D.C., Beranek, L. and Bickerton, L., 2015. Birth of the northern Cordilleran orogen, as recorded by detrital zircons in Jurassic synorogenic strata and regional exhumation in Yukon. Lithosphere, vol. 7, no. 5, p. 541–562.

Colpron, M. and Friedman, R.M., 2008. U-Pb zircon ages for the Nordenskiöld formation (Laberge Group) and Cretaceous intrusive rocks, Whitehorse trough, Yukon. *In*: Yukon Exploration and Geology 2007, D.S. Emond, Blackburn, L.R., Hill, R.P. and Weston, L.H. (ed.), Yukon Geological Survey, p. 139–151.

Colpron, M., Gordey, S., Lowey, G., White, D. and Piercey, S., 2007b. Geology of the northern Whitehorse trough, Yukon (105E/12, 13 and parts of 11 and 14; 105L/4 and parts of 3 and 5; parts of 115H/9 and 16; 115I/1 and part of 8). Yukon Geological Survey, 2007-6. Scale 1:150 000.

Colpron, M., Israel, S. and Friend, M., 2016b. Yukon plutonic suites. Yukon Geological Survey, Open File 2016-37, scale 1:750 000.

Colpron, M., Israel, S., Murphy, D.C., Pigage, L.C. and Moynihan, D., 2016a. Yukon Bedrock Geology Map 2016. Yukon Geological Survey, Open File 2016-1, scale 1:1 000 000.

Colpron, M., Mortensen, J.K., Gehrels, G.E. and Villeneuve, M., 2006b. Basement complex, Carboniferous magmatism and Paleozoic deformation in Yukon-Tanana terrane of central Yukon: Field, geochemical and geochronological constraints from Glenlyon map area. *In*: Paleozoic evolution and metallogeny of pericratonic terranes at the ancient Pacific margin of North America, Canadian and Alaskan Cordillera, M. Colpron and J.L. Nelson (eds.), Geological Association of Canada, Special Paper 45, p. 131–151.

Colpron, M., Murphy, D.C., Nelson, J.L., Roots, C.F., Gladwin, K., Gordey, S.P., Abbott, G. and Lipovsky, P.S., 2002. Preliminary geological map of Glenlyon (105L/1–7,11–14) and northeast Carmacks (115I/9, 16) areas, Yukon Territory (1:125 000 scale). Exploration and Geological Services Division, Yukon Region, Indian and Northern Affairs Canada, Open File 2002-9; *also Geological Survey of Canada, Open File 1457*. Scale 1:125 000.

Colpron, M., Murphy, D.C., Nelson, J.L., Roots, C.F., Gladwin, K., Gordey, S.P. and Abbott, J.G., 2003. Yukon Targeted Geoscience Initiative, Part 1: Results of accelerated bedrock mapping in Glenlyon (105L/1–7, 11–14) and northeast Carmacks (115I/9,16) areas, central Yukon. *In*: Yukon Exploration and Geology 2002, D.S. Emond and L.L. Lewis (eds.), Exploration and Geological Services Division, Yukon Region, Indian and Northern Affairs Canada, p. 85–108.

Colpron, M. and Nelson, J.L., 2011. A digital atlas of terranes for the northern Cordillera. Yukon Geological Survey; *also, BC Geological Survey, GeoFile 2011-11*, https://yukon.ca/en/yukon-geology#bedrock-geology [accessed June 29, 2019].

Colpron, M., Nelson, J.L. and Murphy, D.C., 2006a. A tectonostratigraphic framework for the pericratonic terranes of the northern Cordillera. *In:* Paleozoic Evolution and Metallogeny of Pericratonic Terranes at the Ancient Pacific Margin of North America, Canadian and Alaskan Cordillera, M. Colpron and J.L. Nelson (eds.), Geological Association of Canada, Special Paper 45, p. 1–23.

Colpron, M., Nelson, J.L. and Murphy, D.C., 2007a. Northern Cordilleran terranes and their interactions through time. GSA Today, vol. 17, no. 4/5, p. 4–10.

Colpron, M. and Ryan, J.J., 2010. Bedrock geology of southwest McQuesten (NTS 115P) and part of northern Carmacks (NTS 115I) map area. *In*: Yukon Exploration and Geology 2009, K.E. MacFarlane, L.H. Weston and L.R. Blackburn (eds.), Yukon Geological Survey, p. 159–184.

Cook, F.A., Clowes, R.M., Snyder, D.B., van der Velden, A.J., Hall, K.W., Erdmer, P. and Evenchick, C.A., 2004. Precambrian crust beneath the Mesozoic northern Canadian Cordillera discovered by Lithoprobe seismic reflection profiling. Tectonics, vol. 23, p. TC2010. https://doi.org/10.1029/2002TC001412.

Cui, Y., Miller, D., Schiarizza, P. and Diakow, L.J., 2017. British Columbia digital geology. British Columbia Geological Survey, Open File 2017-8, p. 9.

Dehkordi, B.H., Ferguson, I.J., Jones, A.G. and Ledo, J., 2019. Tectonics of the northern Canadian Cordillera imaged using modern magnetotelluric analysis. Tectonophysics, vol. 765, p. 102–128.

D'el-Rey Silva, L.J.H., Liverton, T., Paradis, S. and Roots, C., 2001. A structural analysis of the upper Swift River area (105 B/3), Yukon, Part I: Dan Zn occurrence and implications for sulphide mineralization. *In*: Yukon Exploration and Geology 2000, D.S. Emond and L.W. Weston (eds.), Exploration and Geological Sciences Division, Yukon Region, Indian and Northern Affairs Canada, p. 289–300.

Duk-Rodkin, A., 1999. Glacial Limits Map of Yukon. Yukon Geological Survey, Geoscience Map 1999-2, 1:1 000 000 scale.

Dusel-Bacon, C., Aleinikoff, J.N., Day, W.C. and Mortensen, J.K., 2015. Mesozoic magmatism and timing of epigenetic Pb-Zn-Ag mineralization in the western Fortymile mining district, east-central Alaska: Zircon U-Pb geochronology, whole-rock geochemistry, and Pb isotopes. Geosphere, vol. 11, no. 3, p. 786–822.

Friend, M., Allan, M.M. and Hart, C.J.R., 2018. New contributions to the bedrock geology of the Mount Freegold district, Dawson Range, Yukon (NTS 115I/2, 6 and 7). *In*: Yukon Exploration and Geology 2017, K.E. MacFarlane (ed.), Yukon Geological Survey, p. 47–68.

Frost, B.R., Barnes, C.G., Collins, W.J., Arculus, R.J., Ellis, D.J. and Frost, C.D., 2001. A geochemical classification for granitic rocks. Journal of Petrology, vol. 42, no. 11, p. 2033–2048.

Gabrielse, H., Murphy, D.C. and Mortensen, J.K., 2006. Cretaceous and Cenozoic dextral orogen-parallel displacements, magmatism and paleogeography, north central Canadian Cordillera. *In*: Paleogeography of the North American Cordillera: Evidence for Major Lateral Displacements in the North American Cordillera, J.W. Haggart, R.J. Enkin and J.W.H. Monger (eds.), Geological Association of Canada, Special Paper 46, p. 255–276.

Gordey, S.P. and Makepeace, A.J. (compilers), 2001. Bedrock geology, Yukon Territory. Exploration and Geological Services Division, Yukon Region, Indian and Northern Affairs Canada, Open File 2001-1; also Geological Survey of Canada, Open File 3754, scale 1:1 000 000.

Gordey, S.P., McNicoll, V.J. and Mortensen, J.K., 1998. New U-Pb ages from the Teslin area, southern Yukon, and their bearing on terrane evolution in the northern Cordillera. *In*: Radiogenic age and isotopic studies: Report 11, Geological Survey of Canada, Report 11, p. 129–148.

Gordey, S.P. and Ryan, J.J., 2005. Geology, Stewart River area (115N,115O and part of 115J), Yukon Territory. Geological Survey of Canada, Open File 4970, scale 1:250 000.

Gordey, S.P. and Stevens, R.A., 1994. Preliminary interpretation of bedrock geology of the Teslin area (105C), southern Yukon. Geological Survey of Canada, Open File 2886, scale 1:250 000.

Grimes, C.B., Wooden, J.L., Cheadle, M.J. and John, B., 2015. "Fingerprinting" tectono-magmatic provenance using trace elements in igneous zircon. Contributions to Mineralogy and Petrology, vol. 170, no. 5-6, p. 1–26.

Grond, H.C., Churchill, S.J., Armstrong, R.L., Harakal, J.E. and Nixon, G.T., 1984. Late Cretaceous age of the Hutshi, Mount Nansen, and Carmacks groups, southwestern Yukon Territory and northwestern British Columbia. Canadian Journal of Earth Sciences, vol. 21, no. 5, p. 554–558.

Hammarstrom, J.M. and Zen, E., 1986. Aluminum in hornblende: An empirical igneous geobarometer. American Mineralogist, vol. 71, p. 1297–1313.

Harris, M.J., Symons, D.T.A., Blackburn, W.H., Hart, C.J.R. and Villeneuve, M., 2003. Travels of the Cache Creek terrane: a paleomagnetic, geobarometric and $^{40}Ar/^{39}Ar$ study of the Jurassic Fourth of July Batholith, Canadian Cordillera. Tectonophysics, vol. 362, no. 1, p. 137–159.

Hart, C.J.R., 1995. Magmatic and tectonic evolution of the Intermontane superterrane and Coast Plutonic complex in southern Yukon Territory. MSc thesis, University of British Columbia, 209 p.

Hart, C.J.R., 1997a. A transect across northern Stikinia: Geology of the northern Whitehorse map area, southern Yukon Territory (105D/13–16). Exploration and Geological Services Division, Yukon Region, Indian and Northern Affairs Canada, Bulletin 8, 112 p.

Hart, C.J.R., 1997b. Geology of Thirty-seven Mile Creek map area, southern Yukon Territory, (NTS 105D/13). Exploration and Geological Services Division, Yukon Region, Indian and Northern Affairs Canada, Geoscience Map 1997-4, scale 1:50 000.

Hart, C.J.R., 1997c. Geology and geochemistry of the Teslin Crossing Pluton: A gold-rich alkalic porphyry target. *In*: Yukon Exploration and Geology, 1996, Exploration and Geological Services Division, Yukon Region, Indian and Northern Affairs Canada, p. 131–137.

Hart, C.J.R., Goldfarb, R.J., Lewis, L.L. and Mair, J.L., 2004a. The northern Cordillera mid-Cretaceous plutonic province: Ilmenite/magnetite-series granitoids and intrusion-related mineralization. Resource Geology, vol. 54, no. 3, p. 253–280.

Hart, C.J.R., Mair, J.L., Goldfarb, R.J. and Groves, D.I., 2004b. Source and redox controls on the metallogenic variations in intrusion-related ore systems, Tombstone-Tungsten belt, Yukon Territory, Canada. Transactions of the Royal Society of Edinburgh: Earth Sciences, vol. 95, p. 339–356.

Hart, C.J.R. and Radloff, J.K., 1990. Geology of Whitehorse, Alligator Lake, Fenwick Creek Carcross and Part of Robinson Map Areas (105D/11, 6, 3, 2 and 7). Yukon Geological Survey, Open File 1990-4.

Hayward, N. and Oneschuk, D., 2011. Geophysical Series, regional geophysical compilation project, Yukon Plateau, Yukon, parts of NTS 105, 106, 115 and 116. Geological Survey of Canada, Open File 6840.

Henneberry, R.T., 1988. 1988 Stage I progress report for assessment credit on the Red Ridge property. Yukon Energy, Mines and Resources Assessment Report 092577.

Héon, D. (compiler), 2003. Yukon Regional Geochemical Database 2003 – Stream sediment analyses. Exploration and Geological Services Division, Yukon Region, Indian and Northern Affairs Canada.

Hodges, K.V., 2014. Geochronology and Thermochronology in Orogenic Systems. *In*: Treatise on geochemistry, volume 3 – The crust, H.D. Holland and K.K. Turekian (eds.), Elsevier Pergamon, p. 263–292.

Holland, T.J.B. and Blundy, J.D., 1994. Non-ideal interactions in calcic amphiboles and their bearing on amphibole-plagioclase thermometry. Contributions to Mineralogy and Petrology, vol. 116, p. 433–447.

Hollister, L.S., Grissom, G.C., Peter, E.K., Stowell, H.H. and Sisson, V.B., 1987. Confirmation of the empirical correlation of Al in hornblende with pressure of solidification of calc-alkaline plutons. American Mineralogist, vol. 72, p. 231–239.

Hood, S.B., Hickey, K., Colpron, M. and Mercer, B.J., 2009. High-grade hydrothermal copper-gold mineralization in foliated granitoids at the Minto mine, central Yukon. *In*: Yukon Exploration and Geology 2008, L.H. Weston, L.R. Blackburn and L.L. Lewis (eds.), Yukon Geological Survey, p. 137–146.

Hood, S.B., 2012. Mid-crustal Cu-Au mineralisation during episodic pluton emplacement, hydrothermal fluid flow, and ductile deformation at the Minto deposit, YT, Canada. MSc thesis, University of British Columbia, Vancouver, British Columbia, 231 p.

Hughes, O.L., 1990. Surficial geology and geomorphology, Aishihik Lake, Yukon Territory. Geological Survey of Canada, Paper 87-29, 23 p., 5 sheets.

Hunt, P.A. and Roddick, J.C., 1987. A compilation of K-Ar ages, Report 17. *In*: Radiogenic age and isotopic studies: Report I, Paper 87-2, Geological Survey of Canada, p. 143–210.

Hunt, P.A. and Roddick, J.C., 1988. A compilation of K-Ar ages, Report 18. *In*: Radiogenic age and isotopic studies: Report 2, Paper 88-2, Geological Survey of Canada, p. 127–153.

Hunt, P.A. and Roddick, J.C., 1991. A compilation of K-Ar ages: Report 20. *In*: Radiogenic Age and Isotopic Studies, Report 4, Geological Survey of Canada, Paper 90-2, p. 113–143.

Hunt, P.A. and Roddick, J.C., 1992. A compilation of K-Ar ages, Report 21. *In*: Radiogenic age and isotopic studies: Report 5, Paper 91-2, Geological Survey of Canada, p. 207–261.

Hunt, P.A. and Roddick, J.C., 1993. A compilation of K-Ar and 40 Ar-39 Ar ages: Report 23. *In*: Radiogenic age and isotopic studies: Report 7, Geological Survey of Canada, Paper 93-2, p. 127–154.

Hunt, P.A. and Roddick, J.C., 1994. A compilation of K-Ar and 40 Ar-39 Ar ages: Report 24. *In*: Radiogenic Age and Isotopic Studies: Report 8, Geological Survey of Canada, Current Research 1994-F, p. 125–155.

Ishihara, S., 1977. The magnetite-series and ilmenite-series granitic rocks. Mining Geology, vol. 27, p. 293–305.

Israel, S., Friend, M. and Borch, A., 2017. Preliminary bedrock geology of the Long Lake and Moraine Lake areas, southwestern Yukon (NTS 115A/15 and 115H/2 and 7). *In*: Yukon Exploration and Geology 2016, K.E. MacFarlane and L.H. Weston (eds.), Yukon Geological Survey, p. 87–102.

Jackaman, W., 2015a. Regional stream sediment geochemical data, Glenlyon area, central Yukon (NTS 105K & L). Yukon Geological Survey, Open File 2015-9.

Jackaman, W., 2015b. Regional stream sediment geochemical data, Carmacks area, southern Yukon (NTS 115I). Yukon Geological Survey, Open File 2015-14.

Jackson L.E., Jr., Barendregt, R.W., Baker, J. and Irving, E., 1996. Early Pleistocene volcanism and glaciation in central Yukon: a new chronology from field studies and paleomagnetism. Canadian Journal of Earth Sciences, vol. 33, no. 6, p. 904–916.

Jackson, L.E., Jr., 1997a. Surficial geology, Victoria Creek, Yukon Territory. Geological Survey of Canada, Map 1876A, scale 1:100 000.

Jackson, L.E., Jr., 1997b. Surficial geology, Tantalus Butte, Yukon Territory. Geological Survey of Canada, Map 1879A, scale 1:100 000.

Jackson, L.E., Jr., 1997c. Surficial geology, Granite Canyon, Yukon Territory. Geological Survey of Canada, Map 1878A, scale 1:100 000.

JDS Energy and Mining Ltd., 2016. NI 43-101 Preliminary economic assessment technical report on the Carmacks project, Yukon, Canada. Copper North Mining Corp., sedar.com, 216 p.

Johnston, S.T. and Timmerman, J., 1997. Geology of Hopkins Lake map area, Yukon (NTS 115H/7). Exploration and Geological Services Division, Yukon Region, Indian and Northern Affairs Canada, Geoscience Map 1997-9, scale 1:50 000.

Johnston, S.T., 1993. The geological evolution of Nisling assemblage and Stikine terrane in the Aishihik Lake area, southwest Yukon. PhD thesis, University of Alberta, Edmonton, 270 p.

Johnston, S.T. and Erdmer, P., 1995a. Magmatic flow and emplacement foliations in the Early Jurassic Aishihik batholith, southwest Yukon: Implications for northern Stikinia. *In*: Jurassic Magmatism and Tectonics of the North American Cordillera, D.M. Miller and C. Busby (eds.), Geological Society of America, Special Paper 299, p. 65–82.

Johnston, S.T. and Erdmer, P., 1995b. Hot-side-up aureole in southwest Yukon and limits on terrane assembly of the northern Canadian Cordillera. Geology, vol. 23, no. 5, p. 419–422.

Johnston, S.T., Mortensen, J.K. and Erdmer, P., 1996. Igneous and metaigneous age constraints for the Aishihik metamorphic suite, southwest Yukon. Canadian Journal of Earth Sciences, vol. 33, p. 1543–1555.

Joyce, N.L., Colpron, M., Allan, M.M., Sack, P.J., Crowley, J.L. and Chapman, J.B., 2016. New U-Pb zircon dates from the Aishihik batholith, southern Yukon. *In*: Yukon Exploration and Geology, K.E. MacFarlane and M.G. Nordling (eds.), Yukon Geological Survey, p. 131–149.

Joyce, N.L., Ryan, J.J., Colpron, M., Hart, C.J.R. and Murphy, D.C., 2015. A compilation of $^{40}Ar/^{39}Ar$ age determinations for igneous and metamorphic rocks, and mineral occurrences from central and southeast Yukon. Geological Survey of Canada, Open File 7924.

Keyser, H., 2001. Report on the 2001 geochemical work on the Mars property. Yukon Energy, Mines and Resources Assessment Report 094290.

Klöcking, M., Mills, L., Mortensen, J.K. and Roots, C.F., 2016. Geology of mid-Cretaceous volcanic rocks at Mount Nansen, central Yukon, and their relationship to the Dawson Range batholith. Yukon Geological Survey, Open File 2016-25, 37 p.

Knight, E., Schneider, D.A. and Ryan, J.J., 2013. Thermochronology of the Yukon-Tanana terrane, west-central Yukon: Evidence for Jurassic extension and exhumation in the northern Cordillera. Journal of Geology, vol. 121, p. 371–400.

Kovacs, N., 2018. Genesis and post-ore modification of the migmatized Carmacks Copper Cu-Au-Ag porphyry deposit, Yukon, Canada. MSc thesis, University of British Columbia, Vancouver, British Columbia, 291 p.

Kovacs, N., Allan, M.M., Zagorevski, A., Milton, J.E. and Hart, C.J.R., 2017. New geological insights into the Carmacks Copper Cu-Au-Ag deposit, central Yukon (Yukon MINFILE 115I 008). *In*: Yukon Exploration and Geology 2016, K.E. MacFarlane and L.H. Weston (eds.), Yukon Geological Survey, p. 117–140.

Kovacs, N., Allan, M.M., Crowley, J.L., Colpron, M., Hart, C.J.R., Zagorevski, A. and Creaser, R.A., 2020. Carmacks Copper Cu-Au-Ag deposit: mineralization and post-ore migmatization of a Stikine arc porphyry copper system in Yukon, Canada. Economic Geology, (in press).

Lang, J.R. and McClaren, M., 2003. Hydrothermal alteration, mineralization and exploration potential of the Mars alkalic copper-gold-molybdenum porphyry occurrence, Laberge map area (105E/7), Yukon. *In*: Yukon Exploration and Geology 2004, D.S. Emond and L.L. Lewis (eds.), Yukon Geological Survey, p. 261–269.

Lang, J.R. and McClaren, M., 2004. The Mars alkalic Cu-Au property, Laberge map area (105E/7), Yukon Territory, Canada: Geology, alteration and mineralization – diamond drilling. Yukon Energy, Mines and Resources Assessment Report 094480.

Le Bas, M.J., Le Maitre, R.W., Streckeisen, A.L. and Zanettin, B., 1986. A Chemical classification of volcanic rocks based on the total alkali-silica diagram. Journal of Petrology, vol. 27, p. 745–750.

Le Bas, M.J. and Streckeisen, A.L., 1991. The IUGS systematics of igneous rocks. Journal of the Geological Society, London, vol. 148, p. 825–833.

LeCouteur, P.C. and Tempelman-Kluit, D.J., 1976. Rb/Sr ages and a profile of initial $^{87}Rb/^{86}Sr$ ratios for plutonic rocks across Yukon Crystalline Terrane. Canadian Journal of Earth Sciences, vol. 13, p. 319–330.

Lee, J.-Y., Marti, K., Severinghaus, J.P., Kawamura, K., Yoo, H.-S., Lee, J.B. and Kim, J.S., 2006. A redetermination of the isotopic abundances of atmospheric Ar. Geochimica et Cosmochimica Acta, vol. 70, no. 17, p. 4507–4512.

LSCFN, 1997. Little Salmon/Carmacks First Nation Final Agreement between the Government of Canada, the Little Salmon/Carmacks First Nation and the Government of the Yukon (1997), https://yukon.ca/sites/yukon.ca/files/eco/eco-ar-little-salmon-carmacks-final-agreement.pdf [accessed September 30, 2019].

Liverton, T. and Casselman, S., 2018. Mod Property, VMS mineralization in the western part of the Yukon-Tanana terrane? (Yukon MINFILE 105B 028, 029, 031). *In*: Yukon Exploration and Geology 2017, K.E. MacFarlane (ed.), Yukon Geological Survey, p. 103–109.

Liverton, T., Mortensen, J.K. and Roots, C.F., 2005. Character and metallogeny of Permian, Jurassic and Cretaceous plutons in the southern Yukon-Tanana Terrane. *In*: Yukon Exploration and Geology 2004, D.S. Emond, L.L. Lewis and G.D. Bradshaw (eds.), Yukon Geological Survey, p. 147–165.

Logan, J.M. and Mihalynuk, M.G., 2014. Tectonic controls on Early Mesozoic paired alkaline porphyry deposit belts (Cu-Au ± Ag-Pt-Pd-Mo) within the Canadian Cordillera. Economic Geology, vol. 109, p. 827–858.

Logan, J.M., Mihalynuk, M.G., Ullrich, T. and Friedman, R.M., 2007. U-Pb ages of intrusive rocks and $^{40}Ar/^{39}Ar$ plateau ages of copper-gold-silver mineralization associated with alkaline intrusive centres at Mount Polley and the Iron Mask batholith, southern and central British Columbia. *In*: Geological Fieldwork 2006, British Columbia Ministry of Energy, Mines and Petroleum Resources, Paper 2007-1, p. 93–116.

Mackie, R., Arne, D. and Pennimpede, C., 2016a. Enhanced interpretation of stream sediment geochemical data for NTS 115N and 115O. Yukon Geological Survey, Open File 2016-30, 13 maps.

Mackie, R., Arne, D. and Pennimpede, C., 2016b. Enhanced interpretation of stream sediment geochemical data for NTS 115J and 115K. Yukon Geological Survey, Open File 2016-15, 13 maps.

Mackie, R., Arne, D. and Pennimpede, C., 2016c. Enhanced interpretation of stream sediment geochemical data for NTS 115I. Yukon Geological Survey, Open File 2016-14, 15 maps.

Mackie, R., Arne, D. and Pennimpede, C., 2016d. Enhanced interpretation of stream sediment geochemical data for NTS 105L. Yukon Geological Survey, Open File 2016-10, 15 maps.

Mackie, R., Arne, D. and Pennimpede, C., 2016e. Enhanced interpretation of stream sediment geochemical data for NTS 115H. Yukon Geological Survey, Open File 2016-11, 13 maps.

Mackie, R., Arne, D. and Pennimpede, C., 2016f. Enhanced interpretation of stream sediment geochemical data for NTS 105E. Yukon Geological Survey, Open File 2016-9, 13 maps.

Mackie, R., Arne, D. and Pennimpede, C., 2016g. Enhanced interpretation of stream sediment geochemical data for NTS 105C. Yukon Geological Survey, Open File 2016-12, 15 maps.

Mackie, R.A., Arne, D.C. and Brown, O., 2015. Enhanced interpretation of regional geochemical stream sediment data from Yukon: catchment basin analysis and weighted sums modeling. Yukon Geological Survey, Open File 2015-10, 9 p.

Maniar, P.D. and Piccoli, P.M., 1989. Tectonic discrimination of granitoids. Geological Society of America Bulletin, vol. 101, no. 5, p. 635–643.

Massey, N.W.D., MacIntyre, D.G., Desjardins, P.J. and Cooney, R.T., 2005. Digital geology map of British Columbia: Whole Province. B.C. Ministry of Energy, Mines and Petroleum Resources, Geological Survey Branch, GeoFile 2005-1, scale 1:250 000.

McCausland, P.J.A., Symons, D.T.A., Hart, C.J.R. and Blackburn, W.H., 2002. Paleomagnetism and geobarometry of the Granite Mountain batholith, Yukon: Minimal geotectonic motion of the Yukon-Tanana Terrane relative to North America. *In*: Yukon Exploration and Geology 2001, D.S. Emond, L.H. Weston and L.L. Lewis (eds.), Exploration and Geological Services Division, Yukon, Indian and Northern Affairs Canada, p. 163–177.

McDonough, W.F. and Sun, S.-s., 1995. The composition of the Earth. Chemical Geology, vol. 120, p. 223–253.

McDougall, I. and Harrison, T.M., 1999. Geochronology and thermochronology by the $^{40}Ar/^{39}Ar$ method. Oxford University Press, 288 p.

McLennan, S.M., 2001. Relationships between the trace element composition of sedimentary rocks and upper continental crust. Geochemistry, Geophysics, Geosystems, vol. 2, 24 p.

Mercer, B.J. and Sagman, J., 2012. Minto Phase VI Preliminary Feasibility Study Technical Report, Minto Explorations Ltd. 320 p.

Middlemost, E.A.K., 1994. Naming materials in the magma/igneous rock system. Earth-Science Reviews, vol. 37, no. 3, p. 215–224.

Mihalynuk, M.G., 1999. Geology and mineral resources of the Tagish Lake area (NTS 104M/8, 9, 10E and 104N/12W) northwestern British Columbia. British Columbia Geological Survey, Bulletin 105, 217 p.

Mihalynuk, M.G., Erdmer, P., Ghent, E.D., Cordey, F., Archibald, D.A., Friedman, R.M. and Johannson, G.G., 2004. Coherent French Range blueschist: Subduction to exhumation in <2.5 m.y.? Geological Society of America Bulletin, vol. 116, p. 910–922.

Mihalynuk, M.G., Nelson, J.L. and Diakow, L.J., 1994. Cache Creek terrane entrapment: Oroclinal paradox within the Canadian Cordillera. Tectonics, vol. 13, p. 575–595.

Mihalynuk, M.G., Smith, M.T., Gabites, J.E., Runkle, D. and Lefebure, D., 1992. Age of emplacement and basement character of the Cache Creek terrane as constrained by new isotopic and geochemical data. Canadian Journal of Earth Sciences, vol. 29, no. 11, p. 2463–2477.

Miller, J.S., Matzel, J.E.P., Miller, C.F., Burgess, S.D. and Miller, R.B., 2007. Zircon growth and recycling during the assembly of large, composite arc plutons. Journal of Volcanology and Geothermal Research, vol. 167, p. 282–299.

Mira Geoscience, 2014. Geologically-constrained inversion of magnetic and gravity data over parts of the Yukon-Tanana terrane and Whitehorse trough. Yukon Geological Survey, Miscellaneous Report MR-10, 85 p.

Monger, J.W.H., Price, R.A. and Tempelman-Kluit, D.J., 1982. Tectonic accretion and the origin of the two major metamorphic and plutonic welts in the Canadian Cordillera. Geology, vol. 10, no. 2, p. 70–75.

Morneau, Y.E., 2017. Tectono-metamorphic evolution of the Snowcap assemblage, Yukon-Tanana terrane, west-central Yukon. Unpublished MSc thesis. Carleton University, 198 p.

Mortensen, J.K., 1992. Pre-mid-Mesozoic tectonic evolution of the Yukon-Tanana terrane, Yukon and Alaska. Tectonics, vol. 11, p. 836–853.

Mortensen, J.K. and Gabites, J.E., 2002. Lead isotopic constraints on the metallogeny of southern Wolf Lake, southeastern Teslin and northern Jennings River map areas, Yukon and British Columbia: Preliminary results. *In*: Yukon Exploration and Geology 2001, D.S. Emond, L.H. Weston and L.L. Lewis (eds.), Exploration and Geological Services Division, Yukon Region, Indian and Northern Affairs Canada, p. 179–188.

Mortensen, J.K., Ghosh, D. and Ferri, F., 1995. U-Pb age constraints of intrusive rocks associated with copper-gold porphyry deposits in the Canadian Cordillera. *In*: Porphyry deposits of the northwestern Cordillera of North America, T.G. Schroeter (ed.), Canadian Institute of Mining and Metallurgy, Special Volume 46, p. 142–158.

Mortensen, J.K., Hart, C.J.R., Tarswell, J. and Allan, M.M., 2016. U-Pb zircon age and Pb isotopic constraints on the age and origin of porphyry and epithermal vein mineralization in the eastern Dawson Range, Yukon. *In*: Yukon Exploration Geology 2015, K.E. MacFarlane and M.G. Nordling (eds.), Yukon Geological Survey, p. 165–185, including appendices.

Murphy, D.C., Colpron, M., Gordey, S.P., Roots, C.F., Abbott, J.G. and Lipovsky, P.S., 2001. Preliminary bedrock geological map of northern Finlayson Lake area (NTS 105G) Yukon Territory. Exploration and Geological Services Division, Yukon Region, Indian and Northern Affairs Canada, Open File 2001-33, scale 1:100 000.

Murphy, D., Mortensen, J.K., Piercey, S.J., Orchard, M.J. and Gehrels, G.E., 2006. Mid-Paleozoic to early Mesozoic tectonostratigraphic evolution of Yukon-Tanana and Slide Mountain terranes and affiliated overlap assemblages, Finlayson Lake massive sulphide district. *In*: Paleozoic evolution and metallogeny of pericratonic terranes at the ancient Pacific margin of North America, Canadian and Alaskan Cordillera, M. Colpron and J.L. Nelson (eds.), Geological Association of Canada, Special Paper 45, p. 75–106.

Nelson, F.E., Barendregt, R.W. and Villeneuve, M., 2009. Stratigraphy of the Fort Selkirk Volcanogenic Complex in central Yukon and its paleoclimatic significance: Ar/Ar and paleomagnetic data. Canadian Journal of Earth Sciences, vol. 46, no. 5, p. 381–401.

Nelson, J.L. and Colpron, M., 2007. Tectonics and metallogeny of the British Columbia, Yukon and Alaskan Cordillera, 1.8 Ga to the present. *In*: Mineral Resources of Canada: A Synthesis of Major Deposit-types, District Metallogeny, the Evolution of Geological Provinces, and Exploration Methods, W.D. Goodfellow (ed.), Geological Association of Canada, Mineral Deposits Division, Special Publication 5, p. 755–791.

Nelson, J.L., Colpron, M. and Israel, S., 2013. The Cordillera of British Columbia, Yukon, and Alaska: Tectonics and metallogeny. *In*: Tectonics, Metallogeny and discovery: The North American Cordillera and similar accretionary settings, M. Colpron, T. Bissig, B.G. Rusk and J.F.H. Thompson (eds.), Society of Economic Geologists, Special Publication Number 17, p. 53–109.

Nelson, J.L., Colpron, M., Piercey, S.J., Dusel-Bacon, C., Murphy, D.C. and Roots, C.F., 2006. Paleozoic tectonic and metallogenic evolution of the pericratonic terranes in Yukon, northern British Columbia and eastern Alaska. *In:* Paleozoic Evolution and Metallogeny of Pericratonic Terranes at the Ancient Pacific Margin of North America, Canadian and Alaskan Cordillera, M. Colpron and J.L. Nelson (eds.), Geological Association of Canada, Special Paper 45, p. 323–360.

Ouellette, O. and Pollries, B., 2010. 2010 Diamond drilling program on the DAD claim block, Northern Tiger Resources Inc. Yukon Energy, Mines and Resources Assessment Report 096148.

Pangman, P.G., 1973. A petrologic study of the Windy Mountain pluton, Yukon Territory. BSc thesis, Queen's University, 69 p.

Pautler, J., 2009. Geological, geochemical, petrographic and compilation Assessment Report of the Stu property. Yukon Energy, Mines and Resources Assessment Report 095195.

Pearce, J.A., 1996. A user's guide to basalt discrimination diagrams. *In*: Trace element geochemistry of volcanic rocks, D.A. Wyman (ed.), Geological Association of Canada - Mineral Deposits Division, p. 79–113.

Pearce, J.A., Harris, N.B.W. and Tindle, A.G., 1984. Trace element discrimination diagrams for the tectonic interpretation of granitic rocks. Journal of Petrology, vol. 25, no. 4, p. 956–983.

Pearson, W.N. and Clark, A.H., 1979. The Minto copper deposit, Yukon Territory; a metamorphosed orebody in the Yukon crystalline terrane. Economic Geology, vol. 74, no. 7, p. 1577–1599.

Phendler, R.W., 1983. Report on the Logjam silver property. Yukon Energy, Mines and Resources Assessment Report 062205.

Phillips, M.P., 1971. Dawson Range Joint Venture summary report: Granite Mountain property, Yukon. Yukon Energy, Mines and Resources Assessment Report 092570.

Piercey, S.J. and Colpron, M., 2009. Composition and provenance of the Snowcap assemblage, basement to the Yukon-Tanana terrane, northern Cordillera: Implications for Cordilleran crustal growth. Geosphere, vol. 5, no. 5, p. 439–464.

Pillsbury, J.N.P., 2016. Characterizing the Bennett batholith: Implications for Early-Middle Jurassic magmatism in southwest Yukon. Unpublished BSc thesis, University of British Columbia, 116 p.

Porter, C., Morin, P., Howat, I., Noh, M.-J., Bates, B., Peterman, K., Keesey, S., Schlenk, M., Gardiner, J., Tomko, K., Willis, M., Cloutier, M., Husby, E., Foga, S., Nakamura, H., Platson, M., Wethington, M., Jr., Williamson, C., Bauer, G., Enos, J., Arnold, G., Kramer, W., Becker, P., Doshi, A., D'Souza, C., Cummens, P., Laurier, F. and Bojesen, M., 2018. ArcticDEM. Harvard Dataverse, V1, https://doi.org/10.7910/DVN/OHHUKH [accessed: 15 October 2018].

Preto, V.A., 1972. Geology of Copper Mountain, British Columbia. British Columbia Ministry of Energy, Mines and Petroleum Resources, Bulletin 59, 87 p.

Rasband, W.S., 1997-2016. ImageJ: Image processing and analysis in Java. U. S. National Institutes of Health, Bethesda, Maryland, USA, https://imagej.nih.gov/ij/.

Read, P.B., Woodsworth, G.J., Greenwood, H.J., Ghent, E.D. and Evenchick, C.A., 1991. Metamorphic map of the Canadian Cordillera: Map 1714A. Geological Survey of Canada, A Series Map 1714A, scale 1:2 000 000.

Relf, C., 2015. Summary of Yukon Geological Survey 2014-15 Activities. *In*: Yukon Exploration and Geology Overview 2014, K.E. MacFarlane and M.G. Nordling (eds.), Yukon Geological Survey, p. 1–16.

Richards, B.G., 1991. VLF – Electromagnetic and geochemical survey on the Irish and Kip claims. Yukon Energy, Mines and Resources Assessment Report 093007.

Roots, C.F., Nelson, J.L., Mihalynuk, M.G., Harms, T., de Keijzer, M. and Simard, R.-L., 2004. Bedrock geology, Dorsey Lake (NTS 105B4), Yukon Territory. Yukon Geological Survey, Open File 2004-2; *also Geological Survey of Canada, Open File 4630*. Scale 1: 50 000.

Roots, C.F., Nelson, J.L. and Stevens, R., 2004. Bedrock geology, Seagull Creek, Yukon Territory. Yukon Geological Survey, Open File 2004-1; *also Geological Survey of Canada Open File 4632*. Scale 1: 50 000.

Ryan, J.J., Colpron, M. and Hayward, N., 2010. Geology, southwestern McQuesten and parts of northern Carmacks, Yukon. Geological Survey of Canada, Canadian Geoscience Map 7 (preliminary version), scale 1:125 000.

Ryan, J.J., Westberg, E.E., Williams, S.P. and Chapman, J.B., 2016. Geology, Mount Nansen – Nisling River area, Yukon. Geological Survey of Canada, Canadian Geoscience Map 292 (ed. prelim.), 1 sheet, scale 1:100 000.

Ryan, J.J., Zagorevski, A. and Piercey, S.J., 2018. Geochemical data of Yukon-Tanana and Slide Mountain terranes and their successor rocks in Yukon and northern British Columbia. Geological Survey of Canada, Open File 8500, p. 11.

Ryan, J.J., Zagorevski, A., Williams, S.P., Root, C.F., Ciolkiewicz, W. and Chapman, J.B., 2013. Geology, Stevenson Ridge (northeast part), Yukon. Geological Survey of Canada, Geoscience Map 116 (2nd edition, preliminary), scale 1:100 000.

Sack, P.J., Casselman, S., James, D. and Harris, B., 2016. Copper-gold ± silver mineralization at the Stu occurrence, central Yukon (Yukon MINFILE 115I 011). *In*: Yukon Exploration and Geology 2015, K.E. MacFarlane and M.G. Nordling (eds.), Yukon Geological Survey, p. 207–222.

Sack, P.J., Kerr, R. and McIlveen, D., 2017. Update on the Minto deposit (Yukon MINFILE 115I 021, 022). *In*: Yukon Exploration and Geology Overview 2016, K.E. MacFarlane (ed.), Yukon Geological Survey, p. 75–87, plus digital appendices.

Sawyer, E.W., 2008. Atlas of migmatites. The Canadian Mineralogist, Special Publication 9. Mineralogical Association of Canada, 386 p.

Schoene, B., 2014. U-Th-Pb geochronology. *In*: Treatise on Geochemistry, 2nd edition, H.D.H.K. Turekian (ed.), Elsevier, p. 341–378.

Seedorff, E., Barton, M.D., Stavast, W.J.A. and Maher, D.D., 2008. Root zones of porphyry systems: Extending the porphyry model to depth. Economic Geology, vol. 103, p. 939–956.

Seedorff, E., Dilles, J.H., Proffett, J.M., Einaudi, M.T., Zurcher, L., Stavast, W.J.A., Johnson, D.A. and Barton, M.D., 2005. Porphyry deposits: Characteristics and origin of hypogene features. *In*: Economic Geology: One Hundredth Anniversary Volume, J.W. Hedenquist, J.F.H. Thompson, R.J. Goldfarb and J.P. Richards (eds.), Society of Economic Geologists, p. 251–298.

Shand, S.J., 1943. Eruptive rocks; Their genesis, composition, classification, and their relation to ore deposits, with a chapter on meteorites. Hafner Publishing Co., New York, 444 p.

Sidhu, G., 2011. Toe property drill program, July 21st to August 13th, 2010. Yukon Energy, Mines and Resources, YMEP Report 2010-025, 119 p.

Sillitoe, D.H. and Perello, J., 2005. Andean Copper Province: Tectonomagmatic settings, deposit types, metallogeny, exploration and discovery. *In*: Economic Geology: One Hundredth Anniversary Volume, J.W. Hedenquist, J.F.H. Thompson, R.J. Goldfarb and J.P. Richards (eds.), Society of Economic Geologists, p. 845–890.

Simard, R.-L., 2003. Geological map of southern Semenof Hills (part of NTS 105E/1, 7, 8), south-central Yukon. Yukon Geological Survey, Open File 2003-12, scale 1:50 000.

Simard, R.-L. and Devine, F., 2003. Preliminary geology of the southern Semenof Hills, central Yukon (105E/1, 7, 8). *In*: Yukon Exploration and Geology 2002, D.S. Emond and L.L. Lewis (eds.), Exploration and Geological Services Division, Yukon Region, Indian and Northern Affairs Canada, p. 213–222.

Sinclair, W.D., 1977. Geology and mineral deposits of the Minto area, Yukon Territory. *In*: Mineral Industry Report 1976, J.A. Morin, W.D. Sinclair, D.B. Craig and M. Marchand (eds.), Indian and Northern Affairs, p. 68–82.

Sinclair, W.D., Morin, J.A., Craig, D.B. and Marchand, M., 1976. Mineral industry Report 1975, Yukon Territory, Indian and Northern Affairs.

Souther, J.G., 1991. Volcanic regimes, Chapter 14. *In*: Geology of the Cordilleran Orogen in Canada, H. Gabrielse and C.J. Yorath (eds.), Geological Survey of Canada, Geology of Canada no. 4; *also Geological Society of America, The Geology of North America, vol. G-2*, p. 457–490.

Stevens, R.A., 1996. Dorsey Assemblage: Pre-mid-Permian high temperature and pressure metamorphic rocks in the Dorsey Range, southern Yukon Territory. Lithoprobe Report no. 50, SNORCLE and Cordilleran Tectonics Workshop, p. 70–75.

Stevens, R.A., Mortensen, J.K. and Hunt, P.A., 1993. U-Pb and $^{40}Ar/^{39}Ar$ geochronology of plutonic rocks from the Teslin suture zone, Yukon Territory. *In*: Radiogenic age and isotopic studies: Report 7, Geological Survey of Canada, Paper 93-2, p. 83–90.

Stevens, R.D., Delabio, R.N. and Lachance, G.R., 1982a. Age determinations and geological studies; K-Ar isotopic ages, Report 16. Geological Survey of Canada, 82-2, 62 p.

Stevens, R.D., Delabio, R.N. and Lachance, G.R., 1982b. Age determinations and geological studies; K-Ar isotopic ages, Report 15. Geological Survey of Canada, Paper 81-2, 56 p.

Sun, S.-s. and McDonough, W.F., 1989. Chemical and isotopic systematics of oceanic basalts: implications for mantle composition and processes. *In*: Magmatism in the Ocean Basins, A.D. Saunders and M.J. Norry (eds.), Geological Society, London, Special Publication 42, p. 313–345.

Tafti, R., 2005. Nature and origin of the Early Jurassic copper (-gold) deposits at Minto and Williams Creek, Carmacks copper belt, western Yukon: Examples of deformed porphyry deposits. MSc thesis, University of British Columbia, 227 p.

Tempelman-Kluit, D.J. and Wanless, R.K., 1980. Zircon ages for the Pelly Gneiss and Klotassin granodiorite in western Yukon. Canadian Journal of Earth Sciences, vol. 17, no. 3, p. 297–306.

Tempelman-Kluit, D.J., 1974a. Geology of Aishihik Lake. Geological Survey of Canada, Preliminary Map 17-1973, scale 1:250 000.

Tempelman-Kluit, D.J., 1974b. Reconnaissance geology of Aishihik Lake, Snag and part of Stewart River map-areas, west-central Yukon. Geological Survey of Canada, Paper 73-41, 97 p.

Tempelman-Kluit, D.J., 1984. Geology of Laberge (105E) and Carmacks (115I) map areas, Yukon. Geological Survey of Canada, Open File 1101.

Tempelman-Kluit, D.J., 2009. Geology of Carmacks and Laberge map areas, central Yukon: Incomplete draft manuscript on stratigraphy, structure and its early interpretation (*ca.* 1986). Geological Survey of Canada, Open File 5982, 399 p.

Tempelman-Kluit, D.J. and Currie, R.G., 1978. Reconnaissance rock geochemistry of Aishihik Lake, Snag, and Stewart River map areas in the Yukon Crystalline terrane. Geological Survey of Canada, Paper 77-8, 72 p.

Tempelman-Kluit, D.J. and Wanless, R.K., 1975. Potassium-argon age determinations of metamorphic and plutonic rocks in the Yukon Crystalline terrane. Canadian Journal of Earth Sciences, vol. 12, no. 11, p. 1895–1909.

Thompson, J.F.H., Sillitoe, R.H., Baker, T., Lang, J.R. and Mortensen, J., 1999. Intrusion-related gold deposits associated with tungsten-tin provinces. Mineralium Deposita, vol. 34, p. 323–334.

Tizzard, A., Johnston, S.T. and Heaman, L.M., 2009. Arc imbrication during thick-skinned collision within the northern Cordilleran accretionary orogen, Yukon, Canada. *In*: Earth Accretionary Systems in Space and Time, P.A. Cawood and A. Kroner (eds.), The London Geological Society, Special Publication 318, p. 309–327.

Topham, M.J., Allan, M.M., Mortensen, J.K., Hart, C.J.R., Colpron, M. and Sack, P.J., 2016. Crustal depth of emplacement of the Early Jurassic Aishihik and Tatchun batholiths, west-central Yukon. *In*: Yukon Exploration and Geology, K.E. MacFarlane and M.G. Nordling (eds.), Yukon Geological Survey, p. 233–251.

Traynor, S., 1999. Evaluation report on the King Lake property (EZE1-24 claims). Yukon Energy, Mines and Resources Assessment Report 094010.

van Straaten, B.I. and Bichlmaier, S., 2018. Late Early to Middle Jurassic Hazelton Group volcanism and its tectonic setting, McBride River area, northwest British Columbia. *In:* Geological Fieldwork 2017. British Columbia Ministry of Energy, Mines and Petroleum Resources, British Columbia Geological Survey Paper 2018-1, p. 39–66.

van Straaten, B.I. and Gibson, R., 2017. Late Early to Middle Jurassic Hazelton Group volcanism and mineral occurrences in the McBride-Tanzilla area, northwest British Columbia. *In:* Geological Fieldwork 2016, British Columbia Ministry of Energy and Mines, British Columbia Geological Survey Paper 2017-1, p. 83–115.

Verweerd, A. and Killin, K. Preface by M. Colpron and B. Mercer, 2010. Report on a Quantec Titan-24 geophysical survey over the Minto Mine, central Yukon. Yukon Geological Survey, Open File 2010-19.

Wanless, R.K., Stevens, R.D., Lachance, G.R. and Delabio, R.N., 1970. Age determinations and geological studies; K-Ar isotopic ages, Report 9. Geological Survey of Canada, Paper 69-2A, 78 p.

Wanless, R.K., Stevens, R.D., Lachance, G.R. and Delabio, R.N., 1978. Age determinations and geological studies; K-Ar isotopic ages, Report 13. Geological Survey of Canada, Paper 77-2, 60 p.

Wark, J.M., 1998. Geophysical surveys on the Mars property. Yukon Energy, Mines and Resources Assessment Report 093874.

Watson, B.E., Wark, D.A. and Thomas, J.B., 2006. Crystallization thermometers for zircon and rutile. Contributions to Mineralogy and Petrology, vol. 151, p. 413–433.

Wheeler, J.O., 1961. Whitehorse map-area, Yukon Territory (105D). Geological Survey of Canada, Memoir 312, 156 p.

Whitney, D.L. and Evans, B.W., 2010. Abbreviations for names of rock-forming minerals. American Mineralogist, vol. 95, p. 185–187.

Wilson, F.H., Hults, C.P., Mull, C.G. and Karl, S.M. (compilers), 2015. Geologic map of Alaska. U.S. Geological Survey, Scientific Investigations Map 3340, scale 1:1 584 000.

Winchester, J.A. and Floyd, P.A., 1977. Geochemical discrimination of different magma series and their differentiation products using immobile elements. Chemical Geology, vol. 20, p. 325–343.

Woodsworth, G.J., Anderson, R.G. and Armstrong, R.L., 1991. Plutonic regimes. *In*: Geology of the Cordilleran orogen in Canada, Chapter 15, H. Gabrielse and C.J. Yorath (eds.), Geological Survey of Canada, Geology of Canada series no. 4, p. 281–327.

Yukon Geological Survey (YGS), 2020a. Yukon Digital Bedrock Geology http://www.geology.gov.yk.ca/update_yukon_bedrock_geology_map.html [Accessed January 10, 2020].

Yukon Geological Survey (YGS), 2020b. Yukon MINFILE - A database of mineral occurrences http://data.geology.gov.yk.ca [Accessed January 10, 2020].

Yukon Geological Survey (YGS), 2020c. Yukon Geochronology database ftp://ftp.geomaticsyukon.ca/GeoYukon/Geological/Geochronology/Geochronology.shp.zip [accessed January 10, 2020].

Zen, E. and Hammarstrom, J.M., 1984. Magmatic epidote and its petrologic significance. Geology, vol. 12, p. 515–518.

Yukon Geological Survey
Energy, Mines and Resources
Government of Yukon

